Combined Mechanical and Command Design for Micro-Milling Machines

A Thesis
Presented to
The Academic Faculty

by

Joel D. Fortgang

In Partial Fulfillment
of the Requirements for the Degree
Doctor of Philosophy

Woodruff School of Mechanical Engineering
Georgia Institute of Technology
May 2006

Combined Mechanical and Command Design for Micro-Milling Machines

Approved by:

Dr. William Singhose
Associate Professor
School of Mechanical Engineering
Georgia Institute of Technology
Committee Chair

Dr. Farrokh Mistree
Professor
School of Mechanical Engineering
Georgia Institute of Technology

Dr. Martha Gallivan
Assistant Professor
School of Chemical and Biomolecular
Engineering
Georgia Institute of Technology

Dr. Warren Seering
Professor
School of Mechanical Engineering
Massachusetts Institute of Technology

Dr. Thomas Kurfess
Professor
School of Mechanical Engineering
Clemson University

Date Approved: January 5th 2006

ACKNOWLEDGEMENTS

I would like to thank all of those that have supported me in my pursuit of a doctorate. The loving support of my family has kept me going. Even the jovial chiding of my friends has kept me at it. My lab mates have provided a priceless resource. The undergraduate researchers, Rory, Alan, Justis, Vlad, and Brian, made things possible I could not hope to do on my own. The professors and staff at ETSII in Madrid especially Dr. Marquez enabled my hands on experience with micro-mills. My committe deserves thanks for shaping my research. Finally, my advisor Dr. Singhose has supported, advised and motivated me throughout this entire journey.

TABLE OF CONTENTS

LIST OF TABLES

LIST OF FIGURES

GLOSSARY

Acceleration Duration   The time it takes a given actuator to accelerate a system to a specified velocity.

AIST   Agency of Industrial Science and Technology, in Japan.

Combined Design   Incorporating system elements other than the mechanical parameters themselves in the design selection.

Command or Move Duration   The time is takes a machine to complete a move or execute a command component.

Command Shaping   The alteration of a command signal for improved dynamic performance.

Continuum Elements   Oscillatory elements whose motion is prescribed by continuous equations of motion.

Cutting Force   The force between a workpiece and a cutting tool.

Cutting Tool   The rotating bit used in a micro-mill to remove material.

ETSII   Escuela Tecnica Superior de Ingenieros Industriales, in Madrid, Spain.

Extra Insensitive Shapers, EI   An input shaper designed specifically to cancel multiple oscillatory frequencies using sensitivity contstraints.

Feedforward Control   A control technique that introduces commands into a feedback control system between the controller and the actuator.

Input Shaping   The use of a series of impulses convolved with the command sent to the system to reduce vibration.

Micro-Milling   The process by which material is removed from a workpiece using a rotating bit, with measurement made in micrometers.

Micro-Turning   The process by which material is removed from a rotating workpiece using a stationary cutter, with measurement made in micrometers.

Modified Acceleration Approach   Command Shaping technique for tracking multi-axis spatial trajectories quickly.

Multi-Mode Input Shapers   Input Shapers designed to cancel multiple oscillatory frequencies simulatenously.

Optimal Command Design   Selection of the entire command for a system based on an optimization routine.

S-curve   A common temporal motion profile in position, consisting of full-on actuator effort followed by full-stop actuator effort.

Sensitivity   A measure of the degredation in system performance if the system cannot be modelled accurately.

Shaper Duration   The increase in move time when an input shaper is convolved with a command.

Spatial Tracking   Attempting to follow a trajectory only defined in spatial dimensions.

Spindle Speed   The rotation rate of the cutting tool.

Stages   Positioning devices used in micro-milling machines to move both the workpiece and the spindle.

Temporal Tracking   Attemping to follow a trajectory defined in both spatial dimensions and in time.

Throughput   The amount of operations a machine can perform in a given period of time.

Trajectory Frequency Ratio   The ratio of the duration of a desired motion to the period of the system to be moved. It is inversely proportional to move speed.

Trajectory Tracking   The ability to follow a predefined trajectory through space and/or time.

Trajectory Tracking Input Shapers   Input Shapers specifically designed by the author for tracking spatial and/or temporal trajectories.

Unity Magnitude Zero Vibration, UMZV, Input Shaper   A common but not robust input shaper designed for fast motions, whose duration is a third of the system oscillatory frequency.

Vibration Absorbers   An auxillary oscialltory element added to a system to improve the dynamic response.

Vibration Isolators   An auxillary oscialltory element added between a system and the ground to limit vibration transmission.

Zero Vibration and Derivative, ZVD, Input Shaper   A common and robust input shaper whose duration is equal to the system oscillatory frequency.

Zero Vibration, ZV, Input Shaper   A common but not robust input shaper whose duration is half the system oscillatory frequency.

SUMMARY

The utilization of micro-scale technologies is limited by the speed of their manufacture. Micro-milling is one particular technology used to manufacture micro-scale parts which could benefit extensively from an increase in throughput. Micro-milling involves a rotating cutter slightly thicker than a human hair removing material while spinning at speeds often over one hundred thousand revolutions per minute.

An obvious solution to the throughput bottleneck is to move current micro-mills faster using existing technology; however, simply increasing the operational speed of existing micro-mills will lead to vibration and trajectory following problems. If a micro-mill cannot be positioned precisely, then part tolerances cannot be maintained. Thus any increase in throughput would be counterproductive in terms of overall performance.

This dissertation presents techniques to improve the performance of micro-mills, as well as other flexible machines. Theses improvements are possible through the utilization of the vibration suppression scheme of input shaping. By thoughtfully altering the commands sent to flexible systems, their vibration can be significantly reduced. Input shaping was effectively applied to an existing micro-mill, which improved part tolerances and increased operational speed. However, at extremely high speeds, traditional input shaping is not effective at following complicated trajectories. Therefore, new input shaping techniques were developed specifically for trajectory tracking of extremely fast motions on micro-mills and other flexible systems. Often machines cannot achieve these high speeds while maintaining their accuracy because of the mechanical design of the machines themselves. If the mechanical design of micro-mills and other machines consider flexible and lightweight design alternatives that utilize input shaping for vibration suppression instead of stiff and heavy designs, then faster machine motion will be possible. By considering input shaped flexible systems as part of traditional mechanical design processes, these flexible solutions allow vast performance improvement. Specifically, embodiment design can be improved through consideration of input shaping performance requirements. Through these advancements, this dissertation improves the design, control, and performance of micro-mills and other flexible machines.

CHAPTER I

INTRODUCTION

1.1 *Problem*

The manufacture of parts with features on the scale of micrometers is time consuming and expensive, thus it is not yet cost effective for many applications. One particular technology used to create metal, plastic, and ceramic micro-scale parts is Micro-Milling. These parts are used for micro-optical devices, biomedical implants, and other miniature machines. In micro-milling a rotating bit typically on the scale of a mechanical pencil lead or smaller is employed. Due to the small size of this cutting tool, many passes must be made to create a complete part. A method is needed to speed up the cutting process so that small scale parts can be manufactured more rapidly while maintaining precise tolerances. If the current generation of micro-mills are sped up, then unwanted vibration occurs, therefore, simply increasing the velocity of the tool is counterproductive. Other problems also occur at high speed like tool wear, however, vibration is still a major bottleneck in the process.

A possible technique for the improving the vibration associated with high speed micro-milling operations is the employment of the vibration reduction scheme of Input Shaping. This technique can cancel unwanted vibration in flexible systems. However, the current mechanical design techniques produce micro-mills that cannot fully exploit the advantages of input shaping.

If a mechanical design for micro-mills can be developed which allows the efficient use of input shaping for vibration cancellation, micro-milling performance can be improved significantly.

1.1.1 Micro-Milling

Micro-milling is a scaled down version of traditional milling, in that it involves a rotating bit removing material. This bit is often between 20 and 200 μm in diameter. Micro-milling has applications in lithography, medicine, optics, and micro-injection molding. It has advantages over other micro-machining techniques in the number of workable materials and the types of surfaces it can generate. A typical micro-mill is shown in Figure 1.1. This particular mill is located at Escuela Tecnica Superior de Ingenieros Industriales (ETSII) in Madrid, Spain, and is the source of much of the experimental work performed for this investigation.

Micro-milling has two significant issues, the first is the tolerances of the final part, and the second is the long process times. To deal with the tight tolerances, high resolution linear
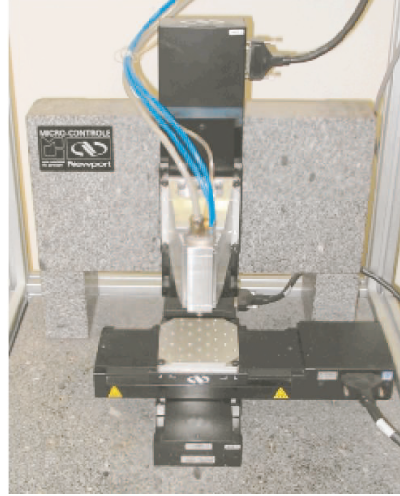
Figure 1.1: A Micro-Mill.
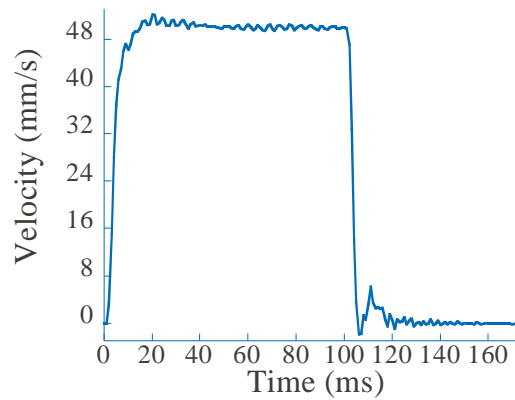
Figure 1.2: Example AIST Mill Velocity Response.

encoders are used for micrometer scale parts. However, the high precision encoders alone do not guarantee precise parts since trajectory deviation can still occur. For example, at the Agency of Industrial Science and Technology (AIST) in Japan, one of their micro-mills exhibits unwanted velocity tracking errors as shown by the velocity profile of Figure 1.2. Likewise, the ETSII mill has a similar problem and its position error can be seen in Figure 1.3. The error on both of these mills results in poor part quality when high-feed-velocity machining is attempted. This tracking problem can be corrected by moving slower; however, this exacerbates the problem of long process times.

Simply increasing the feed velocity of the tool also has a detriment to the cutting dynamics themselves. Because the diameters of the cutting tools are small, large cutting forces will break them. This results in the material removed per pass of each tool tooth also being
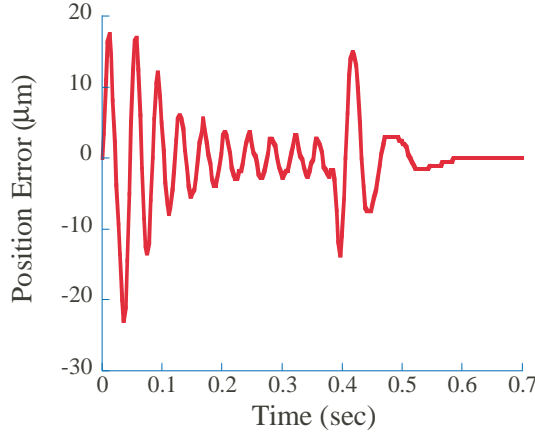
Figure 1.3: Example ETSII Mill Tracking Error.
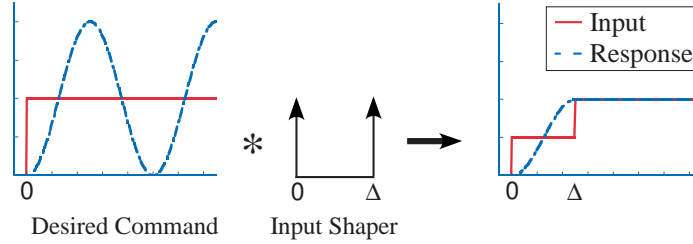
Figure 1.4: Input Shaping Procedure.

small leading to a low throughput. Recent advancements in spindles have pushed speeds to 300,000 RPM allowing the significant reduction of the cutting forces [203]. With these high speed spindles the throughput of the micro-mills is no longer limited by tool breakage, rather it is constrained by the response of the positioning system.

1.1.2 Input Shaping

Command Shaping is a procedure for the alteration of the reference commands sent to a system for the purposes of vibration reduction. One effective version relies on an input shaper which is a series of impulses that are designed to cause minimal vibration when used to drive a system [248]. If this input shaper is convolved with the desired command sent to the system, as seen in Figure 1.4, then the resultant response will have reduced vibration.

One of the drawbacks of this approach is in the difference between the desired and the shaped command. The overall time of the command is increased by the duration of the impulse sequence, and the geometry/shape of the command is also different from the original. Figure 1.5 illustrates this problem for an s-curve position profile (Original) before and after the inclusion of an input shaper (Shaped). The Time Shifted Shaped command is
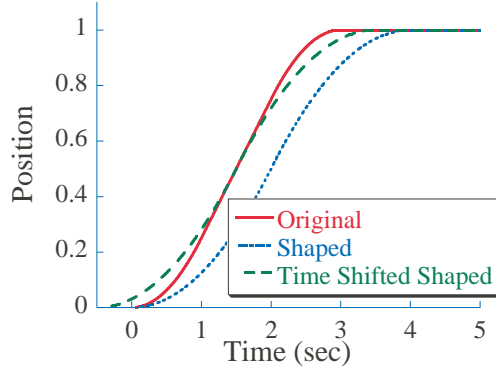
Figure 1.5: Trajectory Comparison.
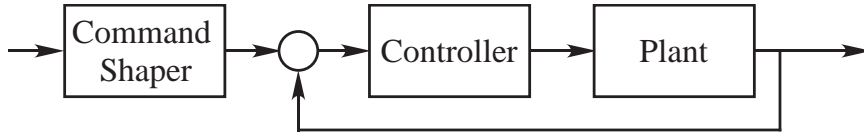
Figure 1.6: Common System Structure.

merely the Shaped command shifted in time to better show how the geometry of the curves differ. These two side effects of input shaping cause problems when implemented on a micro-milling machine. The increased command duration will increase overall process times slowing throughput, while the change in the shape of the trajectory can lead to incorrect patterns being cut if multiple axes are used. However, if these two issues, extended time and differing geometry, can be overcome, input shaping will be better suited for precision trajectory tracking applications. Micro-milling's trajectory tracking is of utmost importance since it is a primary factor in part quality.

Another major shortfall of current system design is that the mechanical systems using input shaping are not designed for its use. Typically the input shaper is an additional corrective procedure added after the machine is constructed. This leads to mechanisms that cannot take full advantage of the benefits input shaping can provide.

1.1.3 Primary Research Question:

How can the consideration of command shaping during the design phase create machine designs with improved performance?

A effective precision machine system structure is shown in Figure 1.6. A desired motion is modified using a command shaper. After the modification, the result is sent to a feedback controller. The controller regulates the motion of the mechanical plant. This dissertation addresses the simultaneous design of two of these elements, the command shaper and the
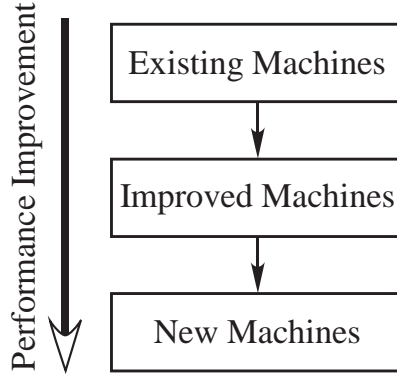
Figure 1.7: Performance Improvement Approach.

plant. While this union of mechanical design and input shaping is the focus of this research, the specific example of micro-milling will lead to design knowledge for other machines.

The goal of this combined design is improved performance. Therefore the research of this dissertation is structured towards improving the performance of machines. However, before the design of new machines is warranted, existing machines must be pushed to their limit. Figure 1.7 diagrams the approach this dissertation takes to improving machines. First existing machines are advanced through the use of new techniques. Once techniques for current machines are found, new machines can be design to benefit from existing as well as the new techniques. This sequential approach to the task is apparent in the secondary research questions that follow.

1.1.3.1   Secondary Research Question 1:

How can the performance of existing micro-milling machines be improved through command shaping?

How both of the problems previously mentioned in this chapter can be improved without the redesign the machine is the focus of this research. The ETSII micro-mill performs poorly when moved at high speeds. Also, traditional input shaping cannot provide for accurate trajectory tracking at high speeds. Once both micro-mill performance and trajectory tracking are addressed, the performance can only be improved by considering different mechanical structures. The other secondary research question addresses this design issue.

1.1.3.2   Secondary Research Question 2:

How can mechanical designs be selected to make the best use of existing and improved command shaping techniques?

If mechanical designs can be selected to utilize existing and new command shaping techniques, then performance can be increased even further.
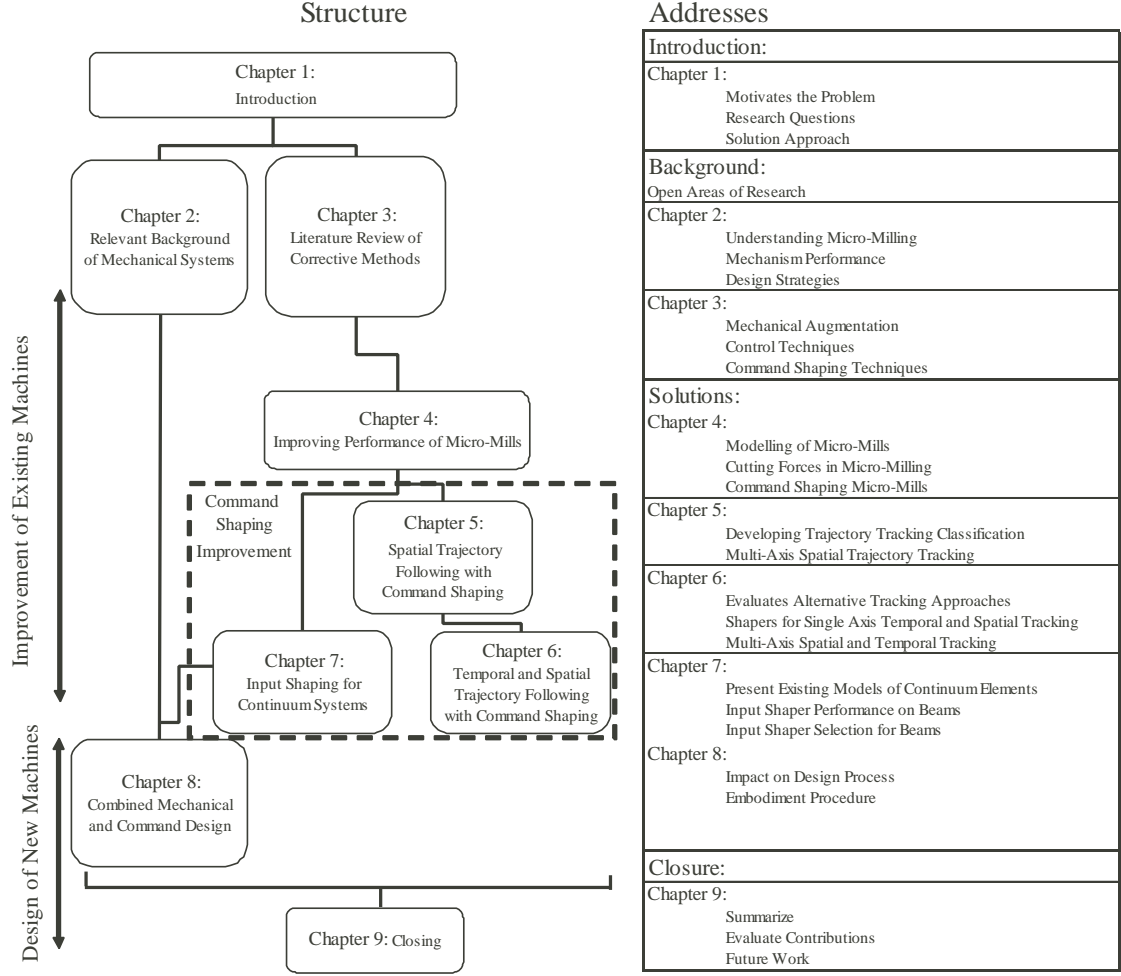
Figure 1.8: Dissertation Overview and Road-map.

1.2 Solution

The approach to answering these research questions is presented in Figure 1.8. This process has three main stages: the evaluate of current technology, the improvement of existing machines, and the design of new machines. By understanding the performance of current machines and motion strategies, the areas in need of improvement are shown in Chapters 2 and 3. Secondary Research Question 1 motivates the improvement of existing machines. This improvement can be subdivided into four distinct areas:

1. The improvement of existing micro-mills using command shaping techniques, Chapter 4.

2. Increasing the accuracy of the spatial trajectories that micro-mills need to perform, Chapter 5.

3. Enabling the tracking of spatial and temporal trajectories, Chapter 6.

4. Developing techniques for continuum mechanical elements like those found in micro-mills, Chapter 7.

Each of these areas is addressed by a separate chapter. However, Chapters 5-7 can be lumped together since all address improvement made to command shaping techniques. An added result from improving the performance of existing machines was an understanding of the physical system criteria necessary for effective exploitation of command shaping techniques. This knowledge of performance criteria specifically in the area of continuum element vibration reduction enabled the design of new elements and complete mechanisms in Chapter 8.

1.2.1 Mechanical System Understanding

In order to address the specific issues of micro-milling when combined with input shaping, the first step is to study existing mechanical systems with an emphasis on micro-mills and other similar manufacturing machines. Input shaping has proven beneficial to other mechanisms like cranes and coordinate measuring machines at reducing the oscillations that will hinder high speed micro-mills. By studying the dynamics and implementation of input shaping on these other machines, useful approaches for input shaping to micro-mills can be seen. Furthermore, by determining the dynamic characteristics of these other examples that work best with input shaping, micro-mills can be better designed to take advantage of input shaping. Finally, existing mechanical design procedures are important to the design of new machines. The development in this dissertation will draw from the previous work in multi-objective design. Specifically techniques that combine the design of control elements and mechanical elements offer insight into how input shaping and mechanical design can be unified. All of these mechanical system techniques will be addressed in Chapter 2.

1.2.2 Corrective Method Investigation

Existing system design procedures deal with mechanical design vibration through a corrective approach. This approach can take the form of a feedback controller tuned after machine construction, or the addition of open-loop techniques like input shaping. These corrective methods must be understood for two primary reasons. First the corrective methods combination with mechanical design in a concurrent design procedures, and second to compare the concurrent procedure results with traditional corrective approaches.

The first important area of correction is the addition of mechanical elements. These techniques are simple to implement since they do not rely on any electronic feedback. The next key area is traditional feedback control, which uses the deviation between the actual and the desired motion to drive the system.

At the crux of unifying input shaping and mechanical design is an understanding of the fundamentals of input shaping, and how it is derived and applied to a real system for
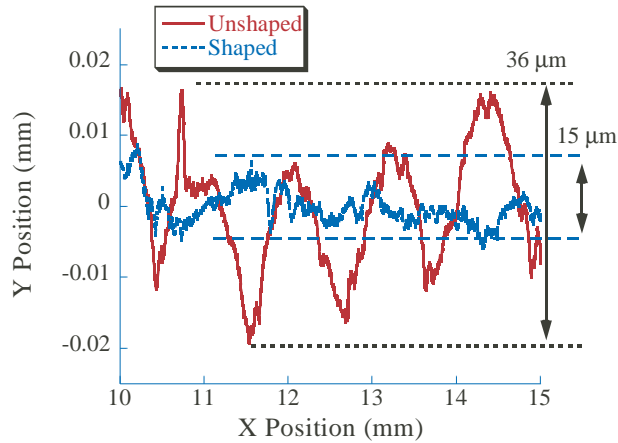
Figure 1.9: Input Shaping's Effect on Part Surface.

both vibration suppression and trajectory tracking. All of these corrective methods will be discussed in detail in Chapter 3.

1.2.3 Micro-Mill Analysis

Before a unified design approach can be created for micro-mills, the sequential application of input shaping must be investigated. That is an existing micro-mill should be retrofitted with an input shaping scheme. This process begins with a full dynamic characterization of the ETSII micro-mill.

The response of the micro-mill to both commanded motions and disturbances is important in the development of an input shaping controller. The response of the mill's positioning system coupled with the feedback controller was studied. Commanded motions at a variety of speeds and directions as well as motions with disturbances of varying magnitudes were made. Finally, a new input shaping scheme was developed to compensate for the specific problems of micro-mills and their CNC controllers. The result was improved quality in the final part, as is shown by Figure 1.9 which compares the surfaces of parts made with and without the new input shaping technique. This new technique will be described in Chapter 4.

1.2.4 Input Shaping Improvement

Although traditional input shaping works for micro-milling, it is not ideally suited for the types of motions made by micro-mills. Input shaping is best suited for straight line motions in one axis. Furthermore, it also has typically been applied to motions that are much longer that the duration of the input shaper.
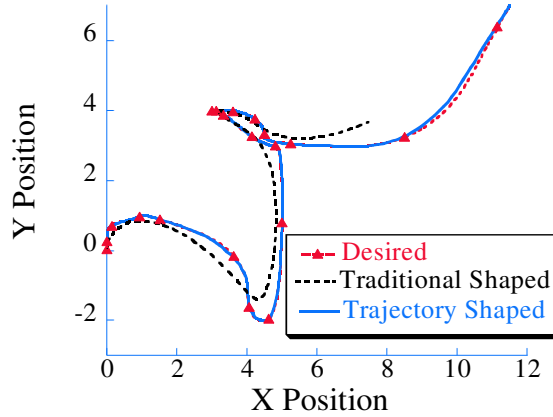
Figure 1.10: Trajectory Following Improvement with Trajectory Tracking Shaping.

For input shaping to be used successfully on machines like micro-mills, better trajectory tracking capabilities are needed. Specifically addressed in this work are the use of input shaping to track complicated trajectory components in both time and position. Also the performance of input shaping schemes was studied for more rapid motions than have been previously considered.

Once techniques for the design of input shapers for these rapid motion segments with both time and position trajectory requirements were developed, tracking of complex trajectories became possible. Figure 1.10 shows how the new technique, Trajectory Tracking Shaping, improves the tracking performance over existing input shaping schemes. This technique of trajectory tracking input shaping will be shown and compared to other approaches in Chapter 6.

Another key area of input shaping that needed to be developed further before input shaping could be used in the design phase was the shaping of continuum systems. Traditional shaping has been used on continuum systems since its inception. However, these systems were always treated as lumped parameter systems before input shaping was applied. By extending the derivation of input shaping theory to continuum systems, it becomes easier to integrate input shaping into continuum system design. This implementation is explored in Chapter 7.

1.2.5 Combined Design

The aforementioned research all build to the final goal of unifying mechanical and command design for micro-milling machines. To accomplish this, the first step was to investigate the design of additional mechanical elements like vibration absorbers with input shaping. The result from this combined design was that simultaneous input shaper and vibration absorber

9
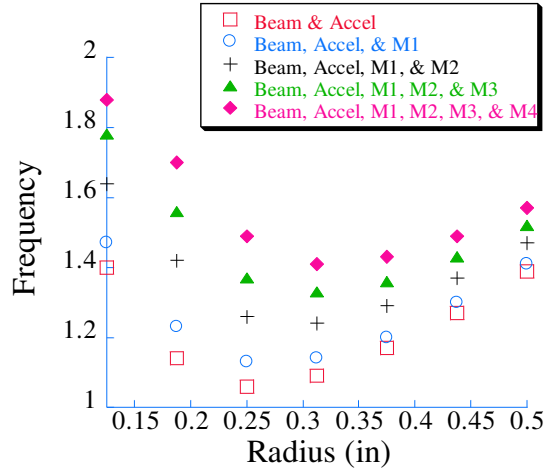
Figure 1.11: Beam Selection with Input Shaping.

selection yielded improved performance over sequential selection.

Once the techniques were developed for vibration absorber and shaping design, the technique could be modified to deal with the design of primary mechanical components. Here the knowledge of input shaping for continuum systems was used to select beam components of a design with an input shaper for maximum speed. The experimental results in Figure 1.11 show how the duration of a shaped move of a transverse beam changes with its radius for a variety of end loads M1, M2, M3, and M4. Note the minimum duration occurs at different radii depending on the carried load. With knowledge of this relationship, ideal mechanical designs can be selected.

The next step was to combine the beam and shaping design with the inclusion of other elements be it other mechanical or control schemes. This enables a procedure to be derived for the integration of input shaping into the mechanical selection of design elements centered around the tradeoff between increased weight and increased natural frequency. This combined approach was then used to show how the positioning system of a micro-mill might be designed. By combining this approach with the shapers derived specifically for trajectory tracking and continuum systems, the next generation of micro-mills integrated with input shaping can be designed.

The integration of input shaping into the design process effects all the stages of the process. Through the clarification of some design stages to eliminate bias, the introduction of new functional solutions, and new approaches for mechanical parameter selection, input shaped solutions gain fair consideration in traditional design procedures. This union of shaping with mechanical design is detailed in Chapter 8.

1.2.6 Closure

The final chapter presents a summary of the research of this dissertation. This chapter also addresses the specific answers to the research questions, and how these answers form the major contributions of the work. Finally, the future research possibilities are presented.

CHAPTER II

RELEVANT BACKGROUND OF MECHANICAL SYSTEMS

By understanding the dynamics and design of current mechanical systems, procedures for the augmentation and design of new mechanical systems, specifically micro-mills can be intelligently developed. This study begins with the modelling of existing system. Emphasis is placed on systems similar to micro-mills. However, systems where input shaping has been successfully employed will also be investigated to find corollaries with the potential next generation of micro-mills. This investigation will allow both secondary research questions to be advanced. First, by investigating micro-milling, the suitability of command shaping as a vibration suppression strategy will be shown. This is the first step toward utilizing input shaping for the improvement of existing micro-mills. Secondly, the design of new mechanical systems will be aided by the study of existing designs and design strategies.

For the modelling of micro-mills, the dynamics of the positioning system are an important aspect. Also important are the forces impacting the mills, specifically from cutting . However, the impact on overall performance of other design elements is also relevant.

Existing design procedures that encompass issues dealing with control rather than the purely mechanical will also be studied. The largest area of such research relevant to the combination of mechanical and command design is Design for Control or DFC where feedback controllers and mechanical elements are designed together. Work on the combination of input shaping with mechanical structure selection and controller design is also relevant.

2.1 Modelling

An understanding of existing system performance is the first step in designing new systems. Modelling of a system is key to that process. Here the previous work on the modelling of micro-mills and other relevant machines is discussed.

2.1.1 Cutting

Understanding the process of how the material is removed from a workpiece is important to understanding the operation of a tool. The primary importance to this research is an understanding of the forces from the cutting process. This is necessary so that their effect on the dynamic response of the overall tool can be predicted. Analysis of the cutting process involves several areas. These are the forces on the tool from the workpiece interaction, the vibration in the cutting tool itself caused by the cutting, the surface finish of the

finished part, the methodology of measurement of the cut, and the design of tools with the aforementioned cutting knowledge. However, the existing research does not explain the phenomenon of cutting at high spindle rotation rates. This understanding of cutting forces at high spindle speeds in necessary for the next generation of micro-mills, since spindle speeds are constantly increasing.

2.1.1.1 Cutting Force Calculations

The cutting force experienced by a machine tool is one of the driving factors in the dynamic response of a tool. Forcing on the tool itself leads to deflection of the cutting tool, the workpiece and the machine's structure as well. The prediction of the forces during a machining operation is an active area of research in order to improve machining quality and speed. Along with the static deflection of a tool, the cutting force often excites chatter, vibration in the tool, which can grow as cutting progresses thus degrading the manufactured part. The prevention of chatter is one of the driving reasons for studying the cutting force. From the standpoint of micro-mill design, chatter is important, but equally important are the forces transmitted from the cutting process onto the positioning system.

2.1.1.1.1 Milling

The forces acting on a mill have been modelled in increasingly complicated ways beginning with the premise that the force is directly related to material removed. A static approximation of this force can be calculated using the power needed for the cut:

$$F_c = \frac{P_{sp}(MRR)}{v} \tag{2.1}$$

Where the cutting force F_c is dependent on the material property specific power P_{sp}, the material removal rate MRR and the tangential velocity of the cutter v [268].

Since the cutter is spinning another level of complexity can be added, this model is a pure sinusoidal forcing such that the thickness of material removed t_c varies with the angle of the cutter:

$$t_c = t_x \sin \theta \tag{2.2}$$

where t_x is a constant coefficient related to the cutting parameters [310]. The force in this model would be proportional to the thickness of the cut at a given instant.

Another simple approach to modelling the forces is to simply make it randomly varying. By using a force distribution of Gaussian white noise, calculations of the kinetics of a machine tool can be made in closed form [244].

More complicated models take into account other variables in the machining besides simply the angle of the cutter. These other variables fall into three categories: the workpiece, the process and the tool variables. Workpiece variables consists of material properties of

the piece. Process variables deal with the way the cutting process is being performed; these include variables such as feed-rate, feed-acceleration, spindle speed, cut depth, cut width, and milling direction. Finally, the tool variables describe the physical nature of the tool. Research considers geometric properties such the radius, the number of teeth, the angle on the teeth, and the type of cutter, as well as the material properties such as stiffness, hardness, and coefficient of thermal expansion. Milling direction is an important aspect for end-mills since climb milling and conventional milling have different physical mechanism for material removal [8, 287]. However, the process of force description becomes more complicated when ball-end milling is considered. In ball milling, the flat end mill properties apply, as well as additional considerations that must be made whether the cut is ramped or contoured. This makes the equations of force prediction have to deal with four separate types of cutting: ramped-conventional, ramped-climb, contoured-conventional, contoured-climb [126].

The actual calculations for the cutting force in mills can be done differently depending on the calculation method. The closed-form solutions rely on the current parameters of the cut to calculate the forcing. However, this is not how actual cutting works. Instead, techniques must and often do take into account the history of the cut in order to calculate the forcing. This is necessary because if previous passes caused an non-uniform surface finish, then the depth of cut will be history dependent.

Also if the tool's deflection is considered, then the surface profile will change, and the past motion of the tool will be necessary to describe its current motion. This flexible tool model of the cutting process can produce more accurate results than a rigid model especially for surface finish and maximum cutting force [126, 317]. The flexibility in the cutting tool prevents the tool from cutting as deeply into the surface thus smoothing the process [277]. Interestingly, a flexible ball-end mill model predicts poor cutting performance at the center of the tool due to the near zero cutting velocity [76]. Additionally, the flexibility of the cutting tool poses a difficult modelling problem due to the mode coupling present. When a tool is excited in one direction, vibration is excited in the perpendicular direction due to the identical modal properties [130]. If the cutter's flexibility can be accurately modelled then control techniques can be used on the cutting process to limit the deflection [59].

In some cases the cutting force equations are never explicitly derived, instead a finite element model is used to estimate the process [326, 304, 305]. A similar approach utilized in ball-end milling modelling uses a series of slices out of the workpiece and tool to predict instantaneous forces on each. Then, a summation over each slice can be used to find the overall forcing [2]. Likewise, often a fit technique is employed to describe the forcing. A multiple sinusoidal regression similar to a Fourier transform was be used to model milling forces in [96].

The analysis of the cutting force is often done with respect to time, however the frequencies of the forcing are often as important as the transient effects. The analysis of these

frequencies can be used to predict the cutting force [310]. Specifically the frequency of the cutting teeth, from an individual cutter's depth of cut, and from the profile of any cut on the workpiece are convolved together to yield a resultant force. While, Volger *et al.* also looked at the frequency spectrum of micro-mill forcing [305].

2.1.1.1.2   Micro-Milling

The prediction of cutting forces in micro-milling is slightly different from the cutting forces in traditional scale milling machines. One difference in the modelling of cutting force is the scale of the cut. For micro-end-milling operations the cutting force is different due to the aggressive feed per tooth of the mill. Bao and Tansel present a model rooted in the angle of interaction between the tool and the part to accurately predict the forcing for a micro-end-mill [16].

The effect of tool run-out is also more pronounced in micro-end-milling operations whereby a run-out that was not noticeable in a conventional operation becomes substantial to the forcing on the tool for micro-operations [17]. The impact of tool wear on micro-milling forces has also be considered. Bao *et al.* expanded on a previous analytical model to include tool wear in [18]. While Kim *et al.* showed that excessive tool tooth wear could lead to intermittent chip formation [143].

To complicate the modelling even further, at small scales, metal grain boundaries become important. The cutting process of each grain may differ greatly depending on the metal. Lee studied the grain's impact on the forces, and found that for materials with grains the cutting process must be considered anisotropic [156]. This grain issues as well as many of the other points about the difference between traditional scale and micro-scale milling cutting forces were reiterated by Liu *et al.* [172].

2.1.1.1.3   Micro-Turning

The calculation of cutting force on a lathe is of similar importance as that of a mill. Understanding the magnitude and the causes of lathe's cutting forces and their relationship to milling forces is necessary if design techniques for mills are to be expanded to lathes.

By knowing the cutting forces for a particular set of cutting conditions, the cutting conditions can be selected to reach desired quality goals. Likewise, if the part quality can be used to determine the maximum cutting force, then the lathe can be controlled to maintain the maximum cutting force thus increasing feed-rate and throughput [292]. Determining this force can be difficult for micro-lathes. Finding a dynamometer with the proper resolution can be difficult and dynamometers can also be size and mass prohibitive. To compensate for this Kim and Kim developed a combination system relying on two piezoelectric accelerometers and a stress measurement in the cutting tool itself [144]

An important distinction between turning and milling is that the cutting force on a

standard lathe is more static than that of a mill do to the nature of the cutting. Wear on the tool is still an issue in micro-turning. Typically this wear comes from chipping of the diamond tool [48].

2.1.1.1.4 Surface Finish

Related closely to the forces made by the mechanical interaction of the tool and the workpiece is the resultant finish which is closely tied to the mode of cutting. The surface finish of the part or the amount of variation in the surface is often the limiting factor in the feature size attainable by a particular machine tool. When surface finish is addressed directly by accurate process modelling, Kim and Kim reduced the waviness of a turned part with a piezo-electric tool positioning system by half [145] while Lim and Meng used the same knowledge to decrease process time in a mill [170].

2.1.1.1.5 Cutting Mode

When the scales of the machining enter the micrometer range, the cutting dynamics themselves can change. Brittle materials will behave as ductile materials, and ductile materials will deform differently than they would at a large depth of cut. For example, glass can be machined in both the brittle and ductile realm in order to allow a high feed-rate and produce precise surface finish. The best approach proposed by Takeuchi *et al.* is to first make a rough cut in the brittle mode and then reducing the material removal rate by one order of magnitude to produce the finish surface in the ductile mode [279]. Matsumura *et al.* showed that for glass the change in cutting mode could significantly impact maximum forcing, going from 0.1 Newton for ductile cutting to 1.25 Newton for brittle cutting with all other parameters the same [184]. Modelling of the physics behind this change has also been attempted for copper and even a model of the motion of individual atoms during machining has been developed [174, 124]. Liang's *et al.* study of micro cutting of crystalline structures showed that cutting force can actually increase as the scale gets smaller due to different cutting mechanisms [167].

For polymers the problem becomes even more evident with temperature playing a more vital roll. Carr and Feger studied the micro-cutting dynamics of a range of polymers over a variety of temperatures including silly putty [36]. All of these other mechanisms impact the cutting force. However, it is hard to develop these relationship, since eliminating noise from the cutting force measurements is difficult. In spite of this difficulty, experimental results have shown the counterintuitive trend that the cutting force may increase as depth of cut decreases. This is opposite of what the larger scale models would predict [124].

Similar changes in the cutting mode from ductile to brittle can be seen in micro-turning. Similarly to the mill, a micro-lathe can cut brittle materials in the ductile mode. This process can also be influenced by the atmosphere present during the cut. By studying what

gas to surround the machine in, linoleic acid was found to be the best atmosphere for one workpiece material in [199]. The crystalline structure of a material are also important in micro-turning especially as the cutter size approaches the crystal size [46].

2.1.1.2 Chatter

The problem of self excited vibration in a machine tool is called chatter. This chatter can be unstable under certain cutting conditions and its frequency is often near the resonant frequency of the system. If this near resonance condition occurs, the continual sinusoidal cutting forces will eventually effect the motion of the tool, thus producing an unacceptable part. Even when stable, chatter can be detrimental. The movement of the tool during chatter causes the surface finish to degrade and an increased stress on the cutting tool, leading to decreased tool life. The chatter phenomenon is predominant in large scale tools, but it less common in smaller tools due to the relationship between overall machine stiffness and forcing magnitude. However, if this relationship changes as could occur if lighter tools are used, then the problem of chatter might become more pronounced and therefore it must be considered for the next generation of micro-machine tools.

Tobias divides chatter sources into three possibilities: [288]

1. Chip thickness variation due to irregularities in the workpiece.

2. Penetration rate variation due to an uneven surface from a previous cutting pass.

3. Dynamic coupling whereby forcing from one direction. excites vibration in another

Welbourn and Smith add another cause of chatter due to the variation of cutting force with cutting speed. A system's velocity will be irregular and this irregularity will cause a variation in the cutting force. This dynamic force can cause chatter in the system [315]. Compensation for this type of irregular velocity and its impact on chatter will be an added benefit to improving the tracking of micro-mills.

Do to its relevance to the machining process, the chatter phenomenon has also been modelled. The structural dynamics of the tool, as well as the cutting interaction can be taken into account. Edhi and Tetsutaro did this in an attempt to find the stability range for a boring tool [63].

Chatter can be controlled by a variety of modifications. Increasing the clamping force on the workpiece can lead to an increase in chatter due to a loss in the damping capacity of the joint [182]. Also, mechanical augmentation of the tool itself can be attempted such as an impact damper for boring chatter [69, 109] or for drilling chatter [68]. Finally, feedback control can be used to reduce the chatter [210].

2.1.1.3   Measurement

Accurately knowing the state of a machine tool allows the prediction of the results of the tool, as well as a useful method for the diagnosis of machining problems [180]. Real time measurement can also be used to adjust cutting parameters to speed the manufacturing process.

The measurement of the cutting process can be done in a variety of ways. The most accurate is the measurement of the workpiece, however this is difficult to do in real time. Measurements from encoders on the axis of the machine, while real time, will exhibit error do to the flexibility between the encoder and the workpiece. In situ measurement is possible of both the cutting force and the workpiece geometry. A dynamometer can be used to measure the cutting forces on a tool. A machine can also utilize accelerometers and/or strain gauges to determine transient and continuous forces respectively [144]. For geometric measurements a capacitive sensor can often be used to measure the part without interfering with the machining operation [160].

Experimentally determined cutting forces can be used to predict surface finish of the part or to give insight into when a tool has been worn. In this manner, Choi *et al.* attempted to use a combination of an accelerometer and dynamometer to monitor the wear of a diamond tool for a precision lathe [48]. However for micro-machine tools measurement is not always a valid option since cutting forces are so small that they could be masked by signal noise. For this reason, measurement of tool wear for micro-mills has been attempted through a predictive equation using a genetic algorithm [18]. This allows the tool life to be estimated from the current workpiece finish.

2.1.1.3.1   Acoustics

The high sound level produced by a machine tool is also a detriment, both as a sign of other problems and as an increase in sound level itself. The acoustic energy produced by a machining operation can be used to monitor the process and gain insight into the current chatter state. Cutting force has been shown to be directly linked to the acoustic response of lathes [319]. However, not all process variables can be discovered by analyzing change in noise level. The noise level itself can produce an unsafe work environment or transfer vibrations to other areas.

2.1.1.4   Design Concerns

The cutter's design is important in determining the quality of the operation. The appropriate cutter must be chosen to meet the desired tolerances while allowing the shortest machining time possible. The cutter itself influences all aspects of the cut. By designing or selecting a cutter appropriately the quality and speed can be increased. Tsai and Hsieh have shown how to accomplish this for a ball-end cutter in [293]. Altinas also mentions that

helical cutter design is advantageous for smoothing the part/tool engagement [8]. Cutter material selection is also an important concern; the surface finish changes dramatically if metal tools are used instead of diamond [238].

Fabrication of micro-mills is another design issue. Traditionally these mills are made in the same manner as the macro/meso scale counterparts, with some being made by direct machining and others being sintered. However, Vasile *et al.* have developed an ion sputtering technique to make a 24 micrometer diameter mill cutter [302].

Grinding error in the edges of the mill's cutter must also be considered as a source for possible excessive force. Gong and Ehmann's work in micro-drilling showed that grinding errors on the drill have significant impact on the response [101]. The impact of grinding error's effects on micro-milling can be deduced from their results.

Modifications to existing cutter designs is another area where the machining process can be improved. Lee *et al.* showed that by adding additional cutting teeth to a milling cutter the stability of the cut could be improved [157]. While Ismail and Batsami showed that by making an asymmetric mill, chatter stability could be increased [130].

Another key aspect of the cutter is its alignment to the tool. For ultra-precision tools this can be quite difficult. A suggested solution is to fabricate the cutter in the spindle, thus eliminating the alignment or run-out issues [183]. This run-out issue has also been address by Sastry *et al.* by altering the spindle speed [235].

2.1.2 Mechanical Plants

Understanding the dynamics of a mechanical system is important to controlling how it operates. Therefore the first step in the control of a mechanical system is to develop a model that captures the important behavior of the system. A generic place to start is Welbourn and Smith's textbook [315]. Models must vary depending on the desired level of fidelity needed. Often first-order linear models are used as a good starting point. From there, increasing the order is common, as well as the implementation of nonlinear terms. The most complicated technique is to utilize a finite element dynamic model to describe the motion of the system. A detailed physical model of a machine tool is often necessary when small disturbances can change the response. For example, micro-positioning stages can be impacted by air currents [39]. The study into existing modelling techniques and the impact of components of the model on the response of the final machine are beneficial in the final design of the machines themselves. However, little research exists into the dynamic modelling of machine tools. Particulary no research exists in the modelling of tools with flexible structures. Therefore, a understand of existing models is needed in order to develop dynamic models.

The selection of what dynamic features to include is an important choice in developing any model. For a machine tool, a variety of features impact the dynamic behavior. Modelling each of these poses its own problems and challenges. Each area chosen to be modelled adds another level of complexity to the overall model of the tool. The sections that follow describe some of these features and how they are typically modelled.

2.1.2.1.1 Cutting Tool

The cutting tool itself is a continuous flexible structure whose vibration is important since it directly effects the work-piece. However, since most tools are small and consequently have higher frequencies than the rest of the tool structure, their dynamics are often lumped together with the cutting force as discussed in 2.1.1.

In boring tools, however, the boring bar is a much larger than the cutting tools of other machines, therefore its detailed dynamics must be considered. A second-order oscillator is a common choice used in both 1951 by Hahn and 1998 by Marui *et al.* [109, 182]. This type of model could be used for smaller cutters if required.

2.1.2.1.2 Friction

Nonlinear or discontinuous effects are the most difficult to model due to their effect on the equations of motion. Friction is a primary example where a piecewise linear function can substantially alter the performance of a machine. The two primary types of friction pose different problems to machine positioning. Kinetic friction acts as a damper and slows the velocity of the machine. Static friction adds position error often reducing part quality. Chen *et al.* and Wei with Lin both looked explicitly at friction in ball screws which are common in micro-mills in [44, 314], while Armstrong-Helouvry *et al.* looked extensively at ways to model friction on a variety of systems [11].

Friction dominates the concerns when machining at low velocities. The stick-slip action alters the dynamic response especially in low velocity operations like precision grinding. A common way to deal with friction is an inverse technique by which the force of friction is compensated by a nonlinear controller such as a feed-forward friction compensator [188, 295, 155] or a Kalman filter [71]. Armstrong-Helouvry *et al.* provide a survey of friction compensation techniques [11]

Another way around the modelling of friction is to simply eliminate it from the plant, this can be done with expensive bearing systems, but also by simply replace sliding interfaces with flexible ones [185, 265]. This reduces the complex effect of friction to a simple spring effect.

Another way friction impacts system modelling is as a catch all for why models are inaccurate. Often friction is left out of a model causing errors to occurs. Specific case of

attributing modelling error to friction can be found in [219, 291]

2.1.2.1.3   Actuators

The actuators found on machine tools are often electric rotational motors. However, sometimes hydraulic or linear motors are employed. Each of these has specific dynamic characteristics and even among electrical rotational motors there exists a variety of dynamic behaviors.

For example, electrical rotational servo motors attached through gearboxes and lead screws are often used to move the cutting tool on a lathe or to position the workpiece on a mill. A simple model of the behavior of such systems is a velocity based first-order model, a mass with viscous damping in [71]. However second-order models are also common assuming an inertia and some electrical effects inside the motor itself [292, 210].

One important issue with actuators are the limits of operation. The saturation limit or maximum output force adds a non-linear transform from input to motion. Likewise, the bandwidth or frequencies of response of the actuator also determine possible motions or non-linear responses to some motions [28].

2.1.2.1.4   Controller

The controller is usually designed to deal with the unwanted dynamics of the system, but if the system is viewed in total, the dynamics as altered by the controller define the total response of the system.

When a control loop is closed, the dynamics of the system are altered by the feedback, as well as introducing the controller dynamics and any sensor dynamics into the overall response. These complex issues in controller design are discussed further in Section 3.2.

2.1.2.1.5   Fixturing

The fixturing or clamping of a workpiece in a tool can have static, as well as dynamic effects on system. Ideally the workpiece would be rigid and rigidly clamped to the structure so that no deformation could occur in the system. However, often this is not the case. A level of flexibility always exists between the workpiece and its mount.

In considering the dynamics of the mount, the clamping force is important. The clamping force affects the pre-load in the clamps. This in turn can alter the natural frequency of the clamps. Also, the amount of clamping force determines the contact conditions between elements. The contact conditions are relevant to the dissipative properties of the tool, since loose clamping allows sliding where friction can dissipate energy.

In precision application, temperature dependence can lead to misalignment. Since the structures expands and contracts, position is a function of temperature. A method to deal with this has been proposed at the design stage of the fixture. Slocum suggest a flexible

mount for the workpiece. By introducing this dynamic component to the fixture through the flexibility of the fixture itself the effect of temperature variation can be decreased [265].

Understanding of the dynamics of fixturing is also important in its relationship to surface finish and chatter. Appropriate fixture dynamics will prevent unstable chatter from being induced the cutting force. In order to understand how the clamping and order of clamping relate to this finite element models have been developed [168].

2.1.2.1.6 Structure

The physical structure of a machine tool is often a dominant contributor to the dynamics of the tool. To avoid flexible dynamics, machine tools are typically designed to be as stiff as possible, since vibration in the structure can be detrimental to the performance of the tool. However, in an attempt to increase the speed of the tool, a lighter structure is often suggested, but lightening the structure usually leads to increased flexibility in the system and therefore a larger unwanted dynamic response.

Dealing with the trade-off between inertia and flexibility can be accomplished by the target removal of material from the tool. Evaluating the sensitivity to vibration of removing material from each of the tool's components allows calculations to be used to determine where to remove mass. This is typically accomplished with a dynamic finite element model. Sadeghipour tried this on a lathe spindle to alter the dynamic response for frequency, as well as deflection considerations [233]

The structure also consists of any auxiliary oscillatory systems mounted to it. The primary example of this is a vibration absorber or mass damper added to the system reduce either transient or continuous vibration. These are discussed further in Section 3.1.2.2.

2.1.2.1.7 Coupled Mechanism

Coupled mechanisms are external dynamic mechanisms added to a machine tool to improve the performance. These fall into two categories: tool mounting elements which go between the machine and ground and the free elements which are not attached to ground.

Tool mounting or the base of a machine tool alters the dynamic response of the tool most commonly by isolating it from the environment. Flexible mounts are often used for these isolation purposes adding another degree of freedom to the motion of the machine.

Vibration isolators can add multiple modes to a system through the addition of another independent mass. These isolators are usually modelled as lumped parameter systems and will be discussed in detail in 3.1.2.1.

Free elements primarily in the form of vibrations absorbers and mass dampers are discussed in 3.1.2.2. They have been used on all types of machine tools such as the boring machines in [109].

2.1.2.1.8   Forces

The forces acting on a machine tool comes from inside the machine itself or from external sources. The external sources force the system either through the mounting of the system or from unwanted direct interaction. An example would be vibration from a adjacent tool transmitting through the floor and the tool base into the tool itself, or the operator flipping a switch on the machine tool while it is cutting.

The internal machine forces can come from machine flaws like rotating imbalance or more likely from the interaction with the workpiece. This interaction of cutting was discussed in detail in 2.1.1.

2.1.2.1.9   Assumptions

What to leave out of a model is as important a decision as what to include. This is typically done by making assumptions about the dynamic response. Any of the above features can be assumed to be irrelevant to the response of a particular machine. Some additional assumptions often made are:

1. Capping the number modes considered

2. Electrical time constants are high

3. Sensors are away from nodes and collocated

4. Temperature is constant

5. Joints are rigid

These types of assumptions must be considered and clearly justified for any model, as was done for the ball screw model in [54]. For example, Honda *et al.* discusses the problems of the assumption of no high modes as the length of a drive screw increases [114]. Zhang *et al.* discuss the problems of assuming rigid joints stating that as much as 60% of the flexibility and 90% of the damping come from joints in some machines [327]. A general approach to show how these assumption and their corresponding error can lead to total machine error can be found in [273].

2.1.2.2   Complete Models

The combination of the various features of the dynamics yield a complete model of a machine. What follows is a discussion of individual modelling choices made by other researchers.

2.1.2.2.1 Milling Machines

The dynamics of milling machines have been typically modelled with simple second-order systems, as well as with finite element approaches. A first-order model of a milling machine was complicated by nonlinear terms dealing with the cutting process in [152] where Lee and Tomizuka used a true first-order model to describe a positioning system like the ones found on mills [155]. While, Futami *et al.* used three different models to describe the response of their positioning system at different scales of motion [97]. Linear second-order models for structural and actuator dynamics have been used by many researchers [28, 37, 269].

A sixth-order model was developed by Shin and Wang with one degree of freedom each for the cutter, the workpiece, and the structure. This lumped model was used with the additional advice that experimental techniques should be used for specific machine tools [244]. Ozisik and Keltie used a fifth-order model to accomplish similar modelling goals [208].

Experimental determination of system model is common as was done for a sixth-order model of a ball screw [231]. When the system dynamics can be determined exactly from physical tests, it allows the application of feed-forward techniques like Zero Phase Error Tracking Control [289]. When this was attempted on a high-speed milling machine, a fifth-order closed loop z-transform model of the mill and a proportional controller was devised and used to allow near perfect trajectory tracking [295]. Continuum models can also be used as in [105] and [301] where a ball-screw is modelled using continuum beam theory.

Finite element models are also used to describe the complete machine dynamics, as well as to help in the design stages of the machine [300, 180]. These models, although difficult to construct, provide more complete frequency response characteristics than lumped parameter or reduced-order models.

In contrast to this Lee *et al.* suggest that ultra-precision machine tools should be designed to be zero-order [158]. They suggest that stiffness should be effectively infinite for these tools to allow high machining accuracy, therefore the dynamics are irrelevant. Advice on how this was to be accomplished with limited actuator forces was not provided.

Another machine that has a similar structure and drive to a milling machine is a coordinate measuring machine. These are used to perform measurements on the dimensions of parts. However, since inspection is often time consuming, coordinate measuring machines are made with low moving inertia in order to perform their tasks quickly. Thus they have a greater flexibility than a traditional milling machine but do show the structural possibilities for low contact force milling structures. Since the moving inertia is low in coordinate measuring machines, flexible modes are more important in the accurate modelling of the system. Seth and Rattan model a coordinate measuring machine as a double integrator coupled with 3 flexible poles. This yielded a fifth-order model to describe the motor and structural vibration [241].

2.1.2.2.2 Turning Machines

Lathes have fewer moving parts than mills. Since the spindle and cross-slide are the only components that move on a traditional lathe they are often at the center of the dynamic modelling. Simple second-order models [146] have been developed all the way to complicated finite element techniques [233].

These models allow implementation of advanced control strategies. For example a second-order actuator model was combined with PD, adaptive filtering, and fuzzy control to improve chatter in a lathe [210]. Second-order models have also been used in turning to describe non-traditional actuators like piezoelectric servos [329] which are often combined with electrical circuit dynamics to form a complete actuator model [145].

Another way to model a lathe is with its frequency response. If the response is known for each frequency, then this data can be used to improve the machine. One way to gather the frequency data is with the impulse response. This can then be analyzed using Fourier techniques to determine the primary frequencies of vibration. These same Fourier techniques have been used to study the responses while the lathe is operating to give cutting conditions and position dependent frequencies [319]. Franse *et al.* used this type of frequency technique to determine that their lathe had significant resonances at over 200 Hz [93].

2.1.2.2.3 Serial Manipulators

The general term of "serial manipulators" can be used to describe many manufacturing machines. While, mills and lathes are serial manipulators, much research has gone into the robot arm type serial manipulators also common in manufacturing for processes such as placement and painting. The kinematics of such manipulators are often difficult to determine. Thus the kinetics are also complicated, and these types of manipulators exhibit challenging vibration problems. Models of these manipulators vary widely. For example, Ferretti *et al.* presented a tenth-order model for an RRR manipulator [77]

The type of serial manipulator, namely the choice and arrangement of actuators alters the dynamic and vibratory characteristics. Tu and Rastegar attempted to find some general correlation between the vibration and the type of serial manipulator [294]. The general approaches used for robotic arm serial manipulators could be used also for the serial manipulators used in milling and turning.

2.1.2.2.4 Parallel Manipulators

Parallel manipulators are robots with closed kinematic chains. These types of machines offer more stiffness than serial manipulators. Parallel manipulator structures for manufacturing machines are beginning to be investigated. For example, a parallel structure allows gross motions to be converted to fine motion in [283]. However, the kinetics are often complicated

by singularities in the workspace; likewise the dynamics are often complicated [149]. In order to deal with these challenges, Jacobians are utilized to describe the motion.

Because of the complicated kinetics, the dynamics of parallel manipulators are often modelled as lump parameter systems. This technique was experimentally verified in [185].

2.1.3 Path Design

Decisions about the path of the machine tool come from a variety of sources. This section will deal with the generation of paths to satisfy process requirements like smoothness and time optimality. However, research into vibration suppression coupled with command design is lacking. Typically vibration is eliminated with simple techniques like moving slowly or smoothing the command. With this type of technique, aggressive motions are not possible. Another important concern in path design is making the dynamic response of the tool follow these paths; this is much more complicated and will be discussed later.

An important area of path design with relevance to machining is surface generation. Generating the most efficient and accurate method of machining a surface involves several key considerations. Minimizing overall process time involves trying to make as few non-cutting motions as possible. While a more advanced technique is to instead try to cut in directions where a high feedrate can be used. For example, Yun *et al.* developed a finite element model of the cutting process which was then used to design a table of feedrates. The knowledge of the cutting forces coming from the finite element simulation allowed the feedrate to be chosen as fast as possible depending on the cutting conditions [326]. Since the depths of cut vary and the material and machine have directional dependent properties these can be considered in designing a surface cutting plan. If this information is known, then a path and feedrate selection algorithm can be developed [170]. This does add complexity to the CNC algorithm and is economically feasible only for large runs of a single part so the increase in efficiency can be traded for increased programming time.

Instead of optimizing for feedrate, a path can be designed to maximize material removed per cut for a complex surface [45]. This approach could be combined with feedrate optimization for continued performance increases.

A similar concern is the precision of the cut. Often fast rough cuts are made with a finishing path used to reach the desired dimension. The path and path parameters also play a part in the creation of surface contours; correctly chosen path parameters can lead to improved surface contours [165].

The mode of cutting used can also dictate machine paths. On a micro-lathe it is possible to cut in both the brittle and ductile regions [199]. This creates different surface conditions, as well as different machining forces. By selecting the appropriate region for a part, the speed can then be increased or decreased as necessary. For ball-end-mill operations the type of surface be it convex or concave should be used to determine the final surface generation

profile.

A combination of minimal time and ductile *vs.* brittle cutting needs to be considered when creating complicated shapes. When many aspheric surfaces (lens) are created on precision mills, the path of the tool needs to be optimal. Thus the continual measurement used for improvement facilitates learning techniques [158]. Since lens creation is an important area in micro-machining, researches often try to create hyperbolic and parabolic shapes in the test runs of their machines. Takeuchi *et al.* were able to create lens shapes with a surface roughness of 35nm with a pseudo-end mill [280].

Some machine tools are over actuated in that they have multiple joint configurations to produce the same position in space. This must also be taken into account. In the creation of diffraction gratings containing many small grooves, several different cutters can be used with different machine configurations to produce the same shape. However, the different configurations do not lead to the same final product. For a mill, the three options are perpendicular, parallel and at any angle in between; using different cutters the same surface can be produced [237]. This micro-grooving can be used to produce fine encoders as well [236].

The mechanical design of a machine tool determines what paths are attainable in a purely position sense. If the tool cannot reach a certain configuration due to an actuator limit, then certain profiles cannot be generated. Therefore, attainable path design is an important step in the machine design process. On micro-lathes certain angles cannot be cut into the face of the workpiece because of the shape of the tool and actuator. To deal with this problem, another actuator can be added to further control the orientation of the tool or manual changes in orientation can be made [281]. The downside of this approach is increased flexibility and error at the expense of a great range of possible paths.

2.2 Specific Mechanism

Obviously a study of the specific mechanisms of micro-milling is needed before beginning the design of micro-mills. However, little work into the dynamics of micro-mills exists. Therefore, micro-lathes are considered since they are similar to milling machines and can be a great source of information, as well as, another application for the techniques developed for micro-mills. Finally, other mechanisms that are commonly used with input shaping can offer insight into the redesign of micro-mills so that they can exploit input shaping. However, the particular features of these other machines that make them well suited for input shaping has not been codified.

2.2.1 Micro-Mills

The micro-milling machining operation allows parts to be created by physical cutting which have features on the scale of $1\mu m$. A rotating cutting tool is moved through a workpiece to

produce a new surface on the part.

Micro-mills typically use the same structural configuration as macro-mills but have several major differences imposed by the scaling. First, since the scale is much smaller than traditional milling, the stiffness from the cutting interface to ground is much smaller. Some of this comes from the milling tool, but the machine structure can also be more flexible, due to its components being significantly smaller than those in traditional milling machines. However, even though the structural stiffness is lower, the forces from material removal are also much lower. A stiffness sufficient to counteract the cutting forces is required on large scale machines [288], but its relationship has not yet been explored for micro-tools. Second, a much higher accuracy is needed for micro-mills. Since the parts are smaller, higher resolution is needed in the positioning system to create parts. Finally, the spindle speeds of micro-mills are significantly higher than macro mills. Several micro-mills are capable of spindle speeds in excess of 100,000 RPM.

An interesting side note is that the evolution of the development of new micro-manufacturing technology has been centered primarily in Japan and Europe due to an American emphasis on silicon planar lithography [58].

2.2.2 Specific Micro-Mills

Research can be found describing the construction of many different micro-mills, with the mills of two different construction groups in Spain and Japan being the most understood.

2.2.2.1 ETSII Mill

The micro-mill at the Escuela Tecnica Superior de Ingenieros Industriales (ETSII) in Madrid, Spain is shown in Figure 2.1. This mill is the experimental testbed for the research in this dissertation and is described in detail in Section 4.

2.2.2.2 AIST Mill

The second mill is located in the National Institute of Advanced Industrial Science and Technology (AIST) in Japan [204, 203]. They have constructed two micro-mills the first is shown in Figure 2.2. This mill "El Chuchito" has a workspace of 60mm by 100mm and is capable of feed velocities of $50\frac{mm}{sec}$. This mill is also capable of turning a cutting tool at 200,000 RPM and as an added feature uses a CCD camera to monitor the operations of the tool. This mill could benefit from improved tracking. Figure 2.3 shows how the velocity profile oscillates. If this error could be decreased, then the machine would both track better and be capable of cutting at higher feed-velocities.

At AIST they have also constructed a newer mill which has a maximum spindle-speed of 300,000 RPM shown in Figure 2.4. This mill is the next stage in their design iterations.

Figure 2.1: ETSII Mill.

Figure 2.2: AIST Mill.
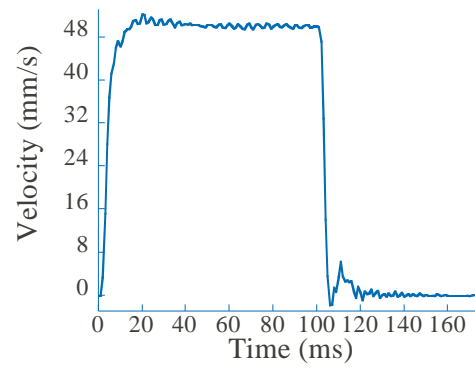
Figure 2.3: AIST Mill Velocity Profile.

Figure 2.4: Next Generation AIST Mill.

2.2.2.3   Other Micro-Mills

Many other micro-mills exist with some researchers using custom designs and others utilizing existing commercial machines. The number of axis can also vary from 2 to 5. Friction is a problem in all of these tools and to deal with it Kawai *et al.* utilizes a "friction-free machine" which uses air bearings for all moving parts [137]. Dow *et al.* constructed a machine with 2-DOF for grooving utilizing a 60,000 RPM air spindle to drive the cutting tool in their force experiments. Additionally, they added an optical detector to determine spindle orientation [59].

Another 2-axis machine was developed by Subrahmanian and Ehmann [275]. This machine uses piezoelectric actuators with a travel of 8mm and a theoretical maximum speed of $50\frac{mm}{sec}$. The response of the systems appears to be first-order from their results. The whole machine fits in a volume of 50 x 50 x 50 mm. A primary design issue in this mill was the spindle, which is powered by an air turbine mechanism and is capable of speeds of 100,000 RPM. A related group of researchers developed a voice coil powered micro-mill [306]. This machine has a half horsepower spindle with a maximum rotational speed of 150,000 RPM. It also uses a stacked structure of the voice coil actuators for positioning, that is the X,Y, and Z actuators are stacked on top of each other while the spindle is fixed to the ground. The travel of the axes is 25, 25, and 20 mm for the X, Y, and Z axes respectively.

A desktop 5-axis machine was constructed by Matsumura *et al.* with a workspace of 40 x 100 mm. This machine is capable of velocities of 150 $\frac{mm}{sec}$ in the primary directions and has been primarily used for the machining of glass. It can be configured with either a spindle for milling or as in the case of [184], it can be set up to scratch a glass surface with a fixed cutter.

One group that focuses on commercial machines is the Bao *et al.* Their research on micro-milling cutting forces utilizes three different machines, a Bridgeport 3,000 RPM machine, and two Fadal CNC machines, one with 3-axes capable of 15,000 RPM and one 5 axis machine capable of 50,000 RPM [16, 18, 17]. By using these different machines, cutting force measurements were possible for a wide range of conditions.

2.2.3   Applications

Micro-mills can process a variety of materials that other techniques cannot. For example, lithography is constrained by part material, primarily silicon. Also, laser machining cannot machine reflective or transparent surfaces [183], and water jets, as well as lasers are not well suited for situations requiring zero tapering of the cut [159]. This diversity in machinable materials and types of finished surfaces leads to a wide range of applications for micro-mills. Micro-mills can be used to create the molds for micro-injection molding [137, 95] or for the creation of micro-fluidics specifically micro-pumps and valves [172].

Micro-milling technology can also be combined with lithography, where micro-milling is

used to generate the mask. Friedrich *et. al.* have sought to use micro-milling to generate metallic masks for X-ray lithography [94]. These resultant parts can be used for thermo-fluidic devices and optical fiber connectors. Optics themselves can be created through micro-milling. Lens, as well as diffraction gratings can be machined out of glass [137, 236, 237, 238].

Another application area is for the mill itself is as part of a micro-factory. This idea is the brainchild of the researchers at AIST. Here the mill would be combined with other micro-scale machine tools in order to create a table-top factory [129, 190]. The mills discussed previously from AIST are designed as eventual components of this system. Many additional issues arise in this application as a factory component including the transport of the workpieces from machine to machine and the dynamic isolation of each tool.

2.2.4 Micro-Turning

High precision turning uses either a traditional lathe setup reduced in size and increased in accuracy or a modified face turning layout. One specific micro-lathe designed for face turning is also at AIST as part of there micro-factory plan. The AIST lathe is a fine example of high precision turning [129, 199, 202]. Mounted on the spindle of the lathe is a disk whose face is machined by a fast servo cutting tool. Another positioning servomotor moves the cutting tool along the disk in order to cut any point on the disk. When the servo's motions are properly coordinated, a complex pattern can be developed. These motions must be coordinated precisely with the rotation of the disk, as measured by the rotary encoder. The speed of the motions therefore limit the part quality.

Another face turning lathe of Takeuchi *et al.* was developed as a psuedo-ball end mill [280, 281]. This machine used a single point to cut surface features in the same structure as the AIST lathe and contained a spindle capable of speeds of 30,000 RPM. This lathe was also able to study the machining of glass and the differences in the ductile and brittle regions of machining [279].

The design of the cutting servomotor in all of these lathes is important to the performance and Okazaki attempted to make the servo as fast as possible [200, 201]. Kim and Kim developed a similar piezoelectric servo for use on a traditionally structured lathe that was used to compensate for waviness in the part [145]. By making the servo fast enough, flexibility in the system's structure could be compensated for using the servomotors's motion. Li and Li developed a similar system but focussed on the measurement of the part *in situ* to improve roundness [160]. Three capacitive sensors were used to measure the part and were fed back into the controller. This type of fast servo can even be affixed to macro-scale lathes. The cutter can be used with appropriate sensors to correct machining errors made by the primary cutter [329].

The wear characteristics of the tool used in face turning lathes were explored by Choi and Kim in [48]. They found that the frequency of the cutting forces was dependent on

the wear of the tool. Another important aspect of the cutting process is the material. Just like in micro-milling the material plays a key role in the micro-turning process. Grains in metals can change surface quality drastically [46].

While most micro-lathes use mechanical cutting to remove material, Feinerman *et al.* developed a lathe that cuts with X-rays. It operates in the same manner as a traditional lathe, but by duration of exposure to X-rays, part profiles can be obtained [75].

2.2.5 Other Micro-Machining Mechanisms

Mills and lathes are not the only precise machine tools. Many other machining operations need to be performed at the micrometer level. These tools encounter similar problems to lathes and mills and the techniques used to counter the problems for these tools can and have been extended to precision mills and lathes.

One such alternative technique is rotary ultrasonic milling. This technique uses a combination of grinding and milling technologies for part creation. A spinning disk is pushed against the surface of a part and vibrated [215]. This type of machining is ideal suited for the manufacture of precise ceramic parts [216].

Jet machining methods are another micro-tool that also have low tool/workpiece contact forces. This technique uses a liquid at high velocity to do the cutting and is often supplemented by particles suspended in the liquid. This technique has also been combined with laser machining [159]. A laser was confined and constrained by the water jet allowing improved cutting. Both laser and water jet machining have little to no contact force and therefore the augmentation techniques developed for low-contact-force machine tools will be applicable on them as well. Another jet like technique is the use of an ion sputter to create micro-solenoids [218].

2.2.6 Other Flexible Systems

An understanding of the work being done on other systems similar to machine tools allows existing techniques to be modified for use on micro-mills. Often similar problems need to be overcome like changes in frequency with configuration, or new techniques need to adapted to use on machine tools like command generation or concurrent mechanical control design. The specific mechanisms addressed here have had their performance improved through the use of input shaping.

2.2.6.1 Cams

Cams have been extensively designed for vibration reduction. A variety of approaches are used to limit the vibration in the cam and follower system. The design of the cam itself is usually seen as a method to avoid excitation of vibration. They are a mechanical element whose design also encompasses command design.

The tradeoffs for vibration suppression are often important in cam systems. In an effort to reduce high frequency vibration, Chew saw the possibility to accomplish this goal at the expense of lower frequency vibration [47]. When using cams, the mechanical profiles are used to generate commands for the attached system. When this occurs, the tradeoffs between design choices are more pronounced than in direct command design. Chew's work showed how careful analysis is required in order to process these tradeoffs whenever implementing a vibration reduction scheme through cams.

The continuation of cam systems as a mechanical command creation scheme occurred in the work of Andresen where the mechanical design rules for cams were combined with the command design rules for input shaping [10]. This combination is a novel approach to combining mechanical design with command generation.

The mechanical augmentation of cam systems to reach performance goals has also be studied. For example, a coulomb damper was used by Dresner and Barkan on the cam follower system [61]. The inclusion of additional mechanical elements into a pseudo-command design scheme is similar in concept to some the of the mechanical and command design techniques presented later in this dissertation.

2.2.6.2 Elevators

Elevators are another application where advanced vibration suppression techniques have been attempted. One dominant feature of elevators that can also be found in milling machines is the change in fundamental frequency dependent on location in the workspace. Elevators exhibit a well behaved nonlinearity associated with the cable length [232]. Techniques deigned for this type of nonlinearity can be expanded to use on other mechanical systems. Agrawal and Pota tried δ-flatness control technique on a simple two-mass model of an elevator [6] to control the nonlinearity. Similarly in the application of advanced control, μ-synthesis was used along with parametric uncertainty discussion [303], while Beldiman *et al.* focused on Heuristic Control techniques for elevators [22]. An alternate approach beside advanced control laws to deal with the uncertainty in the plant has been gain scheduling techniques which rely on simpler controller that change with time. This technique was combined with a robust control law for an elevator to suppress vibration [161].

Elevator control contains two primary realms also found in manufacturing machines. The first is the aforementioned position dependent dynamics; the second is the real-time path optimization necessary for the occupant to be able to change the desired floor at any moment. This is similar to the problem of selecting a cutting path for a tool. The same types of techniques can be used for path optimization be that ladder logic, neural networks, or other decision making controllers.

Aerospace mechanisms have necessitated a move towards optimal design due to the extreme weight requirements on the machines. Many techniques have been developed to design large orbital structures to minimize vibration while keeping weight to some minimal value. This research led into the development of simultaneous optimization of structural parameters and controller parameters as will be discussed in Section 2.3.1

One large vibration problem often encountered in these structures is disturbance rejection. When an orbital vehicle changes positions its appendages tend to vibrate. These appendages like solar arrays, antennae, and structural components vibrate from the acceleration of the satellite or spacecraft. These motions are modelled by actual dynamic motion of the structure or by white-noise forcing functions [206].

Space structures are usually modelled as beams comprising linear and spatial trusses for ease of dynamic prediction. These types of models are typically lumped mass linearized approximations for ease computation. These lumped-parameter models must be augmented by several other factors found on the actual space structures. Actuator force limits from the thrusters can be included in the models. Likewise, the controller and sensor systems will have physical limits on the output. Also, transient deflection limits whereby the structure can only bend to a limited angle sometimes appear [179].

However, sometimes these elements are combined into larger or complete systems of elements like the multiple appendage model in [110]. The structural parameters, namely the size of the members, can then be changed to improve vibration response. Particular to this application, the modal damping is investigated [142]. Robustness to parameter change is also often considered in order to expand the stability margin of the structures [171]. This stability margin measure can also be used to reduce the complexity of the model of the structures [221].

While the robustness and parameter selection techniques can reduce the vibration in the satellite appendages, in order to fully control this vibration several other techniques can be applied. One approach is to design the commands that move the entire satellite not to excite vibration in the flexible appendages. This was done with input shaping for formation flying satellites [29].

Another more common method is to actively control the structures. This involves the addition of actuators at non-joint locations. These are either thrusters which force the structures against the inertial reference frame or internal actuators like piezoelectrics which force the structure against itself [38]. Then, a control law is used to reject the disturbance of the move. A common choice easily combined with structure design are linear quadratic regulators as in [23, 38, 62, 110, 141, 142, 140, 171, 206, 221, 222, 25]. Bang-Bang or on-off controller are also used to model the dynamics of thrusters [179].

Still another method to deal with the vibrations is to implement mechanical filters to

transform the command signal. Yang *et al.* propose the use of non-circular drums to filter the motion commands into the flexible appendages [320].

2.2.6.4   Cranes

A large amount of work in command generation has been done for cranes. The application of command generation on cranes is well suited because the payload position is difficult to sense, thus making them useful for open loop control techniques. They also have a clearly defined vibration problem at one primary frequency which can be completely eliminated by input shaping [91, 247, 261].

Non traditional cranes have also been researched with input shaping. One particular subset is the wire-drive manipulator where the payload of the crane is completely suspended by cables. This approach reduces the inertia that must be moved as would be the case for a new micro-mill. Input shaping research has attempted to cancel the more complicated vibration tendencies of the wire-driven crane, as well as dealing with both the pendulum mode and the cable elongation mode [121, 120]. The solutions for these types of cranes are highly position dependent. In manufacturing machines, the vibrations characteristics are likewise often position dependent.

2.3   Vibration Suppression Design

A good mechanical design usually means one that does not vibrate. In order to accomplish this goal of minimal unwanted vibration many different techniques can be used. The mechanism can independently be designed not to vibrate or the system can be designed in conjunction with a vibration control scheme like a feedback controller as discussed in the following sections. However, little quantitative work has been done in combining command design with mechanical design. Therefore, other combined design strategies will be discussed and their techniques applicability to combined command and mechanical design evaluated.

2.3.1   Design for Control

Mechanical design coordinated with vibration suppression is discussed in this section as an alternative to the simple solution of an increase in stiffness or mass. Coordinated design encompasses many different approaches that involve novel changes in the mechanical design which might increase flexibility but reduce vibration. Also, another technique is selectively choosing flexibility to coincide with an external control methodology. Major gains can first be obtained by considering the structure of the controller at the design phase [324], however more advanced design techniques are possible. The overall goal of combining the element's design is that by integrating the mechanical and controller design, optimal performance can be achieved in positioning, tracking, dynamics, acoustic, *etc.* [299].

2.3.1.1   Machine Tool Fixturing

A cutting machines method for attaching workpiece to the machine itself is vitally important. The clamping force and material properties of the part and fixture define the ability of the system's interfaces to damp the motion through friction [321]. Decreasing the clamping force does increase the flexibility; however, it often improves vibratory performance since the lower clamping force allows sliding and thus frictional energy dissipation and an increase damping ratio in the system. Controlling this frictional interface is important such that the fixture can be design to increase the damping ratio of the system and make it easier to control [11].

The design of fixtures can also deal with cumulative hysteretic errors in the machining as well. If a flexible mount is design correctly as is explained in [265], then the flexibility can be used to eliminate the errors do to cyclical load in both force and temperature.

This clamping principle can be applied to tool holders as well. In [240] the mounting of a lathe cutter was altered in such a way to increase precision. Typical tool mounts will experience hysteretic losses from displacement, as well as thermal deformation. By introducing a known flexibility into the system, the thermal deformation is equal in all directions holding the tool stationary. This mount flexibility must be low enough, however, so that the cutting forces do not cause the tool to move. This appropriate flexibility causes hysteresis loss to decrease since the flexibility in the mount returns the energy instead of the standard loss from a rigid mount. Thus the tool position will remain consistent before and after energy is introduced into the mount from the cut.

2.3.1.2   Novel Mechanical Elements

Another way of altering the vibratory characteristics of a system is to alter the dynamics of the system through the inclusion of additional elements. Some of these methods are well known like the inclusion of external damping, vibration absorbers, and vibration isolators as will be discussed in 3.1. However, there is another class of mechanical elements for vibration suppression which does not fall into these general categories.

One example of such element is the flexure joint which can be used in Gough-Stewart platform design [185]. Here the improved dynamic characteristics of flexure actuators are used for improved response. Specifically, flexure actuators avoid friction and backlash by bending a material to produce motion instead of sliding or rolling. McInroy went one step further in this work by selecting actuators for the overall dynamic effect. Then, he chose system parameters to simplify the Jacobian of the parallel manipulator. A square Jacobian was maintained providing for easier motion calculations.

Gearing can also be selected correctly to provide increased controllability. Planetary gears exhibit vibration in three modes: translational, rotational and in the planets' deformation. Parker showed that by utilizing planet phasing, the vibratory frequencies could

be predicted and thus controlled [214]. Planet phasing is the correct selection of the tooth numbers and planet configuration in order to reduce the internal forces in the gear train.

A corollary to mechanical augmentation is the selection of mechanical components based on the vibration characteristics. A gear train might be used instead of a pulley system for a transmission due to the stiffness of the gears. In a similar way but for a more complicated selection, Tu and Rastegar examined the vibrational tradeoffs for different types of manipulators [294]. Here the frequency characteristics of rotational and prismatic joint manipulators were compared based on actuator selection and location int the serial chain. A similar approach was used with internal architecture of a switch reluctance electric motor in [115]. Differing yoke structures produced different vibratory characteristics in the motor output.

The vibratory characteristics can be used for the purpose of mechanical damping as discussed in detail in 3.1.1.2. An example of such an element is the filling of a box beam with glass balls. These balls interact with each other in such a way as to increase the damping of the beam [307]. The parameters of these glass balls can be chosen in order to achieve different levels of damping with differing costs in terms of material and consequently mass.

More complicated mechanical elements can be used in order to alter the controllability. One type of these is a mechanical filter. A mechanical filter is a device which performs some augmentation of the input to it via mechanical means in order to achieve an output response that is more desirable. This is like an electronic filter which can remove noise from the common voltage or a vibration isolator that removes noise from the base to a machine as discusses in 3.1.2.1. Vibration isolators are a common mechanical filter that are designed to eliminate certain frequencies from entering a system.

Gearing could also be classified as a mechanical filter which merely changes the gains of an input. However, gearing can be more complicated than a speed transformation. Gears can be used to alter an input to a more complicated profile by turning smooth rotation into a shaped rotation for the purpose of vibration suppression as seen in [320]. A series of frictionally connected drums of non-constant radius are used to move a space appendage with minimal vibration. This mechanical element was designed with a regulator control system for the appendage in order to achieve minimal system vibration.

A common mechanical element to add to system in the design phase to reduce the vibration is an actuator. This is not a novel solution for problems where actuation is traditionally used. However, in usually passive situations, the application of an actuator is the first step in active feedback vibration control. Actuator selection is a vast design area which is not addressed here. However, it is important to note that a common solution to an uncontrollable passive problem is to make it an actively controlled vibration like was done in [125] for car suspension to increase damping and in [120, 121] to maintain the frequency

of vibration.

The opposite of this case is for under-actuated systems. The design of nonholonomic machinery involves special care in order to achieve stability and controllability. Nakamura *et al.* studied why it is necessary to combine the design of the controller and mechanism. The specific example was a nonholonomic system of a arm with a spherical gear. The procedure allowed the system to reach both controllability and stability [191]. By combining the mechanical design with the controller design the difficulties in controlling a nonholonomic system were overcome.

2.3.1.3   Mass Redistribution

An alternative strategy for vibration suppression is an augmented balancing scheme with the goal of increased controllability. If the internal forces placed on the actuators of a machine tool can be eliminated through balancing of the machine, then the control forces will be lessened, and the dynamics of the system simplified, thus making the systems and controller response easier to predict.

Closed linkages are a common structure where mass redistribution for force balancing is possible. Since they are typically closed chains, it is possible to move mass from one link to another to balance the machine, whereas the same approach of moving mass on a serial linkage would provide little balancing ability. The technique has been performed on a four-bar linkage in [328] and [163] such that the internal forces were completely cancelled, thus reducing the load on the actuators and simplifying the dynamics model. Furthermore, the moments were balanced as much as possible to further simplify the system. This is done by making the center of mass stationary or by minimizing the rotation of the overall inertia. This balancing procedure can also be done to eliminate gravitational effects.

This approach of simplification of system dynamics is contrary to the techniques discussed in Section 3.1.2, where vibration absorbers and isolators were employed. One must remember that the inclusion of an isolator or absorber is typically a linear component only adding a degree of freedom while the above techniques for mass balancing do not seek to lessen the degrees of freedom but instead eliminate nonlinear forcing on the actuators.

2.3.1.4   Combined Optimization

Design for Control, or DFC, is a general term which could apply to any vibration suppression design scheme, however it usually applies to a technique by which the controller parameters are selected in the same algorithm as the structural parameters. This approach typically utilizes an optimization algorithm with a cost function having weighting on both the structural response and the controlled response.

Table 2.1 summarizes the approaches that have been used in DFC. The constraints and cost function parameters are presented, where C is used for constraints and $ is used for

cost function parameters.

Table 2.1: Constraints Used in Design for Control.

Parameter	1	2	3	4	5	6	7	8	9	10	11	12	13	14	15	16	17
1st Order Time Constant												C					
Avoidance of Singularities													$				
Balance						$											
Controller Force	$		$				$	C			$,C			$			
Controller Gains						C		C		C				$	C		
Damping Ratios		C		C	C	C			C				$	C			
Eigenvalue Robustness						C			$						$		
Force								$	C		$		C			C	C
Harmonic Amplitude																$	$
Manufacturability													C				
Mass		$	$	$	$	$			$		$		C	$	$		
Overall Frequency		C		C	C				C	C			$				
Payload													C				
Position Error	$		$				$	$,C			$		C	$		$	$
Response Time		C											$				
Stability														C			
Stiffness															C		
Structural Frequency														C			
Structural Parameters		C	C	C	C	C		C	C	C	C		C	C	C	C	C
Velocity Error	$		$				$	$					$			$	$

$: Cost; C: Constraint; *where 1:Belvin 1990 [23], 2:Eastep 1987 [62], 3:Hale 1985 [110], 4:Khot 1986 [142], 5:Khot 1988 [140], 6:Khot 1993 [141], 7:Li 2000 [163], 8:Li 2001 [164], 9:Lim 1989 [171], 10:Lust 1988 [175], 11:Manning 1990 [179], 12:Onoda 1987 [206], 13:Park 1994 [212], 14:Rao 1988 [221], 15:Rao 1990 [222], 16:Rastegar 1999 [224], 17: Yang 1994 [320]*

Work has been done using this technique in many areas. For example, Park and Asada designed flexible arms along with controller parameters [212]. They utilize a performance measure containing the dominant close loop pole, λ_{CL}, and a mobility measure, W, associated with the inertia ellipsoid integrated over the joint position space, D, with S being the variable for integration:

$$J = \frac{\int_D Max[Real(\lambda_{CL})]WdS}{\int_D WdS} \qquad (2.3)$$

The variables for the optimization were the geometry of the two link arms as well as the controller gains. Several constraints were also placed in the optimization to deal with problems not covered by the cost function that deal with practical implementation. Actuator size, workspace, vertical deflection, payload, and manufacturable dealing with physically being able to machine to machine to parts. The result was a decrease in inertia of 50% while maintaining the same performance.

This sort of approach can also be extended to include trajectory design in the control and structure design. Rastegar *et al.* has tried to do this utilizing his Trajectory Pattern Method described [223]. In [224], a known trajectory generation technique, TPM, is utilized with a PD control law. A combined optimization is then done to find the optimal response. The trajectory design is not done in the optimization, instead it is off-line approach to generate

trajectories. The optimization then selects from the discrete trajectory alternatives designed by the TPM method The cost function for this work focuses more on modal response amplitude, A, and tracking errors, e, for specific movements with user definable weights w:

$$J = w_A \sum_{j=1}^{n} \left[\sum_{m=n_j}^{n_h^j} w_m^j A_{j,m}^2 \right] + w_e \int_0^t \sum_j \left[w_{p,j} \left(e^j \right)^2 + w_{d,j} (\dot{e})^2 \right] dt \qquad (2.4)$$

The $m, n, d, h,$ and $j's$ are counters to deal with the various weighting and modes of the robot. No constraints are utilized in the optimization.

Another simpler approach is to avoid the complete design of the structure, instead a tailoring or small modification of an existing design can be done as in [23]. By removing strategic masses the with the aid of the Linear Quadratic Regulator, the vibration suppression of a beam was maintained while lowering the mass. The cost function that allowed this to happen needs to be tailored specifically to each problem but the "approximate" cost function is:

$$J \propto \left(\eta + \frac{3}{2} \zeta \right) \gamma^T U^T \Lambda^{\frac{-3}{2}} U \gamma \qquad (2.5)$$

where η and ζ are a scalar proportional and derivative gains respectively, γ is the modal force participation coefficient vector a measure of how a disturbance acts on the modes in the research it is a vector of 1's, Λ is the eigenvalue matrix, and U is the triple matrix product of the mass matrix M and eigenvectors T given by:

$$U = T^T M^{\frac{1}{2}} T \qquad (2.6)$$

No constraints for the optimization are mentioned.

Another option in an attempt to optimize a space structure is to control the sensitivity of the complete control structure scheme in the optimization. In [62] this sensitivity deals with the ability of the closed-loop eigenvalues to deal with changes in structural stiffness. However, this sensitivity is not used in the optimization cost itself, instead it is a constraint on possible solutions. The actual cost function is:

$$J = Weight \qquad (2.7)$$

subject to constraints for specified modal damping and frequency, as well as positive frequency and damping values.

The application of DFC has also been used on complicated large space structures beyond the simple beam, truss, or pyramid. In [110] central hub with spokes extending is optimized. The authors used a cost function that reflects the complexity of the structure using an integration of desired cost function values over an entire desired move length, t_f. Mass was also considered in $\alpha P(\xi)$, which is a structural parameter term related to mass. Also used is control force f, position and velocity u and $\dot{u}$, and weighting terms R, Q_1, and Q_0:

$$J = \alpha P(\xi) + \int_0^{t_f} \frac{1}{2} \left(f^T [R] f + \dot{u}^T [Q_1] \dot{u} + u^T [Q_0] u \right) dt \qquad (2.8)$$

41

Along with this cost function, constraints were placed to keep structural parameters positive. Another option for dealing with the concurrent design in large space structures is to attempt to cancel the subjectivity of a cost function through the comparison of the results from several different cost function optimizations.

Rao attempted this approach in [221, 222] where mass, response time, and two performance indexes were used and the result compared. All four of these relied on constraints on both the smallest modal damping ratio and the area of the structural members. Total mass as a cost function is self explanatory but the response time relies on a more complicated cost function:

$$J = \frac{x_0^T[P]x_0}{x_0^T[Q]x_0} \tag{2.9}$$

where the x vector are the states of the system, P is the Riccatti Matrix and Q is given by:

$$Q = \begin{bmatrix} K & 0 \\ 0 & M \end{bmatrix} \tag{2.10}$$

where K and M are the stiffness and mass matrices. This supposedly yields a solution which has a optimal response time due to the damping properties of the system.

The third and fourth options presented by Rao rely on other means of performance index. A quadratic performance index:

$$J = x_0^T[P]x_0 \tag{2.11}$$

was discussed and yielded the same optimum solution as the fourth, the Frobenius norm:

$$J = trace\left\{[G]^T[R][G]\right\} \tag{2.12}$$

Disturbance rejection is usually the vibration problem to be overcome in these large flexible space structures. The type of forcing is often different in each case. For example, Onoda and Haftka attempt to do design and control optimization using a true white noise forcing on the system in [206]. They hold the interesting view that combining response into the optimization is not good since real application's responses are constrained by practical considerations. Basically, since the response is often given it should not be optimized. Instead they use mass, m_s and control forces, σ_2 to determine the best solution under constraints on parameter limits, displacements and controller forces. The cost function used by Onoda and Haftka is:

$$J = \frac{\left(m_s + \alpha\sigma_2^\beta\right)}{m_N} \tag{2.13}$$

The procedure was tested on a beam with variable thickness being the design parameters along with Linear Quadratic Controller gains.

Lust and Schmit also worked on the DFC problem of disturbance forces. They addressed both static and harmonic loading on beams. Their cost function centers around the mass, M; vector of displacements, $\overline{u}$; and the vector of forces $\overline{F_A}$:

$$J = c_1 M + c_2(Q|\overline{u}| + R\overline{F_A}) \tag{2.14}$$

where c_1 and c_2 are constants, and Q and R are matrix weighting constants. The same optimization of a beam subject to stress on different aspects of the cost function was studied, with constraints placed on displacement, actuator limits, and open loop frequencies.

Mass alone is a common cost function and also appears in the work of Khot *et al.* [142, 140, 141]. This work varied the type of constraints used in the optimization. Sensitivity of the damping, the frequency, and the robustness to changes in the design variables were considered along with the spectral radius, which is a measure of modal robustness. Also considered were physical limits on the design variables.

Methods used to find the optimum solution also vary. Lim and Junkins chose a linear programming technique [171]. This technique was used to compare three different cost function results. The first was total mass of the system. The second was the sensitivity of the eigenvalues to parameter changes, where λ are the eigenvalues, p is the design parameters, and w is a weighting constant over the design parameters counted by i and j:

$$J = \sum_{j=1}^{5} \sum_{i=1}^{6} \left|\frac{\partial \lambda_i}{\partial p_j}\right|^2 w_{ij} \tag{2.15}$$

The third cost function considered was to maximize the robustness of the system stability. This relies on the solution to the Lyapunov equation to find P, which is used in conjunction with the eigenvector u in:

$$J = \bar{u}^T \frac{\partial P}{\partial p_j} \bar{u} \tag{2.16}$$

Once these cost functions were generated, the convergence of the optimization solution was studied. The main result was that the convergence of the measure of stability robustness coincided to a convergence in the actual stability robustness.

Another comparison of optimizations was done in [164]. They chose to use the same type of cost function but change the constraints on the optimization for a four bar linkage. The cost function consists of tracking error, E, actuator power, W, and difference both max and min from the ideal performance S_{max} and S_{min}. Weights α, β, λ and ρ were used as well to form:

$$J = \alpha E + \beta W + \lambda S_{min} - \rho S_{max} \tag{2.17}$$

This combined design approach relied on three different constraint scenarios. The first dealt with the desired path using tracking error and a couple of constraints on the physical implementation of the linkage. The second set of constraints used actuator limits, while the third used a mass balancing technique like that discussed in Section 3.1.2.

The type of controller for these large space structures is typically a Linear Quadratic regulator. However, in orbital environments thruster are the usual actuators. These are on-off actuators and to deal with this limitation, Manning and Schmit developed an optimization scheme based on mass, W, and control force, E, to design the optimum Large Space Structure, LSS, and controller [179]. Constants c_e and c_w were also used in conjunction with an integration over the whole move time t_f:

$$J = c_w W(d) + c_e \int_0^{t_f} E(d, t) dt \tag{2.18}$$

The constraint choices in this problem were acceleration, error, actuator limits, controller limits, and a maximum mass limit. This work, however, only considered one disturbance forcing which would need to be extend for actual application.

2.3.2 Design for Command Generation

Command Generation is typically an afterthought in system design. An existing mechanical system with feedback controller is generally retrofitted with a command modification scheme. However, performance can be improved if the input shaping scheme is designed with the rest of the plant. Previous work referenced later has tried to link the controller design with the command generation design. This work tried primarily to improve the driven response, but did attempt to also deal with disturbances.

The combined design of feedback controller and input shaper allows increased performance from the system. One approach taken by Drapeau and Wang is to choose an appropriate input shaper for the system and then tailor the controller gains to improve performance [60]. This approach adds error from the shapers frequency and the system's new frequency after the controller has been modified. However, this technique is a good starting point and shows a simple first step solution to the problem of designing a controller and input shaper together.

Another technique developed by Kenison and Singhose seeks to design the controller and input shaper concurrently through the use of a numerical optimization [138, 139]. A MATLAB optimization chose a proportional and derivative controller while selecting an input shaper. The advantage of this approach was that damping could be decreased to improve system response time while maintaining strict vibration constraints. The downside of this approach was that it required a complicated optimization that needed to be performed for each system although it yielded improved results over the controller tailoring method.

Input shaping can also be linked with the controller by placing the input shaper inside the feedback loop. This enables the input shaper to have a direct effect on the disturbance response [241]. Here the input shaper effectively becomes part of the controller and the line between controller design and input shaping design becomes blurred. It is important

to note that the input shaping inside the feedback loop's main drawback is that it is not always stable.

These techniques for designing controllers with input shapers indicate how mechanical design and input shaping design might be combined to improve response.

2.3.3 Design for Machining

The current techniques for the design of machine tools have been tested and improved upon by many researchers. However, an understanding of these techniques is necessary for the coupling of mechanical design of components with command design for micro-manufacturing machines. Several comprehensive sources exist for the design of machine tools whose results are too comprehensive to be summarized here including Altinas [8], Crede [50], Marinescu *et al.* [180], Rivin [229], Slocum [266], Tobias [288], and Welbourn and Smith [315]. Instead of these extensive textbooks, the focus will be on the current research into machine design, specifically how it effects the goal of combining mechanical design with input shaping design.

2.3.3.1 Electric Motor Design

One focal area of combined goal design procedures is in the design of electrical actuators. The performance of these primary components drives much of the other design selections. Logical selection algorithms have been developed for choosing motors. For example, Cusimano created a procedure that coupled a database of motors with the power requirement for the in this case a transmission [52]. Considerations were made for continuous and dynamic use.

Haskew and Schinstock also looked at the design of actuators; their study focuses on the optimization problem of actuator selection for space shuttle main engine vector thrust control [112]. The optimization is accomplished through an equivalent circuit technique in the phasor domain.

Electric motor mechanical design has even been coupled with controller design. Reyer and Papalambros attempted an optimal design of a DC motor and a PID controller [227]. They present three approaches to the combined design in increasing complexity: single pass (design one then the other), iterative, decoupled optimization (optimizing structure then controller and iterating), and overall optimization. As more complicated techniques were used in the paper, the resultant design was better suited for the application. The tradeoff between design complexity and final performance is clear from this work.

2.3.3.2 Finite Element Design

One way to design manufacturing machines is to design the machine in a CAD package and then use finite element analysis to determine if the design meets the desired performance criteria. The finite element model can be static or dynamic in nature. Reddy and Sharan

designed a lathe spindle using only a static and dynamic finite element analysis [226]. In a similar problem, Yeh and Liou used finite element techniques to model the static and dynamic loading in a machine tool fixturing set-up [321]. However, the FEA may not be the end of the design iterations. For example Bianchi *et al.* seek to use a finite element model of a mill to develop a second-order dynamic model for use in initial controller response [28].

By creating a dynamic model of the structure and controller at an early stage in the design process, behavior of the machine can be predicted. Wu *et al.* on the other hand used a two-level optimization model based on finite elements [316]. First, the finite element model of a tool's structure was created and optimized. Then, the models of each component were tailored through further optimization to minimize weight and maximize stiffness. A finite element model can also be used to select configurations. Chen *et al.* considered three different headstock configurations and used finite element analysis to determine which one to build [43]. However, their models left out details in the headstocks and therefore general rules about headstock design cannot be deduced from the finite element result.

2.3.3.3   Machine Tool Component Design

Research has also focused on the design of specific components of machine tools. For example, the cutter for a mill offers many design choices. Tsai and Hsieh presented a procedure for the complete design of a ball end cutter [293]. The procedure focuses on the design for manufacture of the cutter. Lee *et al.* chose to focus on designing a face-milling cutter with improved dynamic performance. By selecting inserts for the cutter wear characteristics could be improved [157].

Another integral component in a micro-mill are the linear slides that provide workpiece motion. Mekid presented the procedure he used for the selection of such a slide in [187]. Interestingly, the flexibility of the slide needs to be less than the flexibility of the fluid in the bearings so as to allow proper damping. Singh and Beohar also addressed slide design but used information theory approach to aid in component selection [249]. First, an entropy function was used to define the errors in the slide. Then, the maximum entropy for a given design was calculated, and finally this maximum entropy compared to other designs, with the optimal being the one with the lowest maximum entropy.

The design of the spindles inside the slides are another area of machine tool design that has been investigated. Sadeghipour attempted to reduced the vibration in these slides by inserting small masses at critical locations along the spindle [234]. This process altered the modal response of the spindle to give it better dynamic response. The technique found the receptance sensitivity or the places that a small increase in mass can greatly alter the modal response. A technique similar to this could be used with input shaping design to alter the dynamics of a system to be better suited for input shaping.

Another approach to spindle design is to let a computer optimization select all the radii of the spindle to meet a series of design goals. Taylor *et al.* developed such a program to design the spindle of a grinding machine [284]. A logic based approach coupled with an optimization algorithm make the procedure possible. A similar computer selection approach used by Eskicioglu *et al.* was used to select the bearing arrangement for another spindle [72].

Dequidt *et al.* created another design procedure for machine tool positioning systems [54]. This procedure is quite similar to the one that will be employed in this dissertation for the combination of shaping and mechanical design. A ball screw drive is modelled as a second-order oscillator with several key assumptions: no higher modes are present, sensor are not near vibratory nodes, and the electrical time constant is negligible. For the case of lead screw system first stiffness and inertia are defined in terms of design variables, then test are made to see if these stiffness and inertia values meet minimum performance specifications. If they are then the drive system is suited for the application. Once the motor and configuration are selected, a the gear ratio is selected base on available screw radii.

Yoshimura developed a technique for the design of the machine tool structure to deal with forced and self-induced vibration [323]. This technique relies on finite element analysis to calculate frequencies and damping ratios, and then the developed algorithm is used to determine if design parameters are acceptable. Kulik and Pedchenko took another approach to simplifying the design process of machine tools by creating a complicated model and then reducing the order using a simplification technique [151]. Zhang *et al.* chose to analyze the dynamics of machine tool structures using a technique focussing on the interfaces or joints between structural components [327]. The technique focusses on using "stiff" machine tools, where the main elements are rigid. For their model the primary flexibility is in the joints, where up to 60% of stiffness and 90% of damping is in the joints. While this holds for stiff structures it will not necessarily apply to machines with more flexible members.

2.3.3.4 General Machine Tool Design

Procedure have also been developed for more general design of machine tools. For example, Bohez developed a technique for the selection of the actuator type, either rotational or translational for a 5-axis milling machine [32]. Mishima created design evaluation technique for the same type of problem for a micro-machine tool [190]. Design parameters relating to both the tool and the slides were combined with configuration variables to yield the overall positioning error. From this work, the traditional mill configuration of one slide driving the spindle position and two driving the workpiece was shown to have smaller positioning error than other configurations. Van Brussel *et al.* presented a similar but more comprehensive technique in [300]. First, a genetic algorithm is used to select structural configuration.

Then, a finite element approach is used to determine a simplified model of the tool. Finally, a method to select controller configuration is detailed. By combining all three parts into one procedure, major design decisions become easier, with only detail design remaining.

Several survey style papers also discuss the trends in machine design. Newman *et al.* presents lessons his research group learned about agile or reconfigurable manufacturing systems. By using lightweight tools not only are they able to move faster, but they can also be easily reconfigured. Other survey papers focus on micro-machining and give a broad overview of the current state of micro-manufacturing [183, 129, 64].

2.4   *Synopsis*

By investigating the previous work in mechanical system modelling, operation, and design, the overall goal of the dissertation can be furthered. The modelling of micro-mills and similar systems provides a base point for developing design models for specific and generalized micro-mills. However, the research into micro-mill modelling is an open area. Likewise the specific forces involved in micro-milling is an open although active research area. The forces in the machine process need to be known so that the mechanical designs can effectively deal with them. Finally, investigation of the combined design of commands and mechanical parameters is under-researched. However, similar areas of combined mechanical and control design and combined controller and shaper design do offer some insight into how to formulate the problem.

CHAPTER III

LITERATURE REVIEW OF CORRECTIVE METHODS

Typical design procedures dictate that once a mechanical design is complete, and if vibration is excessive, then corrective techniques should be applied. Three main areas of design correction are relevant to the work here. The first key area is the use of mechanical components. These can be added to a system to alter the performance. Next feedback controllers can be used in a corrective capacity. Finally, the commands sent to the system can be designed to not cause vibration. Command design here is focused on input or command or input shaping. This technique filters systems commands with the goal of vibration suppression.

These three elements are important to the overall goal of combined mechanical and command design for different reasons. Mechanical augmentation elements can be designed in conjunction with command shapers. Also the performance of these augmentations needs to be understood, so that design decisions can be made whether to use command shaping or mechanical augmentation. Control strategies need to be investigated for the same reason as the mechanical augmentation, as a comparison of effectiveness. Particulary, the optimal technique for tracking control are direct competitors of command shaping. Finally and most important, the use and advancement of input shaping is one of the primary areas of this research. Fully understanding command shaping is necessary before it can be expanded to deal with other concerns.

3.1 Mechanical Augmentation

The mechanical augmentation of a machine can have two forms, vibratory mode augmentation or mode addition. Vibratory mode augmentation is important since the effects of changing the characteristics of the modes of a system will be key to later cancelling those modes with input shaping. Mode addition is useful since these additional modes can be designed concurrently with input shapers, although this has not been done outside the research of the author.

3.1.1 Mode Augmentation

Often the dynamic characteristics of each mode of a machine can be altered in order to improve performance. This alteration of elements can change the frequency, the damping, the inertia, and the stiffness of the element allowing improved dynamic performance. Understanding how to make these changes and their resultant tradeoffs allows the designer a

more holistic design approach. This approach allows control and command design to be performed simultaneously with mechanical element design.

3.1.1.1   Inertia and Stiffness Modification

The easiest modal change is an adjustment in the frequency. The frequency is coupled to both the stiffness and the inertia of the tool. It is often necessary to select the frequency specifically to prevent the occurrence of resonances due to some known internal forces. More common, however, is the necessity to alter the stiffness and/or inertia. The stiffness often needs to be changed to alter deflection. Inertia likewise must be changed in order to decrease the size of the actuators, the load on the support structure, or importantly here the speed of the machine. Understanding these types of changes allows the designer get the best performance possible from a machine. These changes are typically done through the addition or subtraction of material. Although the material itself can play an important role. Often composites are designed for specific stiffness and inertia requirements for a task [162].

Riven wrote an entire book devoted to the subject of stiffness and damping as it affects mechanical design [229]. Some of the primary advantages he presents for a reduction in stiffness are:

1. Rigid bodies are brittle

2. Statical indeterminance

3. Stress concentrations

4. Ability to control pre-loading

5. Inappropriate structural natural frequency

While on the other hand reducing stiffness has the drawbacks of:

1. Geometric distortions

2. Change in loads and friction conditions

3. Dynamic instability

4. Increased amplitude of forced vibrations

Rivin goes on to discuss how stiffness changes can be accomplished.

Rivin also specifically discusses stiffness in conjunction with manufacturing tools, specifically a boring bar in [230]. Here the discussion focusses on the stiffness of the boring bar itself. The stiffness impacts the chatter characteristics and because of this has direct correlation to the throughput of a tool. The stiffer a boring bar, the deeper it can cut, and thus

the higher the throughput. Here the stiffness drives the operation of the tool. This case must be considered as a limiting factor for other machine designs.

3.1.1.2 Damping Modification

Another method to augment the modes of a mechanical system is to change the damping properties of the system. Rivin once again gives insight into the effects of damping parameters on a system's response in [229] specific to the areas of:

1. Fatigue strength

2. Wear resistance

3. Efficiency (friction loss)

4. Accuracy and surface finish

5. Vibration stability

6. Manufacturability

Such damping can be linear such as viscous or nonlinear such as frictional damping or cubic dampers [3, 4].

Damping modifications can be accomplished in a variety of ways. The most obvious is to add a mechanical damper externally to the system [50]. Single or multiple dampers have been used [106]. When mechanical or electronic circuits mimicking as mechanical elements are added, a decision must be made about how to implement the damper. The most common approach is to attach the damper to ground. Since this is not possible for mobile machines like car suspensions, sky-hook damping can be employed to accomplish a damping increase [125]. Active dampers usually take the form of traditional viscous dampers where some component of the damper can be altered or the form of actuators controlled with a damping derived control law [125, 132]. The traditional active dampers have orifices that change size [5] or fluid whose viscosity changes as with the electro-rheological fluids in [311].

Another method to change the damping characteristics is to adjust the internal forces. By increasing or decreasing the forces between elements, the normal force is changed. Therefore when the parts slide against each other, the frictional dissipation will change. This coulomb damping can be easily adjust by changing the internal clamping forces [182] or by lubricating the contact surfaces. The clamping force has applicability to both machine tool fixturing and the lubrication method in vibration isolation. In machine tools it is typically concerned with chatter. While in isolation applications, the transmissibility of the isolator is an issue related to damping. For example, earthquake isolators need large damping to dissipate energy, but the damping cannot be too large since that will cause excessive forces on a building [131].

Damping arising from internal forces can be used to increase damping through the inclusion of supplemental moving parts. Here masses are added such that they rub upon each other or on the existing structure. The large number of frictional interfaces increases the damping in the system. One example is the insertion of metal plates into a boring bar in order to reduce chatter [182]. While another novel method is to fill hollow structural elements with balls as in [307] or rods and a viscous fluid as in [267]. These are similar to the vibration absorber or mass dampers that will be discussed in Section 3.1.2.2. Another possibility is the selection of the material for a machine. For instance, cast iron has higher damping than machined steel. Research is also actively trying to create composites with higher damping while maintaining the workability of traditional metals [162].

Coatings are a way to change the material properties with minimal physical change. A coating can be applied to an element, and the internal motions in the coating dissipate energy in the system through hysteresis. If coatings are applied to both sides of a component, losses from tension and compression can be achieved. However, the use of these types of coating is limited due to their temperature dependence [192]. A more advanced coating technology has also been used to increase damping. It relies on an induced magnetic field to increase hysteresis in a magneto-mechanical coating [322]. Coating materials can also be used inside structure elements. If a coating layer is sandwiched between two structural elements damping will not only come from tension and compression but also from shear effects in the interstitial coating [192]. Nashif *et al.* describes a series of coating applications in [192] including a damping wrap for a jet engine inlet guide vane, a constrained shear layer damper for the weapons dispenser of an F-4 phantom, a layer damper for a helicopter cabin, and a free layer coating for an engine exhaust stack.

3.1.2 Mode Addition

If additional dynamic modes are added to a system, then the overall system dynamics will often be complicated. However, if these modes are chose correctly, then the new more complicated dynamics can give better performance than the original system.

3.1.2.1 Vibration Isolators

Vibration isolators seek to eliminate the force transferal either from the environment to a sensitive system, from oscillatory system to the environment, or from both by the inclusion of a flexible system between the main system and the environment. The principle of isolators is a common one and is covered in many standard vibration texts [92, 128, 290]. It relies on mounting the system on a dynamic base which filters out vibration energy. Figure 3.1 diagram a typical isolator application on a system. The isolator prevents vibration from being transmitted from the base into the primary system and vice versa. Typically this is done with spring and mass element dynamics.
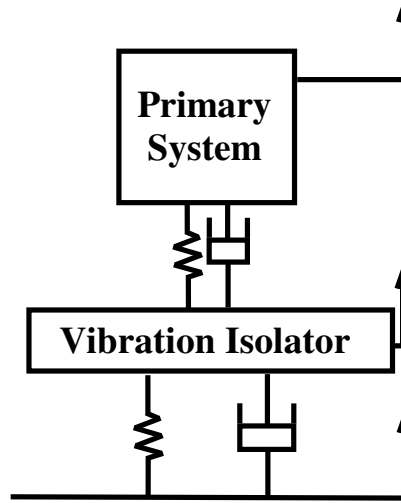
Figure 3.1: Vibration Isolator Schematic.

The application of vibration isolators to machine tools is not a new one [315]; however, for micro-machining, where inertia is low, the role played by vibration isolators is more important due to the susceptibility of the machining process to external disturbances. When the inertia is reduced, the tool itself will be affected by disturbance vibration from the environment in a greater way than before. Therefore, a machine that previously was not affected by the environment will now have its performance affected by the external sources. One area where this new vibration can be especially detrimental is in element interfaces. Often excessive vibration can cause the normal force between components to change and thus the interface to slip, resulting in positioning error [228].

A key performance measure of vibration isolators is the transmissibility, or the ratio of the forces applied at one side of the isolator to the forces transmitted to the other side. In the case of any micro-tool, an isolator is needed so that the transmissibility will be low at all excitation frequencies. This is not a new idea, previous work suggest the isolator needs to be designed to have a lower frequency than the forcing function [111, 49, 272, 50]. Other performance measures are also used in isolator design. Such as structural power transmitted, cancellation of forces, and cancellation of velocities [98]. These are better suited for a non-linear transmissibility or when other specific constraints must be met. Balandin *et al.* propose a another series of performance criteria in [14]:

1. Maximum displacement

2. Maximum angle

3. Maximum force or acceleration

4. Maximum absolute mean square acceleration

5. Maximum isolator force

6. Mean isolator force

Most of the above work in performance measures focuses on vertical vibration. However, Rivin points out that horizontal vibration are often more detrimental to machine performance [228]. Although vibration isolation is an established field, important work continues on isolator development. Active isolators can be used to improve performance even further [98] . A large portion of the current research is the application of isolators to situations where they were not used before [325].

3.1.2.1.1   Passive Isolators

The passive isolator is a fixed design approach that must use novel design techniques to deal with more than one frequency of vibration. One way to accomplish this is to create a cost function of the desired response and utilize optimization techniques to find the "best" isolator [15]. The means of construction of a passive vibration isolator varies greatly. Typically, they are constructed of a flexible mount with inherent mass and stiffness. Modelling this continuous structure can be done in a variety of ways. The simplest is a lumped spring-mass-damper model. However, more complicated modelling approaches have also be used such as Dickens' "four pole parameter models" which have been used to model both the ground to machine response and the machine to ground response [56, 57]. Isolators can also be designed and modelled as nonlinear elements to achieve better precision [131, 272].

In order to choose the best isolator for a given situation, Shekar *et al.* proposed four different techniques; each have a different impact on machine performance [243].

1. Coulomb damper, spring, non-linear damper as isolator

2. Spring in parallel with spring in series with nonlinear damper

3. Spring and non-linear damper isolator with spring and nonlinear damper and mass absorber

4. Two stage isolator with intermediate mass

Another more advanced technique is to use magnetic levitation for vibration isolation [325]. A small superconductor is levitated allowing for vibration isolation through the levitation gap. This is well suited for space applications, since traditional isolator materials like rubber do not perform well at the low temperatures of space. Passive isolators have also been used to deal with earthquake vibrations and the resulting effects they have on structures [131]. In this application, damping is important, along with the acceleration of the top of the structure. Excessive damping can cause the structure to move with the ground resulting in high accelerations for the structure. Whereby low damping can cause too many

cycles of vibration. Jangid looked primarily into friction as the dissipative method, using rubber mounts or sliding steel plates [131]. Another avenue of isolator use is as a mechanical filter. Here the isolator is designed to cancel one specific frequency while allowing others to pass through. Li created a band-stop filter/isolator to cancel the sway in a crane payload [166].

3.1.2.1.2 Active Isolators

Active vibration isolation is the concept of inserting an actuator into the isolator framework. The inclusion of the active element along with some sort of sensor and feedback system allows the isolator to work more effectively [98]. The drawbacks of the active technique are an increase in complexity of the system, in the power consumption of the isolator, and in the increased risk of instability. Active isolator applications are typically in circumstances when a passive isolator would be too large, have to compensate for multiple modes, or have to deal with top broad of variations in system frequency. For example, Blackwood *et al.* studied the effect of a voice coil and piezoelectric isolator on a system with a flexibility in the base of a machine. Here the dynamics of the existing mount must be taken into account and cancelled [30]. Vehicles are another area where passive isolators would be too large. Thus, active techniques show strong promise, if their power consumption can be limited [135]. Another case where weight is an issue is ship-board cranes. By adding a novel passive/active isolator design between the forces of the a disturbed payload and the ship's crane structure, harmonic vibration was decreased [13].

To deal with multiple frequencies of vibration from several different spacecraft components while isolating precision sensors, another active isolation technique is used in [34]. Here a universal isolation component has been developed relying on a fluid filled structure and a piezoelectric actuator to cancel vibration. Often in vibration isolation, if the performance of a passive isolator is unacceptable, then an active element will be proposed. For example, Li plans to expand the capability of his crane mechanical filter by active elements [166]. The active elements themselves can be a variety of devices. Fluid valves can be used to regulate damping, piezoelectric actuators, electric motors, or other actuators can directly effect the isolator force either through force generation or electrical generation [189].

Another application of active vibration isolator technology is in the prevention of earthquake damage. Here actuators are used at the base of the building to help cancel the effects of the earthquake. The control law for these isolators is also an area of research with μ-synthesis being one possibility. In [196, 195] the μ-synthesis approach is tested experimentally, as well as theoretically. Typically isolators are designed for one degree of freedom vibration isolation. However, when actuators are used, the isolator can become a simple positioning system with disturbance rejection capabilities. From this point of view a positioning stage, like a Stewart platform, can be used as an active isolator [274]. In
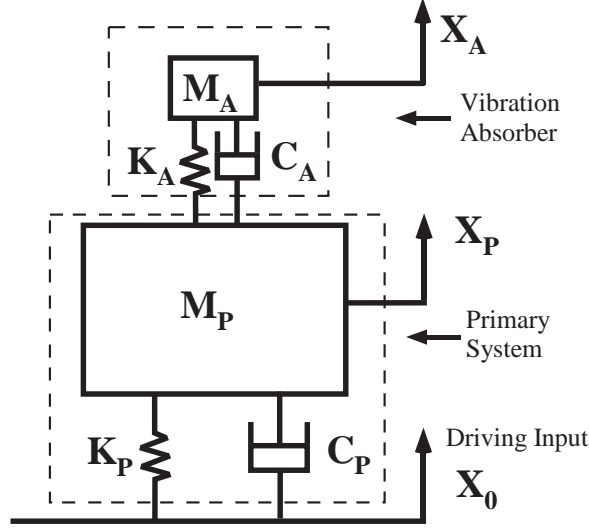
Figure 3.2: Vibration Absorber Schematic.

this approach the actuators static properties coupled with a feedback control law provide vibration isolation in six degrees of freedom.

3.1.2.2 Vibration Absorbers

Vibration of a system can sometimes be reduced by the inclusion of a secondary flexible system tuned to the proper frequency, as shown schematically in Figure 3.2. This secondary system is traditionally known as a dynamic vibration absorber or mass damper. Conventional vibration absorbers have been utilized on systems subject to sinusoidal and random vibrations and their function is described in most standard vibrations texts [111, 92, 50, 128, 266, 271, 290, 198]. Here the motion of the secondary mass creates a reaction force on the original system which can balance forces input to the base system. The technique of adding a vibration absorber has not been rigorously applied to robotics and manufacturing machinery where the desired motion trajectory is known. This application along with the combination of input shaping design with vibration absorber design will be discussed in Section 8.1.

The history of the vibration absorber starts with the absorber mass created by a volume of water in the hull of the HMS Inflexible in 1883 [122]. The secondary mass, the sloshing of the water in the hull, acted to cancel the forces from the waves, resulting in the stabilization of the ship's deck so that the guns were able to track targets more effectively. It was formally patented by Fraham in 1911 as "Device for Damping Vibration in Bodies" [90].

Vibration absorbers appear in a wide range of uses including, but not limited to, architecture: *smoke stacks, windmills, bridges, and cellular towers*; consumer goods: *refrigerators, seating in vehicles, dishwashers and even hair trimmers*; rotational equipment: *pumps, generators, and engines*; and even space structures [122, 113, 148, 276, 309, 147].

56

3.1.2.2.1 Linear Absorbers

Den Hartog did some of the first analytical work on the design of absorbers [111]. Hartog presented a procedure for selecting an absorber for the undamped and partially damped case for sinusoidal excitation at a given frequency. For the undamped case he showed that an absorber tuned to the same frequency as the input to the system would eliminate all steady-state vibration in the primary system. Oniszczuk attempted to find the same procedure for the damped-damped model with more complicated and less implementable results [205]. While Pennestri used Chebyshev's criteria to attempt to solve the damped-damped problem [217]. Another approach is to simply search possible absorbers for the one with the best peak amplitude response [220]. Still another approach is to consider the absorber synonymous with an active controller and use control theory to select the parameters [239].

The vibration absorber for random excitation has been studied but its solution is only analytically definable for non-real world applications, *i.e.* true white noise [194, 12]. Time optimal absorbers have also been designed, but the definition of "time optimal' does not necessarily coincide with the best absorber for a robotic or manufacturing application [19]. Initial condition responses have also been studied [9]. The approach to the optimal absorber solution has also varied widely. Autoparametric study, graph models, system stability, various control techniques, optimization schemes, as well as shear numerical testing have been attempted [118, 119, 42, 53, 312].

The controlled variable in the application of vibration absorbers also changes. Hartog and many others considered steady-state amplitude to be important for both random and sinusoidal excitations [111, 194]. Force transferal is another key issue in absorber design [118]. In time domain analysis, energy remaining in the system was used [12].

The robustness of linear absorbers to parameter variation in the system and/or in the absorber is another issue in their implementation. Chao and Shaw addressed this by studying the impact of small changes in rotational absorber parameters on the overall system response [40, 41]. Large changes in plant dynamics must also be overcome as is the case for anti-galloping absorbers for power lines which can be encumbered with snow and ice [169]

3.1.2.2.2 Non-Linear Absorbers

Since the time of Hartog, many other absorber solutions have been presented, and many have taken advantage of the computational aid provided by the computer. This is true for the non-linear case, where non-linearity in the absorber has been shown to increase absorber performance. The actual approach to the nonlinearity has taken the form of bumpers [102], fluid flow [318, 9], non-linear dampers, cubic springs [242, 207], cubic and linear spring or Duffing springs [193], even continuum string vibrations [286], as well as many others. Once these dynamics are known, a more complete model can be developed. Shaw used this

technique of a more precise nonlinear model to more clearly describe the dynamics of a absorber in order to provide for more precise tuning [242].

3.1.2.2.3 Adaptive Vibration Absorbers

By including an actuator in the absorber, vibration cancellation can be improved further. This same effect of improved performance with active elements was also seen for vibration isolators in Section 3.1.2.1.2. Adaptive absorbers are inherently more complicated to implement and to model but can enable a greater gain in performance [276, 1]. The primary method of implementation of an active absorber is to drive the system directly with the actuator under some sort of control law. Velocity feedback was used in [78]. Whereas position-based control with a delay was used in [116] on a rotational absorber. Magee *et al* used the strain in the main system to create a control law to drive the active absorber [178].

Semi-active absorbers are also an important area, since the active component can be backed up by some passive elements. In the event of a failure of the actuator, the passive components will still offer some vibration suppression [276]. The active component can also be used to magnify the effects of the absorber. This is the case for the wind and earthquake vibration suppression of high-rise buildings in [309, 278, 282]. Here a pseudo-pendulum absorber's length is altered by active elements. Similarly, the frequency of a rotating pendulum absorber can be changed by altering the rate of rotation to cancel different frequencies occurring different operating conditions as in [173]. A change in the stiffness can also be used to modify the frequencies of the absorber as in [308]. The active component can also be used to alter the damping properties of the absorber, instead of changing the frequency or forcing the system directly. This is usually done with hydraulic components like the ones fitted to a cable stayed bridge to cancel seismic waves [5].

Since the models of active absorbers are more complicated, the methods used to determine which absorber to utilize are more detailed. Abe and Igusa, for example, used a Laplace technique in [1]. Anytime actuators are used, saturation can be an issue; in the case of active absorbers saturation can limit the frequencies that the absorber can handle and the magnitudes at each frequency [207]. Another more important problem is stability. Filipovic and Olgac found that their velocity feedback based active absorber required negative gains to maintain the stability of the system [78].

3.1.2.2.4 Vibration Absorbers for Machine Tools

Vibration absorbers have been specifically designed for machine tool applications, typically to deal with problems of chatter which is discussed in Section 2.1.1.2. Absorber principles are even covered in the general machine tool design literature [266, 315, 229]. Typically dampers are applied directly to the cutting tool. Ema and Marui have created these type

of mass dampers through the use of sleeves, either for drill bits [68] or boring bars [69]. Boring bar dampers were also studied by Hahn, who used a second-order model of the bar to aid in the design of the absorber [109]. Marui *et al.* used plates as boring bar dampers to improve the damping ratio from 0.01 to 0.025 [182].

Absorbers can also be applied directly to the structure of a machine tool to reduce chatter. A lathe's part surface finish roughness was improved in one case from 22 to 13 μm by the addition of a properly selected absorber [146]. This absorber had to be adjustable by spring pre-load in order to compensate for slide position based changes in the dynamics. More general techniques have also been developed. Shin presented a experimental technique to reduce the impact of random excitation on machine tools [244]. Machine tools have also been used with active absorbers. Tzou designed a piezoelectrically driven actuator to act as an absorber or an exciter for a generic machine tool [298]. A full mathematical model of the absorber/exciter is given to aid in design of the control algorithm for the actuator.

3.2 Control Techniques

Vibration is often reduced using feedback control techniques. These techniques add additional dynamics to the system in the form of an electronic controller. An understanding of control possibilities is necessary to obtain an adequate system performance. These controllers are classified here into three categories: classical, adaptive, and other. Specific examples relevant to either machine tool control or combining control with mechanical design and input shaping will be detailed in this section. These techniques are important since they are direct competitors with command shaping in the control of vibration. A fully understanding of the alternatives solutions is necessary to select an approach for a particular design.

3.2.1 Classical Control

Classical control consist of a response sent back through a sensor and a control law made up of proportional, derivative, and/or integral gains (PID). This approach is the most common feedback control for all machines and machine tools in particular. This is due to its ease of application and predictable tuning for all types of situations as detailed in all introductory control texts [92, 198]. For example, the Puma robot in [77] utilizes PID control to help combat disturbance, specifically impacts that would occur in a cluttered environment, and Alli *et al.* uses it to deal with vibration of the wave equation [7] in combination with input shaping.

The simple classical control scheme can be advanced with adaptive or scheduled gains for use on machine tools. In [37], an adaptive PID controller is used on a lathe. Gain scheduling was used by Toutant *et al.* on a lathe to keep cutting force constant with change in material [292]. Toutant also controlled the lathe cutting force using classical

control techniques. The classical techniques can be augmented with feedforward control architecture as in [188], where a feedforward friction compensator and PD controller were used on a feed drive system, and in [155] where classical control was used with a Zero Phase Error Tracking feedforward controller for precise stage positioning. More common than these combination techniques is for machine tool drives to be controlled with only a classical controller structure. In Varanasi *et al.* investigation of the control of lead screws, they discovered that actuator collocation, system damping, and whether the screw is minimum-phase are all important when using feedback control on a lead screw [301].

The PID control technique is commonly used in conjunction with other vibration compensation techniques. It has been used in concurrent design with a command generator in [138, 139]; as well as in conjunction with mechanical design as detailed in 2.3.1. Specifically, PID control has been combined with robotic arm design [212] and with mass balancing [163, 328]. Mass balancing can be done to simplify the feedback control technique.

3.2.2   Adaptive Control

Adaptive control is often used when the parameters of the system change drastically over its operation. With respect to machine tools, this could be from the change in forces from different cutting tools or cutting conditions, or from modal variations from different configurations of the axes. For example, a motion to one end of the workspace will lengthen the vibratory element of a machine tool. Compensation for this parameter change can be accomplished with many different techniques. When the controller is changed discreetly then it is termed gain scheduling, whereas continual variation like the PID controller in [37] for turning is usually just called adaptive control.

3.2.2.1   Gain Scheduling

Gain scheduling involves the creation of a list of controller parameters and selecting the parameters from the list based on the conditions of the machine. These parameters are often the gains of the controller but could be the controller architecture as well. The changes are often workspace induced, whereby one area of the workspace uses a different set of gains from another. Another possibility is to change the controller depending on the type of motion desired In [99], small motions used higher gains to compensate for a dead zone in the actuator. Likewise, [292] used different gains for different actuator velocities or feed-rates for a lathe. Also, changes in the forcing on the machine often necessitate the change in controller. In [326], the forces from different types of cuts were used to determine the proportional gain of the drives.

3.2.3 Other Control

There are many controller techniques employed on machine tools. The following is a brief incomplete survey of these types of controllers and where and how they are implemented. An understanding of these allows one to see the range of possibilities when designing a complete machine tool.

3.2.3.1 Observers

Observers are a response prediction tool integrated inside the control architecture. By predicting the response of the system, the observer allows the control force to be adjusted for the responses of the system that cannot be fully sensed. Okazaki implemented such an observer for the tool post or the cutter mount of a precision lathe to reduce the vibration induced from the interaction with the workpiece whose motion was not measured [200]. Likewise, a Kalman filter, a common and powerful observer, was used to model an unmeasured effect on a CNC machine and was implemented to deal with frictional forces [71].

3.2.3.2 Feedforward Control

Feedforward controllers inject control effort based on a model directly into the plant avoiding the sensor feedback. This is often used to compensate for the dynamics of the plant by using an inverse of the plant dynamics for the feedforward controller. The design of the controller is difficult because often the plants model is not exact, the dynamics of the system cannot be inverted, or a phase delay is introduced into the response.

The Zero Phase Error Tracking Controller, ZPETC, is a type of Feed Forward controller for use in digital control which only attempts to cancel the invertible poles of the plant, as well as adjusting for the phase shift in the response of a digitally controlled system [289]. It was applied to a milling machine in [295] showing improvement in the tracking response of the mill. Feedforward techniques can be used to cancel nonlinear phenomenon in the plant as well. Gear backlash can be dealt with [188] or coulomb friction [155].

3.2.3.3 Other Controllers

A couple other relevant controllers are worth noting. Pan devised a fuzzy logic controller to deal with the non-collocated nature of the cutting tip of a lathe [210]. While Zhu *et al.* used sliding-mode control to deal with similar problems of an attached piezoelectric cutter on a CNC lathe [329]. Haber even compared fuzzy logic, an inverting controller, and neural networks in [107].

3.3 Command Methods

The commands to a system play a large role in the determination of the response. The first attempt is usually to use the desired output as the reference command input. However, this can lead to vibration, and therefore, it is often not the best choice. Another problem arises from the selection of what the desired response should be. The ideal response is often known, such as an instantaneous change in position or velocity. These motions cannot usually occur, and therefore, more attainable profiles must be used instead.

3.3.1 Overview of Input Shaping

Input Shaping is a command generation technique that attempts to impart zero energy into a system at the frequencies at which it will vibrate. It originated with Poisicast control in the 1950's, but did not become widely usable until the advent of the digital computer [270]. In order to ensure zero energy at the vibration frequencies, the inputs given to the system must be modified, thus the term Input Shaping. Once a correct command for the system is found, the result will be a system that has no energy at frequencies for which it will vibrate, and thus no vibration. However, this approach for input shaping has not been fully expanded to continuum system. Also, the application of input shaping to nonlinear systems is still an open area of research.

Consider a second-order system given by the transfer function:

$$G(s) = \frac{\omega_n^2}{s^2 + 2\zeta\omega_n + \omega_n^2} \tag{3.1}$$

This is a common real world system, and it is also the base of the input shaping formulation presented here. The input shaping technique attempts to find an impulsive filter which can be used to modify any input so that vibration is reduced. Such a filter can be easily implemented on real machines. To determine such a filter the techniques first laid out in Singer's dissertation will be used [246]. This approach involves considering the impulse response of the system as the base of all derivation.

The time response of this second-order system to a single impulse input is:

$$y(t) = \left[A_0 \frac{\omega_n}{\sqrt{1-\zeta^2}} e^{-\zeta\omega_n(t-t_0)} \right] \sin \omega_n \sqrt{1-\zeta^2}(t-t_0) \tag{3.2}$$

where A_0 is the magnitude of the impulse, ω_n is the system's natural frequency, t_0 is the time the impulse occurs, and ζ is the system's damping ratio. If the damped natural frequency is substituted:

$$\omega_d = \omega_n\sqrt{1-\zeta^2} \tag{3.3}$$

The expression becomes:

$$y(t) = \left[A_0 \frac{\omega_d}{\sqrt{1-\zeta^2}} e^{-\zeta\omega_n(t-t_0)} \right] \sin \omega_d(t-t_0) \tag{3.4}$$

Assuming the system is linear and time invariant, superposition can be used to find the response to a series of impulse. For time greater than the time of the final impulse, the response to an impulse series is:

$$y_\Sigma = \sum_{i=1}^{n} \left[A_i \frac{\omega_n}{\sqrt{1-\zeta^2}} e^{-\zeta\omega_n(t-t_i)} \right] \sin\left(\omega_d(t-t_i)\right) \tag{3.5}$$

This equation can then be used to find a series of impulse magnitudes and times that yield an acceptable level of vibration. In order to find such a series of impulses, an equation for the amplitude of the vibration must be developed. If the following trigonometric identity is used to simplify (3.5):

$$B_1 \sin \alpha t + \phi_1 + B_2 \sin \alpha t + \phi_2 = A_\Sigma \sin \alpha t + \psi \tag{3.6}$$

where the amplitude A_Σ is:

$$A_\Sigma = \sqrt{\left(\sum_{j=1}^{N} B_j \cos \phi_j\right)^2 + \left(\sum_{j=1}^{N} B_j \sin \phi_j\right)^2} \tag{3.7}$$

and when this is then compared to (3.5), the B_i terms become:

$$B_i = \frac{A_i \omega_n}{\sqrt{1-\zeta^2}} e^{-\zeta\omega_n(t-ti)} \tag{3.8}$$

The amplitude of the vibration at any given time can then be found.

If the time of the last impulse is the concerned time, which is a logical time to desire the vibration to be minimized, then the vibration magnitude at the time of the last impulse is:

$$A_\Sigma = \frac{\omega_d}{\sqrt{1-\zeta^2}} e^{-\zeta\omega_n t_n} \sqrt{(C(\omega_d,\zeta))^2 + (S(\omega_d,\zeta))^2} \tag{3.9}$$

where:

$$C(\omega_d,\zeta) = \sum_{i=1}^{n} A_i e^{\zeta\omega_n t_i} \cos \omega_n \sqrt{1-\zeta^2} t_i \tag{3.10}$$

$$S(\omega_d,\zeta) = \sum_{i=1}^{n} A_i e^{\zeta\omega_n t_i} \sin \omega_n \sqrt{1-\zeta^2} t_i \tag{3.11}$$

This result is still complicated. However, it can be simplified by scaling it by the response to a single impulse. The amplitude of such an impulse is:

$$A_\uparrow = \frac{\omega_d}{\sqrt{1-\zeta^2}} \tag{3.12}$$

The division of (3.9) by (3.12) yields a normalized value, the percentage residual vibration:

$$V(\omega_d,\zeta) = e^{-\zeta\omega_n t_n} \sqrt{(C(\omega_d,\zeta))^2 + (S(\omega_d,\zeta))^2} \tag{3.13}$$

63
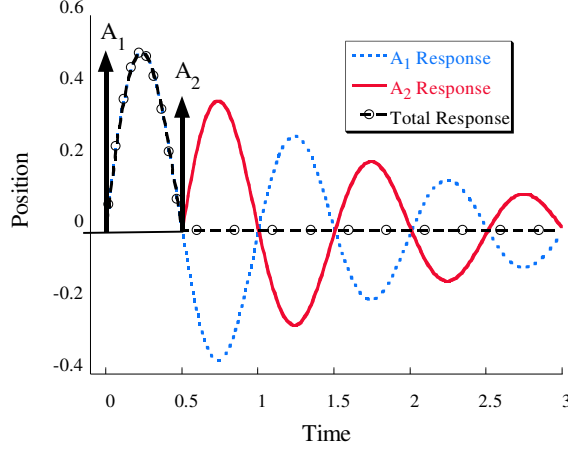
Figure 3.3: Impulse Response Cancellation.

where t_n is the time of the last impulse. If this equation is set equal to zero for a particular set of system parameters, then the damping and frequency, the result will be zero vibration from the impulse sequence. This derivation of (3.13) can also be done graphically using vectors as is discussed in [262].

In order to see more clearly the result of this procedure consider a second-order system with an impulse response like the dotted curve in Figure 3.3. If this response is added to a second appropriately selected response (the solid curve), then the resultant response is the dashed line with circles, which has zero vibration after the second impulse. Another requirement on the input shaper is that it satisfies the equation:

$$\sum_{i=1}^{n} A_i = 1 \qquad (3.14)$$

Once the input shaper is defined, it is implemented as a filter in to the input of the system. This filtering process can be mathematically described by convolution. (3.14) is needed to ensure that a convolution with an input command yields the same final set point as the original. This convolution yields a new reference command for the system as defined by:

$$Shaper * Input = Input_{new} \qquad (3.15)$$

and graphically depicted in Figure 3.4. This convolution can be thought of as a multiplication of functions in the Laplace domain. When one of those functions is a train of impulses, the multiplication is fairly easy to perform and for a step input yields a stair-case command as was demonstrated in Figure 3.4.

Due to the periodic nature of (3.13) another constraint must be placed on the input shaper, a minimal time constraint:

$$min(t_n) \qquad (3.16)$$

64
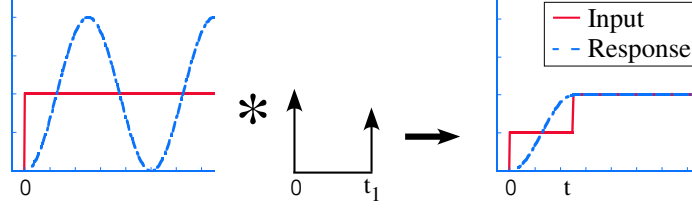
Figure 3.4: The Convolution Process.

where t_n is the time of the last impulse. Other constraints can also be added in order to achieve different qualities for the input shaper. A common one is that all the impulses must be positive. Other constraints are directly related to the performance of the input shaper itself. Several common performance constraints will be discussed in the next section. Kozak *et al.* have researched the impact of these common, as well as some more advanced performance contraints/measures on shaper design [150].

3.3.1.1 Zero Vibration Shapers (ZV)

Zero Vibration, ZV, Input Shaper is the simplest input shaper. The only constraints are minimal time, (3.16), and zero vibration at the modelling frequency, (3.13). If these constraints are satisfied, the positive ZV shaper has the form of impulse amplitudes A_i and times t_i [270, 248]:

$$\begin{bmatrix} A_j \\ t_j \end{bmatrix} = \begin{bmatrix} \frac{1}{1+K} & \frac{K}{1+K} \\ 0 & 0.5T \end{bmatrix} \tag{3.17}$$

where:

$$K = e^{\dfrac{-\zeta \omega_n}{\sqrt{1-\zeta^2}}} \tag{3.18}$$

$$T_d = \frac{2\pi}{\omega_n \sqrt{1-\zeta^2}} \tag{3.19}$$

Notice that the duration of the shaper is one half the damped period of the oscillation. This leads to one of the tradeoffs inherent to input shaping; in order to eliminate the vibration of the move itself, the rise time is increased. The system takes longer to initially reach its desired goal, but if the vibration is eliminated, then the more important settling time is reduced. Also in (3.19), notice that the effect of damping on the shaper magnitude is an increases in the first impulse. This is important, because the larger in magnitude the first impulse, the more aggressive the shaper.

A major problem with the ZV shaper is the robustness to parameter change. If the original system changes or was incorrectly modelled, then the vibration amplitude will not be zero. In order to understand this relationship, a sensitivity curve can be created as seen in Figure 3.5. The frequency modelling error or normalized frequency is:
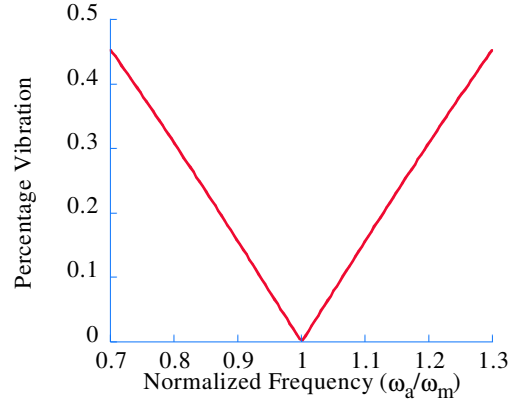
Figure 3.5: ZV Shaper Sensitivity.
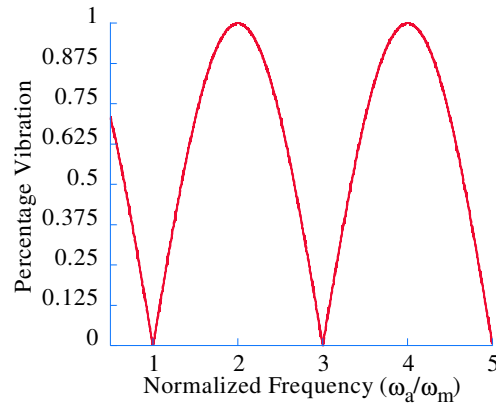
Figure 3.6: ZV Shaper Sensitivity for Large Modelling Errors.

$$\frac{\omega_{actual}}{\omega_{model}} = \frac{\omega_a}{\omega_m} \tag{3.20}$$

which represents the difference between the actual system's frequency and the frequency used to design the shaper. The vertical axis represents percentage residual vibration, which is a ratio of residual vibration between the unshaped and shaped responses. Notice that for the ZV shaper the vibration increases quickly as the frequency changes. However, if the sensitivity curve was expanded over a large frequency range as in Figure 3.6, two facts become apparent. First, the percentage residual vibration never exceeds one hundred percent, meaning a ZV shaper will never increase vibration. Second, the sensitivity curve reaches zero again at every odd multiple of the primary frequency. Although, at these higher frequencies the system will oscillate a number of times (equal to the integer multiple minus one) before the shaper cancels all the vibration. The ZV shaper is useful in situations
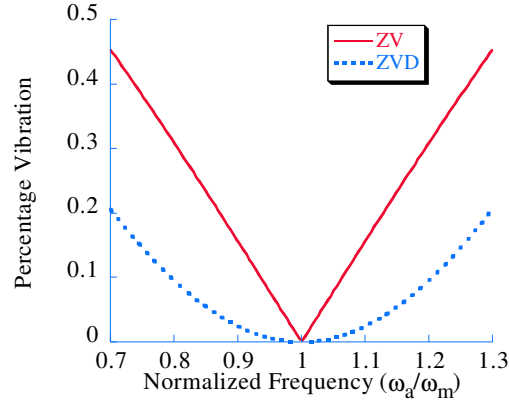
Figure 3.7: ZVD Shaper Sensitivity.

where the parameters of the system are known with a high level of accuracy. Also, if large changes in the vibratory frequency occur, then the application of input shaping will never increase vibration beyond the level before shaping.

3.3.1.2   Zero Vibration and Derivative Shapers (ZVD)

A Zero Vibration and Derivative, ZVD, Input Shaper is a command generation scheme designed to make the input-shaping process more robust to modelling error [248]. If another constraint is added to the formulation of the shaper by setting the derivative of the vibration with respect to frequency equal to zero:

$$\frac{d}{d\omega_n} \left[e^{-\zeta \omega_n t} \sqrt{(C(\omega_n, \zeta))^2 + (S(\omega_n, \zeta))^2} \right] = 0 \tag{3.21}$$

the ZVD shaper results. Its sensitivity curve is shown in Figure 3.7. Notice that the derivative of the curve is zero at $\frac{\omega_a}{\omega_m} = 1$. Physically, the result of this is that if the system parameters change or the model was incorrect, then the vibration will still be close to zero. The times and magnitudes for this shaper are:

$$\begin{bmatrix} A_j \\ t_j \end{bmatrix} = \begin{bmatrix} \frac{1}{1+2K+K^2} & \frac{2K}{1+2K+K^2} & \frac{K^2}{1+2K+K^2} \\ 0 & 0.5T & T \end{bmatrix} \tag{3.22}$$

where K and T are defined by (3.21 and 3.19).

All things have a cost, and the cost of this robustness is a longer shaper duration. For the ZVD shaper, the shaper duration/rise time is the damped period of vibration. Also, the ZVD shaper has three impulses instead of the two in the ZV shaper. Another way to formulate the ZVD shaper is through the use of two ZV shapers. If two identical ZV shapers are convolved together, the result is a ZVD shaper.

67
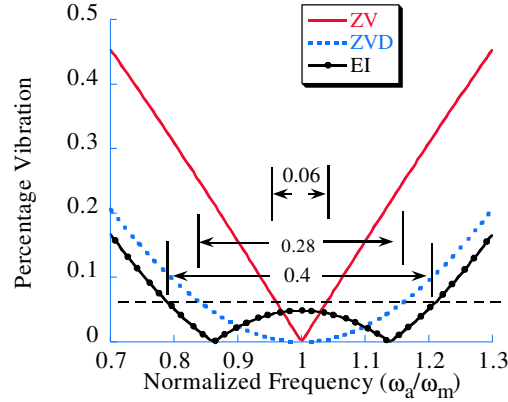
Figure 3.8: EI Shaper Sensitivity.

The application of ZVD shapers is for systems where rise time is still important, but either the system will change with time, or the model is not accurate. If the model's inaccuracy is too extreme for a ZVD shaper then other shaping techniques are available, such as those described in the subsequent sections. The ZVD shaper can also be derived for on-off commands with similar vibration suppression and sensitivity results [260].

3.3.1.3 Extra Insensitive Shapers (EI)

Extra Insensitive, Extra Insensitive Shapers, EI are another shaping technique which can broaden the valley in the sensitivity curve [254]. If the zero vibration constraint at the modelling frequency is relaxed, then it is possible to make even more frequencies fall below some tolerable level of vibration. In order to do this, the residual-vibration constraint is set to a some tolerable level V_{tol}. The derivative of vibration at this value is kept at zero and the resulting shaper for undamped systems has the form:

$$
\begin{bmatrix} A_j \\ t_j \end{bmatrix} = \begin{bmatrix} \frac{1+V_{tol}}{4} & \frac{1-V_{tol}}{2} & \frac{1+V_{tol}}{4} \\ 0 & 0.5T & T \end{bmatrix}
\tag{3.23}
$$

The sensitivity for the EI shaper is shown in Figure 3.8. The range of frequencies for which the vibration is below some tolerable level, for example five percent, is 0.4 for this case. This is the shaper's insensitivity. Notice that the range of frequencies for which vibration is below the five percent tolerable level is larger than either the ZV or ZVD shapers which have 0.06 and 0.28 insensitivity respectively.

The duration of the EI shaper is the same as that of the ZVD shaper, one damped cycle of vibration. Thus, the application of EI shapers is for systems where some small vibration is allowable, and the systems parameters are expected to change considerably.
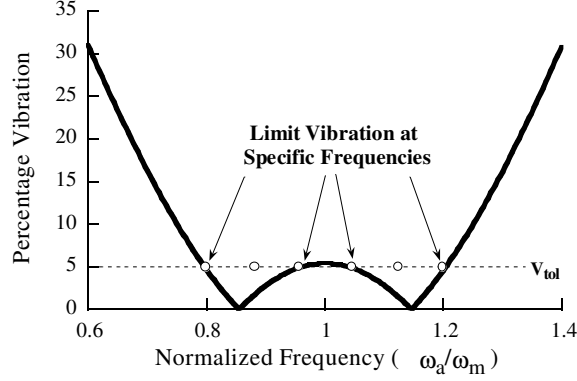
Figure 3.9: SI Shaper Sensitivity.

3.3.1.4 Specified Insensitivity Shapers (SI)

Another robust input shaper is the Specified Insensitivity, SI, Shaper. It does just what it name says, it allows a user to decide where the vibration will be limited [263, 258]. In order to do this a different set of constraints are used. Specific points on the sensitivity curve are used to limit vibration below some tolerable level. This allows the insensitivity to be specified. Figure 3.9 shows how this would be done.

The constraints limit vibration only at the selected frequencies; therefore, the vibration could go above the tolerable level in between them. If the points are chosen close enough together the effect of this phenomenon will be minimal. But if the vibration level is extremely important, the tolerable level could be reduced slightly to counteract the effect. As the desired insensitivity increases so does the shaper duration. This is another tradeoff between rise time and robustness. SI shapers are most useful when there is some information on the expected model variation. The usefulness of the SI shaper was surveyed along with other shapers in Singh and Singhose's tutorial [252].

3.3.1.5 Multi-Mode Input Shapers

In systems with more than one mode of vibration, two schemes can be used to generate commands for the system. The first is by simply convolving together multiple input shapers designed for each specific mode. The result of this process is a longer input shaper, which can deal with each mode specifically [259, 123].

Another method is to design a shaper from the beginning with vibration reduction at both modes. This approach for closely-spaced frequencies can take the form of using the robustness of one shaper to modelling errors so that it engulfs the multiple frequencies. For more broadly spaced frequencies, specific shapers can be designed to meet this goal such as Grosser's High Mode Limiting Shaper [104]. Baumgart and Pao also investigated the design of shapers for multiple modes. Their solution uses an s-plane approach and allowed

multiple shapers to "cooperate" together to eliminate the need to simply convolve existing shapers together [20, 21]. The result is a faster multi-mode shaper that is more complex than the independent design method [211]. Singh found a similar result in his work using time response analysis [251]. He also showed that a two impulse shaper could be used to cancel multiple modes. However, the timing of the impulses can become restrictively long.

3.3.1.6 Negative Input Shapers

Up to this point the input shapers discussed have contained only positive impulses. With positive impulses only, the minimum shaper time is half the period of vibration or the ZV shaper. It is possible to shorten this time by allowing the impulses to have negative magnitudes. This allows the solution of the residual vibration equation to have a total time less than half a period [257].

One common input shaper with negative impulses is the Unity Magnitude shaper. This shaper forces all of the impulses to be of magnitude 1. The constraint equation specifically is:

$$A_i = (-1)^{i+1} \qquad i = 1, ..., n \tag{3.24}$$

This type of shaper is well suited to operation where the actuator is either full on in one direction, full on in the opposite direction, or off. On-Off control is often used to describe machines of this nature. Space applications such as satellites operate under this principle since they have gas thrusters that are either open or closed. If just this constraint is used and the solution with the shortest time span is found, then the solution is called a Unity Magnitude Zero Vibration, UMZV, Input Shaper. For the undamped case it is described by:

$$\begin{bmatrix} A_j \\ t_j \end{bmatrix} = \begin{bmatrix} 1 & -1 & 1 \\ 0 & \frac{T}{6} & \frac{T}{3} \end{bmatrix} \tag{3.25}$$

which is shorter than the ZV shaper by one sixth of a period. The sensitivity of a UMZV shaper can be seen in Figure 3.10. Note that the slope of the UMZV shaper sensitivity is steeper than all the previous shapers. The tradeoff is once again that robustness is inversely related to shaper duration. Another drawback of the UMZV shaper is apparent in Figure 3.11. The UMZV shaper, if designed incorrectly, can actually increase vibration up to three times the original magnitude. Therefore, UMZV shapers are best suited for systems that are well modelled and require a short duration shaper.

Negative shapers are not limited in impulse magnitude; they can have impulses of any magnitude positive or negative. However, it is always important to limit the magnitude of both the positive and negative impulses to prevent actuator saturation. The downside of using negative input shapers is that they place a higher stress on the system and thus can induce high mode vibrations which previously did not appear in the response.

70
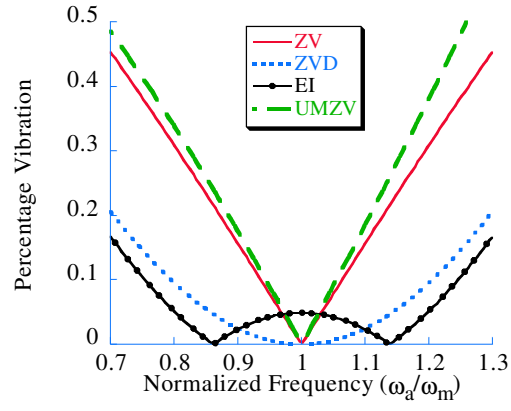
Figure 3.10: UMZV Shaper Sensitivity.
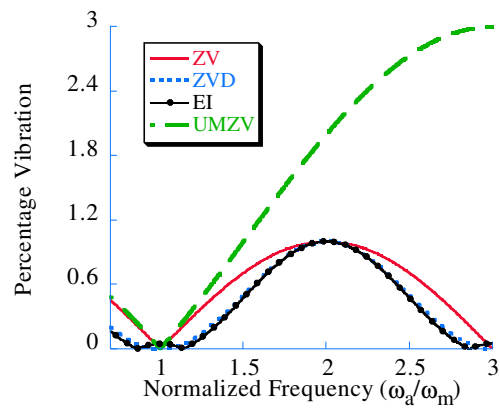
Figure 3.11: UMZV Shaper Sensitivity with Large Modelling Errors.

3.3.1.7 Alternative Derivation of Input Shapers

Input shapers were traditionally found using the previous impulse response techniques. However, other control techniques can be employed in the derivation of shaper parameters. Bhat *et al.* utilized both s-plane analysis, as well as, a linear quadratic regulator based method to determine parameters with time domain analysis [27, 26]. Pao has also used s-plane design for multi-mode shapers [211]. Similar to the s-plane techniques, Park designed digital shapers using the z-plane in [213]. Pole-zero cancellation was used with the digital derivation of the response for shaper design. Tuttle and Seering performed a similar discrete design, but instead of pole-zero cancellation, his work focussed on creating a digital optimization to find shapers faster. By limiting shaper choices digitally, the optimization becomes linear [296]

3.3.1.8 Applications of Input Shaping

Input shaping has been used on a variety of systems. It has often been combined in application or design with feedback control as in [60, 297], and has even been designed concurrently with Proportional and Derivative control to yield improved performance in [138, 139]. Input shaping has also been implemented inside the feedback loop for a system. When this is done, a time delay is introduced into the error signal, which in turn causes stability problems for the system [176, 33].

Coordinate measuring machines (CMM's) are a specific class of machines where input shaping has been applied. Input shaping has been applied directly to motions on existing machines to yield higher accuracy [256, 241, 133]. A CMM's accuracy can be detrimentally effected by friction. Lawrence *et. al.* looked at how input shaping could be specifically tailored to deal with coulomb friction [154].

Another positioning system improved with input shaping is serial manipulators. Drapeau and Wang looked into changing the commands sent to a five-bar linkage. The specific result was an improvement with shaping [60]. Another area of serial manipulators where input shapers have proven helpful is in the realm of long reach manipulators. Magee *et al.* researched this area extensively and successfully applied input shaping on RALF, Robotic Arm Large and Flexible, at Georgia Tech [176, 177, 178]. In another example on RALF, experiments were performed by Grosser *et al.* for the reduction of higher modes and perceived lag [104, 103]. Grosser showed higher modes of vibration can be eliminated with the same shaper as the lower modes, and that the problems associated with an increased rise time, a perceived lag by operator, can be reduced by creative shaping schemes. This author aided in the experimentation and data collection for Grosser's experiments.

Cranes are one area in which input shaping has shown vast performance improvement possibilities [74, 91]. Singer *et al.* discuss the implementation issues of a crane in a hostile environment, the Savannah River Nuclear Facility [247]. In order to test the usability of

Input Shapers by an operator in a cluttered work environment, a path-planning algorithm was developed to mimic an operator's behavior [91]. Singhose investigated the result of changing frequencies due to hoist length in [261]. A mechanical filter approach to vibration suppression similar to input shaping was employed on ship cranes in [166]. Another mechanical filter was tested on a crane to compensate for disturbances without feedback in [13].

Continuum systems are another area where shaping has been applied. Bhat *et al.* investigated shaping on a beam modelled as a second-order oscillator in [26]. While Singh and Alli derived the delayed commands for a generic wave equation [250]. The equations addressed govern string and simple longitudinal and torsional systems. The main difference between this derivation and the work in this dissertation primarily in Chapter 7 is that Singh considered only the first mode of vibration, and the result was directed at time-optimality instead of purely vibration suppression. Also no mention of specific shapers except the optimal bang-off-bang trajectories was made.

Input shapers have been applied to micro-turning machines by Ozisik *et al.* in [208]. A shaper was used on the positioning system of a micro-turning process. However, the lack of multi-mode shaping in their research hindered the application.

3.3.1.9   Trajectory Following with Input Shaping

Most input shaping design has centered around the elimination of vibration after a move. However, input shapers have been designed specifically to address trajectory following issues besides residual vibration. For example, Grosser developed the Reduce Perceived Lag shaper which attempts to track faster trajectories at the expense of temporarily more residual vibration [104, 103]. A shaper is design to move 95 % of the move quickly with some residual vibration and then that vibration is cancelled with the remain 5% move. Singhose specifically studied input shaping's effect on tracking of trajectory components [253, 255]. The result was that input shaping significantly improved trajectory following for the moves attempted. The limits of this work lie in the speed of the trajectories tracked. This issue is address specifically in Chapters 5 and 6.

Another area of trajectory tracking with input shaping is in the combination of input shaping and s-curves. Eloundou and Singhose compared the use of s-curves to input shapers and even derived s-curves as a form of shaper [65, 66]. While Meckl *et al.* also used s-curve and shaping rules to design commands similar to the ones used in this research for the micro-mill [186]. But Meckl only used acceleration residuals as a performance measure and the work did not yield zero vibration in cases with damping in the system.

3.3.2 Trajectory Tracking

Trajectory tracking is an important area of study because machines must not only move quickly without vibration; they must also follow precise motions. While input shaping has been utilized for trajectory tracking, the application of input shaping to track swift trajectories is limited.

3.3.2.1 Command Creation

The simplest forms of trajectory tracking are to select an attainable command for the system to follow. This was done explicitly in [291], where Tounsi *et al.* gave a system a variety of inputs to determine what were attainable outputs, and then relied on those to define a command scheme.

Utilizing command limits is a way to simply determine acceptable commands. If an input acceleration is limited to the acceleration attainable by the machine, then the response will often be close to the input. A primary example of this is the s-curves traditionally used to drive machine tools [8]. For example, the jerk limit aspect was discussed with CNC machines in [70]. Meckl *et al.* discussed the use of command limits for residual vibration reduction [186]. Eloundou and Singhose even compared the s-curve position input technique (which is essentially an acceleration limit) with input shaping in [65, 66].

Another way to design attainable motion paths is by using polynomials. This technique is often used on CNC machines where a series of target locations must be reached while maintaining some velocity or acceleration constraints [70]. This is easily done with polynomial fits often called splines. The same approach as with polynomial command design can be done with trigonometric function, where the function are limited by the real system's response capabilities [245].

A more intuitive command design scheme was developed by Boe in [31]. This technique slows a trajectory if complex motions are needed and then speeds it up for simple motions. Automating this process can save overall motion time and improve the overall tracking. Niu and Tomizuka also used this principle of changed speeds but combined it with an anti-windup controller [197]. On the other end of the spectrum, Dewey *et al.* developed an optimization technique relying on a quadratic cost function to alter an existing trajectory to maximize performance. The end result was that the optimization smoothed the trajectory when necessary [55].

3.3.2.2 Tracking Controllers

Specific use controllers are often needed to track difficult trajectories on a system. These controllers typically need accurate plant models and are burdened with the problem that the faster the move the more likely the system is to behave in a nonlinear manner [51]. Model based controllers can allow a system to track trajectories better than feedback controllers.

Rastegar *et al.* developed the Trajectory Pattern Method which utilizes a command selection algorithm and a plant inverse to reduce tracking error [223, 224, 73]. Other plant inversion technique also exist. Kim and Kim used one on a piezo-cutter for a micro lathe in [145] to combat surface waviness, while Ozisik and Keltie used an inversion technique and a complicated plant model in a purely open loop micro-turning system [208]. Tomizuka's previously mentioned Zero Phase Error Tracking Controller is a plant inversion controller which provides for excellent tracking in certain circumstances. It works by inverting only the invertible parts of a plant and then using phase correction to cancel the other non-invertible components, thus allowing any continuous input to the system [289, 295].

Tracking controller design can also be combined with the command design. Immure and Kaufman presented a piecewise procedure where first the feed-velocities of a machine are optimized based on cutting parameters, then a second optimization is performed to select the best controller gains for the previous feed-velocities [127]. Beldiman *et al.* approached the trajectory control of elevators in a similar manner, by selecting trajectory parameters and then optimizing controllers [22].

All of these aforementioned corrective techniques thoroughly improve performance. This dissertation will seek to expand these techniques specifically input shaping. The corrective method of input shaping will be used to improve the performance of micro-milling machines, as well as generic trajectory tracking problems. Eventually, the input shaping procedure will loose its corrective nomenclature, when it becomes a design as opposed to corrective consideration.

3.4   Synopsis

The thorough study of existing correctional methods for machines, is important to the overall goal of combining mechanical and command design for two reasons. First, understanding other electronic controllers and mechanical system augmentations is necessary as a comparative tool. The decision in the design process to use a concurrent mechanical and command design strategy must be made weighing the options of other approaches including simple input shaping application. The other main justification is in the direct use of these correctional methods in the combined design process. Mechanical augmentation elements can be selected simultaneously with command generators. Most importantly, command generation must be fully understood before it can be advanced or utilized within a design algorithm.

CHAPTER IV

IMPROVING PERFORMANCE OF MICRO-MILLS

The primary motivator of this research is the improved performance of micro-mills. The techniques presented in the previous chapter for the control of vibrations had not been rigourously explored for micro-milling. The vibrations that occur in micro-mills limit the speeds of the mills. Since high speed can cause large levels of vibration, micro-mills are often moved slowly. Micro-milling's uses in industry have been limited due to the slow process speed necessary to eliminate vibration. Typically micro-mills cannot remove much material, since the cutting tool itself is fragile. However, feed-velocity can be increased if the material removed per cutting tooth is held constant. This is accomplished by increasing the rotation rate of the cutting tool itself.

Vibration problems can occur with this increased feed-velocity, thereby limiting the productivity of micro-milling technology. the primary goal of this research is improve micro-milling performance specifically to overcome the vibration problems. The first step is to improve the performance of existing micro-milling machines. To this end, input shaping will be used for vibration compensation. However, before input shaping can be employed the dynamics of micro-mills need to be understood. Once the dynamics were understood, a input shaping scheme for the improvement of current micro-mills was developed. As part of this process several elements necessary to the combination of mechanical and command design will be seen. Specifically, the impact of cutting forces on the motion of the tool and the design issues inherent in micro-milling will be shown.

4.1 ETSII Mill

To research the behavior of micro-mills in general beyond the work of Section 2.2.1, specific experiments were carried out on the Micro-Mill seen in Figure 4.1. This micro-mill is located at the Escuela Tcnica Superior de Ingenieros Industriales (ETSII) in Madrid, Spain. This mill was design and constructed at the ETSII by Juan de Juanes Marquez and Jesus Perez who collaborate on the experiments [79, 81, 181].

The mill diagramed, in Figure 4.2, is of a standard 2.5 degree of freedom mill design and consists of a spindle, three positioning stages, a motion controller, a dynamometer, and the workpiece. The spindle turns the cutting tool while the stages move both the tool and the workpiece into the proper configuration. The motion controller's purpose is to position the stages, overcoming both their internal dynamics and any disturbances that might occur. Finally the dynamometer is used to measure the cutting forces in various operation between

Figure 4.1: ETSII Mill.
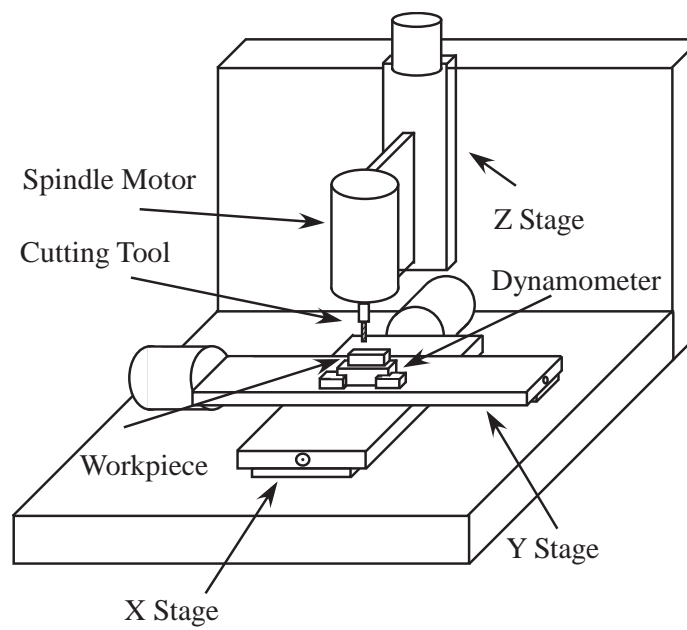
Figure 4.2: Diagram of ETSII Mill.
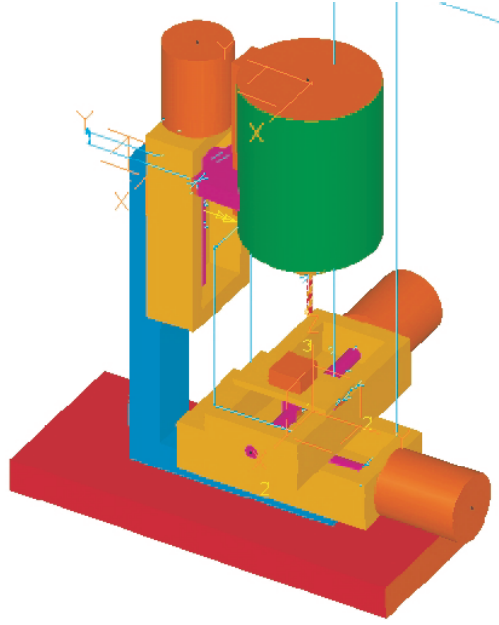
Figure 4.3: CAD Model of ETSII Mill.

the cutting tool and the workpiece. To help understand the spatial interaction between the components, the model in Figure 4.3 was developed.

4.1.1 Spindle

The spindle shown in Figure 4.4 contains and powers the cutting tool. It is comprised of a motor, a chuck, a cutting tool, and a supply tether. The spindle motor provides the for the rotation of the cutting tool. The chuck couples the motor to the cutting tool and allows the exchange of cutters. The cutting tool removes material from the workpiece. Finally, a tether is used to supply power, cooling, and lubricant to the spindle. The entire spindle system rides on the Z-stage, playing a significant role in the vertical motion dynamics of the machine.

The motor for the ETSII mill provides for the rotation of the cutting tool. Its primary performance measure is its rotational speed. The motor is capable of producing rotation rates up to 120,000 RPM. However, at higher rotational speeds, the rotation is not as smooth, therefore the primary operating speeds for the experiments in this dissertation are from 50,000 to 90,000 RPM. In order to accomplish these rotational velocities, it must be cooled and lubricated which is accomplished through the tether.

The chuck of the ETSII mill couples the motor to the cutting tool. This coupling is of primary concern due to the possibility of run-out (an offset between the centers of the cutting tool and its center of rotation). To minimize run-out, the chuck consists of a threaded nut around a collet to provide centering of the cutting tool.

The cutting tool provides for the physical removal of material from the workpiece. On
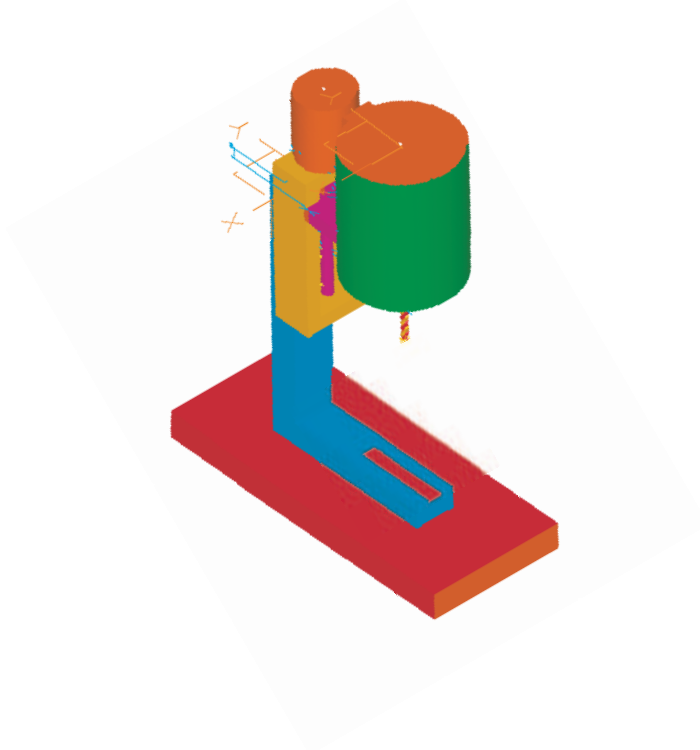
Figure 4.4: ETSII Mill Spindle.

the ETSII mill, two-fluted cutters ranging from 150 to 2,000 μm diameter are used. The wear and breakage of these cutters is a primary operational concern, due to cost, up to \$100 each and calibration time when a tool must be replaced. This calibration must be made to determine the distance between the cutter and the workpiece. This value is not constant, because the chuck/cutting tool interface is not standard, nor are all the cutters fabricated to the same length. Therefore, whenever a tool breaks or a new part is fixtured a timely calibration must be performed.

The tether provides the power, lubrication, and cooling for the micro-mill's spindle motor. The power connection links the motor to the spindle speed controller. The lubrication and some of the cooling is accomplished by an air stream combined with an atomized lubricant blown through the moving parts of the motor. Finally, a cooling line is used to keep the motor temperature down, thus minimize both wear on the motor and thermal deformation in the entire mill.

4.1.2 Stages

Two of the three stages of the ETSII mill are shown in Figure 4.5. All three stages are used to position the machine and are identical. They are each composed of a DC motor, a lead screw and a linear optical encoder. The motor powers the stage, while the screw transforms the rotational motion into translational motion. The linear optical encoders provide for
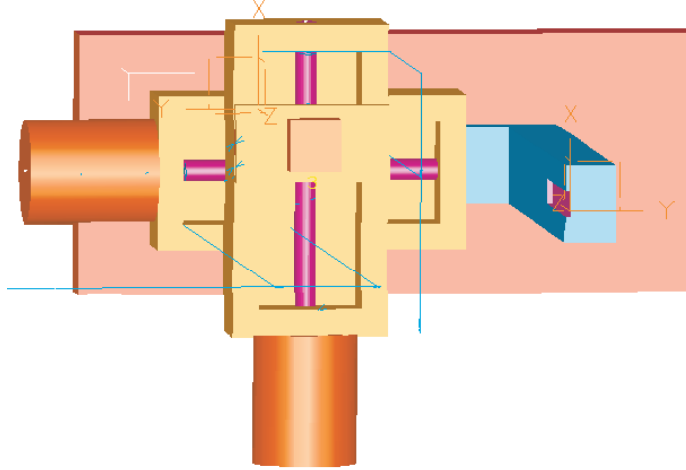
Figure 4.5: X and Y ETSII Mill Stages.
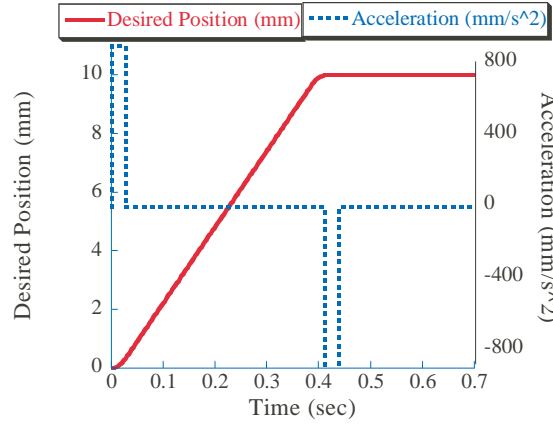
Figure 4.6: Desired Trajectory for the ETSII Micro-Mill.

position feedback of the position of the stages with a resolution of 0.5 μm. The motors are capable of feed-velocities of $100\frac{mm}{s}$, under the constraint of a maximum feed acceleration of $1000\frac{mm}{s^2}$. However, if the motors are moved at this speed, then the vibration in the positioning system is unacceptable. An example desired trajectory profile for the ETSII mill is shown in Figure 4.6. This is a bang-coast-bang acceleration input, which results in an s-curve position input.

4.1.3 Controller

The motion controller provides for feedback control and path interpolation for the motion of the machine. A PID feedback controller is employed. This controller utilizes a series of built in motion commands along with feedback from the optical encoders to produce the motion

profiles. The controller, like most CNC-controllers, is designed for spatial repeatability, *i.e.* it tracks trajectories in space well. However, also like most CNC-controllers it has poor time-based response. The controller is not designed to track trajectories in time and space, and therefore several alternative techniques were developed to overcome this shortcoming.

4.1.4 Dynamometer

A Kistler Type 9256 C1 dynamometer was used to measure the forces between the workpiece and the Y-stage. These forces are equal to the forces on the cutting tool itself. The dynamometer output was recorded by a PC and collected using LABVIEW software. The dynamometer was calibrated using spring scales to ensure proper force measurement.

4.1.5 Workpiece

The workpiece is the most important part of the micro-milling operation as it is the actual product of the machine. For the experiments in this dissertation, the workpiece was either aluminum or plastic, typically 2 by 4 by 1 cm in size. One hurdle in workpiece use for micro-mills is accurate fixturing. Locating the workpiece in the workspace of the mill is a challenge due the scales and precision required. A microscope is used for the analysis of surface features of the workpiece. By taking digital images through the lenses of the microscope, data on the surfaces of machined parts can be created.

4.2 Dynamic Characterization

The primary dynamic response of the ETSII micro-mill is the dynamics of the positioning stages and the controller. Each positioning stage behaves differently due to different loading conditions. However, they each exhibit similar damped oscillatory behaviors. The X-stage example response is shown in Figure 4.7. The X-stage must carry the weight of the Y-stage and the workpiece, fixturing and dynamometer. This response like all those for the micro-mill is the position deviation from a bang-coast-bang feed-acceleration profile. The resultant s-curve position input is tracked well with appropriate controller gains if the machine is moved slowly. However, here the research is concerned with increasing the operating speed of the mill and therefore these experiments are performed at speeds that are not typically used. These speeds are not used because the tracking is so poor as was shown in Figure 4.7. Deviations of over $15\mu m$ often occur at these high speeds.

The Y-stage only has to carry the load of the workpiece, fixturing and dynamometer, therefore its response to the same input is different from the X-stage as apparent by Figure 4.8. The large deviation at the start and stop of the trajectory still occurs, as well as the damped oscillation. However the frequency has changed due to controller gains and loading conditions.
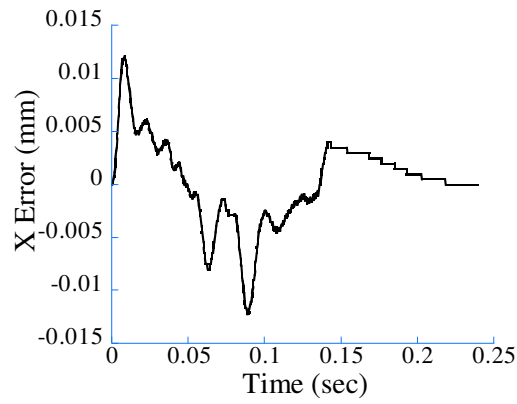
Figure 4.7: Example X-Stage Response.
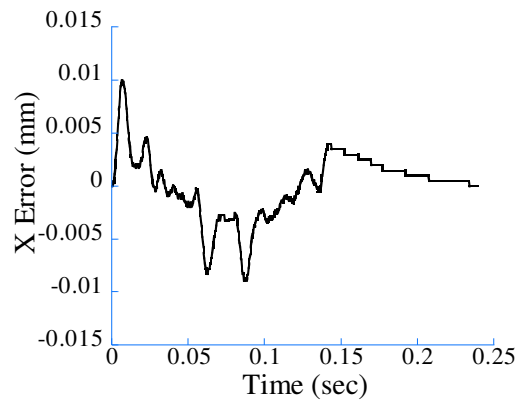
Figure 4.8: Example Y-Stage Response.
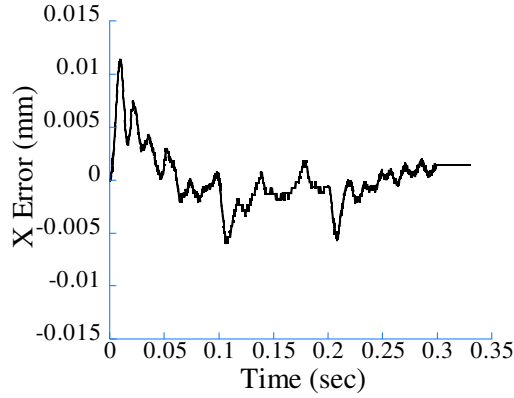
Figure 4.9: Example Z-Stage Response.

The Z-stage's speed is not as important to throughput as the other stages due to the typical operation performed by micro-mills. Its response is different due to having to overcome both the inertia and weight of the spindle system. An example Z-stage response can be seen in Figure 4.9. The same shape of response can be seen for the Z-stage as for the other two stages.

4.2.1 Position Dependence

The responses presented in the previous section, represent example responses for the stages; however, these responses change with the position in the mill's workspace. Understanding this deviation in response is necessary if vibration cancellation is needed in the entire work-area. Also, an understanding of the position dependence of the ETSII mill can lead to mechanical designs for new mills that minimize variability with position.

4.2.1.1 X-Stage

The X-stage's response is directly affected by its configuration, as well as the configuration of the Y-stage. For example, Figure 4.10 shows two following errors for the X-stage for a 4 mm move at a feed-velocity of $50\frac{mm}{s}$ and a feed acceleration of $900\frac{mm}{s^2}$ at two distinct locations in the workspace, near the positive limits for the X and Y axes and the other near the negative limits for those axes as diagramed in Figure 4.11. Both of these moves are under the same feedback controller. Notice that the magnitudes of deviation and even the component frequencies have changed slightly due to this position change.

When these same motions are performed at evenly spaced locations throughout the workspace, then the overall effect of position on the response can be seen. Figure 4.12 shows how the total error over the trajectory (the integral of the following error, with units of mm seconds) changes with the position. Two important trends can be noted from Figure

83
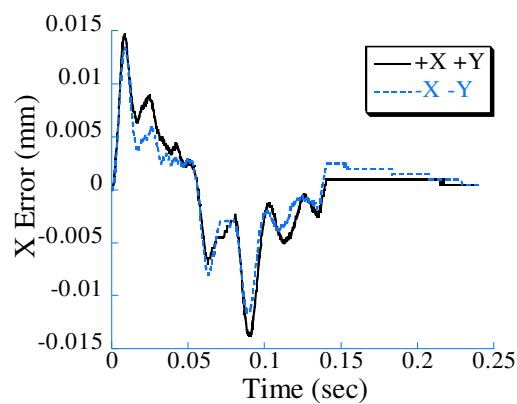
Figure 4.10: Multiple Position X-Stage Response.
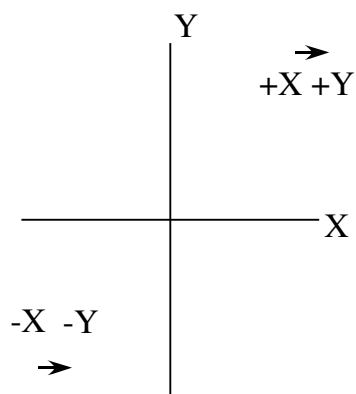
Figure 4.11: Diagram of X-Stage Motions.
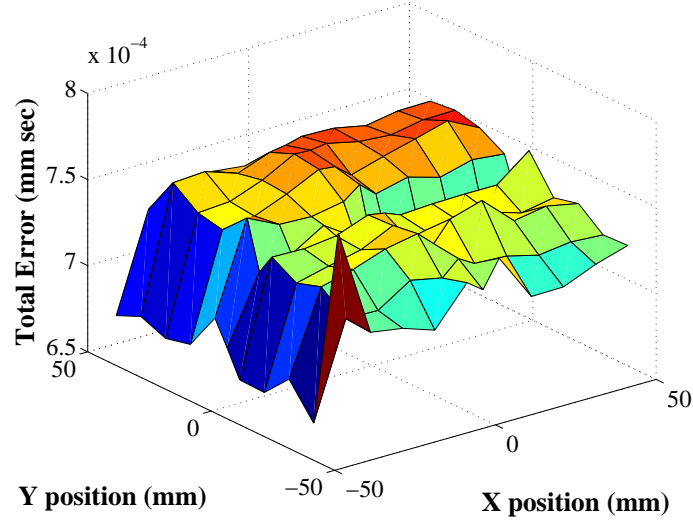
Figure 4.12: X-Stage Response over Workspace.

4.12. First, near the negative limit of the X-axis the error is less. In this configuration the distance and thus flexibility between the motor and the encoder is minimum, thus giving better tracking between the desired and actual response. Also in this configuration, the machine is in its stiffest configuration from workpiece to ground for the same reason. The other trend is dependent on the position of the Y-axis. With the Y-axis at zero or centered on the X-axis the error is also minimum. The x-stage responds better when balanced. The balancing of a system for improved performance is a common technique.

4.2.1.2   Y-Stage

The Y-stage's performance also changes with the configuration of both the X and Y stages. Figure 4.13 shows the tracking response of the Y-stage at two opposite positions in the workspace as diagramed by Figure 4.14. The trajectory parameters are the same as they were for Figure 4.10. Note that the workspace change primarily impacts the magnitude of oscillations. However, the frequency does change slightly.

If the entire workspace is tested for changes in the tracking, as is shown in Figure 4.15, then two trends opposite to those of the X-stage appear. The first is the performance being worst near the minimum X position. The same mechanical interactions that improve the X-stage performance could also be responsible for degrading the Y-stage performance. The second trend is that centering the X-axis also leads to degraded performance. This could be caused by wear on the system near this point on the X-stage from repeated operation, since this is the most heavily employed region. Once the position dependence has been studied, a scheduled control scheme could be used to counteract the changes that occur.
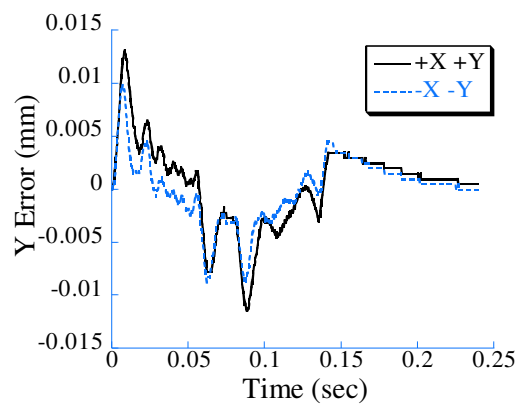
Figure 4.13: Multiple Position Y-Stage Response.
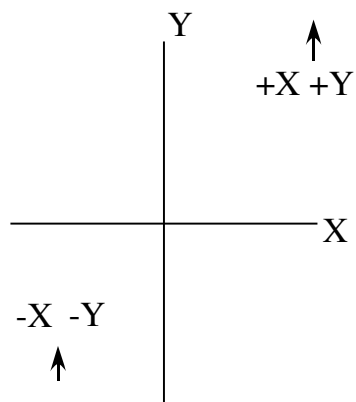
Figure 4.14: Diagram of Y-Stage Motions.
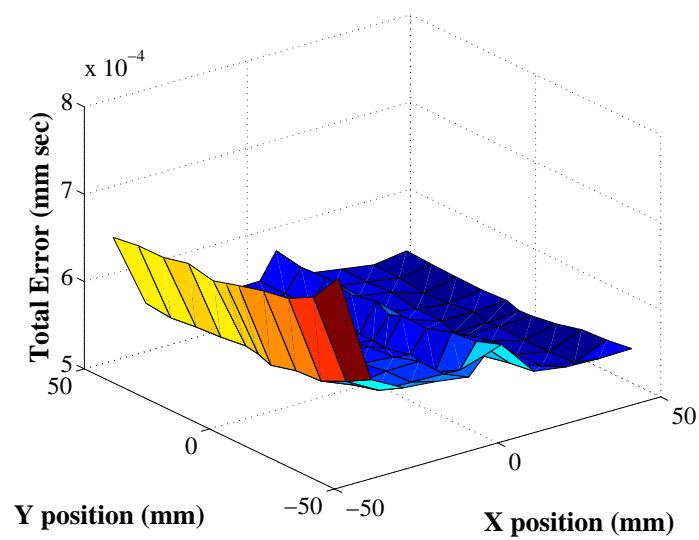
Figure 4.15: Y-Stage Response over Workspace.
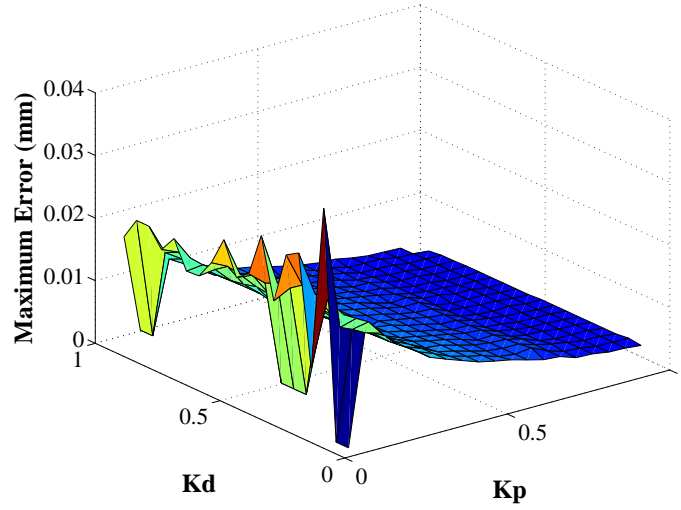
Figure 4.16: Controller Effect on X-Stage Maximum Error.

4.2.2 Controller Gains

Another dominant factor in the dynamics of the micro-mill is the gains in the control scheme. The selection of these gains is the primary tool existing micro-mills have for controlling vibration. The correct tuning of the ETSII mill's gains was necessary for operation. The controller had an impact on all stages of the tracking response. The two primary performance measures used were the maximum tracking error and the frequency of the tracking oscillations. Other conditions like stability, were also considered.

By altering the proportional, K_P, and the derivative, K_D, gains of the X-axis, the maximum error changes as shown in Figure 4.16. The proportional gain has the major impact on the maximum error, beyond the range of the machine's repeatability. The lower the gain the higher the error. However, the proportional gain does not effect the X-stage oscillation period dramatically as shown in Figure 4.17. The period is driven more by the dynamics of the motor and stage than by the controller.

The Y-stage response to various controller gains was also tested and is shown in Figure 4.18 and Figure 4.19. The same trend in the maximum error with low proportional gains as was seen for the X-axis appears in the Y-axis. Also, the period of the Y-stage response is not significantly altered by the gains available to the controller.

4.2.3 Directional Dependence

The previous sections primarily dealt with the variations in the X and Y axes performance. In the Z-axis the primary changes are due to the direction of the motion, either with or against the gravity field. Figure 4.20 shows how the maximum error changes if moves are made up or down. When moves are made against the gravity field, the maximum
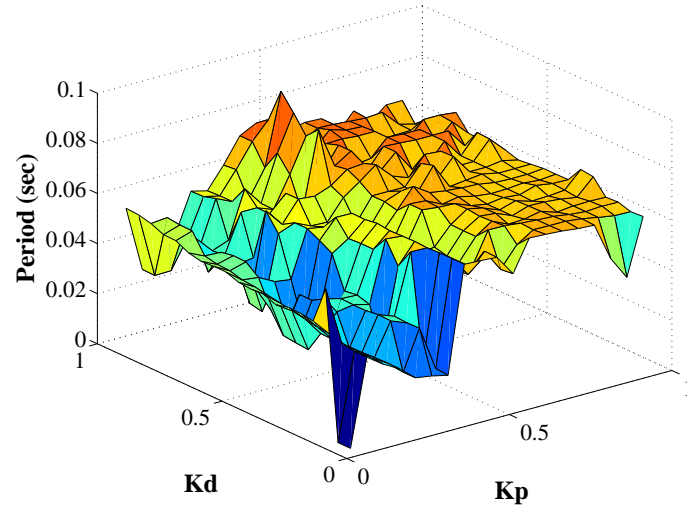
Figure 4.17: Controller Effect on X-Stage Period.
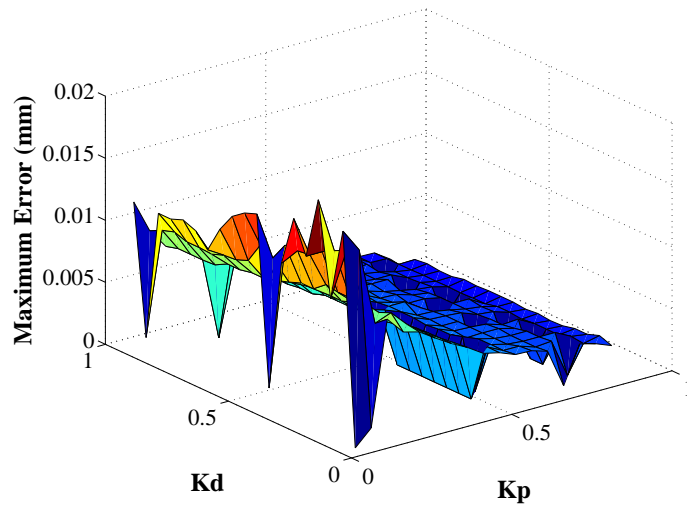
Figure 4.18: Controller Effect on Y-Stage Maximum Error.
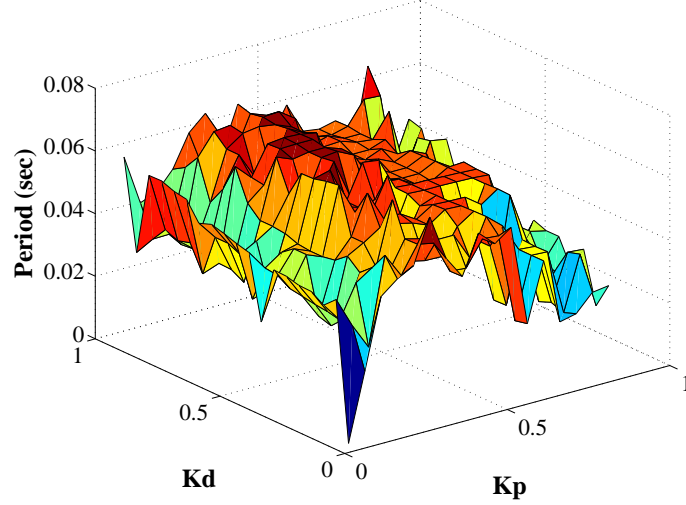
Figure 4.19: Controller Effect on Y-Stage Period.
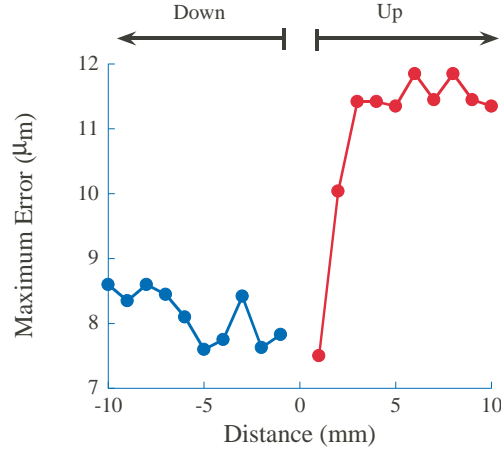
Figure 4.20: Gravity Field Effect on Z Axis.

following error is much larger do to the increased effort needed to accelerate the Z-axis due to the weight of the stage and spindle. This variation can be overcome by moving slower during upwards moves, or by implementing an alternate control scheme for each direction. Directional variation also occurs in the other two stages because of small variation in the mechanics of the system, but their effects are much smaller than that of gravity on the Z-axis.

4.2.4 Cutting Response

One of the primary differences between conventional milling and micro-milling is the magnitudes of the forces involved. The cutting forces on traditional mills are much larger and therefore are more likely to impact the dynamics of the machine. However in micro-milling,
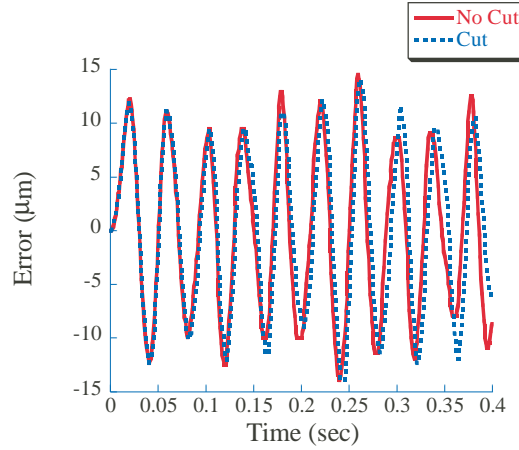
Figure 4.21: Example X-Stage Response With and Without Cutting.

the forces are orders of magnitude smaller and thus do not have the same impact on the machine response.

For example, Figure 4.21 shows a comparison of the tracking error for a swift move with and without a cut. Notice how the machine response does not change while micro-cutting This is consistent with the results of [208] for the similar technique of micro-turning. However, Figure 4.21 only shows the response of one move. Before a general conclusion can be reached about the effect of cutting on the dynamic response of the mill's positioning system can be reached, more complete results need to be considered.

Figures 4.22 and 4.23 show the impact of cutting on the maximum following error of micro-mill for climb and conventional milling respectively. Note that a depth of cut of zero is a move without cutting. Notice that the error does not change significantly with cutting no matter the depth. A general trend does appear that the larger the feed-velocity, the higher the error. This follows logically since the faster the machine is commanded to move the more likely it will deviate from such a trajectory.

The maximum following error is important, but the total error must also be considered in evaluating the relevance of cutting on the dynamics of the micro-mill. Figure 4.24 shows the total error for the same series of cuts with varying feed-velocities and depths of cut as were depicted in Figures 4.22. Note that no major change occurs in the total error by cutting. From these studies, it can be confidently stated that the stiffness of the controller and structure of the micro-mill is not significantly impacted by the cutting force even at aggressive cutting conditions namely high feed-velocities.

4.2.4.1 Excessive Cutting Force Robustness

However, other materials as well as more aggressive cutting conditions could increase the magnitude of the cutting force even further. In order to test this possibility, a calibrated
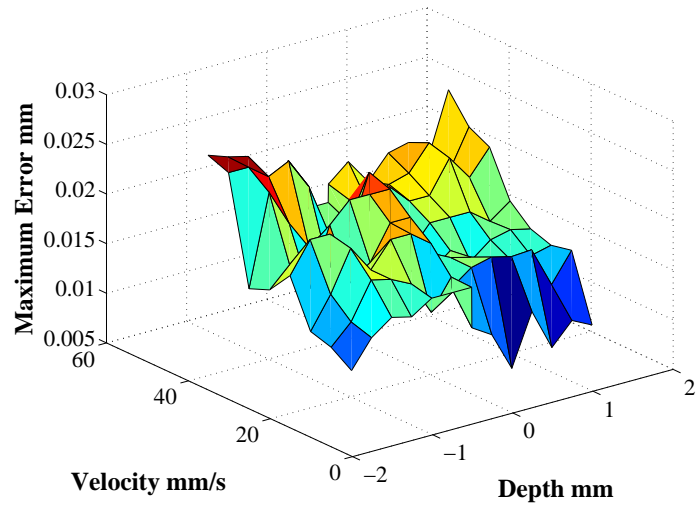
Figure 4.22: Effect of Climb Cutting on Maximum Error.
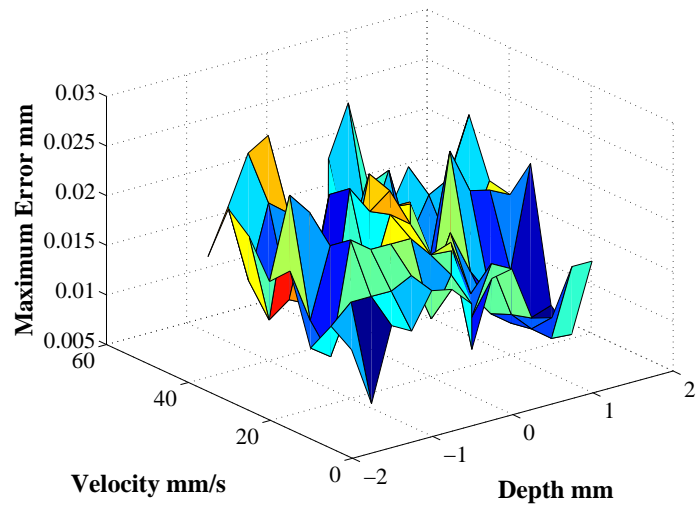
Figure 4.23: Effect of Conventional Cutting on Maximum Error.

91
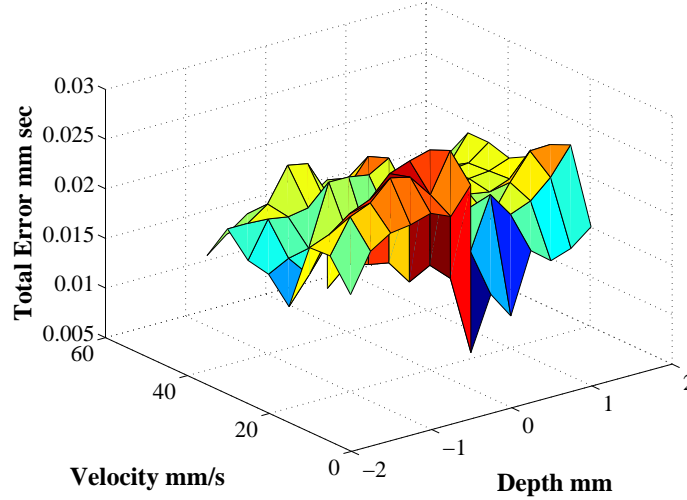
Figure 4.24: Effect of Climb Cutting on Total Error.

Table 4.1: Externally Applied Spring Forces.

	Force at 0 mm	Force at 20 mm
Spring 1	1.4 N	2.4 N
Spring 2	3 N	6.25 N
Spring 3	12 N	16 N

spring scale was utilized to apply a large disturbance force to the micro-mill workpiece. By rigidly attaching the preloaded scale to ground and the workpiece and then moving the workpiece, relatively larger forces could be applied. Table 4.1 describes the forces that the springs exhibited at different deflections. The spring force varies linearly between these extremes. When the response of the motion with the springs attached is compared to the response without the springs, the results show that the maximum and the total error are not markedly impacted by the relatively excessive external disturbance force. Figure 4.25 shows how the maximum error changes with different spring loading conditions for moves of differing lengths. A longer motion distance corresponds to a larger deflection in the spring and thus a larger disturbance force.

Figure 4.26 shows how the total error changes with the move distance for the disturbed cases. Notice that the total error increases with move distance because a longer move will logically have more tracking error. The large disturbance force test show that the performance of the micro-mill is not significantly effected by even excessive cutting forces; these forces would almost certainly break the micro-milling bits. This is fundamental evidence of the over-design of the micro-milling positioning system. The micro-mill's stiffness and consequently mass could be significantly reduced with no degradation in the tracking performance. The result would be a lower moving mass and thus higher possible speeds.
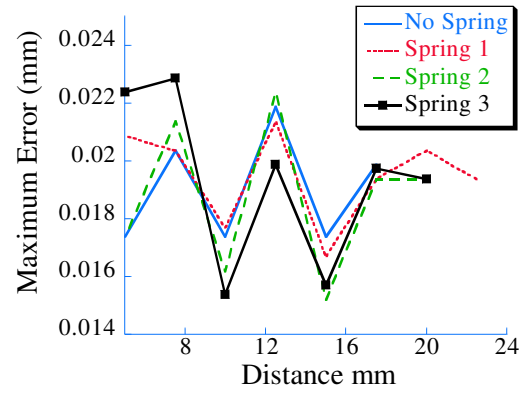
Figure 4.25: Maximum Error With Excessive Disturbance Force.
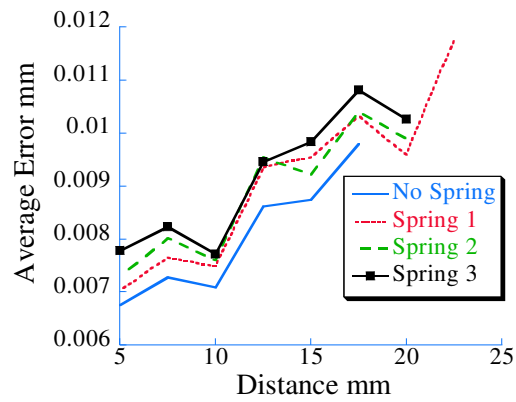
Figure 4.26: Total Error With Excessive Disturbance Force.
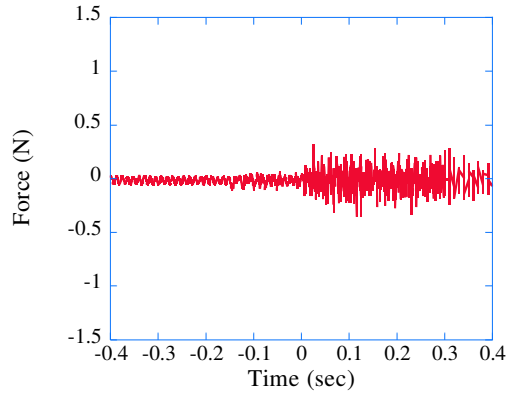
Figure 4.27: Example Cut Direction Cutting Force.
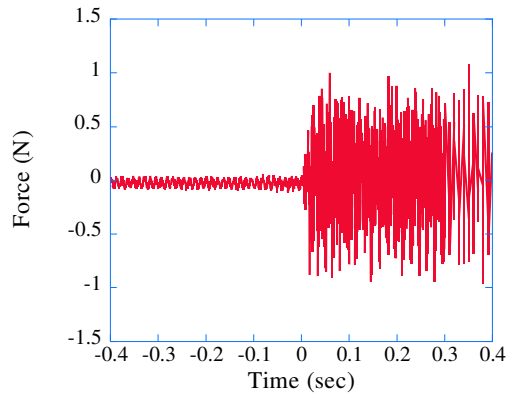
Figure 4.28: Example Normal Cutting Force.

4.3   Cutting/Disturbance Force Characterization

The previous sections focuses on the dynamics of the positioning system itself; this section focusses on the description of the cutting force. The cutting force can also be considered a disturbance to the positioning system. If this disturbance force is fully quantified, then a proper mechanism and control scheme can be employed. The previous study of the magnitude cutting forces on other mills was described in Section 2.1.1. Here the forces of the ETSII mill are presented.

The cutting force is a vector that changes with the spinning of the cutting tool. It can be broken down into components in the cut and the normal direction. Figures 4.27 and 4.28 show an example of the components of the cutting force. Note that the mill engages the part at approximately 0 seconds. This type of force profile is typical for the ETSII mill

Table 4.2: Cut Variable Description.

variable	description
d	mill diameter
h	depth of cut
w	width of cut
ω	spindle speed
V	feed velocity
A	feed acceleration
E_{max}	Maximum following error
t_{zero}	Zero Error Time
E_{total}	Total following error
F_{max}	Maximum cutting force

Table 4.3: Specific Cut Parameters.

Number	Mill Diam (mm)	Depth (mm)	Width (mm)	Accel ($\frac{mm}{s^2}$)	Material
E1	0.6	0.0125	0.125	100	aluminum
E2	0.6	0.025	0.125	100	aluminum
E3	0.6	0.025	0.125	100	plastic
E4	1	0.025	0.25	900	aluminum
E5	1	0.05	0.25	900	aluminum
E6	1	0.05	0.25	900	plastic
E7	2	0.05	0.25	900	aluminum
E8	2	0.1	0.25	100	aluminum
E9	2	0.1	0.25	900	plastic

and is representative of the force profiles characterized by their maximum values in the next section.

4.3.1   Cutting Parameters

The cutting force is dependent on a range of cutting parameters, most relevant to this work being the feed-rate. Table 4.2 describes the important cut parameters. While Table 4.3 gives the numerical values for these parameters for a series of experimental cuts designated E1-E9. Each of these cuts was performed at a variety of feed-velocities and the maximum cut direction and normal forces can be seen in Figures 4.29 and 4.30. Notice that both components of the cutting force increase with feed velocity. However, also note that the maximum force experienced by the micro-mill is 1.4 N. The previous section showed the ETSII mill was capable of withstanding much larger forces with no significant performance degradation. The next generation of micro-mills should be designed for much smaller forces and consequently be much lighter and faster.
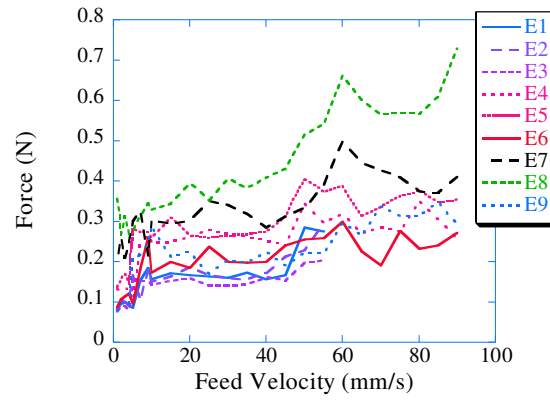
Figure 4.29: Cutting Force Dependence on Cutting Depth.
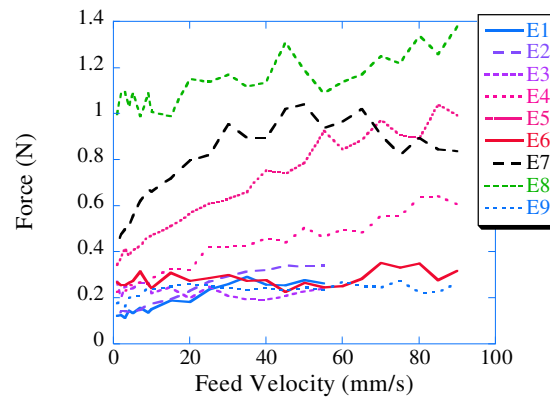
Figure 4.30: Normal Cutting Force Dependence on Cutting Depth.
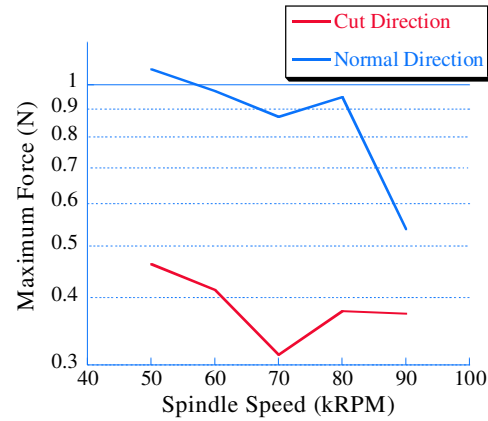
Figure 4.31: Cutting Force Dependence on Spindle Speed.
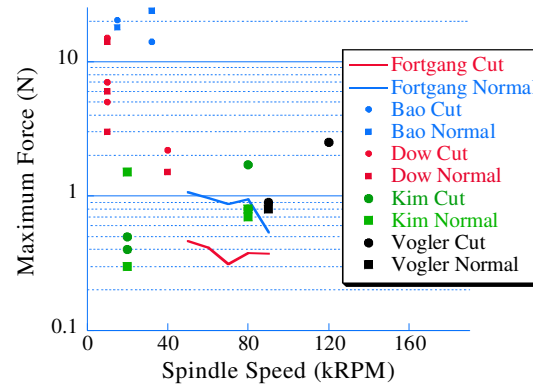
Figure 4.32: Cutting Force Dependence on Spindle Speed Comparison.

4.3.2 Spindle Speed

The primary reason that the cutting force is small is that each tooth of the cutting tool only removes a small amount of material. This is due to the high rotation rate of the spindle. An increase in spindle speed is directly linked to a decrease in the maximum cutting force. Figure 4.31 shows this trend for the ETSII Mill.

The magnitude of the forces change with spindle speed is also reinforced by the work of other researchers. Table 4.4 summarizes the findings of the other micro-milling researchers. This data can also be seen in Figure 4.32, which shows the changes is cutting force for various cutting speeds. The results are complicated by other cut parameters like material removal rate and workpiece material. The details of this other work can be found in Section 2.2.1

Table 4.4: Cutting Forces Other Mills [16, 18, 17, 59, 143, 306, 305].

			Max Force N
Researcher	Spindle Speed KRPM	Feed	Normal
Bao	2	50	90
	32	14	24
	15	41	18
	15	20.5-4.5	
	30	37	
	20	33	
Dow	40	2.2	1.5
	10	7	6
	10	5	3
	10	15	14
Kim	20	0.5	0.5
	20	0.4	0.3
	80	0.8	0.8
	80	1.7	0.7
Vogler	90	0.9	0.8
	120	2.5-0.5	

4.4 Input Shaping

All of the previous study of the dynamics of micro-mills showed that an oscillatory tracking problem exists. Also, the analysis of the cutting operations showed that they did not pose any significant impact on the response of the machine. These two facts together indicate that micro-milling is an excellent candidate for command shaping. Input shaping was described in detail in Section 3.3.1.

On the ETSII micro-mill, input shaping was be used to modify the s-curve input command of the micro-mill as was shown in Figure 4.33. The duration of the acceleration pulses, τ, characterizes the length of time the trajectory takes to complete. When the mill is given this generic input trajectory, the response has the form of Figure 4.34. Several important performance criteria appear in Figure 4.34 dealing with both the magnitude and time components of the response. The magnitude of the following error is defined by two parameters. The maximum overall following error, E_{max}, is a general measure. On the other hand the maximum following error after the acceleration pulse is over, $E_{max}(t > \tau)$, will also be used. The time response is characterized by the times when the error is zero. These response characteristics are number consecutively. Specifically, t_{cross1}, t_{cross2}, and t_{cross4} all play important roles in the time response characterization. These performance measures play a key role in the design of input shapers for the ETSII mill.
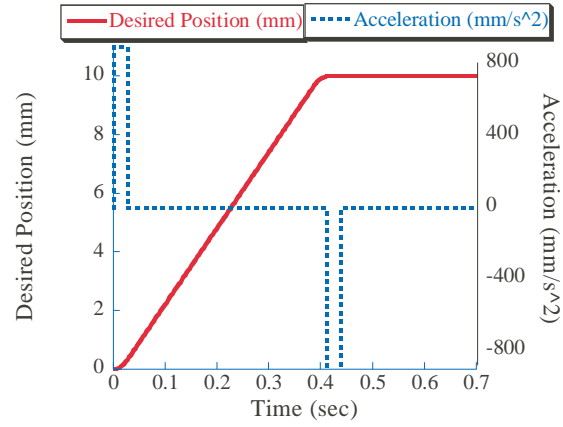
Figure 4.33: Position and Acceleration Input.
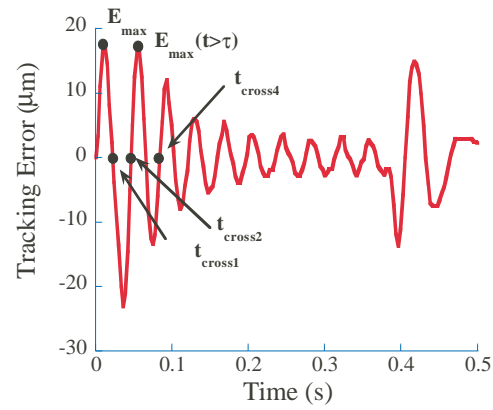
Figure 4.34: Labelled Position Error.

99
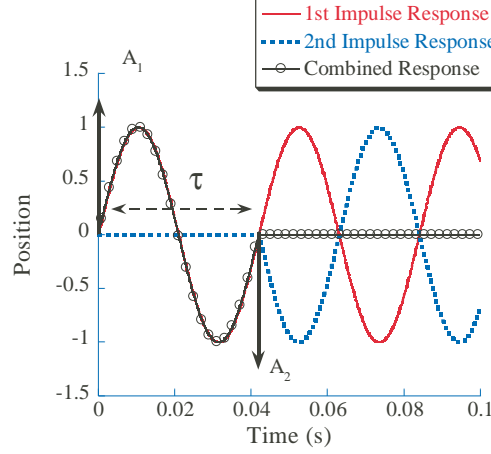
Figure 4.35: Two Impulse Shaper.

4.4.1 Command Duration Input Shapers

The traditional input shaping techniques described in Section 3.3.1 are not possible to implement on the CNC controller of the ETSII mill. Therefore, a different command shaping technique relying on the proper selection of acceleration profiles according to the rules of input shaping is employed. This technique uses the response from different sections of the acceleration input to cancel vibration from other sections. It is called *command duration input shaping* because the shaper is used to select the duration of components of the command. This process is similar to the s-curve work of Meckl in [186], where acceleration residuals were used to select optimum s-curve profiles. Here the impulse response method is used. It is also similar to the patented techniques of [264], used to design trapezoidal motion profiles. The main contributions of the *command duration* input shapers are their application to a CNC-controller, the discussion and quantification of the effects of damping, and the novel inclusion of non-linearity compensation.

4.4.1.1 Impulses Response

The *command duration* shapers are designed as impulses and then transformed into acceleration commands. For example, consider an undamped second-order system given a unit impulse. The response to such an input, A_1, is shown by the solid line in Figure 4.35. If another impulse of opposite magnitude, A_2, is applied to the system at a later time, then the response is the dashed line. However, if both impulses are given to the system, then the resultant response has zero vibration after the second impulse. This principle is used here to design acceleration profiles which cause minimal vibration in the system.

100

Driving a system with impulses is unrealistic. Therefore, for a more reasonable bang-coast-bang acceleration profile (trapezoidal velocity profile) is employed. With this command, the vibration can be reduced by adjusting the acceleration to produce an input command with good vibration characteristics. The acceleration pulses can be viewed as the integral of the two impulses in Figure 4.35, one positive and one negative, and therefore, if these component impulses can be designed correctly, then the corresponding pulse will induce little vibration. The use of the impulses instead of the pulse itself simplifies the derivation. These impulses must be equal in magnitude for the input to be a pulse. Also, the magnitude of the pulses, (the feed-acceleration, A), must coincide with the time between the impulses, τ, to in order to reach the appropriate feed-velocity, V. This relationship is defined by:

$$V = A\tau \tag{4.1}$$

If the values of A and τ are chosen correctly, then the vibration in the system can be minimized.

To find the values of A and τ to reach a desired velocity, a similar technique to that described in Section 3.3.1 is used. It begins by considering a damped second-order response to an impulse of magnitude A_i at time t_i:

$$x(t) = \left[A_i \frac{\omega_n}{\sqrt{1-\zeta^2}} e^{-\zeta\omega_n(t-t_i)} \right] \sin(\omega_n\sqrt{1-\zeta^2}(t-t_i)) \tag{4.2}$$

Where ω_n is the system's natural frequency and ζ is the damping ratio. Assuming the system is linear and time invariant, superposition can be used to find the response to A_1 and A_2, where $A_1 = A$ and $A_2 = -A$. For time greater than the time of the final impulse, τ, the response is:

$$x(t) = \left[A\frac{\omega_n}{\sqrt{1-\zeta^2}} e^{-\zeta\omega_n(t)} \right] \sin(\omega_d t)$$
$$+ \left[A\frac{\omega_n}{\sqrt{1-\zeta^2}} e^{-\zeta\omega_n(t-\tau)} \right] \sin(\omega_d(t-\tau)) \tag{4.3}$$

where the damped natural frequency is $\omega_d = \omega_n\sqrt{1-\zeta^2}$. This equation can then be used to find A and τ to yield a low level of vibration.

The following trigonometric identity can be used to simplify (4.3):

$$B_1\sin(\alpha t + \phi_1) + B_2\sin(\alpha t + \phi_2) = A_\Sigma \sin(\alpha t + \psi) \tag{4.4}$$

Where the amplitude A_Σ is:

$$A_\Sigma = \sqrt{\left(\sum_{j=1}^{2} B_j \cos\phi_j \right)^2 + \left(\sum_{j=1}^{2} B_j \sin\phi_j \right)^2} \tag{4.5}$$

101
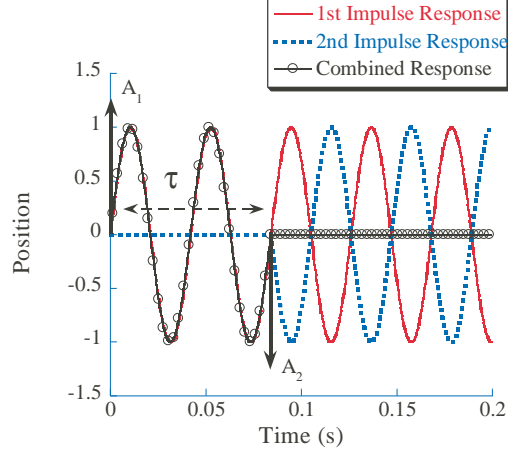
Figure 4.36: Alternative Two Impulse Shaper.

and the B terms are:

$$B_1 = \frac{A\omega_n}{\sqrt{1-\zeta^2}}e^{-\zeta\omega_n t} \tag{4.6}$$

and:

$$B_2 = \frac{A\omega_n}{\sqrt{1-\zeta^2}}e^{-\zeta\omega_n(t-\tau)} \tag{4.7}$$

The amplitude of the boundary of the vibratory response $x(t)$ at any given time after τ can then be found, without having to calculate ϕ_1, ϕ_2 or ψ. This amplitude is:

$$A_\Sigma = \frac{\omega_d}{\sqrt{1-\zeta^2}}e^{-\zeta\omega\tau}\sqrt{(C(\omega_d,\zeta))^2 + (S(\omega_d,\zeta))^2} \tag{4.8}$$

where:

$$C(\omega_d,\zeta) = A\left(1 - e^{\zeta\omega_n\tau}\cos\left(\omega_d\tau\right)\right) \tag{4.9}$$

$$S(\omega_d,\zeta) = -Ae^{\zeta\omega_n\tau}\sin\left(\omega_d\tau\right) \tag{4.10}$$

(4.8) is then used to determine the best command parameters. For the undamped case, A_Σ in (4.8) will be zero when τ is equal to integer multiples of the system period. For example, Figure 4.35 showed the solution when τ is one period of vibration, while Figure 4.36 shows the result when τ is two periods. This result is important because the acceleration/actuator limits on the machine often prohibit the use of the solution of Figure 4.35 to reach the desired feed-velocity.

4.4.1.2 Damping

If there is damping in the system, as is the case for any real micro-mill, then (4.8) can never be equal to zero, except for the trivial case of $\tau = 0$. However, significant vibration
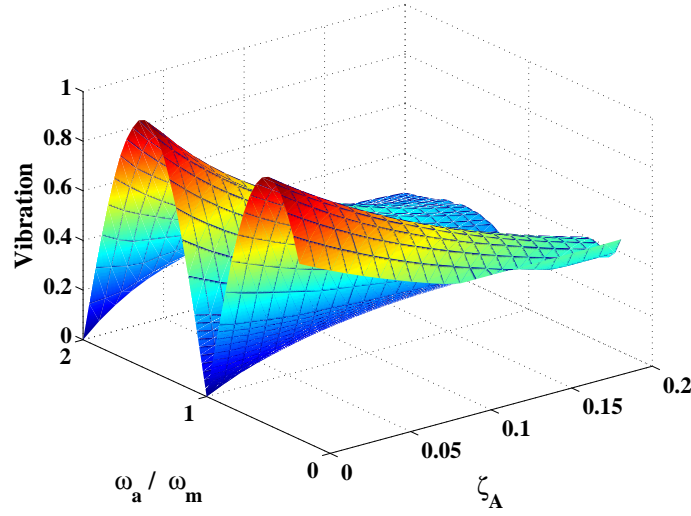
Figure 4.37: Sensitivity of Command Duration Shaper.

reduction is still possible, and the τ that minimizes (4.8) is approximately equal to integer multiples of the system period. The global minimum excluding the trivial case is given by:

$$\tau = \frac{2\pi}{\omega_n} \tag{4.11}$$

while local minimum occur at every integer multiple of τ provided there is damping in the system.

The acceleration input to the system is then designed for a given feed-velocity with an acceleration duration of τ as defined by (4.11) and an acceleration given by:

$$A = \frac{V}{n\tau} \tag{4.12}$$

where V is the desired feed-velocity, and n is the smallest positive integer such that $A \leq A_{limit}$, where A_{limit} is the maximum acceleration possible.

4.4.1.3 Theoretical Sensitivity

The previous derivation assumed perfect modelling of the system, however some error always exists. This deviation from the ideal system for the *command duration* shaper can take the form of damping in the system, or a frequency modelling error. Figure 4.37 shows how frequency modelling error or damping will effect the performance of the *command duration* shaper for a variety of different damping ratios and frequency modelling errors. The figure assumes that the damping is modelled well and error only exists in the frequency of the system. Experimental results for errors in the modelling of damping will be presented later , remember that the technique cannot cancel all the vibration if damping exists as was discussed in Section 4.4.1.2. The parameter $\frac{\omega_a}{\omega_m}$ represents the actual frequency divided by
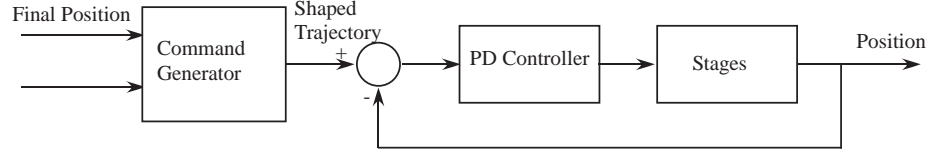
Figure 4.38: Micro-Mill Input Shaping Process.

the modelled frequency while ζ_a represents both the actual and the modelled damping ratio of the system. Notice the minimum occurring in a trough at $\frac{\omega_a}{\omega_m} = 1$, this line represents perfect modelling of the system frequency and obviously the shaping technique performs best here. The minimum trough also shows how the performance of the system degrades with an increase in damping ratio. The curve in Figure 4.37 is steep in the frequency direction near the minimum. This means that the performance degrades quickly with modelling error in frequency. Therefore inaccurate modelling of the frequency has a greater effect than a non-zero damping ratio.

4.4.1.4   Implementation

Above, the theoretical design of the command shaping technique was presented, however a complete understanding of a system and how command shaping works is not necessary in order to implement it. If the system's response is close to that of an under-damped second-order system, then the command shaping technique only needs a frequency measurement to determine τ. Another equally valid approach is to simply look at the time response of the machine and find the second zero crossing, t_{cross2}, which is ideally equal to τ. It is important in this testing of frequency to make sure that the duration of the acceleration pulse sent to the machine is longer than t_{cross2} to ensure that the end of the acceleration pulse does not interfere with the determination of t_{cross2}. Once τ is known, then the technique described above can be used to determine the feed-acceleration and feed-velocity for a particular move to minimize vibration and these values can be sent to the motion controller. To restate, the only values that the controller needs to implement the command shaping technique are the feed-acceleration and velocity, whose relationship causes the rise and the fall in the acceleration command to destructively interfere, thus leading to minimal vibration.

Figure 4.38 shows how the command shaping scheme is implemented on the ETSII mill. First the desired final position and feed-velocity are used by the command generator to produce a *command duration* shaped trajectory. Next, this trajectory is passed to the control loop, which consists of a feedback controller and the stages themselves.

4.4.1.5   Acceleration Dependent Non-linearity

The previous command shaping process is straightforward in its application to linear systems. However, like all real machines the ETSII micro-mill is not linear. This nonlinearity

104
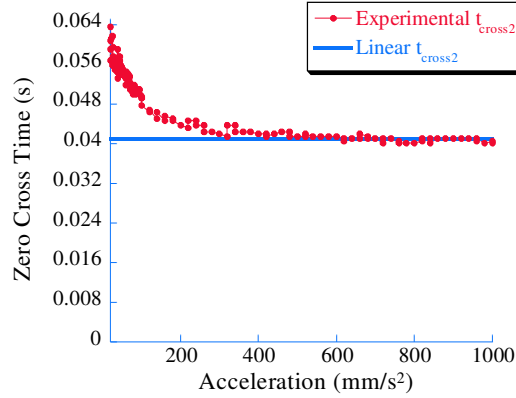
Figure 4.39: Crossover Time Non-linearity.

appears in the time response of the machine as a function of the acceleration. Unfortunately, t_{cross2} is not constant on the physical system. The time at which the error goes to zero is dependent on the acceleration magnitude. This nonlinear effect complicates the trajectory design. This change in the crossing time could be dealt with by introducing a more robust command shaper [254, 248]. However, the motion controller on the ETSII milling machine and other commercial manufacturing machines is limited, and therefore requires a simple shaping scheme to be used. The solution advocated here is to adjust the command shaper parameters, namely τ, depending on the desired acceleration. This requires the command design scheme to consider the acceleration-induced nonlinearity. This process, although simpler for the controller to implement, is more difficult to initially determine. However, it can be designed once and reused for all milling operations.

Compensating for this nonlinearity in the zero crossing times by adjusting the command algorithm yields successful vibration reduction over all accelerations and therefore feed-rates. In order to solve for an appropriate command shaper at a given feed rate, the relationship between all possible accelerations and the zero crossing times must be developed. Figure 4.39 shows how the second time the tracking error is zero changes versus the acceleration of the X-stage. If the mill behaved linearly, then the line would be horizontal. However, since the experimental data deviates from the theoretical value for low accelerations, the experimental data must be used to find the command shaper. This is done with the following three steps:

1. Specify the desired feed-velocity

2. Solve the vibration equation for all attainable accelerations

3. Utilize the acceleration, A, where $\tau = \frac{V}{A}$ is closest to t_{cross2}

105
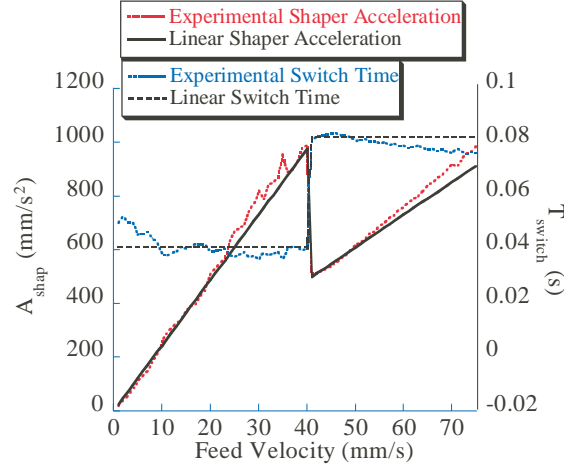
Figure 4.40: Crossover Time Impact on Shaper Parameters.

This process produces a solution for the shaper at each desired feed-velocity. Figure 4.40 shows the command shaper's acceleration and duration, τ, over the feed-velocities attainable by the machine. In order to reduce the vibration at higher feed-velocities, the solution becomes bounded by actuator saturation. This causes the acceleration pulse duration to discontinuously increase by one period of vibration (note the jump at 40 mm/s).

The linear case is also shown in Figure 4.39. The linear solution varies significantly from the nonlinear experimental data at low velocities, where the experimental switch time is 28% greater than the linear. This causes a deviation in the acceleration as well, but because of the scale, it is not noticeable in Figure 4.40. The solution also varies at velocities around $35\frac{mm}{s}$ and above $60\frac{mm}{s}$, due to the effects of approaching the acceleration limits of the machine at both velocities.

4.4.2 Results without Cutting

The above command design technique provides significant improvement in trajectory tracking. For example, Figure 4.41 shows the change in the following error of the machine for a move of $10mm$ at a feed-velocity of $26\frac{mm}{s}$. The peak magnitude $E_{max}(t > \tau)$ after the acceleration pulse is reduced from $17.0\mu m$ to $3.7\mu m$, a reduction of 78%, at a cost of a acceleration pulse duration increase of 0.02 seconds. While the previous discussion focused on the acceleration profile, by setting the trajectory parameters correctly the vibration from the deceleration profile is also reduced. Figure 4.42 shows a complete experimental response with and without command generation. Utilizing command generation improves the settling time of both the initial acceleration and the deceleration of the machine. A low level of vibration occurs in both cases.

The *command duration* shaping technique improves the tracking performance of the ETSII micro-mill at all attainable feed-velocities. Figure 4.43 shows the difference between
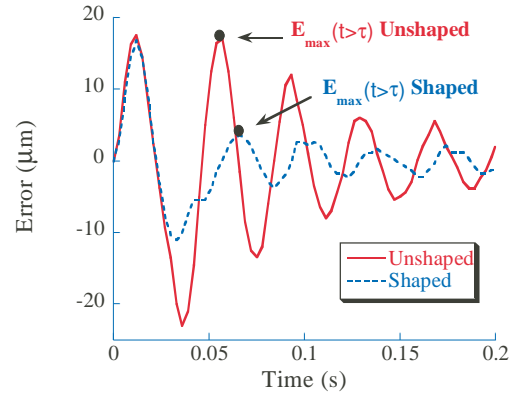
Figure 4.41: Input Shaping Result for $10mm$ X-axis move at $26\frac{mm}{s}$.
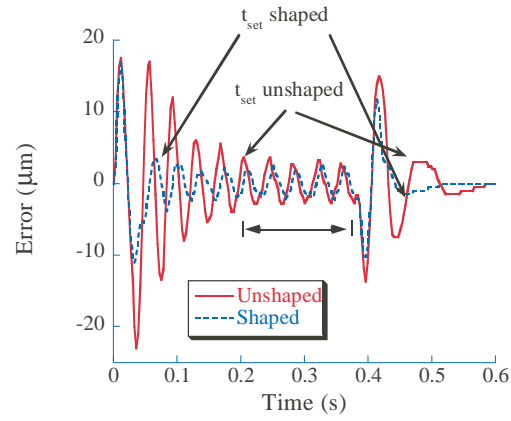
Figure 4.42: Input Shaping Result for Entire $10mm$ X-axis move at $26\frac{mm}{s}$.
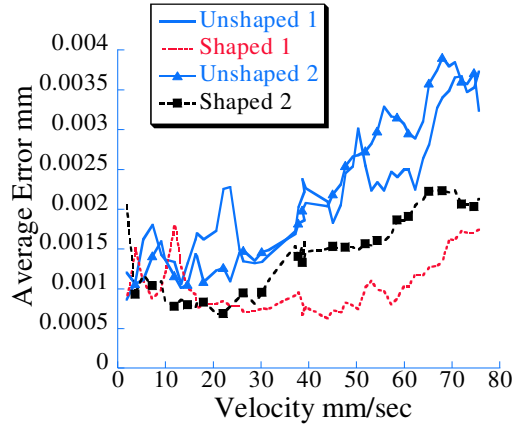
Figure 4.43: Absolute Shaped Error without Cut.

shaped and unshaped total error for a variety of feed-velocities. Shaped 1 and Shaped 2 are the two impulse shaper of Figure 4.35 and the alternative two impulse shaper of Figure 4.36 designed for higher feed velocities respectively. Unshaped 1 refers to a *command duration* τ of t_{cross1}, while Unshaped 2 is a *command duration* τ of t_{cross3}. These represent the worse cases of command design whereby the vibration induced by the changes in the acceleration command will interfere constructively. Not all the command design schemes are capable of reaching all feed-velocities due to the acceleration limits of the stages. Note that the shaped results are significantly better for all feed-velocities.

4.4.3 Results with Cutting

It is of primary importance that the input shaping work for motions involving cutting. Since Section 4.3 showed that the cutting dynamics do not impact of the motion of the stage, it can be correctly deduced that they will not impact the shaped motion of the stage. Figure 4.44 shows how the total error changes with and without shaping while cutting plastic with a variety of feed-velocities. Note that shaping improves the performance with cutting, just as it did without cutting.

It is also important that the command design process not impact the cutting force for purposes of tool breakage and wear. Figure 4.45 shows how the mean absolute value of the cutting force for plastic is not changed by implementing command shaping. Figure 4.46 shows a similar result for cutting aluminum as was shown for plastic in Figure 4.45, that shaping does not impact the mean cutting force. The cutting of aluminum also has little impact on the effectiveness of the shaping technique to counteract vibration in the positioning system, as is shown in Figure 4.47.

108
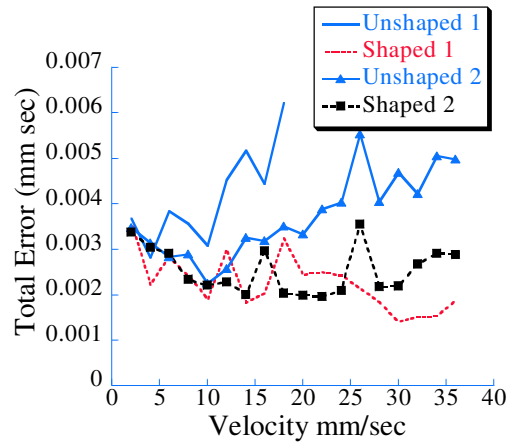
Figure 4.44: Total Error Cutting Plastic.
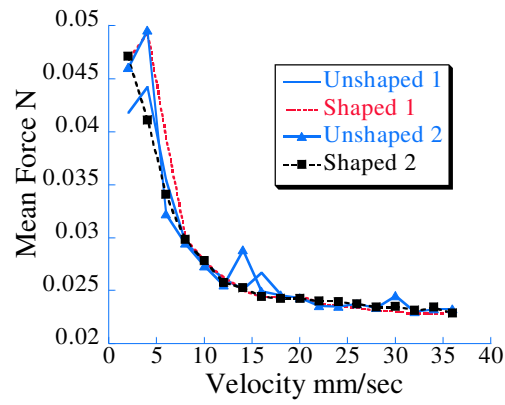
Figure 4.45: Mean Cut Direction Cutting Force for Plastic.
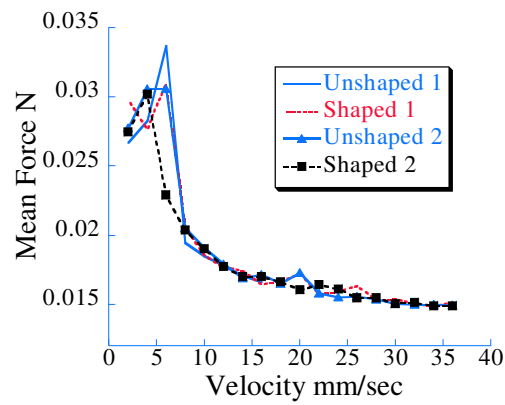
Figure 4.46: Mean Cut Direction Cutting Force for Aluminum.
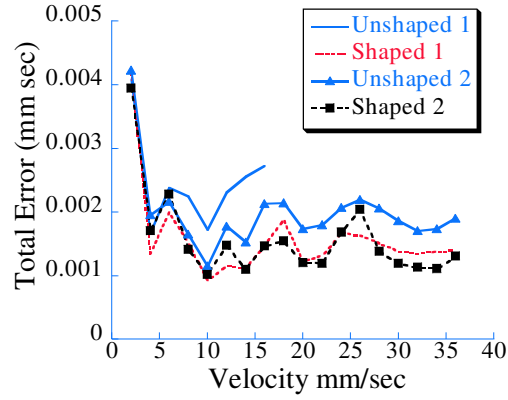
Figure 4.47: Total Error Cutting Aluminum.
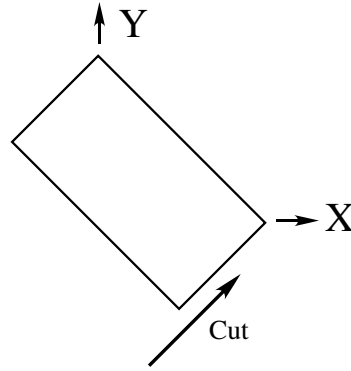
Figure 4.48: Diagram of Part Cutting Procedure.

4.4.4 Actual Part Measurements

The previous results clearly show the effectiveness of the command generation scheme on the position of the stages. However, deflection of the cutting tool or other components not measured by the stage encoders could occur. To test if these deflections occurred, cuts with and without command generation were performed with a feed velocity of $28 \frac{mm}{s}$. These cuts were made using both the X and Y axes in order to see geometric variation in the part. Figure 4.48 diagrams how these cuts were made. In this configuration, input shaping significantly improved the tracking of stages. Figure 4.49 shows a section of the responses of the stage transformed from the encoder frame into the part coordinate frame. Notice how the vibration amplitude is significantly lower in the case of shaping.

The same vibration reduction can be seen in Figure 4.50 which measured the actual surface dimensions of the machined material. The shaping reduces the variation along the actual surface from $36\mu m$ to $15\mu m$, a reduction of 58%. This data was obtained by photographing the machined surface using a microscope. Example photos of the shaped
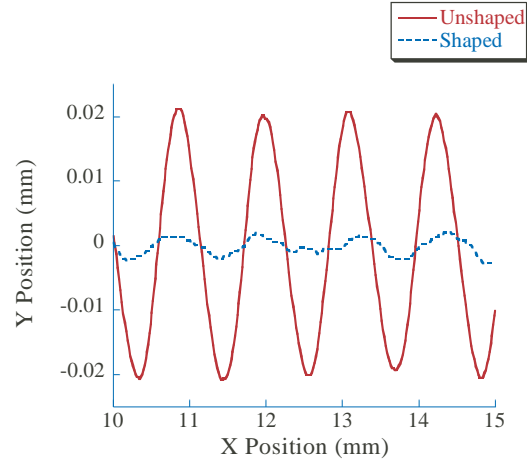
Figure 4.49: Stage Response for Measured Part Experiment with and without Shaping.
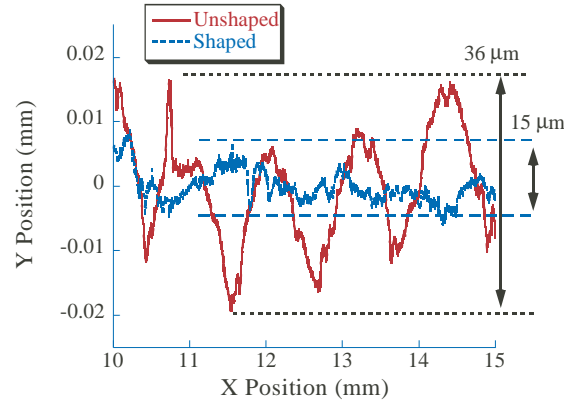
Figure 4.50: Actual Measured Part with and without Shaping.

and unshaped parts can be seen in Figure 4.51 and 4.52 respectively. The improvement in the geometry of these parts was even large enough to see with the unaided eye.

While the command shaping improved the accuracy of the cut, it does not address the small high frequency oscillations in the surface. These are due to the cutting dynamics of the mill and are beyond the capabilities of command shaping. The command shaping scheme applied here does not address tool run-out. However, command shaping could be tailored to reduce vibration of the tool itself if necessary and if the controller and actuators bandwidth was large enough to encompass the cutting tool oscillation frequency.

The effectiveness of the technique for part geometry was tested for a range of feed-velocities. Figure 4.53 shows how the average roughness, like those values shown on Figure 4.50 changes with and without shaping. The average roughness or average peak-to-peak variation in the part surface is decreased in both the stages, as well as the parts dimensions.

111

Figure 4.51: Photo of Unshaped Part.

Figure 4.52: Photo of Shaped Part.
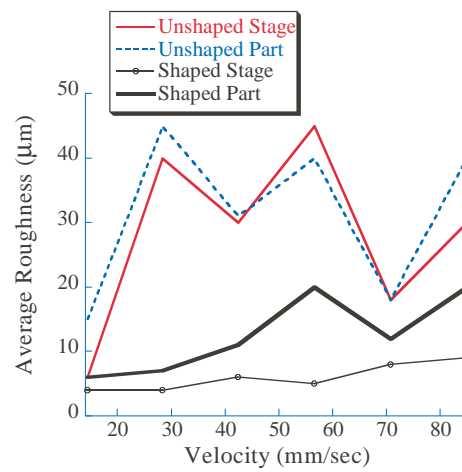
Figure 4.53: Surface Roughness for 45° Parts.
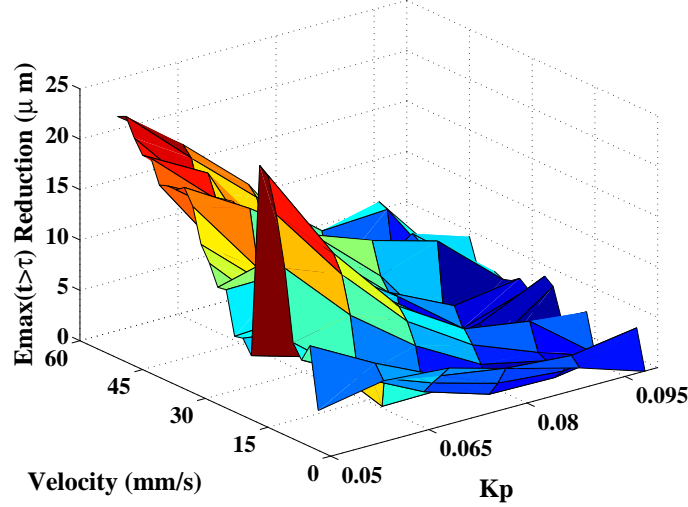
Figure 4.54: Error Reduction with Frequency Modelling Error.

4.4.5 Robustness

The theoretical sensitivity or robustness to modelling errors was discussed in Section 4.4.1.3; however, the physical results of modelling error are more important to actual tool performance. Figure 4.54 shows the improvement in $E_{max}(t > \tau)$ (the maximum error after the initial acceleration pulse) with the use of command shaping for a variety of feed-velocities with modelling error. Modelling error was induced by altering the controller proportional gain without making an appropriate change in the command generator. The magnitude of the improvement drops rapidly as modelling error increases, as predicted by the theoretical results. Also, there is a discontinuity in the surface along the line of velocity at $40\frac{mm}{s}$. This coincides with the discontinuous jump in the value of τ needed to meet the actuator constraints.

Similarly, Figure 4.55 shows the same information, if instead modelling error exists in the damping or derivative gain of the system. The effect of modelling error in damping is not as severe as with frequency, but the performance still degrades. These two graphs show that while the command shaping technique is effective for reducing vibration over a wide variety of feed-velocities, if the system cannot be modelled fairly accurately, then the performance will suffer.

4.4.5.1 Excessive Force Response

Another measure of robustness is the ability to cope with changes in cutting forces. Section 4.2.4, specifically Figure 4.21, showed that the system performed equally well with or without cutting. However, the magnitude of the cutting forces in Figure 4.21 was small - on the order of 1 Newton. Other micro-mills might encounter larger cutting forces, [16, 59]
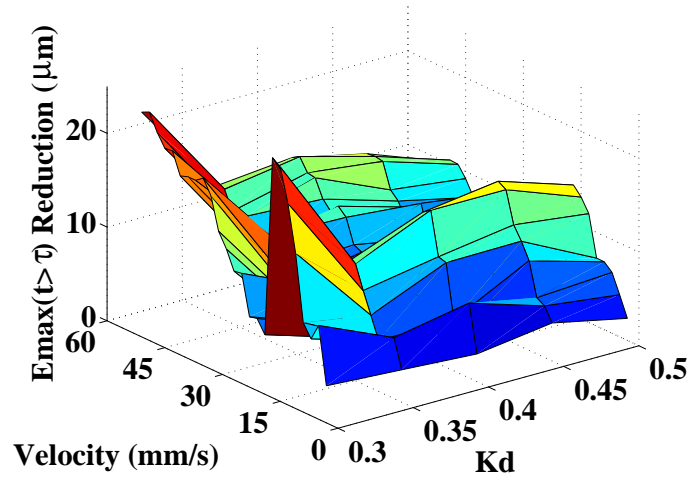
Figure 4.55: Error Reduction with Damping Modelling Error.
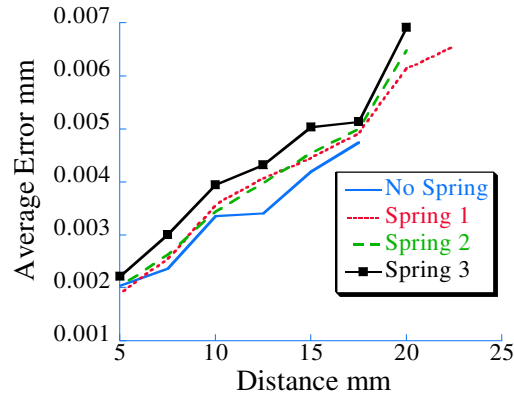
Figure 4.56: Total Shaped Error With Excessive Disturbance Force.

due to differing materials or cutting parameters like spindle speed. Therefore, the command shaping technique needs to be effective when larger forces are present. The larger forces must not alter the dynamics of the machine in such a way that the command shaping technique no longer functions correctly. This was tested by utilizing the same spring scales and setup as Section 4.2.4.1 to apply a quantified disturbance force to the stages. Figure 4.56 shows the performance of the command shaping technique when three different springs were applied. The total shaped error is not effected by disturbance forces, even when they are an order of magnitude larger than the cutting forces.

4.5 Design Sensitivity in Micro-Milling

The experimental work in micro-milling along with the analysis of other researcher's work lead to an improved understanding of the design concerns in the next generation of micro-milling machines. Most of the insight centers around the goal of making the positioning system as fast as possible; however, other considerations also became apparent. A summary of the correlations between the design choices and the performance of the next generation micro-mill is summarized in Table 4.5. These performance measures and design choices are discussed the following sections.

4.5.1 Performance Measures

The measures of the performance of a micro-mill are similar to the measures used on a traditional scale tool. However, on a micro-mill the targets for the measures differ. This section will try to emphasize the differences that will occur in micro-mill design evaluation.

4.5.1.1 Surface Finish

The surface finish or roughness of a final part is always a concern when machining. Micro-milling applications require a finer surface finish than macro-mills primarily due to the scale of the final part. However, more than just the part scaling impacts the need for fine surfaces; the primary applications of micro-milling often require a smooth surface. For example, micro-mills have been use to create optics, specifically lenses and gratings. These types of parts must consider the relationship between wavelength and surface finish, and therefore require stringently smooth finishes. Also, micro-mills have been used to cut the molds for micro-injection molding. The mold finish is imperative to both final part quality and mold release. Another factor that impacts the surface finish for micro-milling operations is the workpieces themselves. The surface finish is impacted by the grains of the material, and possibly even the individual molecules. Dealing with these non-traditional issues is key for the next generation of micro-mills.

4.5.1.2 Part Tolerances

As with the surface finish, the tolerances of the final part for micro-mills are scaled down versions of the macro-scale counterparts. This requires the scale of the resolution to be a fraction of a micrometer.

4.5.1.3 Tool Life

Cutting Tool life is of a primary concern in micro-mills due to the cost of the tools themselves. A micro-cutter will often only be able to cut for centimeters or even millimeters before becoming excessively worn. These cutters can cost over $100 per cutter, and cannot

Table 4.5: Decision Correlation.

Component	Design Choice	Performance Measures	Surface Finsh	Part Tolerances	Tool Life	Throughput	Materials	Energy Consumption	Overall Weight	Cost	Total
Cutter											
	Material		3		3	1	2	1			10
	Shape		3		3	1	2	2			11
Spindle											
	Type			3		1		2	1	1	8
	Stiffness		1	3	1						5
	Speed		3	2	3	3	1	1		1	14
Controller											
	Structure		1	2		2		1			6
	Gains		1	3		2		1			7
Stages											
	Type			2		2		3	3	2	12
	Speed				1	3		2		1	7
	Stiffness		1	3	1	1				1	7
	Encoders			3						2	5
	Dynamics			2	1	2		1	2		8
	Bearings			1		1		1			3
Workpiece											
	Fixturing		1	2		3	3		1	1	11
	Sensing			1	3					3	7
Mount											
	Bandwidth		1	1					3	1	6
	Size		1	1					3	1	6
Total			16	29	16	22	8	15	13	14	

be honed. Another major concern that appears in micro-milling is the inability to effectively monitor the cutting tool condition without some auxiliary equipment. On macro-scale mills, an operator has some knowledge from their eyes and ears into the condition of the cutting tool. For example, surface finish can be quickly judged with the naked eye or by touch as a measure of tool condition. However in micro-mills, other equipment is needed for these measures. A microscope is necessary to judge tool wear or surface finish. Even complete tool failure is often not apparent on a micro-mill. A break in the tool does not change the look or the sound of the operation. Many systems have been developed for monitoring tool wear on macro-scale tools, and they can lengthen the life of each tool. However, a large portion of traditional scale tools simply rely on the operator for tool life assessment. This is not possible on the micro-scale, and consequently the next generation of micro-mills requires techniques be in place for tool monitoring.

4.5.1.4 Throughput

Micro-mills are currently used as prototyping machines. Therefore, any analysis of throughput must consider not only mass production but also prototyping as would be used to generate the molds for micro-injection molding. Current micro-mills require approximately the same time to cut a part as many traditional prototyping tools. However, the non-cutting times are much greater for micro-mills due to the difficulties in fixturing and referencing the part. While mass production macro-tools have developed ways to deal with calibrated fixturing, no economical techniques yet exist for automated fixturing and referencing for micro-tools. Another difference between macro and micro scale tools is the number of parts fabricated at a time in a device. All products are designed to eventually have an impact on the macro-scale world in which humans live. Even nanometer scale circuit boards are designed to convey information that is eventually displayed as 12 point characters on a sheet of paper. Consequently, the usefulness of a product can be measured as its impact on the macro-scale. To impact the macro-scale world more micro-scale parts are needed than macro-scale parts. Even though micro-technology can have increased functionality over macro-technology, micro-part fabrication time must be competitive with the macro-scale. Therefore, micro-machines must be able to produce many parts in a comparable time to macro-technology producing one.

4.5.1.5 Machinable Materials

One of the primary advantages of micro-milling is the ability to machine a wide variety of materials. The materials needed to be machined are often different than those used on macro-scale tools. Micro-mills are being used to cut thinner materials than traditional machine tools due to the scaling. But they are also able to cut softer materials due to the decreased cutting forces. Likewise, brittle materials can be machined due to the change in

cutting regions when the scale becomes small. For example, glass can be cut in the ductile region with a micro-mill. Conversely, other materials suited for macro-scale machining cannot be scaled down to the micro-scale due to issues such as grain size and other heterogenous characteristics.

4.5.1.6 Energy Usage

Another primary concern is energy consumption. Obviously micro-tools consume much less energy than their macro-scale counterparts. However, two main issues still arise. The first is the location of micro-mills. Due to their size and quietness, micro-mills can be set up in non-traditional manufacturing settings, like in an office building. Here available power is much less than in a dedicated manufacturing facility. The other main issue is temperature variation. Because the scales are so much smaller, micro-machines are especially susceptible to changes in temperature. For this reason alone energy consumption of micro-mills must be considered in the design phase and weighed as a measure of machine repeatability.

4.5.1.7 Machine Weight

Micro-mills are by their nature lightweight. However, due to their increased susceptibility to vibration from external sources, vibration isolation is a primary concern. This isolation typically involves a substantial block of granite, which can weigh an order of magnitude more than the micro-mill's other structure.

4.5.1.8 Cost

Cost of micro-mills is a primary concern as it is with macro-mills. Many issues contribute to this cost, but one of the primary differences is the relative cost between the components. Much of the cost of macro-scale tools is the structure itself, while in micro-scale tools the structure is usually much smaller and therefore the cost becomes dominated by higher technology components. Many of the components of large scale tools become cheaper when scaled down, like amplifiers for the motors. However, other component costs, like encoders, increase as scales go down.

4.5.2 Mill Component Design

This section will try to outline the design choices in each component of the micro-mill design process. The specific impact on the next generation of lighter and faster tools will be addressed with impacts on cutter, controller, positioning system, workpiece and mount selection.

4.5.2.1 Cutter

The design selection of a cutter for a micro-mill is of primary importance to the overall performance. However, a variety of cutters can be used on any given mill and the selection of a particular cutter is easy to change after the mill is constructed. Therefore, consideration of the cutter at the design phase is not as important as some other more fixed mill components. Nevertheless, some important observations about the cutter's impact on the performance of the next generation of micro-mills can be made. Cutter selection, both in the shape of the cutter and the material, primarily impact the surface of the final part and the life of the cutter itself. For example, using a four-fluted cutter instead of a two-fluted cutter halves the material removed for each cutter flute which will improved the surface finish of the cut and make each flute wear slower. However, the flutes on the four-fluted mill will not be as strong and therefore more susceptible to breakage from other factors. This tradeoff is one of the key factors in choosing a milling cutter.

4.5.2.2 Spindle

The desire to design a new, lighter, and faster micro-mill is driven by the recent advances in spindle technology. These new air powered motors allow speeds of 300,000 RPM which is a vast improvement over the AC and DC motors that are used on larger machine tools. This choice of spindle motor be it air, DC, AC, or stepper along with the related stiffness and attainable rotation rate are the primary design choices for the new micro-mills. In order to improve throughput, the primary concern is the rotation rate, which is highly dependent on the type of motor selected. As spindle speed increases the amount of material removed for each revolution of the spindle decreases. Thus decreasing the force on the cutter itself and the positioning system. Both benefit from the this decreased force. Lower force on the cutter allows the feed-velocities to be increased, while lower force on the positioning system allows lightweight stages. Another added benefit from high spindle speeds on both tool life and part tolerances is the reduction of chatter. If the spindle speed is significantly higher than the natural frequency of the system, chatter will not occur.

There are a couple detrimental effects of this new approach of faster spindles. The first is the control of tool run-out, or the offset between the cutter's center and the center of rotation. Tool run-out is more prominent in high speed air systems and directly effects the workpiece's shape. Secondly the higher the speeds the more energy that will be consumed by the machine. These issues need to be fully addressed if spindle speeds are to continually increase. Finally, as spindle speeds increase so do spindle accelerations. For high acceleration spindles, gyroscopic forces must be considered in the spindle mount.

4.5.2.3 Controller

The motion controllers needed for the next generation of micro-mills will need to be more advanced than those of current machine tools. The increased speeds and lighter overall weight will require advanced techniques to deal with system vibration from commanded moves. While traditional machine tools rely on controllers with simple PID architectures, new machines could use command shaping techniques, feed-forward components, or even learning algorithms for motion control. The ability of these controllers to follow tool paths will have primary impact on the final part tolerances, and following these paths becomes increasingly difficult as machine flexibility or speed increases. Likewise, the gains or parameters of these new controllers need to be chosen to provide adequate trajectory tracking, but also to maintain a fast response in order to improve throughput.

4.5.2.4 Stages

A primary motivation for the redesign of micro-mills is that the current positioning systems are much stiffer than they need to be. By choosing a lighter-weight positioning stage, the machining process could be faster and consume less energy. In the selection of these positioning stages, the primary tradeoff is between the attainable speeds and the stiffness or ability to reject disturbances. Chapter 8 deals with this issue specifically. However, other considerations besides the speed of the stage must be made. The type of system used to position the machine, be it a ball screw powered by a conventional motor, a piezoelectric actuator, or a linear actuators, is an important choice. Each type of stage will have a particular impact on both the speed and the repeatability, and thus tolerances of the final part. Encoder selection is also important, as finer encoders will allows finer positioning of the stages, and thus finer details on the final part.

Another issue, in the selection of a light positioning system is the increased dynamic complexity. Any flexible mode of vibration, if not successfully dealt with through the controller could degrade the tracking of the machine. It is also important to note that poor tracking can lead to decreased tool life. Errant motions can cause excessively deep cuts and consequently cutting forces large enough to break the cutter. Also related to the linear dynamic of the stages are the non-linear dynamics often caused by friction in the bearings. Bearing selection should be made to reduce friction within the cost limits of the machine tool. However, the friction in the bearings does add important damping to the structure, and thus the damping/accuracy tradeoffs must be considered.

4.5.2.5 Workpiece

The workpiece selection does not deal with the actual workpiece, but instead the components needed to integrate the workpiece into the machine. The workpiece must be mounted into the machine, and as mentioned previously in Section 4.5.1.4 sensing of the workpiece

condition is important due to the scales involved. This sensing of tool breakage and other tool wear is typically done with a dynamometer which can be quite costly. Other techniques such as optical inspection under a micro-scope are possible. The mounting or fixturing of the workpiece is strongly correlated to the throughput of the machine. This is due to the long times that must be spent referencing the workpiece in the workspace of the tool. A fixture that reduces the degrees of freedom of the workpiece in space could improve this setup time significantly.

4.5.2.6 Mount

The mounting of the machine tool is important when operated in traditional machining environments where vibration can be transferred from other machines into the new micro-mill. The new mills would be especially susceptible to vibration due to their increased flexibility. Therefore, an adequate vibration suppressing mount is needed. The mount needs to large/massive enough to provide a rigid structure for the machine tool to sit, but also have an acceptable bandwidth of vibration suppression from external disturbances. Both of these issues are typically overcome with large and massive isolators. However, these are both expensive and obviously massive, (expensive to support and transport). An intelligent isolator selection process must therefore balance the isolation requirements, with the environment of the machine. For example, a machine in a traditional factory would need better isolation equipment, but the factory would have the capability to accommodate a massive machine. Likewise, a machine in an office setting would need less vibration isolation, and consequently could be lighter, which would be helpful in installation of the machine.

4.6 Synopsis

The major result of this chapter was the improved performance of existing micro-milling machines. This is required to answer the secondary research question of how existing mechanical design performance can be improved further. This is a fundamental step towards coupling mechanical and command design for micro-milling machines. By the application and evaluation of the command shaping scheme on an existing micro-mill, the performance was improved and the shortcoming of the current systems discovered.

The development of techniques for use on existing machines builds the framework for the design procedures presented later in Chapter 8. Specifically, several key results of this chapter further the combined design in the following ways:

- Micro-mill dynamic behavior is similar to other machines. This similarity allows techniques for micro-mill design to be expanded to other machines.

- The positioning system of micro-mills are unaffected by the low magnitude cutting

forces. Therefore, the cutting forces can be ignored in the positioning system design process.

- Since input shaping techniques are effective on existing micro-mills, they should also be effective on the next generation of micro-mills.

- Experience with micro-mills enabled design criteria and performance measures necessary for the design selection to be codified. These measures and criteria are important in any micro-mill design selection.

Each of these results will directly aid the development of micro-mill mechanical and command designs, but also create an example case for generic mechanical and command design.

CHAPTER V

SPATIAL TRAJECTORY FOLLOWING WITH COMMAND SHAPING

In the previous chapter, input shaping was successfully applied to the tracking of simple trajectories on micro-mills. These traditional trajectories were simple straight line motions. However, manufacturing machines often require the accurate tracking of very complex trajectories. If input shaping can be tailored for use with complex trajectories, then the performance of manufacturing machines, specifically micro-mills, can be improved even further. This chapter will show techniques for tracking spatial trajectories using standard input shapers. The resultant improvement in tracking using existing mechanical designs advances the overall goal of combined design by showing what mechanical parameters allow for fast motions.

This chapter focuses on the use of traditional input shaping implementation, not the command selection shapers of the previous chapter for three reasons. First, the command selection shapers are limited by the attainable acceleration and speeds. Second, the command selection shapers do not deal well with damping, and thirdly, they cannot be convolved with any arbitrary command input. Remembering that the motivation for the command selection shapers was the use with simple controllers, an argument can be made that a system designed for complex trajectory tracking will have a controller with significant capabilities, thereby allowing the use of traditional input shaping structures.

5.1 *Trajectory Tracking Classification*

The tracking of trajectories can be divided into three main areas: spatial tracking, temporal tracking, and spatial/temporal tracking. This chapter focuses on the tracking of spatial trajectories while the other two subjects will be covered in Chapter 6. Each of these areas can benefit from the simple use of input shapers as described in Section 3.3.1; however, advancements are needed in order to use input shaping to track very fast trajectories.

5.1.1 Spatial Tracking

Spatial tracking is the geometric difference between the desired position of a machine and its actual position. For example, a micro-mill might need to cut the desired path in X and Y shown in Figure 5.1. However, the machine's actual response might differ from the desired. The difference between these curves is the spatial tracking error. This error would lead
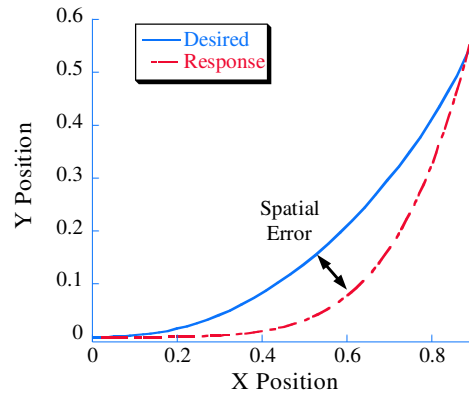
Figure 5.1: Example of Spatial Trajectory Tracking.
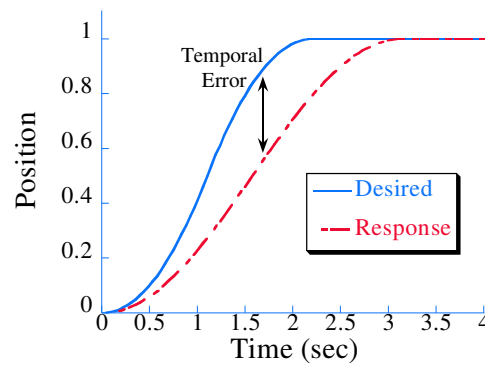
Figure 5.2: Example of Temporal Trajectory Tracking.

to form error in the produced part; and therefore, its minimization is important to micro-milling, as well as other motion applications. In all tracking application speed is important. Spatial error is particularly influenced by the speed of the move, where typically the faster the motion, then the larger the spatial error. However, spatial trajectories only require an overall duration of the move as opposed to the time specificity imposed by temporal tracking.

5.1.2 Temporal Tracking

Temporal Tracking is attempting to follow a position and time profile simultaneously. These time/position profiles define positions in the workspace along with the time to be at those positions. An example of such a trajectory and its tracking error is shown in Figure 5.2. Note that the figure only depicts one spatial dimension, because when times are specified,

tracking error can occur in only one spatial dimension. The tracking of temporal trajectories is important in many machines where exact locations at specific times are needed. Temporal tracking's importance only grows as speeds are increased, since it is a more in depth approach to trajectory tracking. In the specific case of micro-milling, motions profiles need to be followed in order to avoid cutting related problems. However, micro-mills typically are faced with the larger problem of spatial/temporal tracking.

5.1.3 Spatial and Temporal Tracking

Spatial and temporal tracking is attempting to follow a trajectory in time and in more than one spatial dimension. It is the coupling of multiple temporal tracking problems together. When multiple temporal trajectories are combined together, the individual temporal errors combine to form spatial errors. Consider a milling machine like the one described in Chapter 4. If this machine is in the wrong place in the X-axis, the Y-axis could be tracking perfectly, then the resulting part would still be the wrong shape. However, if the temporal trajectories of each axis are tracked well, then minimal spatial error will exist. These temporal issues will be discussed further in Chapter 6.

5.1.4 Trajectory Speed Through Trajectory Frequency Ratio

Tracking error both spatial and temporal is directly related to the speed of a motion. The higher the speed through a trajectory, the more difficult it is to follow. To quantify the speed of a desired trajectory, the trajectory frequency ratio can be used. The trajectory frequency ratio is the relationship between the frequency of the desired command and the frequency of the system, and in the S-curve case it is given by:

$$R_{freq} = \frac{\omega_{sys}}{\omega_{command}} = \frac{T_{des}}{T_{sys}} \tag{5.1}$$

Conversely, the trajectory frequency ratio can be defined as the relationship between the shortest duration components of the trajectory and the period of the system. A trajectory component being a constant, acceleration or velocity portion of the trajectory. The lower the trajectory frequency ratio, the faster the motion and thus more difficult to track.

For spatial trajectories in particular, the trajectory frequency ratio is related to the time of the overall move by:

$$R_{freq} = \frac{T_{traj}}{T_{sys}} \tag{5.2}$$

where T_{traj} is the duration of the move. For some complicated trajectories this overall move time will be substituted with duration of a move component. These trajectory components are discussed in the next section.
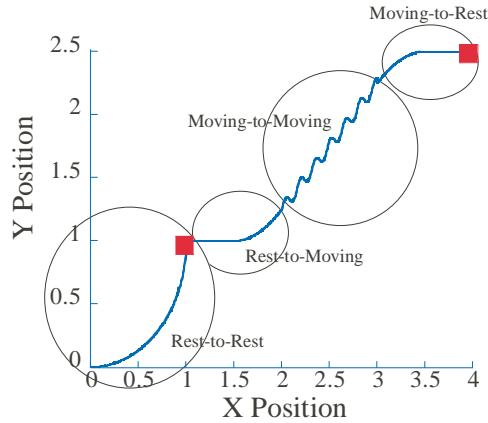
Figure 5.3: Two Axis Spatial Trajectory Component Breakdown.

5.2 Two Dimensional Trajectory Characterization

A preliminary step in tracking a wide range of trajectories is to characterize the trajectories that might be encountered. These trajectories can then be combined to form larger trajectories. If these trajectories can be input shaped effectively, then the shapers could be combined to shape complex motions. An example of how to break down a complicated two-axis trajectory into its components is shown in Figure 5.3. The squares on the figure represent complete halts to motion. breaking down a complicated motion into its components needs to consider these stops in particular, as they are obvious breaks between trajectory components. Figure 5.3 shows the four types of trajectory components:Rest-to-Rest, Moving-Rest, Rest-Moving, and Moving-Moving . Each of these components is discussed in detail in the following sections.

5.2.1 System Model

Before the performance of any tracking approach could be studied, a representative system needed to be selected. One system that exhibits spatial tracking problems is the two degree of freedom uncoupled oscillator. Figure 5.4 shows a diagram of an undamped symmetric oscillator in X and Y. This system will be used as a test case for all the multi-axis tracking techniques presented in this chapter. This system exhibits unwanted vibration for simple motions. For example, the tracking of a trajectory composed of three straight line segments is shown in Figure 5.5 The tracking of this command could be improved. Simply convolving an input shaper with this desired command and using that to drive the system will significantly improve the response. However, tracking error will still exist.

126
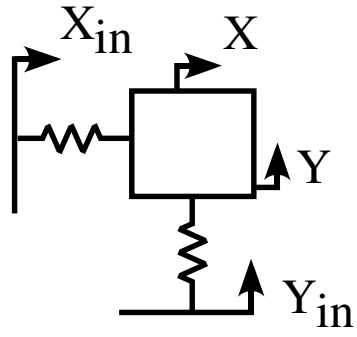
Figure 5.4: Multi-Axis System Model.
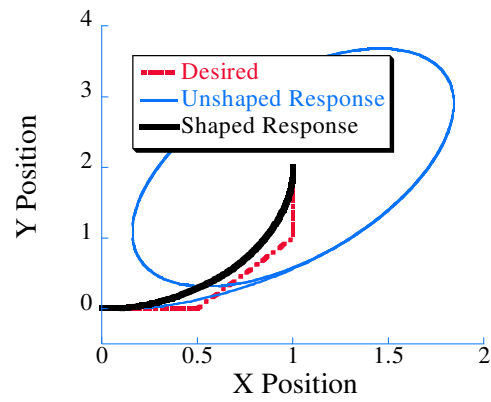
Figure 5.5: Multi-Axis Move Following Error.
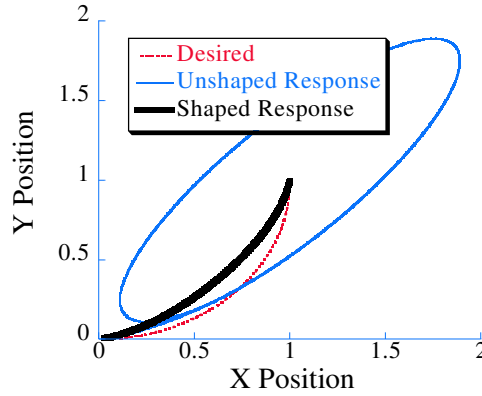
Figure 5.6: Stop-Stop Motion in 2 Axis with Error.

5.2.2 Trajectory Components

5.2.2.1 Rest-to-Rest

The most common motion is the rest-to-rest motion. Here both axis start and finish with zero velocity. This was the first type of motion made in Figure 5.3. A specific rest-to-rest motion is shown in Figure 5.6 for an arc with these zero velocity conditions. Without shaping the tracking is unacceptable. Even with input shaping, the tracking error can be large for fast moves. For one axis trajectories, the S-curve approach could be used in tracking this type of motion.

5.2.2.2 Moving-Rest

Another common trajectory component is the moving-stop motion where the system starts at a constant velocity and after completing some motion stops. This would be useful if attempting to string many smaller trajectory components into a larger trajectory in conjunction with the stop-moving component discussed next. Figure 5.7 shows such a command where an initial velocity in the X direction leads into an arc in X and Y. Both the shaped and unshaped trajectories deviate from the desired. In the one-axis case, the acceleration approach discussed previously could be used for tracking. For the trajectory shown in Figure 5.3, a moving-rest motion is used to complete a portion of the trajectory initially moved by a rest-moving component. The moving-rest component is typically combined with the rest-moving component, although intermediate, moving-moving, trajectory components can be used.
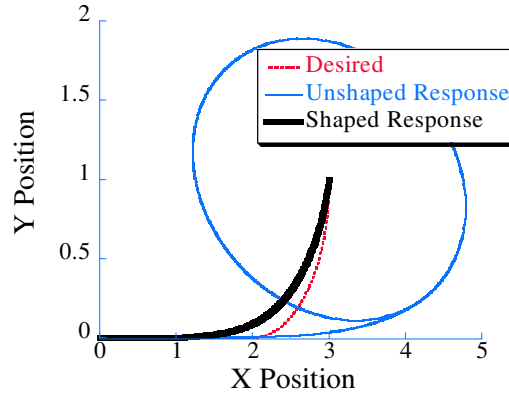
Figure 5.7: Moving-Rest Motion in 2 Axis with Error.
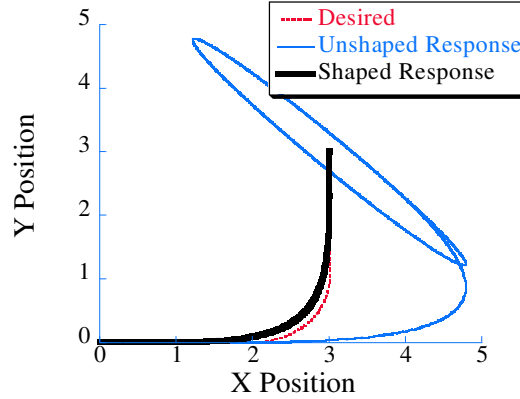
Figure 5.8: Moving-Moving Motion in 2 Axis with Error.

5.2.2.3 Rest-Moving

The rest to motion case is the same as the moving-rest case discussed previously, just in reverse. If a rest to moving component was used to describe the beginning of a long complex trajectory, then the ending could be a moving-stop trajectory component as was demonstrated in Figure 5.3.

5.2.2.4 Moving-Moving

Often the middle of long trajectories, the moving-moving motions have velocities at both the beginning and end of trajectories. Figure 5.8 shows this type of motion with initial velocity in X and a final velocity in Y with and without shaping. This type of motion can have unwanted deviation in both the shaped and unshaped case as was shown in Figure

5.8. Figure 5.3 depicts a more complicated moving-moving trajectory. However, the basic principles are the same. One important characteristic about the moving-moving component is that it can always be subdivided without changing the component type. This flexibility allows the trajectory component selection to be altered to work best with whatever tracking approach is utilized.

5.3   Modified Acceleration Approach

A possible approach to the problem of spatial tracking is to simply move slowly. Slowly moving systems will not deflect significantly and therefore can track spatial trajectories exactly. However, speed is typically an issue in machine usage, and therefore for faster motions requiring spatial tracking traditional input shaping like that employed in the previous section can be used. When traditional input shaping does not yield acceptable spatial tracking, then the modified acceleration approach can be used [88].

One possible solution for the tracking of complex trajectories is to alter simple commands until they result in accurate tracking. This approach is used here to improve the tracking of the model of Figure 5.4. As an example case, the tracking of a quarter circle in a fixed time will be considered. While a quarter circle is not an extremely complicated trajectory, it is complicated by the addition of one feature not addressed before. The quarter circle has continuously varying acceleration and jerk. Also the quarter circle is a common trajectory for manufacturing equipment, and therefore, it needs to be tracked well. A reasonable command to give the system is the desired trajectory as the input:

$$X_{in} = cos\left(t - \frac{\pi}{2}\right) \tag{5.3}$$

$$Y_{in} = sin\left(t - \frac{\pi}{2}\right) + 1 \tag{5.4}$$

This leads to unacceptable trajectory tracking as is shown in Figure 5.9 for fast motions.

5.3.0.5   Procedure of Modified Acceleration Technique

A similar approach to the tracking of S-curves in one axis will be used for the tracking of multiple axes. That is a simplified trajectory will be shaped and sent to the system as opposed to shaping the desired trajectory. One solution for this simplified trajectory is to drive the system with simple shaped bang-bang acceleration commands. These commands are essentially position S-curves; however, they are altered directly in the acceleration domain for clarity of parameter variation. Figure 5.10 diagrams a bang-bang acceleration profile and its resultant position and velocity components.

Figure 5.11 shows an example bang-bang acceleration command and the important parameters that will be adjusted for improved tracking. Once the bang-bang commands are specified, then they will be shaped using a ZV input shaper and used to drive the system.
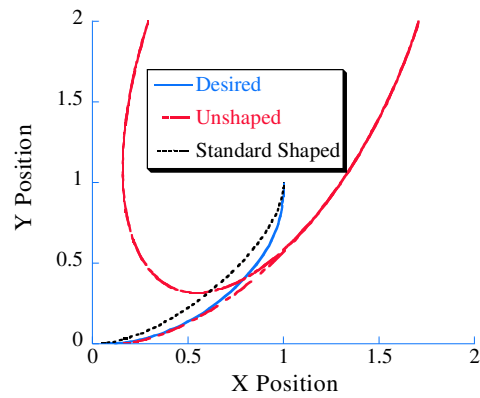
Figure 5.9: Quarter Circle Tracking.
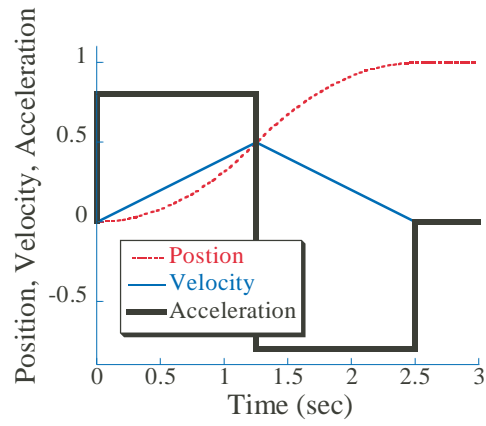
Figure 5.10: Bang-Bang Acceleration, Position, and Velocity Corollary.
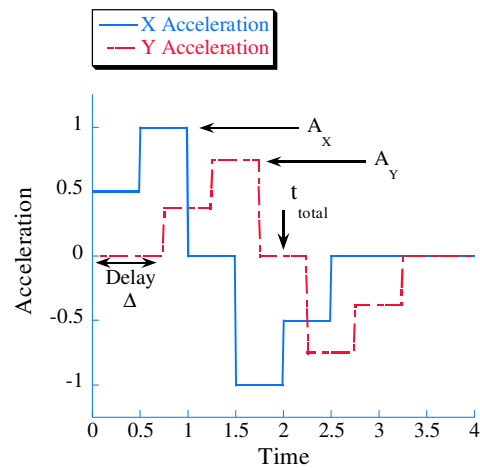
Figure 5.11: Bang-Bang Input Parameters.
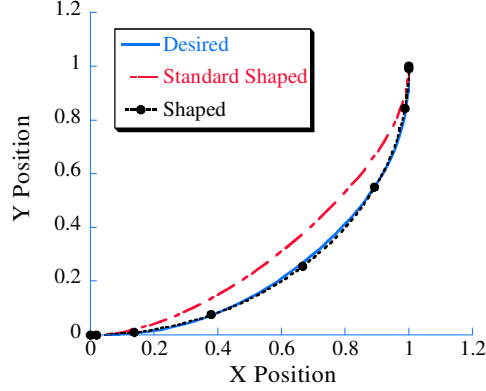
Figure 5.12: Modified Acceleration Quarter Circle Tracking.

The first parameter of the acceleration command relates the acceleration in each axis. These parameters must also comply with any maximum overall acceleration constraints on the machines. These accelerations are defined by the acceleration ratio R_{accel} as the percentage of the total acceleration of the move corresponding to the X-Axis acceleration:

$$R_{accel} = \frac{A_x}{A_x + A_y} \tag{5.5}$$

Another dimensionless parameter, the delay ratio, R_D, determines the time offset between the motions of the different axes. This allows the moves to include straight line motion in one axis, as well as more complicated curves. The delay ratio is defined as delay duration divided by the total move time:

$$R_D = \frac{\Delta}{t_{total}}. \tag{5.6}$$

where Δ is the time between when the first axis begins to move and the second axis starts moving, and t_{total} is the duration of the baseline X axis bang-bang command.

By altering these two ratios, the motion can be completed with a trajectory frequency ratio of 0.3 and with minimal tracking error as shown in Figure 5.12. Figure 5.13 shows how the input and the output of this system differ. Note that the deflection in the system causes the output that track the trajectory. Therefore, the inputs are plant dynamic specific.

5.3.0.6   Single Parameter Impact

The bang-bang commands that are shaped with a ZV shaper and then sent to the system can produce a wide range of trajectories if the delay and the acceleration are changed intelligently. By only altering a either of the parameters, the result of changing the bang-bang commands has an intuitive effect on the response, so reference commands can be easily created to provide excellent trajectory tracking.
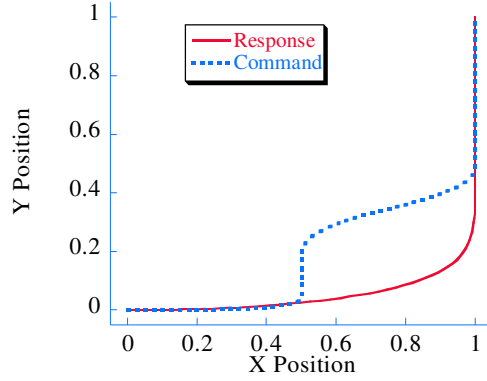
Figure 5.13: Modified Tracking Command.
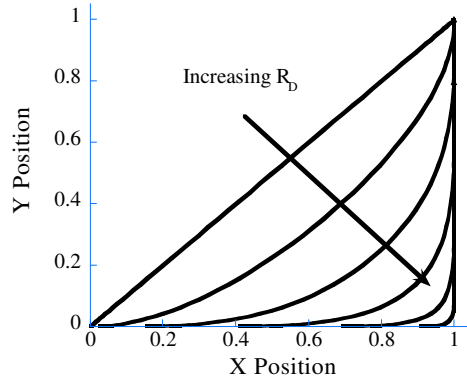
Figure 5.14: Delay Variation Effect.

By altering only the delay ratio, R_D, symmetric trajectory curves can be produced. Figure 5.14 shows how increasing the delay R_D produces a sharper corner. Note that with no delay, a straight line is produced since the X and Y axis have the same input and thus respond identically for the symmetrical case. By choosing the appropriate delay, the arc shaped responses that were shown in Figure 5.14 can be generated.

This approach of rounding the corners can be beneficial to the machine motion since a square corner in a trajectory forces the machine to come to a complete stop. By rounding the corner of an X-Y command the machine vector velocity can be maintained and the process speed thus increased over the square corner. If the square is required for the trajectory, then input shaping alone can improve the performance of this move, as was shown in [255]. The techniques developed here are applicable not only to simply rounding corners but to producing any curved trajectory that is symmetric about the position midpoint of the
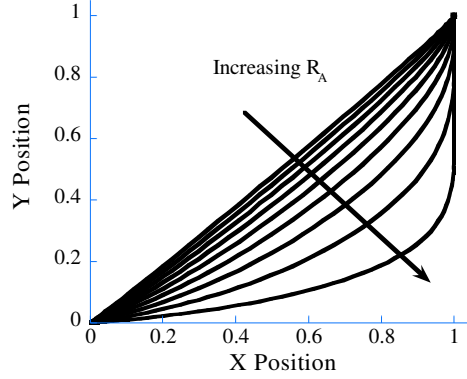
Figure 5.15: Acceleration Variation Effect.

trajectory.

If an asymmetric arc is desired in order to produce a more complicated trajectory such as an ellipse, then only the acceleration ratio, R_{accel}, between the X and Y directions can be altered. Figure 5.15 shows how altering the acceleration ratio can change the response. For $R_{accel} = 0.5$, *i.e.* the X and Y accelerations are the same, the response is a straight line.

A low trajectory frequency ratio, or the nondimensional measure showing the speed of the move, is the reason that the traditional method of input shaping does not work well here. However, if the trajectory frequency ratio is changed, then the resulting trajectory from a given R_{accel} and R_D values will change as well. Figure 5.16 shows how the response with a 0.5 acceleration ratio and 0.25 delay ratio changes with the trajectory frequency ratio. The larger the trajectory frequency ratio or the slower the move, then the more curvature in the trajectory, up to a maximum point around $R_{freq} = 1$ where curvature no longer increases.

5.3.0.7 *Multi-Variable Impact*

The effects on the modified acceleration technique's responses by altering only one variable is simple. However, if multiple variable ratios are utilized simultaneously, then the resultant curves are more complicated, specifically the symmetric nature of the curves is gone. For example, the dashed curve in Figure 5.17 shows a command with a delay ratio of 0.34 and acceleration ratio of 0.95.

In order to classify the response in Figure 5.17, four variables, *X Scale*, *Y Scale*, *X Center*, and *Y Center*, are used. The variables define the midpoint of the curve in X and Y (X and Y Center), as well as the time the curve travels only in the X and Y direction, (X Scale and Y Scale respectively). A variety of trajectories can be described with these 4

134
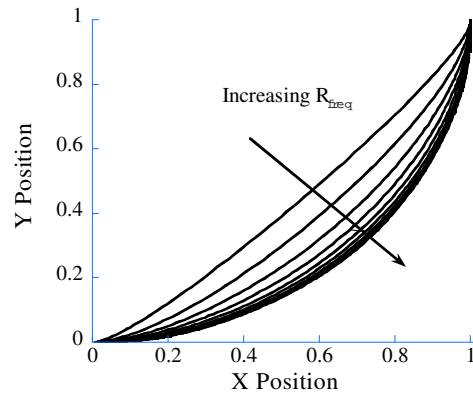
Figure 5.16: Trajectory Frequency Ratio Effect.
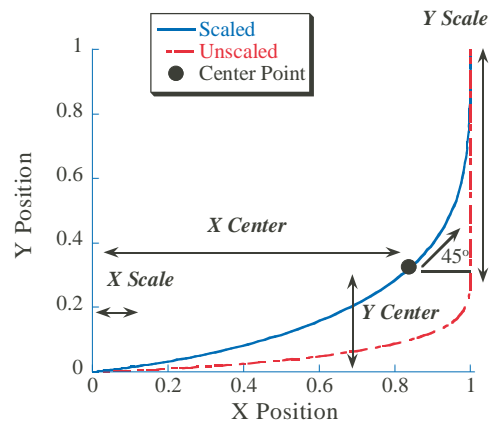
Figure 5.17: Modified Acceleration Response Classification.

variables. Once these parameters are known for a desired trajectory, then they can be used by the bang-bang generator to select the appropriate delay and acceleration ratios. Note that in the following, only trajectories including a 90° turn are considered in this section, due to the complexity of the technique. Other techniques will be presented later in this chapter for dealing with other curves.

In order to track a curve in two axis, the following procedure should be used which relies on characterizing the curve so that the correct bang-bang parameters can be chosen:

1. Classify desired trajectory with *X Scale*, *Y Scale*, *X Center*, and *Y Center*).

2. Define duration of desired trajectory, which fixes R_{freq}.

3. Determine range of R_{accel} and R_D values which meet desired *X Scale*.

4. Use *Y Scale* to select specific R_{accel} and R_D values from *X Scale* subset.

5. Check to see if resultantc *X Center* and *Y Center* are acceptable, if not, change R_{freq} and return to step 2.

The procedure will be used to determine the bang-bang profile parameters needed to track the desired trajectory in Figure 5.17.

The first step in the process of determining the values of R_D and R_{accel} needed to follow a curve begins with the determination of *X Scale* and *Y Scale* of the desired trajectory. This classifies the trajectory based on the desired motion along each of the primary axes. *X Scale* and *Y Scale* are the percentages of the move distance in each direction where the curve follows the axes. *X Scale* and *Y Scale* in Figure 5.17 show that the dashed response is straight along the X axis for only a short distance, while the *Y Scale* is large showing that the desired trajectory is straight along the Y axis for a longer distance. The result is that the *X and Y Scale* values are 0.0039 and 0.32 respectively.

Once the scaling values are known, then the curvature of the trajectory must be classified by using the center point. In order to decouple the center values from the scale values, the desired trajectory is first normalized before *X and Y Center* are determined. This normalization by *X and Y Scale* produces a scaled curve, which for the example is also shown in Figure 5.17 by the solid line. This process ensures that any scaled curve will begin at the same point and end at a different yet constant point, thus decoupling the scale values from the center values. Once the response has been scaled, the response's curvature can be classified by its center point. The center point is the point on the curve where the tangent line is at 45°. This point's X and Y coordinates in the scaled curve, *X Center* and *Y Center*, along with the scaling parameters allow the complete characterization of the desired trajectory. In the example the *X and Y Center* values are 0.95 and 0.2 respectively. Once these variables are known for the desired trajectory, the next hurdle is finding which
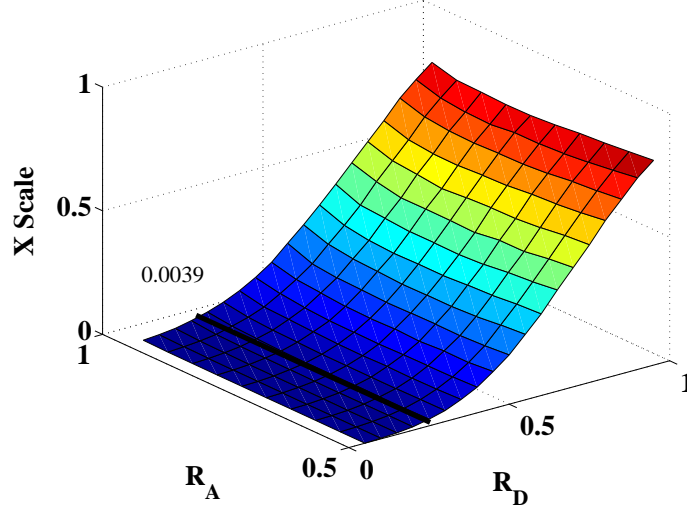
Figure 5.18: Modified Acceleration *X Scale* Dependence.

bang-bang profile parameters, R_{accel} and R_D, will act in conjunction with the ZV input shaper to produce accurate tracking. The ZV input shaper reduces the vibration after the move is complete.

The next step is to determine the duration of the move, since for any particular trajectory frequency ratio, R_{freq}, and move distance, the attainable curves are limited. Here only one move distance is considered, although the technique is the same no matter the move distance.

For a particular trajectory frequency ratio, in the example case 0.3, the attainable scaling values are limited and are a function of R_D and R_{accel}. Figure 5.18 shows how on the bang-bang profile parameters relate to *X Scale*. Note how the X scale is dependent primarily on the delay ratio. This can be seen more clearly for the simple case in Figure 5.15 where the response remains on the X axis for the same distance independent of the changes in acceleration ratio. The example required an *X Scale* value of 0.0039, which is possible with a range of R_D and R_{accel} values and is depicted as the solid line on Figure 5.18.

The *Y Scale* value like the *X Scale* value varies with both the acceleration and delay ratio. This relationship is shown in Figure 5.19. Figures 5.18 and 5.19 can be used when the desired trajectory classification parameters, *X Scale* and *Y Scale*, are known in order to determine the appropriate R_D and R_{accel} values. In the example case, the subset in bang-bang profile parameters produced by the *X Scale* values is further reduced to specific values of $R_D = 0.34$ and $R_{accel} = 0.95$ shown by the dot on Figure 5.19. For these two values the center location is fixed. Therefore, if different center locations are required, then a new trajectory frequency ratio should be considered.

The same procedure for finding the R_D and R_{accel} values from scale classifications can be done for desired center locations. Figures 5.20 and 5.21 show the center positions dependence on R_D and R_{accel} for the 0.3 trajectory frequency ratio. If the acceleration ratio
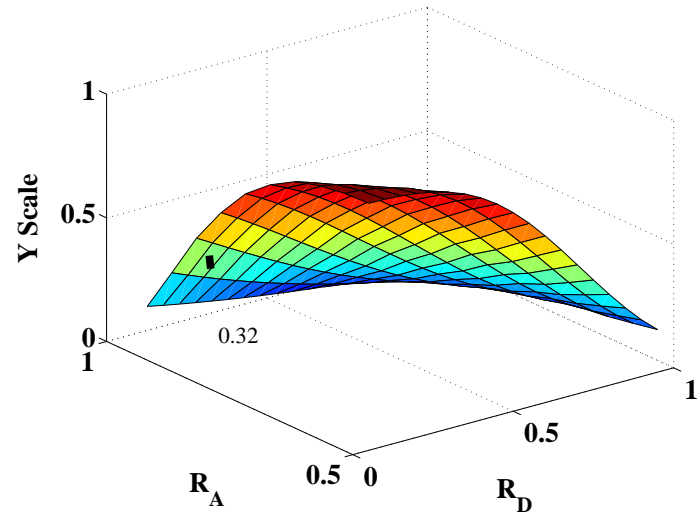
Figure 5.19: Modified Acceleration *Y Scale* Dependence.
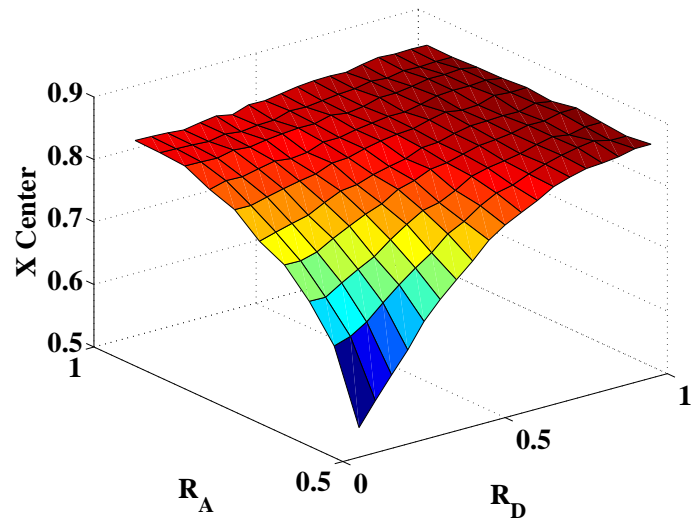
Figure 5.20: Modified Acceleration X Center Dependence.
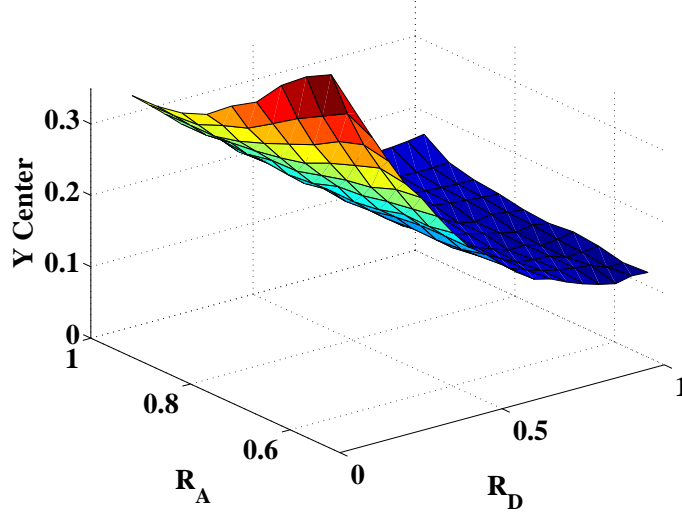
Figure 5.21: Modified Acceleration Y Center Dependence.

is 0.5, (the acceleration of X and Y are equal), then the center values are the same for X and Y as in Figure 5.14. These four Figures 5.18-5.21 can be used together to determine what curves are attainable for a given move distance and trajectory frequency ratio.

Previously, the specific relationship between the scale and center values for a given trajectory frequency ratio was mentioned. Therefore, it is also important to study the direct effects of changing the trajectory frequency ratio. For the case of an acceleration ratio fixed at 0.5 different trajectory frequency ratio can be considered The results will always yield symmetrical curves. If the delay ratio is changed while altering the trajectory frequency ratio, then the symmetric response can be characterized by the *X center* position in Figure 5.22.

5.3.0.8 Modified Acceleration Evaluation

The modified acceleration technique for tracking arcs has several key advantages. The main advantage is that it is a combination of simple techniques that can be explained as just change these three parameters, (R_{freq}, R_{accel}, and R_D), until the desired response occurs. Specifically one or two variables can be altered with logical consequences to reach the desired arc trajectory. This is possible because it relies on existing input shapers and simple initial commands. The other main benefit is the variety of arcs that can be created.

There are, however, a few disadvantages to this technique. The first is that it is spatially based, *i.e.* positions in space are specified and a total move time. If the time/space relationship is required at all locations along the trajectory, this technique will not reach that goal. The other main disadvantage is that it is a coupled technique, the trajectories have to be designed together. This results in the ability to achieve a multitude of rest-to-rest moves, while not being able to link them together. Finally, it is derived only as a two
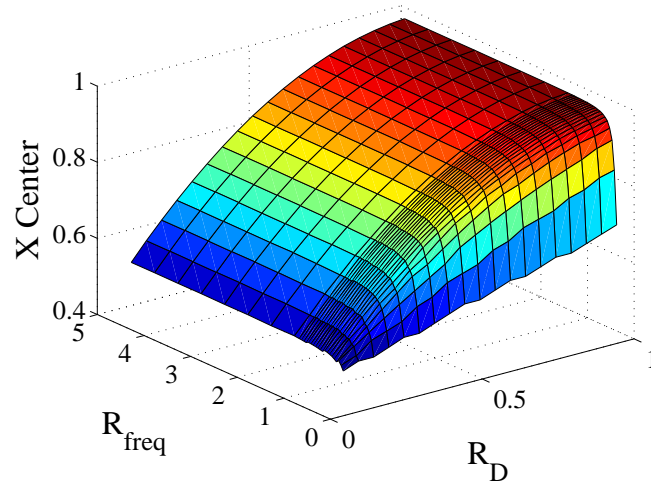
Figure 5.22: Frequency and Delay Ratio Effect.

degree of freedom technique. To deal with these shortcomings a new technique building on the S-curve and acceleration tracking of Sections 6.2 and 6.3 has been developed.

5.4 Synopsis

Many machines must make accurate motions in space. To accomplish this goal, oscillations in the machine must be limited. The use of input shaping to eliminate these oscillations can still allow for spatial tracking error. Therefore the techniques presented in this chapter are necessary to track spatial trajectories accurately with input shaping. The modified acceleration approach leads to improved positioning performance of existing flexible hardware. The improvement for existing machines is key to the secondary research question of how the performance of existing mechanical designs can be improved.

The modified acceleration approach of this chapter also impacts the larger goal of combined design by providing techniques to make flexible systems have the same trajectory tracking components as stiff systems. Therefore, the ability to track trajectories accurately is no longer an advantage of heavy/stiff designs over lightweight/flexible options.

CHAPTER VI

TEMPORAL AND SPATIAL TRAJECTORY FOLLOWING WITH COMMAND SHAPING

If a system deviates from its desired path, then the result is often poor quality output. For micro-mills in particular, any deviation from the desired trajectory can lead to a multitude of problems. For example, if the micro-mill is moving in only one axis, but does not follow the prescribed motion, then the surface finish can be adversely effected due to varying feedrates. The same deviation when extended to two axes can result in the part being the wrong shape. Most concerning is damage to the tool itself from tracking error. Excessive deviation from the desired trajectory can result in dangerously large material removal, if the cutting tool moves into an incorrect section of the workpiece, which can snap the cutting tool. These trajectory tracking problems grow as speed increases, therefore for the throughput of micro-milling machines to be successfully increased, all of these issues tracking the desired motion must be addressed. The solution to each of these issues will further improve the performance of existing machines. In so doing, the benefits possible from combined design will be increased.

The previous chapter dealt with improving the spatial tracking characteristics of flexible system through input shaping. This chapter seeks to not only prevent spatial deviation from the desired motion but also deviation related to time. The major steps in addressing temporal tracking error are to characterize the error and common solutions, develop approaches suited for one spatial dimension, and finally develop a technique that can be used for multiple spatial dimensions.

6.1   Temporal Trajectory Tracking Error

Temporal tracking error is the deviation in both the time and the position of a machine. The differences of temporal tracking and spatial tracking were discussed in depth in the Chapter 5, Section 5.1. Figure 6.1 shows an example of temporal tracking error. The temporal tracking error is defined as the difference at any specific time between the desired and actual position of a machine. This tracking error is influenced by the system dynamics, the command shapers if applicable, and the commands themselves. In this study of temporal tracking the system dynamics and the commands will be limited, while changes to the command shaper will be investigated.
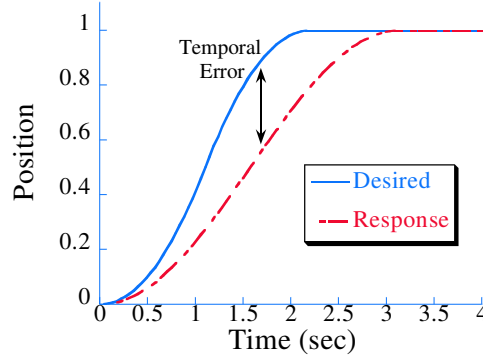
Figure 6.1: Example of Temporal Trajectory Tracking.
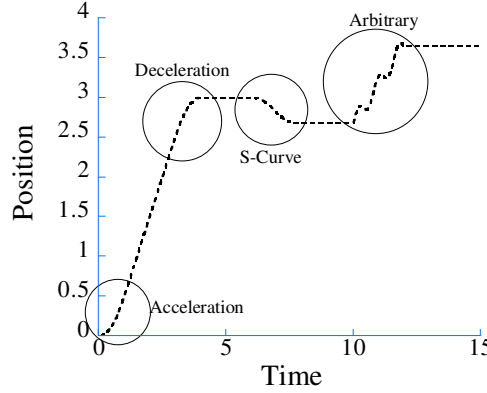
Figure 6.2: Trajectory Component Examples.

6.1.1 Complex Trajectory Decomposition

The baseline system for the initial analysis of temporal tracking is a second-order oscillator with minimal damping. Other more complicated systems will also be considered later in this chapter. The tracking of both the second-order and the more advanced systems is effected by the types of trajectories that need to be tracked. Often these trajectories are complicated and consist of many components. Figure 6.2 shows an example one-axis temporal trajectory. This trajectory can be decomposed in a number of ways, but the three that will be directly addressed here are the S-curve, the acceleration/deceleration, and the arbitrary components. The S-curve components involve constant acceleration and deceleration with no coast time in between. For trajectories requiring a coast, it is advantageous to break the trajectory into acceleration, coast, and deceleration components and track those independently. This is because no tracking is required in a coasting portion. The final component is

Table 6.1: Tracking Discussion by Components.

Component	Technique	Section
S-Curves	Three-Impulse Trajectory Tracking Shapers	6.2.1
	Four-Impulse Trajectory Tracking Shapers	6.2.2
	Multi-Axis S-Curve Technique	6.4
	Optimal Command Design	6.1.4
Accel/Decel	Acceleration Three-Impulse Trajectory Tracking Shapers	6.3.2
	Acceleration Four-Impulse Trajectory Tracking Shapers	6.3.2
	Multi-Axis S-Curve Technique	6.3.2
	Optimal Command Design	6.1.4
Arbitrary	Optimal Command Design	6.1.4
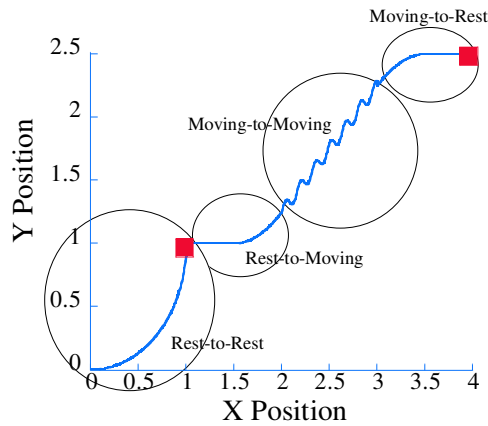
Figure 6.3: Trajectory Component Example In Two Axes.

an arbitrary trajectory element, which must be addressed by more complicated techniques particulary optimal command design. The arbitrary components do not necessitate constant accelerations and will be the most difficult to track. Table 6.1 detail each of the these components and the approaches and sections that will discuss them.

A similar compartmentalized approach will be discussed for multi-axis trajectories. Chapter 5 dealt extensively with the issue of dividing a large trajectory into smaller trajectory components for spatial trajectories. Figure 6.3 shows an example two axis trajectory and some possible ways to divide it into trajectory components. The trajectory can be viewed in total as a rest-to-rest motion, or into a set of components, beginning with a rest-moving component, then a moving-moving component, and finishing with a moving-rest component. The decomposition of the entire trajectory into these component is dependent on the methods used. The tracking of this sort of multi-axis trajectory will be discussed later in Section 6.4.
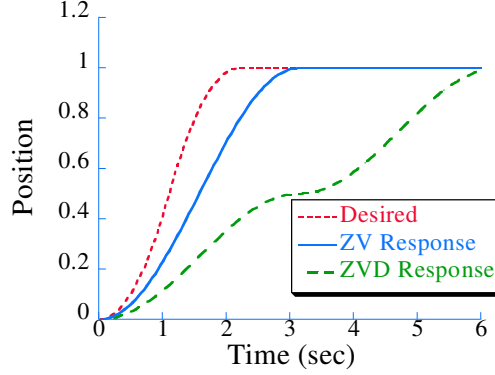
Figure 6.4: Example Trajectory Error.

6.1.2 Investigation of S-Curve Temporal Tracking Error

On particularly common trajectory component shown in Figure 6.2 is the S-curve. If input shaping is attempted as a method for tracking S-curves, often deviation will occur. When an input shaper modifies a desired trajectory, no longer is the trajectory tracking only a function of the system dynamics. Instead it is composed of both dynamic and input shaped effects.

6.1.2.1 Input Shaping's Effect on System Input

Input shaping by its nature modifies the input to a system. Figure 6.4 shows the response of an aggressive S-curve input when it is convolved with ZV and ZVD input shapers and sent to the system. If just the desired response was used as an input to the system, then it would oscillate excessively. Notice that response differs from the desired in both the shape and the duration when the ZV shaper is used; specifically, the slope of the command is reduced, and as a result the duration is increased. For the ZVD case, the slope of the response is reduced even further, and the duration is near tripled over the desired trajectory.

6.1.2.2 Location of Error

As mentioned previously input shaped responses decrease the slope and increase duration of the desired trajectory. These modifications lead directly to tracking error. Figure 6.5 diagrams these errors when the desired S-curve convolved with a ZV shaper drives the system, where T_{des} and T_{shap} are the desired and shaped durations respectively. The period of the system, T_{sys} is shown. The relationship between this period and the durations of the command and shaper will later be used as a measure of the aggressiveness of the trajectory. Finally, E_{abs} is the total absolute error between the shaped and unshaped trajectories.

Minimizing the error between the desired and the shaped command could be important
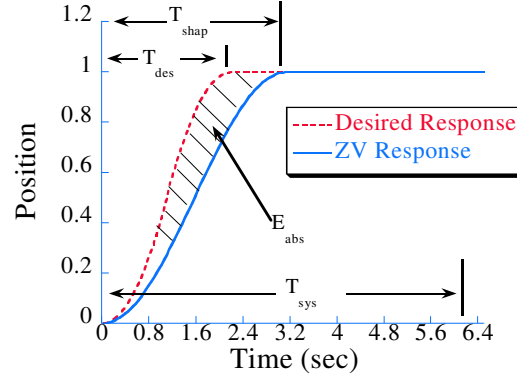
Figure 6.5: Labelled Trajectory Error.
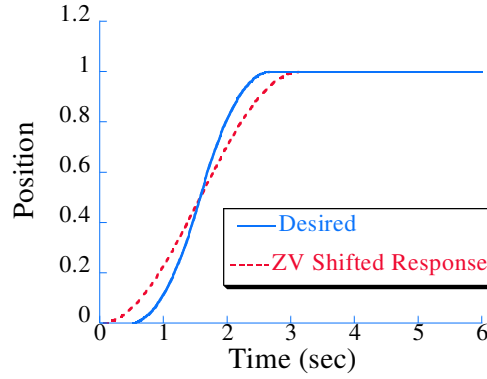
Figure 6.6: Shifted Input Response Comparison.

to the performance of the machine, if exact trajectories are needed as in the case in micro-milling. Any deviation from the desired trajectory can lead to form errors in the part. If this minimal error is needed, then a time shift correcting some of the difference between T_{des} and T_{shap} can be introduced. For example, the start of the shaped input to the system can be shifted back in time half the duration of the shaper. While, this approach is not always possible due to motion constraints, when feasible, time-shifting the input can improve the tracking significantly. Figure 6.6 shows the improvement in the response tracking if this shift is introduced. This process or any other process where a desired trajectory is altered before being shaped is called preshaping. In this example, the preshaping does significantly reduce the error in the tracking. However, significant tracking errors still exist, and the preshaped command must start before the desired trajectory, which may not be a practical solution. Although preshaping is an acausal technique, it can be implement if flexibility exists in the start time of the desired trajectory. If the start time is delayed, then the
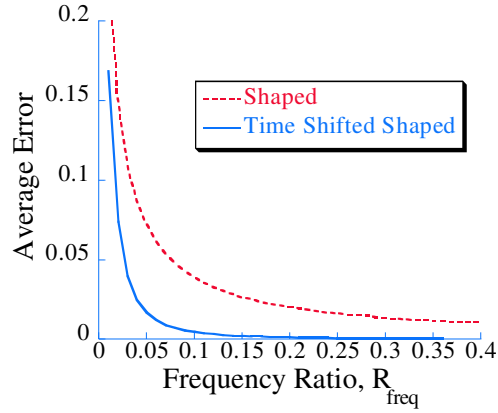
Figure 6.7: Trajectory Frequency Ratio Impact on ZV Maximum Following Error.

acausal preshaping technique could be introduced in the same manner as derivatives are implemented in discrete control algorithms.

6.1.3 Trajectory Frequency Ratio Impact

The trajectory frequency ratio is used to measured the speed of a motion and was presented in the previous chapter in Section 5.1.4. Their the trajectory frequency ratio was defined as the relationship between the duration of the command and the duration of the system or:

$$R_{freq} = \frac{\omega_{sys}}{\omega_{command}} = \frac{T_{des}}{T_{sys}} \tag{6.1}$$

For example, a low trajectory frequency ratio is a fast motion. Since the trajectory frequency ratio is a measure of speed, input shaping approaches performance over changing trajectory frequency ratios are important.

For a given command, there exists a decaying relationship between the trajectory frequency ratio and the shaped tracking error. Figure 6.7 shows how the trajectory frequency ratio affects the average tracking error for both the ZV-shaped and the time-shifted shaped, where the average tracking error is the mean difference between the shaped response and the desired trajectory during the move. Of course the time shifted average error is less, however it still degrades for low trajectory frequency ratios like the unshifted. This figure shows that for fast, low trajectory frequency ratio moves, time shifting the command will improve tracking up to a certain point near a $R_{freq} = 1$. After that point, accurate tracking is no longer possible with simple time shifting.

The choice of input shaper also has a major impact on the ability to track fast trajectories. Figure 6.8 compares the ZV, ZVD, and UMZV shapers performance at low trajectory frequency ratios. Notice that the shorter the duration of the shaper, the better the tracking.
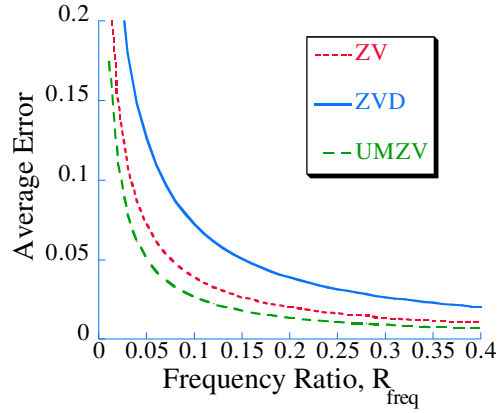
Figure 6.8: Trajectory Frequency Ratio Impact on Shaper Average Following Error.

The UMZV being the fastest shaper outperforms the ZV and ZVD shaper at all trajectory frequency ratios particularly those less than one. Shorter shapers improve the tracking for two reasons. First, the larger impulses found in short shapers allow for greater slope congruity between the shaped and unshaped. Second, the shorter duration shapers also minimize the duration difference in the commands, thus reducing tracking error.

By selecting short duration input shapers and combining them with time-shifted or preshaped commands, tracking can be improved at lower trajectory frequency ratios. However, the time-shifted technique inherently slows the system, and without the time shifting, unacceptable tracking error will occur for low trajectory frequency ratios. Even with time-shifted command, at trajectory frequency ratios around and less than one, the tracking error is large. If these fast moves need to be followed precisely, then another technique is needed to provide for both vibration suppression and trajectory tracking.

6.1.4 1-DOF Optimal Command Design

One current solution to tracking trajectories with low trajectory frequency ratios is to move slower (increase the trajectory frequency ratio), which is often unacceptable since it will increase process time. Another solution not requiring a change in the trajectory is to use optimal command design techniques. These techniques attempt to minimize tracking error by optimizing the actual system input. This can be accomplished through either plant inversion techniques like zero-phase-error tracking control [289] or through direct optimization of the input to the system. The direct optimization technique will always yield superior results, and therefore it will be used for comparison here.

The direct optimization technique chooses the value of the input at each time step of the system. This process is computationally intensive, however it will always lead to exceptional tracking, if actuator limits are not imposed. It is accomplished by stepping through each
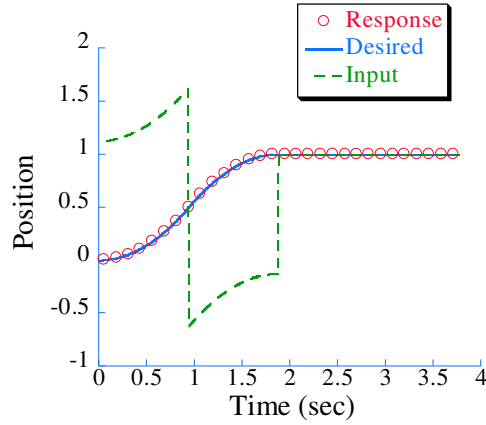
Figure 6.9: Optimal Command Design Example.
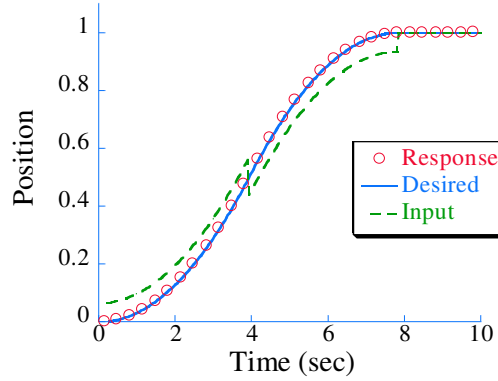
Figure 6.10: Optimal Command Design Slow Example.

time step of the command. At each time step, the input magnitude is selected so that with the combination of all previous inputs, tracking is perfect.

For a move with a $R_{freq} = 0.6$, theoretically perfect tracking is possible as shown by comparing the response and the desired trajectory in Figure 6.9. Note both the complexity and magnitude of the input. Both of these factors motivate the search for a simpler trajectory tracking solution.

For a less aggressive desired trajectory where $R_{freq} = 2.5$, optimal command design works equally well as shown in Figure 6.10. In this case the input/actuator effort is much less. The downside is that the technique required even more computation than the shorter case since more time steps were considered. This computational intensity is the primary motivation for a simpler technique. The other is a better understanding of the resultant actuator effort. By knowing what trajectory frequency ratio trajectories require excessive
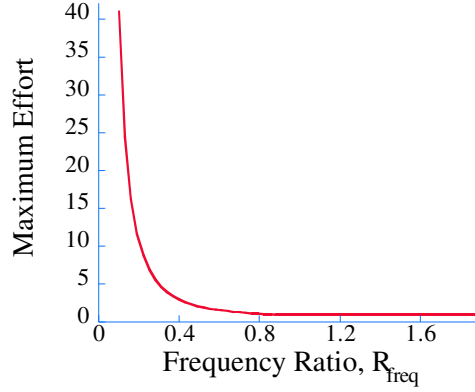
Figure 6.11: Optimal Command Design for Various Trajectory Frequency Ratios.

actuator effort, those types of trajectories can be avoided or actuators selected appropriately. Figure 6.11 shows how the maximum actuator effector for the optimal command design technique decreases with the trajectory frequency ratio. At trajectory frequency ratios less than 0.5, the actuator effort is greater than one or greater than the desired acceleration of the system. Of course, the actuator effort can be constrained in the optimization at the cost of poorer tracking and more computational complexity.

6.1.5   Analytical Description of Error

One approach to determining the best shaper for trajectory tracking is to analytically derive a tracking error cost function in terms of the shaper parameters. This cost function could then be used to select the best shaper parameters. The problem with this technique is that the equations for tracking error become complicated quickly. The obvious solution is to determine the tracking error numerically. This technique, however, involves similar complexity to the optimal command design technique; therefore, a simpler to implement technique is needed. Nevertheless, a study of the analytical error can offer two important insights. First is the aforementioned complexity, while the second is a solid understand of how trajectory frequency ratio will effect tracking error.

6.1.5.1   *Trajectory Frequency Ratio Effect on Analytical Error of Ramped Step*

Consider a desired response of a ramped step of magnitude one shown in Figure 6.12, with a ramp duration of τ_{ramp}. To track this trajectory, a new technique will be used, instead of convolving the shaper with the desired trajectory, the shaper will be convolved with a simpler command, in this case a step. The result shown in Figure 6.12 is somewhat adequate tracking, with the added benefit of a much simpler implementation process. Also when this approach is used, the time-shifting of the shaped command might not be necessary.
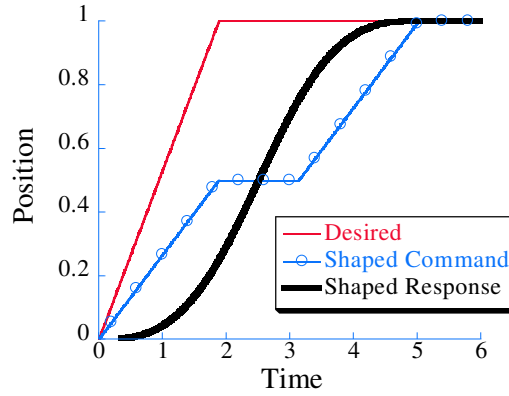
Figure 6.12: Ramped Step Trajectory.

If a the ZV shaper is used, then the integral of the absolute difference between the desired ramped step and actual shaped-step response can yield the total tracking error E_{total}. There are two cases to consider. In the first case the shaper is longer than the desired trajectory, or $R_{freq} > 0.5$. The other case is if the shaper is shorter than the desired trajectory, or $R_{freq} < 0.5$.

For the specific case of $\tau >$ shaper duration, $R_{freq} > 0.5$, the total error is:

$$E_{total} = \frac{\tau}{3} - \frac{5\tau^2}{3} + \frac{5\tau^3}{3} + \frac{-2\tau\pi + \pi + \tau^2\pi}{\omega} +$$
$$\frac{\cos(\tau\omega)\tau + 4\tau - 2}{\omega^2} + \frac{-\cos(\tau\omega)\pi + \pi + 2\frac{\sin(\tau\omega)}{\tau} - 5\sin(\tau\omega)}{\omega^3} \tag{6.2}$$

and for the case where $\tau <$ shaper duration, $R_{freq} < 0.5$, the total error is:

$$E_{total} = \frac{\tau}{3} - \frac{5\tau^2}{3} + \frac{4\tau^3}{3} + \frac{2\tau^2\pi + \pi - 2\tau\pi}{\omega} + \frac{5\tau - 2 - \pi^2\tau}{\omega^2} +$$
$$\frac{-\sin(\tau\omega)\cos(\tau\omega) + 2\frac{\sin(\tau\omega)}{\tau} + \frac{1}{3}\pi^3 - 4\sin(\tau\omega)}{\omega^3} \tag{6.3}$$

These equations represent a simple desired response, a ramped step, and a simple input, a ZV shaped step. For more complicated trajectories and shapers, often the error is not obtainable in closed form.

These error functions offer insight into the effectiveness of the ZV shaper for tracking a variety of ramped trajectories. Figure 6.13 shows how the total absolute error changes with trajectory frequency ratio. Notice that for the ramped step, the ZV shaper tracks best at a trajectory frequency ratio near 0.6. Also notice that the slope in Figure 6.13 is gentle around $R_{freq} = 0.6$. Therefore, the ZV shaper will work well for ramped commands near this frequency ratio as well. The error is smaller for low trajectory frequency ratios merely because the input is essentially a step in these locations and the command duration

150
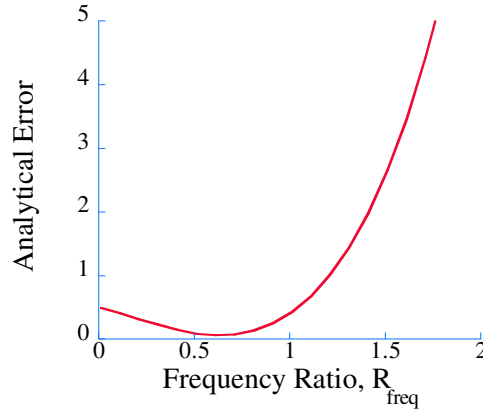
Figure 6.13: Total Error versus Trajectory Frequency Ratio for a Ramped Step Motion.

is shorter. In fact, the error for the ramp case approaches the tracking error for a step as the trajectory frequency ratio approaches zero:

$$E_{total} = \frac{\pi}{2\omega} \tag{6.4}$$

These trends dealing with trajectory frequency ratio and error hold for other more complicated motions. However, the technique of analytically calculating this error is not practical for motions more complicated than a ramp, and therefore other techniques must be used in shaper design.

6.2   Tracking Specific S-curves

One of the most common trajectory profiles is the S-curve. The S-curve can be by itself or part of a large trajectory like the one in Figure 6.2. In either case, a technique was developed to track S-curves in time and space accurately, so that the procedure could be extrapolated to deal with many common trajectories. This technique focusses on fast motions, where the duration of the motion is smaller than the period of the system, a trajectory frequency ratio less than 1. Here the same approach is used as was used for the ramped step, *i.e.* a simple shaped step is input to the system to track a complicated S-curve. The resultant output to the shaped step is a smooth motion due to the dynamics of the system. The benefits are the similar to the ramped step case and are fourfold: a simpler implementation, an avoidance of command delays, a decoupling of the shaper and the input from the desired response, and a minimization of design variables. The shaped step input is much simpler to implement than a shaped S-curve, since complex changes in the input are eliminated. The delay is avoided by the correct selection of shaper parameters. Also, by sending a shaped input into the system, the direct impact of shaper parameters on the output response can be seen. If the shaper was convolved with something more complicated than a step, then
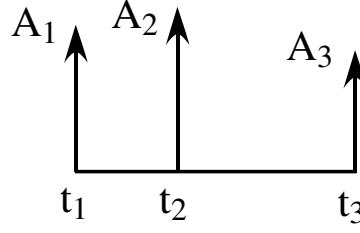
Figure 6.14: Three-Impulse Shaper Diagram.

the shaper parameter impact on the response would not be clear. Finally, this shaped step input is preferable to the shaped S-curve due to its lack of trajectory design variables (slope, acceleration, jerk, *etc.*).

The technique involves deriving the input shaper for a fixed duration, then testing different shaper parameters to determine which shaper best tracks the S-curve best. The baseline system used in this tracking investigation is the undamped second-order oscillator. More complicated plants will be considered in Section 6.3.4.

6.2.1 Trajectory Tracking Three-Impulse Input Shapers

The first input shaper developed to track S-curves was an arbitrary three-impulse shaper, that is a three impulse shaper with variable impulse times and magnitudes. Figure 6.14 diagrams this shaper, which has three impulses of magnitudes A_1, A_2, and A_3 at times t_1, t_2, and t_3, where t_1 is always equal to zero. The vibration response of an undamped second-order system of frequency ω to these impulses convolved with a step after time t_3 can be described by the total vibration from each impulse. This vibration from each impulse convolved with a step is defined by:

$$V_1 = A_1\omega \sin\left(\omega t\right) \tag{6.5}$$

$$V_2 = A_2\omega \sin\left(\omega(t - t_2)\right) \tag{6.6}$$

for $t > t_2$:

$$V_3 = A_3\omega \sin\left(\omega(t - t_3)\right) \tag{6.7}$$

for $t > t_3$, where the total response is given by:

$$V_{tot} = V_1 + V_2 + V_3 \tag{6.8}$$

This response will be identically zero if the following identities are satisfied using the same procedure as was described in Section 3.3.1. First, the impulses must sum to one:

$$A_1 + A_2 + A_3 = 1 \tag{6.9}$$
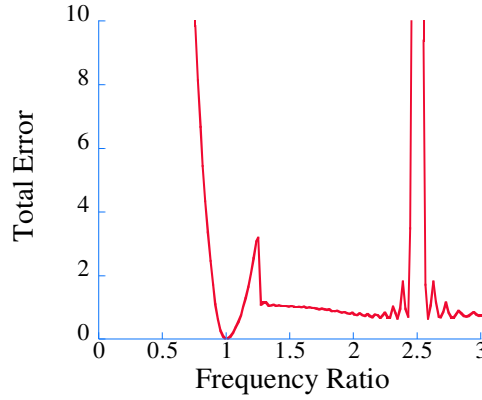
Figure 6.15: Three-Impulse Shaper Error.

The impulses must also satisfy the zero vibration equation (3.13):

$$A_1 + A_2 * \cos t_2 * \omega + A_3 * \cos t_3 * \omega = 0 \tag{6.10}$$

and:

$$A_2 * \sin t_2 * \omega + A_3 * \sin t_3 * \omega = 0 \tag{6.11}$$

so that the command does not induce any oscillations into the system. This represents three equations and five unknowns. The solution strategy is to select the duration of the impulse sequence, t_3, and then test a discrete set of values of t_2 such that $0 < t_2 < t_3$ to determine which one has the best S-curve tracking performance when convolved with a step input.

To determine which duration is best for the shaper, simulated trajectory errors from the desired S-curve were calculated for a variety of cases. For example, consider a desired trajectory whose duration is four times the period of the system. The best possible total error for any t_2 can be plotted versus the normalized duration *i.e.* shaper duration divided by command duration, or trajectory frequency ratio. The result shown in Figure 6.15 is that minimum tracking error occurs when the shaper duration is the same as the duration of the desired trajectory. The observation follows logically since the least tracking error will occur when the command and the desired output occur at the same time. Anomalies do occur in Figure 6.15 due to the nature of the algorithm. The sharp changes at frequency ratios of 1.25 and 2.5 occur because different local minimums become the global minimum. From this simulation and others, it was concluded that the best shaper to use for tracking an S-curve would have a duration equal to the duration of the S-curve. This reduces the unknowns in the shapers design to t_2, A_1, A_2, and A_3, with three equations (6.9-6.11). The result is one unknown to select for the best tracking performance.

This specific rule of setting shaper duration equal to desired command duration created the trajectory tracking input shaper. This three-impulse shaper diagramed in Figure 6.14
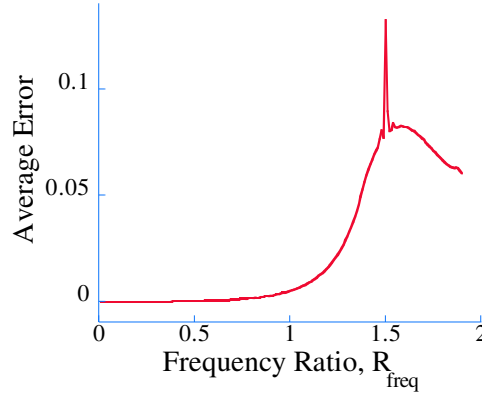
Figure 6.16: Three-Impulse Shaper Error over Trajectory Frequency Ratios.

is design using the following procedure to track an S-curve profile with a shaped step as input.

- t_3 is set equal to the command duration

- t_2 is varied and the resultant shaper parameters (A_1, A_2, and A_3)determined from Equations (6.9-6.11)

- The total tracking error is calculated for each t_2

- The shaper parameters (A_1, A_2, A_3, and t_2) resulting in the lowest tracking error are selected

The resultant shaper is capable of tracking any trajectory with a trajectory frequency ratio less than one with minimal error. Figure 6.16 shows how the average tracking error for a fixed system changes with command duration or trajectory frequency ratio using this trajectory tracking shaping technique. Notice that error is larger for trajectory frequency ratios greater than one. For these type of motions, traditional techniques of shaping the desired output and using that as the input to the system should be chosen. The spike occurring at $R_{freq} = 1.5$ is due to the discrete nature of the design choices. This spike can be eliminated by considering a finer discretization of t_2. However, even without the spike, this region is not well suited for the three impulse shaper as will discussed in Section 6.3.5.

The individual shapers that give the results of Figure 6.16 are explored further in the following sections. Interestingly, many common input shapers were found to be subsets of the trajectory-tracking shaper. In the following sections, the solutions for various trajectory frequency ratios and their similarities to existing shapers will be documented. Also note that the three impulse technique will be compared to other approaches later in Section 6.2.3.
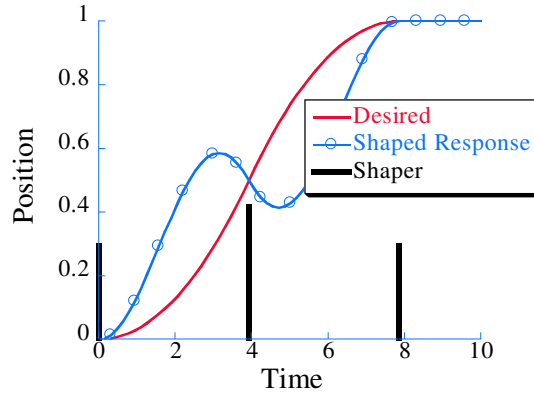
Figure 6.17: Three-Impulse Shaper and Response for $R_{freq} > 1$.

6.2.1.1 Trajectory Duration > T

The first case of shaper design for trajectory tracking is for slow moves or moves where the desired response duration is greater than the period of the system. In this case, as was shown in Figure 6.16, the performance is not ideal. However, it is important to document the performance of this three impulse trajectory-tracking shaper in this region so that the selection of alternative schemes can be made objectively. Consider the case of a trajectory frequency ratio of 1.25 shown in Figure 6.17. The trajectory tracking three-impulse shaper was derived using the previous technique and the solution with the minimum error is shown in the figure. The tracking of desired command is poor for the transient region, however, zero residual vibration occurs. Another important attribute is that the shape of the impulse sequence is similar to the ZVD shaper. In fact, the trajectory-tracking shaper approaches the ZVD shaper for trajectory frequency ratios of one. The conclusion illustrated by Figure 6.17 is that the trajectory tracking input shaping technique is not the ideal solution for commands with trajectory frequency ratio's greater than one. However, it does perform well in vibration suppression after the move is complete.

6.2.1.2 T/2 < Trajectory Duration < T

Shorter desired response durations are better suited for the trajectory-tracking shapers. In the region where the command duration is less than the period of the system and greater than half the period, the trajectory-tracking shapers perform well. Figure 6.18 shows the case of a trajectory frequency ratio of 0.65. Notice the improved tracking over the slower case of Figure 6.17. Another example of this range of trajectory frequency ratios is shown for the case of a trajectory frequency ratio of 0.525 in Figure 6.19. The tracking is improved further in this case. Also notice the shape of the impulse sequence. The trajectory-tracking
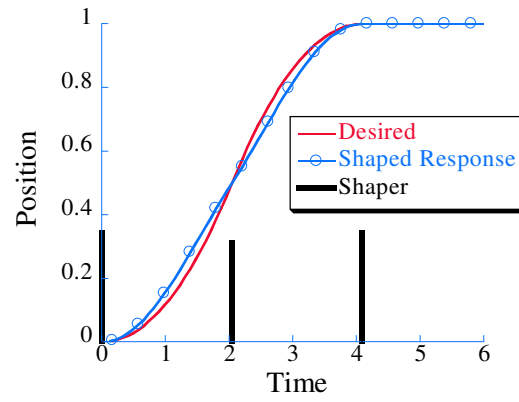
Figure 6.18: Three-Impulse Shaper and Response for $0.5 < R_{freq} < 1$.
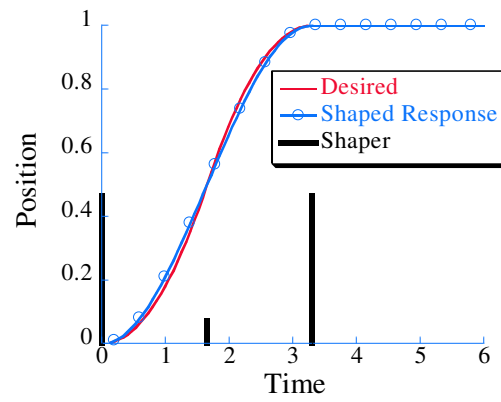
Figure 6.19: Three-Impulse Shaper and Response for $R_{freq} \simeq 0.5$.
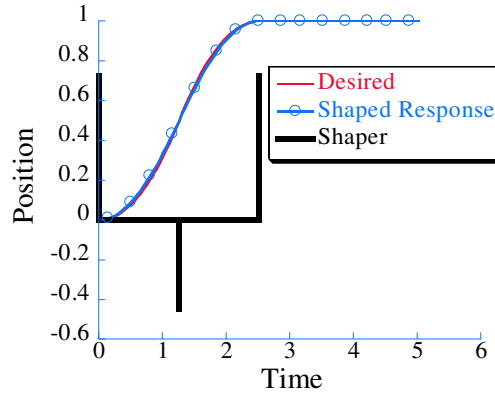
Figure 6.20: Three-Impulse Shaper and Response for $1/3 < R_{freq} < 0.5$.

shaper actually approaches the ZV shaper for a trajectory frequency ratio of 0.5.

6.2.1.3 $T/3 < $ Trajectory Duration $< T/2$

As the trajectory frequency ratio gets smaller, the trajectory-tracking shaper contains a negative middle impulse. For example, Figure 6.20 shows the three-impulse trajectory-tracking shaper also works well for a trajectory frequency ratio of 0.4.

Figure 6.21: Three-Impulse Shaper and Response for $R_{freq} < 1/3$.

The downside of the negative impulse is not first apparent in Figure 6.20. Negative shapers are more demanding on a system, requiring both positive and negative velocities. Also negative shapers often excite higher modes of vibration due to the increased acceleration and jerk.

6.2.1.4 Trajectory Duration $< T/3$

As the duration get shorter another major problem appears, impulse magnitude. For trajectory frequency ratios less than $1/3$, at least on impulse will have a magnitude greater than one. That means that the actuators must move at a greater acceleration than the commanded motion, and often this is beyond the limits of the actuator. For example the case of a trajectory frequency ratio of 0.25 is shown in Figure 6.21. Notice that the negative impulse is approximately -2.5. This motion may be impossible for the actuator to perform. This problem gets significantly more important for lower trajectory frequency ratios. The limiting case of a trajectory frequency ratio of zero would require infinite actuator effort.

Another important note in this region is the case of a trajectory frequency ratio of $1/3$. For this case the trajectory-tracking shaper is the same as the UMZV shaper discussed in Section 3.3.1. This case can be seen for trajectory frequency ratio of 0.3 in Figure 6.22.

6.2.1.5 Three-Impulse Input Shapers Parameter Variation

The shapers that result in the best tracking change depending on the period ratio for which they were designed. The time of the middle impulse, for example, typically remains centered between the first and last impulse as shown in Figure 6.23. The time of the final impulse increases linearly, since it is equal to the duration of the desired motion.

The magnitudes of impulses also exhibit some general trends as shown in Figure 6.24 and detailed in Figure 6.25. The magnitudes of all the impulses increase for low frequency
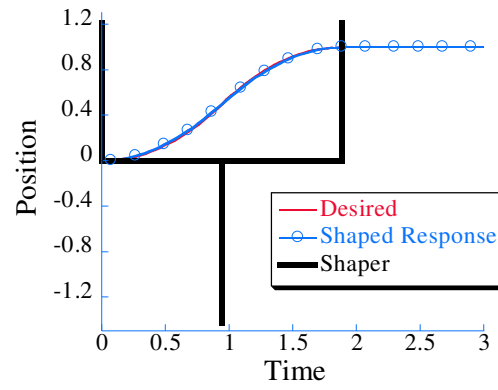
Figure 6.22: Three-Impulse Shaper and Response for $R_{freq} \simeq 1/3$.
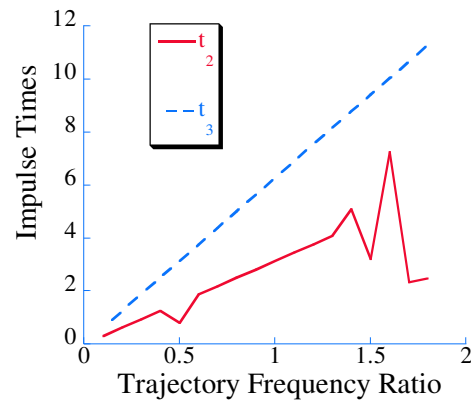
Figure 6.23: Three-Impulse Shaper Impulse Time Variation with Trajectory Frequency Ratio.
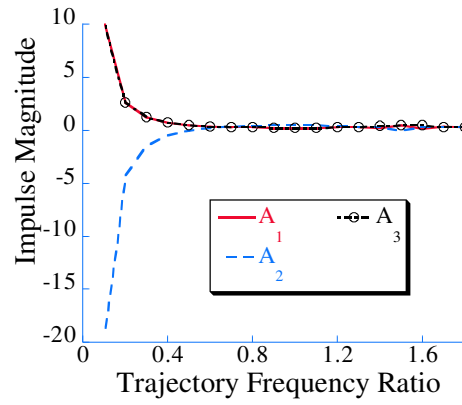
Figure 6.24: Three-Impulse Shaper Impulse Magnitude Variation with Trajectory Frequency Ratio.
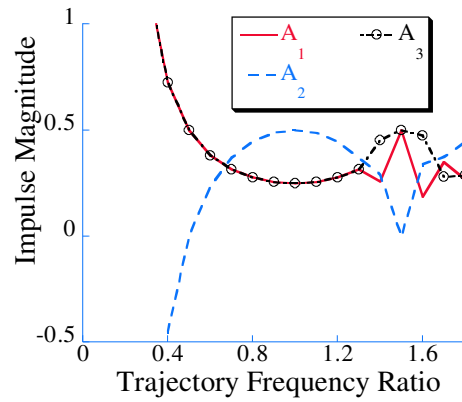
Figure 6.25: Detailed Three-Impulse Shaper Impulse Magnitude Variation with Trajectory Frequency Ratio.
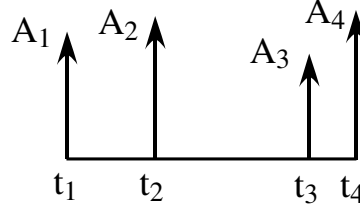
Figure 6.26: Four-Impulse Shaper Diagram.

ratio. This is due to the more effort being required to move the system quickly. Likewise, for quicker motions, a negative middle impulse is required. The issues of impulse magnitude and negative impulses will be discussed later. Also notice in Figure 6.25 like Figure 6.23, that the shaper parameters are not well behave at trajectory frequency ratios above 1.25. This region of R_{freq} also has poor tracking performance, therefore the three impulse technique is not advisable for large frequency ratios. The specific application of three impulse technique will be discussed further in Section 6.2.3.

6.2.2   Trajectory Tracking Four-Impulse Input Shapers

The previous sections detailed an input shaper design for trajectory tracking utilizing three impulses. However, this tracking can be improved by using more impulses. The tradeoff with more impulses is more complexity in the command design. The four-impulse shaper has two more variables than the three-impulse shaper, and therefore, many more possible shapers exist that satisfy the duration constraint and the zero vibration constraints. A four-impulse shaper can been seen diagramed in Figure 6.26. The variables in this case are $A_1, A_2, A_3, A_4, t_1, t_2, t_3$, and t_4, where $t_1 \equiv 0$. To begin, a second-order undamped system's response to a series of four impulses convolved with a step, forces the shaper to satisfy three constraints. The first is the amplitude of the impulses:

$$A_1 + A_2 + A_3 + A_4 = 1 \tag{6.12}$$

The other two are constraints on the vibration such that:

$$A_1 + A_2 * \cos t_2 * \omega + A_3 * \cos t_3 * \omega + A_4 * \cos t_4 * \omega = 0 \tag{6.13}$$

and:

$$A_2 * \sin t_2 * \omega + A_3 * \sin t_3 * \omega + A_4 * \sin t_4 * \omega = 0 \tag{6.14}$$

If these three equations are satisfied, then any command convolved with the shaper will induce zero vibration after the move. Furthermore, the time of the final impulse should be set equal to the duration of the command, since the result of Section 6.2.1 showed this would lead to minimal error. Due to the nature of the equations many solutions exist that satisfy all the constraints. However, satisfying these constraints is only part of the goal of these

shapers, therefore the selection between the multiple solutions will be made by trajectory tracking performance.

The problem has three equations and seven unknowns, as well as a constraint that the duration of the shaper must be equal to the duration of the desired command. Therefore, three values must be specified to find the shaper. To accomplish this, a search method is used which involves the following steps.

- Create search mesh for all possible impulse times, (t_2, t_3)

- At each node in the mesh, test several values for the first impulse magnitude

- From t_2, t_3 and A_1 compute the other shaper parameters, and find the tracking error

- Compile the results for each test case and find the shaper with the best tracking performance

This procedure allows a discrete testing of all possible shapers to find the best four-impulse shaper for trajectory following. The resolution of the discretization of the process is variable, but here it is constant. The times of the second impulse are limited to 100 discrete choices between the first and last impulse, and once the second impulse time is chosen, t_3 is further limited to 100 discrete choices between the newly defined t_2 and the previously defined t_4. Furthermore, the magnitude of the first impulse is limited to 100 discrete choices from 0.01 to 2. This is constrained only to positive numbers since all discussed trajectories require the system to move positively first. Also, the magnitude of the first impulse is limited to two to avoid actuator saturation.

This entire process could be performed much more efficiently using a numerical optimization. However, for the initial phases of its the four impulse technique's development, it is important to gain insight into all the trends in the solution which could be overlooked by simply implementing an optimization algorithm. The behavior of the variables has shown that an optimization algorithm with intelligently chosen starting point could speed this process if it were necessary.

The resultant trajectory following when this four-impulse shaper is convolved with a step input to the system for a variety of S-curve speeds can be seen in Figure 6.27. Notice that the maximum average error is low, less than 0.01 for frequencies ratios up to 2. This is much better than the results of the three shaper case that was shown in Figure 6.16 for which the maximum average error is an order of magnitude larger. The improvement is due to the extra impulse being able to further alter the command. A decision must be made by the designer whether the extra complexity of design and implementation of the four-impulse shaper is necessary for a given application.

The specific four-impulse shapers designed by this approach will be discussed in the following sections. For many cases, these four-impulse shapers mimic more standard shapers

162
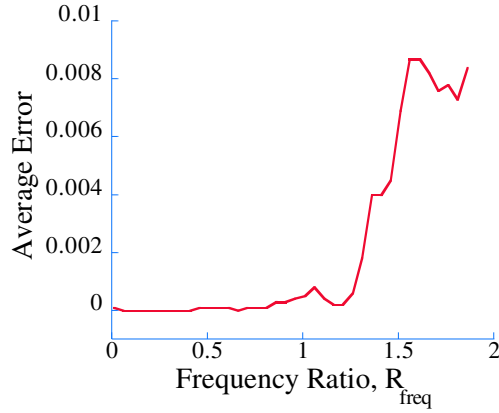
Figure 6.27: Four-Impulse Shaper Duration Error for Trajectory Frequency Ratio.
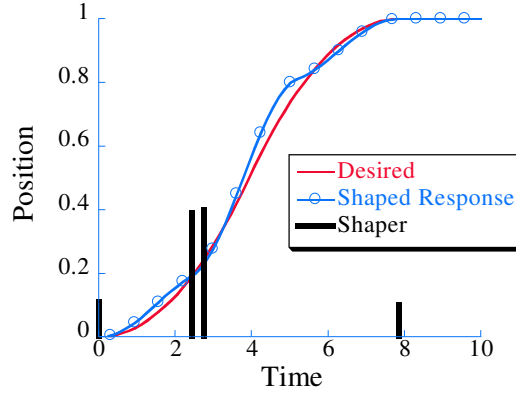
Figure 6.28: Four-Impulse Shaper and Response for $R_{freq} > 1$.

just as the three-impulse shapers did. Likewise, in some cases the four-impulse shapers are just minor variation from the three-impulse trajectory-tracking shapers. Also note that the four impulse trajectory-tracking input shapers will be compared to the three-impulse, as well as the time-shifted shaped and simply shaped later in Section 6.2.3.

6.2.2.1 Trajectory Duration > T

The limiting factor of the effectiveness of specifically designing input shapers for trajectory tracking is the speed of the motion. For some moves the improvement in tracking with this technique is not worth the extra complexity. This breakdown occurs at a trajectory frequency ratio greater than one. For example consider a trajectory frequency ratio of 1.25 whose trajectory following shaper is shown in Figure 6.28. This shaper tracks the desired
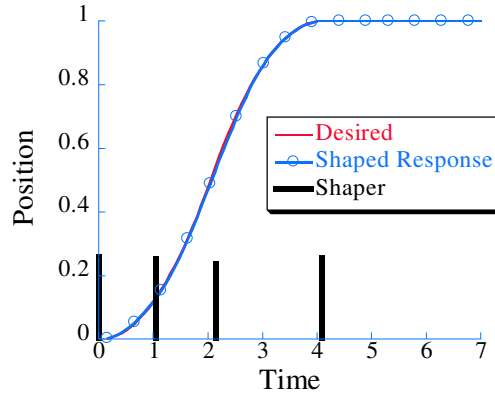
Figure 6.29: Four-Impulse Shaper and Response for $0.5 < R_{freq} < 1$.

trajectory better than the three-impulse shaper of Figure 6.17 at the larger trajectory frequency ratio, however the tracking error is still large. In comparison the three-impulse shaper This shaper does not resemble any common input shaper. Instead, trajectory following shapers near this trajectory frequency ratio rely on small first and last impulses to make minor changes in acceleration while doing most of the moving of the system with large impulse in the middle of the trajectory.

6.2.2.2 $T/2 <$ Trajectory Duration $< T$

For faster trajectories than the previous section, the four-impulse shaper design technique works better. For example, Figure 6.29 shows the trajectories for a trajectory frequency ratio of 0.65. Notice that for this case the impulses are approximately equal in magnitude and equally spaced in time. As the trajectory speeds up, the first impulse increases in magnitude to cope with the increase in initial acceleration.

While the shaper for this case does not resemble any traditional shapers, its limiting case of $T \simeq T/2$ does share similarities with a ZV shaper. Figure 6.30 shows the shaper and trajectories for the four-impulse technique for a trajectory frequency ratio of 0.525. The impulse times and combined magnitudes of the impulse pairs suggest the ZV shaper. Digitized ZV shapers can even exhibit the same impulse splitting, if no discrete time aligns with the correct continuous shaper duration.

6.2.2.3 $T/3 <$ Trajectory Duration $< T/2$

For faster motion than half the period of vibration, negative-magnitude impulses must be introduced in order to satisfy the vibration constraints. Such is the case for a trajectory frequency ratio of 0.4 which is shown in Figure 6.31. This shaper's negative impulse is greater than -1, which can be a problem for some systems in terms of actuator saturation.

164
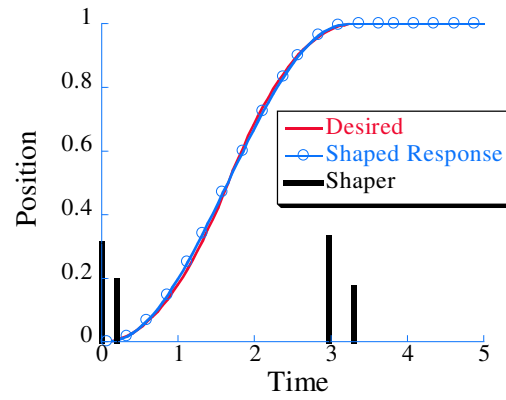
Figure 6.30: Four-Impulse Shaper and Response for $R_{freq} \simeq 0.5$.
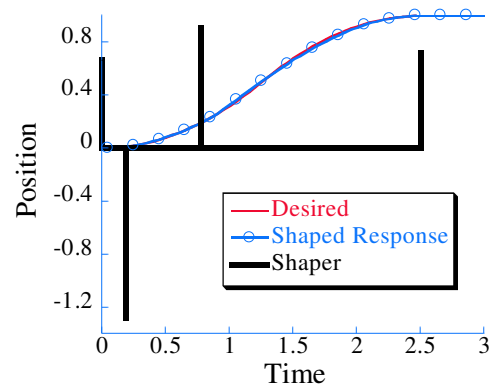
Figure 6.31: Four-Impulse Shaper and Response for $1/3 < R_{freq} < 0.5$.
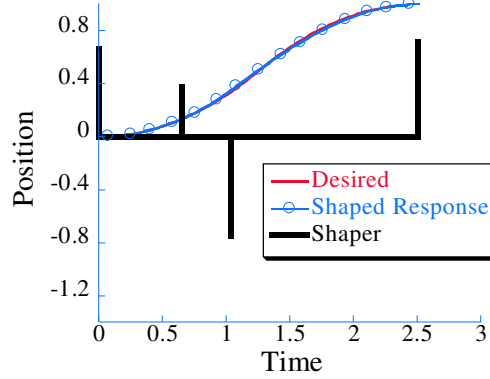
Figure 6.32: Limited Four-Impulse Shaper and Response for $1/3 < R_{freq} < 0.5$.

Moving at this speed puts increased strain on the system's actuators and therefore may not be physically possible on some equipment. This can be corrected by limiting the impulses to a maximum magnitude of 1. If this limited is imposed on the shaper design, the result for a trajectory frequency ratio of 0.4 is shown in Figure 6.32. This shaper has slight worse performance than the unlimited case of Figure 6.31; however, the lower impulse magnitudes mean less actuator effort. The magnitude limiting case will not work for more aggressive moves ($R_{freq} < 1/3$), because not solution exist for zero vibration while meeting the maximum impulse magnitude of 1.

6.2.2.4   Trajectory Duration < T/3

As trajectory duration decreases even further the shapers become even more aggressive with both positive and negative impulses having magnitudes greater than one. For example, a trajectory frequency ratio of 0.25 shown in Figure 6.33 leads to significant magnitude changes. This type of motion can be extremely harmful for some system while completely possible on others with more responsive actuators. The impulse magnitude problem is only further exacerbated as the speeds increase. In this realm the three-impulse shaper could be advantageous since its impulse are of a typically lower magnitude as was the case for the same trajectory frequency ratio shown in Figure 6.21.

The four-impulse shaper does resemble a traditional shaper, the UMZV, near a trajectory frequency ratio of 1/3. Figure 6.34 shows a trajectory frequency ratio of 0.3. While on the surface this four-impulse shaper does not resemble a typical UMZV shaper, on closer inspection it has many similarities. The first and last impulse magnitude are near one as they are for the UMZV shaper. Second, the average time of the second and third impulse is around half the shaper duration, and will get close as the trajectory frequency ratio approaches 1/3. Finally, if the two middle impulse are summed together their magnitude is

166
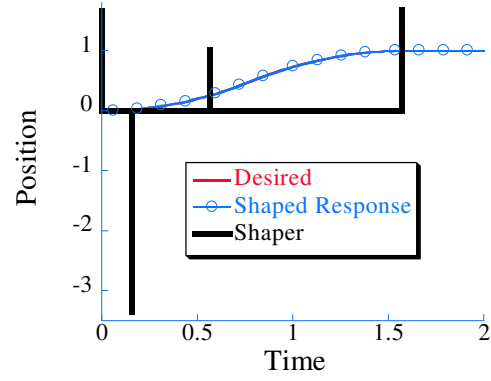
Figure 6.33: Four-Impulse Shaper and Response for $R_{freq} < 1/3$.
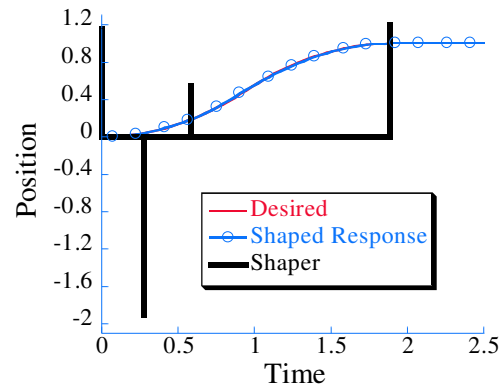
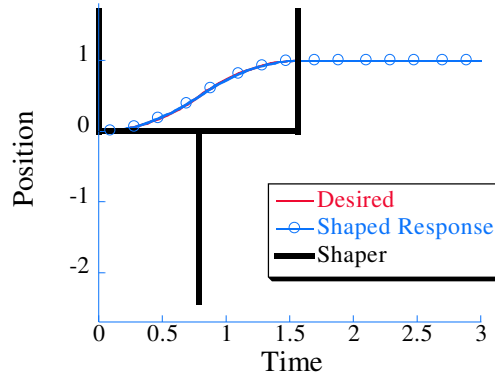**Figure 6.34:** Four-Impulse Shaper and Response for $R_{freq} \simeq 1/3$.
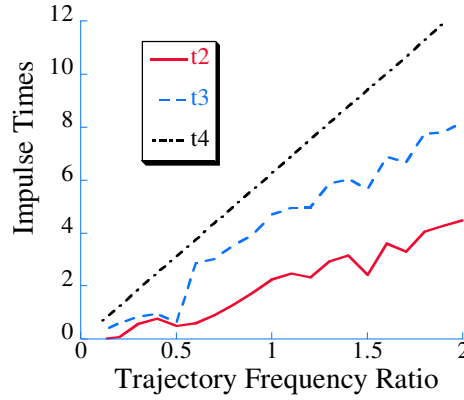
Figure 6.35: Four-Impulse Shaper Impulse Time Variation with Trajectory Frequency Ratio.

near one, the same as for the UMZV shaper.

6.2.2.5 Trajectory Design for Specific Shapers

Many of the aforementioned input shapers designed for trajectory tracking had similarities to existing shapers when their durations were equal. This leads to an interesting aside from the idea of shaper design for a specific trajectory, that is trajectory design for specific shapers. If a designer wants to work with existing shapers but still operate at high speeds, then all that designer needs to due is select trajectories with durations equal to common shapers. This choice seems obvious but since the field of input shaping coupled with trajectory design is new, it has not been a first choice in many applications. While this is not particularly useful, it would provide for a simple input shaped trajectory tracking solution.

6.2.2.6 Four-Impulse Input Shapers Parameter Variation

The four impulse trajectory tracking input shaper's performance is highly dependent on the trajectory frequency ratio for which it was designed. The impulse times vary shown in Figure 6.35. The time of the final impulse increases linearly, while the other two impulse are approximately equally spaced.

Trends also exist in the magnitudes of impulses as shown in Figure 6.36 and detailed in Figure 6.37. For the four-impulse shaper at low trajectory frequency ratios, only one impulse is negative. Also, the magnitudes of all the impulses are large for low frequency ratios. The justification is the same as for the three impulse case, *i.e.* more effort is required to move the system quickly. Unlike the three impulse case, the shaper parameters are well behaved for all trajectory frequency ratios. The four impulse techniques effectiveness compared to other approaches will be presented in Section 6.2.3.

168
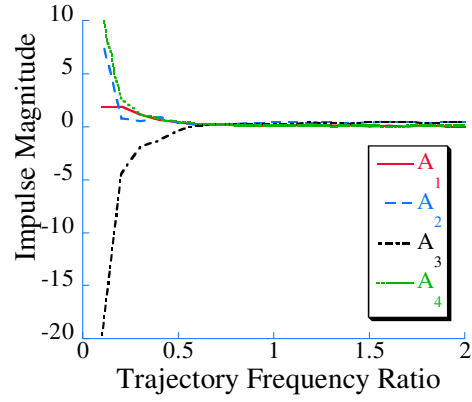
Figure 6.36: Four-Impulse Shaper Impulse Magnitude Variation with Trajectory Frequency Ratio.
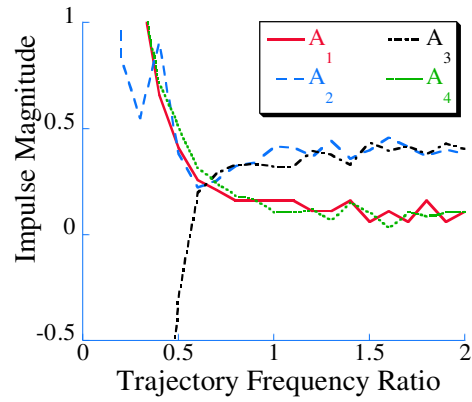
Figure 6.37: Detailed Four-Impulse Shaper Impulse Magnitude Variation with Trajectory Frequency Ratio.
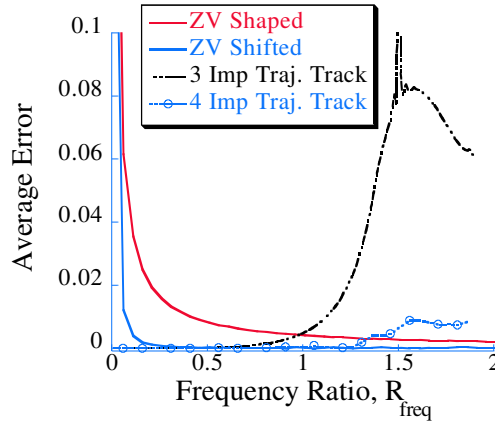
Figure 6.38: Comparison of Tracking Error Among Various Shapers.

6.2.3 Comparison to Other Shaping Techniques for Various Speeds

The previous sections detailed how to design input shapers for trajectory tracking applications. However, these trajectory tracking input shapers have limited regions where they work effectively. For the three and four-impulse trajectory tracking shapers, impulse magnitudes can be large for low frequency ratios. Also at large frequency ratios, the performance of the three and four-impulse trajectory tracking shapers degrades. In terms of performance, the opposite is true for the traditional approaches of using the shaped desired response as the input to the system, or time shifting this shaped input. A comparison of the average tracking error for all four of these techniques can be seen in Figure 6.38. Note that while the ZV Shifted approach seems effective at low trajectory frequency ratios, it introduces a delay of a quarter system period into motion. Eliminating this delay is one of the primary advantage of the trajectory tracking input shapers.

If the shifted approach is unacceptable, then Figure 6.38 shows that the three-impulse trajectory tracking shapers are preferable to traditional ZV techniques for all frequency ratios less than one. The four impulse approach is preferable to the traditional approach for larger trajectory frequency ratios, those less than 1.4. Figure 6.39 shows this relationship closer. From Figure 6.39, it can be seen that the four-impulse technique is preferable in effectiveness to the three-impulse technique for $R_{freq} > 0.5$. However, there are other considerations to be made when choosing a trajectory tracking scheme. These concerns will be discussed further in Section 6.3.5.

6.3 Acceleration/Deceleration Tracking

The previous section dealt with tracking rest-to-rest motions; however, often rest to a constant velocity or a constant velocity to rest is desired. An example of such a trajectory
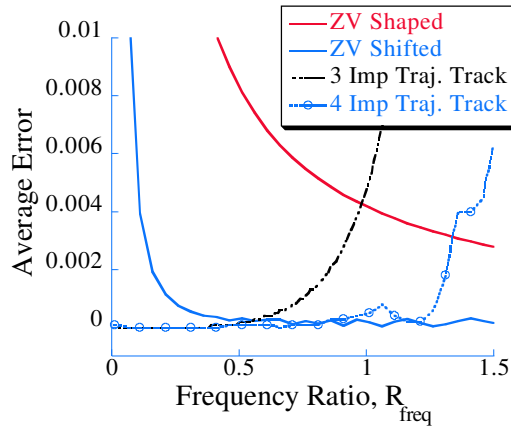
Figure 6.39: Detail of Comparison of Tracking Error Among Various Shapers.
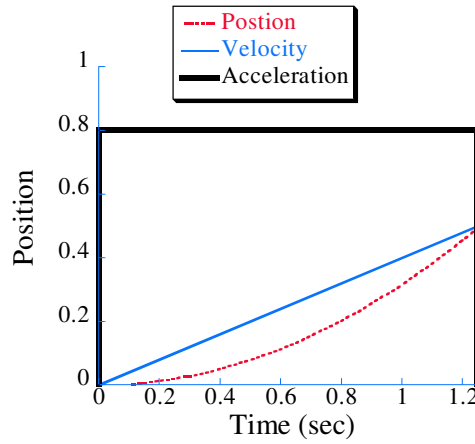
Figure 6.40: Acceleration/Deceleration Diagram.

is shown in Figure 6.40. It is called an acceleration or deceleration trajectory, because the response is simply from a pulse in acceleration/deceleration. Input shapers can be designed specifically for these types of trajectory elements as well. To demonstrate this problem consider tracking an acceleration pulse with a trajectory frequency ratio of 0.4. For acceleration and deceleration tracking, instead of using the input shaper convolved with the step change, the shaper will be convolved with a ramp. This distinction is made because of non-zero final velocity needed in the acceleration case. Figure 6.41 shows how a typical ZV shaper convolved with a ramped input changes the input trajectory. A continuous offset in position is introduced. Another solution to this problem is to preshape the command, which is also shown in Figure 6.41. While this solution effectively solves the following error, it introduces a delay into the motion. For many applications, eliminating this delay would be beneficial. Obviously any situation where speed is of utmost concern could use a new
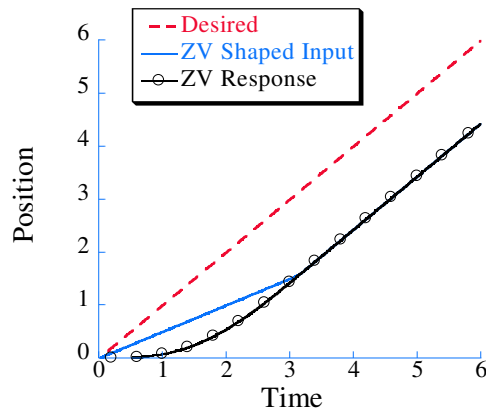
Figure 6.41: Acceleration/Deceleration Problem.

shaping scheme. Also benefiting from removing a delay in the system would be situation where many trajectory elements are strung together, such as painting robots or milling machines.

6.3.1 Acceleration Trajectory Tracking Three-Impulse Input Shapers

The trajectory-tracking shapers for acceleration and deceleration are designed in the same manner with the same goals as for the S-curve cases previously described. The difference is in the trajectory attempted to be followed. Specifically, the bang acceleration profile to reach a constant velocity is tracked. This profile is also equal to the first part of the S-curve discussed previously. In order to track this profile, the shapers are convolved with a ramp position profile with a slope equal to the desired velocity. The shaped ramped input has benefits of limited parameters, avoiding preshaping, and being simpler to implement than a shaped polynomial input. Also, here only the accelerations of the system are discussed. The same techniques can be used to design deceleration tracking shapers.

The three-impulse technique operates by fixing the shaper duration and then determining the other parameters based on tracking performance. This approach works well for a variety of acceleration durations as shown in Figure 6.42. To refresh, the trajectory frequency ratio is the duration of the acceleration divided by the period of the system. Note that the three-impulse design technique has similar performance for acceleration tracking as it did for S-curve tracking. That is, for slower moves, *i.e.* a trajectory frequency ratio greater than 1, the shaped ramp has trouble following the desired motion.

The resultant shapers design by the three-impulse technique for acceleration tracking are nearly identical to the shapers for the S-curve tracking due to the nature of the problem as the integral of the first half of the S-curve case. However, since locations and magnitudes of error are different, it is important to study several test cases.
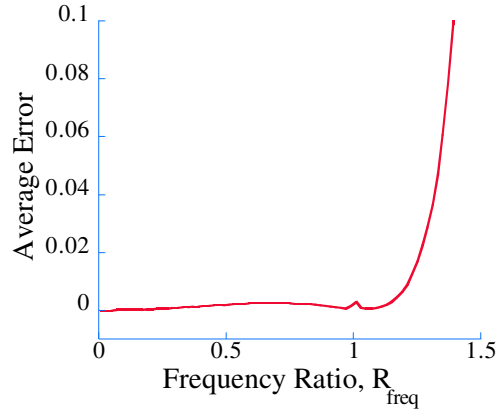
Figure 6.42: Acceleration Three-Impulse Shaper Duration Error.
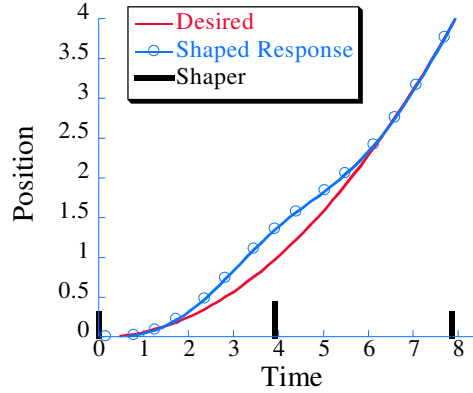
Figure 6.43: Acceleration Three-Impulse Shaper and Response for $R_{freq} > 1$.

6.3.1.1   Trajectory Duration > T

Like all of the previous cases, the acceleration tracking three-impulse shapers have problems in accurately tracking trajectories with a trajectory frequency ratio greater than one. For example, the 1.25 trajectory frequency ratio case in Figure 6.43 shows a major deviation from the desired velocity about half-way through the move. This deviation shows the faults of this technique at this frequency ratio. This ratio is presented to show the need to switch to other approaches in this region as will be discussed later in Section 6.3.5. Note that this three-impulse shaper has a similar form to the ZVD shaper. On the positive side, the shaper also manages to provide for accurate trajectory tracking after the acceleration, *i.e.* the system is in the correct position with the correct velocity. This post acceleration condition is primarily due to two factors. First, the input shaper eliminates all oscillation,

173
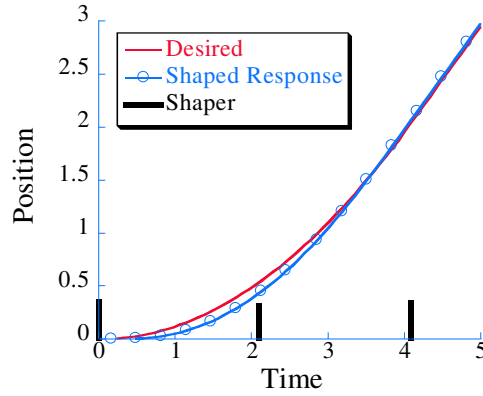
Figure 6.44: Acceleration Three-Impulse Shaper and Response for $0.5 < R_{freq} < 1$.
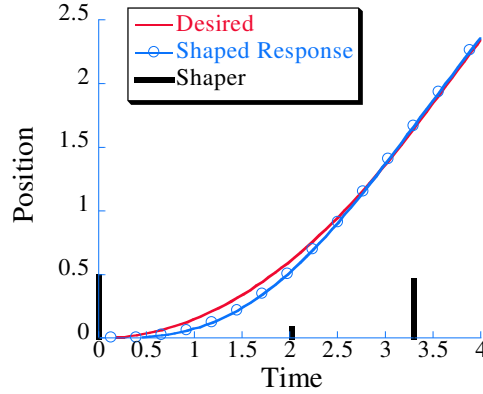
Figure 6.45: Acceleration Three-Impulse Shaper and Response for $R_{freq} \simeq 0.5$.

and second, the duration of the two commands are the same yielding zero position offset.

6.3.1.2   *T/2 < Trajectory Duration < T*

For faster moves, the performance of this technique improves, showing it usefulness as only a niche solution. For example, a trajectory frequency ratio of 0.65 is shown in Figure 6.44 The shaper has three impulses of near identical magnitudes, and is identical to the shaper shown in Figure 6.18. Figure 6.45 present the acceleration tracking result at a trajectory frequency ratio of 0.525. The shaper only differs from a ZV shaper in a small centered impulse. This region of trajectory durations between T/2 and T is the most promising for the trajectory tracking techniques. This is because the tracking is improved substantially, yet the shaper impulses are still always positive and of a magnitude less than one.
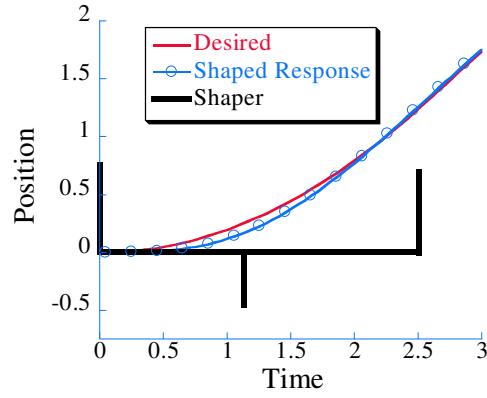
Figure 6.46: Acceleration Three-Impulse Shaper and Response for $1/3 < R_{freq} < 0.5$.

6.3.1.3 $T/3 <$ *Trajectory Duration* $< T/2$

As the speed increases, the tracking performance is still good, but the demands on the actuators increase. Figure 6.46 shows the tracking of an acceleration command with a trajectory frequency ratio of 0.4.
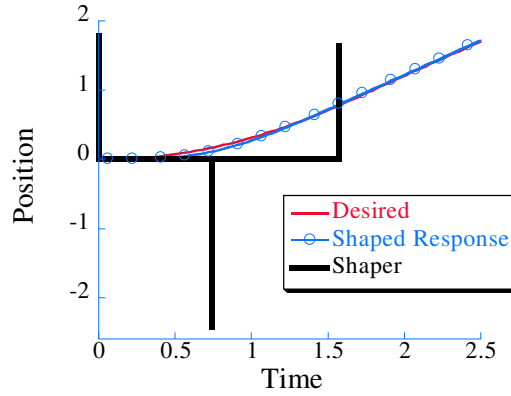
Figure 6.47: Acceleration Three-Impulse Shaper and Response for $R_{freq} < 1/3$.
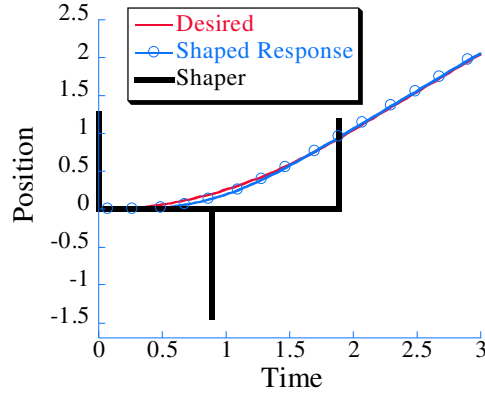
Figure 6.48: Acceleration Three-Impulse Shaper and Response for $R_{freq} \simeq 1/3$.

In the region where the trajectory duration is between T/3 and T/2, the input shaper designed for acceleration command tracking is still useful, if a system's actuators can deal with negative impulses. In this region, the effort is still constrained and the tracking is good.

6.3.1.4 Trajectory Duration < T/3

For even faster trajectories the technique still provides excellent tracking in theory. However, actuator effort is increased. For example in the case of a trajectory frequency ratio of 0.25 the maximum effort is -2.5 as shown in Figure 6.47. This region also resembles the three impulses of the UMZV shaper. Figure 6.48 shows how the tracking designed shaper is like the UMZV shaper for a trajectory frequency ratio of 0.3. In this region, unlike the others the shaper design technique is severely limited by the magnitude of effort required from
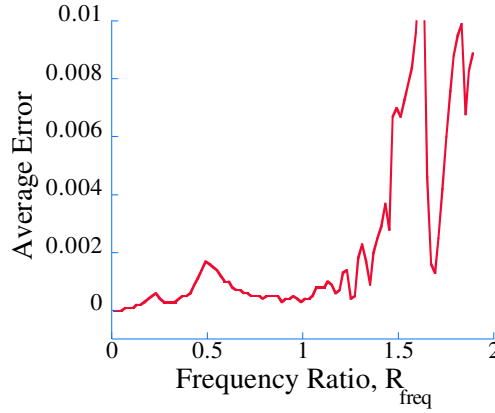
Figure 6.49: Acceleration Four-Impulse Shaper Error for Trajectory Frequency Ratio.

the actuators. For a system to be driven effectively in this realm, the actuators need to be carefully considered.

6.3.2 Acceleration Trajectory Tracking Four-Impulse Input Shapers

If the tracking performance of the three-impulse shapers is not acceptable, the number of impulses can be increased to four. For the acceleration tracking case this requires the same technique as the S-curve case and has the same drawbacks of increased complexity in design and implementation. The design requires the solution to a more complicated problem. The implementation requires the use of an additional impulse. This impulse is not difficult to include in the command hardware; however, this extra impulse can cause problems for the actuators since it typically leads to much larger shifts in the input command.

The four-impulse acceleration tracking technique performs well for a wide range of trajectory frequency ratios as is shown in Figure 6.49. The worst-case tracking is improved over the three-impulse technique of Figure 6.42 by an order of magnitude again and trails off as the trajectory frequency ratio increases. It is important to note the difference in the shape of the S-curve tracking of Figure 6.27 and the acceleration tracking of Figure 6.49. While theoretically, the shapers should be the same in both case due to the acceleration being the integral of the S-curve case, the complexity of the problem and the solution approach allows for slightly different results and thus shaper performance, leading to differences between Figures 6.27 and 6.49.

6.3.2.1 Trajectory Duration $> T$

The four-impulse case tracks the acceleration commands better than the three-impulse approach especially for slower moves where the trajectory frequency ratio is greater than 1. For example, for a trajectory frequency ratio of 1.25 as shown in Figure 6.50, the
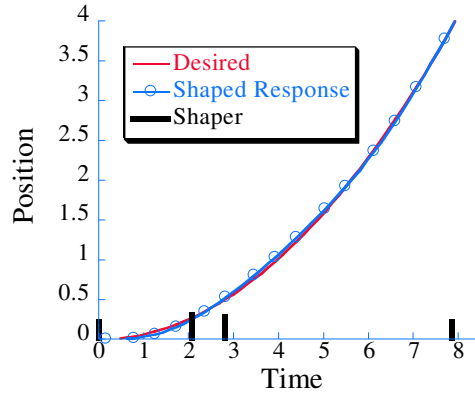
Figure 6.50: Acceleration Four-Impulse Shaper and Response for $R_{freq} < 1$.
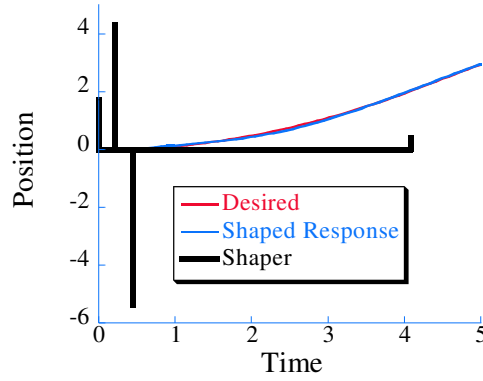
Figure 6.51: Acceleration Four-Impulse Shaper and Response for $0.5 < R_{freq} < 1$.

appropriately shaped ramped input causes the system to track the desired trajectory well. However, in the three-impulse case of Figure 6.43, the response exhibited a small bump halfway through the acceleration.

6.3.2.2 T/2 < Trajectory Duration < T

For the faster cases, the four-impulse technique also works well in tracking the acceleration profile. Figure 6.51 shows this tracking for a trajectory frequency ratio of 0.65 while Figure 6.52 shows it for a trajectory frequency ratio of 0.525.   The downside in both these cases is requiring impulses both positive and negative greater than one. This would be especially problematic for the case of Figure 6.52 for some systems due to the location of two impulse close together. This type of input would be simple on some systems with fast actuator response. However, un-modelled effects could cause the two impulse to smeared.

178
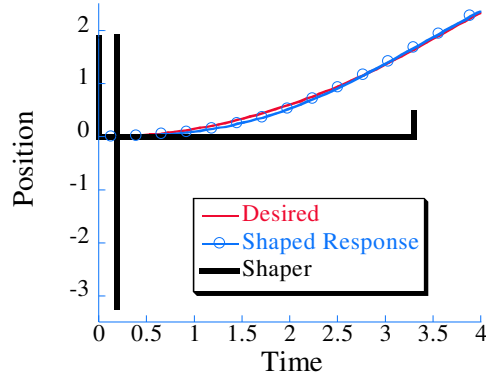
Figure 6.52: Acceleration Four-Impulse Shaper and Response for $R_{freq} \simeq 0.5$.
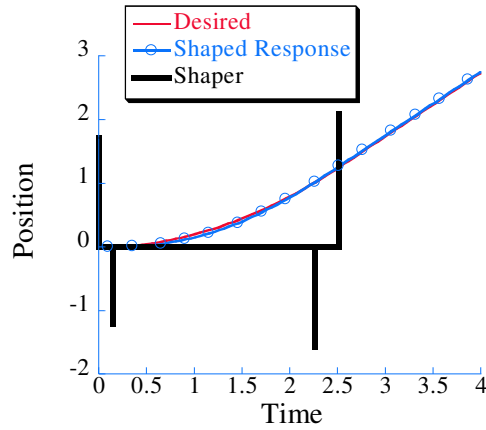
Figure 6.53: Acceleration Four-Impulse Shaper and Response for $1/3 < R_{freq} < 0.5$.

These considerations must be made when using the four-impulse shaper for these trajectory frequency ratios. The trajectory frequency ratio of 0.525 case unlike the three impulse case does not resemble the ZV shaper.

6.3.2.3 $T/3 <$ Trajectory Duration $< T/2$

The necessity to consider actuators effort becomes more important for faster moves. Figure 6.53 shows the tracking using the four-impulse technique for a trajectory frequency ratio of 0.4. At this trajectory frequency ratio, the shaper actually resembles a ZV shaper. If the impulse pairs are summed together, the correlation with the ZV shaper can be seen. Once again in this region, impulse magnitudes are greater than one in both the positive and negative directions.
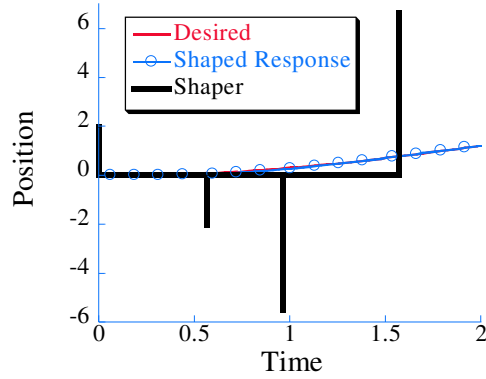
Figure 6.54: Acceleration Four-Impulse Shaper and Response for $R_{freq} < 1/3$.
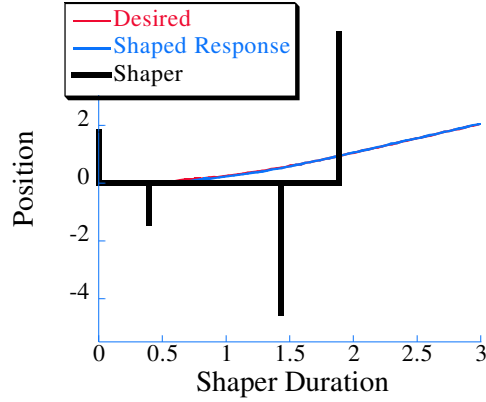
Figure 6.55: Acceleration Four-Impulse Shaper and Response for $R_{freq} \simeq 1/3$.

6.3.2.4 Trajectory Duration $< T/3$

For still faster moves, the technique is still valid with some minor caveats as have been seen previously, actuator saturation and negative impulses. As an example, consider the two cases of trajectory frequency ratios of 0.25 and 0.3 shown in Figures 6.54 and 6.55 respectively. Both cases rely on large magnitude impulse in both directions but provide excellent tracking performance.

6.3.2.5 Multi-Impulse Input Shapers

Four-impulse and often three-impulse shapers provided adequate tracking for most commands. Of course the tracking could be improved using more impulses, since the shaper

180
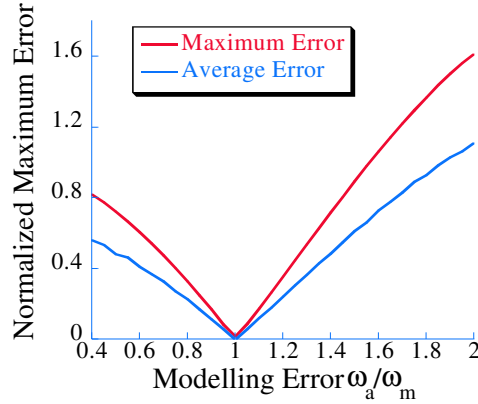
Figure 6.56: Sensitivity of Three-Impulse Trajectory Tracking Shaper.

selection would approach the optimal command design discussed in Section 6.1.4. Simulations were performed with five impulse shapers. However, the improvement in tracking is negligible compared to the four impulse shapers and the complexity grows considerably with each additional impulse. Also, as impulses are added the problem become less of an input shaping problem and more of a complete optimal command profile design problem. This optimal command problem has already been addressed by others and presents its own problem, although it is not considered in detail in this dissertation.

6.3.3 Robustness

The susceptibility of a vibration suppress scheme to modelling error or parameter variation is one of the primary performance measures. Likewise, robustness is a primary concern for a trajectory tracking techniques. To measure this robustness, sensitivity curves like those previously discussed in Section 3.3.1 are used to study the effectiveness of trajectory tracking input shapers, as well as optimal command design .

The three-impulse trajectory tracking input shaper's sensitivity to modelling errors for S-curve tracking with a trajectory frequency ratio of 0.4 is shown in Figure 6.56. The vertical axis represents the normalized maximum difference between the desired trajectory and the actual response computed at each instant of the motion. Obviously both the maximum and the average error are minimal at perfect modelling, and the error will increase with modelling error. The interesting aspect is the slope of the sensitivity. The sensitivity curve increases quickly with modelling error. It is also important to note that the normalized maximum error is greater than one, meaning that utilizing this scheme could lead to greater following error than if no shaper was used at all. However, this measure is not as concrete as with the previous sensitivity curve, since a following error is extremely trajectory dependent. In this case it is specific to the S-curve tracking.

181
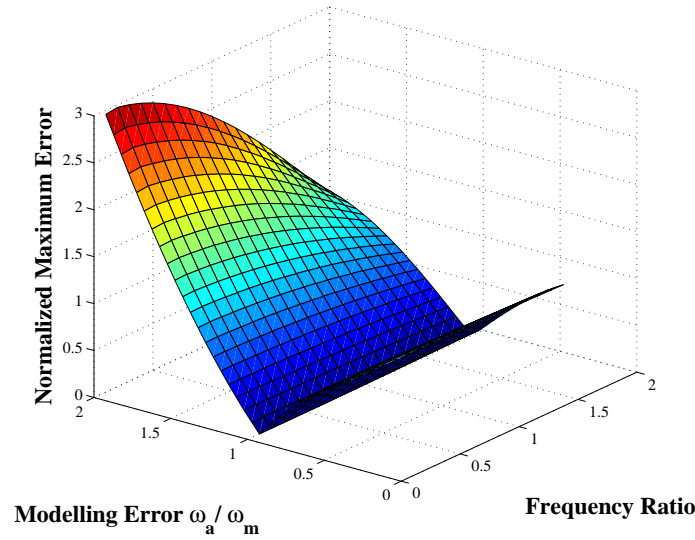
Figure 6.57: Sensitivity of Three-Impulse Trajectory Tracking Input Shapers with Trajectory Frequency Ratio Variation.

Like all other factors dealing with the trajectory tracking input shapers, the trajectory frequency ratio plays an important role in the robustness. Figure 6.57 shows the sensitivity curve for the three-impulse shaper for a variety of trajectory frequency ratios. Notice that the effect of modelling error is much greater than the effect of larger trajectory frequency ratios. Also important to note is that although the slope changes slightly with changes in trajectory frequency ratio, for all trajectory frequency ratios tracking error increases quickly with frequency modelling errors. Another important observation on the magnitude of the error is that the motions with higher trajectory frequency ratio are less aggressive and therefore less susceptible to extreme vibration.

Similar results occur for the four-impulse trajectory tracking input shaper. Figure 6.58 displays the sensitivity curve for a trajectory frequency ratio of 0.4. The deviation due to modelling error is nearly identical to the three-impulse case at this particular frequency ratio. Deviation does occur when other trajectory frequency ratios are considered as shown in Figure 6.59 The four-impulse shaper performs similarly to the three-impulse shaper over a range of trajectory frequency ratios.

For comparison, the optimal tracking algorithm presented earlier is considered in the robustness evaluation. This algorithm is a sequential digital command design procedure and uses the following steps:

- Compute the response of all previous inputs at the current time step

- Subtract the current desired location from the response of all previous inputs

- Compute the magnitude of the current input to yield the difference found from the
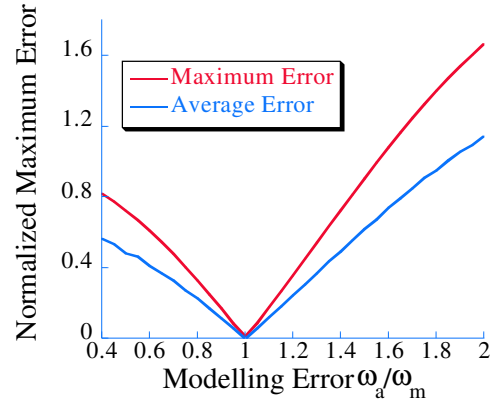
Figure 6.58: Sensitivity of Four-Impulse Technique.
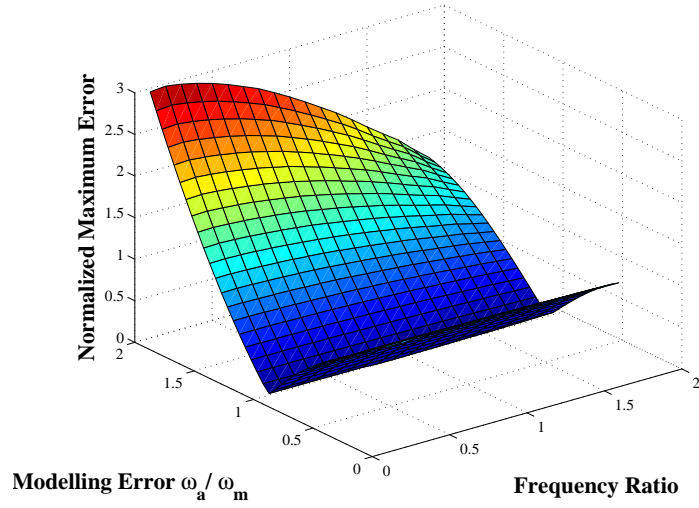
Figure 6.59: Sensitivity of Four-Impulse Trajectory Tracking Input Shapers with Trajectory Frequency Ratio Variation.
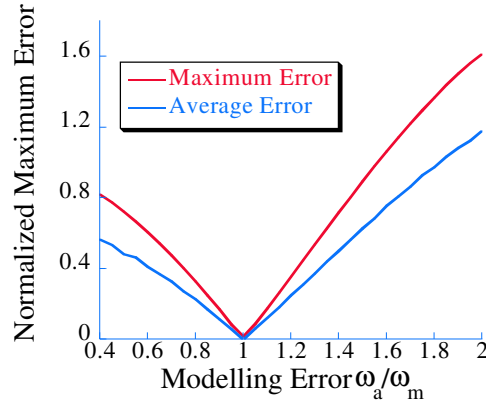
Figure 6.60: Sensitivity of Optimal Command Technique.

previous step

- Repeat this process until all time step's inputs have been found

The tracking of this technique is perfect if the inputs are not constrained, and the model is perfect. However, this technique is time consuming and reliant on computing a new total response to the equations of motion at every time step.

Nevertheless, this technique is the baseline for trajectory tracking since it gives perfect tracking at the expense of computational intensity. The sensitivity of this technique is similar to the other techniques for the case of a trajectory frequency ratio of 0.4 as shown in Figure 6.60. When other trajectory frequency ratios are considered, the result is the same. The sensitivity of the scheme is similar to the input shaping techniques as shown in Figure 6.61. This results shows how closely related the trajectory tracking input shapers are to the optimal command. It also reiterates that any techniques for tracking fast trajectories accurately are parameter sensitive.

The net result of the robustness investigation is that all three approaches are not robust to large variations in the system parameters. Also, only minor difference occur in the sensitivities of the three different techniques with none being significantly more robust than the others. From this, it can be concluded that sensitivity should not be part of the selection process between the algorithms for trajectory tracking scheme selection. If sensitivity is an important consideration due to change system frequency, then slower trajectories should be used, where the robustness of the shaping schemes are greater.

6.3.4 Trajectory Tracking on Other Advanced Plants

The previous sections only considered second-order plants, specifically a mass spring with position input. While this plant is synonymous with a mass under P control, many other
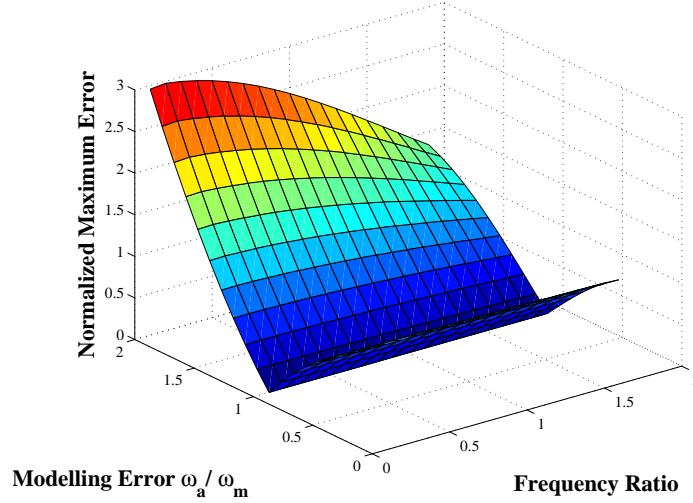
Figure 6.61: Sensitivity of Optimal Command Technique with Trajectory Frequency Ratio Variation.

plants exist in the real world. While this section does not attempt to show that the techniques developed for the trajectory tracking input shaper will work for any real system, it will instead discuss a few example cases. These cases will show that the techniques can be followed to design trajectory tracking schemes for more complicated systems.

6.3.4.1   Viscously Damped Plants

Damping is a major concern that has not been considered yet. Damping in the system increases the complexity of the constraint equations of the trajectory tracking input shapers as it did for the normal input shapers of Section 3.3.1. However, the technique still works to develop system commands for trajectory tracking. For example, consider a second-order system with a damping ratio of 0.1. The system can follow an S-curve move with a trajectory frequency ratio of 0.4 well, as is shown in Figure 6.62 for a three-impulse shaper, if the damping is considered throughout the design process. Note that the three-impulse shaper is similar to those seen previously for similar trajectory frequency ratios on undamped systems.

A more general study of the effect of damping was performed for a variety of damping ratios, as well as trajectory frequency ratios. Figure 6.63 shows how the normalized maximum error changes with these two parameters. For zero damping the results are the same as Figure 6.15. As damping increases so does the maximum tracking error, but for low damping ratios, this error is still small. This result is counterintuitive, since normal error, namely overshoot, is reduced with increased damping. However, damping slows the response of a system making it harder to make changes in the trajectory and thus leading to increased tracking error. Also notice that the trend of increased trajectory frequency
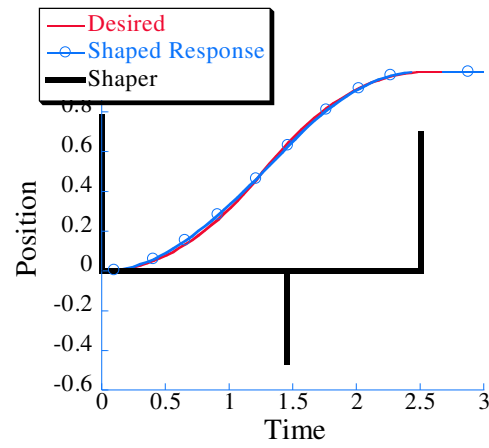
Figure 6.62: Example Tracking of Viscously Damped 2nd-Order Plant.
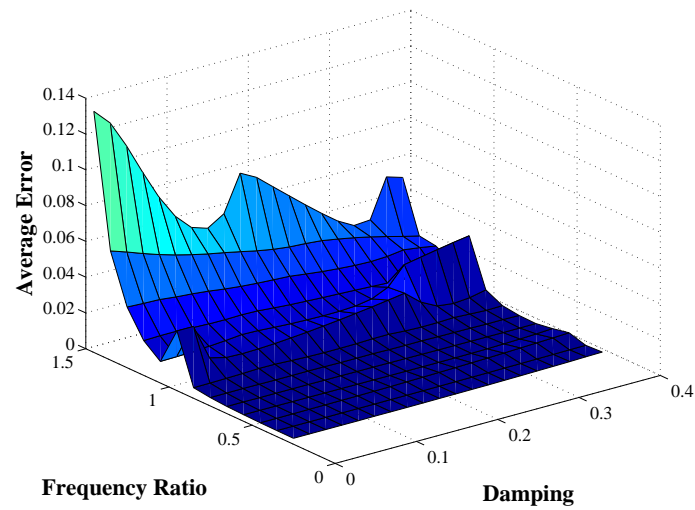
Figure 6.63: Tracking of Viscously Damped 2nd-Order Plant with Trajectory Frequency Ratio Variation.
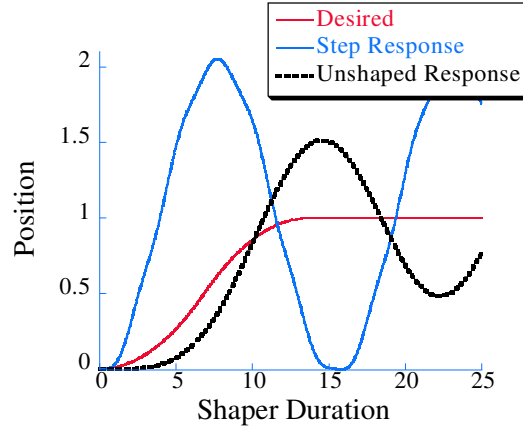
Figure 6.64: Unshaped Tracking of 4th-Order Plant.

ratio yielding increased error also holds generally for the damped cases.

6.3.4.2   Fourth-Order Plants

Another important classification of mechanical plants is those with two modes of vibration or fourth-order plants. The trajectory tracking input shapers can successful track motions of these plants as well. Figure 6.64 shows how a fourth-order plant might respond, if the desired trajectory was used to drive the system, or if this desired trajectory convolved with a simple input shaper was used. Obviously many techniques exist for dealing with multiple modes with input shaping, as were discussed in Section 3.3.1. Here the technique of using two different shapers convolved together will be employed.

The approach to designing a trajectory tracking input shaper for a fourth-order system is to initially simplify the problem by using a ZV shaper for the faster mode of vibration and a trajectory tracking shaper for the slow mode. The slow mode shaper is designed using the rules of Section 6.2 to be convolved with the ZV shaper and then have its tracking evaluated. The results are similar to those of the second-order systems with small changes in the shapers. For a trajectory frequency ratio for the slow mode of the plant of 0.4 and 0.8, the results can be seen in Figures 6.65 and 6.66, respectively.   For both cases the ZV shaper's effect on the impulse sequence can be seen. All the impulses of the sequence are repeated approximately one second later. From these results, the trajectory tracking input shapers are shown effective on more complicated systems than the simple second-order undamped oscillator.

6.3.5   Summary of the Usefulness of Each Approach

The previous section detailed the use of the three and four-impulse command shaping techniques for both S-curve and acceleration commands. In different regions some shaping
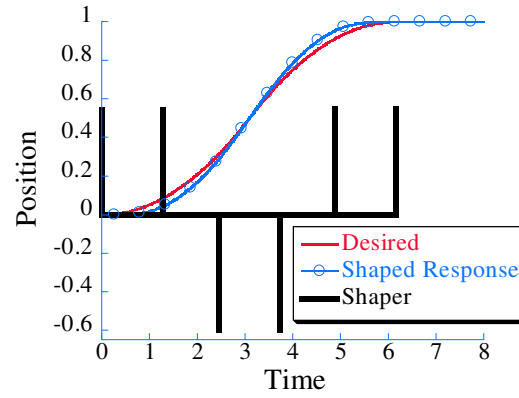
Figure 6.65: Example Tracking of 4th-Order Plant with $R_{freq} = 0.4$.
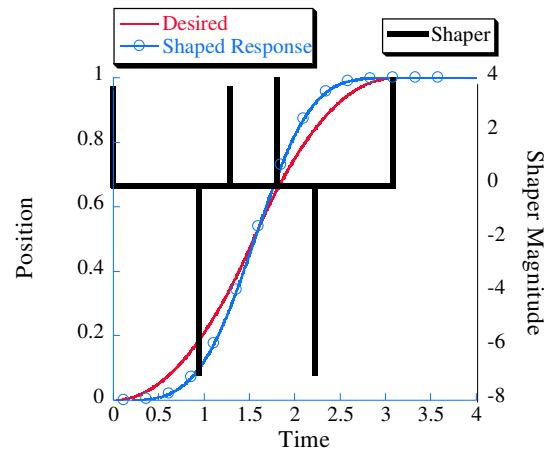
Figure 6.66: Example Tracking of 4th-Order Plant $R_{freq} = 0.2$.

Table 6.2: Approach Comparison for Trajectory Tracking for Various Trajectory Frequency Ratios.

Approach	$\leq 1/3$	$1/3 \leq R_{freq} \leq 0.5$	$0.5 \leq R_{freq} \leq 1$	> 1	$\gg 1$
Moving Slow					X
Shaping					$\otimes$
Pre-Shaping				$\otimes$	
3-Imp. Traj. Shap.	$\otimes$	$\otimes$	$\otimes$		
4-Imp. Traj. Shap.	X	X	X	X	
Opt. Com. Des.	X	X	X	X	X

approaches are better suited than others. Table 6.2 indicates the effective regions for each technique with an X for both acceleration and S-curve commands. The technique that should be attempted first is marked with $\otimes$. The best choice for a shaping scheme based on tracking performance and minimal effort is further explained for each trajectory frequency ratio in the following sections.

6.3.5.1 Trajectory Frequency Ratio $\gg$ 1

In this region it is best to use traditional input shaping convolved with the desired trajectory to yield the best tracking. Other techniques could be used to improve the tracking slightly, but the gains would not be worth the increased complexity in design.

6.3.5.2 Trajectory Frequency Ratio $>$ 1

For this region a grey area exist between when to use traditional shaping convolved with the desired trajectory, time shifted shaped trajectories, or shapers specifically design for tracking convolved with simple commands like steps and ramps. Here, a designer should first attempt the simple shaping solution and the preshaped solutions and if those do not provide sufficient tracking consider the four-impulse trajectory shapers. The three-impulse shapers performance is significantly less than that of the four-impulse shapers for these trajectory speeds.

6.3.5.3 Trajectory Frequency Ratio $\leq$ 1

In this region three-impulse shapers should be used primarily due to the simplicity of their design. The tracking error is the same with the four-impulse and the three-impulse shapers.

6.3.5.4 Trajectory Frequency Ratio $\leq$ 0.5

In this region of faster motion than previous sections, the three-impulse shaper is preferred over the four-impulse shaper even though they have similar tracking performance for two reasons. First, the three-impulse shaper is simpler, but more importantly the three-impulse shaper in this region does not exceed 1 in its impulse magnitudes.
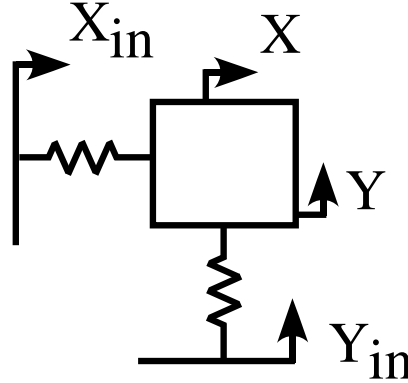
Figure 6.67: Multi-Axis System Model.

For the fastest motion, the three-impulse shaper is preferred even though tracking performance is similar. The justification is that the three-impulse shaper has lower impulse magnitudes than the four-impulse shaper, and has fewer closely spaced impulses that may be difficult to implement. However, actuator saturation needs to be carefully considered for any trajectory in this region.

6.4 Shaping Two-Dimensional Trajectories

Chapter 5 dealt with tracking two axis trajectories spatially. Often, however, multi-axis trajectories also need to be tracked temporally. While the modified acceleration technique of the previous chapter was only spatial it was effective. A more useful technique has been developed which allows segmental design of a tracking algorithm and is based on the trajectory tracking input shapers. If, instead of considering the complete multi-axis trajectory, the trajectory is reduced to any number of single axis tracking problems, then the trajectory tracking input shapers can be employed.

6.4.1 System Model

The same model will be used for two-dimensional tracking as was used in the previous chapter. The two degree of freedom uncoupled oscillator diagramed in Figure 6.67 is undamped and symmetric in X and Y. Even before complicated trajectories are considered, this system suffers from tracking problems. For example, the system attempting follow a trajectory composed of three line segments is shown in Figure 6.68. Although shaping improves the tracking, it does not provide for acceptable tracking of fast motions. The difference with and without shaping and the shortcomings that still exist with input shaping are more obvious in Figure 6.69. The previously mentioned problems of the introduced delay and slope change when input shaping is utilized combine together on the two axes to lead to the
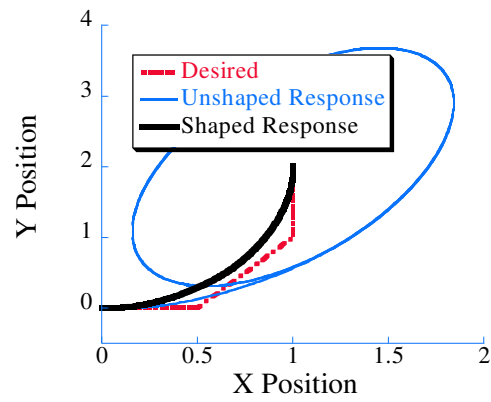
Figure 6.68: Multi-Axis Move Following Error.
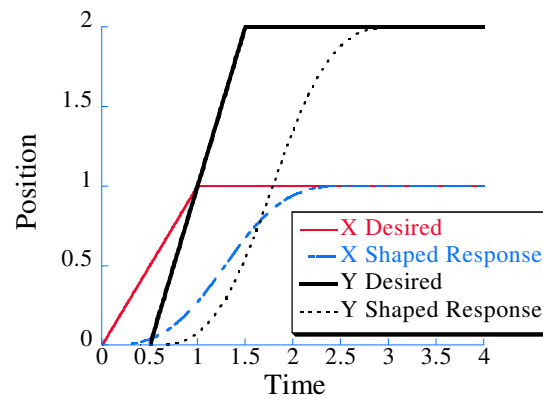
Figure 6.69: Multi-Axis Move Following Error Axis Breakdown.

191
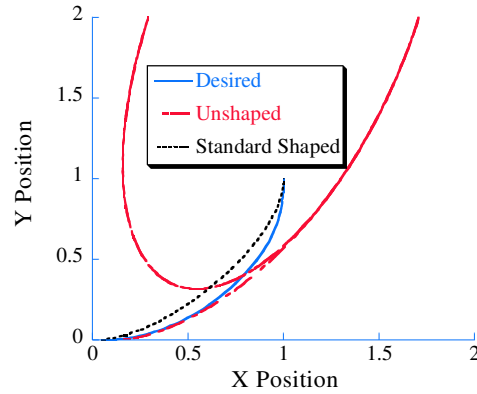
Figure 6.70: Quarter Circle Tracking with and without Input Shaping.
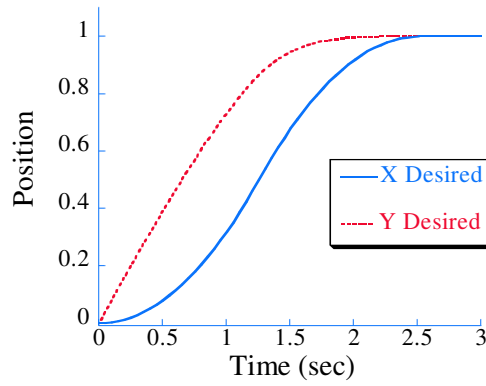
Figure 6.71: X and Y Breakdown of Quarter Circle.

tracking error. It is clear from these two figures how even minor deviations in the tracking can have a significant impact when trying to move a system quickly.

6.4.2 Multi-Axis Temporal Tracking Procedure

The first step in applying the trajectory tracking input shapers to a complex multi-axis trajectory is to break the trajectory down into several single axis trajectories. As a test case, again consider the quarter circle shown in Figure 6.70. This system obviously exhibits poor tracking when no shaping is used. However, even with shaping, tracking error exists, primarily due to the delay introduced by a standard input shaper.

If the X-axis component of the circle is assumed to be an S-curve (forcing the time response along the X-axis into the well known form), then the equations for the circle dictate the Y-axis trajectory as is shown in Figure 6.71. At this point the X-axis can be
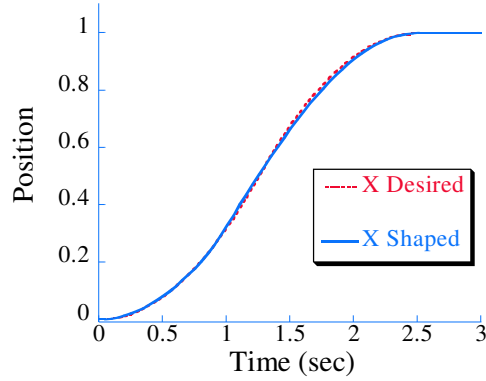
Figure 6.72: Quarter Circle Best Fit X Axis S-Curve.
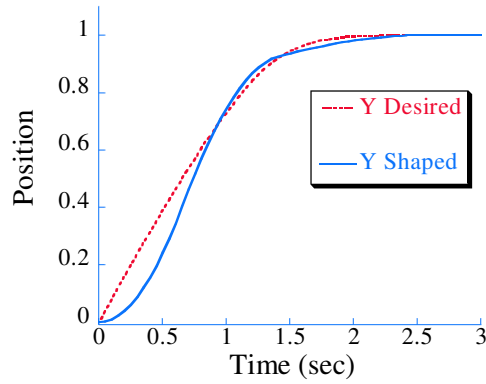
Figure 6.73: Quarter Circle Best Fit Y Axis S-Curve.

tracked well using the previous techniques, however, the Y-axis trajectory is not exactly an S-curve. To remedy this, the S-curve that is the closest approximation of the Y trajectory is needed so that the previous S-curve tracking techniques can be employed. This Y-axis S-curve can be obtained from a simple parameter search. The best match S-curve for the Y-axis deviates from the needed trajectory near the start of the move due to the non-zero initial velocity.

Now that two S-curves exist, the techniques from Section 6.2 can be used to find shapes and thus commands to follow them. The X-axis is tracked well using the three-impulse trajectory tracking input shaper as shown in Figure 6.72. The Y-axis however does not track exactly due to the difference between the desired S-curve and the actual desired motion. Figure 6.73 shows the desired and actual response for the new Y-axis shaped trajectory. The responses of the two axes can be combined together to find the overall response of the

193
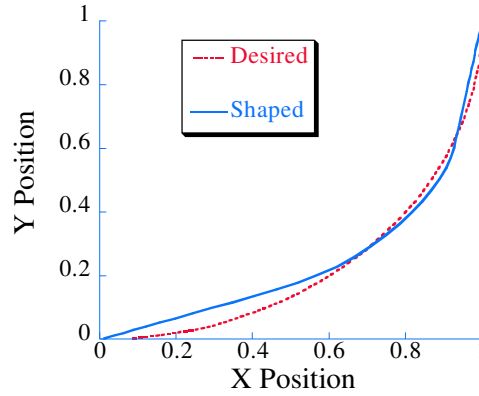
Figure 6.74: Quarter Circle Tracking with S-Curve Technique.
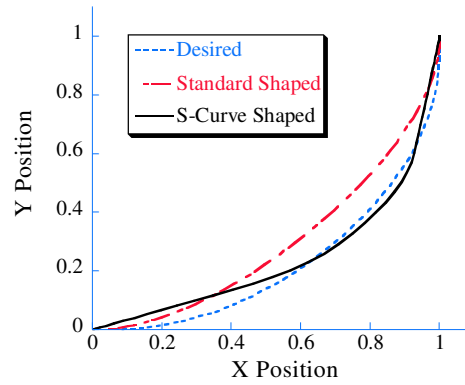
Figure 6.75: Quarter Circle Tracking Technique Comparison.

system. Figure 6.74 shows the desired and actual tracking for this new technique of the multi-axis S-curve. The tracking in this case is not ideal, however it is a vast improvement over the unshaped or simply shaped cases as seen in Figure 6.75. The deviation is due to the inability to find an S-curve to correctly match the Y-axis, not the S-curve tracking algorithm which is working well.

This deviation from the desired trajectory is dependent on the speed of the motion, as are all shaped trajectories. Figure 6.76 shows how the average error tracking a quarter circle in both X and Y change with the trajectory frequency ratio for the three-impulse trajectory-tracking shaper. Note that the X-axis error is the same as would be seen in Figure 6.15, while the Y-axis error changes due to the nature of the S-curve approximation. The deviations are still small for both axis at all trajectory frequency ratios. The quarter circle is a special case, because many other trajectories can be more easily broken down
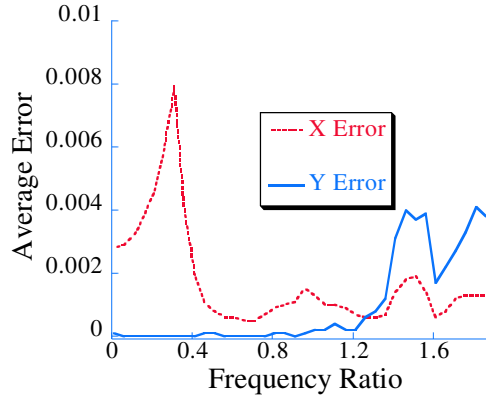
Figure 6.76: Frequency Ratio Effect on S-Curve Quarter Circle Response.

into S-curves. These trajectories will be discussed next.

6.4.3 Combined Trajectories

The previous section detailed how specific trajectory components, specifically a quarter circle, can be tracked using trajectory tracking input shapers. The process of how this could be used for a complete trajectory is shown in the flow chart in Figure 6.77. The process begins by dividing the command into its respective single axis trajectories. These single axis trajectories can be further broken down into single axis components. Once these components are created, S-curves are chosen to best fit the components. Also at this time, a duration for the S-curve or a speed for the move is selected. These preliminary curves are then shaped and the overall error for the trajectory component is calculated. If the error is too large, then the speed should be reduced. If this is not possible, then the breakdown of the total trajectory into components should be reconsidered. For example, rest-to-rest motions should be divided into separate acceleration and deceleration components. Once a shaped trajectory for all the components is complete, the process is done. However, one caveat exists, if no acceptable scheme is possible at a desired speed, then a more complicated tracking technique must be employed. For the quarter circle example this could be the modified acceleration technique. For other trajectories this could be plant inversion or total command optimizations.

To test this technique, a complicated trajectory was designed out of S-curves as is shown in Figure 6.78. The trajectory was chosen exclusively from S-curves for two reasons. First, the vast trajectory possibilities with S-curves are shown, and second, the parameter search for the best fit S-curves is avoided, thus simplifying the process. If this desired response is given to the symmetrical two degree of freedom oscillator of Figure 6.67 as an input, then the result has large tracking errors, as is shown in Figure 6.78. If instead a ZV shaper is used on

195
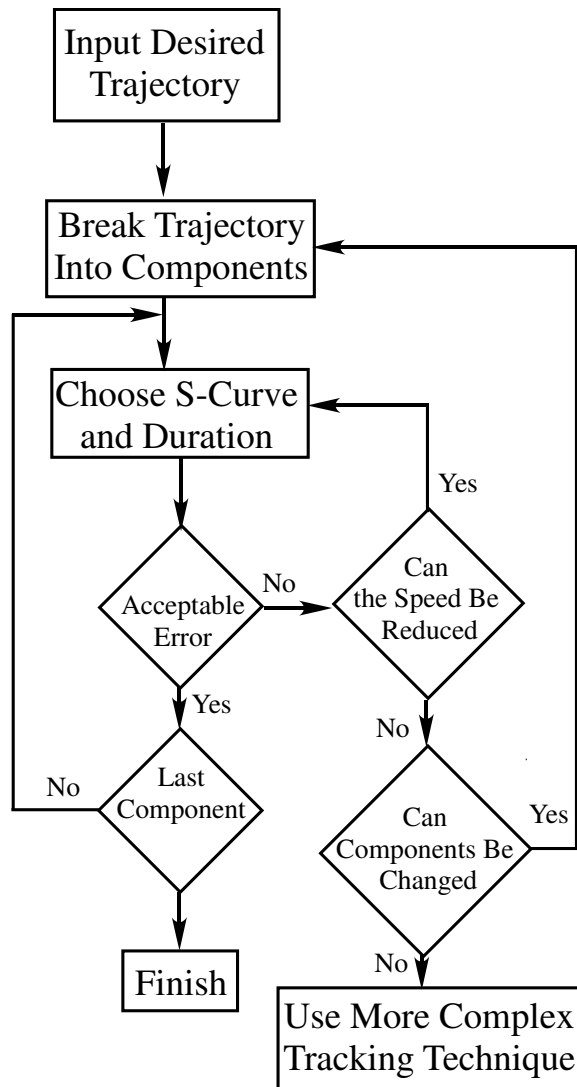
Figure 6.77: Flow Chart for Shaped Trajectory Design.
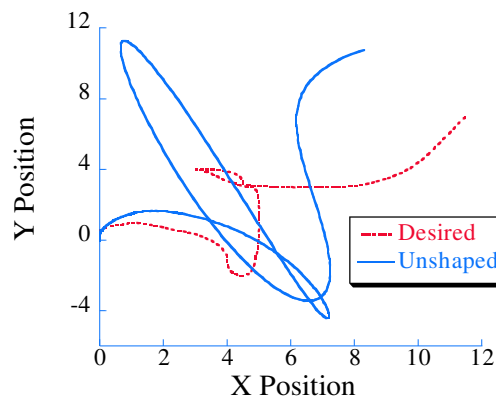
Figure 6.78: Example Combined Trajectory Unshaped Tracking.
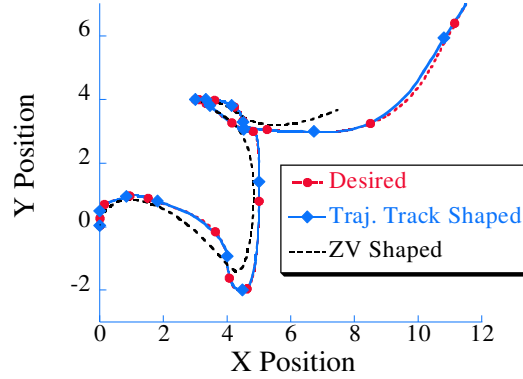
Figure 6.79: Example Combined Trajectory Tracking.
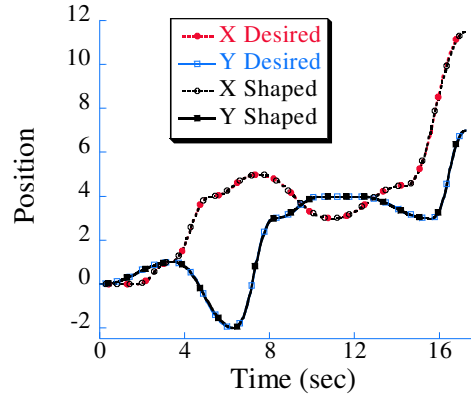
Figure 6.80: Example Combined Trajectory Tracking for Each Axis.

the desired response as the input command, then the tracking can be improved significantly as is shown in Figure 6.79. Notice the lag in the response, as well as the smoothing of sharp corners with traditional input shaping. If instead the multi-axis S-curve technique is employed, whereby shapers are designed and convolved with step changes in the reference command, then the tracking can be improved significantly as is shown in Figure 6.78. The components of this trajectory can be seen in Figure 6.80. For this trajectory it was possible to break down the components into S-curves with little error. The larger the trajectory the more likely this is to occur due to multiple options for the design of components.

The multi-axis S-curve technique is successful in tracking complicated trajectories provided they can be decomposed with little error to either S-curves or the accelerations/decelerations discussed earlier with the trajectory tracking input shapers. The complete technique does suffer from the same limitations as the trajectory tracking input shapers that compose it.

Table 6.3: Comparison of Two-Axis Tracking Techniques.

	Optimal Commands	Modified Acceleration	Traj. Input Shapers
Tracking	3	2	2
Robustness	1	1	1
Computation	3	1	2
Complexity	1	3	2
Extendability	3	1	3
Implementation	1	2	2

3-Good, 2-Average, 1-Poor

Another of these limitations not previously discussed is the robustness of the trajectory tracking input shapers themselves.

6.4.4 Comparison of Two-Axis Tracking Techniques

Three approaches have be shown for tracking multi-axis moves, the first existing technique of optimal command design is computationally intensive. The modified acceleration technique involves only three design parameters and only solves the spatial problem, while the S-curve technique is applicable to trajectories consisting of many components. The benefits of each approach are evaluated and summarized in Table 6.3 where three is good performance, two is average, and one is poor. The tracking performance is good for all three techniques. Note should be made that the modified acceleration technique only addressed spatial tracking. The optimal commands are the best by their nature. However, the optimal technique does not perform better than the others in robustness, where all three techniques showed issues, not with complexity where optimal techniques are the most difficult. Complexity is how difficult it is to understand the choices the trajectory designer is making. The modified acceleration technique performs well at this due to only varying two parameters. The trajectory tracking input shapers are easy to understand for some cases, when they align with existing shapers. The optimal approach's input to the system is the most difficult to follow since it has the most variables. In extendability to multiple axis and linked trajectory components, the modified acceleration technique performs poorly since it is a stop-stop motion technique developed for two axis moves. All three techniques require some sort of path designer for implementation, but the shaping techniques only need the system to implement step or ramp changes to the input. From Table 6.3 a decision can be made about which technique is best suited for an application in multi-axis trajectory tracking.

6.5   Comparison to Existing Techniques

This section outlines when to use different trajectory tracking techniques. Comparisons are made between the following techniques.
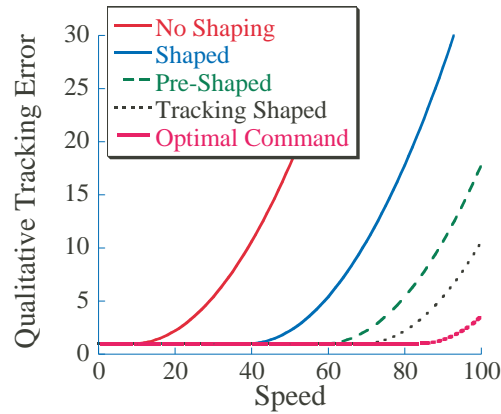
Figure 6.81: Tracking Versus Speed of Motion.

- Moving Slow: Accelerating slowly enough not to excite vibration, and using the desired response as the input

- Traditional Shaping: Using a standard input shaper convolved with the desired response to deal with command induced vibrations

- Pre-Shaping: Slightly altering the desired response before convolving it with a traditional shaper

- Trajectory Tracking Input Shaping: Designing an input shaper to be convolved with a simple command to be used as input to the system

- Optimal Command Design: Utilizing an optimization algorithm or plant inversion technique to select the commands for the system

The first comparison is in how the trajectory tracking performance changes increasing speed. Figure 6.81 shows qualitatively how tracking error changes with increases in desired speed. The speed is unit-less and is only to represent general trends. For low desired speeds, all the techniques will provide good trajectory tracking. As the speeds increase, moving at those speeds will cause vibration in the system and therefore moving slowly is no longer an option for trajectory tracking, in these cases input shaping is needed. At still higher speeds, input shaping alone will introduce an unwanted delay into the system causing increased error. Time shifting the command, (Preshaping), can alleviate this problem, but eventually preshaping will no longer be able to compensate for this delay due to the duration of the command elements being shorter than the required preshape. This will occur at a trajectory frequency ratio around 1. Finally, at extremely high speeds near a trajectory frequency ratio of 0.3, trajectory tracking input shaping will fail due to the large actuator efforts required to move the system. Since the optimal commands can change the input at
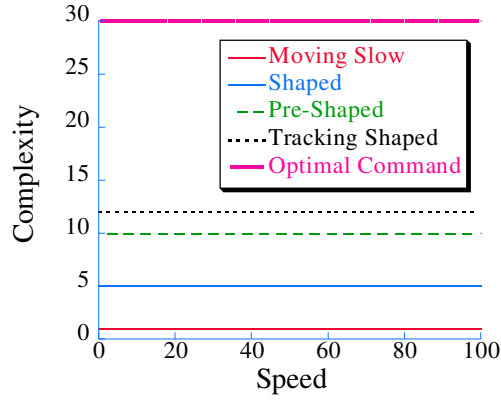
Figure 6.82: Speed Versus Complexity.

all time locations, they can more aggressively change the system motion with less actuator effort. This smoothing of effort over several times steps allows the actuator saturation to occur at slightly faster trajectories than the trajectory tracking shaped cases.

Depending on the speed of the desired trajectory, many different tracking schemes could be effective. The selection can be made on the complexity of designing the tracking scheme. Figure 6.82 shows qualitatively how the complexity of each of the schemes changes with the speed. Although complexity does not change with speed, the figure does offer insight into the relative complexity of the techniques. Therefore, it is advisable to use the simplest tracking scheme that will provide adequate tracking for a given application. For most real systems the simplest scheme is to move slowly, relative to the system natural frequency. For faster motions that will induces vibration into the system, standard input shaper application is simple and effective. Fewer machines operate at the higher speeds than do at low speed. Thus the techniques suited for slower motions will be the more common solutions.

6.6 Synopsis

The previous section detailed the appropriate techniques for trajectory tracking. For fast motions, the use of trajectory tracking input shapers is recommended. The ability to perform fast and accurate motions is the primary motivation for combining mechanical and command design. This chapter offered a method for improving the performance of existing machines, but also supports the idea that fast and accurate motions will be possible for combined design solutions.

CHAPTER VII

INPUT SHAPING FOR CONTINUUM SYSTEMS

All real systems, including micro-milling machines, are composed of continuum vibratory elements; however, these continuum elements are typically modelled by lump-parameter approaches. Lumped-parameter models, while accurate for some machines, are unable to deal with dynamic effects that occur when machines are moved rapidly or when machines are excessively flexible. Both of these issues are relevant to the modelling of micro-mills as discussed in Section 4.2. By considering micro-mills to be composed of continuum elements, more accurate models can be developed and thus more effective command and control schemes. The result of more effective control schemes is improved performance. Therefore through effective modelling and control of continuum elements, the secondary research question of how to improve existing micro-mills can be answered. Likewise the derivation of input shaping for continuum elements provides the relationship necessary between mechanical and input shaper parameters necessary for answering the primary research question of how to design mechanical and command components simultaneously.

On a micro-mill drive-screw positioning stage, three types of vibration can occur: rotational, torsional, and transverse. Figure 7.1 diagrams a typical drive-screw stage with the motor and workpiece. The workpiece is connected to the motor through a long flexible threaded shaft. Torsional vibration in the shaft can occur from the rotation of the motor, while transverse and longitudinal vibration can occur from the cutting forces and from the motion of the stage itself. Moving the workpiece to the left and right will cause longitudinal vibration. If the entire stage is moved up and down by another stage, transverse vibration will occur. Accurately modelling all these types of vibration is necessary for their suppressing. The technique used in this dissertation for vibration suppression is input shaping.

While, command shaping has been used extensively on continuum vibratory systems,
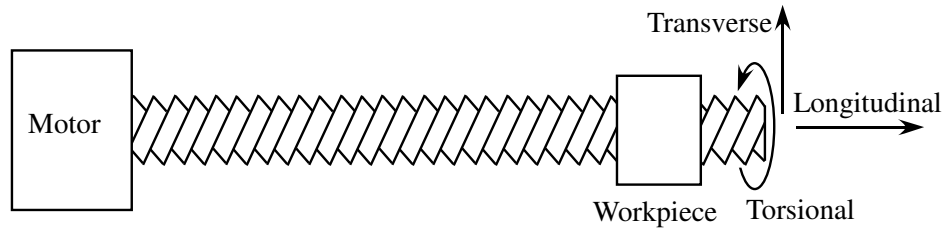
Figure 7.1: Diagram of Continuum Elements in Drive-Screw Stage.

most of this work has simplified real systems by modelling them with lumped parameter models. This approach has been successful for many problems, yet it can be improved by studying the effect of input shaping on continuum models directly. Currently, the issues with using input shaping on continuum systems are overcome by introducing robustness into the shaper to deal with the higher modes, that are neglected by the lumped-mass treatment. In this chapter existing input shapers will be explicitly studied on continuum systems in an attempt to validate the theory that lumped parameter input shaping is effective on continuum elements.

For each of the three types of continuum vibration previously mentioned, rotational, torsional, and transverse, the following procedure will be used to study the impact of command shaping.

1. The equation of motions for the beams will be presented. Both simple beams, as well as beams with attached masses or inertias will be addressed.

2. ZV, ZVD, and UMZV input shapers will be derived in terms of the continuum beam equations of motion.

3. The effectiveness of each of theses shapers for the beams will be studied for case of external forces and base motion.

4. The impact of higher modes will investigated.

5. The sensitivity to modelling error will be studied.

6. Recommendations will be made as to which shaper is best suited for each beam type.

This work is a corrolary to the work of Singh and Alli [250]. They derived new time-optimal shapers for simple longitudinal beam vibration, where here existing shapers use on a variety of beams is explored. Singh and Alli also did not consider the effect of additional mass on the end of the beam, which significantly complicates the dynamics. Although not specifically address in [250], the relationships between the modes, simplified the resultant time-optimal shaper and effectively reduced the system to one mode. The modal relationships will be explored in detail here as a primary factor in input shaper performance. Singh and Alli's work basically used an optimization routing and the equations of motion of a longitudinal beam to derived a time-optimal shaper similar to a ZV input shaper for the first mode of longitudinal beams with no attached mass. Singh and Alli searched and found the solution to one specific continuum problem, where this chapter seeks to re-derive the fundamental principles of input shaping for continuum beams.
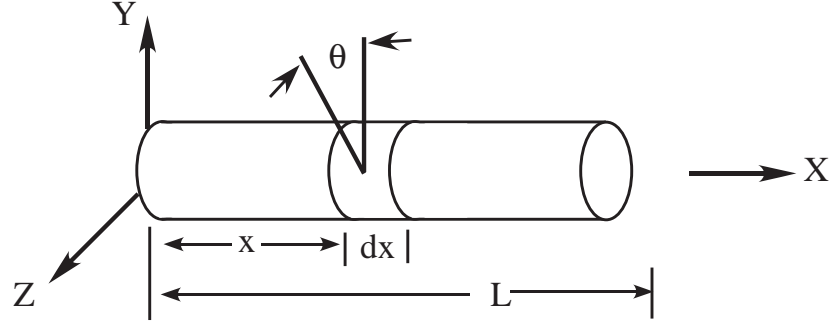
Figure 7.2: Diagram of Torsional Beam.
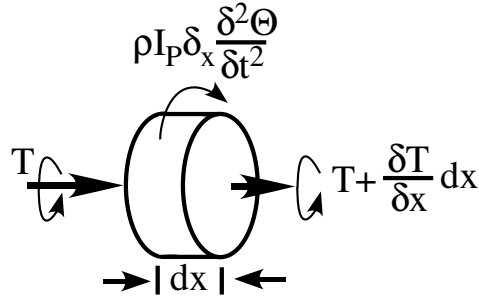
Figure 7.3: Diagram of Torsional Beam Element.

7.1 Modelling of Continuum Systems

The first step in understanding how input shaping will effect the dynamics of continuum systems is to study the motion of the systems to simple inputs. Three different beams will be considered both with and without end attached masses/inertias, *i.e.* torsional, longitudinal, and transversely vibrating beams. These beams represent the majority of vibratory continuum systems. For the purposes of derivation of the equations of motion for the beams, several vibration texts were consulted [313, 225, 136]

7.1.1 Torsional Beam

The first beam to be considered is the torsionally vibrating beam. This element can be used to model shafts in particular. Figure 7.2 diagrams the torsional beam of length L considered here. In order to determine equations of motion for the torsionally vibrating beam, first consider a differential element of the beam. Figure 7.3 shows a free body diagram of this differential torsional element with the generic torque, T, the change in the torque over the element, $\frac{\delta T}{\delta x}dx$, and the inertial torque $\rho I_P \delta x \frac{\delta^2 \Theta}{\delta t^2}$, where ρ is the density and I_P is the polar moment of inertia.

These variables and the parameters for the torsional beam are presented in Table 7.1.

In order to describe the motion of the entire beam, the first step is to sum the torques

Table 7.1: Torsional Beam Parameters.

Variable	Definition
D	Diameter
ρ	Density
L	Length of Beam
I_A	Attached Inertia
θ	Rotational Deflection of Element
I_P	Polar Moment of Inertia
G	Shear Modulus of Elasticity
x	Position Along Beam
b	Wave Velocity
ω_i	Beam Natural Frequencies
t	Time
r_T	Torsional Rigidity
I_{tot}	Mass Moment of Inertia
X_i	Mode Shape
P_{stat}	Static Force Magnitude
A_i and B_i	Modal Time Coefficients
C_i and D_i	Mode Shape Coefficient
K	Static Stiffness
ϕ_i	Time Dependent Response
θ^*	Inertial Forces Response
θ_g or g(t)	Base Motion
i	Mode number
Q	Forcing Function
P	Sinusoidal Forcing Magnitude
Ω	Sinusoidal Forcing Frequency
T	Elemental Torque

of Figure 7.3. The relationship exists between the torques of:

$$T + \frac{\delta T}{\delta x}dx - T - \rho I_P \delta x \frac{\delta^2 T}{\delta t^2} = 0 \qquad (7.1)$$

Since mechanics theory prescribes the relationship between the torque and the change in deflection according to:

$$T = GI_P \frac{\delta \theta}{\delta x} \qquad (7.2)$$

where G is the shear modulus of elasticity. For beam with a circular cross section of diameter D, the polar moment of inertia is:

$$I_P = \frac{\pi D^4}{32}; \qquad (7.3)$$

Therefore, (7.1) simplifies to:

$$GI_P \frac{\delta^2 \theta}{\delta x^2}dx - \rho I_P \delta_X \frac{\delta^2 \theta}{\delta t^2} = 0 \qquad (7.4)$$

which can be further simplified using the wave velocity in the beam which is:

$$b = \sqrt{\frac{G}{\rho}} \qquad (7.5)$$

To yield the primary equation of motion:

$$\frac{\delta^2 \theta}{\delta x^2} = \frac{1}{b^2}\frac{\delta^2 \theta}{\delta t^2} = 0 \qquad (7.6)$$

This equation must be satisfied for any torsional beam, with only the end conditions and initial conditions needed for a complete description of the motion.

The end conditions considered here are fixed on one end and free to vibrate on the other, since this is the motor and drive-screw relationship in a micro-mill as shown in Figure 7.1. This creates boundary conditions for the fixed end of:

$$\theta_{(x=0)} = 0 \qquad (7.7)$$

and at the free end gives the condition:

$$\left(\frac{d\theta}{dx}\right)_{x=L} = 0 \qquad (7.8)$$

The next step is to assume the form of the solution to (7.6). Traditionally, (7.6) is assumed to have the form of [313]:

$$\theta_i = X_i \left(A_i \cos \omega_i t + B_i \sin \omega_i t\right) \qquad (7.9)$$

where A_i and B_i are constants for each mode. Furthermore, X_i, the spatial component of the response, the mode shapes, are assumed to be [313]:

$$X_i = C_i \cos \frac{\omega_i x}{b} + D_i \sin \frac{\omega_i x}{b} \qquad (7.10)$$

Since the position changes in (7.9) are only dependent on X, substituting the boundary condition of (7.7) into (7.10), yields $C_i = 0$ and for (7.8) to be satisfied:

$$\cos \frac{\omega L}{b} = 0 \tag{7.11}$$

Thus the natural frequencies of the system are given by the solutions to the previous equation and are:

$$\omega_i = \frac{\pi b i}{2L} \qquad (i = 1, 3, 5, ..., \infty) \tag{7.12}$$

The mode shapes can be determined from these frequencies:

$$X_i = D_i \sin \frac{\omega_i x}{b} \tag{7.13}$$

leading to a generalized form for the behavior of the torsional beam:

$$\theta = \sum_{i=1}^{\infty} \sin \frac{\omega_i x}{b} \left(A_i \cos \omega_i t + B_i \sin \omega_i t \right) \tag{7.14}$$

where A_i and B_i encompass D_i and are determined by the initial conditions of the beam.

7.1.1.1   Static Deflection

If a constant torque, P_{stat}, is applied to the beam, then the deflection at the end, after all transient effect dissipate, is given by:

$$\theta_{(x=L)} = \frac{P_{stat}}{K} \tag{7.15}$$

where the static stiffness K is:

$$K = \frac{I_P G}{L} \tag{7.16}$$

7.1.1.2   Forced Response

Once the natural frequencies and modes of the beam are determined the response can be calculated for any force or torque defined in time and position along the beam. The forced response of the torsional beam model is based on the equation of motion for a differential element:

$$I_{tot} \ddot{\theta} dx - r_T \theta'' dx = Q(x, t) dx \tag{7.17}$$

where $Q(x, t)$ is the applied torque on the element defined for all time and $I_{tot} = \rho I_P$. If θ is assumed to have the same form as (7.14):

$$\theta = \sum_i \phi_i X_i \qquad (i = 1, 2, 3, ..., \infty) \tag{7.18}$$

where ϕ is the time dependent portion of the response and is defined as:

$$\phi_i = A_i \cos \omega_i t + B_i \sin \omega_i t \tag{7.19}$$

206

Then, the forced response only has an effect on ϕ_i and is given by employing the Duhamel's integral:

$$\phi_i = \frac{1}{\omega_i} \int_{x=0}^{L} X_i \int_{t=0}^{t} I_{tot} Q(x,t') \sin\left(\omega_i(t-t')\right) dt' dx \tag{7.20}$$

where $Q_{(x,t')}$ is the torque on the beam at time t'. The result for an arbitrary forcing function is:

$$\theta_i = \sum_{i=1}^{\infty} \frac{X_i}{\omega_i} \int_{x=0}^{L} X_i \int_{t=0}^{t} I_{tot} Q(x,t') \sin\left(\omega_i(t-t')\right) dt' dx \tag{7.21}$$

substituting in X_i yields:

$$\theta_i = \sum_{i=1}^{\infty} \frac{D_i \sin \frac{\omega_i x}{b}}{\omega_i} \int_{x=0}^{L} D_i \sin \frac{\omega_i x}{b} \int_{t=0}^{t} I_{tot} Q(x,t') \sin\left(\omega_i(t-t')\right) dt' dx \tag{7.22}$$

where D_i is defined by the orthogonality and normalization condition:

$$\int_{0}^{L} X_i^2 dx = 1 \tag{7.23}$$

This relationship forces the mode shapes to have equal magnitude and be orthogonal to each other, yielding:

$$D_i = \sqrt{\frac{L}{2}} \tag{7.24}$$

7.1.1.3   Base Motion

Another relevant source of vibration is the rotation of the base of the beam. If the beam's base is given a displacement $g(t)$, with a given acceleration of $\ddot{g}(t)$, then the continuum response of the beam can be calculated in closed form. First, $\theta(x=0,t) = g(t)$ is the prescribed motion. In order to calculate the beam response, it must be noted that the rotation of the beam with respect to ground will have two components, the rotation of the base, θ_g, and the response due to the inertia torques, θ^*, which represent the rotational displacement from the moved base:

$$\theta(x,t) = \theta^*(x,t) + \theta_g(t) \tag{7.25}$$

This same relationship also holds in acceleration:

$$\ddot{\theta}(x,t) = \ddot{\theta}^*(x,t) + \ddot{\theta}_g(t) \tag{7.26}$$

These relationships can then be used to write the equation of motion for each beam element. Since $g(t)$ does not vary with position, the equation for a beam element is similar to (7.17):

$$I_{tot}\ddot{\theta}^*(x,t) - r\theta^*(x,t)'' = -I_{tot}\ddot{g}(t) \tag{7.27}$$

This is the same as the forced response where:

$$Q(x,t) = -I_{tot}\ddot{g}(t) \tag{7.28}$$

207
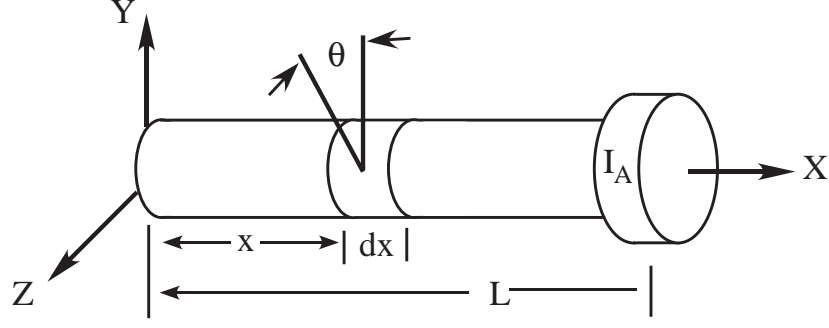
Figure 7.4: Diagram of Torsional Beam with Attached Inertia.

Thus the response of the beam due to the deflection caused by resistance to the motion of the base is:

$$\theta^* \left(x, t\right)_i = \sum_{i=1}^{\infty} \frac{X_i}{\omega_i} \int_{x=0}^{L} X_i \int_{t=0}^{t} \ddot{g}(t') \sin \left(\omega_i(t - t')\right) dt' dx \tag{7.29}$$

If this is combined with the motion of the base, then the total response of θ to a base motion $g(t)$ is:

$$\theta \left(x, t\right) = g(t) + \theta^* \left(x, t\right) \tag{7.30}$$

7.1.2 Torsional Beam with Attached Mass

If instead of a free end, an added inertia, I_A is attached to the end of the torsional beam, the response will be significantly different, although the derivation procedure is similar. This case of an attached inertia is important, because in real machines often some load must be carried by a beam. In the micro-mill stage shown in Figure 7.1, the load was the workpiece. Figure 7.4 diagrams this loaded beam, which has the same differential elements as Figure 7.3 and whose parameters are also defined in Table 7.1. The attached inertia creates boundary conditions of:

$$\theta_{(x=0)} = 0 \tag{7.31}$$

at the fixed end, and at the attached inertia end:

$$r_T \left(\acute{\theta}\right)_{(x=L)} = -I_A \ddot{\theta}_{(x=L)} \tag{7.32}$$

This boundary condition encompasses the torques that will be applied by the attached inertia.

The same procedure of using the equations of the differential elements to derive the overall response is used. Therefore, (7.6) is the primary equation for the motion of the beam, and its solution is once again assumed to have the form of:

$$\theta_i = X_i \left(A_i \cos \omega_i t + B_i \sin \omega_i t\right) \tag{7.33}$$

208

where A_i and B_i are constants. Since again the position changes in (7.33) are only dependent on X, the boundary conditions of (7.31 and 7.32) become for the free end:

$$X_{i(x=0)} = 0 \tag{7.34}$$

and for the attached inertia end:

$$r_t \acute{X}_{i(x=L)} = I_A \omega^2{}_i X_{i(x=L)} \tag{7.35}$$

The form of the mode shapes, X_i, can also be assumed to be the same as the case without the attached inertia:

$$X_i = C_i \cos \frac{\omega_i x}{b} + D_i \sin \frac{\omega_i x}{b} \tag{7.36}$$

However, the results from the boundary conditions of (7.34 and 7.35) on (7.36) yield a different result from the free case, the coefficients C_i are:

$$C_i = 0 \tag{7.37}$$

and the natural frequency are given by the relationship:

$$\frac{r_T \omega_i}{b} \cos \frac{\omega_i L}{b} = I_a \omega_i^2 \sin \frac{\omega L}{b} \tag{7.38}$$

(7.38) can be simplified to:

$$\zeta_i \tan \zeta_i = \eta \tag{7.39}$$

where $\zeta_i = \frac{\omega_i L}{b}$ and $\eta = \frac{\rho I_p L}{I_A}$. The multiple solutions to (7.39) yield the natural frequencies, ω_i's, of the system.

7.1.2.1 Orthogonality

The orthogonality of the modes is an important concept which forces describes the phenomenon that energy in one mode will not be transfer to other modes. The orthogonality will be used later to aid in the response description, specifically the orthogonality conditions are used to derive the mode shapes which are an integral part of the response description. To begin, the modes can be characterized by the eigenvalue problem:

$$r_T X''{}_i = -I_{tot} \omega_i^2 X_i \tag{7.40}$$
$$r_T X''{}_j = -I_{tot} \omega_j^2 X_j$$

If these equations are multiplied by X_j and X_i respectively and integrated over the length of the beam, then:

$$r_T \int_0^L X''{}_i X_j dx = -I_{tot} \omega_i^2 \int_0^L X_i X_j dx \tag{7.41}$$
$$r_T \int_0^L X''{}_j X_i dx = -I_{tot} \omega_j^2 \int_0^L X_j X_i dx$$

209

The boundary condition (7.35) for the attached inertia can also be transformed by multiplying by X_j and X_i:

$$r_T \acute{X}_{i(x=L)} X_{j(x=L)} = I_A \omega_i^2 X_{i(x=L)} X_{j(x=L)} \tag{7.42}$$

$$r_T \acute{X}_{j(x=L)} X_{i(x=L)} = I_A \omega_j^2 X_{j(x=L)} X_{i(x=L)}$$

If (7.42) is subtracted from (7.41), then:

$$r \int_0^L X''_i X_j dx - r \acute{X}_{i(x=L)} X_{j(x=L)} = -\omega_i^2 \left(I_{tot} \int_0^L X_i X_j dx + I_A X_{j(x=L)} X_{i(x=L)} \right) \tag{7.43}$$

$$r \int_0^L) X''_j X_i dx - r \acute{X}_{j(x=L)} X_{i(x=L)} = -\omega_j^2 \left(I_{tot} \int_0^L X_j X_i dx + I_A X_{i(x=L)} X_{j(x=L)} \right)$$

The left hand side can be integrated by parts to yield:

$$r_T \acute{X}_{i(x=0)} X_{j(x=0)} - r \int_0^L \acute{X}_i \acute{X}_j dx = -\omega_i^2 \left(I_{tot} \int_0^L X_i X_j dx + I_A X_{i(x=L)} X_{j(x=L)} \right) \tag{7.44}$$

$$r_T \acute{X}_{j(x=0)} X_{i(x=0)} - r \int_0^L \acute{X}_j \acute{X}_i dx = -\omega_j^2 \left(I_{tot} \int_0^L X_j X_i dx + I_A X_{j(x=L)} X_{i(x=L)} \right)$$

$X_{i(x=0)}$ and $X_{j(x=0)}$ are both identically equal to zero in this case since the base is fixed.

If the two equations from (7.44) are subtracted from each other, then the left-hand side cancels leaving:

$$\left(\omega_i^2 - \omega_j^2 \right) \left(I_{tot} \int_0^L X_i X_j dx + I_A X_{i(x=L)} X_{j(x=L)} \right) = 0 \tag{7.45}$$

For the nontrivial case of $\omega_i \neq \omega_j$ the right must be equal to zero such that:

$$I_{tot} \int_0^L X_i X_j dx + I_A X_{i(x=L)} X_{j(x=L)} = 0 \qquad i \neq j \tag{7.46}$$

This with $X_{i(x=0)} = 0$ substituted into (7.44) yields:

$$r_T \int_0^L \acute{X}_j \acute{X}_i dx = 0 \qquad i \neq j \tag{7.47}$$

When this is used with (7.43), the result is:

$$r_T \int_0^L X''_i X_j dx - r_T \acute{X}_{i(x=L)} X_{j(x=L)} = 0 \qquad i \neq j \tag{7.48}$$

For the case of $i = j$, the results of the previous equation will instead be a constant, I_{tot}. This yields three orthogonality relationships:

$$I_{tot} \int_0^L X_i^2 dx + I_A X_{i(x=L)}^2 = I_{tot} \tag{7.49}$$

$$r_T \int_0^L X''_i X_i dx - r \acute{X}_{i(x=L)} X_{i(x=L)} = -\omega_i^2 I_{tot} \tag{7.50}$$

210

$$- r_T \int_0^L \left(\acute{X}_i\right)^2 dx = -\omega_i^2 I_{tot} \qquad (7.51)$$

These orthogonality relationships can be used to compute the scaling D_i for the modes of the system given by:

$$X_i = D_i \sin \frac{\omega_i x}{b} \qquad (7.52)$$

7.1.2.2 Static Deflection

The static response of the beam to a constant torque applied at the end of the beam is the same as for the case with no attached inertia that is, it is governed by:

$$\theta_{(x=L)} = \frac{P_{stat}}{K} \qquad (7.53)$$

where:

$$K = \frac{I_P G}{L} \qquad (7.54)$$

7.1.2.3 Forced Response

The derivation of the forced response of the torsional beam model is based on the equation of motion for a differential element:

$$I_{tot} \ddot{\theta} dx - r_T \theta'' dx = Q\left(x, t\right) dx \qquad (7.55)$$

where $Q\left(x, t\right)$ is the applied torque on the element. This can be combined with the differential equation for the attached mass:

$$I_A \ddot{\theta}_{x=L} + r_T \acute{\theta}_L = 0 \qquad (7.56)$$

to find the overall response. If θ is assumed to have a form of:

$$\theta = \sum_i \phi_i X_i \qquad (i = 1, 2, 3, ..., \infty) \qquad (7.57)$$

Then this can be substituted into (7.56) as well as multiplied by X_j and integrated over the length of the beam:

$$\sum_i^\infty \left(I_{tot} \ddot{\phi}_i \int_0^L X_i X_j dx - r_T \phi_i \int_0^L X''_i X_j dx\right) = \int_0^L X_j Q\left(x, t\right) dx \qquad (7.58)$$

The same substitution into (7.56), multiplication by X_j and integration over the length of the beam can be made for the attached inertia and (7.57) to yield:

$$\sum_i^\infty \left(I_A \ddot{\phi}_i X_{i(x=L)} X_{j(x=L)} + r_T \phi_i \acute{X}_{i(x=L)} X_{j(x=L)}\right) = 0 \qquad (7.59)$$

These two can be added together to yield the overall equation:

$$I_{tot}\ddot{\phi}_i \int_0^L X_i X_j dx + I_A \ddot{\phi}_i X_{i(x=L)} X_{j(x=L)} - r_T \phi_i \int_0^L X''_i X_j dx + r_T \phi_i \acute{X}_{i(x=L)} X_{j(x=L)} \quad (7.60)$$

$$= \int_0^L X_j Q(x,t)\, dx$$

This can be simplified with the orthogonality and normalization relationships of (7.49) and (7.50) for $i = j$, yielding:

$$I_{tot}\ddot{\phi} + I_{tot}\omega_i^2 \phi_i = \int_0^L X_i Q(x,t)\, dx \quad (7.61)$$

In order to find the complete response, the factor D_i from (7.36 and 7.52) needs to be found. If (7.52) with $C_i = 0$ is substituted into (7.49), then the result is:

$$\int_0^L D_i^2 \left(\sin \frac{\omega_i x}{b}\right)^2 dx + \frac{I_A}{I_{tot}} D_i^2 \left(\sin \frac{\omega_i L}{b}\right)^2 = 1 \quad (7.62)$$

Taking the integral over x yields:

$$D_i^2 \left(\frac{L}{2} - \frac{\sin \frac{2\omega L}{b}}{\frac{4\omega_i}{b}} + \frac{I_A}{I_{tot}} \left(\sin \frac{\omega_i L}{b}\right)^2 \right) = 1 \quad (7.63)$$

The result is an expression for D_i:

$$D_i = \sqrt{\frac{1}{\frac{L}{2} - \frac{\sin \frac{2\omega L}{b}}{\frac{4\omega_i}{b}} + \frac{I_A}{I_{tot}} \left(\sin \frac{\omega_i L}{b}\right)^2}} \quad (7.64)$$

Returning to (7.61), this can be solved utilizing Duhamel's integral which state that the solution to:

$$\ddot{u} + \omega u = q \quad (7.65)$$

for a real vibratory system is:

$$u = \frac{1}{\omega} \int_0^t q \sin \omega (t - t') dt' \quad (7.66)$$

Equation (7.61)can be rearranged to give:

$$\ddot{\phi} + \omega_i^2 \phi_i = \frac{1}{I_{tot}} \int_0^L X_i Q(x,t)\, dx \quad (7.67)$$

which by Duhamel's integral yields:

$$\phi = \frac{1}{\omega_i I_{tot}} \int_0^L X_i \int_0^t Q(x,t') \sin \omega (t - t') dt' dx \quad (7.68)$$

This derivation applies to a generic torque function $Q(x,t)$.

7.1.2.4 Base Excitation Response

For the computation of the base excitation response, the same procedure is used as for the torsional beam without and end inertia. The rotation of the beam with respect to ground is composed of two components, the rotation of the base θ_g and the response from deflection θ^*, which represents the rotational displacement from the base:

$$\theta(x,t) = \theta^*(x,t) + \theta_g(t) \tag{7.69}$$

The same relationship exists in the beam accelerations:

$$\ddot{\theta}(x,t) = \ddot{\theta}^*(x,t) + \ddot{\theta}_g(t) \tag{7.70}$$

This is then used to create an equation of motion for each beam element. Since $g(t)$ is independent of position, the beam element equation is similar to (7.55):

$$I_{tot}\ddot{\theta}^* - r\theta^{*''} = -I_{tot}\ddot{g}(t) \tag{7.71}$$

The equation of motion for the attached inertia is given by the inertia's mass, the beams stiffness, and is forced by the inertial effects from the acceleration of the beam:

$$I_{tot}\ddot{\theta}^*_{(x=L)} - r\theta^{*''}{}_{(x=L)} = -I_{tot}\ddot{g}(t) \tag{7.72}$$

If θ^* is assumed to once again be equal to $\sum_{i=1}^{\infty} \phi_i X_i$, then the same procedure as for the simpler beam must be used. The equations of motion are multiplied by X_j and integrated over the length of the beam and then added together the result in an overall equation of:

$$I_{tot}\ddot{\phi}_i \int_0^L X_i X_j dx + I_A \ddot{\phi}_i X_{i(x=L)} X_{j(x=L)} - r_T \phi_i \int_0^L X''_i X_j dx + r\phi_i \acute{X}_{i(x=L)} X_{j(x=L)} \tag{7.73}$$

$$= -I_{tot} \int_0^L X_j \ddot{g}(t)\, dx - I_A X_{j(x=L)} \ddot{g}(t)$$

Utilizing orthogonality rules of (7.49) and (7.50) for $i = j$, (7.73) simplifies to:

$$\ddot{\phi}_i + \omega_i^2 \phi = -\int_0^L X_j \ddot{g}(t)\, dx - \frac{I_A}{I_{tot}} X_{j(x=L)} \ddot{g}(t) \tag{7.74}$$

If Duhamel's integral is used, then the equation becomes:

$$\phi = -\frac{1}{\omega_i} \left(\int_0^L X_i dx + \frac{I_A}{I_{tot}} X_{i(x=L)} \right) \int_0^t \ddot{g}(\acute{t}) \sin\left(\omega_i\left(t-\acute{t}\right)\right) d\acute{t} \tag{7.75}$$

which can be used to describe the base motion of the beam, leading to an overall response of:

$$\theta(x,t) = \left(D_i \sin\frac{\omega_i x}{b}\right)\left(-\frac{1}{\omega_i}\left(\int_0^L X_i dx + \frac{I_A}{I_{tot}} X_{i(x=L)}\right) \int_0^t \ddot{g}(\acute{t}) \sin\left(\omega_i\left(t-\acute{t}\right)\right) d\acute{t}\right) + \theta_g(t) \tag{7.76}$$
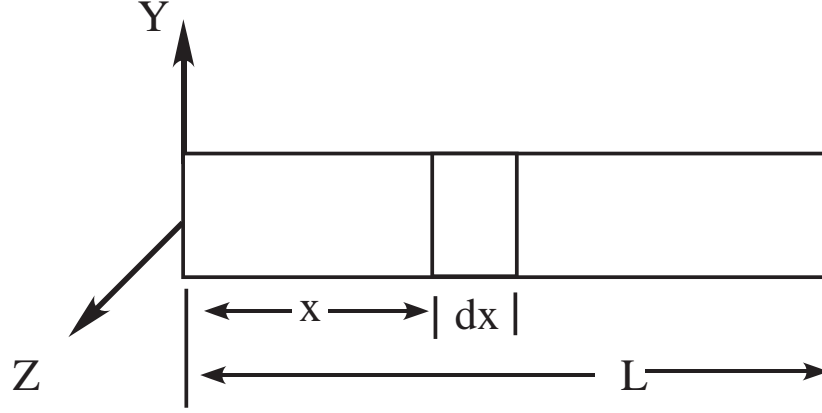
Figure 7.5: Diagram of Transverse Beam.
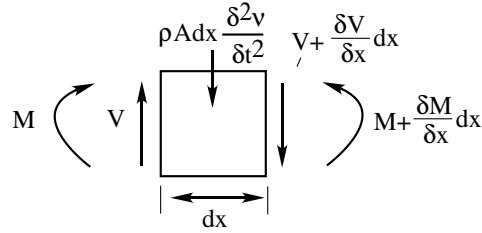
Figure 7.6: Diagram of Transverse Beam Element.

7.1.3 Longitudinal Beam

Longitudinal beams are also important in machine tools. The micro-mill drive screw of Figure 7.1 will oscillate longitudinally every time the workpiece is moved. The equations of motion for such longitudinal beam are quite similar to those of the torsional beam. Consequently, the longitudinal beam's equations are presented in the Appendix in Section A.1.

7.1.4 Transverse Beam

Transverse beams are used as an important building block for many machines. The consideration of transverse vibration is perhaps the most important, since most beams are the least stiff in the transverse direction. A diagram of a fixed free transversely vibrating beam can be seen in Figure 7.5. If a differential element of the beam is considered, then both shear and moment loads affect the response as shown in the diagram of Figure 7.6. The transverse beam parameters and variables are described in Table 7.2. Writing the equation for the equilibrium of the beam element in the vertical direction yields:

$$V - V - \frac{\delta V}{\delta x} - \rho A dx \frac{\delta^2 \nu}{\delta x^2} = 0 \tag{7.77}$$

214

Table 7.2: Transverse Beam Parameters.

Variable	Definition
ρ	Density
L	Length of Beam
ν	Transverse Deflection of Element
m	Elemental Mass
M_A	Attached Mass
E	Modulus of Elasticity
x	Position Along Beam
a	Wave Velocity
ω_i	Beam Natural Frequencies
t	Time
A	Area
V	Shear Load
M	Moment Load
X_i	Mode Shape
F_{stat}	Static Force Magnitude
A_i and B_i	Time Response Coefficients
C_i and D_i	Mode Shape Coefficients
K	Static Stiffness
ϕ_i	Time Dependent Response
i	Mode Number
Q	Forcing Function
I_P	Moment of Inertia

While the sum of the moments assuming $dx \cong dx/2$ yields:

$$- V\,dx + \frac{\delta M}{\delta x}dx = 0 \tag{7.78}$$

Combining these two equations together with the relationship between deflection and moment of:

$$M = EI\frac{\delta^2 \nu}{\delta x^2} = 0 \tag{7.79}$$

yields the governing equation for the motion of the transverse beam:

$$EI_P\frac{\delta^4 \nu}{\delta x^2} = -\rho A\,dx\frac{\delta^2 \nu}{\delta t^2} \tag{7.80}$$

The wave velocity is given by:

$$a = \sqrt{\frac{EI_P}{\rho A}} \tag{7.81}$$

With this equation, (7.80) can be further simplified to:

$$\frac{\delta^4 \nu}{\delta x^2} = -\frac{1}{a^2}\frac{\delta^2 \nu}{\delta t^2} \tag{7.82}$$

The specific case considered here is fixed on one end and free on the other. This creates two boundary conditions at each end. For the fixed end:

$$y_{(x=0)} = 0 \tag{7.83}$$

$$\left(\frac{dy}{dx}\right)_{x=0} = 0 \tag{7.84}$$

and at the free end, the conditions are:

$$\left(\frac{d^2 y}{dx^2}\right)_{x=L} = 0 \tag{7.85}$$

and:

$$\left(\frac{d^3 y}{dx^3}\right)_{x=L} = 0 \tag{7.86}$$

If the solution for the vibration of the beam is assumed to have the form of:

$$\nu_i = X_i\left(A_i \cos \omega_i t + B_i \sin \omega_i t\right) \tag{7.87}$$

where A_i and B_i are constants, then the mode shapes, X_i, can be assumed to be:

$$X_i = C_{1i}(\cos k_i x + \cosh k_i x) + C_{2i}(\cos k_i x - \cosh k_i x) + C_{3i}(\sin k_i x + \sinh k_i x) + C_{4i}(\sin k_i x - \sinh k_i x) \tag{7.88}$$

where:

$$k_i = \sqrt{\frac{\omega_i}{a}} \tag{7.89}$$

Table 7.3: Transverse Beam Frequency Solutions.

k_1L	k_2L	k_3L	k_4L	k_5L	k_6L
1.875	4.694	7.855	10.996	14.37	17.279

Note the increase in complexity over the torsional case due to the fourth derivative in (7.80). Using (7.87), (7.83) and (7.84) yields $C_{1i} = C_{3i} = 0$ and for (7.85) and (7.86) to be satisfied:

$$\cos k_i L \cosh k_i L = -1 \tag{7.90}$$

The first few solutions to (7.90) are given in Table 7.3. The table can be used to simply calculate the important natural frequencies of the transverse beam.

The next important step is to determine the mode shapes of the beam. By using the constraints and the assumed mode shape of (7.87), the result is:

$$X_i = C_{2i}(\cos k_i x - \cosh k_i x) + C_{4i}(\sin k_i x - \sinh k_i x) \tag{7.91}$$

C_{2i} and C_{4i} are determined by using the boundary conditions of (7.85) and (7.86) in conjunction with the spatial derivative of (7.91). This yields a proportional relationship between C_{2i} and C_{4i}, specifically $C_{4i} = \alpha C_{4i}$ where α is a constant determined by the particular parameters of the problem. This resultant relationship can then be used with the normalization property:

$$1 = \int_0^L X_i^2 dx \tag{7.92}$$

to find the specific values of C_{2i} and C_{4i}.

7.1.4.1 Static Deflection

The static stiffness of the transverse beam is given by:

$$k = \frac{3EI_p}{L^3} \tag{7.93}$$

This value can be relevant in both static analysis of the system and in simple dynamic modelling.

7.1.4.2 Forced Response

The same procedure is used for the computation of the forced response as was used for the other beams. That is Duhamel's integral is used with the mode shapes whose magnitudes C_{2i} and C_{4i} are calculated from the normalization. The result is that the deflection ν is:

$$\nu_i = \sum_{i=1}^{\infty} \frac{X_i}{\omega_i} \int_{x=0}^{L} X_i \int_{t=0}^{t} I_{tot} Q(x,t') \sin\left(\omega_i(t-t')\right) dt' dx \tag{7.94}$$

The major difference is that X_i contains two terms, and that the calculation of the magnitudes is much more complicated.
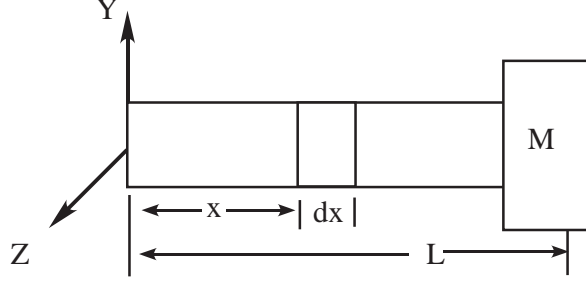
Figure 7.7: Diagram of Transverse Beam with Attached Mass.

7.1.4.3 Base Motion

The base motion of the transverse beam is not considered due to the complexity in modelling the rotary effects as described by the work of Kane, Ryan and Banerjee in [134].

7.1.5 Transverse Beam with Attached Mass

Often transverse beams must carry a load on the end. This load could be a sensor, an end-effector, or simply a load to be moved. For the case of transverse loading where there is an attached mass as described by Figure 7.7, the equations are the same as the case without the mass except that the boundary conditions at the mass end are instead:

$$\left(\frac{d^2 y}{dx^2}\right)_{x=L} = 0 \tag{7.95}$$

and:

$$\left(\frac{d^3 y}{dx^3}\right)_{x=L} = -M_a \left(\frac{d^2 y}{dt^2}\right)_{x=L} \tag{7.96}$$

Again the solution for the vibration of the beam is assumed to have the form of:

$$\nu_i = X_i \left(A_i \cos \omega_i t + B_i \sin \omega_i t\right) \tag{7.97}$$

Where X_i is assumed to be:

$$X_i = C_{1i}(\cosh k_i x) + C_{2i}(\sinh k_i x) + C_{3i}(\cos k_i x) + C_{4i}(\sin k_i x) \tag{7.98}$$

7.97 can be combined with (7.96) to write the equation of motion for the attached mass:

$$\left(\frac{d^3 X_i}{dx^3}\right)_{x=L} = -M_a \omega_i^2 (X_i)_{x=L} \tag{7.99}$$

The boundary conditions of (7.83) and (7.84), when combined with (7.97) yield:

$$C_{1i} = -C_{3i}$$
$$C_{2i} = -C_{4i} \tag{7.100}$$

218

Table 7.4: Frequencies of Transverse Beam with Attached Mass.

$k_i L$	$\alpha = 0$	$\alpha = 0.2$	$\alpha = 0.4$	$\alpha = 0.6$	$\alpha = 0.8$	$\alpha = 1$
$k_1 L$	1.875	1.616	1.472	1.375	1.304	1.248
$k_2 L$	4.694	4.267	4.144	4.086	4.053	4.031
$k_3 L$	7.855	7.318	7.215	7.173	7.149	7.134
$k_4 L$	10.996	10.401	10.317	10.285	10.267	10.256
$k_5 L$	14.137	13.506	13.436	13.410	13.376	13.388

The third boundary condition, (7.95), with (7.100) leads to the relationship:

$$C_{1i} = -C_{2i}\frac{\sinh kL + \sin kL}{\cosh kL + \cos kL} \tag{7.101}$$

When (7.100) and (7.101) are substituted into (7.99), the result is a complicated expression whose zeros can be used to determine the frequencies of the system. To ease this calculation, the equation has been parameterized and the result tabulated. Example values are included in Table 7.4 where α is the relationship of the attached mass M_a to the beams total mass $\rho * A * L$. While interpolating for values using the table is effective. A numerical solution was used for the results presented in this dissertation. The data in Table 7.4 was obtained from [24, 153, 108] and agreed with the numerical approach used here.

The modes shapes remain of the same form as the before the mass was added:

$$X_i = C_{1i}(\cosh k_i x) + C_{2i}(\sinh k_i x) - C_{1i}(\cos k_i x) - C_{2i}(\sin k_i x) \tag{7.102}$$

However, the values of C_{1i} and C_{2i} are significantly changed and can be determined by the normalization of (7.102) by the same procedure as the longitudinal and torsional beams with attached masses.

7.1.5.1 Static Deflection

The static stiffness of the transverse beam with an attached mass is the same as the case without the attached mass. That is:

$$K = EI_P \tag{7.103}$$

7.1.5.2 Forced Response

The forced response of the transverse beam with an attached mass, follows exactly the same procedure as the other beams. However, the normalization of the mode shapes is difficult and can only be solved numerically in many cases. However, once the values are normalized the same equation as the transverse case without a mass can be used with the new mode shapes and natural frequencies:

$$\nu_i = \sum_{i=1}^{\infty} \frac{X_i}{\omega_i} \int_{x=0}^{L} X_i \int_{t=0}^{t} I_{tot}Q(x,t')\sin\left(\omega_i(t-t')\right)dt'dx \tag{7.104}$$

7.1.5.3   Base Motion

Like the case with no mass, the base motion of the transverse beam is not considered but [134] is a good source for developing a Finite Element model for the base motion case.

7.2   Input Shaping for Continuum Systems

Now that models exist for the motion of continuum systems, these models can be used to explore input shaping theory directly on continuum systems. While input shaping has been applied to these systems before, a derivation of its effectiveness and sensitivity has not been made except by the author [80]. Throughout this discussion both the first mode as well as the higher modes will be addressed. Often the higher modes will be presented separately, as their impact cannot always be seen when coupled with the dominant first mode.

7.2.1   Input Shaped Response

The first step in using input shaping to reduce continuum beam vibrations is to study how input shaping effects multi-mode continuum system dynamics. For this study of continuum beams, the vibration of a torsional beam will be considered as an example using the same procedure as was used for discrete systems in Section 3.3.1. Equation (7.75) depicts the time response of the continuous torsional beam to any arbitrary base position input $g(t)$. The solution to this equation is simplified if the input is assumed to be a series of impulses or an input shaper. Also if the time dependent portion of the beam response is zero, then the overall response will also be zero. Therefore, henceforth only the time dependent portion of (7.75) will be considered:

$$\int_0^t \ddot{g}\left(\acute{t}\right) \sin\left(\omega_i \left(t - \acute{t}\right)\right) d\acute{t} \tag{7.105}$$

If $\ddot{g}(t)$ is a dirac impulse of magnitude A_j at time t_j then the previous equation becomes:

$$\int_0^t A_j \delta\left(t - t_j\right) \sin\left(\omega_i \left(t - \acute{t}\right)\right) d\acute{t} \tag{7.106}$$

whose solution is given for various times t by:

$$\int_0^t \ddot{g}\left(\acute{t}\right) \sin\left(\omega_i \left(t - \acute{t}\right)\right) d\acute{t} = \begin{cases} 0 & \text{if } t < t_j \\ \frac{A_j}{2} \sin\left(\omega_i \left(t - t_j\right)\right) & \text{if } t = t_j \\ A_j \sin\left(\omega_i \left(t - t_j\right)\right) & \text{if } t > t_j \end{cases} \tag{7.107}$$

Thus the time dependent portion of the response for the ith mode after an impulse sequence of length j will be given by V:

$$V = \int_0^t \ddot{g}\left(\acute{t}\right) \sin\left(\omega_i \left(t - \acute{t}\right)\right) d\acute{t} = \sum_{j=1}^{j} A_j \sin\left(\omega_i \left(t - t_j\right)\right) \tag{7.108}$$

This equation can be used to prove the effectiveness of different input shapers, since if the time dependent portion is identically zero then the overall response will also be zero.

7.2.1.1 Zero Vibration (ZV) Shapers

The traditional Zero Vibration or ZV shaper for an undamped system is given by:

$$\begin{bmatrix} A_j \\ t_j \end{bmatrix} = \begin{bmatrix} \frac{1}{2} & \frac{1}{2} \\ 0 & \frac{\pi}{\omega_n} \end{bmatrix} \tag{7.109}$$

where ω_n is the frequency it is designed to cancel.

If this input shaper is used on the first mode of the continuum torsional beam model of (7.108), then the resultant time dependent portion of the response after the shaper is:

$$V = \frac{1}{2} \sin(\omega_i t) + \frac{1}{2} \sin(\omega_i t - \pi) \equiv 0 \tag{7.110}$$

This equation is identically equal to zero, which means that the response of the beam coming from the first mode of vibration will be zero. However, the response of the other modes will still need to be calculated using (7.108) and (7.75).

7.2.1.2 Zero Vibration and Derivative (ZVD) Shapers

The ZV shaper does not deal well with significant modelling error in the system. To combat this the Zero Vibration and Derivative, ZVD, shaper was developed which requires the derivative of vibration magnitude to also be zero at the modelled frequency. This derivative of the vibration equation, (7.108), for an arbitrary impulse sequence with respect to the designed frequency is:

$$\frac{\delta V}{\delta \omega_i} = \sum_{j=1}^{j} A_j (t - t_j) \cos(\omega_i (t - t_j)) \tag{7.111}$$

If (7.108) and (7.111) are zero after the input shaper, then the ZVD constraints are met.

The standard ZVD shaper for undamped systems has the form:

$$\begin{bmatrix} A_j \\ t_j \end{bmatrix} = \begin{bmatrix} \frac{1}{4} & \frac{1}{2} & \frac{1}{4} \\ 0 & \frac{\pi}{\omega_n} & \frac{2\pi}{\omega_n} \end{bmatrix} \tag{7.112}$$

If these impulse are used in (7.108), then the result is:

$$V = \frac{1}{4} \sin(\omega_i t) + \frac{1}{2} \sin(\omega_i t - \pi) + \frac{1}{4} \sin(\omega_i t - 2\pi) \equiv 0 \tag{7.113}$$

which is also identically zero. Using the ZVD shaper in the derivative constraint of (7.111) yields:

$$\frac{\delta V}{\delta \omega_i} = \frac{t}{4} \cos(\omega_i t) + \frac{t - \frac{\pi}{\omega_n}}{2} \cos(\omega_i t - \pi) + \frac{t - \frac{2\pi}{\omega_n}}{4} \cos(\omega_i t - 2\pi) \tag{7.114}$$

which can be expanded to:

$$\frac{\delta V}{\delta \omega_i} = \frac{t}{4} \cos(\omega_i t) + \frac{t - \frac{\pi}{\omega_n}}{2} (\cos(\omega_i t) \cos(\pi) + \sin(\omega_i t) \sin(\pi)) \tag{7.115}$$

$$+ \frac{t - \frac{2\pi}{\omega_n}}{4} (\cos(\omega_i t) \cos(2 * \pi) + \sin(\omega_i t) \sin(2 * \pi))$$

The derivative equation can then be further reduced to:

$$\frac{\delta V}{\delta \omega_i} = \cos\left(\omega_i t\right)\left(\frac{t}{4} - \frac{t}{2} + \frac{\pi}{2\omega_i} + \frac{t}{4} - \frac{2\pi}{4\omega_i}\right) \equiv 0 \tag{7.116}$$

This equation is also equal to zero any time after the duration of the shaper. Thus the ZVD input shaper's vibration and derivative of vibration criteria work on the first mode of the torsional continuum model. However, vibration will still exist coming from the other modes.

7.2.1.3 Unity Magnitude Zero Vibration (UMZV) Shaper

The Unity Magnitude Zero Vibration Shaper, UMZV, is another common input shaper which has a shorter duration than the standard ZV shaper. It duration is only $\frac{1}{3}$ of the period compared to $\frac{1}{2}$ for the ZV. This is accomplished using both positive and negative impulses with all impulse magnitudes equal to one. The UMZV shaper is defined for the undamped case by:

$$\begin{bmatrix} A_j \\ t_j \end{bmatrix} = \begin{bmatrix} 1 & -1 & 1 \\ 0 & \frac{\pi}{3\omega_n} & \frac{2\pi}{3\omega_n} \end{bmatrix} \tag{7.117}$$

where $\frac{2\pi}{\omega_n}$ is the period of vibration to be cancelled. The vibration (7.108) becomes:

$$V = \sin\left(\omega_i t\right) - \sin\left(\omega_i t - \frac{\pi}{3}\right) + \sin\left(\omega_i t - \frac{2\pi}{3}\right) \tag{7.118}$$

Through trigonometric identities the previous equation can be simplified to:

$$V = \sin\left(\omega_i t\right) - \left(\sin\left(\omega_i t\right)\cos\left(\frac{\pi}{3}\right) - \cos\left(\omega_i t\right)\sin\left(\frac{\pi}{3}\right)\right) + \left(\sin\left(\omega_i t\right)\cos\left(\frac{2\pi}{3}\right) - \cos\left(\omega_i t\right)\sin\left(\frac{2\pi}{3}\right)\right) \tag{7.119}$$

The terms can be collected to yield:

$$V = \sin\left(\omega_i t\right)\left(1 - \frac{1}{2} - \frac{1}{2}\right) + \cos\left(\omega_i t\right)\left(\frac{\sqrt{3}}{2} - \frac{\sqrt{3}}{2}\right) \tag{7.120}$$

which is identically equal to zero. Thus the UMZV shaper cancels the vibration perfectly in the mode it is trying to cancel, although again the other modes of the system are not constrained.

7.2.2 Torsional Beam

Using the previously derived equations of motion for the torsional beam, the effectiveness of input shaping particular to this been can be investigated. This process involves first defining the impulse response of the beam, then combining those responses together to yield a total shaped response. As part of this process, the effect of higher modes will be considered along with the sensitivity of the input shaping process to parameter variation.
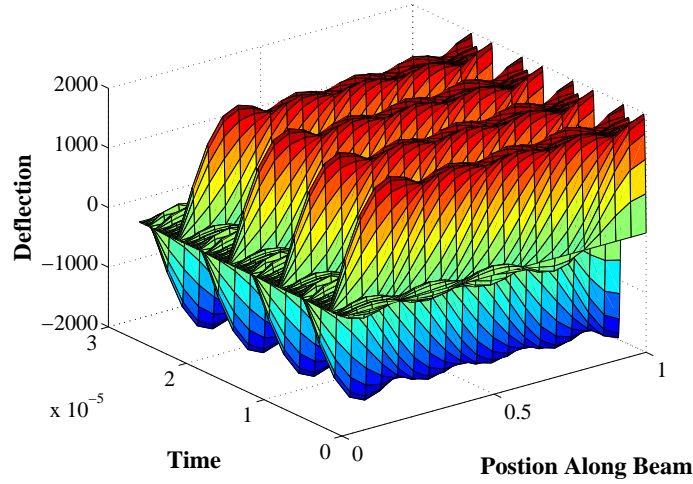
Figure 7.8: Impulse Moment Response of Torsional Beam.

7.2.2.1 Impulse Response

The first step in the input shaping process is to find the response of the torsional beam to an impulsive torque. Figure 7.8 shows how a torsional beam might respond to such a torque applied to the free end of the beam. This figure format for the presentation of beam vibration will be used extensively in the remainder of this chapter. It shows the deflection along the beam as time progresses into the page. From this particular figure, the dominant first mode can be seen. The higher modes impact on the response is secondary for this beam, as is shown in the response of modes 2,3,4, and 5 in Figure 7.9. These modes occur at the odd integer multiples of the first mode and are responsible for a large portion of the response as shown by their large magnitude in the figure.

7.2.2.2 Forced Input Response

The forced response of the torsional beam refers to directly applying an sequence of impulsive torques to the end of the beam. Later the motion of the base will be considered. Here the impact of ZV, ZVD, and UMZV shapers will be discussed.

7.2.2.2.1 Zero Vibration Shaper

If a fixed-free torsional beam is given two impulsive torque that obey the rules for a ZV shaper, then the deflection along the beam with time is shown in Figure 7.10. After the second impulse occurs theoretically all vibration in the beam is eliminated. The first mode is cancelled as was predicted by the theory. The other modes are also cancelled as is shown in Figure 7.11, the response of modes 2 through 5. The higher modes are cancelled due to the relationships between the frequencies. The higher frequencies of the torsional beam are

223
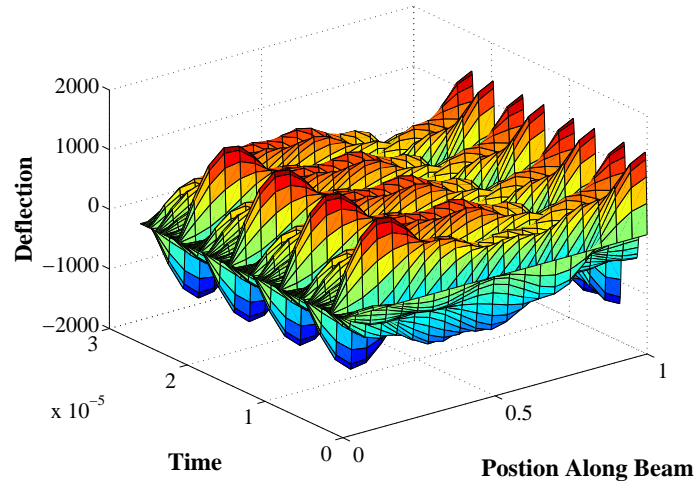
Figure 7.9: Modes 2 through 5 Impulse Moment Response of Torsional Beam.
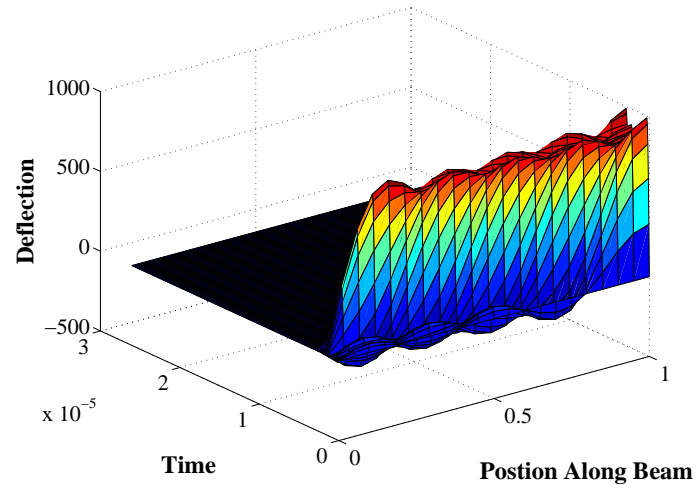
Figure 7.10: Zero Vibration Moment Response of Torsional Beam.
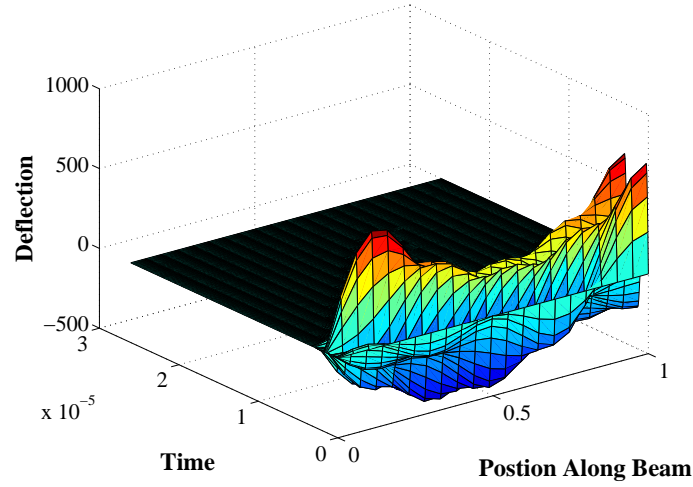
Figure 7.11: Modes 2 through 5 ZV Moment Response of Torsional Beam.
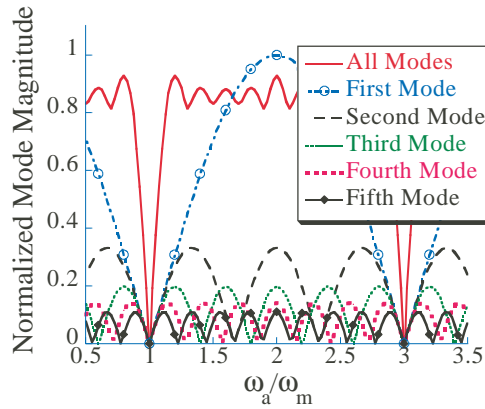
Figure 7.12: Zero Vibration Sensitivity of Torsional Beam.

odd integer multiples of the fundamental frequency. Odd integer multiples of the designed frequency are also cancelled by the ZV shaper. From this result, ZV input shapers are ideally suited for this type of beam.

The relationship between the modes can further be seen from the sensitivity of the shaper. Figure 7.12 shows the normalized error of each mode with modelling error in the first natural frequency of the system. All five modes have zero error at exact modelling. This leads to the response also having zero error when modelling is exact. Note that the natural frequency of the second mode would occur at 3 on this figure, the third mode at 5 and so on. The ZV shaper inherently cancels these modes.

The sensitivity of the overall beam response is also important. The curve that represents the summation of all modes is much steeper than the traditional ZV shaper, for which the
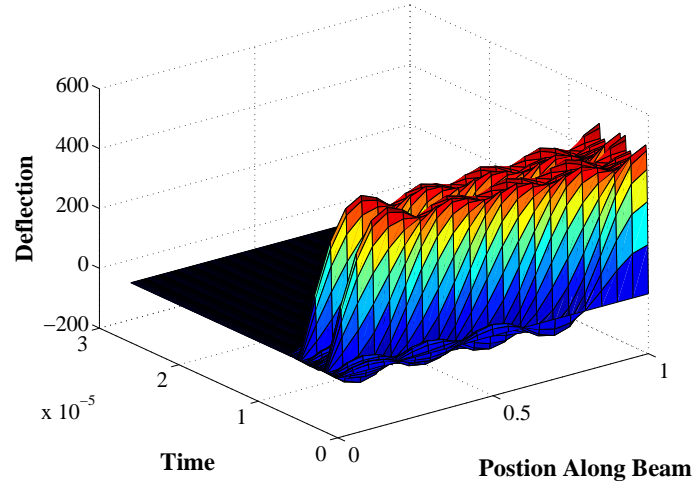
Figure 7.13: Zero Vibration Derivative Moment Response of Torsional Beam.

first mode is a good example. This means that even small modelling errors can cause a significant degradation in performance. Another important observation from the sensitivity is the magnitude of the curve for large modelling errors. The error is never larger than in the unshaped case. Therefore, implementing a ZV input shaper will never make the vibration worse than with no shaper at all, no matter the modelling error.

7.2.2.2.2 Zero Vibration and Derivative Shaper

The ZV shaped torsional beam was sensitive to modelling errors. If this is unacceptable, then a ZVD shaper might be employed to improve the response of a torsional beam. Figure 7.13 shows the response of an entire torsional beam to three impulsive torques governed by the ZVD shaper applied at the end of the beam. The duration of this command is twice that of the ZV shaper, allowing the beam to vibrate for an entire period, but also notice that just like the ZV case, all vibration is cancelled after the shaper. This is because like the ZV shaper the ZVD shaper cancels all odd integer multiples of the design frequency. This can be seen clearly if the response of the higher modes only is plotted, as it is in Figure 7.14.

Again the sensitivity of all the modes of the beam offers some insight into the sources of the excellent performance. Figure 7.15 shows how the normalized performance of the shaping scheme changes with modelling error in the shaper. The higher modes are once again zero at perfect modelling. The shape of the overall curve is also important. The curve is less steep than for the ZV case. This comes at the cost of a shaper with twice the duration of the ZV shaper. Also notice that while the curve is steep, it does maintain one of the primary features of the ZVD shaper, a zero-derivative with respect to modelling error at perfect modelling. This derivative relationship occurs in all the modes. Finally the ZVD
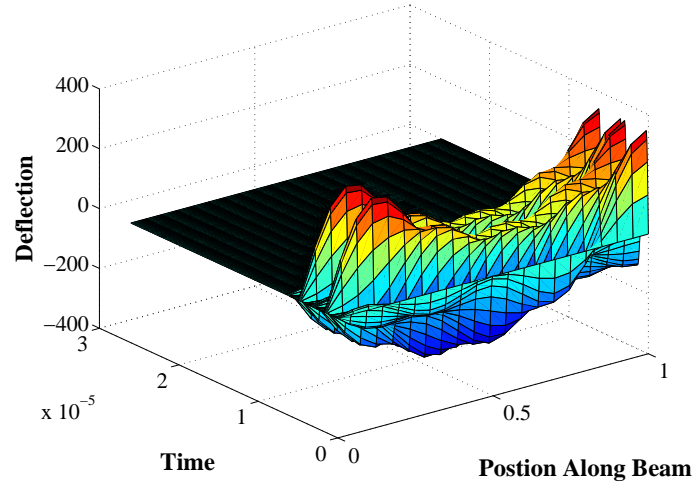
Figure 7.14: Modes 2 through 5 ZVD Moment Response of Torsional Beam.
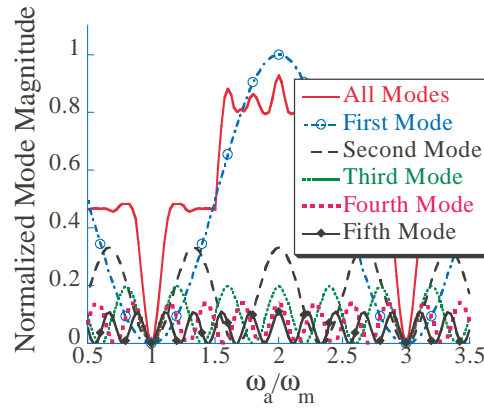
Figure 7.15: Zero Vibration Derivative Sensitivity of Torsional Beam.
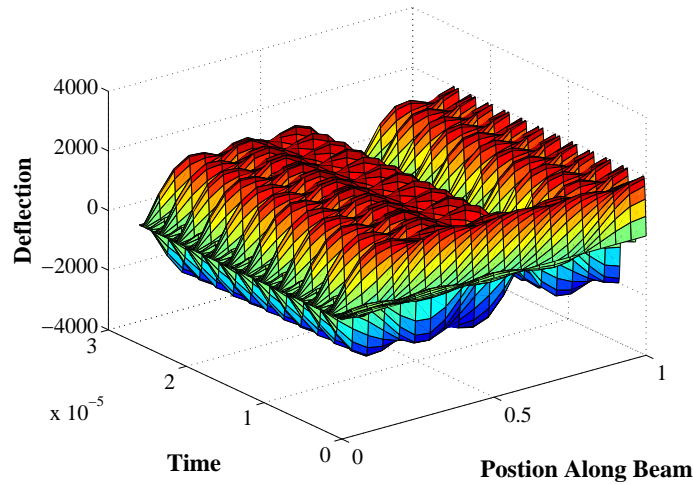
Figure 7.16: UMZV Moment Response of Torsional Beam.

shaper never increases the vibration over the unshaped case.

7.2.2.2.3 Unity Magnitude Zero Vibration Shaper

Another common input shaper designed for swift motion is the UMZV shaper. This shaper utilizes both positive and negative impulses to drive the system, and thus is capable of faster motion. If a series of impulse coinciding with a UMZV shaper is given the torsional beam, the result is less than ideal as is shown in Figure 7.16. The first mode of vibration is completely cancelled, however some of the other modes of vibration are excited instead of suppressed. Figure 7.17 shows how these higher modes are increased by the aggressive UMZV shaper. The odd integer multiple relationship that enabled the ZV and ZVD shaper to work well for the torsional beam are the decline of the UMZV shaper. A UMZV shaper excites frequencies at 3, 5, 7, *etc.* times the natural frequency to three times their original magnitude. For the torsional beam's impulse response, these modes contribute a third of the overall vibration. Since these modes are excited to three times their unshaped magnitude with the UMZV shaper, the vibratory magnitude remains approximately the same after UMZV shaping.

The sensitivity curve of the first five modes of the torsional beam for the UMZV shaper is shown in Figure 7.18. It offers insight into the lack of vibration reduction. Every even mode is increased in magnitude three times. The result is that at perfect modelling the vibration is the same as without shaping. A further drawback of this technique is that the vibration can be made even worse if significant modelling error occurs. The first mode can be excited to three times its unshaped magnitude if the modelling error is severe.

The result of this investigation into the UMZV shaper is that the UMZV shaper is a poor choice for multi-mode system that have significant modes at 3, 5, or 7 times the designed
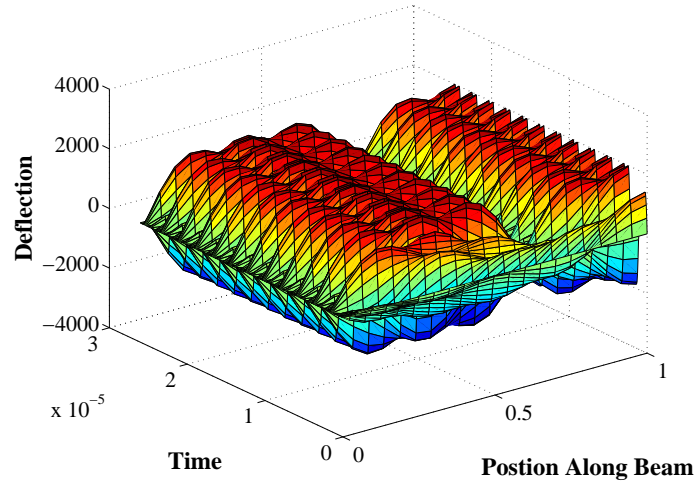
Figure 7.17: Modes 2 through 5 UMZV Moment Response of Torsional Beam.
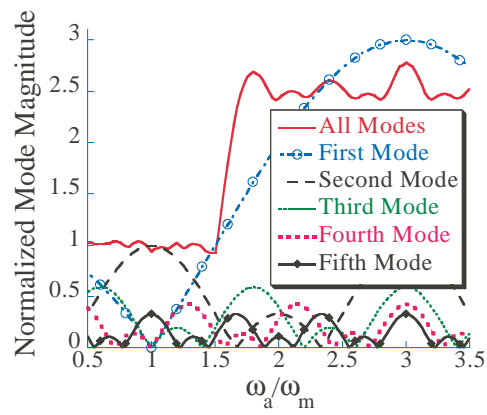
Figure 7.18: UMZV Sensitivity of Torsional Beam.
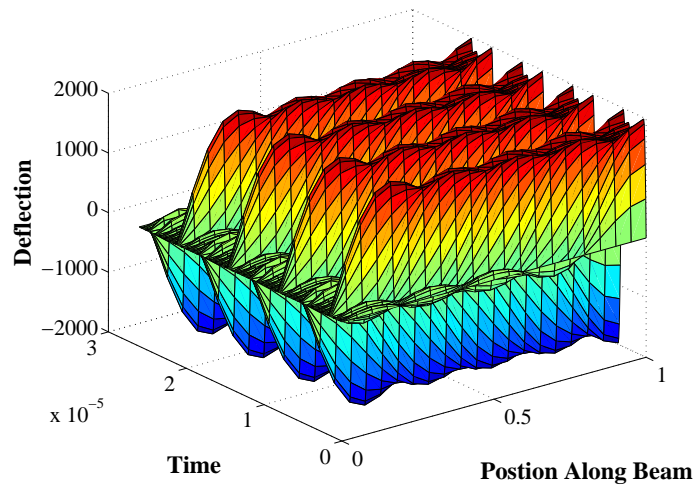
Figure 7.19: Step Acceleration Response of Torsional Beam.

frequency. This fact has been known since the development of the UMZV shaper, however, the problems exacerbation by this torsional beam is novel.

7.2.2.3   Base Motion

Beams are not only driven by applied forces or torques but also by motion of the base of the beam. One of the most common motions that a beam might undergo is an S-curve displacement of the base. In such a case, an input shaper would need to work effectively for all the changes in acceleration of the move. To study the effectiveness of input shaping on continuum torsional beams, input shaping was applied to a step change in acceleration of the base of the beam, the most basic component of S-curve position profiles.

The unshaped response of the beam to a step change in the acceleration of the base produces unwanted vibration. Figure 7.19 shows the deflection along the beam from the moving base. Note, that although difficult to see, after the change in acceleration the beam oscillates about a new non-zero set-point. This new set-point is due to the beam now being constantly accelerated, forcing a continuous deflection. As was the case for the forced motion, the higher modes of the beam contribute significantly to the response as seen in Figure 7.20. The oscillation about a new set-point is more clear in these higher modes. A successful shaping scheme will have to compensate for these higher modes in order successfully move the system.

7.2.2.3.1   Zero Vibration Shaper

The zero vibration input shaper was effective at multi-mode vibration suppression for the torsion beam. Likewise, it is effective for base acceleration motions. Figure 7.21 shows the response of the beam theoretically has zero post-shaper vibration when the ZV shaper is
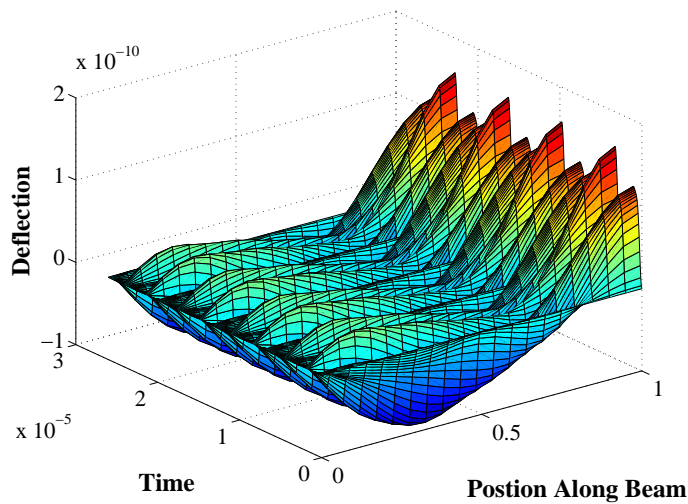
Figure 7.20: Modes 2 through 5 Step Acceleration Response of Torsional Beam.

employed. The beam has a constant deflection synonymous with the constant acceleration load. Also the higher modes have been successfully restricted. Figure 7.22 details how the higher modes undergo a constant deflection during the acceleration with no vibration. A few transient oscillations in the higher modes do occur during the shaper. Also the higher modes exhibit there original contribution to the motion, that is the combined higher mode deflection is an order of magnitude less than the overall response.

7.2.2.3.2 Zero Vibration and Derivative Shaper

Parameter variation is also an important concern when accelerating a beam's base. The ZVD shaper can be used to compensate for this issue. Figure 7.23 shows that the ZVD shaper is also effective at cancelling vibration resultant from base accelerations. The constant acceleration set-point is clear as well as the middle impulse of the shaper, which is the hump halfway through the transient of the deflection. Since the ZVD shaper is longer than the ZV shaper, more transient deflection occurs, especially in the higher modes as seen in Figure 7.24. Although, these transients last longer, the magnitude is still the same.

7.2.2.3.3 Unity Magnitude Zero Vibration Shaper

The UMZV shaper is not well suited for forced motions of torsional beams, and likewise it does not perform well for base accelerations. Figure 7.25 shows the overall beam response, where some of the higher modes once again are excited by the shaper. The higher mode oscillation can be seen clearly in Figure 7.26. Once again the UMZV shaper successfully cancels the first mode, but excites the third, fifth, *etc.* modes to three times there original magnitude, making it a poor choice for vibration suppression in this beam.
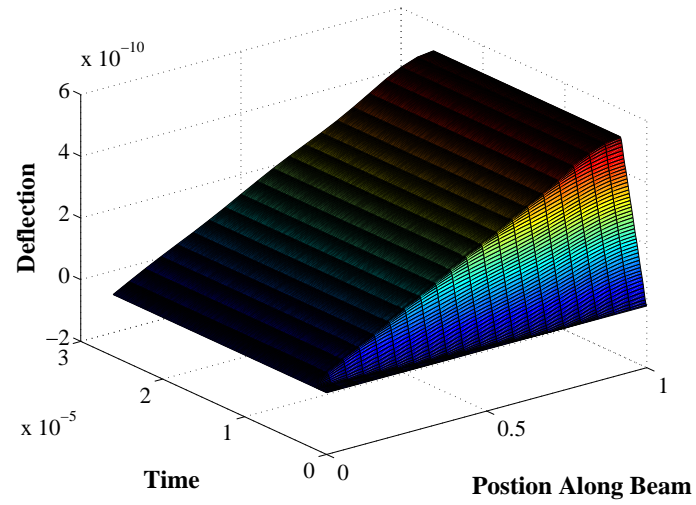
Figure 7.21: Zero Vibration Acceleration Response of Torsional Beam.
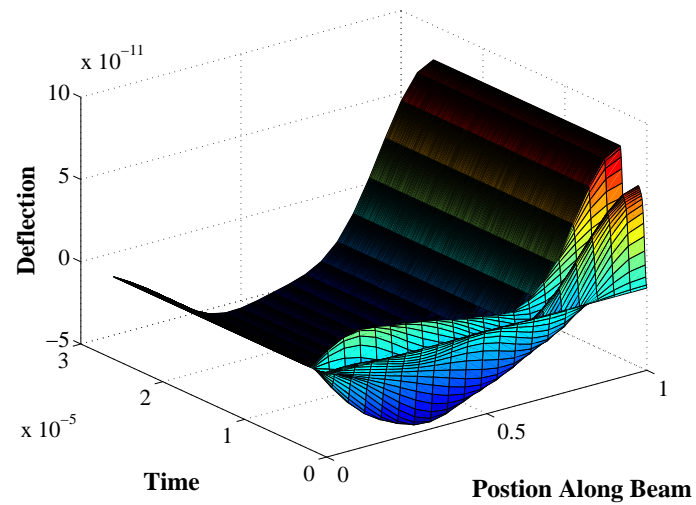
Figure 7.22: Modes 2 through 5 ZV Acceleration Response of Torsional Beam.
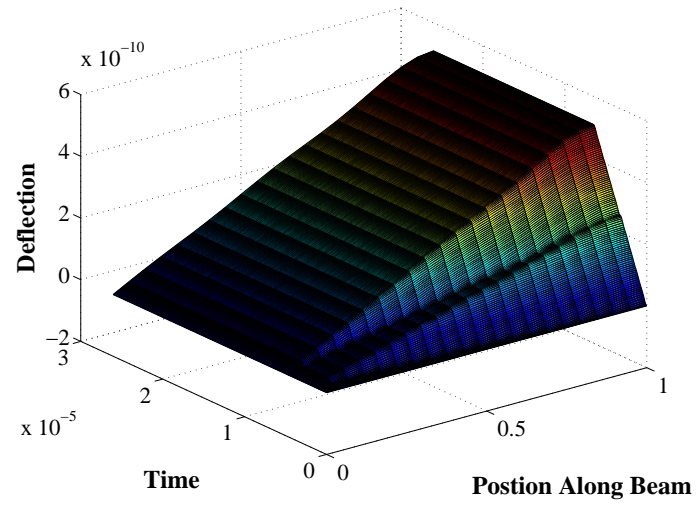
Figure 7.23: Zero Vibration Derivative Acceleration Response of Torsional Beam.
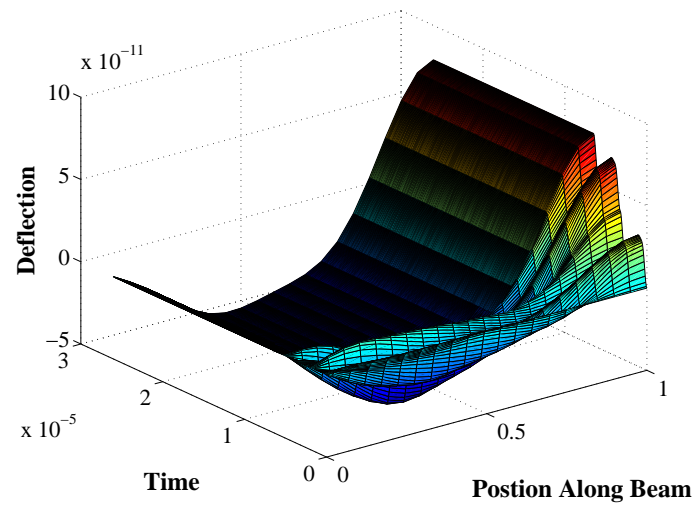
Figure 7.24: Modes 2 through 5 ZVD Acceleration Response of Torsional Beam.
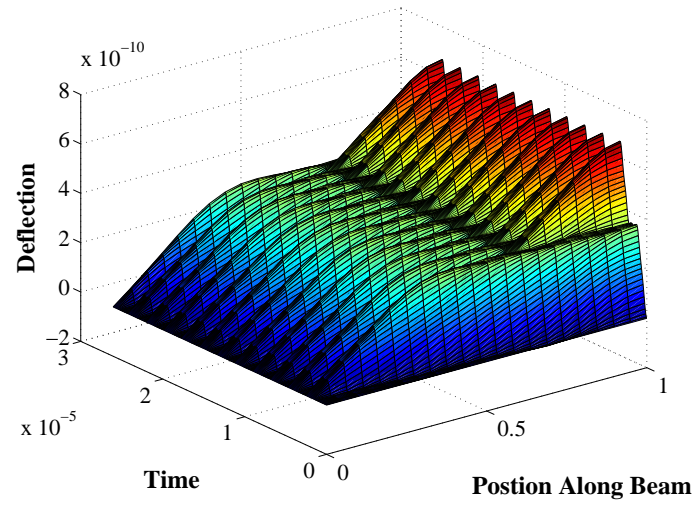
Figure 7.25: UMZV Acceleration Response of Torsional Beam.
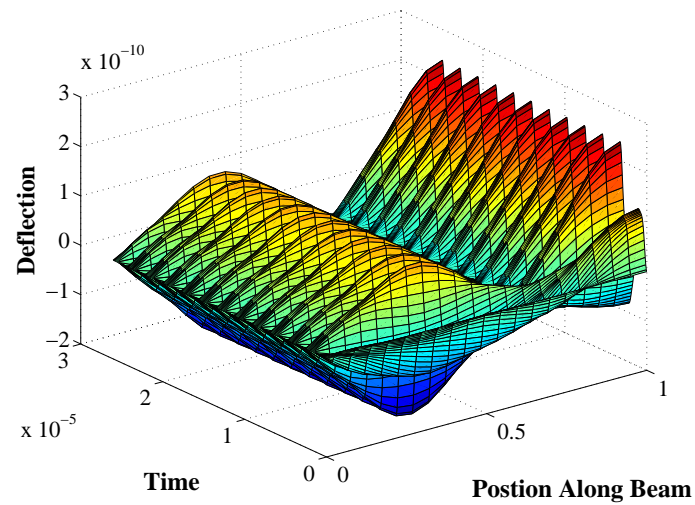
Figure 7.26: Modes 2 through 5 UMZV Acceleration Response of Torsional Beam.
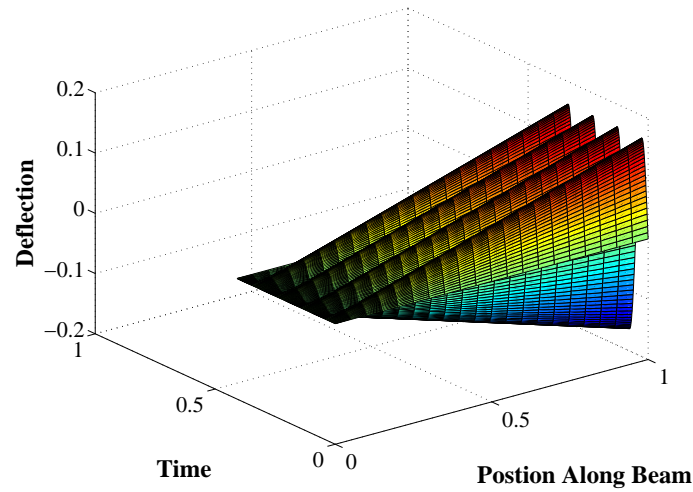
Figure 7.27: Impulse Moment Response of Torsional Beam with Attached Inertia.

7.2.3 Torsional Beam with Inertia

Attaching an inertia to the end of a torsional beam can drastically alter the motion of the beam. The ability of input shaping to deal with this new oscillatory system will be investigated as it impacts both forced and base motion responses. The sensitivity of the system to modelling error as well as the impact of higher modes will be studied.

7.2.3.1 Impulse Response

The first step in studying the effects of input shaping for the torsional beam with an attached inertia is to investigate the impulse response. Figure 7.27 shows an example impulsive torque response if applied at the free end of the beam. Notice the difference in shape now that the attached inertia has been added. The beam now deflects essentially linearly between the attachment point and the forced end. This is due to different mode shapes, as well as a lesser impact of the higher modes. Figure 7.28 shows the impulse response of only the higher modes. The influence of these higher modes is negligible in this attached inertia case, as evident by the scale of the deflection in the higher modes. For cases with lower attached inertia, these modes could still impact the motion of the beam. But here the impulse response shows that the system is behaving like a second order oscillator with only one mode, that is the beam is essentially a spring.

7.2.3.2 Forced Input Response

This attached inertia case behaves quite differently than the case with no inertia when forced. The major difference is that for large attached inertias, the beam behaves as essentially a second-order system. Input shaping has already been proven effective on these
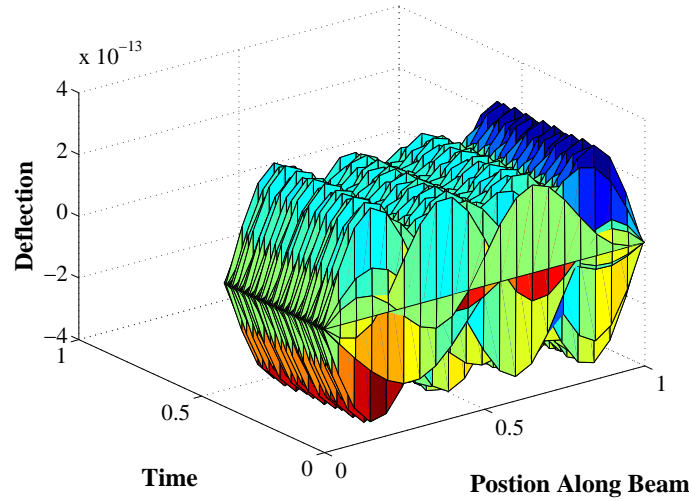
Figure 7.28: Modes 2 through 5 Impulse Moment Response of Torsional Beam with Attached Inertia.

types of systems.

7.2.3.2.1 Zero Vibration Shaper

When a ZV input shaper is applied to the beam in the form of a sequence of impulsive torques at the inertia end of the beam, the input shaper is effective as shown in Figure 7.29. The first mode of vibration is successfully cancelled while the higher modes do not offer any significant vibration into the system as shown by their response in Figure 7.30. However, the modes still oscillate. The ZV shaper does not cancel the higher modes of the torsional beam with an attached inertia. Instead the magnitude of the modes is always low.

The sensitivity of the ZV shaper on the torsional beam with an attached inertia is effectively the same sensitivity as a ZV shaper on any second-order system as shown in Figure 7.31. Since the scales from the higher modes are so small they have no impact on the response.

However, as the attached inertia is reduced the beam behaves more like a beam with no attached inertia. Figure 7.32 shows the change in the sensitivity curve for different inertia ratios or the ratio between attached inertia and beam inertia. With even small attached inertia, the impact of the higher modes is reduced. That is, with attached inertia, although the frequencies no longer align with the odd multiples of the primary frequency, the magnitude of the modes is reduced. Thus the higher modes have little impact.

7.2.3.2.2 Zero Vibration and Derivative Shaper

The behavior of the ZVD shaper on this system is as expected from the ZV case, that is it mimics a second order system. Figure 7.33 depicts the total response to a ZVD input.
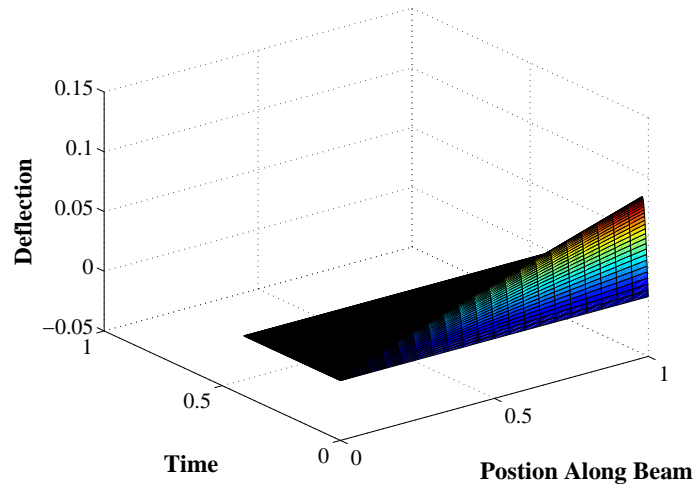
Figure 7.29: Zero Vibration Moment Response of Torsional Beam with Attached Inertia.
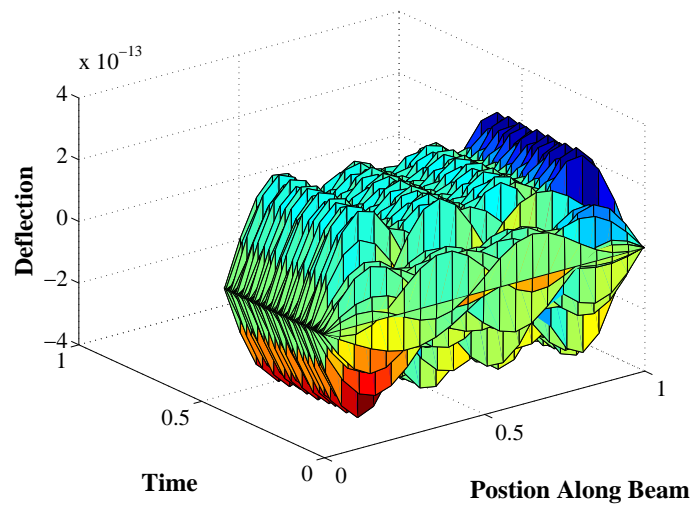
Figure 7.30: Modes 2 through 5 ZV Moment Response of Torsional Beam with Attached Inertia.
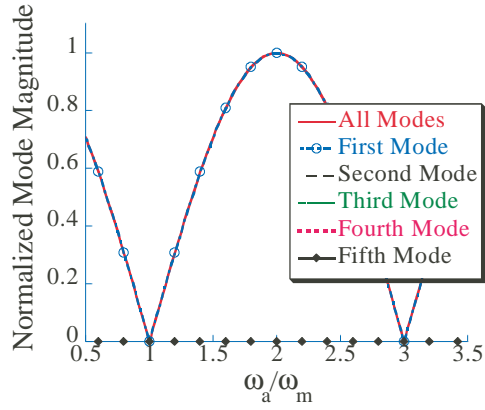
Figure 7.31: Zero Vibration Sensitivity of Torsional Beam with Attached Inertia.
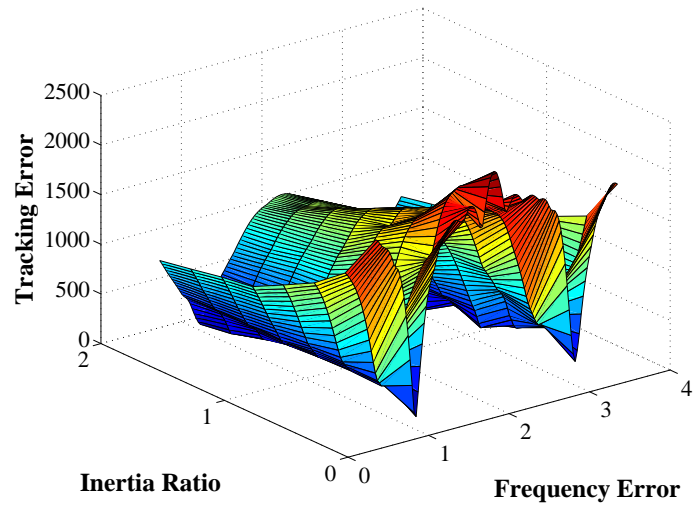
Figure 7.32: Zero Vibration Sensitivity of Torsional Beam for Various Attached Inertia.
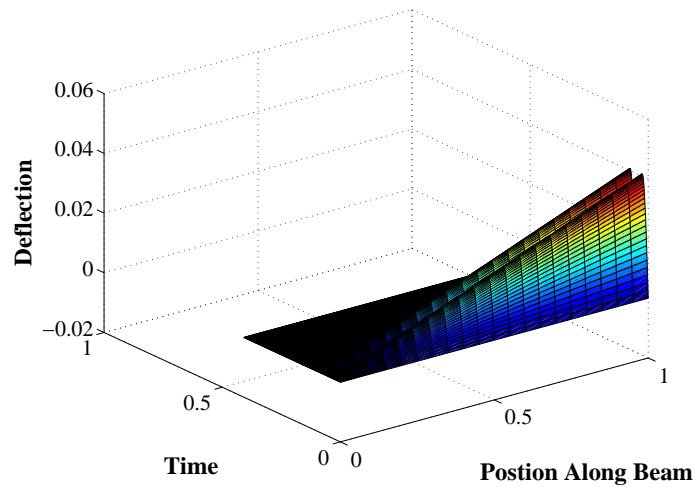
Figure 7.33: Zero Vibration Derivative Moment Response of Torsional Beam with Attached Inertia.

An entire period of vibration does occur before the vibration is eliminated, but the first mode as well as the other modes are successfully cancelled as shown for the higher modes in Figure 7.34.

The ZVD shaper's sensitivity on the torsional beam with an attached inertia also resembles the second-order oscillator case. Figure 7.35 shows how the zero vibration and the derivative constraint are met, and that the higher modes contribute little if anything to the motion of the beam.

7.2.3.2.3   Unity Magnitude Zero Vibration Shaper

The UMZV shaper was inappropriate for the torsional beam without an attached inertia, however when an inertia is added to the beam, the UMZV shaper becomes an effective vibration reduction tool. Figure 7.36 shows an example case for the application of a UMZV shaper. For this level of attached inertia, the higher modes do not adversely affect the response. This is for two reason, first the contributions are significantly less, and second the modes no longer line up exactly with the worst case scenarios of the UMZV shaper. Figure 7.37 shows how the higher mode oscillations are significantly lower in magnitude.

The negligible impact of the higher modes for the attached inertia case can be seen clearly in the sensitivity curve, which closely resembles the lumped-parameter case. However, for small attached inertias, UMZV shaping can still excite the higher modes to an unacceptable level. Figure 7.39 show how for various attached inertias the sensitivity curve changes. In fact, near zero vibration cannot be obtained from the UMZV shaper until an inertia ratio near one. That is the attached inertia must be equal to the inertia of the entire beam. From this analysis, it is not a good idea to use UMZV shapers on this type of beam due to the

239
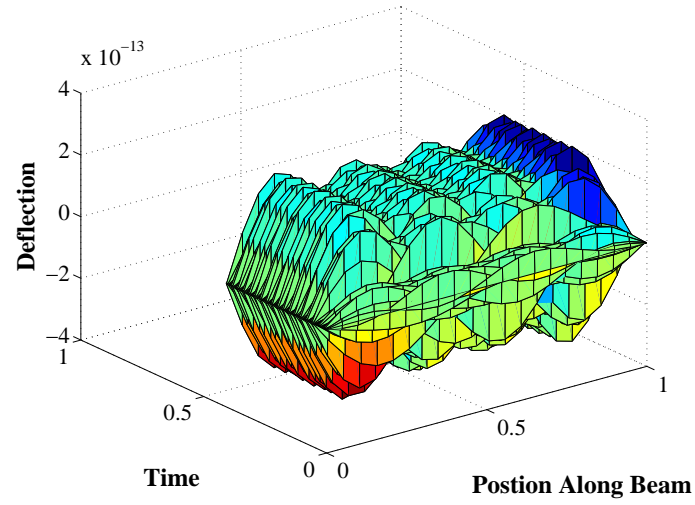
Figure 7.34: Modes 2 through 5 ZVD Moment Response of Torsional Beam with Attached Inertia.
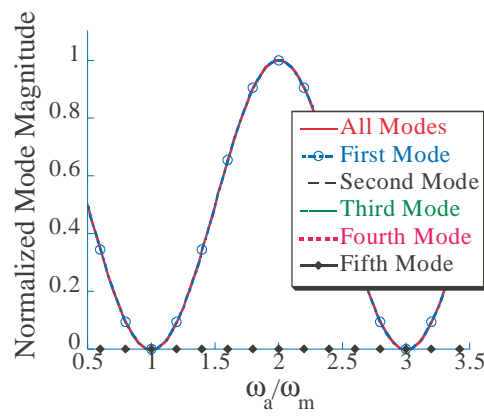
Figure 7.35: Zero Vibration Derivative Sensitivity of Torsional Beam with Attached Inertia.
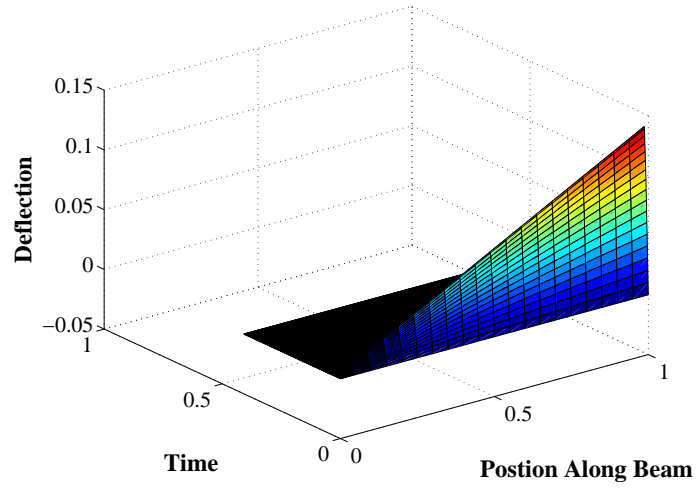
Figure 7.36: UMZV Moment Response of Torsional Beam with Attached Inertia.
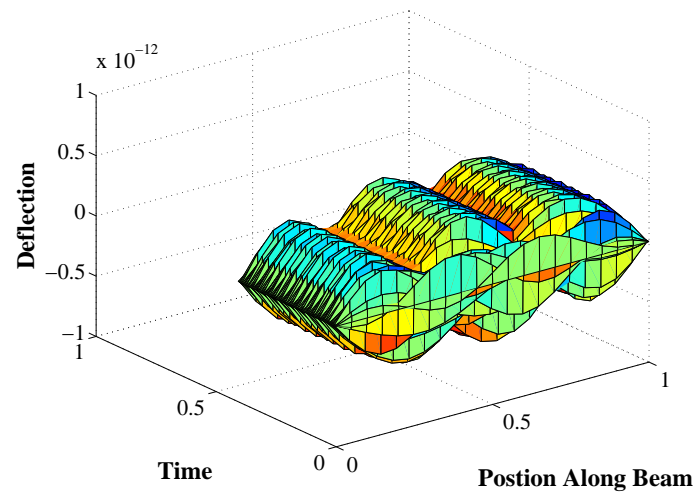
Figure 7.37: Modes 2 through 5 UMZV Moment Response of Torsional Beam with Attached Inertia.
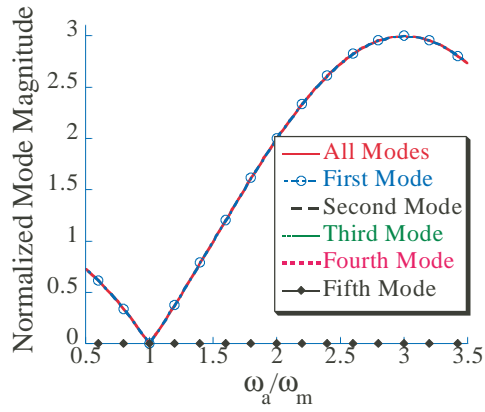
Figure 7.38: UMZV Sensitivity of Torsional Beam with Attached Inertia.
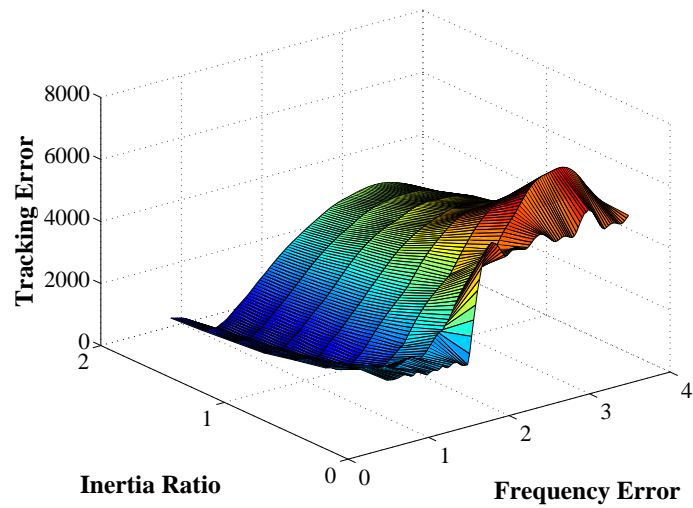
Figure 7.39: UMZV Sensitivity of Torsional Beam with Various Attached Inertias.

danger of exciting the higher modes.

7.2.3.3 Base Motion Response

The attached inertia on the end of the beam also affects the base motion response of the beam. Once again the simple step change in acceleration of the base will be used as a test case. Since, the responses and insight are the same as those for the forced response case, the base motion responses are included in Appendix A.2 without discussion.

7.2.4 Longitudinal Beams

The results of input shaping for longitudinal beams are the same as for torsional beams. Consequently, Appendix A.3 shows the results for longitudinal beam examples, both with and without attached masses.

7.2.5 Transverse Beam

Transversely vibrating beams have more complicated dynamics than either the torsional or longitudinal beams due to the multiple term mode shapes. Therefore, input shaping may have a different effect. Specifically, the impulse responses with respect to forced motion will be investigated for the transverse beam. Considerations will be made for the sensitivity of the process.

The transversely vibrating beam is a more complicated oscillatory problem due to the complexity of the modes. However, the application of input shaping is the same. The input shaper can be used to completely cancel the first mode, and then only the vibration in the higher modes needs to be considered.

7.2.5.1 Impulse Response

The simple vibration of the transverse beam offers some insight into how input shaping will work. Figure 7.40 shows the response of a transverse beam to an impulse applied at the end. The shape of this curve mimics the first mode of the beam, which is the amalgam of sines, cosines and their hyperbolic counterparts. Notice that the higher modes only contribute about a third as much as the first mode to the response as can be seen in Figure 7.41. Since the higher modes are low in magnitude, simple input shapers should be effective in eliminating the vibration in the beam. To test this hypothesis input shapers will be applied to the transversely vibrating beam.

7.2.5.2 Forced Input Response

7.2.5.2.1 Zero Vibration Shaper

If a ZV input shaper is used on the transverse beam in the form of forces applied at the free end, the vibration is significantly reduced. Figure 7.42 shows how the entire beam responds
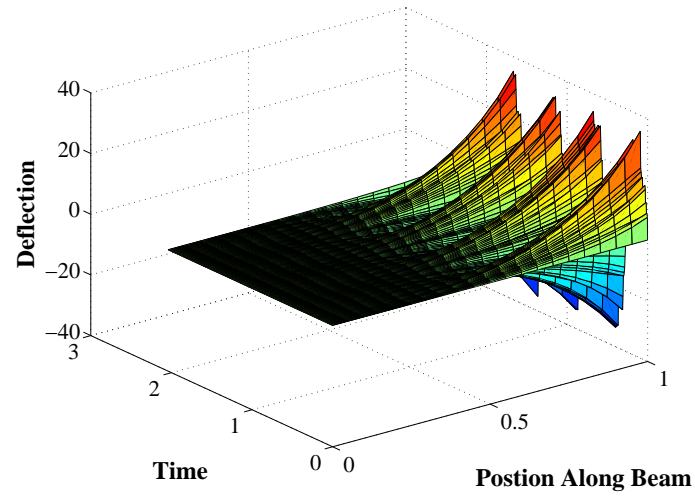
Figure 7.40: Impulse Force Response of Transverse Beam.
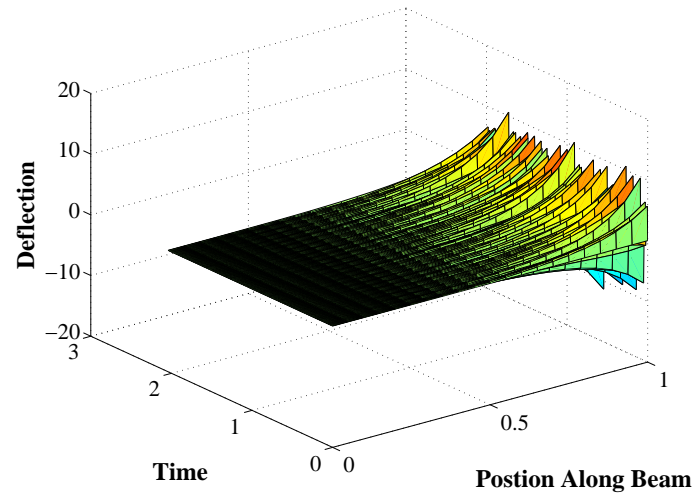
Figure 7.41: Modes 2 through 5 Impulse Force Response of Transverse Beam.
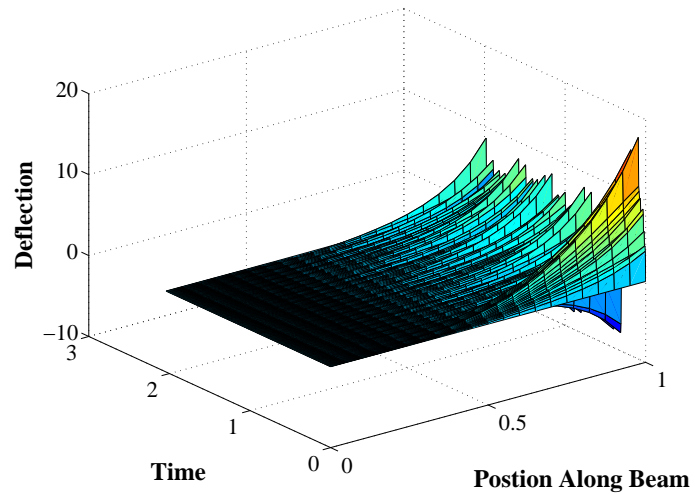
Figure 7.42: Zero Vibration Moment Response of Transverse Beam.

to the ZV input shaper. However, the higher modes still vibrate, and their vibration allows only a 66% reduction in vibration magnitude over the unshaped case. The higher mode response can be seen specifically in Figure 7.43. Investigation of this figure shows that all of the vibration in the beam after the shaper is due to the higher modes alone. That is, the first mode's oscillation has been eliminate completely.

The Zero Vibration input shaper is effective in reducing the vibration of a transverse beam. However, it does not eliminate the vibration like it did for the other beams. It reduces the vibration to a third of the unshaped vibration for perfect system modelling as is shown in Figure 7.44. This sensitivity curve has a minimum near perfect modelling and a maximum as expected at a modelling error of 2. Interestingly, with incorrect modelling, the vibration can be increased beyond the unshaped amplitude. This does not occur with lumped parameter systems and the ZV shaper and should be consideration before using a ZV shaper on a transverse beam with low confidence in the model. ZV input shaping for transverse beams is a helpful technique, however, it is not the complete solution to all vibration as it is in the case for many other simpler oscillatory systems.

7.2.5.2.2 Zero Vibration and Derivative Shaper

The ZVD shaper is marginally more effective than the ZV shaper for transversely vibrating beams. When a ZVD shaper is applied as a force to the end of the beam, the first mode is eliminated, but the other modes still vibrate as shown in Figure 7.45. The robustness built into the ZVD shaper reduces the higher modes slightly more than the ZV case as shown in Figure 7.46. Comparing Figure 7.46 for the ZVD case with the higher mode response of the ZV shaper in Figure 7.43 shows that the ZVD shaper reduces vibration 75% compared to 66% for the ZV shaper. However, the ZVD shaper is twice as long as the ZV shaper. The
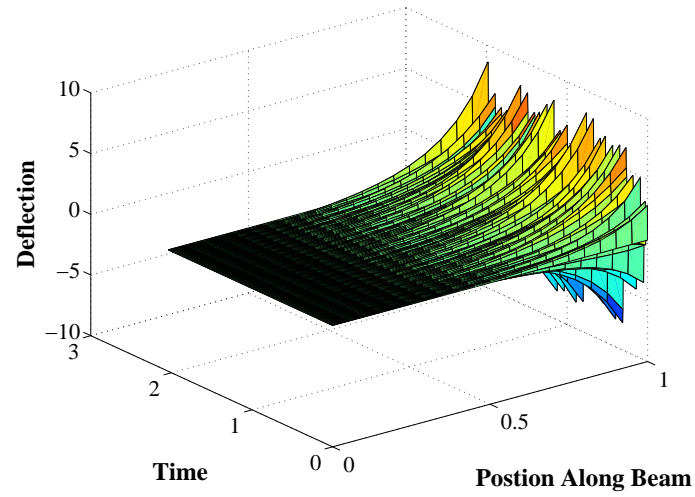
Figure 7.43: Modes 2 through 5 ZV Moment Response of Transverse Beam.
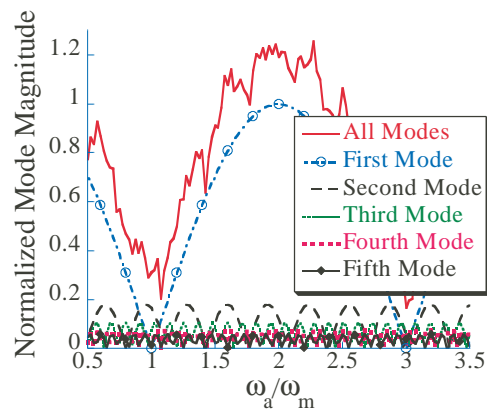
Figure 7.44: Zero Vibration Sensitivity of Transverse Beam.
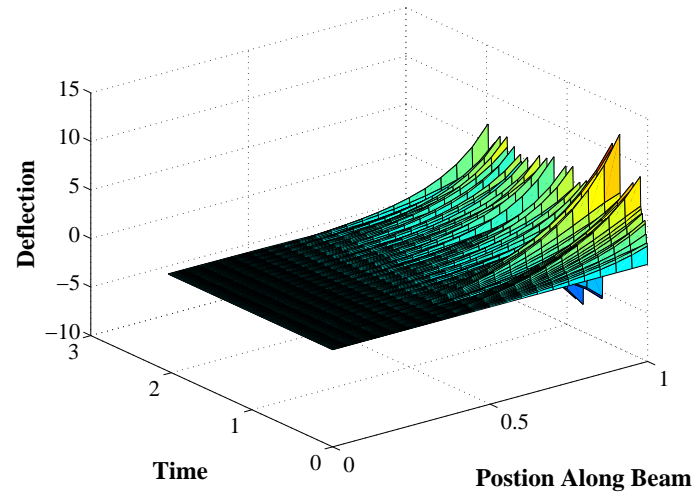
Figure 7.45: Zero Vibration Derivative Moment Response of Transverse Beam.
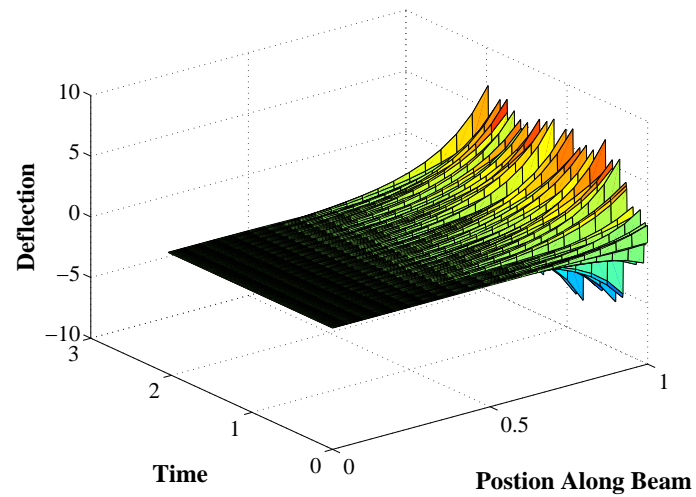
Figure 7.46: Modes 2 through 5 ZVD Moment Response of Transverse Beam.

247
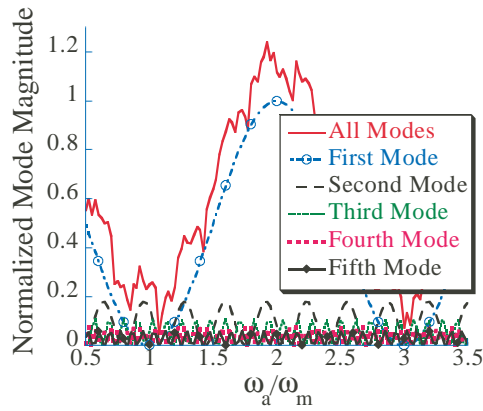
Figure 7.47: Zero Vibration Derivative Sensitivity of Transverse Beam.

tradeoff between the two is made more nebulous by investigating the sensitivity.

Figure 7.47 shows the sensitivity curve for a ZVD shaper when applied to a transversely vibrating beam. While the derivative of the first mode of vibration is zero at perfect modelling, this fact does not significantly improve the performance with modelling error over the ZV case. The error does approach zero near 1.1. However, the slope is steep in this region, and therefore the low value is probably an artifact of the simulation process, not a new way to design input shapers for beam vibration.

The result of the study of ZV and ZVD shapers is that both are capable of significant vibration improvement; however, the difference in performance between the two is minimal. Therefore, the ZV shaper is recommended over the ZVD shaper for transverse beams due to its shorter duration.

7.2.5.2.3 Unity Magnitude Zero Vibration Shaper

Like the ZV and ZVD shaper, the UMZV shaper is effective in the reducing the vibration of transverse beams. However, also like the other shapers, the UMZV shaper leaves substantial vibration after its application, resulting from the excitation of the higher modes. Figure 7.48 shows how the entire beam vibrates when a UMZV shaped force is applied to the free end. Once again the first mode is virtually eliminated while the other modes continue to vibrate as is shown by the high mode only response of Figure 7.49. The vibration is once again reduced about 66%. This result is similar to the ZV case, but is obtained with a shorter duration shaper. This shorter duration including negative impulses is responsible for a much less robust suppression scheme.

The UMZV shaper is inherently not robust even for lumped parameter system. Figure 7.50 shows how sensitive the UMZV shaper is to modelling errors. First notice that the minimum is of similar scales as the ZV and ZVD shapers. More importantly is that the
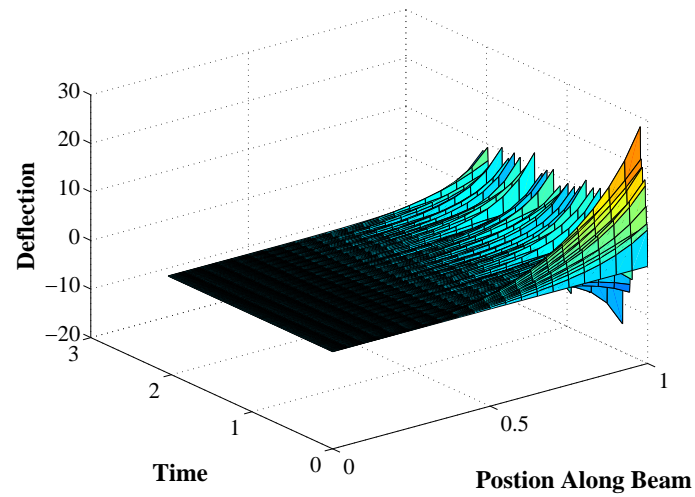
Figure 7.48: UMZV Moment Response of Transverse Beam.
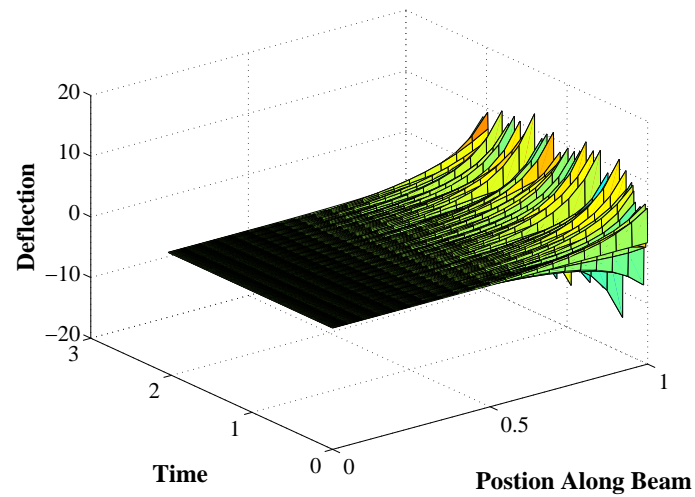
Figure 7.49: Modes 2 through 5 UMZV Moment Response of Transverse Beam.

249
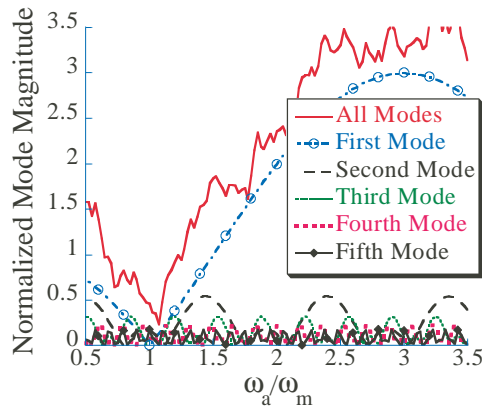
Figure 7.50: UMZV Sensitivity of Transverse Beam.

vibration magnitude can be greatly increased by using the UMZV shaper on the transverse beam. This propensity for increasing instead of reducing vibration is a great concern in any case where modelling is an issue.

The application of the UMZV shaper shows the major differences among the transverse, the longitudinal, and the torsional beams, that is the modes are not odd integer multiples of each other in the transverse beam. This fact makes the transverse beam more suitable to UMZV shapers.

7.2.6 Transverse Beam with Mass

The final beam under consideration is the transverse beam with an attached mass. This beam's dynamics interfacing with traditional input shapers will show that input shaping works effectively for this beam. However, higher modes and well as sensitivity to modelling errors still remain an issue in this type of beam.

Transverse beams used in manufacturing environments often have some end load, like an end effector or sensor. These types of beams can also benefit from input shaping for vibration reduction. Transverse beams with attached masses on the free end exhibit the same trends as were seen for the torsional beam with an attached mass. Specifically the more mass is attached the less the impact of the higher modes, and thus, the better all one-mode input shapers perform.

7.2.6.1 Impulse Response

If a transverse beam with an attached mass is given an impulsive force on its free end, then all of the modes will oscillate as shown in Figure 7.51. The first mode is more dominant than it was in the case without an attached mass. Figure 7.52 details the response of these higher modes to the impulse. This reduced response of the higher modes only increases
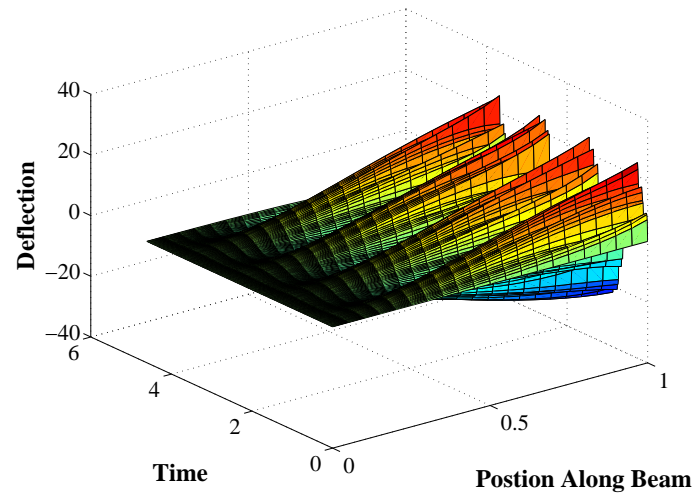
Figure 7.51: Impulse Force Response of Transverse Beam with Attached Mass.
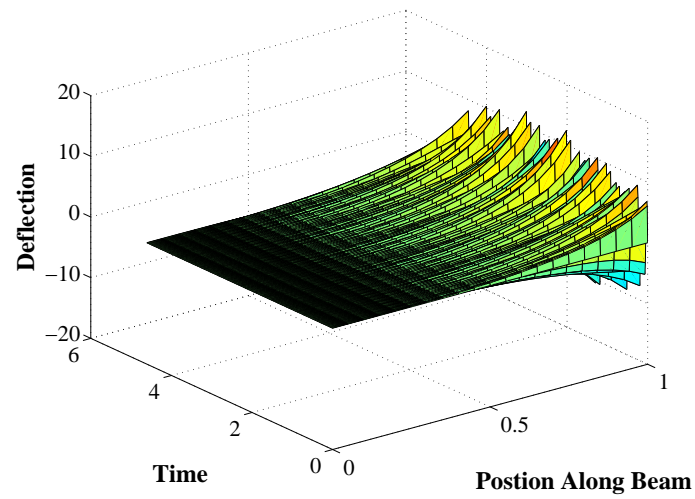
Figure 7.52: Modes 2 through 5 Impulse Force Response of Transverse Beam with Attached Mass.
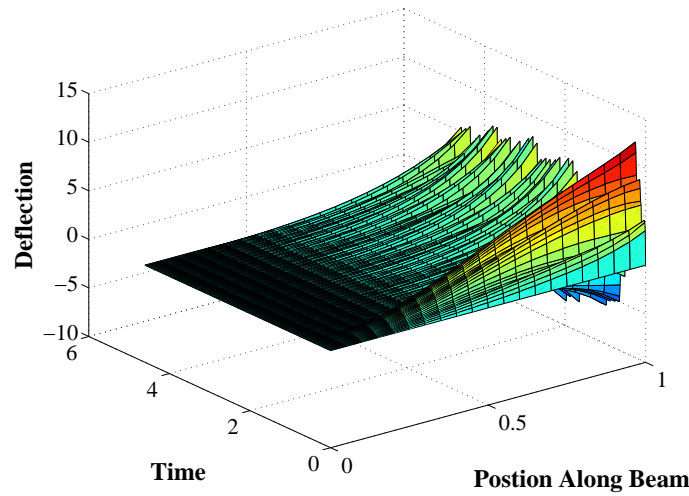
Figure 7.53: Zero Vibration Force Response of Transverse Beam with Attached Mass.

with the attached mass and likewise results in an improved input shaping performance for higher attached masses.

7.2.6.2   Forced Input Response

7.2.6.2.1   Zero Vibration Shaper

The higher the attached mass the better the performance of ZV input shaping on the beam. For example, Figure 7.53 shows how the attached mass beam performs under ZV input shaping. The vibration is reduced more than for the case without the mass, however the vibration in the higher modes is still significant as shown in Figure 7.54.

This higher mode vibration also effects the sensitivity of the ZV shaper on the beam. Figure 7.55 shows how the vibration is reduced about 70% at perfect modelling. The vibration does always remain below the unshaped level, but the ZV shaper is still not capable of eliminating all the vibration. However, if the attached mass is increased, then the beam will perform more like a lumped parameter system. The sensitivity curve for various attached mass ratios in Figure 7.56 shows that for higher attached masses, shaping is more effective at vibration reduction.

7.2.6.2.2   Zero Vibration and Derivative Shaper

The ZVD shaper is more effective at reducing the vibration in the transverse beam with an attached mass than the ZV shaper. Figure 7.57 shows that the ZVD shaper can reduce the vibration by more than 80%. The higher modes are significantly reduced as is apparent from the vibration response of only these modes in Figure 7.58. The robustness of the ZVD shaper successfully reduces some of the higher modes, thus reducing the overall shaped
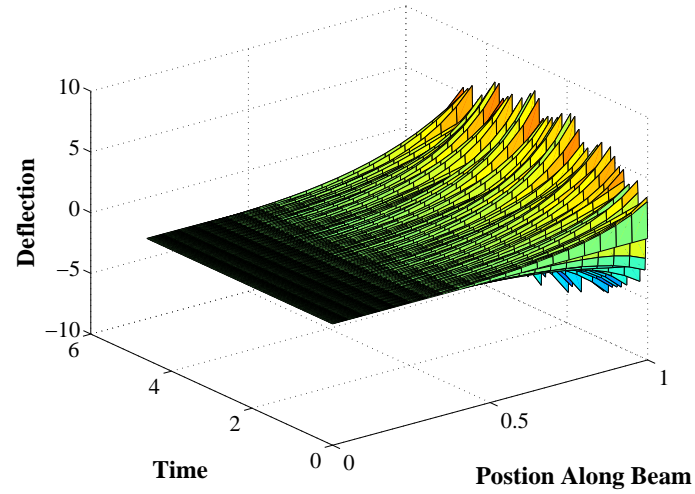
Figure 7.54: Modes 2 through 5 ZV Force Response of Transverse Beam with Attached Mass.
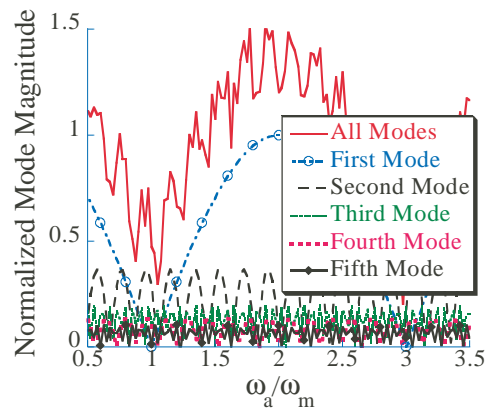
Figure 7.55: Zero Vibration Sensitivity of Transverse Beam with Attached Mass.
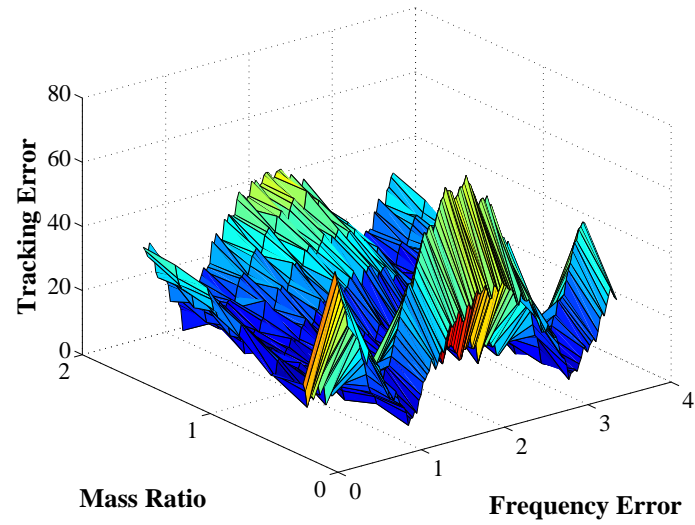
Figure 7.56: Zero Vibration Sensitivity of Transverse Beam for Varying Attached Masses.
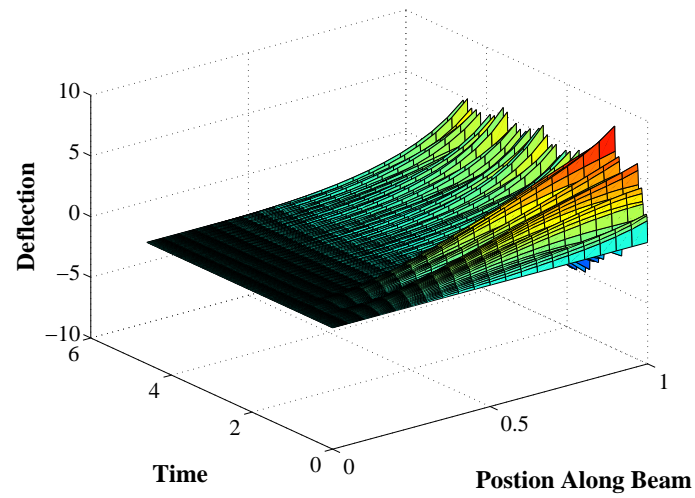
Figure 7.57: Zero Vibration Derivative Force Response of Transverse Beam with Attached Mass.

254
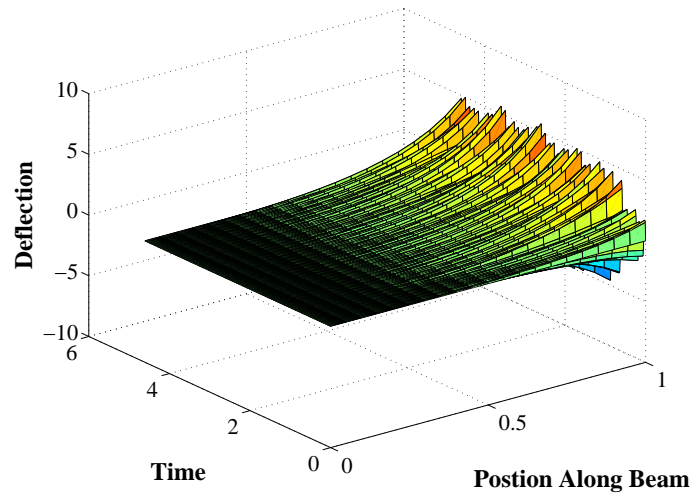
Figure 7.58: Modes 2 through 5 ZVD Force Response of Transverse Beam with Attached Mass.

response.

This shaper robustness can be seen in the sensitivity curve of Figure 7.59. This curve shows that the vibration is never increased beyond the unshaped magnitude. The total response curve does exhibit an oscillation equal to the second mode. In this case, vibration in the second mode can significantly alter the response of the system. As the shaper excites this mode, the vibration magnitude increases significantly.

7.2.6.2.3 Unity Magnitude Zero Vibration Shaper

The UMZV shaper performed well for the transverse beam with no attached mass, and likewise the UMZV shaper significantly reduces vibration in the transverse beam with a mass. Figure 7.60 shows how the vibration is reduced from UMZV shaping. Only a 50% reduction in vibration occurs due to the excitement of the higher modes as shown in Figure 7.61. These modes' vibration is increased by the nature of the UMZV shaper to excite modes at three times the design frequency to three times their unshaped magnitude.

The excitement of the higher modes can be seen in Figure 7.62 a sensitivity curve for the transverse beam with mass and UMZV shaping. Like the ZVD shaper, the excitement of the second mode causes an oscillation in the sensitivity curve. If excitement of the second mode is kept to a minimum, the UMZV shaper is effective at reducing the vibration in the system. This effectiveness is highly dependent on the attached mass. As the mass increases so does the effectiveness of the UMZV input shaper. Figure 7.63 documents this change. Although difficult to see in the figure due to the oscillations from the second mode, the effectiveness of the UMZV shaper increases with an increase in the mass. If the attached mass is significant, then UMZV shaping can be a useful technique for vibration suppression
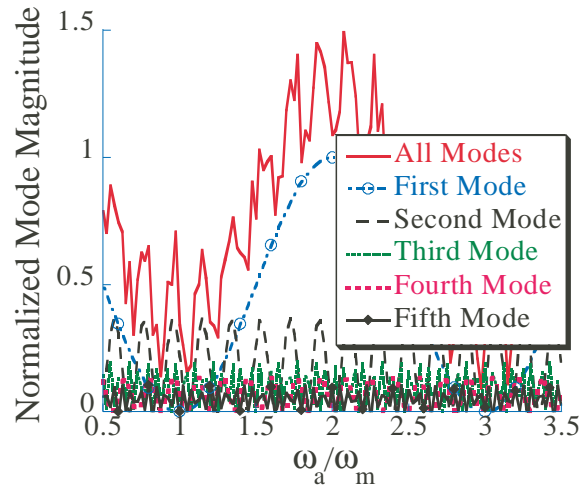
Figure 7.59: Zero Vibration Derivative Sensitivity of Transverse Beam with Attached Mass.
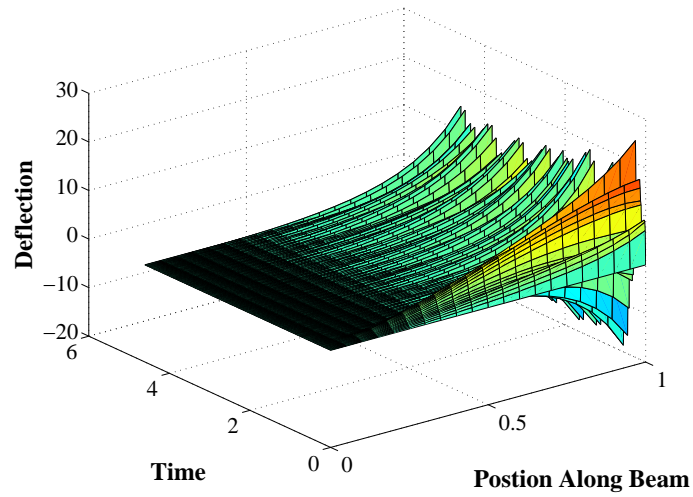
Figure 7.60: UMZV Force Response of Transverse Beam with Attached Mass.
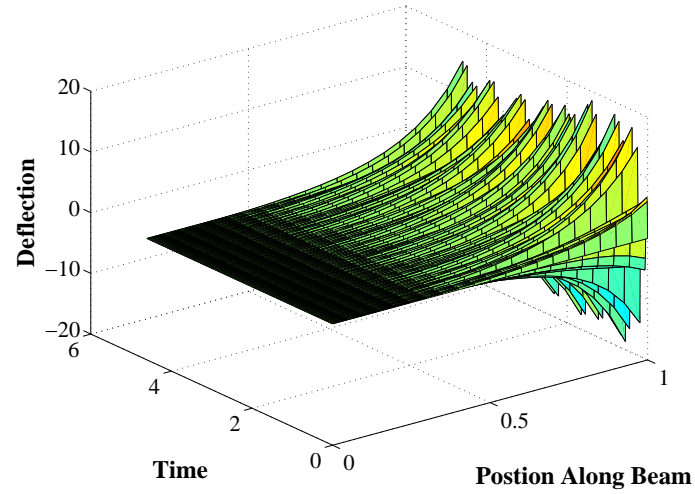
Figure 7.61: Modes 2 through 5 UMZV Force Response of Transverse Beam with Attached Mass.
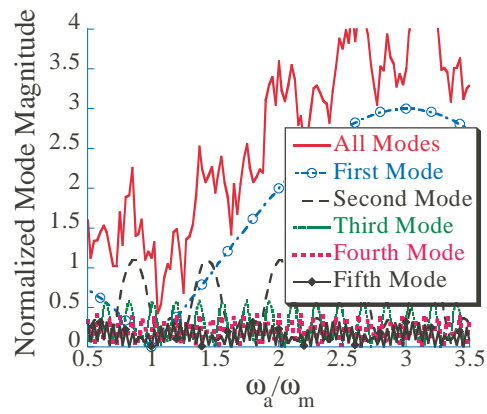
Figure 7.62: UMZV Sensitivity of Transverse Beam with Attached Mass.
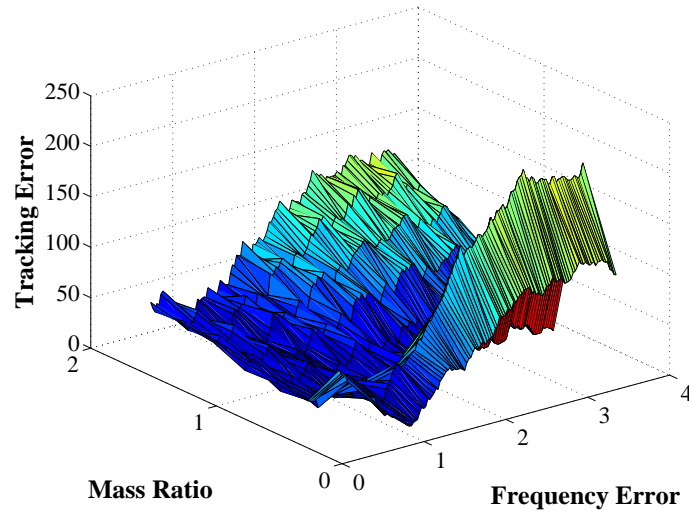
Figure 7.63: UMZV Sensitivity of Transverse Beam for Varying Attached Masses.

Table 7.5: Input Shaping Effectiveness for Continuum Systems.

	ZV	ZVD	UMZV
Torsional	Full⋆	Full	None
Torsional: Low Inertia	Full⋆	Full	Partial
Torsional: High Inertia	Full⋆	Full	Full
Longitudinal	Full⋆	Full	None
Longitudinal: Low Mass	Full⋆	Full	Partial
Longitudinal: High Mass	Full⋆	Full	Full
Transverse	Partial	Partial⋆	Partial
Transverse: Low Mass	Partial	Partial⋆	Partial
Transverse: High Mass	Full⋆	Full	Full

in transverse beams.

7.3 Input Shaper Selection for Continuum Systems

The previous sections detailed how input shaping can be derived and applied to various continuum systems. Depending on the type of continuum system, some input shapers are preferred for vibration reduction, while for others, shapers did not reduce the vibration at all. Table 7.5 summarizes the results of each input shaper for each beam. Note that Full refers to complete vibration reduction in all modes; Partial is the reduction in the first mode, but with significant vibration in the other modes; and None is no reduction in overall vibration by the inclusion of input shaping. The starred ($\star$) cases represent the recommended shaper for each beam.

In most cases of the torsional and longitudinal beam, the result of using traditional input shaping on the continuum systems was full vibration elimination due to the integer

relationship of the modes. This relationship, however, also causes the UMZV shaper to be an unwise choice for these same beams. The UMZV shaper is only useful on transverse beams, and only provides near total vibration elimination for those beams with large attached loads. A large load on any of the beams makes the system behave as a mass and spring for which input shaping has already been proven effective.

Interestingly, input shaping performs the least well on transversely vibrating beams, which are the most common beam on which it has been used. This discrepancy is due to the ubiquitous nature of transverse beams, and the large reductions, of over 60% of the unshaped vibration amplitude, that are possible with simple input shaping. Typically the remainder of oscillations in transverse beams are explained by non-linear or higher order effects. Chapter 8 will show experimental results for transverse beam vibration reduction through input shaping as part of the description of input shaping design combined with mechanical design.

CHAPTER VIII

COMBINED MECHANICAL AND COMMAND DESIGN

The previous chapters of this dissertation have dealt with tailoring input shaping to a particular mechanical system to yield improved performance answering the secondary research question of how existing machine performance can be improved. These previous systems, be it micro-mills, multiple degree of freedom oscillators, or continuum beams, were all designed for some set of performance criteria (independent of input shaping), and then input shaping was added. This is the traditional approach to machine design, that is to develop the machine and then develop a vibration control strategy. That strategy could be feedback control or an open loop technique like input shaping. However, these two elements must work effectively together in the final machine. Therefore, it should be possible to use knowledge of the vibration suppression scheme, specifically input shaping, to change the mechanical design of the plant for improved performance and find an answer to the primary research question of: *How can the consideration of command shaping during the design phase create machine designs with improved performance?*

Previously in Section 2.3.1, the combination of mechanical design and feedback control was discussed. Here, instead of feedback control, input shaping will be included in the mechanical design decision making process. Specifically, the performance of the machine with input shaping will be used to make mechanical design choices. Inclusion of input shaping in the design process will be presented at a variety of levels, from rules of thumb to exacting procedures for selecting mechanical elements such that their motions are as fast as possible.

The union of input shaping with mechanical design influences all four stages of the traditional engineering design process of [209] as shown in Figure 8.1. The Definition and Clarification of the Task needs to be unbiased towards input shaping alternatives. Conceptual Design needs to consider flexible input-shaped structures as functional alternatives. Also, the functional evaluation must consider input-shaped solutions strengths and weaknesses. If input-shaped function solutions are selected, then Embodiment Design should consider input-shaped based performance measures. Finally, the Detail Design should make minor adjustments for the input-shaped functional solutions. The influence of input shaping directly on the stages of the traditional engineering design process will be discussed in Section 8.4. However, the remainder of the chapter focuses on introducing input shaped functional alternatives and presenting techniques for their parameter selection in embodiment design. This will begin with the combination of auxiliary mechanical elements, specifically vibration
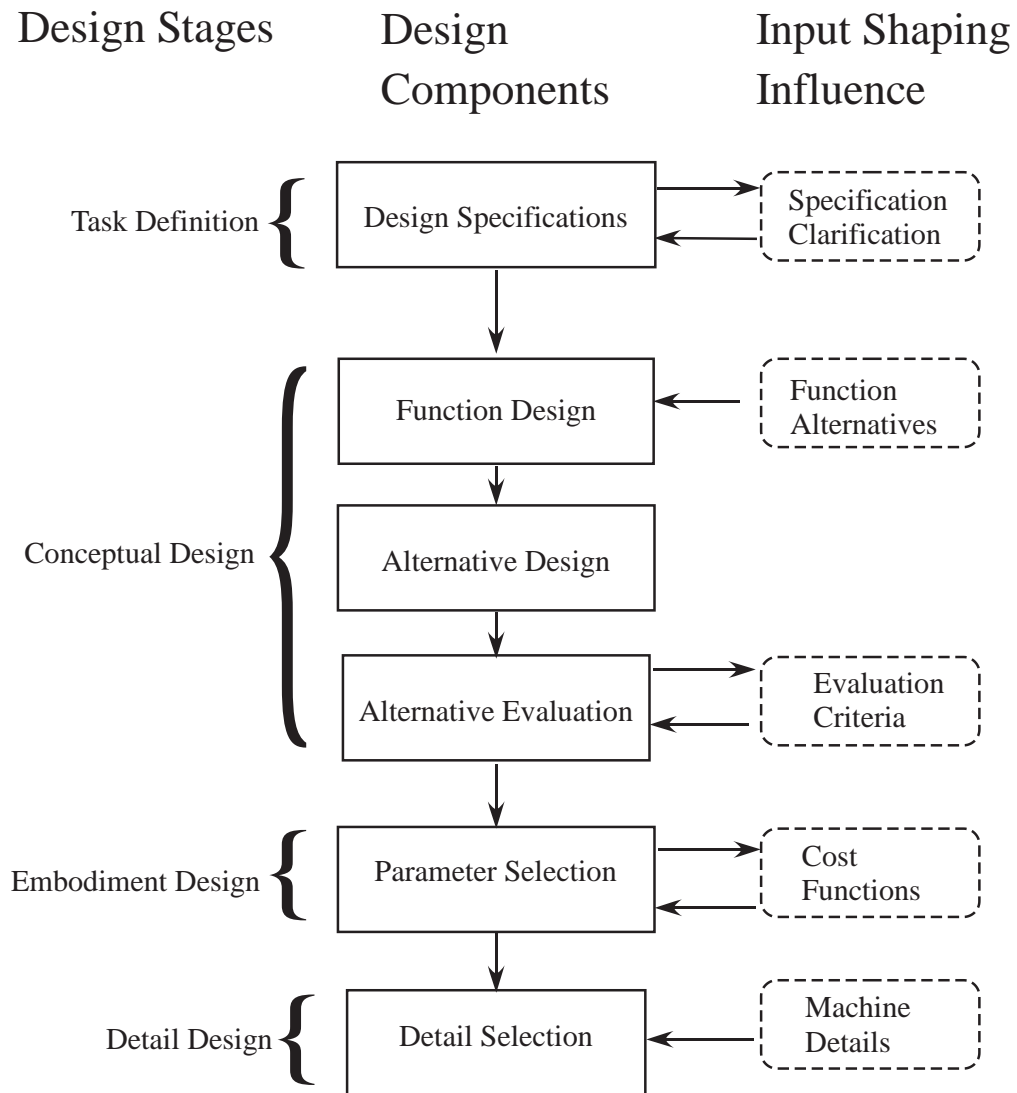
Figure 8.1: Input Shaping Impact in Design Process.

absorbers and input shapers. Then input shaping will be integrated with the mechanical design of beams like those discussed in the previous chapter. Next, these beam elements will be combined with other mechanical elements to demonstrate a realistic initial phase mechanical embodiment process, specifically tailored to a micro-mill positioning system.

8.1 Vibration Absorber Design

An easy and useful approach to combining mechanical design with input shapers is not to tackle overall machine design, instead modify existing machines by using auxiliary mechanical elements and input shaping [35, 84, 85, 86, 82, 89, 87, 285]. By limiting the problem to an existing mechanical structure, with the addition of a vibration absorber like the ones presented in Section 3.1.2.2, input shaping and mechanical element tradeoffs can be addressed. Specifically, vibration absorbers will be developed here for the non-traditional purpose of eliminating step disturbances. Step disturbances are common in manufacturing machines. These disturbances can take the form of mass being added to a machine when it picks up a part or a internal clamp engaging to hold a workpiece. Once absorber are designed for these class of disturbances, then the design of these step disturbance absorbers will be modified to include the selection of their mechanical parameters simultaneously with input shapers.

8.1.1 Absorber Design For Step Disturbances

The first issue addressed here is the development and implementation of a dynamic vibration absorber that improves the response of a system subject to step functions either from a reference command or from an external disturbance. A step motion, or motion from one place to another, is common in manufacturing machines; and therefore, eliminating the vibration step motions can cause would be useful. Likewise, step disturbances cause vibration in the system when machines pick up loads or internal actuators are used to clamp workpieces. It is also important to control these disturbance vibrations.

The benchmark system shown in Figure 8.2 is the spring-mass-damper system with base excitation X_0, where the position of the primary mass, X_P, is the desired state to be controlled. If this system is disturbed by a step either from the input or as an applied force, then the primary mass will oscillate as shown in Figure 8.3. The reduction of this vibration is the goal of including a vibration absorber.

When a dynamic vibration absorber is added, the system has fourth-order dynamics described by:

$$\frac{X_P(s)}{X_0(s)} = \frac{b_3 s^3 + b_2 s^2 + b_1 s + b_0}{a_4 s^4 + a_3 s^3 + a_2 s^2 + a_1 s + a_0} \tag{8.1}$$

Where, the following definitions have been made:

$$a_4 = M_p M_A$$
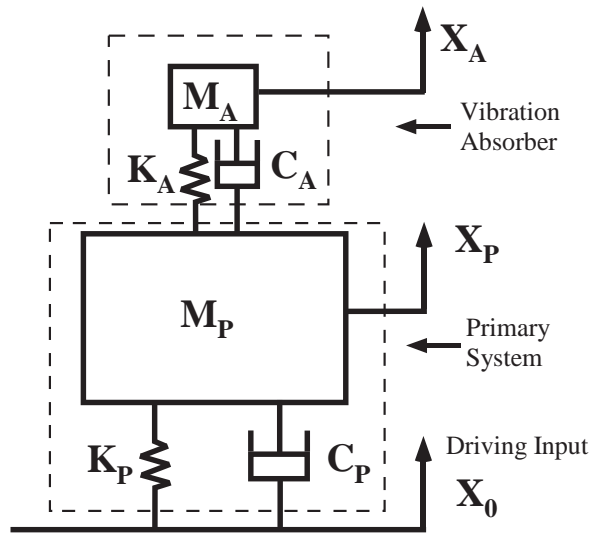
Figure 8.2: Vibration Absorber Diagram.
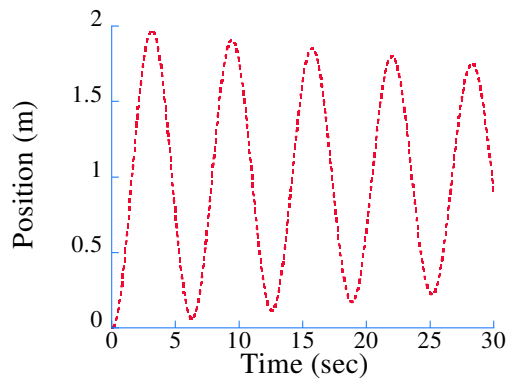
Figure 8.3: Step Disturbance and Driven Responses.

263

$$a_3 = (C_P + C_A) M_A + M_P C_A$$
$$a_2 = (K_P + K_A) M_A + C_P C_A + M_P K_A$$
$$a_1 = K_P + C_A + C_P K_A$$
$$a_0 = K_P K_A \quad (8.2)$$
$$b_3 = C_P M_A$$
$$b_2 = K_P M_A + C_P C_A$$
$$b_1 = K_P C_A + C_P K_A$$
$$b_0 = K_P K_A$$

M_P, K_P, and C_P represents the primary system's mass, spring constant, and damping coefficient, respectively, and M_A, K_A, and C_A represent the absorber's parameters. The absorber-mass-to-primary-mass ratio, μ is given by:

$$\mu = \frac{M_A}{M_P} \quad (8.3)$$

The absorber-frequency-to-primary-frequency ratio, r, is:

$$r = \frac{\sqrt{\frac{K_A}{M_A}}}{\sqrt{\frac{K_P}{M_P}}} = \frac{\omega_A}{\omega_P} \quad (8.4)$$

If (8.3) and (8.4) are substituted into (8.1) the variables become:

$$a_4 = \mu M_P^2$$
$$a_3 = 2\mu M_P^2 (\zeta_p \omega_p + \zeta_a \omega_a \mu + \zeta_a \omega_a)$$
$$a_2 = M_P^2 \mu (\omega_P^2 + \omega_A^2 \mu + 4\zeta_P \omega_P \zeta_A \omega_A + \omega_A^2)$$
$$a_1 = 2\omega_P M_P^2 \omega_A \mu (\omega_P \zeta_A + \zeta_P \omega_A)$$
$$a_0 = \omega_P^2 M_P^2 \omega_A^2 \mu \quad (8.5)$$
$$b_3 = 2\zeta_P \omega_P M_P^2 \mu$$
$$b_2 = \omega_P M_P^2 \mu (\omega_P + 4\zeta_P \zeta_A \omega_A)$$
$$b_1 = 2\omega_P M_P^2 \omega_A \mu (\omega_P \zeta_A + \zeta_P \omega_A)$$
$$b_0 = \omega_P^2 M_P^2 \omega_A^2 \mu$$

Traditionally, approximations have been made by assuming light or proportional damping. Unfortunately, in the quest for an effective absorber for step-like motions, the absorber damping ratio is often greater than 0.2 and the light damping assumption is invalid. Also, the absorber damping is not known *a priori*; and therefore, any light damping approximation cannot be guaranteed.

8.1.1.1   Solution Approach

Two methods are presented here for designing the ideal absorber for a step trajectory application, the simulated response and the modal method. The simulated response method relies on a simulation of the step response of the absorber augmented system to determine the best absorber with regards to both settling time and overshoot. The modal method seeks only to minimize settling time and does so by utilizing the slowest eigenvalue of the system.

The procedure proposed here for designing a vibration absorber for a system subject to step motions and step disturbances with either method has four components:

1. Perform step-response simulations or modal analysis of the fourth-order system over a wide range of absorber parameters.

2. Evaluate the time response performance characteristics, peak overshoot,M_P, and settling time, t_S, or the slowest modal frequency ω_{slow}.

3. Search the space of performance characteristics to locate optimal absorber parameters.

4. Refine the search with finer parameter spacing near the optimal value determined in step 3.

8.1.1.2   Performance Characteristics

The performance of an absorber is quantified in the simulation approach by two parameters peak overshoot, M_P, and settling time, t_S, of the primary mass. These parameters characterize fourth-order responses with commonly accepted second-order terminology.

The first performance characteristic, peak overshoot of the primary system is defined for a unity magnitude step as:

$$M_P = max\left(X_P(t)\right) - 1 \tag{8.6}$$

The second response parameter is settling time, defined by the time it takes for the system to fall within a percentage of the step size and remain within those bounds. To calculate this value, the response of the system is analyzed using an exponential boundary fit technique. The exponential-boundary-fit technique balances accuracy with computational complexity. Its goal is to find the exponential decay equation that bounds the maximums of the step response. From the equation of this curve, the settling time is computed by calculating the time it takes the exponential curve to decay to 5% of the step size.

A unique quality of the exponential-boundary-fit method is the continuity of the settling time as the damping ratio changes. Figure 8.4 compares the exponential-boundary-fit settling time to a technique that determines settling time by scanning backward from the end of the response data. When the damping changes slightly and one peak in the response
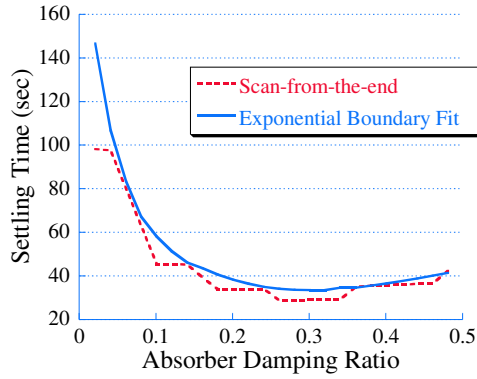
Figure 8.4: Exponential-Boundary-Fit Technique.

leaves the 5% settling envelope, the Scan-From-The-End method predicts a sharp change in the settling time. This is not the case with the exponential-boundary-fit method; it gives a smooth performance measure. This quality is useful because it avoids sharp changes in the performance measures for the design. These sharp changes could mask the best parameters for a design.

For the case of the modal method, the desired performance is the fastest decay of the step excitation. This is quantified by numerically calculating the eigenvalues of the system, then looking at the eigenvalue with the lower real part. This is the slow eigenvalue and the imaginary part is the slow natural frequency ω_{slow}. Increasing the value of ω_{slow} makes the system settle faster.

8.1.1.3   Parameter Search

The solution to the absorber selection entails a brute force optimization by which many possible combinations for absorber parameters, *i.e.* μ, r, and ζ_A are considered and then compared to find the optimal absorber. This brute force technique is employed to ensure full coverage of possible absorbers. The parameters for the primary system, as well as the desired mass percentage for the absorber, μ, are treated as given design parameters. The absorber mass is selected at the highest tolerable value, because previous work shows that the effect of the absorber increases with mass of the absorber [276]. Therefore, absorber mass must be chosen by the designer, otherwise the optimal solution would be undefined because the absorber mass would increase without bound.

After the mass ratio and primary system parameters are known, then an initial search over a mesh in the r-ζ_A space is performed to find the best absorber, followed by a secondary, refined-mesh, search. From preliminary tests with a large range of absorber frequencies and damping values, as well as consideration of existing absorber techniques, a range was

266
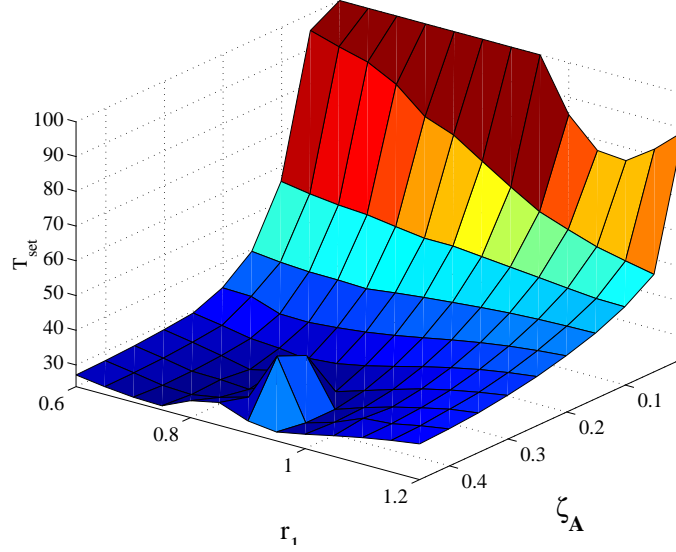
Figure 8.5: Absorber Settling Time.

established in which the optimal absorbers can be found.

$$0.1 \leq r \leq 2$$

$$0.01 \leq \zeta_A \leq 0.45 \tag{8.7}$$

Within this two-dimensional mesh in r and ζ_A, the performance characteristics, M_P and t_S or ω_{slow} are calculated and stored in a performance array. Examples of these performance arrays for the settling time and peak overshoot can be seen in Figure 8.5 and 8.6 respectively. Note the surfaces are "smooth" functions of the parameters. Once the performance array is created, a selection algorithm searches through the performance array for the absorber parameters that enable the greatest improvement to the system.

8.1.1.4 Simulation Method

The simulation method allows the absorber to be designed with the tradeoffs between settling time and peak overshoot considered. A weighting scheme can be used to balance the tradeoff between peak overshoot and settling time. For example, the performance measure used in this section gives more weight to settling time and is given by:

$$J_{sim} = t_S + 0.1 M_P \tag{8.8}$$

where M_P is the peak overshoot from a unit step.

An example of a mesh created by this cost function is shown in Figure 8.7, where the relationship of the cost function value to the absorber damping ratio, ζ_A, and frequency ratio, r, is shown. Once the initial absorber parameters are selected, the search mesh is refined around them. This second mesh consists of smaller cells of higher resolution in the
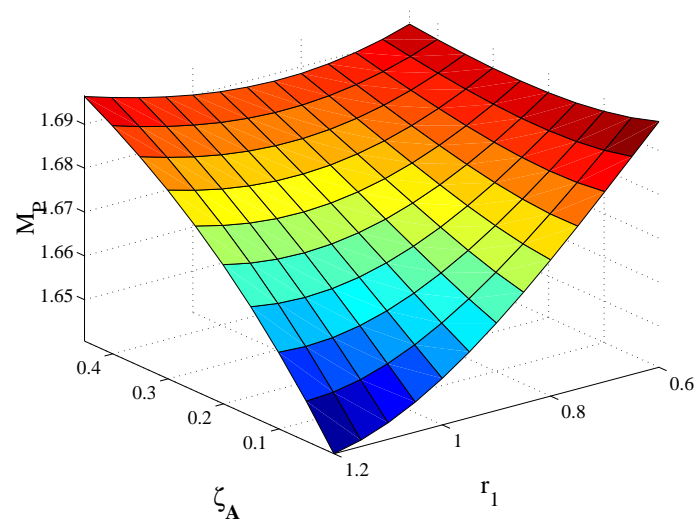
Figure 8.6: Absorber Peak Overshoot.
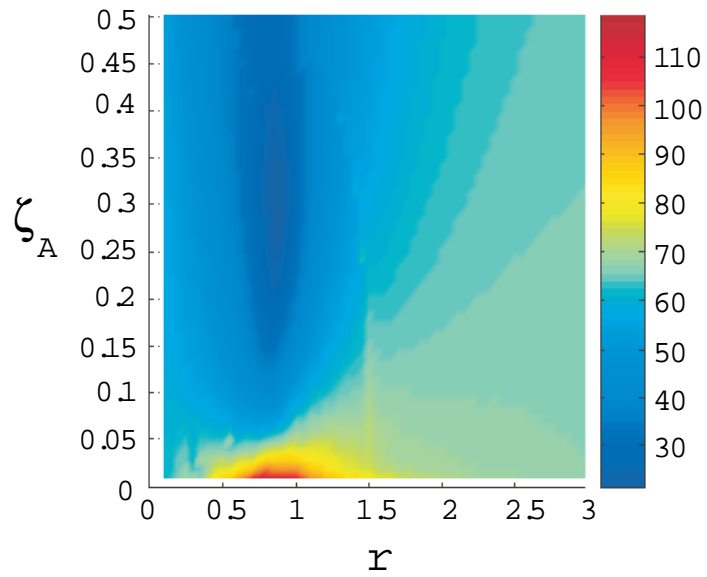
Figure 8.7: Cost Function Mesh for Simulation Method.
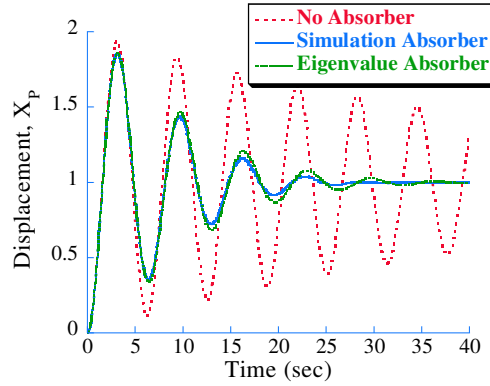
Figure 8.8: Comparison of Step Response of System with and without Simulated and Eigenvalue Absorber.

r-ζ_A space, and therefore, when its series of simulations is complete, the results enable the precise selection of the desired absorber using the aforementioned weighting and selection algorithm. This process could be repeated; however, the level of precision involved in modelling the system and constructing the absorber make it difficult to justify a tertiary search. Even the second search is unnecessary in many cases. A typical result using this optimal step-response vibration absorber is shown in Figure 8.8. The peak overshoot is reduced 9%, but the settling time has been greatly improved by 82%.

An auxiliary approach, that eliminates the need for weighting factors and shows the benefit of the simulation method, is to impose a desired performance specification, such as settling time, and then minimize the other performance measure. Again a computational technique is used whereby a large mesh is generated. Unacceptable performance character-istics eliminate absorbers from consideration. After this truncation is made, the absorber with the greatest improvement in the secondary performance specification is selected. The results of this process are shown in Figure 8.9 for a primary system with a damping ratio of 0.1. For each value of improvement in settling time, an absorber was chosen to minimize the peak overshoot. The resulting line provides a boundary on the absorber performance. Figure 8.9 also shows the relationship between the line of ideal absorbers developed here and previously designed absorbers described by Pennestri in a survey paper [217]. Note that the absorbers designed by the simulation method with the cost function as defined by (8.8) are in the bottom right corner of the graph due to their emphasis on settling time. Absorbers in the upper left correspond to weighting settling time improvement heavily. From this figure, it can be concluded that this approach not only provides added flexibility to the designer, but also yields improvement over previous methods in the step trajectory case. This should not be surprising because previous methods were not directly aimed at improving the step response characteristics.

269
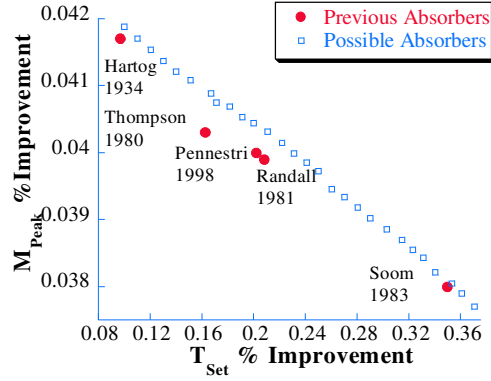
Figure 8.9: Step Vibration Absorber Comparison.
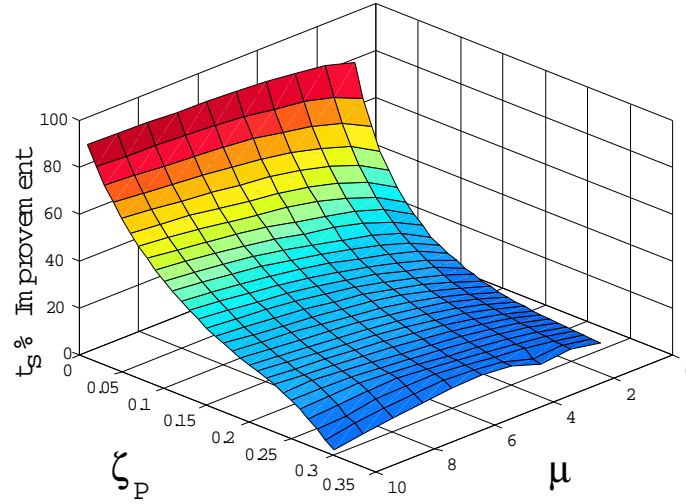
Figure 8.10: Percent Improvement in Settling time over a Variety of Primary Systems.

8.1.1.4.1 Simulation Results

The inclusion of the dynamic vibration absorber on a lightly damped system subjected to step motion can reduce settling time by close to 90%. Figure 8.8 showed a primary system with a 0.02 damping ratio before and after the absorber with $\mu = 0.1$, $r = 0.89$, and $\zeta_A = 0.271$ is added. This drastic improvement is only possible for systems that are lightly damped. For primary systems with large damping ratios, the system's response decays at a large enough rate, that the vibration absorber's additional dynamics do not have time to drastically alter the system response. This is shown in the possible settling time improvement with respect to primary system damping ratio, ζ_P, and absorber mass ratio, μ, in Figure 8.10. Figure 8.10 shows that absorber performance is highly dependent on the original system damping ζ_P. The mass of the absorber does not play as dominant a role
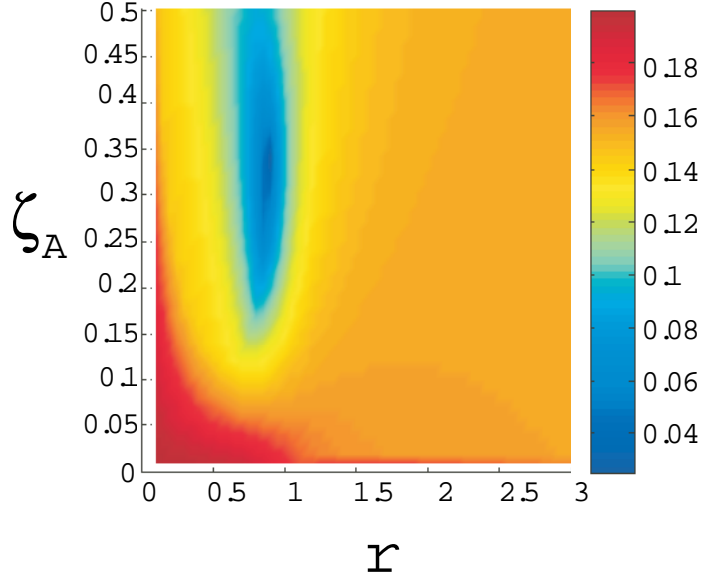
Figure 8.11: Cost Function Mesh for Eigenvalue Method.

as the damping ratio. However, the higher the absorber mass, the better the improvement. Therefore, the highest absorber mass for the application should be used. The absorber that accomplishes these improvements are tuned in the region:

$$0.26 \le \zeta_A \le 0.45$$
$$0.75 \le r \le 0.9 \tag{8.9}$$

8.1.1.5 Eigenvalue Method

The eigenvalue method follows the a similar procedure as the Simulation method with the exception of different performance characteristics and a different cost function. The mesh technique is utilized to determine numerically the slow frequency eigenvalue of the system at each possible absorber r and ζ_A. The slow eigenvalue for each absorber then is used to select the best absorber using the cost function:

$$J_{eig} = \frac{1}{\omega_{slow}} = T_{slow} \tag{8.10}$$

or simply minimizing the period of the slowest vibration frequency, T_{slow}. This technique is much faster than the simulation technique since it only requires the calculation of the eigenvalues of each absorber system and not a complete dynamic response followed by a settling time search.

An example mesh for the eigenvalue method is shown in Figure 8.11. The best absorber using the cost function and this mesh was also shown in Figure 8.8. The absorber with a mass ratio of $\mu = 0.1$ designed for system with a damping ratio $\zeta_P = 0.002$ has a 87.7%

improvement in the modal slow period of vibration. This absorber's design parameters are $r = 0.9$ and $\zeta_A = 0.31$.

8.1.1.6 Method Comparison

Notice in Figure 8.8 that the simulation method absorber performs better in terms of settling time and peak overshoot than the eigenvalue method. This is because the simulation method is based exclusively on the result of the simulation, so it is obvious it would work better for the simulation. The eigenvalue method absorber is better suited for applications in unknown conditions, however in many machine tasks the trajectory is repetitive and known exactly; and therefore, it makes sense to optimize for that trajectory instead of some general case.

The cost function meshes shown in Figures 8.7 and 8.11 are quite similar in shape. From this it can be inferred that solutions for the eigenvalue or simulation approach will be close to the best possible for the other. Therefore the usefulness of each can be chosen for a particular application. If speed of design or a wide range of disturbance/motions are needed, then the eigenvalue method is preferable. However, if a repetitive machine tool that only performs one motion needs vibration suppression, then the simulation method should be used.

The simulation absorber performs better with respect to peak overshoot as well since it was a performance characteristic. The trade off between the simulation and eigenvalue method is that the simulation method has better accuracy for a specific step motion and allows the tradeoffs between peak overshoot, M_P, and settling time, t_S, to be made, while the eigenvalue method is easier, faster, and presents a solution that is applicable over a wider range of circumstances.

8.1.1.7 Experimental Results

The applicability of the proposed vibration absorbers was tested on the experimental setup sketched in Figure 8.12. The motion of a gantry stage was used to drive the primary flexible system. This system is composed of a mass on linear bearings coupled to the gantry through springs. A vibration absorber consisting of flexible steel bar and an attached mass was tuned by height adjustments and used to reduce vibration in the primary system. Damping was performed and adjusted by a variable air damper between the absorber bar and the primary system mass. By adjusting the orifice in the air damper, the damping values could be changed. The primary system performs close to a second-order linear system with a frequency of 2.25 Hz and a damping ratio of $\zeta_P = 0.1$ without the vibration absorber attached. The additions of the vibration absorber greatly improves the step response as shown in Figure 8.13. The absorber parameters for this experiment were $r = 1$ and $\zeta_A = .4$. These were determined experimentally by a similar search technique as described in the

272
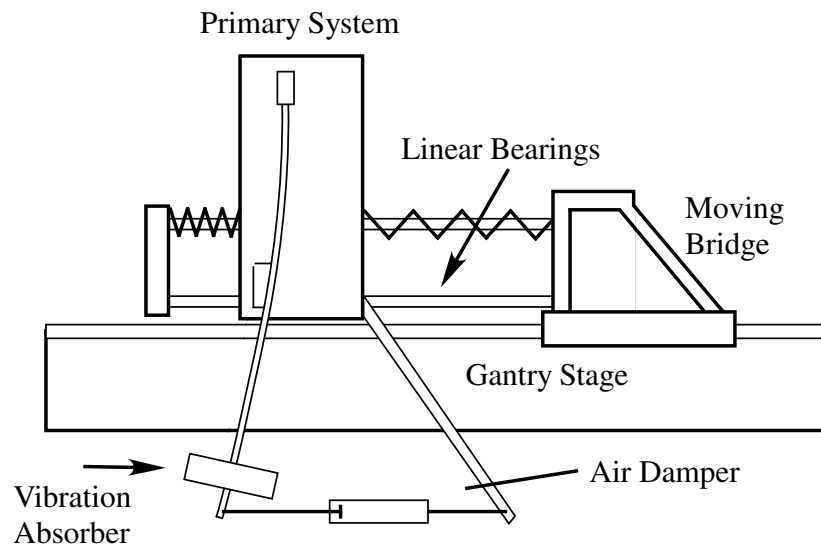
Figure 8.12: Experimental Vibration Absorber Setup.
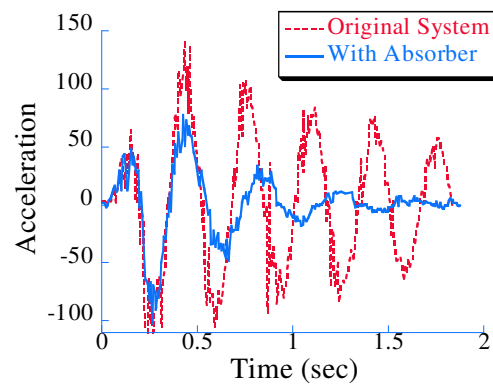
Figure 8.13: Experimental Absorber Design.

273

previous sections. An absorber was tuned to the values theoretically predicted by both methods and experiments run and analyzed by the exponential fit algorithm. Then, the absorber tuning was altered creating a search mesh. The best areas of performance in the mesh was explored further until the best possible absorber for the mechanism was found. Although the absorber and the system are nonlinear due primarily to frictional forces, the differences in the model and the actual system do not prevent the absorber from significantly reducing the step-induced vibration.

These results also show that solutions obtained from both methods are not necessarily the ideal solution for real nonlinear problems. The overcome this shortcoming there are two possible solutions. First a more complicated primary system model could be created and used with the simulation method. The other option is to implement an adjustable parameter absorber like the one in the experimental setup. This absorber could be initial tuned according to the eigenvalue or simulation method. Then the absorber could be adjusted using a series of experiments, until the best absorber parameters were found. However, simply applying the absorber from either method will substantially reduce the vibration from a step motion and could be all the vibration suppression necessary for a particular machine.

8.1.2 Combined Absorber and Shaper Design

Now that it has been shown possible to design vibration absorbers specifically for step disturbances and motions, this same type of absorber will be combined with input shaping. The resultant system will be capable of rejecting disturbances, as well as moving quickly without vibration when commanded. A simple method to accomplish this goal is to first design the absorber for a generic step disturbance, then design an appropriate input shaper. This sequential approach first designs the vibration absorber to compensate for the external disturbances to a system, then finds an input shaper to cancel the multiple modes of the augmented system. In order to achieve the best possible performance the vibration absorber and input shaper parameters should be selected concurrently. This concurrent approach will offer some insight into how more complicated mechanical designs can be combined with input shaping.

8.1.2.1 *Sequential Design Of Vibration Absorbers and Input Shapers*

A well-designed step vibration absorber can improve the settling time from disturbances by up to 90% as discussed previously, shown with simulation in Figure 8.8, and experimentally in Figure 8.13. There exists one best absorber for the settling time reduction from a step disturbance for a given peak overshoot and settling time cost function; however more criteria are needed to determine the best input shaper. Settling time, overshoot, robustness and the duration of the shaper are the important criteria used here to evaluate input shapers.
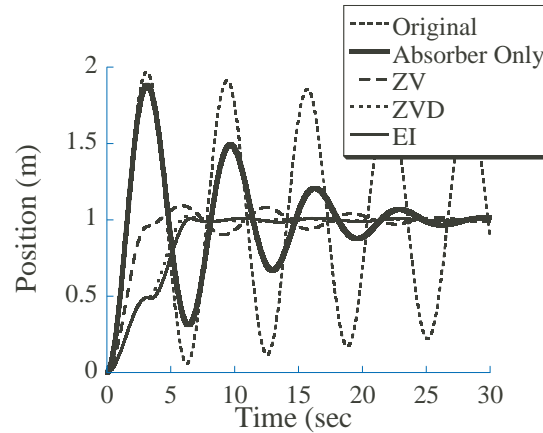
Figure 8.14: Simulated Response to a Variety of Input Shapers.
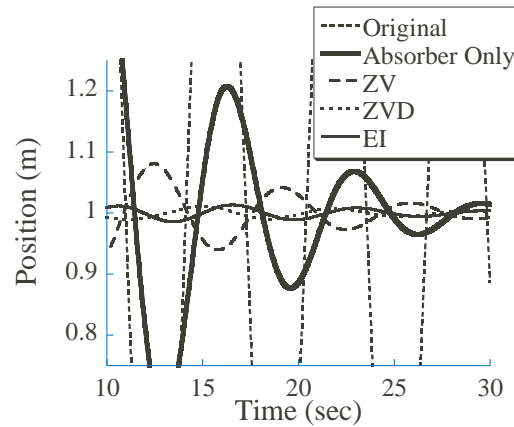
Figure 8.15: Detail of Simulated Response to a Variety of Input Shapers.

One option is to use either a ZV or a ZVD input shaper for the primary mode of vibration in the system. These shapers are designed to eliminate one frequency and therefore do not cancel the multi-mode vibration completely as shown in Figure 8.14. The ZVD shaper does a better job due to its robustness and the close proximity of the vibratory modes. These shapers when combined with a vibration absorber significantly reduce the vibration while also providing a fast rise time.

Another possibility is to use an input shaper designed for multiple modes of vibration like the Extra Insensitive shaper where the vibration sensitivity is zero for two closely-spaced frequencies. If an EI shaper is design for both modes of the system augmented with the vibration absorber, then the residual vibration can be reduced further as shown in Figure 8.15. Note the EI shaper in Figure 8.14 has virtually the same rise time as the ZVD shaper.

This sequential approach can be used in the design phase if accurate modelling is possible, or it can be employed on existing machines. First, if the system can be modelled
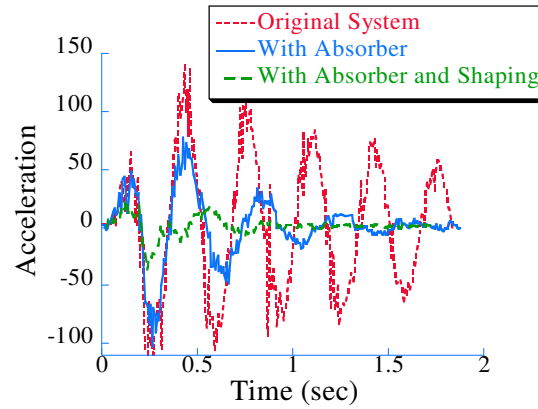
Figure 8.16: Experimental Sequential Solution.

accurately, either before construction or on an existing piece of hardware, then an absorber and input shaper designed exclusively by theory can be used. The experimental setup discussed previously meets this criteria and therefore the simulation based techniques can be used. Figure 8.16 shows the system response with and without the absorber and with the application of a ZV input shaper.

However, if an exist system cannot be modelled accurately, the sequential technique can still be used to improve performance. A search for the best absorber parameters by altering absorber parameters can be made on the actual system. This entails many experiments while altering the absorber parameters. Once this absorber is found then an input shaper can be designed in the same manner from an exhaustive set of experiments. This technique is much more consuming than the simulation based technique, but can be implemented when a good model is not available. However, the simulation technique is much better suited as an initial design tool, since it requires only an accurate system model.

8.1.2.2 *Concurrent Design Of Vibration Absorbers and Input Shapers*

Although useful, the sequential design approach will not lead to the best possible results. In order to attain peak performance, vibration absorbers and the complimentary input shapers need to be designed concurrently. To achieve this goal, a numerical optimization can be performed to select both the absorber and input shaper parameters. The MATLAB Optimization Toolbox can be utilized along with the simulation capabilities of MATLAB and a settling time calculation of the fourth-order response of the combined system. The net result is a solution that optimally decreases vibration from both externally-induced and command-induced step disturbances. The process consists of the following steps.

1. Create a dynamic model of the system

2. Parameterize the vibration absorber and input shaper

3. Optimize parameters while minimizing a cost function.

8.1.2.2.1 Optimization Parameters

Before the optimization can be formulated, the possible solution set has to be defined, *i.e.* the set of variables that the optimization can select. These parameters fall into two subcategories: absorber variables, and shaper variables. The absorber variables are the physical properties of the absorber namely, the damping ratio and the spring constant (the absorber mass must be fixed by the designer). For the input shaper, the variables are the number of impulses and their time locations and magnitudes.

The optimization parameters cannot take on arbitrary values; instead, they are limited by the laws of physics, by the desired outcome and by the knowledge gained from previous input shaper design and the absorber design of Section 8.1.1. Therefore, the range of the absorber parameters in the concurrent approach are limited to be : $0.001 < \zeta < 0.5$ and $0.5 < r < 2$. These limits form the basis of the constraints and cost functions of the optimization.

8.1.2.2.2 Constraints and Cost Functions

The limits on the optimization fall into three categories, Physical Constraints, Response Constraints, and Cost Function Values. The Physical Constraints are products of a simulation-based environment and are used to limit the options of the optimization algorithm. For example, a negative damping ratio for the absorber is not physically realizable. The mass of the absorber is also considered a physical constraint. An increase in the mass of the absorber increases its effectiveness at disturbance rejection. A larger mass is able to exert more force on the primary mass and can control the undesired vibration better. Therefore, if absorber mass is considered a variable it will be driven towards infinity. The designer must, therefore, choose an appropriate absorber mass for the application.

The Response Constraints are used as a binary condition for the possible solutions of the optimization. If these constraints are satisfied, then the current candidate solution of the optimization becomes an acceptable solution. These Response Constraints define the desired response of the absorber and input shaping scheme. For example, if a peak overshoot of 2 inches is the maximum permitted, then a response constraint can be used to limit the possible solutions to only those less than 2 inches. Here, the primary response constraint is the peak overshoot of the system when driven by a shaped step. This constraint takes the form:

$$M_{P_{shap}} - M_{P_{allow}} < 0 \tag{8.11}$$

where $M_{P_{shap}}$ is the peak overshoot of the shaped step response and $M_{P_{allow}}$ is the maximum allowable overshoot.
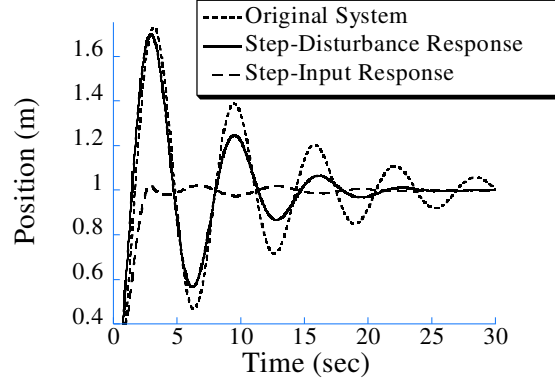
Figure 8.17: Combined Design Driven and Disturbed Response.

Finally, the Cost Function Values determine how the optimization is driven towards the solution. The cost function used here is:

$$J = T_{set} + \alpha M p_{shap} \tag{8.12}$$

where the scaling α is increased for a more important shaped response or decreased for improved disturbance response. The 5% settling time of the combined system subject to an external step-disturbance is the most heavily weighted value in the cost function. However, the inclusion of the peak overshoot of the augmented system provides resolution in the optimization routine. The settling time of the externally disturbed system, T_{set}, is not affected by any of the shaper variables. If a shaper-affected variable is not included, then a distinct solution does not exist for the entire scheme. In (8.12), T_{set} primarily drives the selection of the vibration absorber parameters, while Mp_{shap} primarily drives the shaper parameters. Any small value of α will be sufficient to find an effective shaper.

8.1.2.2.3   Results

The concurrent design of input shaping and vibration absorbers yields a solution that rejects vibrations caused by both the input to the system and external disturbances. Figure 8.17 shows an example of this improvement for a system with $\omega_n = 2\pi$ and $\zeta = 0.1$. The settling time from a step disturbance is reduced by 31.4% with the aid of the vibration absorber and the peak overshoot caused by a step change in the reference command is reduced 94.6% through the inclusion of the input shaper. The vibration absorber mass was limited to 10% of the original system's mass, and $\alpha = 0.01$. The resulting vibration absorber has:

$$
\begin{aligned}
r &= 0.7878 \\
\zeta_A &= 0.4000
\end{aligned}
\tag{8.13}
$$

278
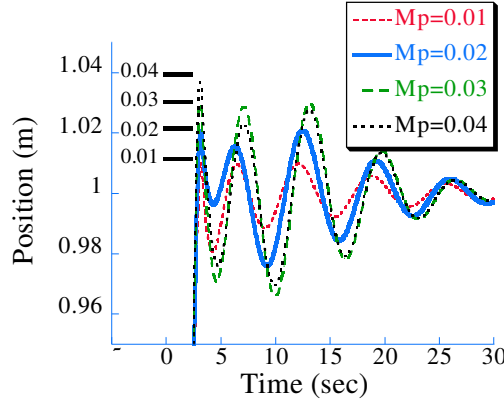
Figure 8.18: Peak Overshoot Constraint Effect on Driven Response.

This damping ratio is much larger than traditional continuous sinusoidal absorber applications. The input shaper is given by:

$$
\begin{bmatrix} t_i \\ A_i \end{bmatrix} = \begin{bmatrix} 0 & 3.3451 \\ 0.6051 & 0.3949 \end{bmatrix}
\tag{8.14}
$$

In this example, a two-impulse shaper is used. Using only two impulses forces a fast rise time and simplifies the optimization routine. More impulses or different response parameters can be tuned to better suit the needs of a particular application. For example, if the problem required large robustness to modelling errors, then the shaper would need more impulses.

Several trends arise in the solutions provided by this concurrent design approach, most notably relating to the allowable peak overshoot. The peak overshoot's worth as a constraint is related both to its applicability to the problem and its direct relation to the shaper parameters. Lowering the peak overshoot constraint obviously reduces the maximum excursion, as seen in Figure 8.18. However, more importantly and unexpectedly, Figure 8.19 shows that increasing the limit on overshoot provides an improvement in the disturbance rejection properties. Therefore, a designer can trade off directly between disturbance rejection and vibration induced by the reference command.

This concurrent technique also works for real systems even if the model is not perfect. Figure 8.20 shows the response of the experimental setup when fitted with the concurrent absorber and input shaper predicted by the simulation. The absorber parameters are $\mu = 0.1$, $\zeta_a = .4$, and $r = 1.28$ and the shaper is given by:

$$
\begin{bmatrix} t_i \\ A_i \end{bmatrix} = \begin{bmatrix} 0 & .1753 \\ 0.5832 & 0.4168 \end{bmatrix}
\tag{8.15}
$$

Notice that the concurrent design shaped result in Figure 8.20 is better than the sequential design result in Figure 8.16. The reverse is true for the absorber only results. Namely,

279
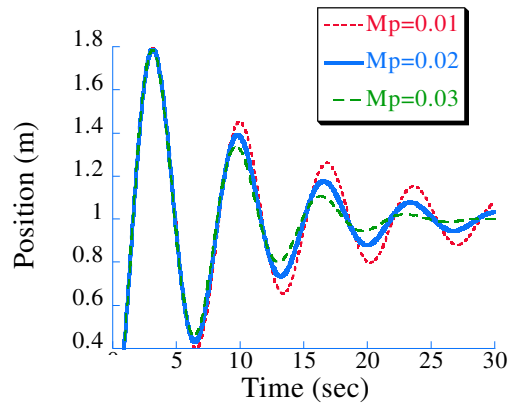
Figure 8.19: Peak Overshoot Constraint Effect on Disturbed Response.
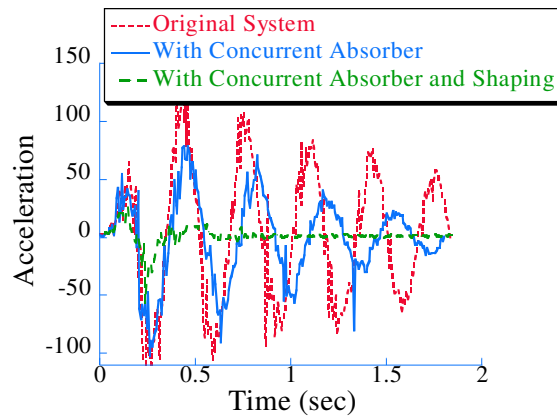
Figure 8.20: Experimental Combined Solution.

the absorber designed with the sequential method preforms better than the concurrent absorber for disturbance rejection. This shows that the concurrent design method obtains the improvement in the shaped result by sacrificing a small amount of the disturbance rejection ability.

There exist certain instances when the concurrent approach should be utilized to push the performance limit. However, the sequential technique is preferable in cases where design time or cost is an issue, since it does not require a simultaneous optimization. Also when the absorber cannot be designed precisely due to difficulty modelling the system, the sequential method is preferable since the improved performance from the concurrent approach would be lost due to modelling inaccuracies. The concurrent solution does allow a significantly better commanded motion than the sequential approach at the cost of increased difficulty in design.

8.1.3 Summary of Vibration Absorber Usage

Vibration absorbers can be developed specifically for the reduction of step disturbances. This application of vibration absorbers led into the investigation of input shaping design with the mechanical design of vibration absorbers. This process pointed out that direct tradeoffs could be made between mechanical design choices and input shaper design choices. Specifically, increasing the mechanical vibration reduction caused by the absorber caused a decrease in the input shaper performance. In this application, a direct tradeoff exists between these two parameters. This tradeoff was shown both in simulation and experiment. The same basic techniques for designing auxiliary mechanical elements with input shapers can be used to design mechanical elements that compose the basic structure of a machine with input shapers as will be discussed in the following sections. However, when the basic structure design is combined with input shaper design, the input shaper has a more direct effect on the speed of the response. The tradeoffs between mechanical performance and the input shaper still exist. Therefore, in the following sections where larger scale design implementation will occur, the input shaper's impact on speed will be considered concurrently with other mechanical performance measures.

8.2   Single Beam Design

The previous section presented a method for concurrently designing input shapers with auxiliary mechanical elements. This section will show how to design simple system elements, namely beams, with input shaping. The focus will be on creating designs consisting of simple beams driven with input shapers that move as fast as possible. This process has two major components; first the relationships between beam parameters and response will be investigated. Once these relationships are known, they will be combined with a selection

approach to choose beams and input shapers together. For the investigation in this dissertation only circular cross-section beams are considered; however, the same techniques and calculations can be used for any cross-section beam. Beams as were discussed in Chapter 7 are an integral part of a micro-mill structure. A micro-mill position system could benefit from selecting beams and input shapers concurrently.

8.2.1 Design Requirements

The relationships between the design parameters, specifically radius and length of circular beams and the mass of any load, and the response of the beam are important to design selection. One of the primary influences on beam speed is the natural frequency. Therefore understanding how natural frequency changes with the beam design parameters is important. However, the natural frequency of a system is not the only design concern, therefore, other design requirements, the static stiffness and total mass are utilized. A combination of these parameters will be used for design selection. This beam selection process will utilize the design requirements, natural frequency, mass, and static stiffness, in combination to select beam design parameters, radius, length and attached mass.

8.2.1.1 Frequency

A fundamental measure of the speed of a system is its natural frequency. A system with a high natural frequency can respond more quickly than a system with a low natural frequency. Selection of mechanical designs based on system frequency is not a new approach; however, here the frequency data will be used to design input shapers to move the system. The duration of these shapers is a primary factor in the speed of the machine. Consequently, to know how the speed of a system changes with its basic parameters, the relationship between the frequency and the physical parameters are needed. The frequency relationships will be developed for the beams presented in Chapter 7. Each beam's physical parameters impact on frequency will be discussed. Specifically radius, length and, where appropriate, attached endpoint mass will be considered as physical parameters.

In terms of speed or duration of the input shaper, the fastest natural frequency can be shaped by the fastest or shortest duration shaper. This effect will later be limited by system mass, but from a purely frequency standpoint, higher frequencies are better for rapid shaped motion. Note that longitudinal beam design will not be discussed due to their similarities to torsional beams except as presented in Appendix B.

8.2.1.1.1 Torsional Beam Frequency

The first beam under consideration is the torsional beam with no attached inertia seen in Figure 8.21 that was presented in Sections 7.1.1 and 7.2.2. Remember that the ith natural
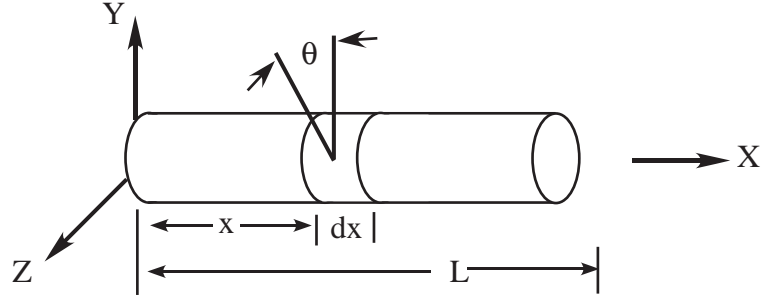
Figure 8.21: Diagram of Torsional Beam.
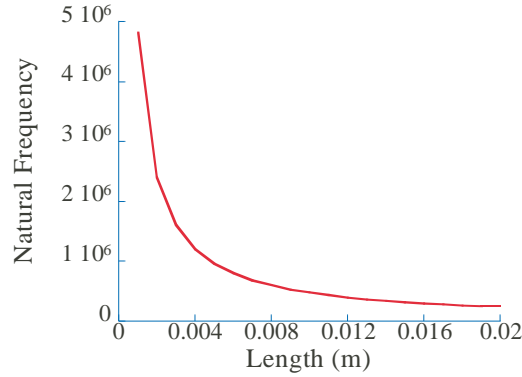
Figure 8.22: Torsional Beam: Frequency Variation with Length.

frequency of the torsional beam is given by:

$$\omega_i = \frac{\pi b i}{2L} \qquad (i = 1, 3, 5, ..., \infty) \tag{8.16}$$

where L is the length and b is the wave speed in the beam, and is defined for a Shear Modulus, G, and density ρ by:

$$b = \sqrt{\frac{G}{\rho}} \tag{8.17}$$

Interestingly, the torsional natural frequency of the beam is not affected by the diameter of the circular fixed-free beam. While the diameter of this torsional beam does not affect the frequency, the diameter will later play an important role in the speed of the beam's response, since it directly effects total inertia.

The length of the beam, on the other hand, has a direct correlation to the natural frequency. Figure 8.22 shows that the longer the beam, the lower the natural frequency. This relationship will be important later in beam selection. While for the torsional beam, the frequency does not change for varying diameters, for many other beams this relationship will not be true. Therefore, it is important to introduce a way of examining how changes in both diameter and length affect the frequency. For the torsional beam with no attached

283
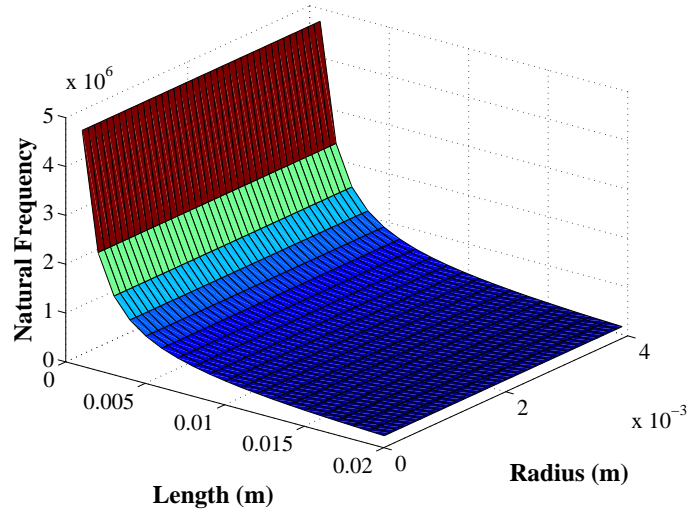
Figure 8.23: Torsional Beam: Frequency Variation with Length and Diameter.
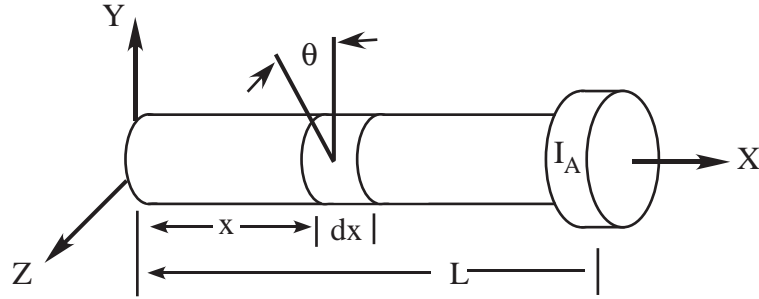
Figure 8.24: Diagram of Torsional Beam with Attached Inertia.

inertia, Figure 8.23 shows how the diameter and length relate to frequency. The frequency is obviously unaffected by changes in the diameter. The figure also shows that the shortest possible beam will have the highest frequency, and the higher the frequency the shorter the shaper duration, and therefore, the faster the machine.

8.2.1.1.2 Torsional Beam with Attached Inertia Frequency

While determining the frequency determination for torsional beam without any attached inertia is straightforward, as the frequency is only a function of the length; attaching an inertia to the end of the beam complicates the process. The attached inertia torsional beam is diagramed in Figure 8.24 and was discussed previously in Sections 7.1.2 and 7.2.3. Another design variable is required for the attached inertia case, the percentage attached inertia, η, which is the attached inertia divided by the inertia of the beam alone. The percentage attached inertia changes the frequency calculation to the solution to:

$$\kappa_i \tan \kappa_i = \eta \tag{8.18}$$
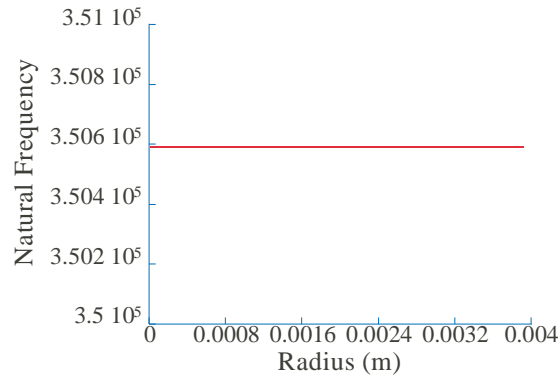
Figure 8.25: Torsional Beam with Fixed Inertia Ratio: Frequency Variation with Diameter.
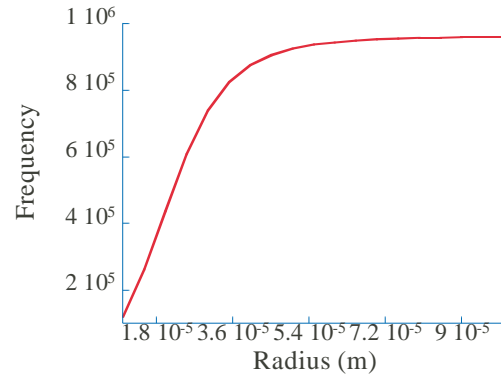
Figure 8.26: Torsional Beam with Variable Inertia Ratio: Frequency Variation with Diameter.

where $\kappa_i = \frac{\omega_i L}{b}$ and the percentage attached inertia $\eta = \frac{\rho I_p L}{I_A}$. I_p is the polar moment of inertia of the beam, and I_A is the attached inertia.

For a fixed attached inertia ratio, the frequency does not change with diameter as shown in Figure 8.25. The independence of diameter from frequency is only possible because inertia ratio, not actual attached inertia, is considered in the figure. Since inertia ratio depends on the diameter of the beam, it is also important to consider how the frequency changes for a fixed endpoint inertia instead of inertia ratio. Figure 8.26 shows how the frequency changes with diameter for a fixed inertia. Notice that the frequency is asymptotically approaching the constant value that would occur if no inertia was attached. As the radius grows significantly large enough, the attached inertia no longer has a significant impact. At lower radii, however, an increase in radius causes an increase in frequency, but after a certain point, it does not help to alter the radius of the beam. The result from this
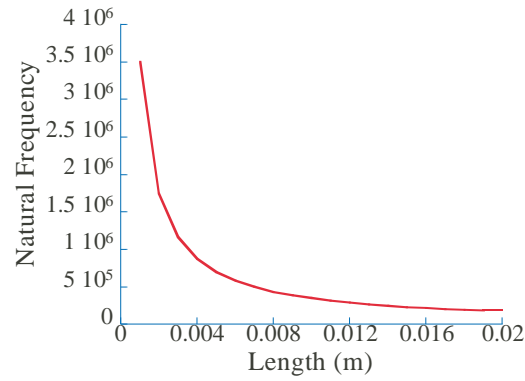
Figure 8.27: Torsional Beam with Fixed Inertia Ratio: Frequency Variation with Length.
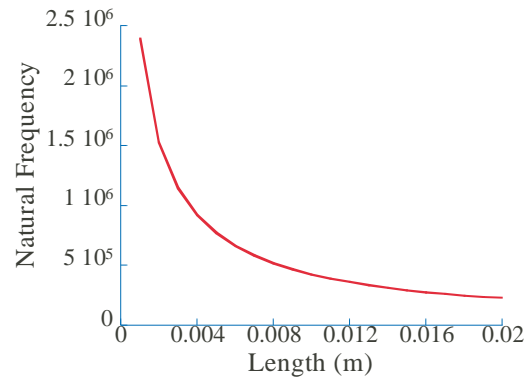
Figure 8.28: Torsional Beam with Fixed Inertia: Frequency Variation with Length.

frequency analysis is to select the largest possible radius if the highest natural frequency is desired.

The length of the beam also has an impact on natural frequency. Figure 8.27 shows how the frequency of the beam decreases as length increases for a fixed inertia ratio of 0.9. A similar trend occurs, if instead of fixing the inertia as a percentage of the overall beam inertia, the attached inertia is fixed to a specific value. Figure 8.28 shows that the same general trend occurs independent of considering a fixed inertia ratio or a fixed inertia. Thus, these figures show that once again, a shorter torsional beam is recommended for a high natural frequency and a shorter input shaper duration.

It is clear from considering only the length or the radius, that the frequency of a torsional beam with an attached endpoint inertia is dependent on both the beam length and the radius. An increase in radius or a decrease in length, both increase the natural frequency of the system. When a length and radius are investigated simultaneously, both variables are
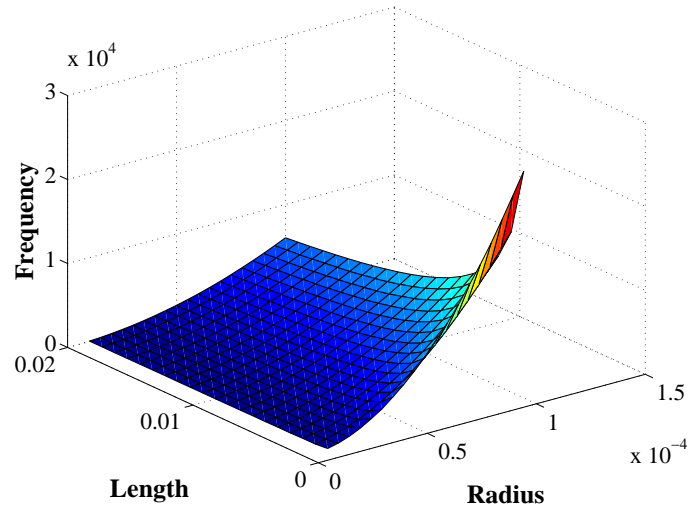
Figure 8.29: Torsional Beam with Fixed Inertia: Frequency Variation with Length and Radius.

shown to contribute to the natural frequency on the same order of magnitude for a fixed inertia, as displayed in Figure 8.29. Unlike the case of the beam with no endpoint inertia, design choices involving the attached inertia beam need to consider the radius and length simultaneously.

Up to this point, the attached inertia was considered fixed in value or in ratio. If the attached inertia of the beam is allowed to vary, the frequency of the beam will certainly change. If just the percentage attached inertia is investigated, then the lighter the attached inertia will yield a higher the frequency, as seen in Figure 8.30. If the radius of the beam is also considered, then the frequency appears not change with the radius of the beam, as shown in Figure 8.31. The frequency remains constant for a given inertia ratio no matter the radius. However, this is an artifact of using the inertia ratio and not the actual inertia. Figure 8.32 shows the same parameter variation but for fixed inertia values. The relationship previously seen of lower inertia yielding higher frequencies is less prominent in this figure especially for larger radii. Figure 8.32 shows that if the radius is large enough, then the attached inertia must change considerably in order to effect the frequency of the system. Therefore, for beams with relatively small attached inertias, once again radius is not important in the torsional frequency determination.

A definitive relationship also exists between the attached inertia ratio and the length of the beam. Figure 8.33 shows that the lower the inertia, the greater of an impact length changes have on the dominant frequency of the system. By investigating the physical parameters on the torsional beam with an attached inertia, it was found that the shortest length beam with lowest attached inertia is needed if high frequencies are desired. Also, when the attached inertia is significant, the radius should be made as large as possible.

287
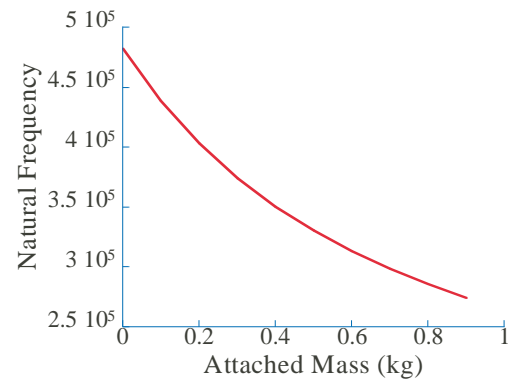
Figure 8.30: Torsional Beam with Inertia: Frequency Variation with Attached Inertia.
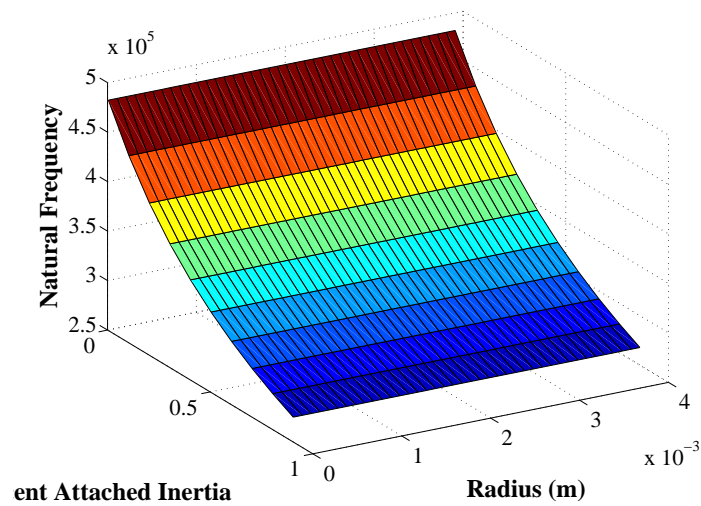
Figure 8.31: Torsional Beam with Inertia: Frequency Variation with Radius and Percentage Attached Inertia.
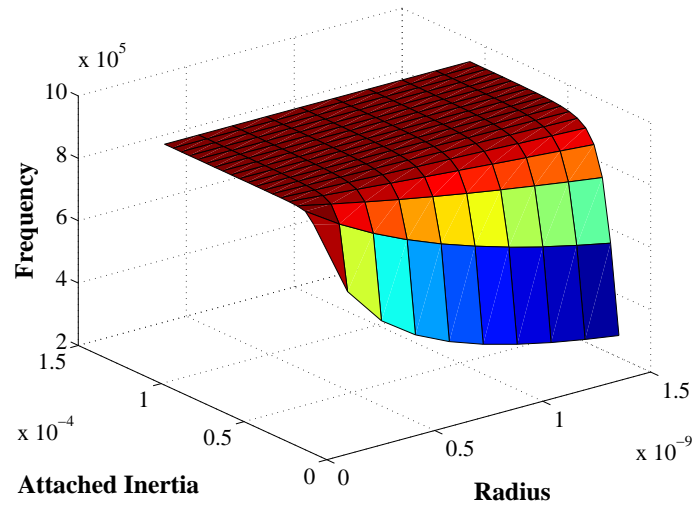
Figure 8.32: Torsional Beam with Inertia: Frequency Variation with Attached Inertia and Radius.
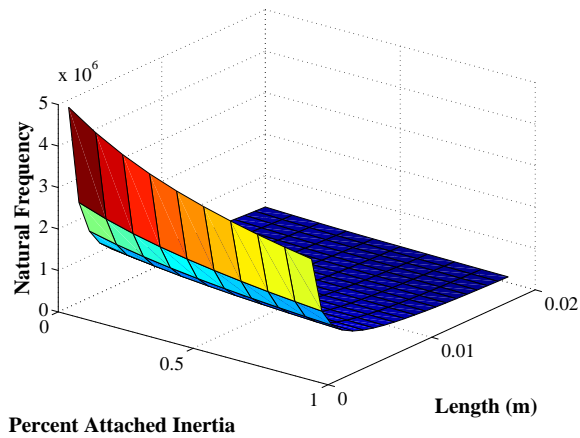
Figure 8.33: Torsional Beam with Inertia: Frequency Variation with Length and Inertia.
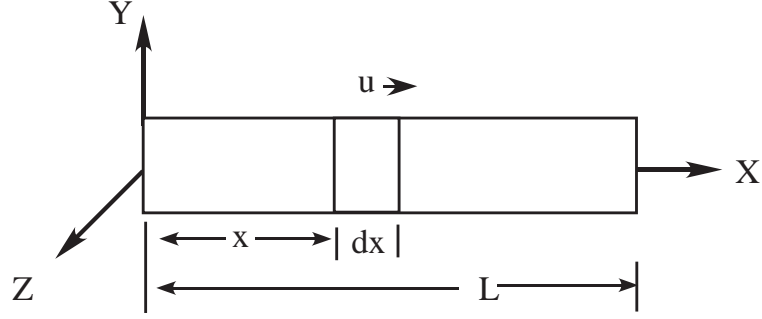
Figure 8.34: Diagram of Longitudinal Beam.
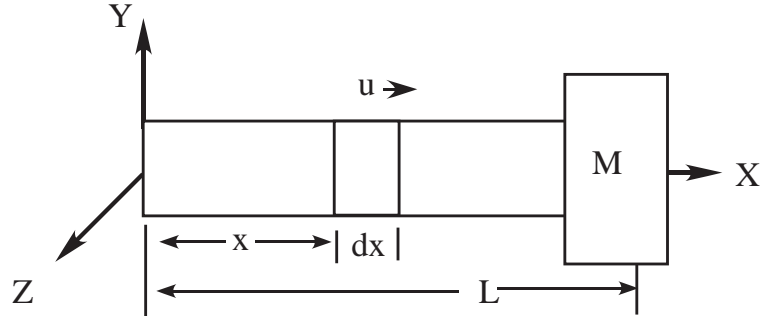
Figure 8.35: Diagram of Longitudinal Beam with Attached Mass.

8.2.1.1.3 Longitudinal Beam Frequencies

The longitudinal beam with and without attached masses performs in the same way as the torsional beam. The longitudinal beam is diagramed in Figure 8.34, while the longitudinal beam with attached mass is diagramed in Figure 8.35. Both are also discussed in Appendix A.1. The input shaping of both of these beams was presented in Appendix A.3. Because the longitudinal beam is so similar to the torsional beam, the frequency analysis is relegated to Appendix B.

8.2.1.1.4 Transverse Beam Frequencies

The study of input shaping on continuum beams in Chapter 7 showed the differences in behavior between the torsional/longitudinal and transversely vibrating beams. These differences also make themselves apparent when the relationships between the physical parameters and frequency are studied. For the transverse beam diagramed in Figure 8.36 and presented previously in Sections 7.1.4 and 7.2.5, both the length and the radius are directly coupled to the frequency. An increase in the radius of the beam causes a linear increase in frequency as shown in Figure 8.37. This relationship is governed by the equations for natural frequency. The ith frequency for the transverse beam is the solution to:

$$\cos k_i L \cosh k_i L = -1 \tag{8.19}$$

290
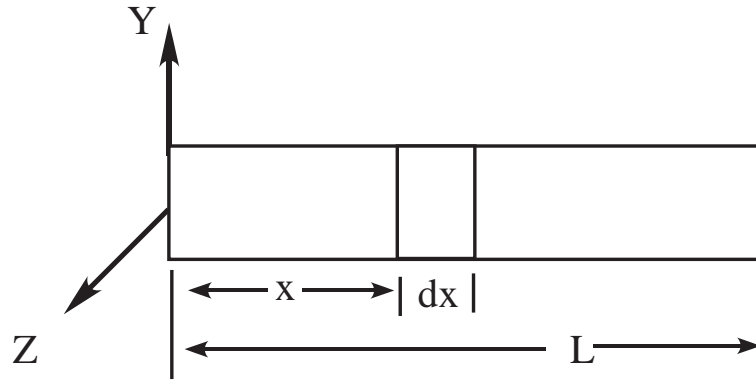
Figure 8.36: Diagram of Transverse Beam.
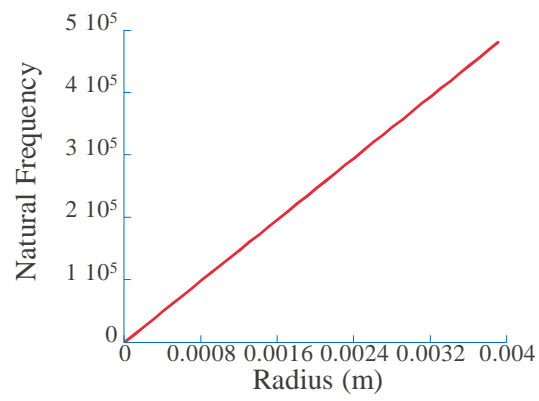
Figure 8.37: Transverse Beam: Frequency Variation with Radius
.
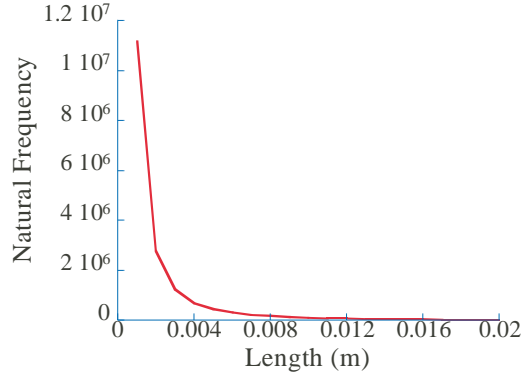
Figure 8.38: Transverse Beam: Frequency Variation with Length.

where:

$$k_i = \sqrt{\frac{\omega_i}{a}} \tag{8.20}$$

with L is the length and a is the wave speed in the beam given by:

$$a = \sqrt{\frac{EI_P}{\rho A}} \tag{8.21}$$

where E is Young's Modulus, I_P is the polar moment of inertia, ρ is the density, and A is the area. The area and polar moment of inertia are where the radius impacts the frequency equation. The relationship between frequency and radius cannot be derived directly due to the trigonometric and hyperbolic properties of (8.19). But the general trend of a larger radius leading to a higher frequency still holds as it did for the loaded torsional/longitudinal beams.

Similarly, the relationship between length and frequency cannot be solved in closed form. However, if it is investigated numerically, then the frequency of the beam is shown to decrease with length as shown in Figure 8.38. The exponential decay in the figure shows how important it is to make the beam as short as possible in order to maximize frequency. Shorter beams have a higher natural frequency irrespective of the beam radius. Figure 8.39 shows how the length and radius impact the first natural frequency. From the figure it is clear that a short and wide beam is preferred when attempting to increase the natural frequency. To reiterate, increasing the natural frequency shortens the duration of any particular input shaper, thus allowing the beam to move faster with input shaping.

8.2.1.1.5 Transverse Beam with Attached Mass Frequency

Often transverse beams must carry a payload. Therefore, transverse beam frequencies must also be investigated. Figure 8.40 diagrams a transverse beam with an attached mass; this type of beams was also discussed previously in Sections 7.1.5 and 7.2.6. Attaching an inertia

292
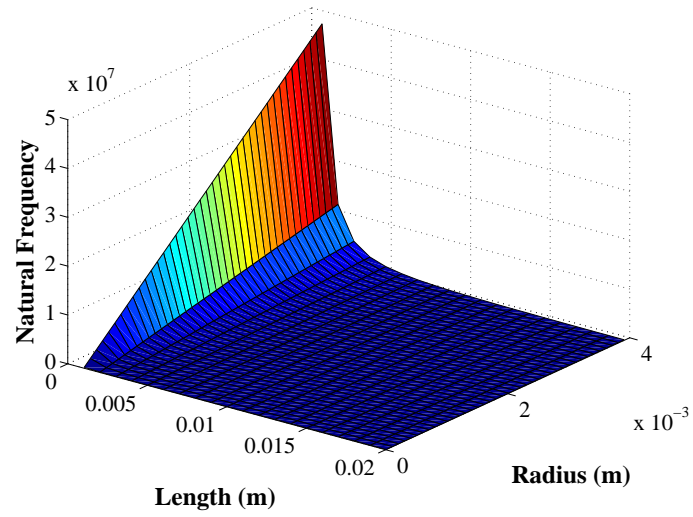
Figure 8.39: Transverse Beam: Frequency Variation with Length and Radius.
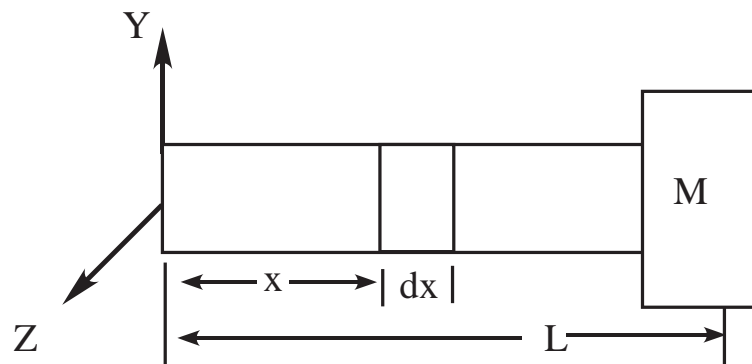
Figure 8.40: Diagram of Transverse Beam with Attached Mass.
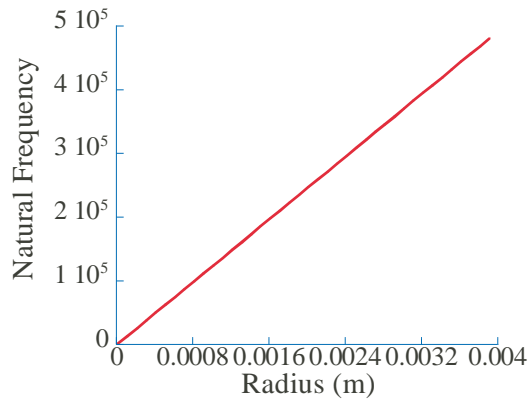
Figure 8.41: Transverse Beam with Inertia: Frequency Variation with Radius.
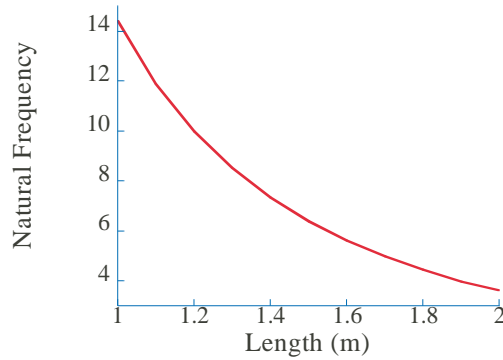
Figure 8.42: Transverse Beam with Inertia: Frequency Variation with Length.

to a torsional beam alters the natural frequency calculations depending on the magnitude of inertia added. Likewise, the relationships between frequency of the transverse beam with an attached mass and the beam parameters are somewhat different from beam without an attached mass. However, the desired for a high natural frequency mandates a short beam with a large radius no matter the attached mass. Figure 8.41 shows the radius/frequency relationship for a beam with a constant attached mass. This figure was obtained using the derivation in Section 7.1.5.

The attached mass also changes the relationship between length and frequency as shown in Figure 8.42. While this curve still exponentially decays with larger lengths, its shape is different depending on the attached mass. Yet, the ideal highest frequency case is still the shortest beam, no matter the mass. The relationship among the attached mass, the length, and the dominant natural frequency is also important

If attached endpoint mass can also be considered as a design variable, then like the
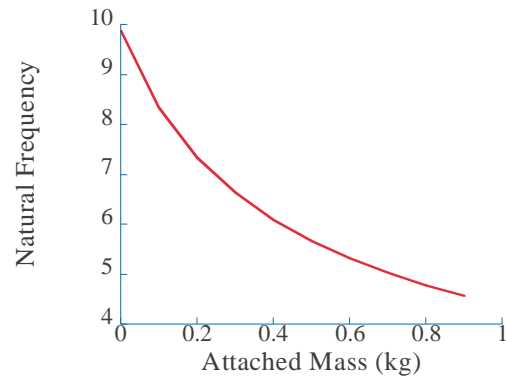
Figure 8.43: Transverse Beam with Inertia: Frequency Variation with Mass.
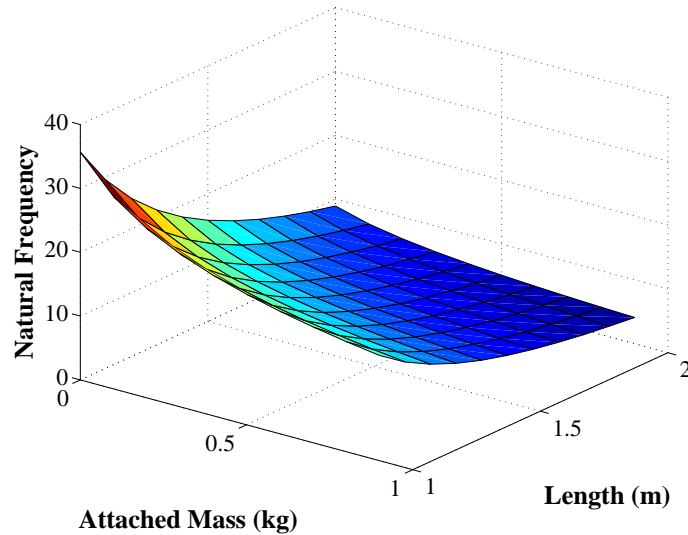
Figure 8.44: Transverse Beam with Inertia: Frequency Variation with Length and Mass.

torsional beam with an attached inertia it is desirable to minimize the value of this mass. Figure 8.43 show how increasing the mass decreases the natural frequency. The limiting case is the unloaded beam, like those discussed in the previous section, shown as the back left edge of the surface in Figure 8.43. Therefore, in order to keep the beam frequency large, so that the input shaper is short, it is necessary to minimize the mass, no matter the other beam parameters. Figure 8.44 shows the mass minimization impact for length; the relationship shown in the figure of an increases mass decreases the frequency holds for all beam lengths. Also notice how the relationship between beam length and frequency changes with attached mass. As mass increases the length/frequency relationship becomes shallower. Therefore, the larger the attached mass, the less relevant beam length is in the calculation.
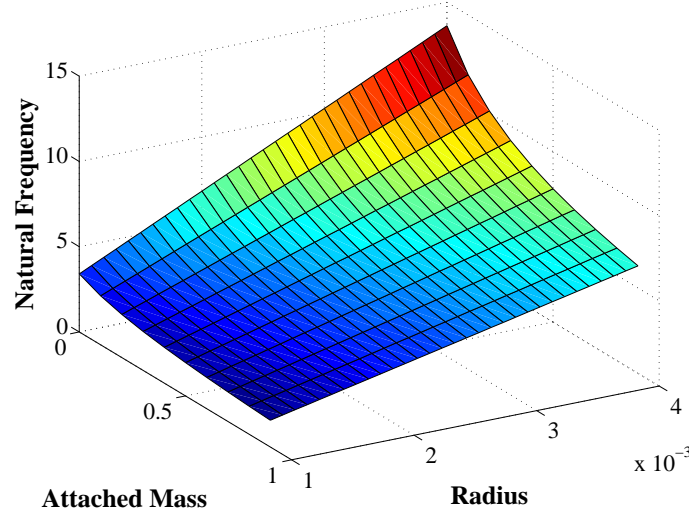
Figure 8.45: Transverse Beam with Inertia: Frequency Variation with Radius and Mass.

The same relationship between the relevance of radius at larger attached masses is seen. Figure 8.45 shows that for larger masses, the radius has a smaller contribution to the frequency, just as the length did. This result coincides with the torsional beam result. That is, for larger masses, the beam parameters cease to be as important, and the beam behaves more like a lumped parameter spring mass system. Consequently the relationship between increased mass and decreased frequency shown in the figure becomes even more important.

The study of frequency response for the transverse beam with an attached mass, showed that the length, radius and attached mass are all directly related to the frequency and thus the speed of the corresponding input shaper. However, as the attached mass increases, the relevance of the beam parameters trails off as the attached mass increases. Therefor,e when selecting transverse beam with attached masses it is primarily important to minimize mass, and if that is not possible by some design constraint, then the length and radius need to be addressed as will be discussed later.

8.2.1.2   Static Stiffness

While the frequency is a performance measure related to the motion limits of the system, another important measure is related to the static behavior of the beam, that is its static stiffness. Often static deflection requirements are placed on beams, and therefore, it is important to understand the relationship between the static stiffness and the physical parameters of the system. Note that the static stiffness of a beam with an attached mass or inertia is the same as an unloaded beam. Typically the static stiffness has the same trends as the natural frequency. Specifically beams with high natural frequencies are usually stiff. However, when endpoint inertias are added they blur this relationship.
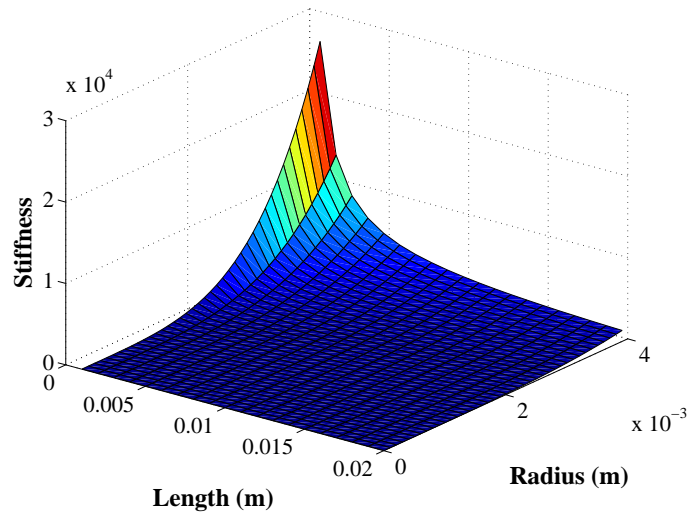
Figure 8.46: Torsional Beam Stiffness.

8.2.1.2.1   Stiffness of Torsional Beams and Torsional Beams with Attached Inertias

Remembering that the torsional beams stiffness is defined by:

$$k = \frac{GI_p}{L} \tag{8.22}$$

where G is the Shear Modulus, I_p is the polar moment of inertia and L is the length. The polar moment of inertia is directly related to the radius and for a circular cross section is defined by:

$$I_P = \frac{\pi R^4}{2}; \tag{8.23}$$

These straightforward relationships between radius, length, and stiffness can be seen for a variety of cases in Figure 8.46. An increase in radius or a decrease in length both lead to an increase in static stiffness of the beam. Noting that a high static stiffness is desired in beam design, this relationship can be used to select acceptable beam parameters.

8.2.1.2.2   Stiffness of Longitudinal Beams and Longitudinal Beams with Attached Masses

Since the dynamics of the torsional beam and the longitudinal beam are the same except for different variables, the relationships among radius, length, and stiffness are the same as well. Remember that the stiffness of a longitudinal beam with or without a mass is defined by:

$$k = \frac{EA}{L} \tag{8.24}$$

where E is Young's modulus, A is the area, and L is the length. Figure 8.47 shows how these parameters change the static stiffness. Once again the length and radius contribute approximately the same order of magnitude to the static stiffness of the system. Also large radii and short lengths are desirable to maximize stiffness.
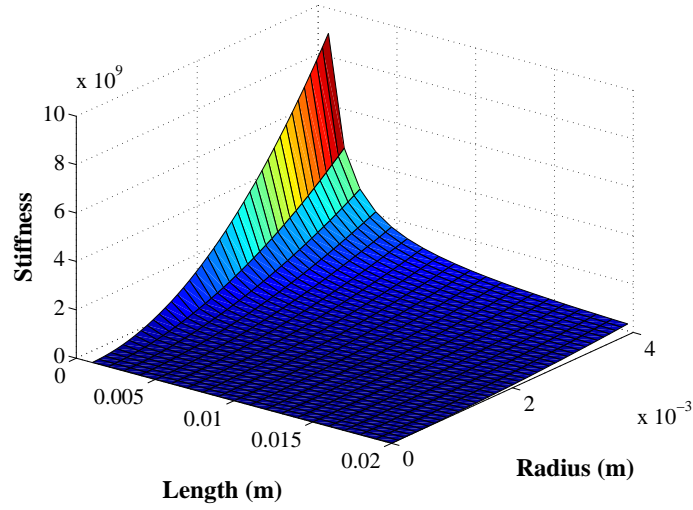
Figure 8.47: Longitudinal Beam Stiffness

8.2.1.2.3 Stiffness of Transverse Beams and Transverse Beams with Attached Masses

Even though the dynamics of transverse beams differ from those of torsional beams, the same general relationships among stiffness, length, and radius exist. Since the stiffness of the transverse beam is given by:

$$k = \frac{3EI_P}{L^3} \tag{8.25}$$

where the parameters as defined as before, the same trends occurs in the transverse beam as the longitudinal and torsional beams. This can be clearly seen by comparing Figure 8.47 for the longitudinal beam and Figure 8.48 for the transverse beam. Both show an increase in length or a decrease in radius detrimental to the static stiffness of the beam. However, differences do exist in the shape of the curve, particularly along the length axis. While stiffness decreased with length linearly for the longitudinal beam, it falls off as the cube of length for the transverse beam. Therefore, it is more important to consider minimizing length in the transverse beams when attempting to maximize stiffness.

8.2.1.3 Total Mass

Previously, both static and dynamic measures of performance were presented. Dynamically, frequency is control system bandwidth and thus the speed of the machine, while static stiffness only describes the rest performance of a machine. The total mass of a beam has impact in both of these realms. The more massive a beam, then the harder it is to accelerate with a given actuator. Mass also is important to the static machine, since larger masses require larger support structures, as well as larger bearings. Since the total mass of a beam is important in both the static and dynamic performance analysis, the relationships of the physical parameters to the total mass must be well understood. Even though the
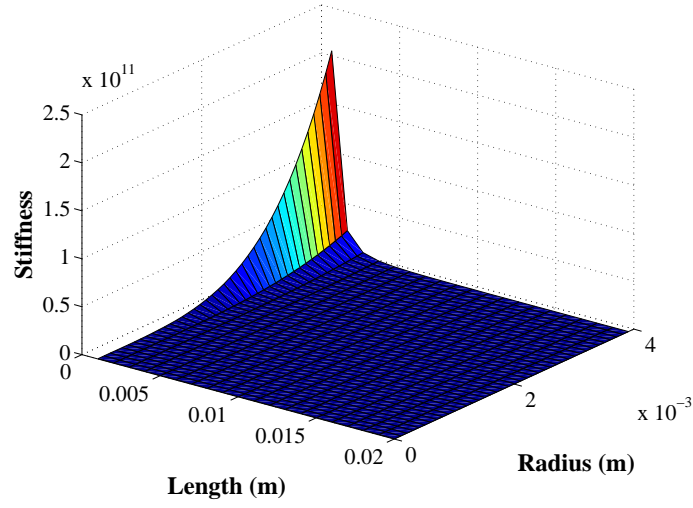
Figure 8.48: Transverse Beam Stiffness

calculation of total mass can be trivial, later the relationships between total mass and the beam parameters will be important in designing beams with input shaping.

8.2.1.3.1   Torsional Beams: Total Inertia

First, the torsional beam's overall inertia will be considered and is defined by:

$$I_{tot} = \rho I_p L \tag{8.26}$$

where for a circular cross section specifically, it is:

$$I_{tot} = \frac{\rho \pi R^4 L}{2} \tag{8.27}$$

As expected, the inertia varies with the length and radius. Figure 8.49 shows how increases in either parameter parameters increase the mass. While this result is obvious, the relationships between the desired result of lower mass and the physical parameters must be combined with other design considerations. Thus tradeoffs in the design will have to be made to balance mass with stiffness and frequency.

8.2.1.3.2   Torsional Beam with Attached Inertia: Total Inertia

When inertia is added to the end of a torsional beam, the total inertia is:

$$I_{tot} = \rho I_p L + I_A \tag{8.28}$$

and for a circular cross section:

$$I_{tot} = \frac{\rho \pi R^4 L}{2} + I_A \tag{8.29}$$
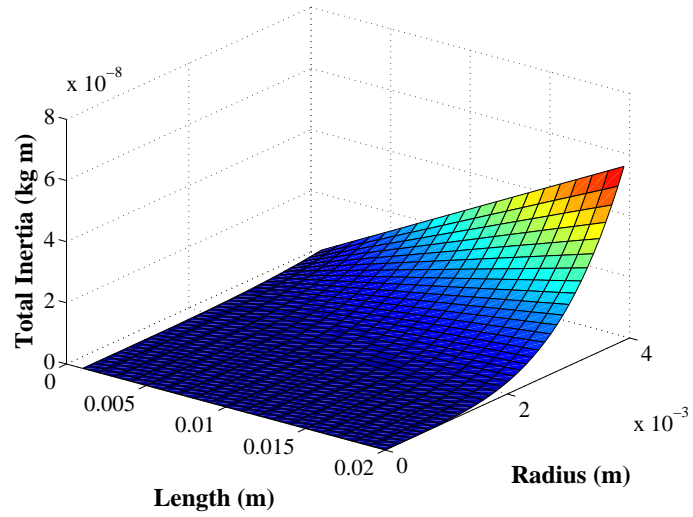
Figure 8.49: Torsional Beam: Inertia
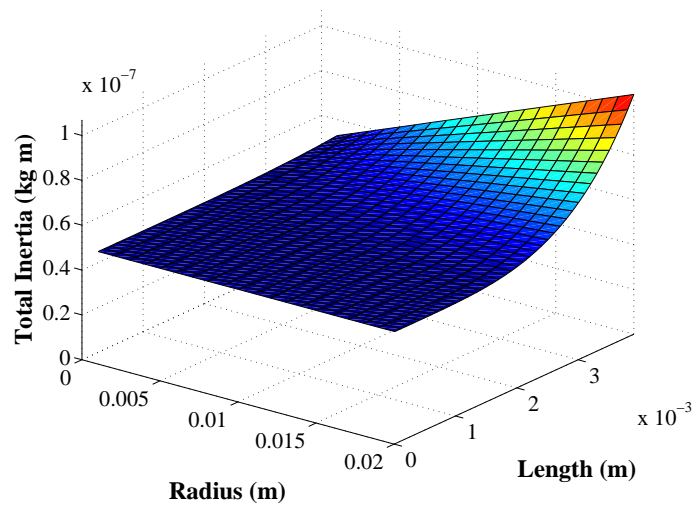
Figure 8.50: Torsional Beam with Attached Inertia: Total Inertia
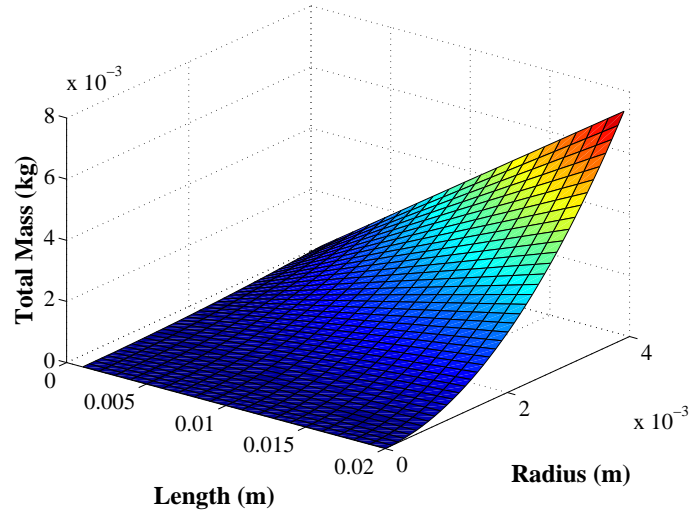
Figure 8.51: Longitudinal Beam: Mass.

This relationship is obviously the same as the previous torsional case plus a constant for the attached inertia. Figure 8.50 shows how the mass changes with length and radius. The design tradeoff is dependent on the magnitude of the attached inertia, as well as the length and radius of the torsional beam.

8.2.1.3.3 Longitudinal Beam: Total Mass

Longitudinal beams are quite similar to torsional beams in all aspects. They do differ in that, the mass changes with the square of the radius for a longitudinal beam while the inertia of a torsional beam changes with R^4. The total mass for a longitudinal beam is:

$$m_{tot} = \rho A L \tag{8.30}$$

and for a circular cross section:

$$m_{tot} = \rho \pi R^2 L \tag{8.31}$$

The length and radius parameters effect on total mass is logical and can be seen in Figure 8.51. This figure will be useful when selecting a beam design for a specific application later in this chapter.

8.2.1.3.4 Longitudinal Beam with Attached Mass: Total Mass

Attaching a mass, M_A, to the end of a longitudinal beam has the obvious effect of shifting the total mass of the beam as defined by:

$$M_{tot} = \rho A L + M_A \tag{8.32}$$
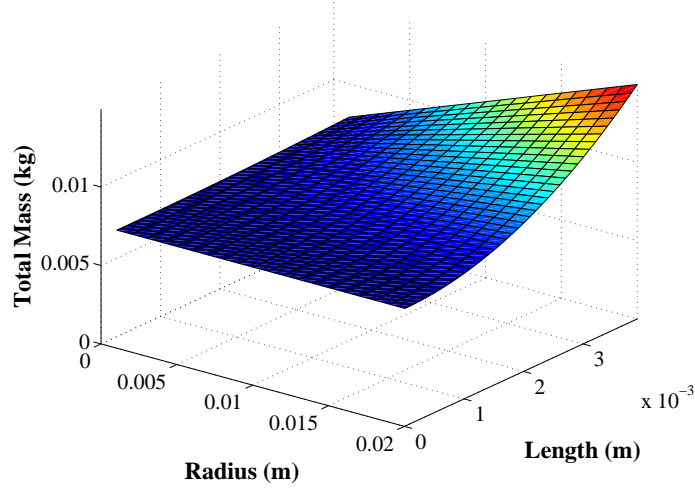
Figure 8.52: Longitudinal Beam with Attached Mass: Total Mass

For a circular shape, the total mass is:

$$M_{tot} = \rho \pi R^2 L + M_A \tag{8.33}$$

While this relationship is similar to the unloaded beam, adding the mass at the end of the beam will make it more difficult to meet a required maximum mass constraint on the beam, and consequently could effect the selection of the radius and the length of the beam. Figure 8.52 shows the relationship among mass, length, and radius. Note that since the total mass in higher in Figure 8.52 than for the unloaded case of Figure 8.51, a constraint on the total mass of a design would require the selection of a thinner and/or shorter beam.

8.2.1.3.5   Transverse Beam With and Without Attached Mass: Total Mass

The same trends exist for the transverse beam as were seen in the total mass calculations of the other beams. The total mass calculations are even identical to the previous longitudinal beam case. It is still important to note that the trends in total mass with respect to the design parameters are at odds with the relationships for static stiffness and frequency. Particularly maximizing either stiffness or frequency would require as large a beam radius as possible, while minimizing the mass measure would require a small radius.

8.2.1.4   Speed of Motions

The goal of this combined design approach is selecting beams that can move as fast as possible with input shaping for vibration suppression. This attainable speed is composed of two components. The first is the input shaper duration, or the length of time that the the input shaping process will add to any move. Shaper duration, as stated before, is highly dependent on the beam's frequency. The other component in the speed of a beam is the ability of an actuator to accelerate the beam. This acceleration is related to the power of

Table 8.1: Shaper Duration for Different Input Shapers.

Shaper	Duration
Zero Vibration (ZV)	$\frac{\pi}{\omega_n}$
Zero Vibration and Derivative (ZVD)	$\frac{2\pi}{\omega_n}$
Unity Magnitude Zero Vibration (UMZV)	$\frac{2\pi}{3\omega_n}$
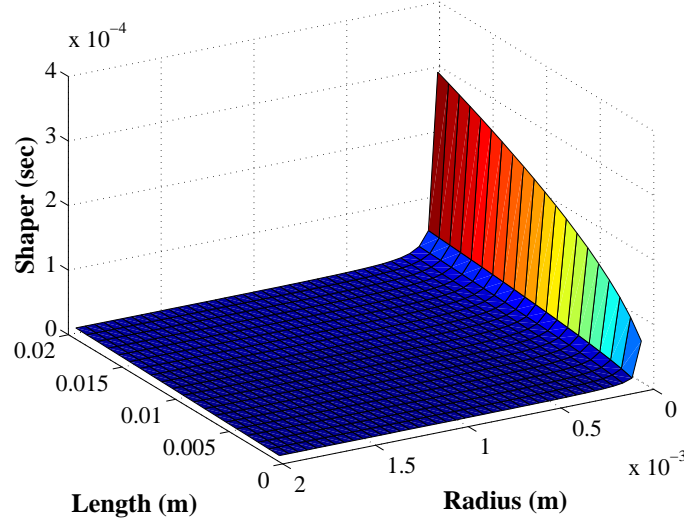
Figure 8.53: Example Shaper Duration for Longitudinal Beam with Attached Mass.

the actuator and the previously calculated inertia of the beam. By combining these two effects, the total duration of a particular motion can be calculated.

8.2.1.4.1 Shaper Duration

By selecting beams considering the shaper duration, t_{shap}, the beams capable of the fastest motion will be possible. The shaper duration of several shapers for a beam with a natural frequency ω_n can be seen in Table 8.1.

Depending on the shaper being used for a particular beam, the shaper duration will change (Note: shaper selection for different beams was discussed throughout Chapter 7 but specifically in Section 7.3). Since the shaper duration is simply a scaled value of the inverse of the natural frequency, (whose values were presented in Section 8.2.1.1), all possible shaper duration combinations will not be presented here. Instead, the example case of a longitudinal beam with an attached mass will be considered, as shown in Figure 8.53. This figure shows how the duration of an appropriate ZV shaper for a longitudinal beam would change with the beam length and radius. Here the shortest shaper duration is desirable. Design for minimal shaper duration has the same parameter relationships as designing for maximum frequency, a short length and large radius are preferred. The surface in Figure
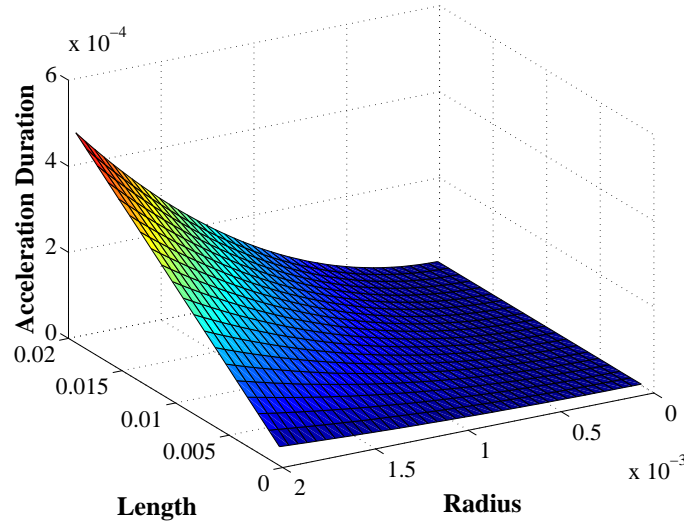
Figure 8.54: Example Base Command Duration for Longitudinal Beam with Attached Mass. Change Y to Acceleration Duration.

8.53 could be easily scaled to show the ZVD or UMZV input shaper cases, if a particular application necessitated these shapers (Section 7.3 addresses shaper selection for specific beams). Once the shaper duration is calculated, it can be combined with acceleration duration to calculate the shaped move time. This acceleration duration will be discussed next.

8.2.1.4.2 Acceleration Duration

Acceleration duration is the length of time it will take a given actuator to accelerate a beam to a desired velocity. This value added to the shaper duration will yield the overall shaped move time. The acceleration duration is directly related to the total mass of a beam, but also to other parameters dealing with actuator and the desired motion of the beam.

First consider the simplest case of the longitudinal beam with an attached mass, where the acceleration duration, t_{accel}, is the time it takes to accelerate the beam to a desired velocity, $V_{desired}$, with a given actuator force, F_{act}. In this case acceleration duration is defined by:

$$t_{accel} = \frac{V_{desired}M_{tot}}{F_{act}} \tag{8.34}$$

where M_{tot} is the total beam mass. If the acceleration duration is plotted for the same longitudinal beam used to generate Figure 8.53, then Figure 8.54 shows that shaper duration decreases with radius. Conversely, acceleration duration increases with radius. Specifically, minimal acceleration duration requires a small radius to keep overall mass low, while minimal shaper duration requires a large radius to keep frequencies high. Dealing with these two opposing effects is the crux of the combined beam and input shaper design problem.
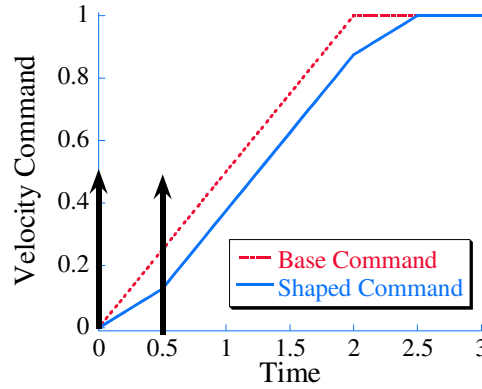
Figure 8.55: Diagram of Command Duration.

Acceleration duration may depend not only on the mass of the beam, but also several parameters separate from the beam, specifically, desired velocity and attainable actuator force. Most systems are required to move at several velocities; therefore, single acceleration duration value will not suffice. If that is the case, then several approaches discussed in Section 8.2.2.5 could be used. Likewise, actuator selections are usually not fixed in the physical system design phase; this issues will also be investigated later in Section 8.2.2.5.

8.2.1.4.3   Command or Move Duration Calculation

The fastest overall speed of motions is the goal of combining input shaping and beam parameter selection. The overall speed of a move is calculated here as the total time it takes to accelerate to a desired velocity when an appropriate input shaper is included to deal with vibration. This command duration is equal to the shaper duration added to the acceleration duration:

$$t_{com} = t_{shap} + t_{accel} \tag{8.35}$$

Minimizing this command time will yield the fastest beam and shaper combination for a given actuator and desired velocity. The command duration can be seen more clearly diagrammed in Figure 8.55. Notice how the unshaped command is extend by the input shaper represented by the impulses in the figure. This increased time is necessary if little vibration is required after the acceleration.

Now that a performance measure exists that relates the overall speed of the beam and shaper combination, the effect of mechanical parameters on this speed measure can be investigated. Figure 8.56 shows how the command duration of a ZV shaped longitudinal beam with an attached mass changes with the physical parameters. At small radii the long command duration is due to a long shaper duration, while at large radii the long command

305
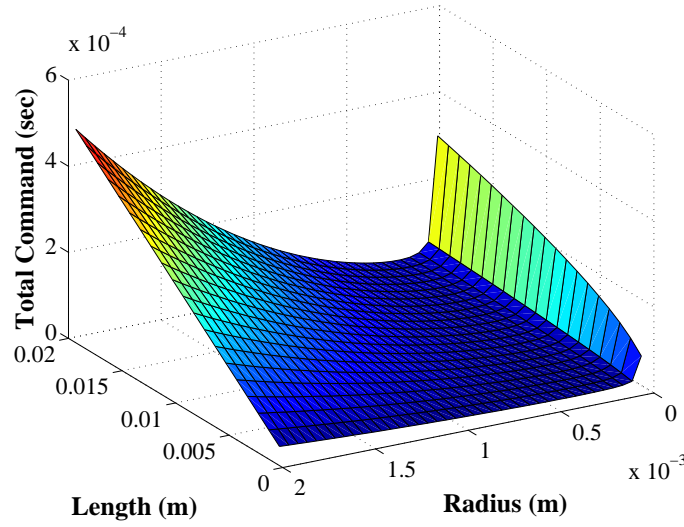
Figure 8.56: Example Total Command Duration for Longitudinal Beam with Attached Mass.

duration is because of large acceleration duration. The fastest possible beam in the figure would have an infinitely short length, the bottom right of the figure. Since this is not possible, a fixed minimal length must be included in the selection process. For any fixed length of the beam, their exist a radius that provides the globally fastest move time.

Figure 8.56 shows the basic cost function when designing input shapers and mechanical plants together. Now that this relevant cost function exist, mechanical parameters can be selected to best perform when input shaping is used. The determination of the minimum or fastest beams in terms of command duration under design constraints will be discussed in the next section.

8.2.2 Single Beam Design Selection

Now that beam performance measures and a useful cost function exist, beam design with integrated input shaping can be rigorously developed. First, the selection process will be detailed. Then the selection process will be tested on increasingly complicated examples. The examples will incorporate constraints on the designs, as well as the issues of variable desired velocity and multiple actuators previously discussed in conjunction with acceleration duration. This beam selection process's place in the overall design process is detailed in Section 8.4.

8.2.2.1   Beam Selection with Input Shaping Process

A design process for the selection of continuum beam parameters knowing that input shaping will be used has been developed. That process involves the following steps:

1. Define Beam Type and Beam Constraints.

2. Identify Appropriate Input Shaper Form (ZV, ZVD, UMZV, *etc.*.

3. Determine Beam Design Variables.

4. Identify Actuator Related Constraints.

5. Compute Command Duration as Part of a Overall Cost Function.

6. Implement Design Constraints.

7. Select Beam and Shaper Parameters.

The first step is selecting the type of beam to be used and any constraints on the beam parameters, like a minimum length, a material, a fixed attached mass, or even limited beam parameter availability. Limited availability is when beam parameters are not available with continuous variation. For example, it may be possible to obtain a 10 mm diameter beam but not a 9.86832 mm diameter beam.

Second an appropriate input shaper form, (ZV, ZVD, *etc.*) for the beam should be chosen using the guidelines presented in Section 7.3. Third, the beam design variables should be identified. For the cases presented here, these will be geometric variables; however, they could be material or load related, such as density or attached mass.

Actuator related constraints are the desired velocities of the system and the possible forces or torques attainable by the actuators. These constraints could be complicated by multiple velocities or various actuator design choices. These specific cases will be discussed later in Section 8.2.2.5.

Once the design variables and all the constraints on the system have been identified, then a search over the design variables can be made using the command duration as part of a cost function. The cost function can be the command duration alone, or could incorporate other values like total mass. The search of the design parameters can be made explicitly as it is in this chapter, or with numerical optimization, depending on the complexity of the problem. This cost function will be subject to the aforementioned constraints on the problem. Finally, a beam and input shaper can be selected.

While this process is complete for simple beam design, other parameters such as cost or interaction with other design elements would alter it. Combining this process within the context of a larger design will be discussed in Section 8.4.

8.2.2.2   Example 1: Maximum Speed Example, Longitudinal Beam with Attached Mass

Problem: *The first example case is the design of a longitudinal beam with a fixed length and attached mass for the fastest possible motion with a fixed actuator. This beam will also*
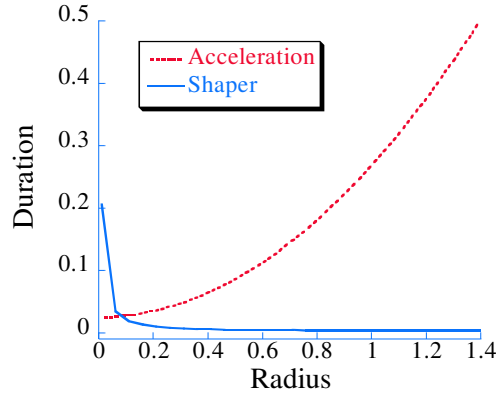
Figure 8.57: Cost Function Components of Maximum Speed Example.

be subject to two constraints, maximum total mass and minimum allowable static stiffness. Finally the beam selection process will be limited to only commercially available beam radii.

Following the procedure, the first step is to identify the beam: longitudinal with an end mass. The constraints are a fixed length and a fixed attached mass. Also, the beam must meet a minimum stiffness requirement, as well as not exceed a given mass. Finally, the beam selection process will be limited to the discrete beam diameter choices commercially available.

From Section 7.3, the ZV input shaper is chosen to move the beam. Since the length and the attached mass are fixed, the only design variable is the radius. In terms of the actuator, a fixed applied force will be used, as well as a fixed desired velocity. From these values a cost function consisting solely of command duration can be computed. The command duration has two components, the acceleration duration and the shaper duration. For this beam, the component values vary as in Figure 8.57 for various beam radii. Notice the conflicting effect on command duration of the shaper and acceleration duration. The minimal shaper duration requires the radii to be increased to increase the natural frequency, while minimal acceleration duration requires a small radius to minimize the mass. If the two components are added together to form the command duration, then Figure 8.58 shows that a minimum exists near a radius of 0.2. If there were no further constraints on the beam, and all radii were possible, then a radius of 0.2 would be the ideal beam for input shaped motion.

However, the beam design is further constrained. The minimum allowable stiffness constraint effectively sets a minimum allowable radius. Figure 8.59 shows how this would limit the design process. No radius lower than the 0.1 would be acceptable. Similarly, Figure 8.59 shows the maximum mass constraint, which for the fixed length and attached mass is a maximum beam radius. These two constraints effectively create a parameter subspace for beam selection. In this case the global minimum lies between the two extremes. In
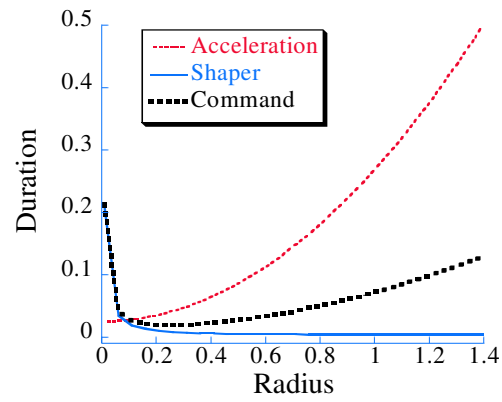
Figure 8.58: Cost Function of Maximum Speed Example.
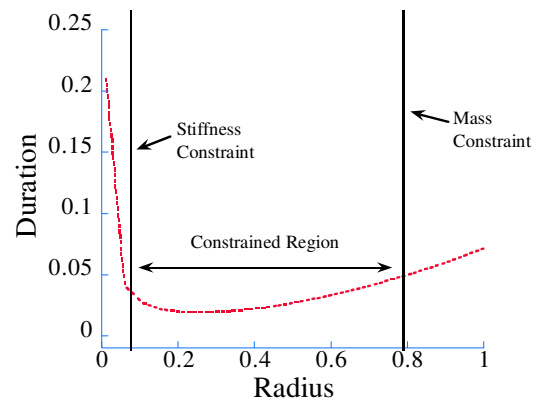
Figure 8.59: Maximum Speed Example Design Constraints.
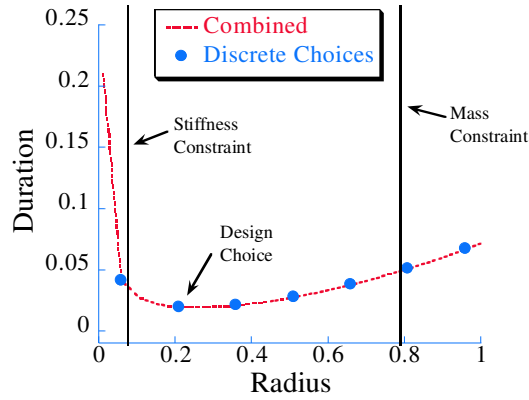
Figure 8.60: Maximum Speed Example with Discrete Design Choices.

other cases, the fastest allowable beam might lie directly on a constraint surface because the global minimum had been excluded.

The final issues to be overcome is the discrete nature of the selection process, where only certain beam radii are available. Figure 8.60 shows the cost function curve at the available beam radii. In this case the lowest cost function value radius is at 0.2.

This example was a straightforward, single goal case. However, it showed how input shaping knowledge could be combined with beam design. A more complicated example and an experimental technique will be presented next, while this selection process impact on the overall design process will be discussed in Section 8.4.

8.2.2.3 Example 2: Combined Goal Example, Torsional Beam with Attached Inertia

Problem:*A torsional beam of fixed length is needed to carry an inertia whose value must be within a set of limits. Minimal beam vibration is important to this process and therefore both the first and the second vibratory modes need to be input shaped. No additional constraints exist for this beam*

Since the design process has been explained during the previous example, only the new issues relevant to this torsional beam will be considered. Specifically, the design variables are both the radius and the attached inertia, although the inertia is limited to a maximum and a minimum value.

The addition of another design variable does not significantly complicate the process, except now the cost function will depend on two variables. The cost function here is the command duration. The command needs to include input shaper for both modes, and both these modes will impact the duration. A decision will first have to be made as to what input shaping approach should be used for the beam. Some of the possibilities are using ZV or ZVD shapers for the first mode. Figure 8.61 shows the shaper duration for several

310
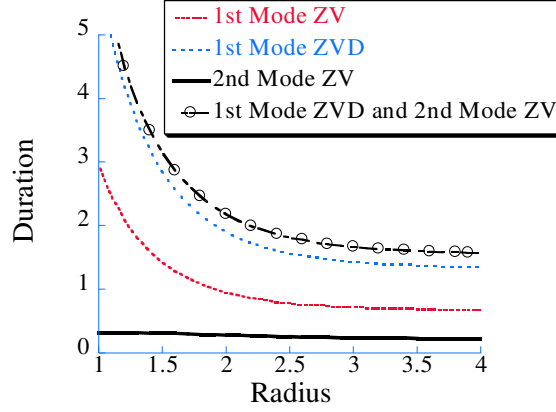
Figure 8.61: Effect of Mode and Shaper on Shaper Duration.

different shaping approaches for one example attached inertia. Notice that the ZVD shaper will lead to a significantly longer shaper duration than the ZV shaper. Also notice that since the higher modes have higher frequencies, their shaper durations are shorter. There is relatively low command duration cost to shape for these higher modes, if that is necessary.

Figure 8.61 also shows the combined shaper duration of using a ZVD shaper for the first mode and a ZV shaper for the second mode. Because of the robustness and effectiveness of this combination, this ZVD-ZV combination will be used in this example. This choice was made using the experience garnered from the references in Section 3.3.1. The combination of the two input shapers alters the calculation of the command duration. Now the command duration includes the duration of both shapers and is:

$$t_{com} = t_{shap} + t_{accel} = \frac{\pi}{\omega_1} + \frac{2\pi}{\omega_2} + \frac{V_{desired}m_{tot}}{F_act} \tag{8.36}$$

The new command duration can be tested for acceptable values of radius and attached inertia. Figure 8.62 shows the relationship between these beam parameters and the multi-mode shaped command duration. Here only allowable inertia values are used. The figure shows that the minimum allowable inertia is preferable, since the command duration surface decreases with attached inertia. At that minimum inertia, a global minimum once again exists for a particular radius. The solution including minimum attached inertia could have been predicted from the results of both the mass and frequency calculations. For both of acceleration and shaper duration, minimum attached inertia leads to a faster response of the torsional beam.

The design procedure is capable of selecting multi-mode shaped beams. The shaper selection for multiple modes has a direct impact on the beam choice. Also, the knowledge gained from the investigation of the simple design requirements can be used to simplify the problem. Here, attached inertia could have been fixed at the minimum allowable value and
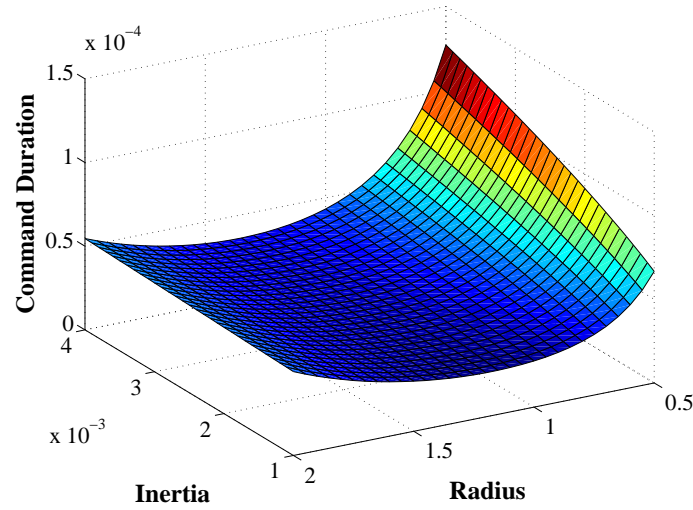
Figure 8.62: Cost Function of Combined Design Example.

minimal command duration beam would still be found.

8.2.2.4 Example 3: Experimental Maximum Speed Example: Transverse Beam

Problem: *Transverse beams with a rotational position input are needed to carry different loads as fast as possible. The existing actuator is limited in the torque it can provide to move the beam. The beam selection is limited by available diameters.*

Here the fastest motion of a transverse beam is needed. This response is not solvable in closed form as was discussed in Chapter 7 and [134]. Therefore, the solution to the transverse beam will be obtained experimentally. For a variety of attached masses, transverse beams will be selected that move each mass as fast as possible using an existing actuator with a software imposed torque limit.

The experimental setup is shown in Figure 8.63. This servomotor is driven with input shaping using Labview motion control. The actuator was then connected through a 100 to 1 reduction eccentric gear box to the base of the beam. An accelerometer was attached at the end of the beam. The accelerometer was also connect to a PC running Labview to capture the acceleration data. The setup was variable, since different diameter steel beams, and various masses at the end of the beam were possible. Since the problem is rotational, all the experimental values are needed in terms of inertia. The beam and attached mass parameters are summarized in Table 8.2. These experiments sought to find the fastest shaped transverse beam for each possible attached mass. [1]

The first step was to test the effectiveness of ZV input shaping on the experimental

---

[1]Most experiments presented here were performed by undergraduate research assistant Brian Fatkin under supervision from the author.
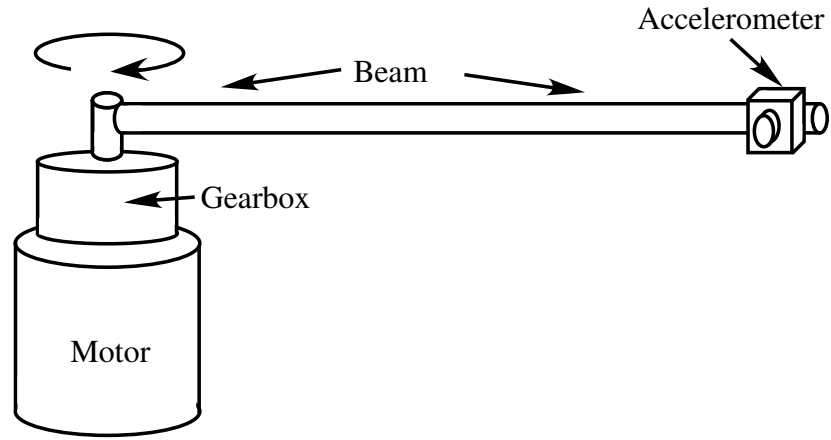
Figure 8.63: Beam Experimental Setup.

Table 8.2: Beam Experiment Parameters.

	Element	Mass(g)	Inertia (g-cm)
Rods	0.125"	94	7191
	0.1875"	211	16141
	0.25	373	28534
	0.3125	588	44982
	0.375	841	64336
	0.4375	1154	88281
	0.5	1507	115285
Attached Masses	Accelerometer	91	13923
	M1	29	4437
	M2	65	9945
	M3	65	9945
	M4	64	9792
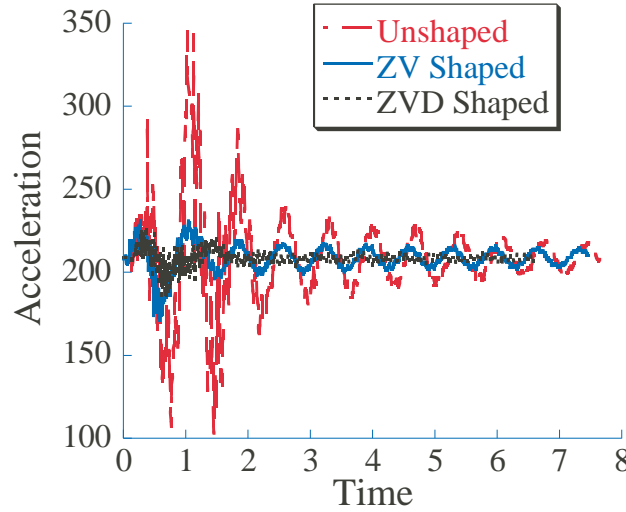
Figure 8.64: Experimental Example Solution.

setup. Figure 8.64 shows the accelerometer output for a 180° rotation of the beam with no shaping and with ZV and ZVD input shapers. While their is no theoretical derivation for input shaping in this case, the results are clear; input shaping is effective at eliminating transverse beam vibrations with rotational base input. Some vibration still remains due to the higher modes of the beam, as well as the nonlinearities caused by the base rotation input.[2] The ZVD shaper performs better in this case because its robustness cancels some of these effects.

The first step in determining the fastest beam and shaper solution for a given load was to determine the natural frequencies of each beam under each possible load. This was done experimentally since the setup led itself well to this approach. Figure 8.65 shows the primary frequencies of each beam for each loading condition related to beam diameter. The $M_i's$ values represent additional masses. Multiple masses were added together to increase the end condition of the beam. The natural frequencies were then used to determine ZV input shapers for each beam mass combination. The shapers were then tested on the system. All the shapers were as effective at vibration suppression as the example case shown in Figure 8.64. Recall, the length of these shapers is one component of the total command duration.

The other component in command duration is the acceleration duration. Because the actuator in this case had more torque than was need to move the beams at a safe speed, a

---

[2]An interesting side result did come from input shaping flexible beams rotating in the plane parallel to the ground. The beams started each motion deflected due to gravity. This ground perpendicular deflection was decreased due to the centripetal acceleration of the beam. That is as the beams were spinning, energy was introduced into the vertical motion of the beam. After input shaping had stopped the beam, little vibration occurred in the rotation direction; however, the beam had residual vibration in the vertical direction.

314
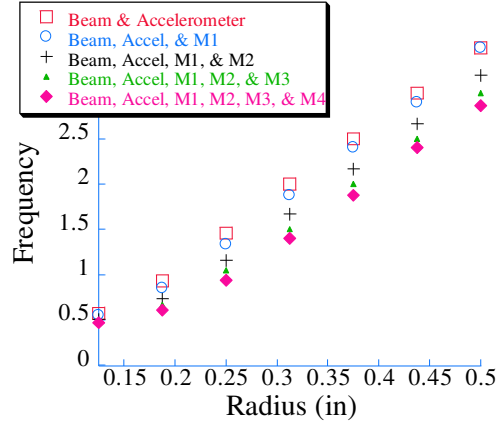
Figure 8.65: Experimental Natural Frequencies.

torque limit was imposed using the software. This was done by calculating the inertia of each beam and mass combination. These inertias were then used to compute the maximum allowable acceleration of the motor. By fixing a maximum theoretical torque, the allowable acceleration could be found using the equation:

$$A_{allowable} = \frac{T_{theoretical}}{I_{tot}} \tag{8.37}$$

The allowable torque was less than the maximum torque of the motor; however, this same procedure could be used with an actual torque limit.

In this case, the command duration was also altered to become a move duration. Instead of using acceleration duration, the entire move duration was used, since the motions were made for a fixed rotation using a shaped bang-bang acceleration profile. That is, the motor accelerated at the previously calculated $A_{allowable}$ for a 90° rotation and then decelerated with the same magnitude for the remaining 90°. This resulted in an S-curve position profile. The duration of this profile is defined by:

$$t_{s-curve} = \sqrt{\left(\frac{\theta}{A_{allowable}}\right)} \tag{8.38}$$

where θ is the angle of rotation in these cases 180°. This S-curve duration was used to compute the shaped move time in the same manner acceleration duration was used previously in Section 8.2.1.4.3 to compute the shaped move time.

When the move duration is computed from the experimentally determined frequencies and the S-curve duration presented above, the resultant move duration is given by:

$$t_{move} = t_{shap} + t_{s-curve} = \frac{\pi}{\omega_{exp}} + \sqrt{\left(\frac{\theta}{A_{allowable}}\right)} \tag{8.39}$$

The result of this calculation for each of the beam setups is shown in Figure 8.66. For
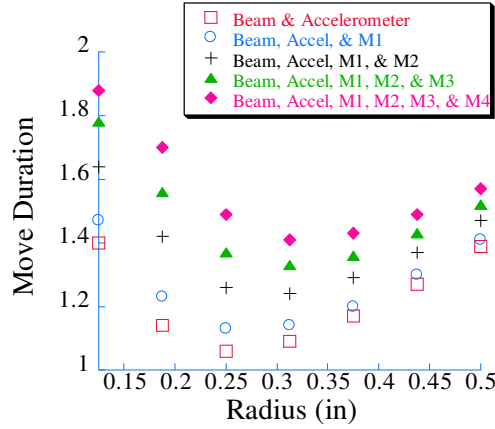
Figure 8.66: Cost Function of Maximum Speed Example with ZV Shaper.

each beam loading condition, there exist a beam with the fastest response or the minimum value in the figure. For lower attached masses the 0.25 inch diameter beam was the fastest. However, for larger masses with the same torque limit, the 3/8 inch beam was superior. The beam design procedure for fastest shaped motion works for experimental, as well as theoretical design approaches. Specifically, a beam can be design to move as fast as possible using any input shaper and given actuator.

Figure 8.64 showed that the vibration suppression performance of the ZVD shaper was superior to the ZV shaper for this beam. If this level of vibration suppression is needed, then ZVD shaping should be used, and consequently the beam chosen for the system should be designed using ZVD parameters. Since the duration of the ZVD shaper is twice that of the ZV shaper, the move duration becomes:

$$t_{move} = t_{shap} + t_{s-curve} = \frac{2\pi}{\omega_{exp}} + \sqrt{\left(\frac{\theta}{A_{allowable}}\right)} \tag{8.40}$$

When a ZVD shaper is used on the experimental setup, the results are shown in Figure 8.67. Again, a minimum duration motion is possible. However, the beam to accomplish this goal is different than in the ZV case. Because the ZVD shaper is longer, it contributes more to the duration of the move. Thus the shaper term is more dominant. However, the cost of using a ZVD shaper is a longer move time, as apparent from the move times in Figure 8.67 being significantly higher than those in the ZV case of Figure 8.66. These results demonstrate that the shaper selection will directly impact the beam selection, as well as the attainable move durations.

8.2.2.5 *Actuator Related Issues*

The previous sections assumed a fixed actuator and fixed desired velocity in determining the fastest beam design. However, a fixed actuator is often not the case, since machines

316
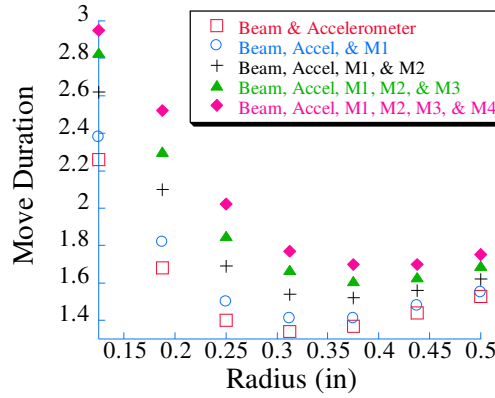
Figure 8.67: Cost Function of Maximum Speed Example with ZVD Shaper.

are asked to perform at a variety of velocities. Also, actuator selection is often up to the designer of the system and consequently complicates the design process. Both of these challenges can be accommodated within the proposed design protocol.

8.2.2.5.1 Multiple Desired Velocities

Designing a beam to operate at a variety of velocities is a simple matter of recalculating the acceleration duration over the desired velocity range. The simplest solution is to use the average operating velocity and perform the design process as before. Another possible solution is to select several discrete velocities and compute the average acceleration times. For a set of k velocities the acceleration duration would become:

$$t_{accel} = \frac{m_{total}}{k F_a ct} \sum_{i=1}^{k} V_i \tag{8.41}$$

This average value could then be used for the determination of the fastest beam for a set of velocities. A probability distribution of possible operating velocities could also be utilized as a weighting on the velocities in (8.41).

8.2.2.5.2 Actuator Selection

Actuator selection along with beam selection adds another design variable to the process. The simplest solution to this problem is to develop the beam design algorithm with the actuator force/torque as an input variable. Then the process can be performed for multiple possible actuators. Figure 8.68 shows how multiple actuators would affect the design problem presented in Example 1. The minimum of the curves shifts to higher radii as the actuator force increases. By simply considering the actuator effort as a discrete design variable, the fastest beam can once again be selected. Obviously, the larger the actuator

317
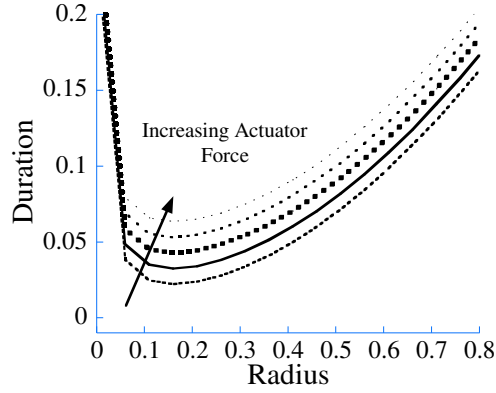
Figure 8.68: Cost Function for Various Actuators Forces.

force, then the faster the attainable motion. Likewise, the ideal radius will be larger for a larger actuator force, since large actuators lessen the dominance of acceleration duration in the command duration calculation. By utilizing these simple techniques, beams can be designed with many different constraints. Combining these techniques with more complicated oscillatory mechanical elements will be presented in the next section.

8.2.3 Complex Mechanical Element Design

The previous section discussed the combined design of input shaping with simple beam elements. This section seeks to show that the technique of minimizing move time will work well for other continuum elements. Two areas will be investigated: more complex continuum elements and multi-state simple beams, where length or endpoint mass change.

8.2.3.1 Transverse Vibration of a Tapered Beam

The first complex continuum element considered is the rectangular tapered transversely loaded beam. This type of beam is common in machines because it is stiffer for a given mass than an un-tapered beam. Considered here is a beam tapered only in the direction of deflection, δ, diagramed in Figure 8.69. It has a width along the entire beam of b, and a starting height of h_0 and tapers to a point after a length L. Many researchers have derived the equations of motion of tapered beams [100, 117, 67, 136]. From their work the natural frequency of the beam can be calculated by:

$$\omega_i = \frac{\lambda}{L^2} \sqrt{\frac{EI_0}{\rho A_0}} \tag{8.42}$$

with $\lambda_1 = 5.315$, where the base area, A_0, is:

$$A_0 = bh_0 \tag{8.43}$$

318
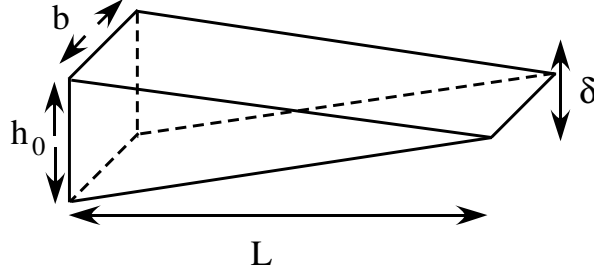
Figure 8.69: Tapered Beam Diagram.
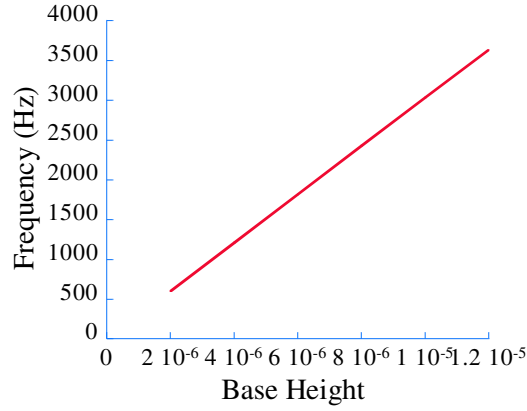
Figure 8.70: Tapered Beam Frequency.

and the base moment of inertia is:

$$I_0 = \frac{bh_0{}^3}{12} \tag{8.44}$$

These equations can be used to find the relationship between the beam frequency and the base height. This frequency relationship is depicted in Figure 8.70. The same trends that held for the radius of the circular transverse beam also hold for the base height of this type of beam.

The command duration for tapered beams is the same as previously discussed command duration in Section 8.2.1.4.3 except that the total mass is particular to the tapered beam:

$$m_{tot} = \frac{h_0 \rho L b}{2} \tag{8.45}$$

This total mass when transformed into an acceleration duration for a desired velocity, $V_{desired}$, and given actuator force, F_{act}:

$$t_{accel} = \frac{2V_{desired}}{F_{act} h_0 \rho L b} \tag{8.46}$$

results in the command duration curve shown in Figure 8.71. Again, a true minimum exists, showing that even if utilizing the design parameters of more complicated beams, the design

319
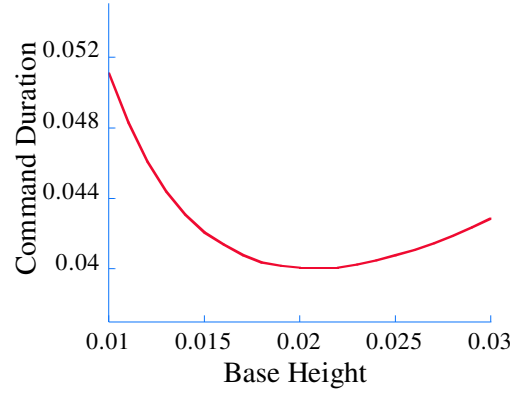
Figure 8.71: Tapered Beam Command Duration.

procedure still works. The equations for tapered beams and tapered cones behave in the same manner, such that the design technique of using input shaping to aid in physical parameter selection also holds for cones.

8.2.3.2   Plate Design

Theoretically plate vibration can also be suppressed with input shaping, and plates are common structure components in machines. A plate is essentially a wide beam, and likewise, the same trends in shaped command duration appear when the thickness of the plate is a design variable. Weaver *et.al* presented the equations for the natural frequency and the wave propagation for a plate in [313]. The derivation of input shaping for plates was not included in Chapter 7 because the wave propagation is essentially that of the transverse beam in two dimension, if the plate is symmetrical. The first natural frequency of a square plate of thickness h and width a is given by

$$\omega_1 = \frac{2*\pi^2}{a^2}\sqrt{\frac{D}{\rho h}} \tag{8.47}$$

where D is the flexural rigidity:

$$D = \frac{Eh^3}{12(1-\nu^2 0} \tag{8.48}$$

and ν is Poisson's Ratio. The natural frequency of the plate exhibits the same trends with increase in thickness and length as have often been seen before. Figure 8.72 shows that as thickness increases so does the natural frequency. Likewise, as width increases the frequency decreases. Since an increase in thickness will also increase the mass of the plate, a tradeoff between low mass and high frequency exists in the plate problem. This is the same tradeoff between acceleration and shaper duration that has been seen in the previous design examples.
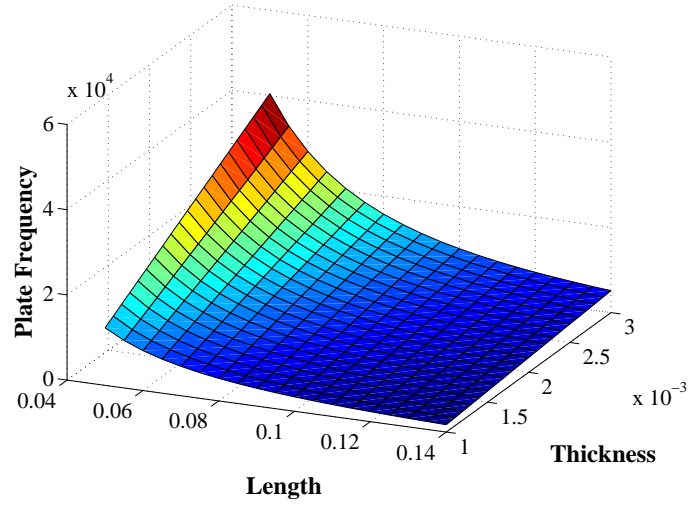
Figure 8.72: Plate First Natural Frequency.

The plates total mass of a plate is given by:

$$m_{tot} = a^2 \rho h \qquad (8.49)$$

The mass can be used with the above frequency expression to find the command duration for a plate. Figure 8.73 shows the familiar curve, where a particular thickness will enable the fastest shaped motions. Although difficult to see in the surface, a minimum exists for a particular thickness at each possible length. Again, the smaller the plate's length, the faster the possible motions. This trend will continue to be found in other continuum elements, no matter the complexity, because when mass or inertia is added to the structure of an element, it increases the stiffness which in turn increases the frequency. However, adding inertia decreases the maximum acceleration. The consideration of the opposed command duration effects of increased mass versus increased stiffness is vitally important when designing with input shaping.

8.2.3.3 Changing Mass

The techniques developed here have been shown effective for single state beams. However, the design of these beams gets more complicated if they are asked to carry more than one load. For example, a mill might need to utilized different size and mass workpieces. One way of selecting a beam for multiple end-load conditions is to use a similar technique to the one used in actuator selection. That is, test both conditions, lightly and heavily loaded and select the beam that performs best at both. Figure 8.74 shows how a longitudinal beam command duration behaves with two different end-load masses. By using the information in the figure, a beam radius can be selected between the light and heavy load radii depending on occurrence of each condition. If the beam is usually lightly loaded, then the thinner
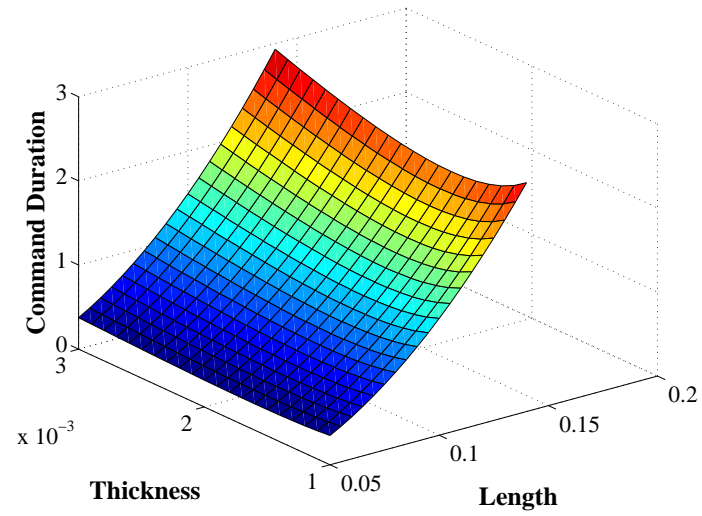
Figure 8.73: Plate Command Duration.
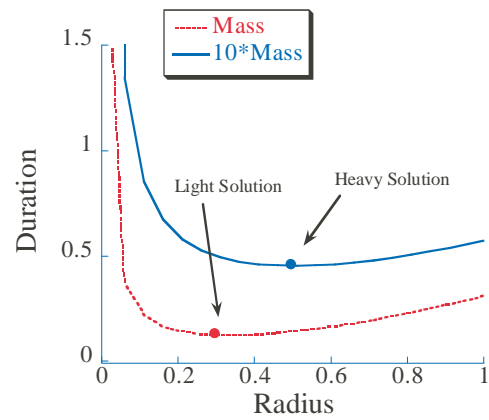
Figure 8.74: Longitudinal Beam Command Duration For Two Masses.

322
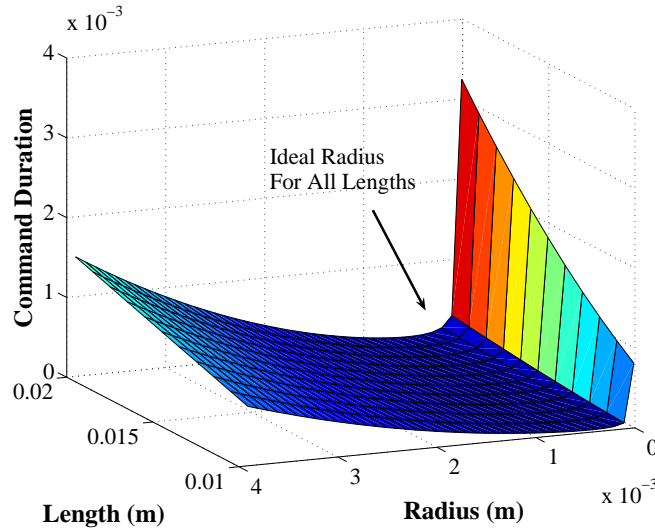
Figure 8.75: Longitudinal Beam Command Duration for Changing Length.

beam should be selected. The converse is also true. A probability or average load technique could also be used as was discussed for the changing velocity case in Section 8.2.2.5.1. This sort of technique can be used to understand the nature of combining input shaping with mechanical design. That is mass should be decreased in all forms until the point where the system frequency starts to decrease. This will be discussed further in Section 8.4.3.2.

8.2.3.4   Changing Length

Another common occurrence is for a beam's effective length to change. This is typical of ball stages. The effective length between the actuator and the load changes often with the position of the load. This issue can be addressed by studying a range of possible lengths. Figure 8.75 shows how length and radius effect the command duration of a loaded torsional beam. By selecting a radius in the trough of the curve, performance over the entire workspace will be good. This technique will require the input shaper to change with the location in the workspace, since the frequencies also change with the length. Likewise, the changing load problem presented previously will need the same sort of shaper adjustment. Many solutions have already be proposed to deal with this including the work by the author and an undergraduate assistant Vlad Patrangenaru in [83], where an input shaping technique similar to gain scheduling was employed on an elevator as it moved between floors. Another option to deal with frequency variation is the continuously vary technique of Chapter 4 for where the shaper was changed depending on the desired acceleration to deals with the acceleration dependent nonlinearities of the micro-mill.
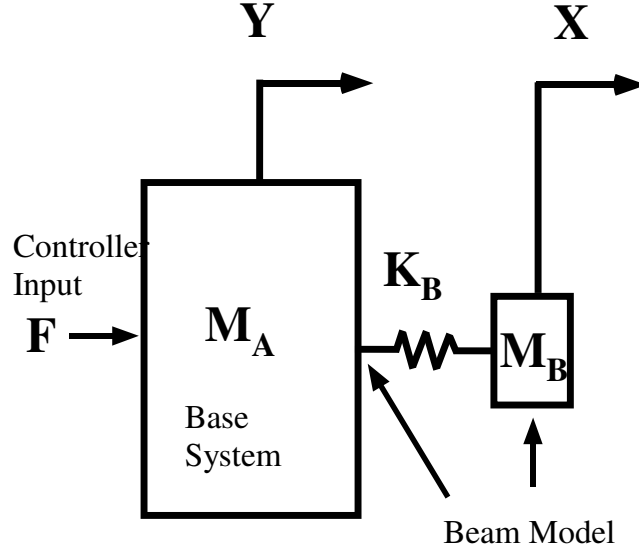
Figure 8.76: Diagram of Longitudinal Beam and Controller.

8.2.4 Beams with Fixed Controllers

All of the previous examples of beam design dealt with the motion of only one mechanical element. However, in typical applications, flexible systems are under feedback control. While designing feedback controllers, mechanical plants, and input shapers concurrently is beyond the scope of this work, it is possible to use a fixed control strategy on a flexible beam system and then select the beam and shaper simultaneously. Using a fixed controller design approach allows the mechanical parameter variation to be studied. While this approach is an interesting proof of concept, it is not recommended for use on real world systems, because of the high controller gains it can require.

The example case considered here is a longitudinal beam affixed to a much larger mass. This mass is under proportional and derivative feedback control. For simplification in the model, the longitudinal beam will be modelled as a lumped parameter spring and mass, whose parameters are determined from the previous derivation of longitudinal beam vibration in Chapter 7. This simplification is made because incorporating a continuum equation of motion in a feedback control simulation is extremely difficult. A diagram of the system can be seen in Figure 8.76.

The motion of the system in Figure 8.76 is described by:

$$M_A \ddot{Y}(t) + K_B Y(t) = F + K_B X(t) \tag{8.50}$$

$$M_B \ddot{X}(t) + K_B X(t) = K_B Y(t) \tag{8.51}$$

and the feedback control law is:

$$F = K_P(Y(t) - Y_{des}(t)) + K_D(\dot{Y}(t) - \dot{Y}_{des}(t)) \tag{8.52}$$

324
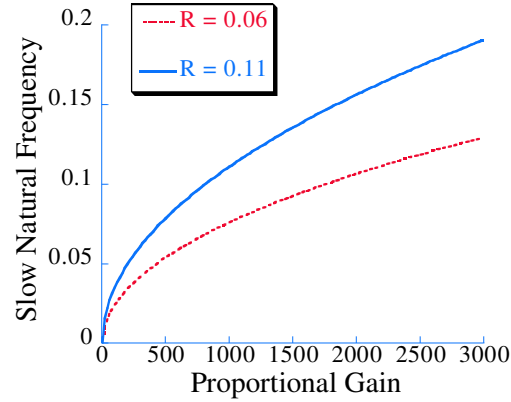
Figure 8.77: Controller Gains For Maintained Frequency.

where Y_{des} is the desired position of Y, K_P and K_D are the proportional and derivative gains respectively, and the physical parameters are defined by Figure 8.76. This system will exhibit two natural frequencies depending on the physical and controller parameters.

The approach suggested here to segregating the beam design from the controller design is to hold the lower mode of vibration to a constant value much lower than the frequency by altering the controller gains. If controller gains can be selected to maintain the lower mode frequency, then the beam design problem can be isolated from the controller design. Figure 8.77 shows the relationship between controller gains and the low natural frequency of vibration for two different radii beams. Notice that the gains are substantially different for the two beams, when the natural frequencies are equal. Therefore, the controller will have to be altered significantly to hold the frequency constant.

When the controller gains are used to hold the low natural frequency of the system constant for varying beam radius, the higher mode of vibration in the system changes in the same general manner as for the beam alone. If the combined system is moved with a two-mode input shaper, then the first input shaper would remain constant due to the fixed low frequency. The other input shaper would change with the radius of the beam. The duration of the changing frequency input shaper is shown in Figure 8.78. The shaper duration decreases with increase in radius; this decrease would help counteract the increase in mass that the larger radius would incur. This is the same trend that has been seen in all of the other beam design problems.

While this approach to controller design is not advisable for real world systems due to possible large feedback gains, it did enable the beam parameters to be considered independent of the controller. The result is that even when working within the confines of controller dynamics, the trade-off still exists between increasing acceleration duration and decreasing shaper duration. Therefore, for more complicated design problems than those presented
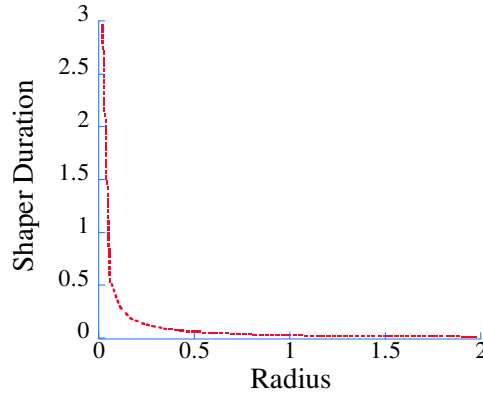
Figure 8.78: Shaper Duration for Longitudinal Beam and Feedback Controller.

here, the tradeoff in design parameter selection exists. Increasing some design parameters both increases mass and increases natural frequency. These increases have opposite effects on the speed of the shaped beam motion, by simultaneously increasing acceleration duration while decreasing shaper duration.

8.3   Design for Micro-Mill Positioning System

The techniques of combining of mechanical design with input shaping were developed with the goal of designing the positioning stages of a micro-mill. The X-Y stages of a micro-mill are required to move quickly, and the stages are subject to minimal external forcing due to the low cutting forces as discussed in Chapter 4. This is the ideal situation for flexible systems relying on input shaping for vibration suppression. This section will detail how the design procedures used to develop simple beams can be combined to design a micro-mill's X-Y positioning system.

8.3.1   Micro-Mill Model

The first step is to develop a reasonable model of a micro-mill positioning system. It should incorporate flexibility in both the X and Y stages, as well as the coupled nature of the loads on the stages. Only one configuration will be considered in this section, although Section 8.2.3.4 does discuss considerations for multiple beam lengths and configurations.

To design the stages with integrated input shaping, the stages are modelled as transversely vibrating beams. If two of these beams are affixed perpendicular to each other, then a basic model of the positioning system as depicted in Figure 8.79 can be developed. The beams' mass, length, natural frequency and deflection are indicated for each axis by M, L, ω, and δ.
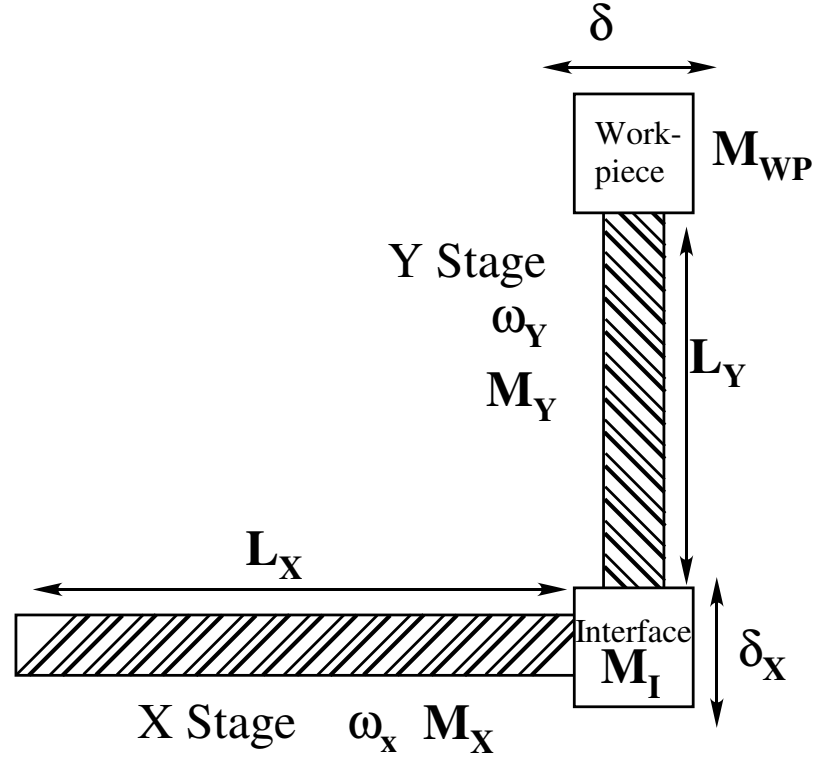
Figure 8.79: Diagram of Positioning System Model.

The coupled nature of the X-beam's load is apparent if the model is broken down into the separate axes. Figure 8.80 shows that the transverse vibration in the Y-axis is unaffected by any parameter selections in the X-axis. Note that M_{WP} is the mass of the workpiece and all fixturing hardware carried on the end of the Y-stage. The X-axis, on the other hand, depicted in Figure 8.81, is highly dependent on the parameters of the Y-axis because the X-axis must carry all of the mass of the Y-axis. Here the simplification was made, that from the X-axis point of view, the Y-axis appears as a lumped mass at the tip of the X-axis. Making the total load at the end of the X-axis M_T equal to:

$$M_T = M_I + M_Y + M_{WP} \tag{8.53}$$

where M_I is the mass of the interface with the Y-axis including the Y-axis motor. M_Y is the mass of the Y stage beam, and M_{WP} is the same workpiece and fixturing load carried by the Y-axis. Although the real system's vibration would be coupled, if the vibration can be greatly reduced through input shaping, then this coupling should be significantly reduced. Thus, an uncoupled parameterized vibrational model was developed, which can be used to design both beams.
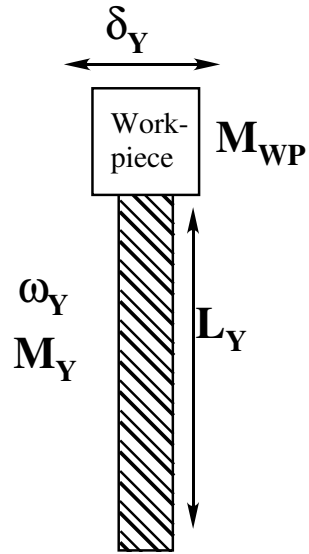
Figure 8.80: Diagram of Y-Stage Model
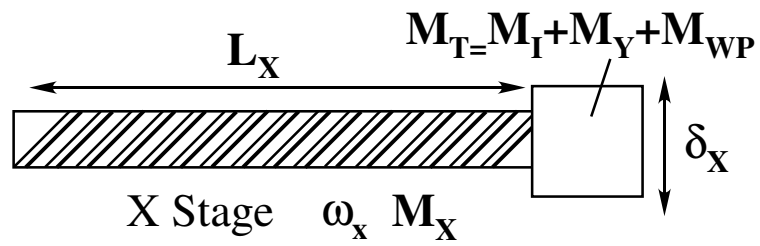
Figure 8.81: Diagram of X-Stage Model

8.3.2 Design Procedure for Micro-Mill Beam Selection

The procedure to design multiple beams of a micro-mill positioning system in conjunction with input shaping utilizes the command duration for moves of both those beams. Revisiting the procedure for one beam design in Section 8.2.2.1, allows a similar approach to be used for the multiple-beam system. This procedure develops parameter relationships for both beams independently and then merges them into a solitary cost function. The procedure for the micro-mill positioning system's beams is summarized in the following:

1. Define Beam Types and Beam Constraints.

2. Select Appropriate Input Shapers.

3. Determine Beam Design Variables.

4. Identify Actuator Related Constraints.

5. Compute Command Duration of Each Beam.

6. Combine Command Durations through Weighted Usage.

7. Implement Design Constraints.

8. Select X and Y Stage Beam Parameters.

The differences in this procedure compared to the single beam procedure of Section 8.2.2.1 is the addition of a step combining the command durations into a single value. The command durations of each beam will be weighted by the percentage of all motions that utilize each axis in determining the final beam design.

8.3.3 Micro-Mill Stage Parameter Selection Process

The first step in the design of the micro-mill positioning system is to identify both beams as transverse with end loads. Both will be shaped using ZV input shapers, and the only design variable for each beam is the radius. The actuator force and desired velocity along each axis will be the same, F_{act} and V_{des}. With these values known the command duration of each axis can be found. The Y-axis command duration is:

$$t_{Y-com} = \frac{\pi}{\omega_Y} + \frac{V_{des}\left(M_{WP} + \pi R_Y^2 \rho L\right)}{F_{act}} \tag{8.54}$$

The shaper duration component of the command duration for the Y stage alone is shown in Figures 8.82 for varying radius. Figure 8.83 shows how changes to the radius effect the acceleration duration. Then the same general trends can be seen in these two figures as were seen for all other transverse beams. That is, an increase in radius increases mass which slows the system, but the larger radius also increases frequency which allows a faster shaped
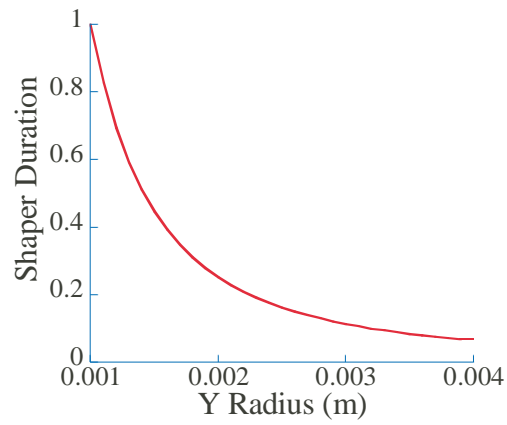
Figure 8.82: Shaper Duration in Y Direction.
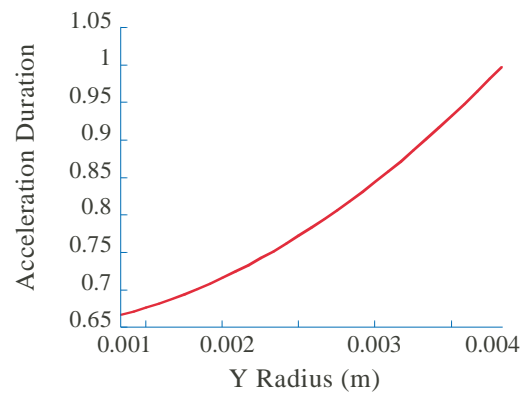
Figure 8.83: Acceleration Duration in Y Direction.
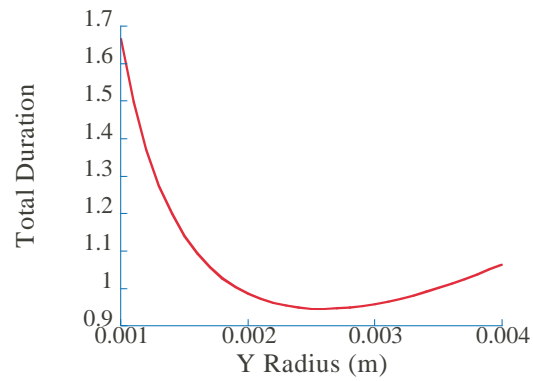
Figure 8.84: Total Command Time in Y Direction.
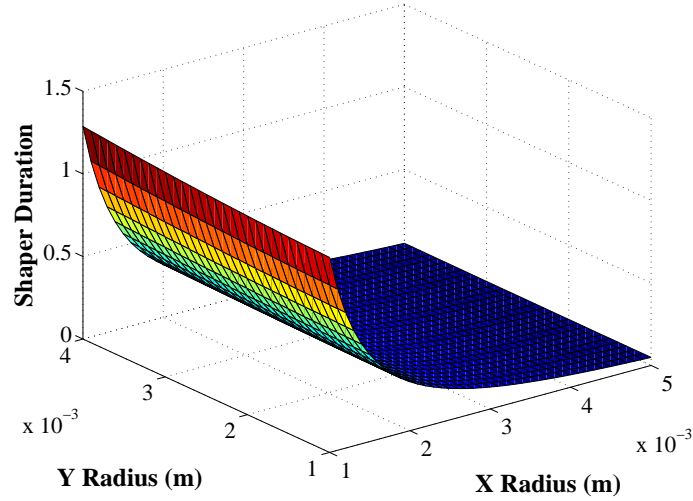
Figure 8.85: Shaper Duration for the X Direction.

motion. The total command duration for the Y-axis combines these effects as depicted in Figure 8.84

The X-axis command duration is a more complicated calculation since it involves additional masses, including the mass of the Y-axis. Its components, the shaper duration and the acceleration duration, depend on radius of both the X and Y-axis. Figure 8.85 shows how the shaper duration changes for various X and Y-axis radii. The shaper duration is effected slightly by the Y-axis radius because the Y-axis radii changes the attached mass at the end of the X-axis beam. Still the general trend of increased radius leading to higher frequencies still holds for the X-axis radius. However, the Y-axis radius has the opposite effect. An increase in R_Y leads to a larger end mass for the X-axis which reduces the frequency. This effect would be more prominent if the interface and workpiece mount masses were significantly lower than the mass of the Y-axis beam.

The other important component of the command duration of the X-axis is the acceleration duration. This acceleration duration is shown in Figure 8.86 for various axis radii. An increase in the radii of either axis increases the overall mass of the beam and thus the acceleration duration.

If these two components, shaper and acceleration duration, are added together, then the X-axis command duration is:

$$t_{X-com} = \frac{\pi}{\omega_X} + \frac{V_{des}\left(M_{WP} + M_I + \pi * R_Y^2 \rho L + \pi * R_X^2 \rho L\right)}{F_{act}} \tag{8.55}$$

The total command duration as a function of changes in both radii are shown in Figure 8.87. If only a constant Y-axis radius is considered, then the figure shows a command duration variation as expected from previous transverse beams. However, multiple Y-axis radii need to be considered. The addition of the Y-axis radius as a design variable gives
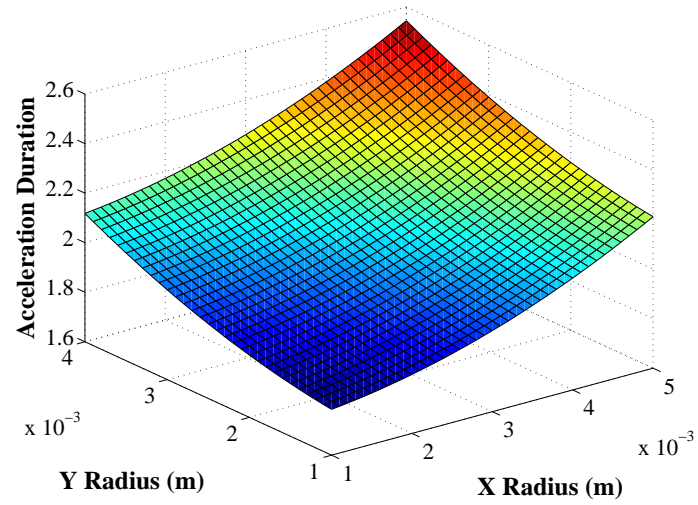
Figure 8.86: Acceleration Duration for the X Direction.
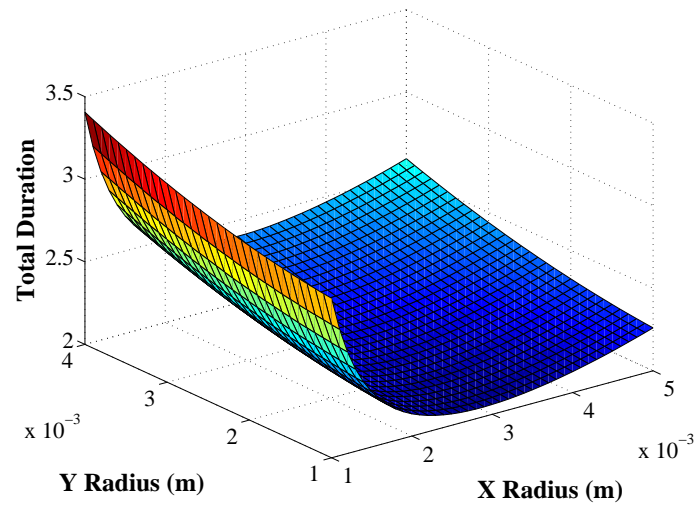
Figure 8.87: Total Command Time for the X Direction.
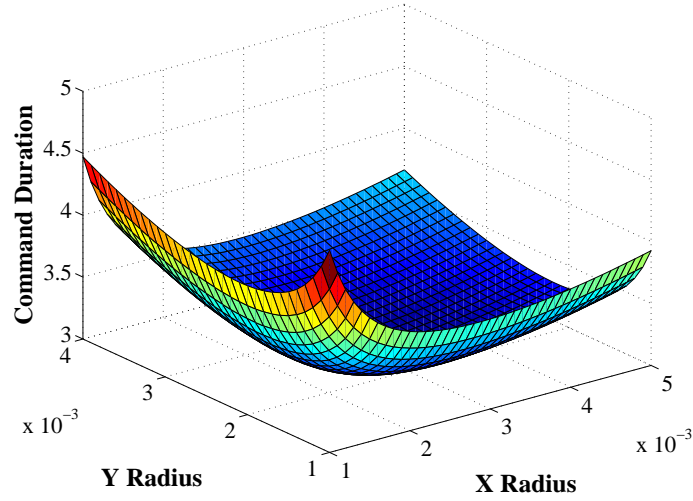
Figure 8.88: Total Command Time in X and Y Directions.

more design parameters but does not makes the X-axis radius selection significantly more complicated, if only the X-axis command duration is being minimized. For minimum X-axis command duration, R_Y should be as low as possible, obeying the previous result that minimal attached mass leads to the fastest beam motion.

The difficulty comes when selecting the radii of both the X and Y-axis for the overall performance. This determination can be made by using a weighted sum of the command durations to determine the fastest beams. This cost function is:

$$J = t_{X-com} + \alpha t_{Y-com} \qquad (8.56)$$

where α is the weights on the frequency of motion in the Y-axis relative to the X-axis. If a mill were operated primarily in the X-direction, then α should be less than one. In most micro-mills, the axis are used equally and therefore $\alpha = 1$ is a good choice. The results of equally weighting the two axis can be seen in the average command duration relative to both axis radii in Figure 8.88. Notice that a global minimum again exists. There is one set of beam radii that will produce the fastest motion. Because the Y-axis radius effects the motions of both axes, the surface slopes more steeply with changes in the Y radius than for the X radius. Therefore, the Y radius is a more important design decision.

The results of this mill positioning system design has resulted in another example when input shaping and mechanical system parameters were design concurrently for improved performance. These techniques can be expanded to a larger design process, and this generalization will be discussed in the next section.

8.4   Effect of Input Shaping on the Design Process

The overall engineering design process is typically subdivided into four separate stages: Defining and Clarifying the Task, Conceptual Design, Embodiment Design, and Detail Design [209]. The possibility of using input shaping will impact all stages in the engineering design process. Specifically, the ability to use input-shaped flexible components in a system will clarify the definition of the task, as well as introduce new design possibilities into the conceptual design. While this is not a new idea, direct study of input shaping's influences on these stages is novel. Furthermore, the techniques developed earlier in this chapter for the direct selection of mechanical components are useful in the embodiment and detail design phases.

The specific impact of input shaping on each of the four stages of the design process will be discussed. Particular stress will be placed on the use of the mechanical parameter selection techniques developed previously in this chapter for design embodiment and detail selection. Whenever possible the previously discussed examples, specifically, vibration absorbers, solitary beam elements, and multiple-beam element configurations, will be used to further the design analysis.

8.4.1   Task Definition

The formulation of the task for a design should not be influenced by any design decision that will be made later in the process. The task definition should be independent of the solution. Therefore, the application input shaping as part of the design process should not change the design definition. However, this independent task definition does not always occur. This section seeks to point out the common mistakes in task definition which could adversely impact the utilization of input shaped flexible design alternative. These clarifications of the task are shaped by input shaping accomplishing functions in new ways. To restate, it is not that the task definition needs to be changed to encompass an input shaping solution; instead, the task definition process needs to be objectively viewed such that the design requirements are solution independent. Specifically several traditional design requirements are often unknowingly solution specific and need to be clarified and complicated. Also, the desired "wishes" for a design might need to be expanded since the combining of input shaping with lightweight mechanical components allows vast improvements over rigid and heavy structures in certain areas. These issues will be studied for the general design case, as well as the specific example of the micro-mill. It is important to note that the steps presented here might not be necessary if the task definition is sufficiently solution independent.

8.4.1.1   General Approaches

The objective consideration of design requirements requires two main components, the clarifying of design specifications and the expansion of design wishes. Both are important

Table 8.3: Existing and Improved Common Design Specifications.

Type	Specification
Existing	Machine Mechanical Stiffness
Improved	Allowable Deflection to a Specified Condition
Improved	Controlled Stiffness
Existing	Machine Mechanical Damping
Improved	Disturbance Vibration Decay Time
Improved	Planned Motion Vibration Decay Time
Existing	Maximum Velocity
Improved	Maximum Velocity performing specific operation
Improved	Process Time Requirement
Existing	Specific Trajectory Maximum Deviation
Improved	Generic Trajectory Maximum Deviation
Existing	Operators Separated from Machine
Improved	Operators Unharmed by Machine

to making the task definition less aimed at a particular solution or set of solution principles.

8.4.1.1.1   Clarifying Design Requirements

The task of clarifying the design requirements to make them less linked to particular solutions needs to be made in light of the alternative solutions possible with input shaping. Several traditional machine specifications are unknowingly solution specific and consequently could make the implementation of an input-shaped flexible solution impossible. Examples of these specifications are listed in Table 8.3. Also shown in Table 8.3 are the proposed expansions and clarifications of these design objectives.

The first and primary areas of design requirements that should be clarified deal with machine stiffness and machine deflection. Often a machine's static stiffness will be required at a particular value; while these types of specifications are valid, they are often excessively scaled. Instead of requiring a fixed stiffness, requirements should be made on performance from the required operations. For example, a satellite antenna's stiffness should not be required; instead, its deflection from reorientation should be specified. By moving away from static parameters to dynamic requirements, the design task is made clearer and more open to various alternative solutions.

A related area is the requirements placed on the motion of the design. Often, these requirements are made briefly and generally. For example, a desired maximum velocity, a desired damping ratio, and desired maximum deviation from a set motion profile could be specified. Addressing these each individually, a maximum velocity constraint should be broken down into velocity requirements for different types of motions and different directions of motions. Likewise a damping ratio constraint is too general and should be separated into vibration oscillation duration for commanded motions and vibration duration from

Table 8.4: New Design Specification "Wishes".

Lower Power Consumption
Lower Overall Mass
Lower Machine Size
Lack of Closed Loop Control
Lower Total Cost
Ease of Transport
Ease of Assembly

disturbances. Finally, setting the deviation or tracking error to a specific motion profile, should be expanded to also include generic tracking error, as well as placing additional criteria on different trajectory types. A machine might require fast motions with low error, or the machine might need to be resistant to a specific disturbance force.

Another area of task definition that needs to be re-evaluated is safety. Since many existing machines have large moving masses and consequently large internal forces, they are quite dangerous. To overcome this, design requirements forcing operators away from the machines have been introduced. These requirements should be reevaluated in terms of their original intent. Actual worker safety, not safety equipment should be included in the design requirements. A lightweight machine does not need the same type of separation from its operator as a massive machine.

The final task definition issue is one that always appears in innovative designs. That is the unwritten design requirement that a design fit into preconceived notions of the correct solution. While this prejudice should never impact a design process, it is especially import if input shaped flexible system solutions are to be given equal consideration. These flexible solutions can be counter to most common notions of machine design.

The design specifications presented here are not new, and they could be used to improve the design process of machines even without the possibility of an input shaped flexible element solution. However, they are specifically important to the input-shaped designs discussed here. The new approach of flexible systems replacing stiff ones forces the reevaluation of ingrained design specifications from an objective point of view.

8.4.1.1.2 Reformulated with Design Requirements

While the consideration of an input shaped flexible system requires an increased watchfulness in design requirement selection, it also allows additional design wishes to be included. The application of input shaping allows machines to be built with improved performance in many areas as summarized in Table 8.4. By including these previously unattainable wishes into the task design, creativity in the design process is fostered, which can only lead to more design possibilities being considered.

Most of these new wishes are made possible by a reduced overall mass from the use

Table 8.5: Micro-Mill Traditional Design Specifications.

D/W	Specification
D	Following Error of 2 μm
D	Maximum Velocity of 50 mm/s
D	Deflection of 1 μm at 100 N
D	Power Consumption under 1 KW
D	10 KHz isolation bandwidth
D	Operator Separated From Machine by Clear Shield

of more flexible structural members. Lower mass reduces energy consumption, both from actuators and from transportation equipment. Similarly, lighter components are easier to assembly by machine or by hand, as well as costing less. Also, the open loop nature of input shaping vibration suppression can eliminate the need for feedback control, or at least sophisticated feedback control. Finally, thinner and lighter components require less support structures, thus leading to smaller machines overall. While adding additional wishes like these to the task formulation is not required, it can motivate the design process.

8.4.1.2 Micro-Mill Example

To show how the proposed alterations to task determination are altered for a specific design process, micro-mill specifications are presented. Two different subsets of specifications for the micro-mill have been developed. Neither addresses the total machine design; instead they focus on the areas altered by the proposed clarifications presented in Section 8.4.1.1.1. The specifications for current micro-mills are shown in Table 8.5, while Table 8.6 shows how the proposed changes alter the specifications.

Most of the specifications in the tables are self explanatory. However, a few need further description. If the workpiece mass substantially effects the motion of the machine, then the machine should be able to move faster with no workpiece or when carrying light workpieces. This condition is possible with a lightweight positioning system. Also, the vibration isolation is typically specified for the overall machine. However, if the machine's natural frequencies are low as is the case for lightweight machines, then the vibration isolation scheme does not need as large a bandwidth to prevent vibration from being induced in the machine. Finally, low-power actuators lead to less heat being introduced into the system and therefore less thermal deformation of the system. While this is not required is can improve a micro-mill's performance.

The specification lists for the mills are in no way complete, however they do show how simple changes can be made. These changes enable the solution of input-shaped flexible components to be considered equally with more traditional solutions of stiff and massive elements.

Table 8.6: Micro-Mill Proposed Design Specifications.

D/W	Specification
D	Following Error of 2 μm while Cutting
D	Following Error of 50 μm while not Cutting
D	Maximum Velocity of 50 mm/s in X and Y while Cutting
W	Maximum Velocity of 500 mm/s in X and Y while not Cutting
D	Maximum Velocity of 10 mm/s in Z while Cutting
D	Maximum Velocity of 30 mm/s in Z while not Cutting
W	Maximum Velocities 50% higher when no workpiece
D	Deflection of 3 μm from commanded move
D	Deflection of 1 μm with Specified Cutting Conditions
D	Power Consumption under 1 KW
W	Power Consumption under 100 W
D	Isolation bandwidth covers important system frequencies
D	Operator Not in Danger from motion of machine
D	Operator separated from cutting interface
W	Total Mass under 20 kg
W	Total Temperature Change under 2° C

Table 8.7: Design Function Comparison.

Goal	Traditional Solution	Input Shaped Solution
Flexible Element Motion	Feedback Control	Input Shaping
Long Appendage	Stiff Element	Flexible Element
Multiple Degrees of Freedom	Heavy Stages	Lightweight Serial Manipulator

8.4.2 Conceptual Design

The conceptual design phase has two important elements where input shaping can alter the process. The first is in the solution to the design functions. By utilizing input shaping, new functions become possible. The other area where input shaping requires clarification of the process is in the concept evaluation. Evaluation criteria that might not have been applicable with other designs should be included when designing with input shaping.

8.4.2.1 Functional Solutions

While the creation of input shaping did not lead to any new functional solutions, it did make designs that were previously regarded as unworkable valid design solutions. All of these now valid solutions utilize flexible elements whose vibration is constrained through input shaping. These flexible elements can be used to solve design problems traditionally requiring stiff mechanical elements. Some design functions, their traditional solutions, and their input shaped solutions are presented in Table 8.7. The first additional functional solution is substituting input shaping for another controller. Since input shaping is an open loop technique, it has inherent advantages in simplicity. Before input shaping, open

338

Table 8.8: Design Evaluation Criteria Important with Input Shaping.

Positive	Negative
Total Mass	Disturbance Rejection
Cost	Operator Interaction
Power Requirements	Implementation
Machine Size	Programming
Transport Size and Weight	Transport Fragileness
Noise Output	Noise Susceptibility

loop designs might be discarded due to their poor performance. The other two areas of useful design solutions involve using low stiffness elements to replace high mass elements. Before input shaping, the low stiffness solutions would have too much vibration for many applications.

The vibration absorber coupled with input shaping presented in Section 8.1 is an example of this type of new functional solution. Traditionally, the primary solution to both disturbance and commanded vibration was a massive, stiff physical structure coupled with a feedback controller. However, the application of input shaping to deal with commanded motion enables the new design alternative of the vibration absorber and input shaper together. By allowing more alternative solutions to be considered, input shaping increases machine design possibilities.

8.4.2.2 Evaluation

Input shaping should have no impact on design evaluation and selection. However, often evaluation criteria, like design specifications, are skewed towards traditional design solutions. If input shaping is to get equal consideration in the design process, then the evaluation criteria must be objectively chosen. To clarify, input shaping only requires that design evaluation be made fairly and clearly.

To this end, it is important to included criteria that might have been previously omitted, but for which input shaping performs well. Likewise, to equalize the process, it is also important to consider evaluation criteria for which input shaping does not perform well. Table 8.8 shows some examples of each type of criteria. The criteria's location in the Table is by no means the definitive evaluation of all designs including input shaping. However, each of the criteria is specifically impacted by input shaping and, therefore, needs to be considered in a successful alternative evaluation. For example, programming is listed on the negative criteria because although input shaping is simple to program, it is not available from the manufacturer on many off-the-shelf controllers. Therefore, the controller's programming will need to be modified. Conversely, cost is listed as a positive criteria. Input shaping allows the use of lighter weight components which should cost less. However, smaller does not always mean cheaper to produce. Also, input shaping requires some sort of logic to implement

which can increase cost over simply manually controlled actuators. By considering these criteria that might have been previously neglected due to all the alternatives having similar evaluation performance, the design process in general can be improved. Specifically, by thoughtfully selecting and implementing evaluation criteria, input shaping can prove to be an exceptional machine element.

8.4.3 Design Embodiment

The design embodiment phase involves three steps, with much iteration among them. First, the relationships between components must be finalized. Next, the parameters for the components must be selected, and finally the components' parameters adjusted to final values. All of the previous discussion of input shaping as it relates to the design process is based on general input shaping theory. The embodiment design phase allows the specific introduction into the design process of the procedures for mechanical parameter selection for input-shaped motion developed earlier in this chapter.

8.4.3.1 Function Assembly

The assembly of functional components is not significantly effected by input shaping. Minor allowances related to the types of functional solutions that involve input shaping might need to be made. For example, since an input-shaped beam deflects more during a motion than a massive, stiff beam, a clearance should be allowed. For the most part, however, input shaping will not impact this process.

8.4.3.2 Parameter Selection

Design parameter selection is the primary design component that can benefit from the techniques developed earlier in this chapter. By selecting mechanical parameters based on the input-shaped response, faster machines can be produced. The procedures developed for vibration absorber design with input shapers for disturbance rejection could be used to select both absorber and shaper parameters. Likewise, the procedures for beam parameter selection will allow fast machine motions.

Specifically, as cost functions are created for the parameters of the machine design, they should include terms relating to command duration. By including command duration with input shaping in the mechanical parameter selection, the important tradeoffs between speed and other design factors can be seen.

Including command duration in the cost functions of the machine design is one possibility of how to implement mechanical design with input shaping. Another possible method relies on a simpler procedure to obtain a fast moving machine. This process involves designing the lightest system possible and then testing the derivative of its speed with respect to the design parameters. This process involves the following steps:
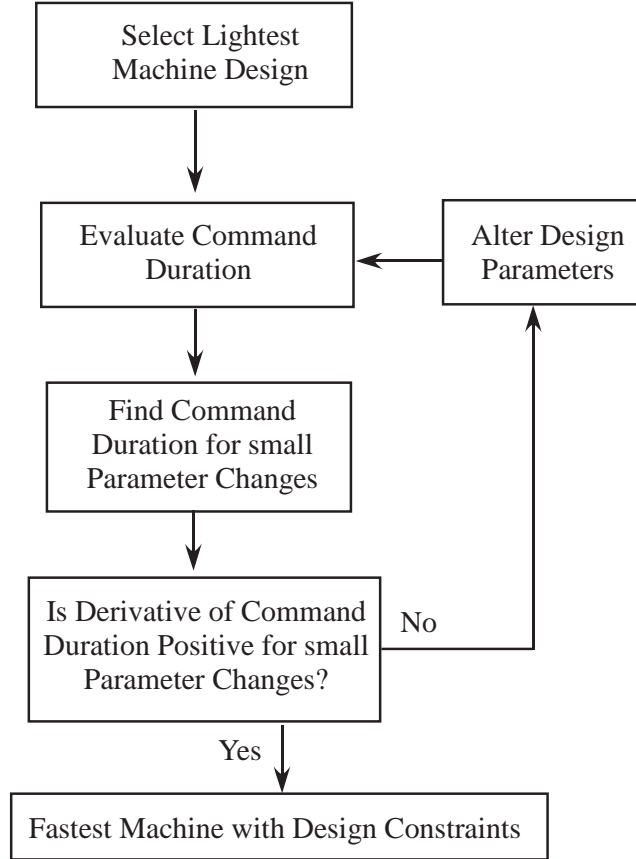
Figure 8.89: Derivative Test for Parameter Selection.

1. Select design parameters to result in the lowest moving mass, while satisfying all other design constraints.

2. Compute command duration at these design parameters.

3. Compute command duration for small changes to the design parameters.

4. If command duration decreases with all mechanical parameters, then stop.

5. Else, increase some parameters until the previous item is satisfied.

This process can also be seen schematically in Figure 8.89.

This process relies on considering the slope of the command duration curves for beam design. Specifically for all the design parameters, P_i for $i = 1, 2, 3, ...n$, the following relationship should hold:

$$\frac{\delta t_{com}}{\delta P_i} \geq 0 \tag{8.57}$$

where t_{com} is the command duration. If this relationship is true, then generally the speed of the design cannot be increased by changing any of the design parameters. This also assumes that the design is constrained in it minimum mass, which is typically the case.

341

This relationship derives from the guidelines for designing beams. Specifically, for the beams discussed earlier, the design parameters should be decreased until the command duration starts to rise. This will only occur if a designer begins with traditional mechanical designs where the mass component dominates the command duration. If the designer chooses to start with an excessively lightweight design, then the opposite approach should be implemented.

By selecting the lowest moving mass for a design, typically the other design constraints will limit the design before the frequency component of the command duration becomes prevalent. If this is not the case, then increasing a mechanical parameter will result in a decrease in command duration. Then the designer will know that a faster solution is possible with a more massive system.

8.4.3.3 Parameter Tuning

The final stage in embodiment design is parameter tuning. The influence of input shaping in this process is much the same as for parameter selection and, therefore, the same techniques can be utilized.

8.4.4 Detail Design

The detail design phase is influenced slightly by input shaping inclusion. This influence is limited to a few concerns that are typical with flexible systems. While these considerations should be made for any system, they are especially important to input-shaped systems. These concerns are:

- Ensure Linear Vibration, for ease of Input Shaping.

- Leave Room for Deflection from Commanded Motion.

- Inspection Schedules Specific to Deflecting Parts.

- Procedures to Avoid Damage of Lightweight Components.

Making sure these issues are addressed is the only impact of input shaping on the detail stage of the design process, beyond the fine tuning of the system parameters according to the embodiment design rules.

8.4.5 Summary of Input Shaping's Impact on the Design Process

The previous sections detailed how traditional input shaping, as well as combined input shaping and mechanical parameter selection improve the design process. Here the general application of these techniques is summarized.

Figure 8.90 shows the stages of the design process, as well as one way to break these sections into components. Also shown are the roles that input shaping should play in the
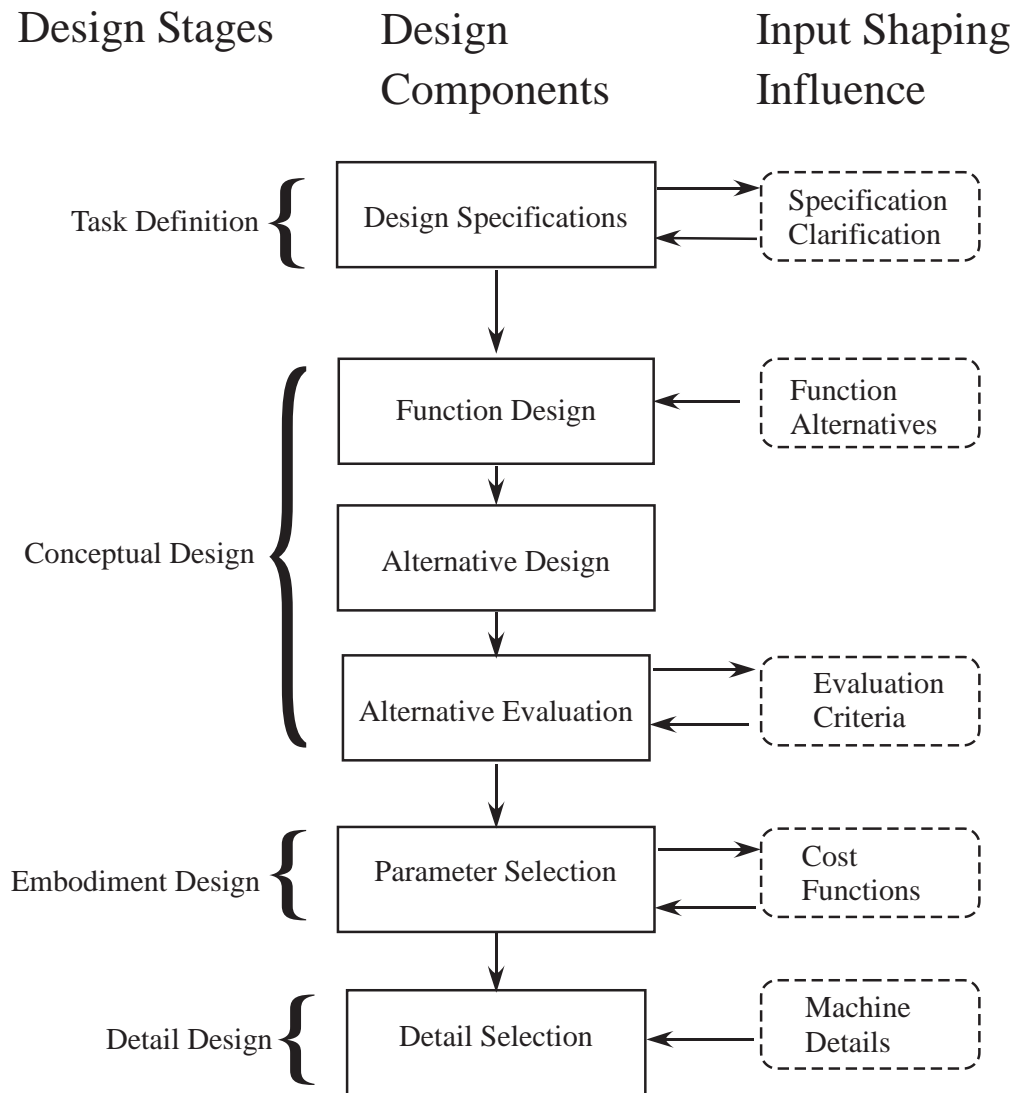
Figure 8.90: Input Shaping Impact in Design Process.

design process. These roles take two forms, the impact of using input shaping and the specific machine parameter selection with input shaping. These input shaping roles are:

- **Specification Clarification**: Input shaping requires that design specification be made impartially. Therefore, existing design requirements that are solution specific should be clarified to give equal ground to lightweight solution alternatives.

- **Function Alternatives**: Input shaping adds additional functional alternatives to the design process. Flexible lightweight solutions become acceptable for consideration if input shaping is used.

- **Evaluation Criteria**: Like the specifications, the evaluation criteria need to be unbiased. Therefore, special attention should be payed to included the criteria where input shaping performs well, as well as poorly.

- **Cost Functions**: The selection of mechanical parameters should be made with the goal of the fastest input-shaped motion. This can be done in two ways. First, a cost function including command duration can be used. Or, a study of the trends of command duration with mechanical design can be combined with test points for design parameter selection.

- **Machine Details**: The details of the final design should give attention to the issues resulting from repeated deflection of mechanical elements.

By adding these concepts to a design process, input shaping can be given a fair consideration, which should increase the application of the technology and result in better overall machine design.

CHAPTER IX

CLOSING

9.1 Summary

This dissertation addressed several issues relating to the design and application of input shaping on micro-milling machines. The contributions were often presented in the context of micro-milling, but they have applications to other micro-positioning machines, as well as larger-scale systems. The contributions fall into three distinct areas, micro-mill characterization and design, trajectory tracking with input shaping, and mechanical design coupled with input shaping. All three can be viewed as developments that address the vibratory issues of micro-milling machines.

Existing micro-milling machines have good dynamic behavior if they are moved slowly. However, if they are moved quickly, then unwanted vibration will occur. In order for micro-mills to become economically viable, they must operate much faster than current machines. Input shaping is a good solution to the problem of motion induced vibration because the cutting forces in micro-milling are negligible. For input shaping to be thoroughly successful, the dynamics of the micro-mill must be linear or techniques employed to deal with the non-linearities. Once these issues are overcome, input shaping can be applied to existing micro-mills to improve their performance.

However, current input shaping techniques do not offer extremely accurate tracking for fast machine motions. Therefore, to track the complicated trajectories required for micro-milling, input shapers developed specifically for trajectory tracking are essential. These shapers allows the improvement of the tracking of current micro-mills, as well as the next generation of micro-milling machines.

The next generation of micro-mills needs to be as fast as possible to make the machining processes more cost efficient. To reach this goal, it is possible to design micro-mills with knowledge that an input shaper will be used to control the motion-induced vibration. This combined design approach allows faster machine motion and consequently higher micro-mill throughput. This goal is summarized in the primary research question of this work.

9.2 Research Questions

How can the consideration of command shaping during the design phase create machine designs with improved performance?

The goal of any mechanical designer is to produce the best machine possible. For that to
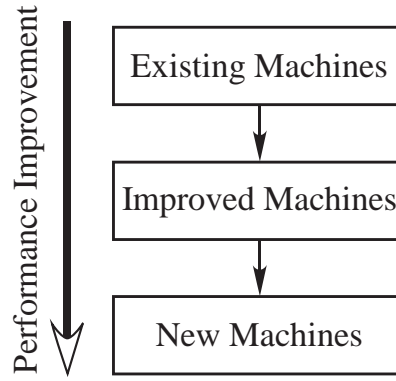
Figure 9.1: Performance Improvement Approach.

occur, the mechanical design must be selected in conjunction with the other machine components. By concurrently selecting a command shaper and mechanical parameters, a faster machine is possible than if they were selected independently. However, existing command shaping schemes do not offer adequate performance in several key areas. Therefore the approach presented in Figure 9.1 is utilized. First, existing technology is investigated. Then, new techniques to improve existing machines are generated. Finally, combined mechanical and command shapers designs are created using the knowledge of the existing technology and improved techniques. The primary research question can therefore be divided into existing machine improvement and combined design. A road-map for the approach taken to addressing these research questions is shown in Figure 9.2. Each chapter has sought to answer part of each of the research questions. The following section will review the procedure used to find answers to the research questions.

9.2.1   Secondary Research Question 1.

How can the performance of existing micro-milling machines be improved through command shaping?

The improvement of existing machines was necessary for three reasons. First, micro-mills needed to be proven a candidate for the open-loop technique of command shaping. Second, the limits of existing machines need to be known to justify the need for combined design. Third, combined design solutions will be more flexible than current machines, and therefore effective techniques for trajectory tracking and vibration suppression will be needed.

9.2.1.1   Micro-Milling Characterization

By investigating the performance of existing micro-mills, the candidacy of command shaping for vibration suppression on the micro-mill was shown, as was the need for increased throughput. Both the work of other researchers and the results presented here showed slow process speeds. When speeds were increased, an oscillation problem developed as is shown

Structure

Addresses

Introduction:
Chapter 1:
Motivates the Problem Research Questions Solution Approach
Background:
Open Areas of Research
Chapter 2:
Understanding Micro-Milling Mechanism Performance Design Strategies
Chapter 3:
Mechanical Augmentation Control Techniques Command Shaping Techniques
Solutions:
Chapter 4:
Modelling of Micro-Mills Cutting Forces in Micro-Milling Command Shaping Micro-Mills
Chapter 5:
Developing Trajectory Tracking Classification Multi-Axis Spatial Trajectory Tracking
Chapter 6:
Evaluates Alternative Tracking Approaches Shapers for Single Axis Temporal and Spatial Tracking Multi-Axis Spatial and Temporal Tracking
Chapter 7:
Present Existing Models of Continuum Elements Input Shaper Performance on Beams Input Shaper Selection for Beams
Chapter 8:
Impact on Design Process Embodiment Procedure
Closure:
Chapter 9:
Summarize Evaluate Contributions Future Work

Figure 9.2: Dissertation Overview and Road-map.
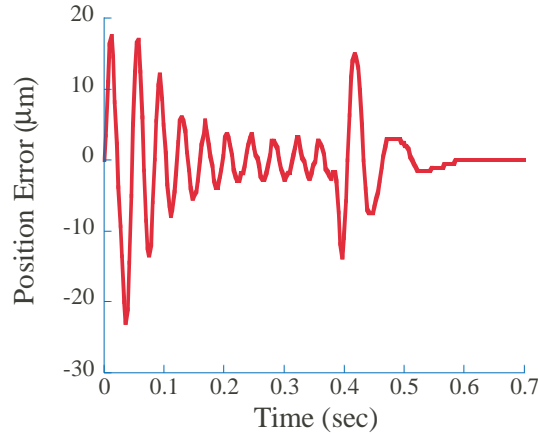
Figure 9.3: Example ETSII Mill Tracking Error.

in Figure 9.3. Also, for input shaping to be an effective solution to vibratory problems, there must be minimal disturbance forces. Both the experiments performed here and by other researchers prove this point. Figure 9.4 shows that forces on the positioning system are minimal. Once the validity of micro-mills as a platform for command shaping was proven, the next step to improving the performance of existing machines was to develop command shapers for micro-mills.

9.2.1.2   Input Shaping on Micro-Mills

Before combined mechanical and command design for micro-mills could be completed, the validity of command shaping on micro-mills had to be shown. By effectively implementing a command shaping scheduling algorithm on the ETSII micro-mill, the validity of the approach was confirmed. The improvement possible from the command shaping algorithm selected is shown as a part surface in Figure 9.5. However, previous command shaping schemes do not allow for precise trajectory tracking of fast motions. Therefore new shaping techniques were needed before flexible design solutions could be implemented.

9.2.1.3   Trajectory Tracking

Previous command shaping approaches are not capable of producing accurate motions either spatially or spatially/temporally when speeds are increased. Therefore, for fast motions to be possible on the next generation micro-milling machines, techniques were needed to provided for both spatial and spatial/temporal tracking of complex trajectories. The resultant improved command shaping techniques is shown tracking a complex multi-axis trajectory in Figure 9.6, and also offered insight into system design. Specifically, the command shaping
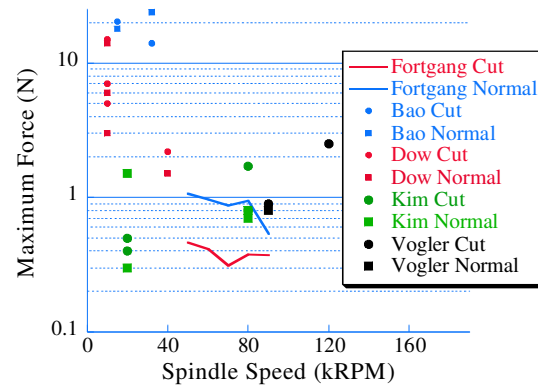
Figure 9.4: Cutting Force Dependence on Spindle Speed Comparison.
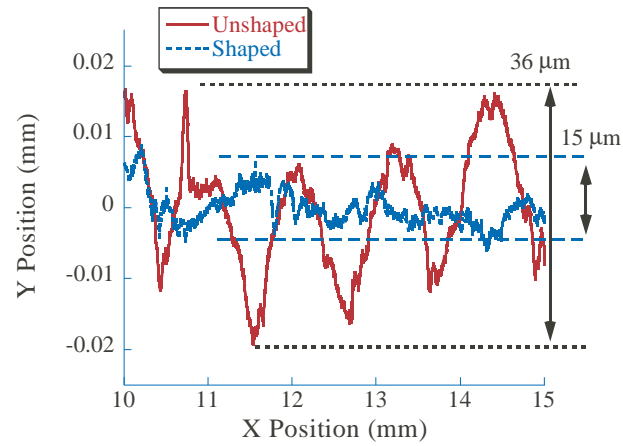
Figure 9.5: Input Shaping's Effect on Part Surface.

349
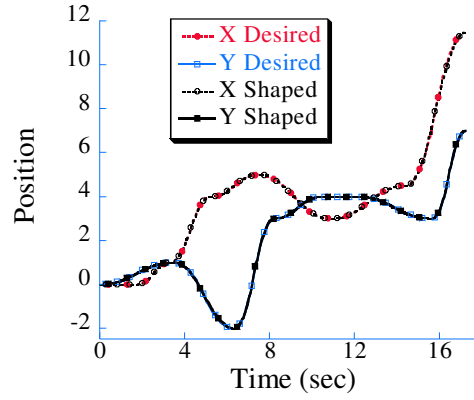
Figure 9.6: Example Combined Trajectory Tracking for Each Axis.

Table 9.1: Approach Comparison for Trajectory Tracking for Various Trajectory Frequency Ratios.

Approach	$\leq 1/3$	$1/3 \leq R_{freq} \leq 0.5$	$0.5 \leq R_{freq} \leq 1$	> 1	$\gg 1$	
Moving Slow					X	
Shaping					$\otimes$	
Pre-Shaping				$\otimes$		Desired
3-Imp. Traj. Shap.	$\otimes$	$\otimes$	$\otimes$			
4-Imp. Traj. Shap.	X	X	X	X		
Opt. Com. Des.	X	X	X	X	X	

X; Recommended $\otimes$

approach should be selected depending on the speed of a motion as detailed for various trajectory frequency ratios in Table 9.1. This information allows designers to select the shaping approach for specific speed requirement. However, as speed increases so does the impact of un-modelled effects. Therefore, for command shaping schemes to function on newly designed fast machines, the shaper design should include the continuum nature of some of the machine elements.

9.2.1.4 Command Shaping for Continuum Beams

Most real machines are actually composed of continuum elements, although they may have been traditionally modelled as lumped parameter systems. As speeds increase, the continuum effects increase, therefore at high speeds a command shaping scheme is needed to deal with the particular concerns of continuum elements. Traditional input shapers are capable of eliminating large amounts of vibration in continuum beams as shown in the experimental transverse beam response of Figure 9.7. The results of the investigation into which shapers work best for which beams are summarized in Table 9.2. This table allows designers to

350
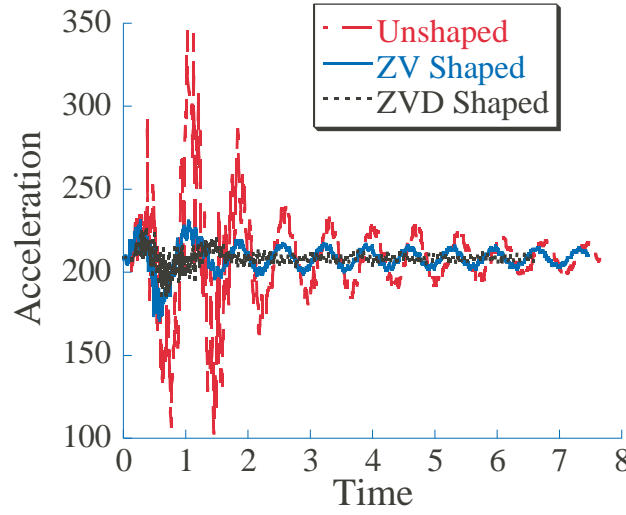
Figure 9.7: Experimental Example Solution.

Table 9.2: Input Shaping Effectiveness for Continuum Systems.

	ZV	ZVD	UMZV
Torsional	Full★	Full	None
Torsional: Low Inertia	Full★	Full	Partial
Torsional: High Inertia	Full★	Full	Full
Longitudinal	Full★	Full	None
Longitudinal: Low Mass	Full★	Full	Partial
Longitudinal: High Mass	Full★	Full	Full
Transverse	Partial	Partial★	Partial
Transverse: Low Mass	Partial	Partial★	Partial
Transverse: High Mass	Full★	Full	Full

Recommended (★)

appropriately choose shaper type at the design stage. In this way the continuum input shapers are both a solution to a current problem and a shaper design selection guide at the same time. However, simply having shaper selection guidelines does not constitute a design procedure. Therefore, another research question is needed.

9.2.2   Secondary Research Question 2.

How can mechanical designs be selected to make the best use of existing and improved command shaping techniques?

The direct implementation of design selection utilizing existing and new command shaping techniques was completed with the goal of improved machine performance. This research
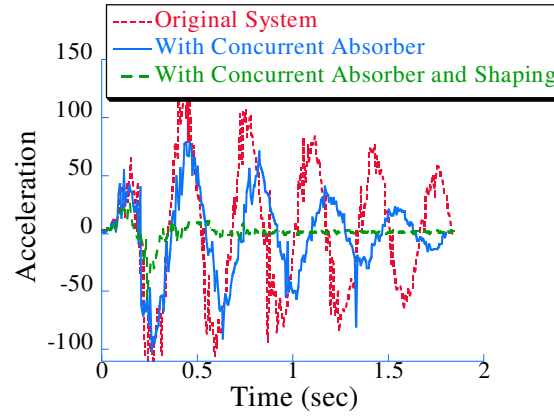
Figure 9.8: Experimental Combined Solution.

question like the primary research question centers around the design of micro-milling machines; however, other applications of combined design are addressed, specifically vibration absorber design. By designing these auxiliary oscillatory elements simultaneously with input shapers, a corrective approach to the combined design process was shown. This corrective process aided in the complete design of continuum elements, which were combined together to create micro-mill position system design scenarios. Finally the previous research was synthesized together to create a general procedure for the impact of command shaping on the design process.

9.2.2.1 Micro-Mill Design

By studying the work of others in the design of micro-mills and the behavior and issues of the ETSII mill, it was possible to formulate the design variables and criteria for micro-mills. The correlation analysis shown in Figure 9.3 showed that the design decisions of the positioning system could be used to increase the throughput of the mill. This enabled the positioning system to be separated from the other design parameters. This separation is key to reducing the complexity of the combined design problem for micro-mills.

9.2.2.2 Vibration Absorber Design

The next major step in the combination of mechanical and command design was to consider the design of a secondary mechanical element. A vibration absorber was chosen, since the absorber could be used to deal with disturbances that the input shaper could not cancel. Figure 9.8 shows experimental performance of the concurrent design approach for the vibration absorber. This specific application of the combined strategy introduced concepts and procedures which were later combined into the overall design process strategy.

352

Table 9.3: Decision Correlation.

Component	Design Choice	Performance Measures	Surface Finsh	Part Tolerances	Tool Life	Throughput	Materials	Energy Consumption	Overall Weight	Cost	Total
Cutter											
	Material		3		3	1	2	1			10
	Shape		3		3	1	2	2			11
Spindle											
	Type			3		1		2	1	1	8
	Stiffness		1	3	1						5
	Speed		3	2	3	3	1	1		1	14
Controller											
	Structure		1	2		2		1			6
	Gains		1	3		2		1			7
Stages											
	Type			2		2		3	3	2	12
	Speed				1	3		2		1	7
	Stiffness		1	3	1	1				1	7
	Encoders			3						2	5
	Dynamics			2	1	2		1	2		8
	Bearings			1		1		1			3
Workpiece											
	Fixturing		1	2		3	3		1	1	11
	Sensing			1	3					3	7
Mount											
	Bandwidth		1	1					3	1	6
	Size		1	1					3	1	6
Total			16	29	16	22	8	15	13	14	

Figure 9.9: Total Command Time in X and Y Directions.

9.2.2.3 Continuum Beam Design

Another important area of research towards the goal of general combined mechanical and command design is the combined design of beam elements and command shapers. This provided procedures that could be modified for the general design case. The continuum beam design also enabled the study of the design of a micro-mill positioning system. By selecting stage parameters according to Figure 9.9, the fastest possible shaped motion design can be selected. This selection process, however, only focused on the embodiment stage of the design process. Therefore the other portions of the design process had to be considered.

9.2.2.4 Design Process Impact

The overall goal of the research is summarized as the effect of considering input shaping on the overall design process. Figure 9.10 summarizes the effects of input shaping on all stage of the design process. Specifically input shaping requires prejudices to be eliminated in the task definition and conceptual design phases. In the area of embodiment and detail design, the combined command and mechanical design strategy both introduces new methods of selection, but also, specific concerns only relevant to flexible systems. Together, the modification of the design process allows the design of machines with simultaneous consideration of command shapers and mechanical parameters to yield machines with better performance.

9.3 Contributions

This research makes contributions to many different areas leading to the introduction of an approach to the simultaneous design of mechanical and command components. Specifically the areas of micro-milling, command shaping, and mechanical design have been advanced.

Design Stages   **Design Components**   **Input Shaping Influence**
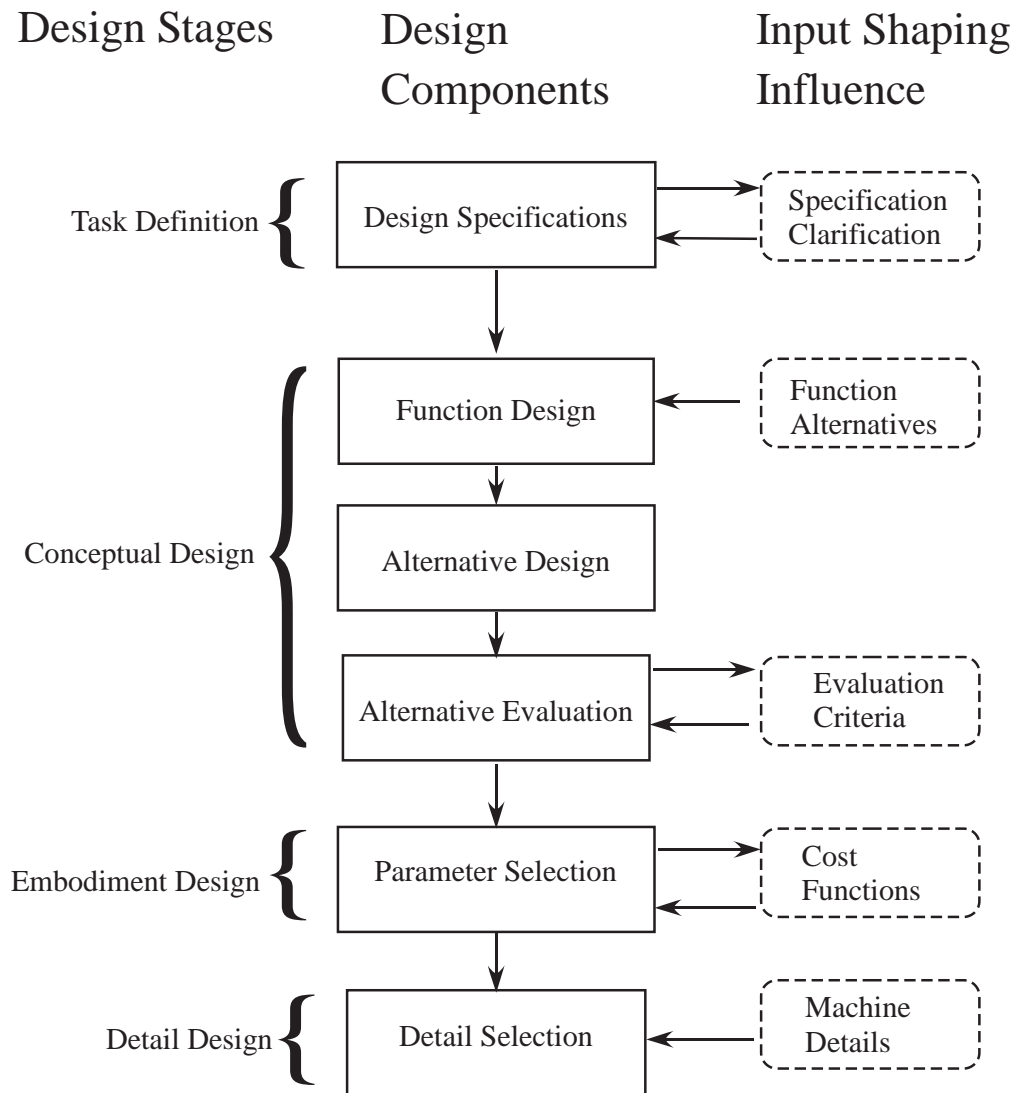
Figure 9.10: Input Shaping Impact in Design Process.

9.3.1 Micro-Milling

In the areas of micro-milling, this work has contributed in three main ways. First the dynamics of the micro-milling process have been described. Second, the performance of existing micro-mills has been improved through command shaping. Finally, the design knowledge for the next generation of micro-mills has been expanded.

The performance of existing micro-mills has been quantified and described in detail. Including the following specific contributions:

- Description of Cutting Forces.

- Observation of Directional Dependence on Motion.

- Observation of Position Dependence on Motion.

- Lack of Cutting Force Impact on Positioning System.

Together these can be used by others to better understand specific micro-mills and the performance of micro-mills in general.

Micro-mill performance was not only studied; but it was improved through the use of command generation. This modification to the ETSII micro-mill contributed the following:

- Development of Shapers for Acceleration Dependent Nonlinearity.

- Method for Improved Micro-Mill Stage Positioning.

- Method for Improved Micro-Milling Part Quality.

These contributions should motivate others to employ command shaping on their micro-mills.

Finally, the design of the next generation of micro-mills has been aided through both observations and design procedures, including:

- Study of Micro-Mill Design Sensitivity.

- Procedure for the Combined Design of the Micro Positioning System.

- Generalized Design Approach for Improved Micro-Milling Performance.

This work enables designers to create better micro-mills with or without the simultaneous consideration of command shaping.

9.3.2 Command Shaping

In the area of command shaping, four important areas have been advanced in this dissertation: nonlinear systems, spatial tracking, spatial/temporal tracking, continuum system performance.

The specific application of command shaping on the ETSII micro-mill motivated the development of new command shapers with the following contributions:

- Method of Implementing Nonlinear Shaping on a CNC Controller.

- Another Successful Application of Command Shaping.

- Shaping Procedure for Dealing with Acceleration Dependent Nonlinearities.

This should motivate the use of command shaping on micro-mills, nonlinear systems, and systems with limited command design capabilities.

In the are of tracking of accurate trajectories in multiple spatial dimensions as fast as possible, the following contributions were made:

- Develop of Measure for Speed of Trajectories.

- Technique for Accurately making Complex Motions with Simple Shaped Commands.

These should enable the performance of command shaped machines to be improved further.

In the more complicated area of tracking spatial and temporal trajectories, several contributions were made including:

- Analytical Technique for Shaper Selection Based on Tracking Error.

- Shapers Specifically Design for Tracking S-Curves.

- Shapers Specifically Design for Tracking Acceleration Profiles.

- Shaping Techniques for Multi-Axis Spatial/Temporal Trajectories.

- Guidelines for the Use of Different Tracking Techniques.

The guidelines should lead to designers selecting existing or the new trajectory tracking input shapers for applications requiring accurate tracking.

Although command shaping has been used on continuum elements before, the derivation and analysis of this dissertation provides the following contributions:

- Derivation of Command Shaping for Continuum Elements.

- Analysis of Shaping Sensitivity for Different Beams.

- Impact of Higher Modes on Shaper Selection.

- Shaper Selection Guideline For Continuum Elements.

Now when command shaping is utilized on continuum system, there is a theoretical basis and a guide for which shaper to employ.

9.3.3 Mechanical Design

The largest contributions of this work are in the area of mechanical design, specifically for micro-mills. The consideration of command shaping has lead to techniques for the design of vibration absorbers, continuum elements, and general procedures for embodiment design. Culminating in the general impact of input shaping on all stages of the design process.

Micro-milling design has been advanced in two ways:

- Analysis of Design Sensitivity.

- Procedure for Design of Positioning System.

These along with the general design impact should lead to new lightweight micro-mill designs.

This research has expanded the uses of vibration absorbers, as well as introducing new design strategies; these lead to the following contributions:

- Vibration Absorbers Specifically for Step Disturbances.

- Sequential Technique for Vibration Absorber and Command Shaper Design.

- Concurrent Technique for Vibration Absorber and Command Shaper Design.

This new application of vibration absorber makes them useful for non-rotating machinery.

The design of continuum elements has been advanced by this research in the following ways:

- Procedure for Constrained Parameter Selection of Simple Beams.

- Procedure for Parameter Selection of Tapered Beams.

- Procedure for Parameter Selection of Symmetric Plates.

- Input Shaper Selection Guidelines for Various Beams.

This should lead to more flexible continuum elements with command shaping replacing traditional massive and stiff elements.

The area of design embodiment with command shaping has been advanced in both specific examples as well as general procedures including:

- Continuum Beam Embodiment Procedure.

- Vibration Absorber Beam Embodiment Procedure.

- Method for Embodiment Design of Micro-Mill Positioning System.

- Generalized Cost Function Formulation Based on Shaped Command Duration.

- Derivative Based Analysis for Shaped Design Embodiment with Speed Goal.

All of these techniques allow a designer to select parameters of the mechanical system and command shaper simultaneously.

Finally, this dissertation has created an approach to considering command shaped flexible systems as valid alternatives in the design process. The following recommendations should contribute to better command shaped design solutions.

- Discussion of Removal of Prejudice from Task Definition.

- Previously Discarded Functional Alternatives being Useful.

- Discussion of Removal of Prejudice from Evaluation.

- Shaped Motion Based Method for Cost Function Creation in Design Embodiment and Detail Design.

- Discussion of Specific Issues for Flexible Systems in Detail Design.

Together these form a complete approach to considering command shaping in the design phase of a machine.

9.4 Future Work

The research presented in this dissertation has several opportunities to be expanded and continued in future work. This future research can be divided into three categories, micro-milling, command shaping, and mechanical design.

9.4.1 Micro-Milling

In the area of micro-milling there are three major areas where the research in the dissertation can be expanded.

1. Cutting Dynamic Investigation: The dynamics and methods of cutting with micro-scale tools, while not presented significantly in this dissertation, are an important and promising area of research. The theory of the cutting operation has not yet approached prediction of the cutting process for high RPM spindles.

2. More Advanced Command Shaping Application: The mill at ETSII had a limited motion controller, therefore the command shapers were constrained. More advanced and robust command shapers should enable greater micro-mill process speeds.

3. Construction of New Micro-Mill: The culmination of the micro-milling design research presented in this dissertation would be the construction of a flexible and lightweight micro-mill using the principle of combined mechanical and command parameter selection. The actual implementation of the procedure would offer insight.

9.4.2 Command Shaping

Although this dissertation presented several key advancements to the area of command generation, command generation knowledge could still be expanded by both investigating trajectory tracking input shaping and shaping for continuum elements.

1. Automated Tracking Algorithm: The technique of multi-axis trajectory tracking command shapers is limited by the necessity for a user to break the desired motion into trajectory components. If an automated algorithm could select the components, then the trajectory tracking process could be completely automated.

2. Specific Guidelines for Shaper Selection for Trajectory Tracking: The guidelines for selecting a shaping scheme for trajectory tracking could be expanded to encompass other issues such as actuator force, and robustness.

3. Shaping Advanced Continuum Elements: While this work presented techniques for fixed-free beams of various types, many other continuum elements exist. Plates, membrane, non-uniform beams, as well as finite element model input shaping still needs to be considered.

9.4.3 Mechanical Design

Although the impact of command shaping on the entire design process is discussed in this dissertation, several areas of mechanical and command design can be further studied.

1. Design Embodiment of Other Systems: In this work only micro-mills and simple elements were considered in the embodiment design process. The study of command shaping's impact on other specific machines would enable the refinement of the generalized impact.

2. Usefulness of Combined Design Approach: The combined design approach can be used to yield faster moving machines, however a study of the occurrence of combined design being selected in the evaluation design stage over other more traditional approach would show the merit of the technique.

APPENDIX A

CONTINUUM BEAMS

A.1 Equations of Motion For Longitudinal Beams

A.1.1 Longitudinal Beam

Another common mechanical element is the axially or longitudinally vibrating beam. This beams motion is similar to that of the torsional beam in Section 7.1.1, therefore the derivation will be abbreviated where possible. Figure A.1 diagrams a longitudinal beam while Table A.1 describes the primary parameters for the beam.

The first step is to once again consider the forces on a differential element. Figure A.2 shows a free body diagram of a longitudinal differential element with the generic Force, S, the change in the force over the element, $\frac{\delta S}{\delta x}dx$, and the inertial Force $\rho A \delta x \frac{\delta^2 u}{\delta t^2}$. A relationship exists between these forces of:

$$S + \frac{\delta S}{\delta x}dx - S - \rho A \delta x \frac{\delta^2 S}{\delta t^2} = 0 \tag{A.1}$$

The force S is related to the change in deflection by:

$$S = EA\frac{\delta u}{\delta x} \tag{A.2}$$

allowing (A.1) to simplify to:

$$EA\frac{\delta^2 u}{\delta x^2}dx - \rho A \delta_X \frac{\delta^2 u}{\delta t^2} = 0 \tag{A.3}$$

$$\frac{\delta^2 u}{\delta x^2} = \frac{1}{a^2}\frac{\delta^2 u}{\delta t^2} = 0 \tag{A.4}$$
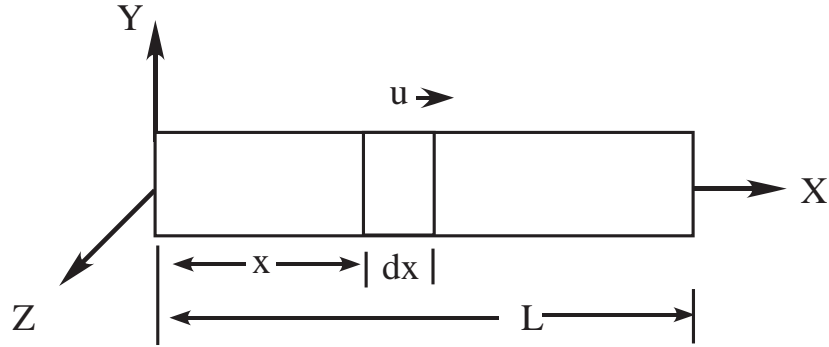
Figure A.1: Diagram of Longitudinal Beam.

Table A.1: Longitudinal Beam Parameters.

Variable	Definition
ρ	Density
L	Length of Beam
M_A	Attached Mass
u	Longitudinal Deflection of Element
m	Elemental Mass
E	Modulus of Elasticity
x	Position along Beam
a	Wave Velocity
ω_i	Beam Natural Frequencies
t	Time
r_L	Longitudinal Rigidity
A	Area
X_i	Mode Shape
F_{stat}	Static Force Magnitude
A_i and B_i	Time Response Coefficients
C_i and D_i	Mode Shape Coefficients
K	Static Stiffness
ϕ_i	Time Dependent Response
u^*	Inertial Forces Response
u_g or g(t)	Base Motion
i	Mode Number
Q	Forcing Function
S	Elemental Force
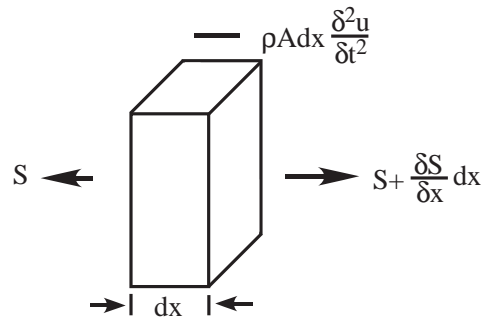
Figure A.2: Diagram of Longitudinal Beam Element.

where for a round bar the longitudinal wave velocity, a, is given by:

$$a = \sqrt{\frac{E}{\rho}} \tag{A.5}$$

Again, the fixed-free case is considered with boundary conditions of:

$$u_{(x=0)} = 0 \tag{A.6}$$

$$\left(\frac{du}{dx}\right)_{x=L} = 0 \tag{A.7}$$

The solution to (A.4) is assumed to have the form of:

$$u_i = X_i \left(A_i \cos \omega_i t + B_i \sin \omega_i t\right) \tag{A.8}$$

where A_i and B_i are constants. Where X_i is assumed as:

$$X_i = C_i \cos \frac{\omega_i x}{a} + D_i \sin \frac{\omega_i x}{a} \tag{A.9}$$

Inserting the boundary conditions into (A.9); (A.6) yields $C_i = 0$ and (A.7) forces:

$$\cos \frac{\omega L}{a} = 0 \tag{A.10}$$

giving the natural frequencies of the system:

$$\omega_i = \frac{\pi a i}{2L} \qquad (i = 1, 3, 5, ..., \infty) \tag{A.11}$$

The mode shapes are described by:

$$X_i = D_i \sin \frac{\omega_i x}{a} \tag{A.12}$$

with a general form of the solution:

$$u = \sum_{i=1}^{\infty} \sin \frac{\omega_i x}{a} \left(A_i \cos \omega_i t + B_i \sin \omega_i t\right) \tag{A.13}$$

where A_i and D_i encompass D_i and are determined by the initial conditions of the problem.

A.1.1.1 Static Deflection

If a static longitudinal force, P_{stat}, is applied to the beam then the deflection at the end is given by:

$$u_{(x=L)} = \frac{P_{stat}}{K} \tag{A.14}$$

where:

$$K = \frac{EA}{L} \tag{A.15}$$

A.1.1.2   Forced Response

The forced response of the longitudinal beam model uses the same basic procedure as the torsional beam and centers around the equation of motion for a differential element:

$$m\ddot{u}dx - ru''dx = Q\left(x,t\right)dx \tag{A.16}$$

where $Q\left(x,t\right)$ is the applied force for the element. u is assumed to have the form:

$$u = \sum_i \phi_i X_i \qquad (i = 1, 2, 3, ..., \infty) \tag{A.17}$$

The forced response only changes ϕ_i which is found with Duhamel's integral by:

$$\phi_i = \frac{1}{\omega_i} \int_{x=0}^{L} X_i \int_{t=0}^{t} mQ(x,t') \sin\left(\omega_i(t-t')\right)dt'dx \tag{A.18}$$

where $Q_(x,t')$ is the forcing on the beam. The result for an arbitrary forcing Q is:

$$u_i = \sum_{i=1}^{\infty} \frac{X_i}{\omega_i} \int_{x=0}^{L} X_i \int_{t=0}^{t} mQ(x,t') \sin\left(\omega_i(t-t')\right)dt'dx \tag{A.19}$$

substituting in X_i yields:

$$u_i = \sum_{i=1}^{\infty} \frac{D_i \sin\frac{\omega_i x}{a}}{\omega_i} \int_{x=0}^{L} D_i \sin\frac{\omega_i x}{a} \int_{t=0}^{t} mQ(x,t') \sin\left(\omega_i(t-t')\right)dt'dx \tag{A.20}$$

where D_i must satisfy the normalization and orthogonality conditions:

$$\int_0^L X_i^2 dx = 1 \tag{A.21}$$

giving:

$$D_i = \sqrt{\frac{L}{2}} \tag{A.22}$$

A.1.1.3   Base Motion

Base motion of the longitudinal beam will also be considered. A displacement of the fixed end of the beam of $g\left(t\right)$, with a given acceleration of $\ddot{g}\left(t\right)$, can be used to find the overall response. First, $u\left(x=0,t\right) = g\left(t\right)$ will constrain the motion. The two component approach will be used, with the displacement of the fixed end being u_g and the response from the inertia forces u^* which represent the deflection with reference to the moving fixed end:

$$u\left(x,t\right) = u^*\left(x,t\right) + u_g\left(t\right) \tag{A.23}$$

The acceleration conditions give:

$$\ddot{u}\left(x,t\right) = \ddot{u}^*\left(x,t\right) + \ddot{u}_g\left(t\right) \tag{A.24}$$

These relationships yield the equation of motion for each differential beam element. $g(t)$ does not change with x, yielding an equation of motion of:

$$m\ddot{u}^* - r_L u^{*\prime\prime} = -m\ddot{g}(t) \tag{A.25}$$

A forced response only yields:

$$Q(x,t) = -m\ddot{g}(t) \tag{A.26}$$

The inertial component of the response is thus:

$$u_i^* = \sum_{i=1}^{\infty} \frac{X_i}{\omega_i} \int_{x=0}^{L} X_i \int_{t=0}^{t} \ddot{g}(t') \sin\left(\omega_i(t-t')\right) dt' dx \tag{A.27}$$

allowing the overall response to be found:

$$u = g(t) + u^* \tag{A.28}$$
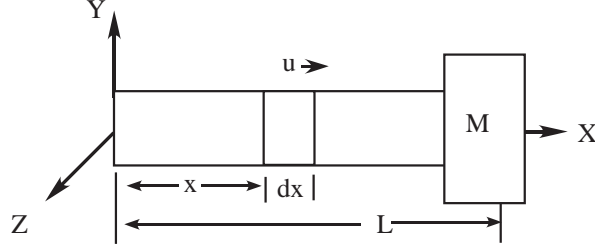
Figure A.3: Diagram of Longitudinal Beam with Attached Mass.

A.1.2 Longitudinal Beam with Attached Mass

Another common occurrence is for the longitudinal beam to have a mass affixed to the end here an attached inertia of M_A as shown in Figure A.3. The derivation for the motions of this loading on a longitudinal beam is similar to the attached inertia case discussed in Section 7.1.2. The boundary conditions are thus:

$$u_{(x=0)} = 0 \tag{A.29}$$

$$r_L \left(\acute{u} \right)_{(x=L)} = -M_A \ddot{u}_{(x=L)} \tag{A.30}$$

Equation's (A.4) solution has the form:

$$u_i = X_i \left(A_i \cos \omega_i t + B_i \sin \omega_i t \right) \tag{A.31}$$

where A_i and B_i are constants. The boundary conditions of (A.29 and A.30) can be transformed to:

$$X_{i(x=0)} = 0 \tag{A.32}$$

$$r_t \acute{X}_{i(x=L)} = M_A \omega^2{}_i X_{i(x=L)} \tag{A.33}$$

$X_i's$ form is:

$$X_i = C_i \cos \frac{\omega_i x}{a} + D_i \sin \frac{\omega_i x}{a} \tag{A.34}$$

The boundary conditions with (A.34) yield:

$$C_i = 0 \tag{A.35}$$

and:

$$\frac{r_L \omega_i}{a} \cos \frac{\omega_i L}{a} = I_a \omega_i^2 \sin \frac{\omega L}{a} \tag{A.36}$$

Equation (A.36) can be simplified in order to find the natural frequencies:

$$\zeta_i \tan \zeta_i = \eta \tag{A.37}$$

where $\zeta_i = \frac{\omega_i L}{a}$ and $\eta = \frac{mL}{M_A}$. The multiple solutions to (A.37) are the natural frequencies (ω_i).

The orthogonality is once again important and begins with:

$$r_L X''_i = -m\omega_i^2 X_i \tag{A.38}$$
$$r_L X''_j = -m\omega_j^2 X_j$$

If these two equations are multiplied by X_j and X_i respectively and then integrated over the beam:

$$r_L \int_0^L X''_i X_j dx = -m\omega_i^2 \int_0^L X_i X_j dx \tag{A.39}$$
$$r_L \int_0^L X''_j X_i dx = -m\omega_j^2 \int_0^L X_j X_i dx$$

The boundary condition (A.33) is also multiplied by X_j and X_i:

$$r_L \acute{X}_{i(x=L)} X_{j(x=L)} = M_A \omega_i^2 X_{i(x=L)} X_{j(x=L)} \tag{A.40}$$
$$r_L \acute{X}_{j(x=L)} X_{i(x=L)} = M_A \omega_j^2 X_{j(x=L)} X_{i(x=L)}$$

Equation (A.39) - (A.40) yields:

$$r \int_0^L X''_i X_j dx - r \acute{X}_{i(x=L)} X_{j(x=L)} = -\omega_i^2 \left(m \int_0^L X_i X_j dx + M_A X_{j(x=L)} X_{i(x=L)} \right) \tag{A.41}$$
$$r \int_0^L)X''_j X_i dx - r \acute{X}_{j(x=L)} X_{i(x=L)} = -\omega_j^2 \left(m \int_0^L X_j X_i dx + M_A X_{i(x=L)} X_{j(x=L)} \right)$$

integration yields:

$$r_L \acute{X}_{i(x=0)} X_{j(x=0)} - r \int_0^L \acute{X}_i \acute{X}_j dx = -\omega_i^2 \left(m \int_0^L X_i X_j dx + M_A X_{i(x=L)} X_{j(x=L)} \right) \tag{A.42}$$
$$r_L \acute{X}_{j(x=0)} X_{i(x=0)} - r \int_0^L \acute{X}_j \acute{X}_i dx = -\omega_j^2 \left(m \int_0^L X_j X_i dx + M_A X_{j(x=L)} X_{i(x=L)} \right)$$

$X_{i(x=0)}$ and $X_{j(x=0)}$ are both identically zero. The difference between the two part of (A.42) leaves:

$$\left(\omega_i^2 - \omega_j^2 \right) \left(m \int_0^L X_i X_j dx + M_A X_{i(x=L)} X_{j(x=L)} \right) = 0 \tag{A.43}$$

The nontrivial case of $\omega_i \neq \omega_j$ forces the right side of the equation to equal to zero thus:

$$m \int_0^L X_i X_j dx + M_A X_{i(x=L)} X_{j(x=L)} = 0 \qquad i \neq j \tag{A.44}$$

$X_{i(x=0)} = 0$ substituted into (A.42) gives:

$$r_L \int_0^L \acute{X}_j \acute{X}_i dx = 0 \qquad i \neq j \tag{A.45}$$

In conjunction with (A.41) gives:

$$r_L \int_0^L X''_i X_j dx - r_L \acute{X}_{i(x=L)} X_{j(x=L)} = 0 \qquad i \neq j \tag{A.46}$$

When $i = j$ the results is the mass, m giving three orthogonality equations:

$$m \int_0^L X_i^2 dx + M_A X_{i(x=L)}^2 = m \tag{A.47}$$

$$r_L \int_0^L X''_i X_i dx - r \acute{X}_{i(x=L)} X_{i(x=L)} = -\omega_i^2 m \tag{A.48}$$

$$- r_L \int_0^L \left(\acute{X}_i\right)^2 dx = -\omega_i^2 m \tag{A.49}$$

A.1.2.2 Static Deflection

The static deflection results are identical to the longitudinal beam with no attached mass. Thus, if a static longitudinal force, P_{stat}, is applied, then the end deflection is:

$$u_{(x=L)} = \frac{P_{stat}}{K} \tag{A.50}$$

where:

$$K = \frac{EA}{L} \tag{A.51}$$

A.1.2.3 Forced Response

The differential element is once again used for the forced response of the longitudinal beam with an attached mass:

$$m\ddot{u}dx - r_L u'' dx = Q(x,t)\, dx \tag{A.52}$$

where $Q(x,t)$ is the applied force on the element. The motion of the attached mass is given by:

$$M_A \ddot{u}_{x=L} + r_L \acute{u}_L = 0 \tag{A.53}$$

$u's$ form is assumed as:

$$u = \sum_i \phi_i X_i \qquad (i = 1, 2, 3, ..., \infty) \tag{A.54}$$

Used with (A.53), multiplied by X_j and integrated over the length of the beam gives:

$$\sum_i^\infty \left(m\ddot{\phi}_i \int_0^L X_i X_j dx - r_L \phi_i \int_0^L X''_i X_j dx \right) = \int_0^L X_j Q(x,t)\, dx \tag{A.55}$$

The same procedure is used for the attached inertia and (A.52) to yield:

$$\sum_i^\infty \left(M_A \ddot{\phi}_i X_{i(x=L)} X_{j(x=L)} + r_L \phi_i \acute{X}_{i(x=L)} X_{j(x=L)} \right) = 0 \tag{A.56}$$

368

Summing the two equations describes the overall motion:

$$m\ddot{\phi}_i \int_0^L X_i X_j dx + M_A \ddot{\phi}_i X_{i(x=L)} X_{j(x=L)} - r_L \phi_i \int_0^L X''_i X_j dx + r_L \phi_i \acute{X}_{i(x=L)} X_{j(x=L)} \quad (A.57)$$

$$= \int_0^L X_j Q(x,t) \, dx$$

The orthogonality and normalization relationships of (A.47) and (A.48) simplify the result for $i = j$ to:

$$m\ddot{\phi} + m\omega_i^2 \phi_i = \int_0^L X_i Q(x,t) \, dx \qquad (A.58)$$

D_i from (A.34) is also needed. When (A.34) with $C_i = 0$ is substituted into (A.47) gives:

$$\int_0^L D_i^2 \left(\sin \frac{\omega_i x}{a} \right)^2 dx + \frac{M_A}{m} D_i^2 \left(\sin \frac{\omega_i L}{a} \right)^2 = 1 \qquad (A.59)$$

Integrating over x yields:

$$D_i^2 \left(\frac{L}{2} - \frac{\sin \frac{2\omega L}{a}}{\frac{4\omega_i}{a}} + \frac{M_A}{m} \left(\sin \frac{\omega_i L}{a} \right)^2 \right) = 1 \qquad (A.60)$$

giving a described value of D_i of:

$$D_i = \sqrt{\frac{1}{\frac{L}{2} - \frac{\sin \frac{2\omega L}{a}}{\frac{4\omega_i}{a}} + \frac{M_A}{m} \left(\sin \frac{\omega_i L}{a} \right)^2}} \qquad (A.61)$$

Equation (A.58) used with Duhamel's integral can yield to total response:

$$\ddot{u} + \omega u = q \qquad (A.62)$$

where:

$$u = \frac{1}{\omega} \int_0^t q \sin \omega (t - t') dt' \qquad (A.63)$$

Equation (A.58) can be changed to:

$$\ddot{\phi} + \omega_i^2 \phi_i = \frac{1}{m} \int_0^L X_i Q(x,t) \, dx \qquad (A.64)$$

which when used with Duhamel's integral gives:

$$\phi = \frac{1}{\omega_i m} \int_0^L X_i \int_0^t Q(x,t') \sin \omega (t - t') dt' dx \qquad (A.65)$$

If a specific a sinusoidal force is applied at the attached mass, then $Q(x,t) = F \sin \Omega t$, where F is the magnitude of the force and Ω is the forcing frequency. Equation (A.65) simplifies with $Q(x,t)$ to:

$$\phi = \frac{F X_{i(x=L)}}{\omega_i m} \int_0^t \sin (\Omega t') \sin (\omega (t - t')) dt' \qquad (A.66)$$

369

yielding ϕ_i:

$$\phi_i = \frac{F X_{i(x=L)}}{\omega_i m} \left(\Psi_i \right) \tag{A.67}$$

Where Ψ_i is given by:

$$\Psi_i = \sin \omega_i t \left(-\frac{\cos \left(\left(\Omega - \omega_i \right) t \right)}{2 \left(\Omega - \omega_i \right)} - \frac{\cos \left(\left(\Omega + \omega_i \right) t \right)}{2 \left(\Omega + \omega_i \right)} + \frac{1}{2 \left(\Omega - \omega_i \right)} + \frac{1}{2 \left(\Omega + \omega_i \right)} \right) \tag{A.68}$$
$$+ \cos \omega_i t \left(\frac{\sin \left(\left(\Omega - \omega_i \right) t \right)}{2 \left(\Omega - \omega_i \right)} - \frac{\sin \left(\left(\Omega + \omega_i \right) t \right)}{2 \left(\Omega + \omega_i \right)} \right)$$

Prescribing the overall response to be:

$$u = \sum_{i=1}^{\infty} \phi_i X_i \tag{A.69}$$

where ϕ_i is defined in (A.67) and X_i in (A.34) where $C_i = 0$ and D_i by (A.61)

A.1.2.4 Base Excitation Response

Motion of the base of the beam follows the same procedure as the other beams. A displacement $g(t)$, and acceleration $\ddot{g}(t)$ are used to describe the beam position:

$$u(x, t) = u^*(x, t) + u_g(t) \tag{A.70}$$

and acceleration:

$$\ddot{u}(x, t) = \ddot{u}^*(x, t) + \ddot{u}_g(t) \tag{A.71}$$

The differential equations of motion of the beam are thus:

$$m\ddot{u}^* - r u^{*\prime\prime} = -m\ddot{g}(t) \tag{A.72}$$

and the attached inertia:

$$m\ddot{u}^*_{(x=L)} - r u^{*\prime\prime}_{(x=L)} = -m\ddot{g}(t) \tag{A.73}$$

If $u* = \sum_{i=1}^{\infty} \phi_i X_i$, then multiplication by X_j and integrated over the beam gives:

$$m\ddot{\phi}_i \int_0^L X_i X_j dx + M_A \ddot{\phi}_i X_{i(x=L)} X_{j(x=L)} - r_L \phi_i \int_0^L X^{\prime\prime}{}_i X_j dx + r \phi_i \acute{X}_{i(x=L)} X_{j(x=L)} \tag{A.74}$$
$$= -m \int_0^L X_j \ddot{g}(t) \, dx - M_A X_{j(x=L)} \ddot{g}(t)$$

Orthogonality of (A.47) and (A.48) for $i = j$, makes the motion:

$$\ddot{\phi}_i + \omega_i^2 \phi = - \int_0^L X_j \ddot{g}(t) \, dx - \frac{M_A}{m} X_{j(x=L)} \ddot{g}(t) \tag{A.75}$$

Duhamel's integral gives ϕ which can be used to find the overall motion:

$$\phi = -\frac{1}{\omega_i} \left(\int_0^L X_i dx + \frac{M_A}{m} X_{i(x=L)} \right) \int_0^t \ddot{g}\left(\acute{t}\right) \sin\left(\omega_i \left(t - \acute{t} \right) \right) d\acute{t} \tag{A.76}$$
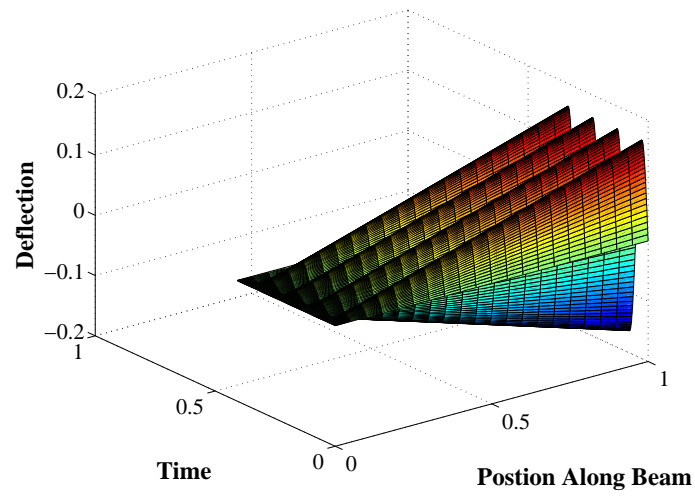
Figure A.4: Step Acceleration Response of Torsional Beam with Attached Inertia.

A.2 Base Motion Response of Torsional Beams with Attached Masses
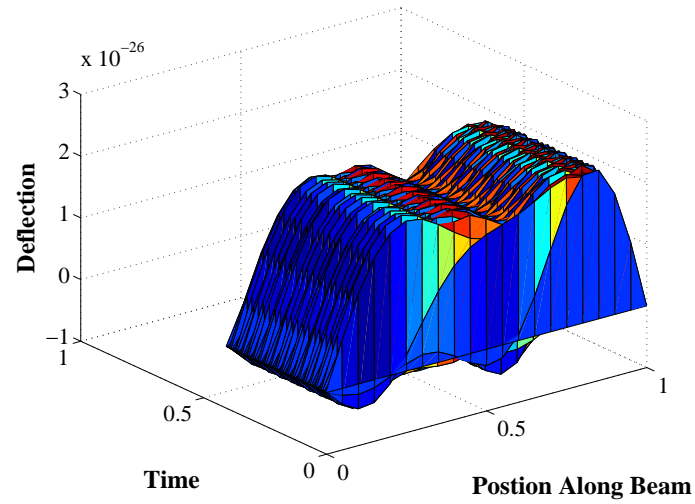
Figure A.5: Modes 2 through 5 Step Acceleration Response of Torsional Beam with Attached Inertia.
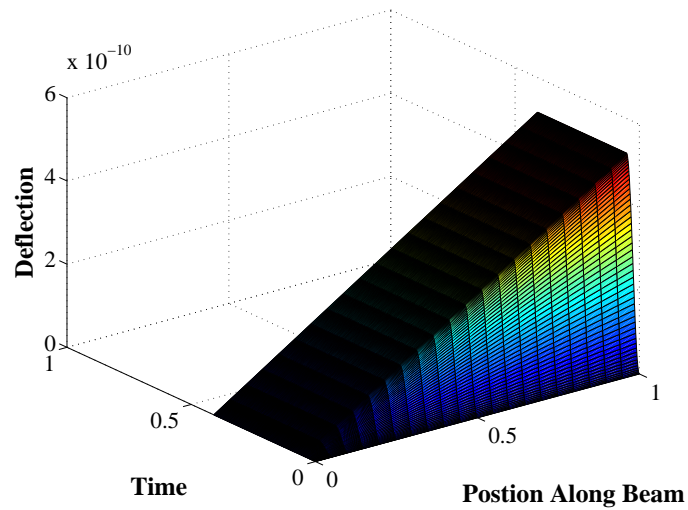
Figure A.6: Zero Vibration Acceleration Response of Torsional Beam with Attached Inertia.

Figure A.7: Modes 2 through 5 ZV Acceleration Response of Torsional Beam with Attached Inertia.
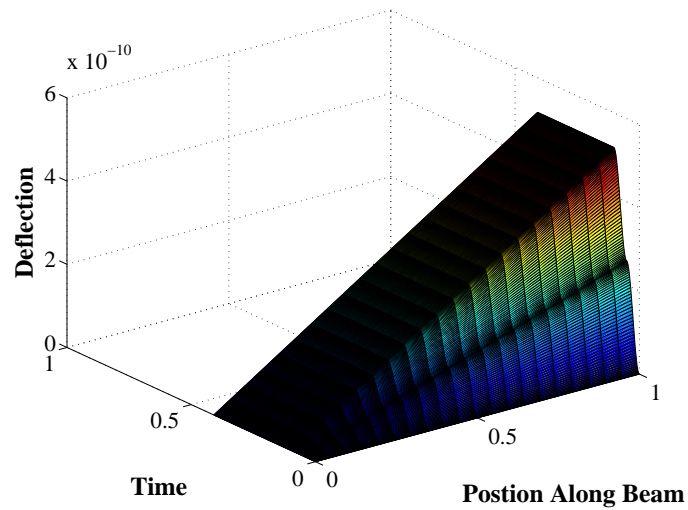
Figure A.8: Zero Vibration Derivative Acceleration Response of Torsional Beam with Attached Inertia.
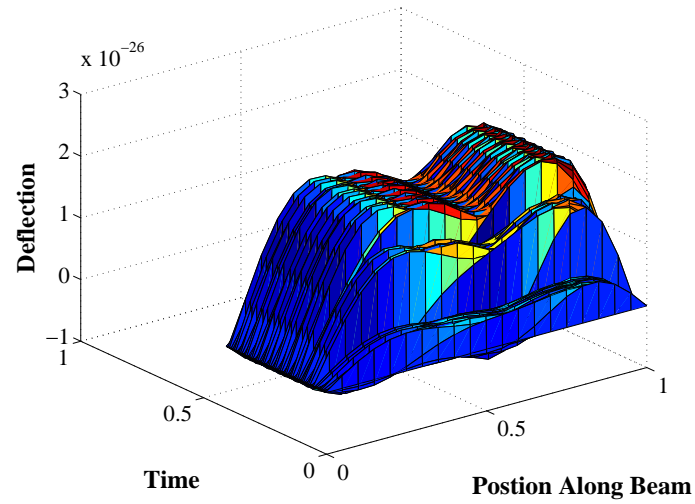
Figure A.9: Modes 2 through 5 ZVD Acceleration Response of Torsional Beam with Attached Inertia.

Figure A.10: UMZV Acceleration Response of Torsional Beam with Attached Inertia.
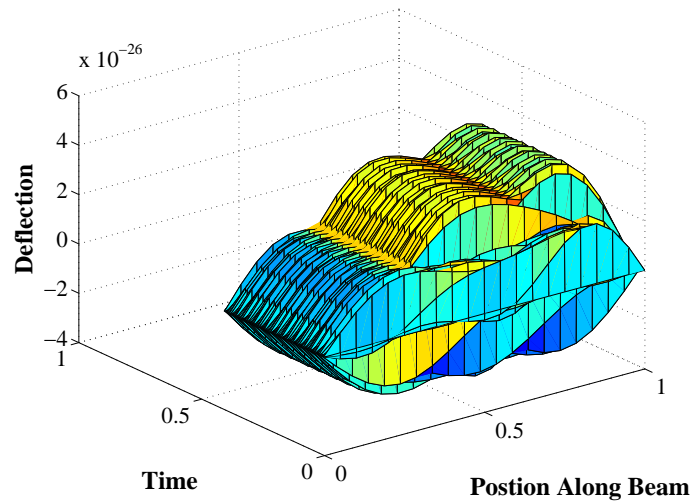
Figure A.11: Modes 2 through 5 UMZV Acceleration Response of Torsional Beam with Attached Inertia.

A.3   Input Shaping Results For Longitudinal Beams

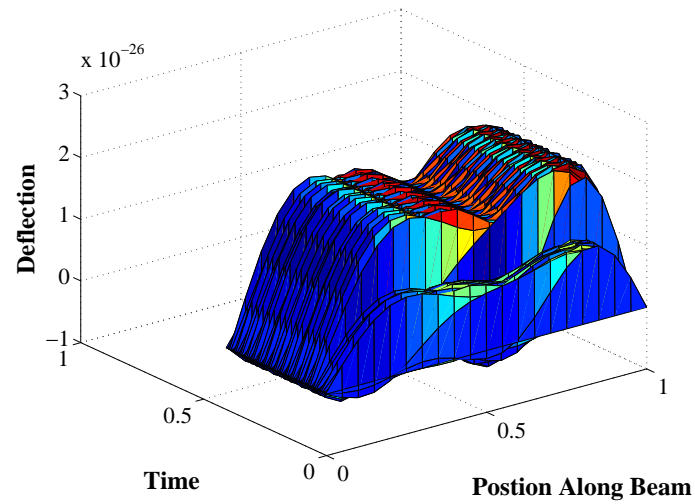### A.3.1   Longitudinal Beam

The longitudinally vibrating beam is similar to the torsional beam in the definition of the vibration. However, due to the differences in modes, its usefulness with input shaping also needs to be investigated. Specifically, the use of traditional input shapers the ZV, the ZVD, and the UMZV shaper will be studied for the multiple modes of the system. Considerations into the sensitivity of the shapers will also be made. The analysis and results are the same as for the torsional case of Section 7.2.2 . Therefore only the Figures are presented in this appendix.

A.3.1.1   Forced Response
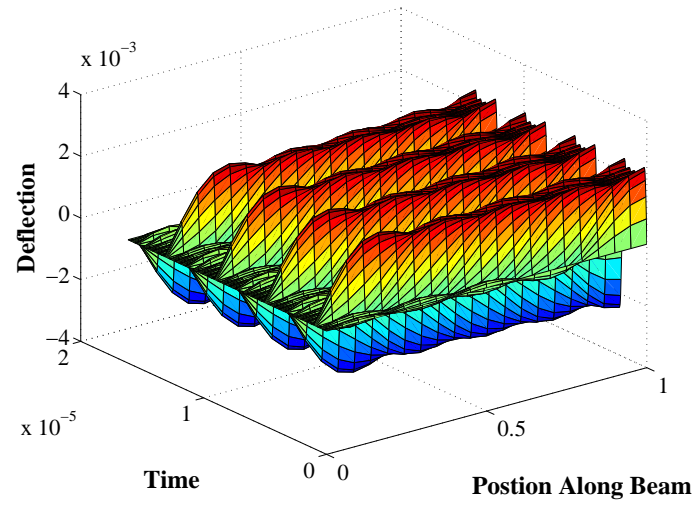
Figure A.12: Impulse Force Response of Longitudinal Beam.
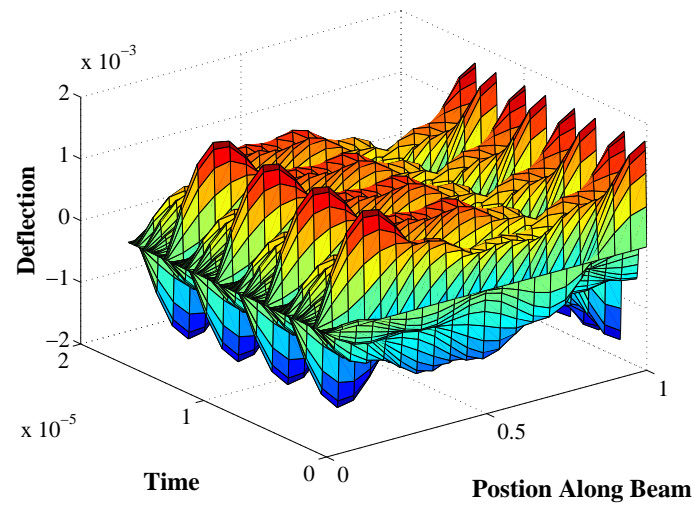
Figure A.13: Modes 2 through 5 Impulse Force Response of Longitudinal Beam.

Figure A.14: Zero Vibration Force Response of Longitudinal Beam.

Figure A.15: Modes 2 through 5 ZV Force Response of Longitudinal Beam.
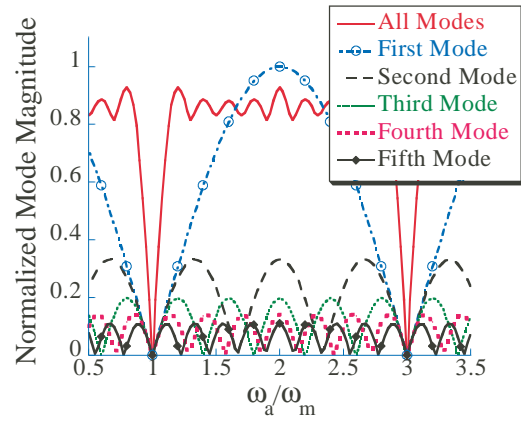
Figure A.16: Zero Vibration Sensitivity of Longitudinal Beam.
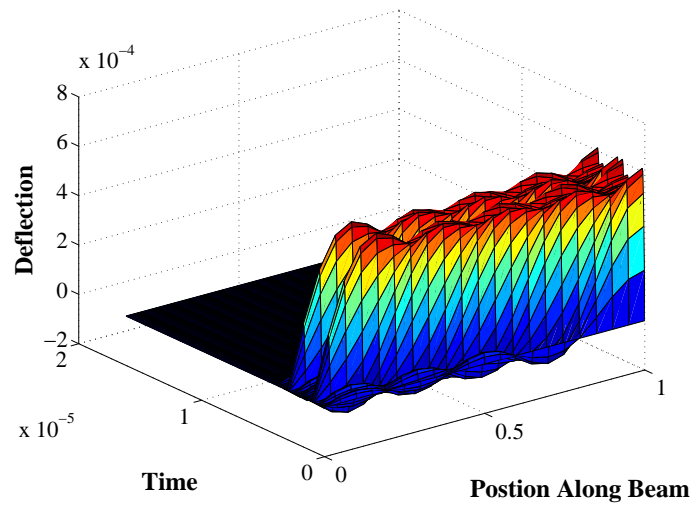
Figure A.17: Zero Vibration Derivative Force Response of Longitudinal Beam.
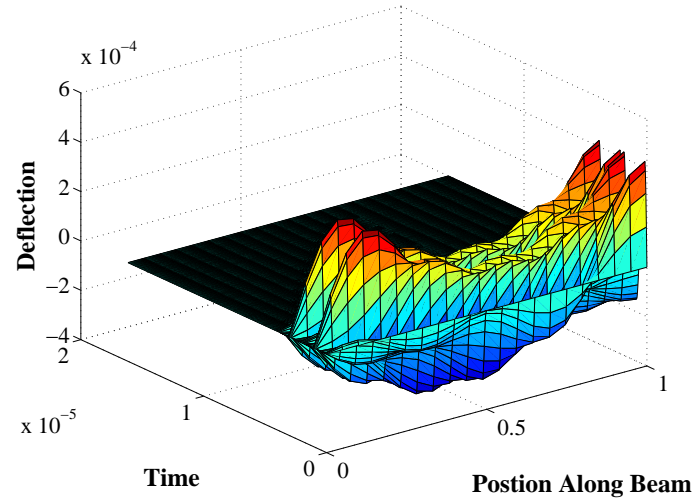
Figure A.18: Modes 2 through 5 ZVD Force Response of Longitudinal Beam.
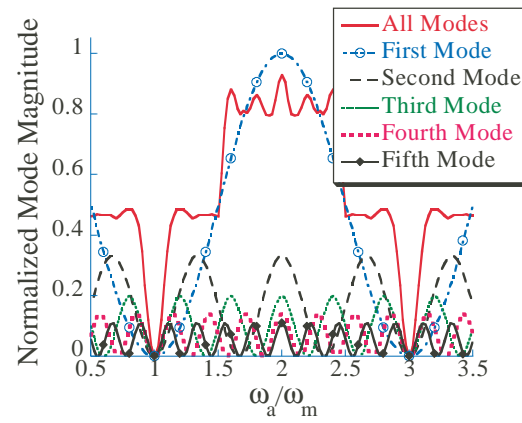
Figure A.19: Zero Vibration Derivative Sensitivity of Longitudinal Beam.
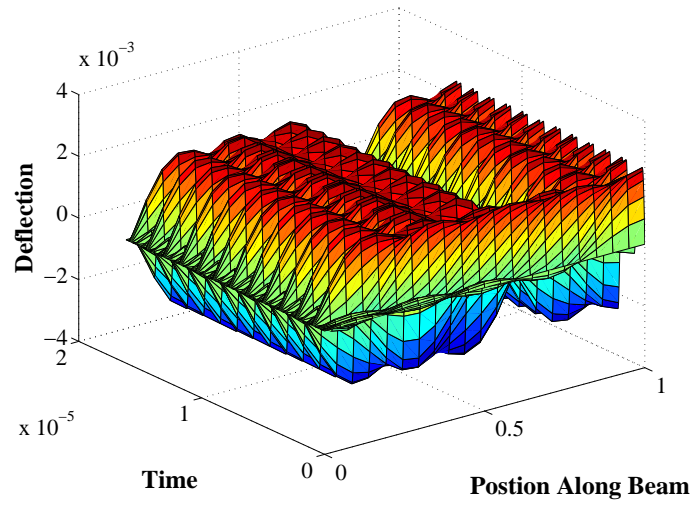
Figure A.20: UMZV Force Response of Longitudinal Beam.
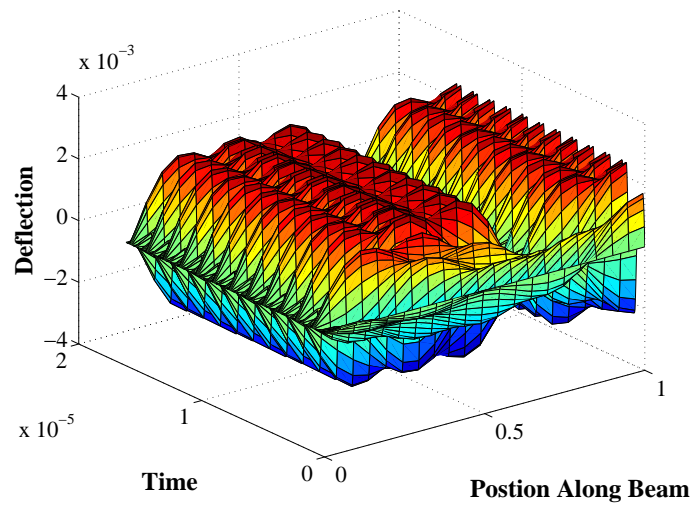
Figure A.21: Modes 2 through 5 UMZV Force Response of Longitudinal Beam.
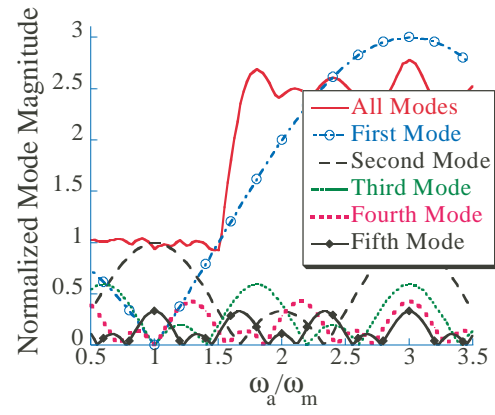
Figure A.22: UMZV Sensitivity of Longitudinal Beam.

A.3.1.2   Base Motion Response
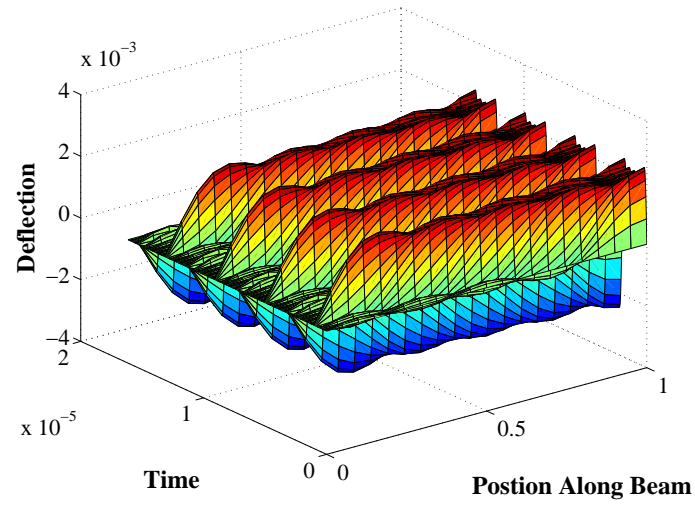
Figure A.23: Step Acceleration Response of Longitudinal Beam.
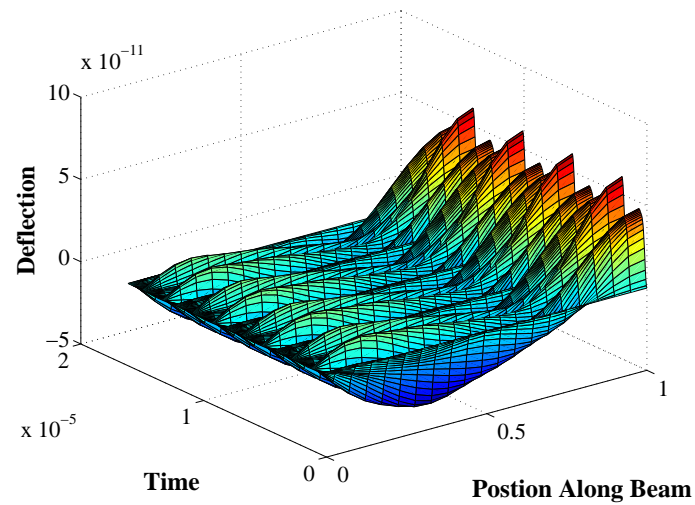
Figure A.24: Modes 2 through 5 Step Acceleration Response of Longitudinal Beam.
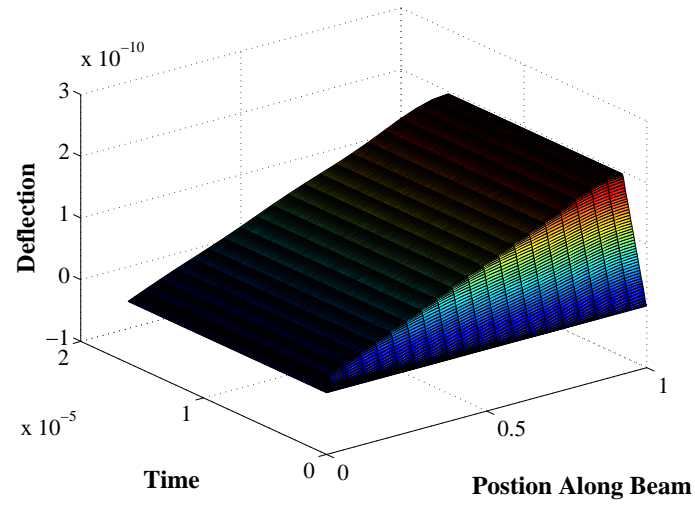
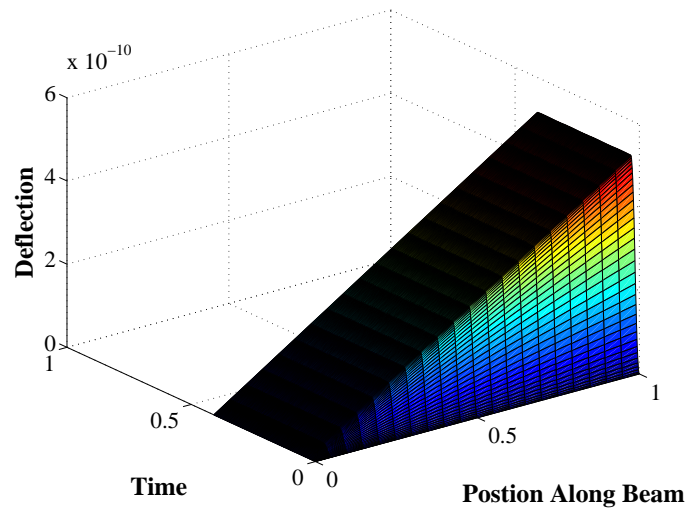**Figure A.25:** Zero Vibration Acceleration Response of Longitudinal Beam.
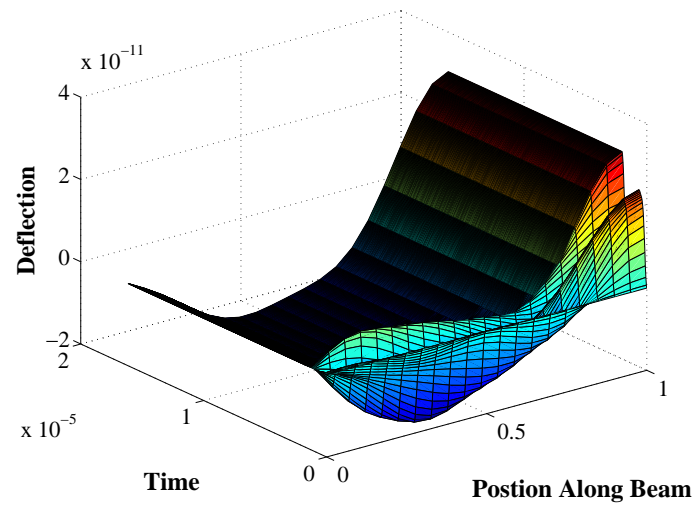
Figure A.26: Modes 2 through 5 ZV Acceleration Response of Longitudinal Beam.
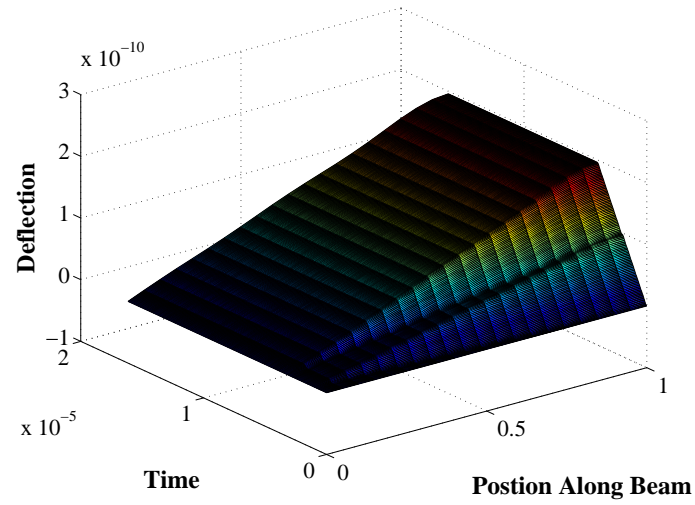
Figure A.27: Zero Vibration Derivative Acceleration Response of Longitudinal Beam.
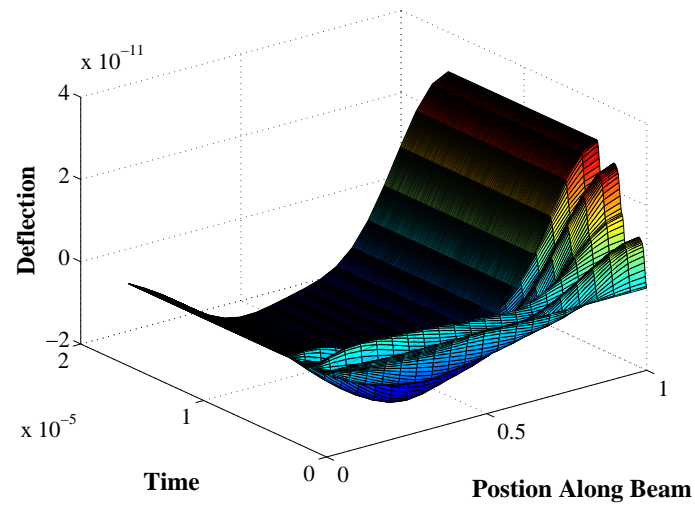
Figure A.28: Modes 2 through 5 ZVD Acceleration Response of Longitudinal Beam.

384
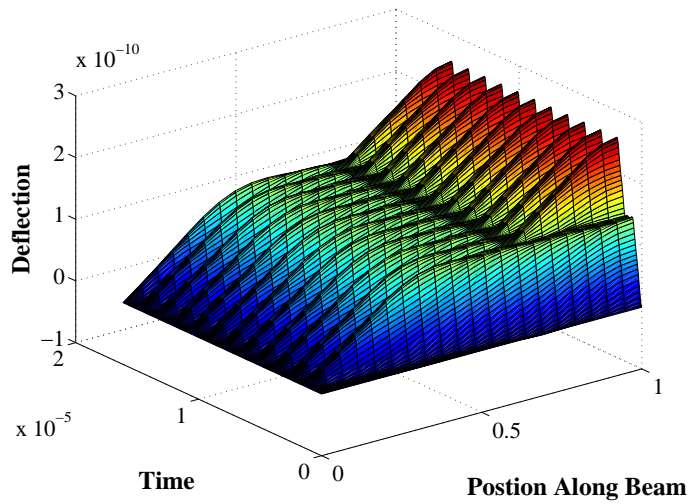
Figure A.29: UMZV Acceleration Response of Longitudinal Beam.

A.3.2 Longitudinal Beam with Mass

Like attaching an inertia to a torsional beam, affixing a mass to a longitudinal beam significantly alters the dynamics, primarily in the relationships between the natural frequencies. A longitudinal beam with an attached mass no longer has natural frequencies that are integer multiples of each other. This changes impact is significant when combined with traditional shapers. The results with and without modelling error will be studied for the beam. The analysis is the same as for the torsional case presented in Section 7.2.3 . Therefore only the figures are presented in this appendix.

A.3.2.1 Forced Response
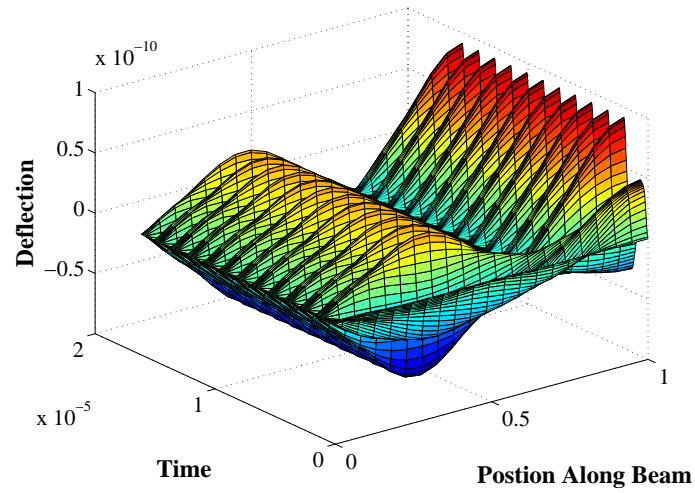
Figure A.30: Modes 2 through 5 UMZV Acceleration Response of Longitudinal Beam
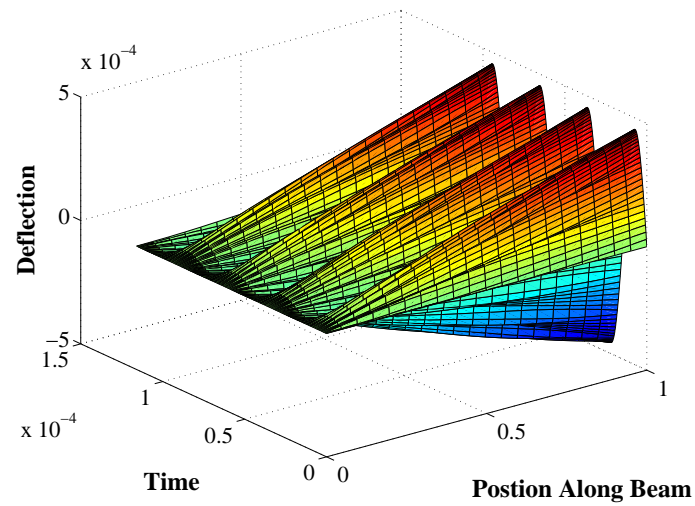
Figure A.31: Impulse Force Response of Longitudinal Beam with Attached Mass.

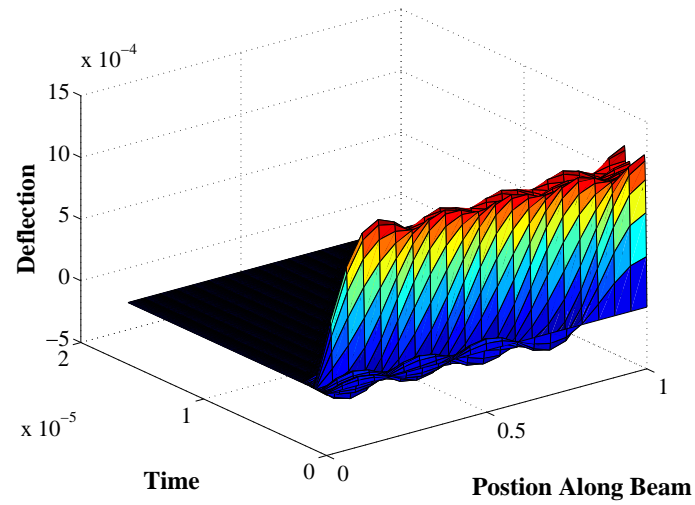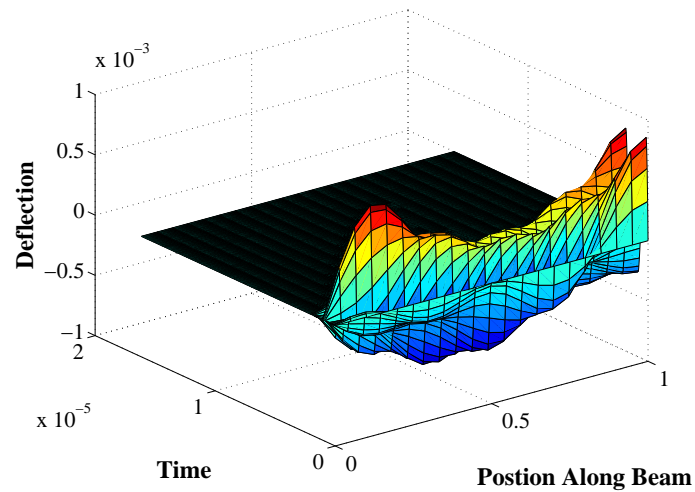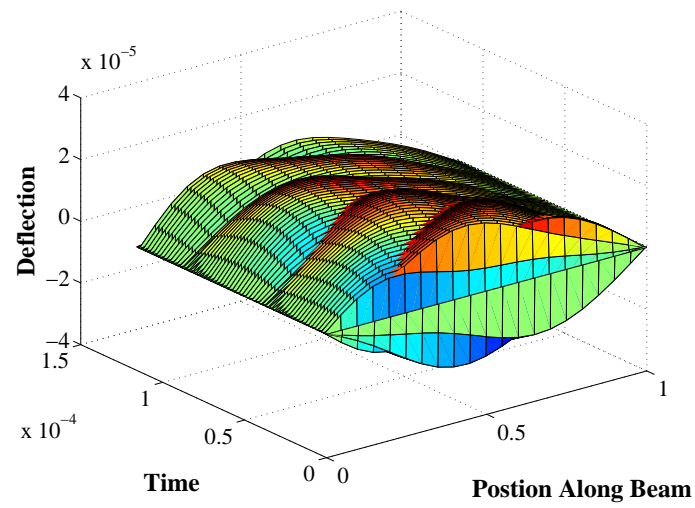**Figure A.32:** Modes 2 through 5 Impulse Force Response of Longitudinal Beam with Attached Mass.

A.3.2.2   Base Motion Response
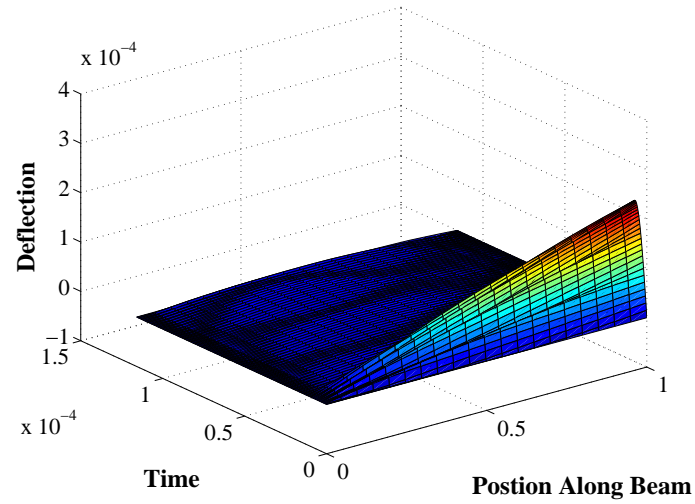
Figure A.33: Zero Vibration Force Response of Longitudinal Beam with Attached Mass.
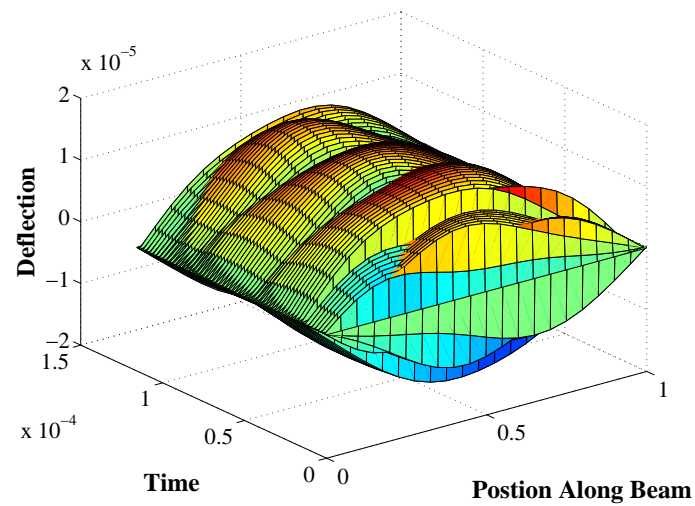
Figure A.34: Modes 2 through 5 ZV Force Response of Longitudinal Beam with Attached Mass.
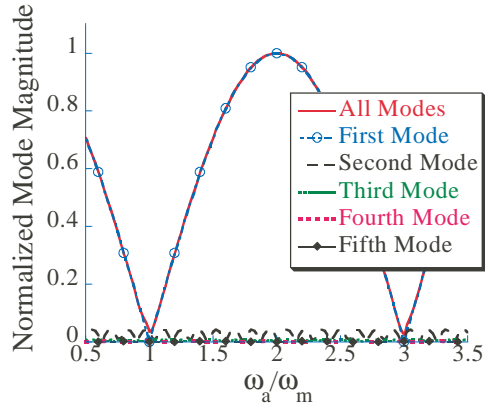
Figure A.35: Zero Vibration Sensitivity of Longitudinal Beam with Attached Mass.
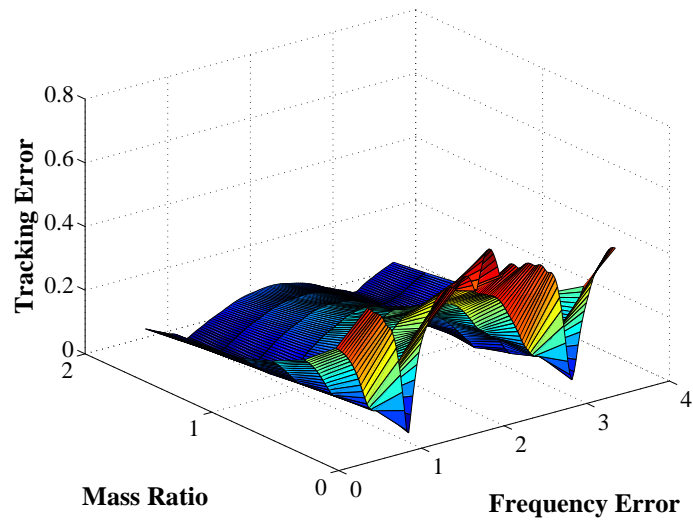
Figure A.36: ZV Sensitivity of Longitudinal Beam with Various Attached Masses.
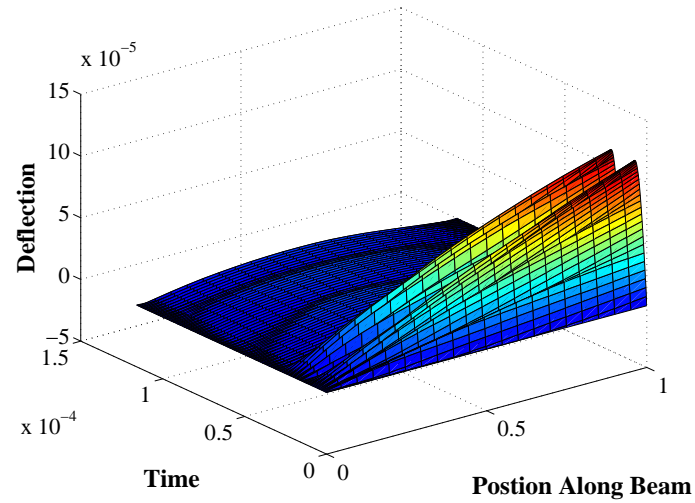
Figure A.37: Zero Vibration Derivative Force Response of Longitudinal Beam with Attached Mass.
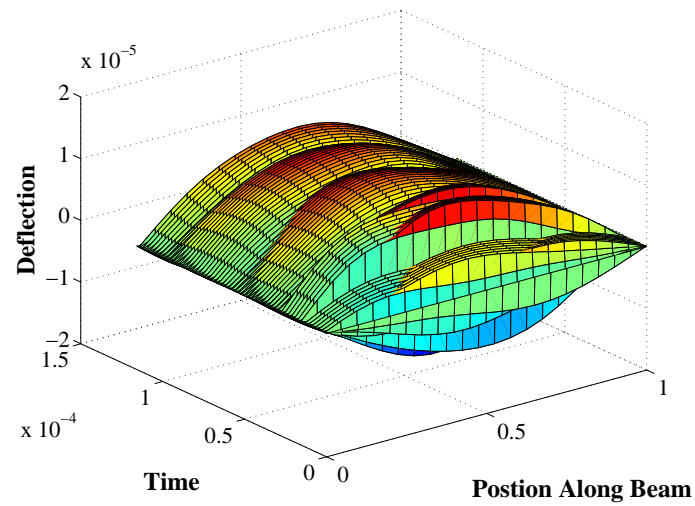
Figure A.38: Modes 2 through 5 ZVD Force Response of Longitudinal Beam with Attached Mass.
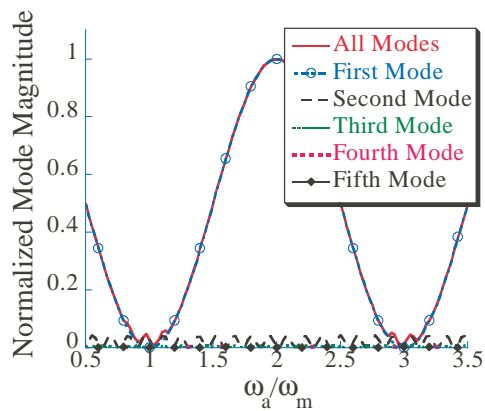
Figure A.39: Zero Vibration Derivative Sensitivity of Longitudinal Beam with Attached Mass.
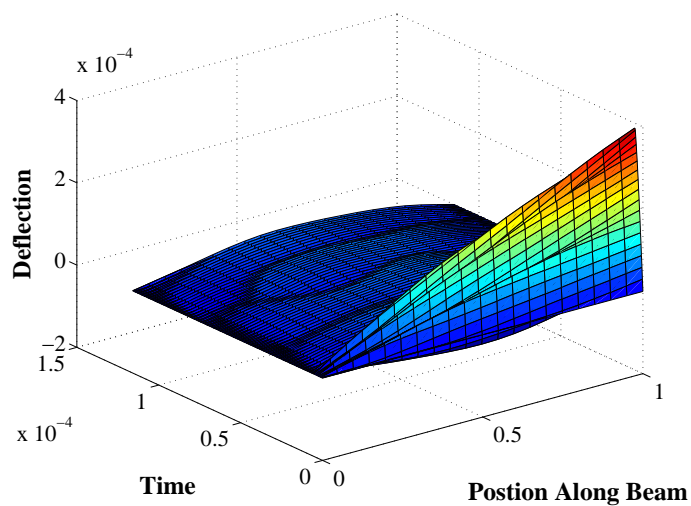
Figure A.40: UMZV Force Response of Longitudinal Beam with Attached Mass.
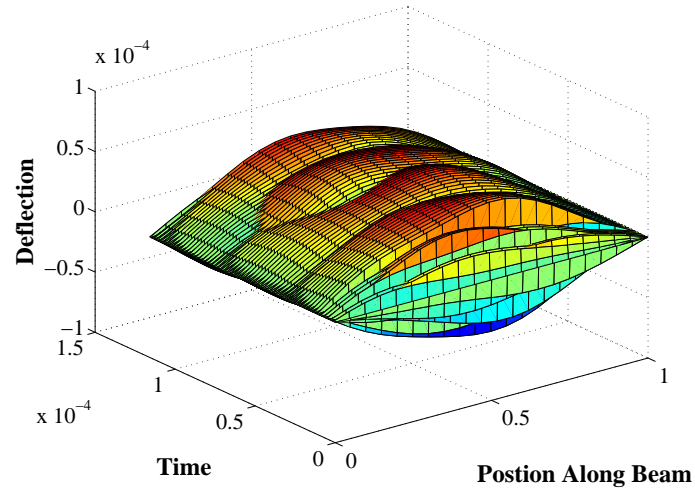
Figure A.41: Modes 2 through 5 UMZV Force Response of Longitudinal Beam with Attached Mass.
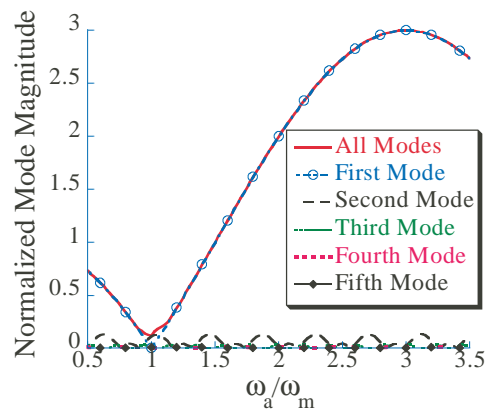
Figure A.42: UMZV Sensitivity of Longitudinal Beam with Attached Mass.
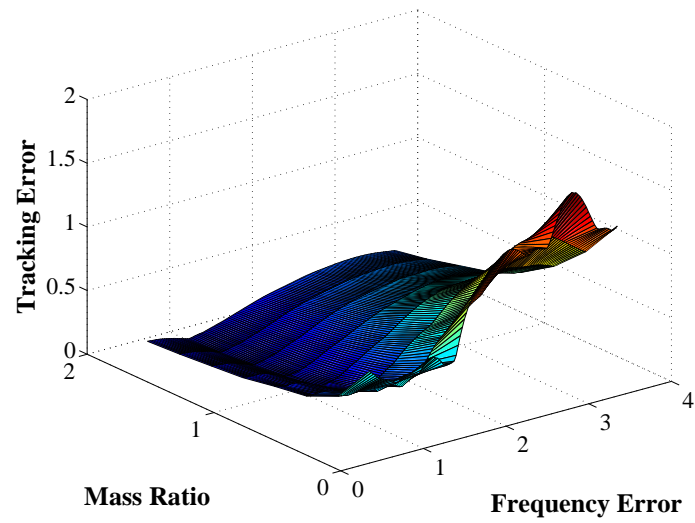
Figure A.43: UMZV Sensitivity of Longitudinal Beam with Various Attached Masses.
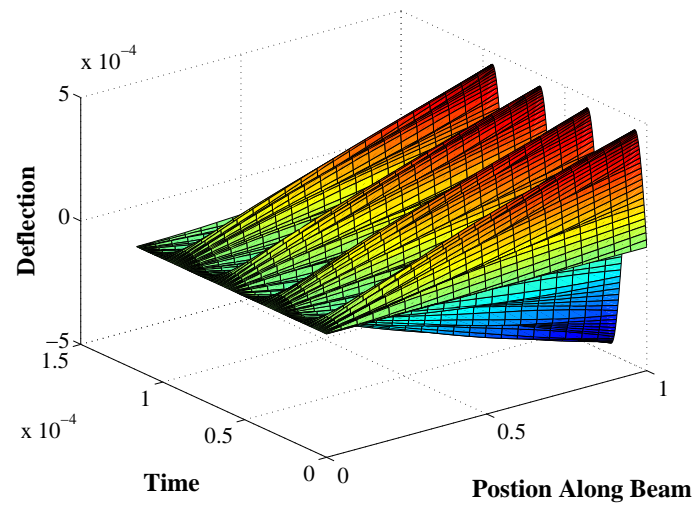
Figure A.44: Step Acceleration Response of Longitudinal Beam with Attached Mass.
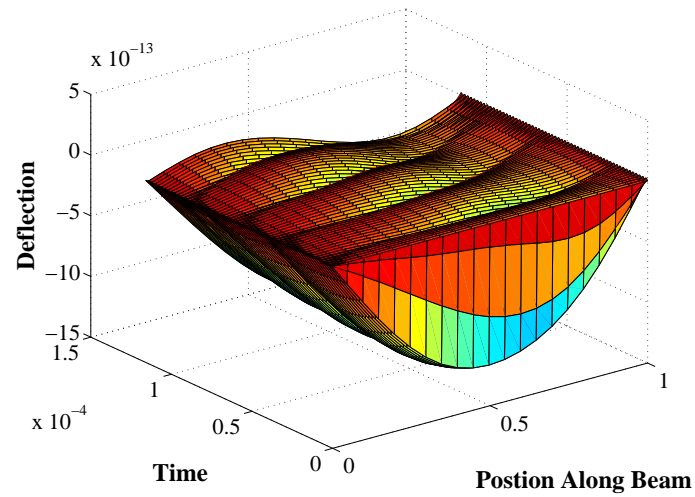
Figure A.45: Modes 2 through 5 Step Acceleration Response of Longitudinal Beam with Attached Mass.
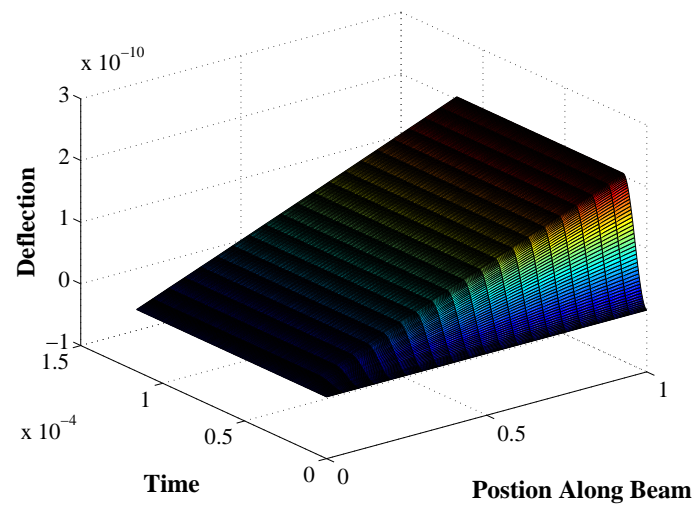
Figure A.46: Zero Vibration Acceleration Response of Longitudinal Beam with Attached Mass.
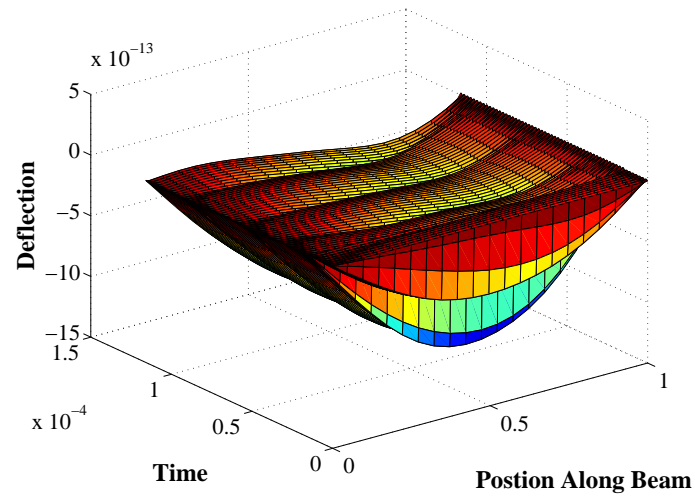
Figure A.47: Modes 2 through 5 ZV Acceleration Response of Longitudinal Beam with Attached Mass.
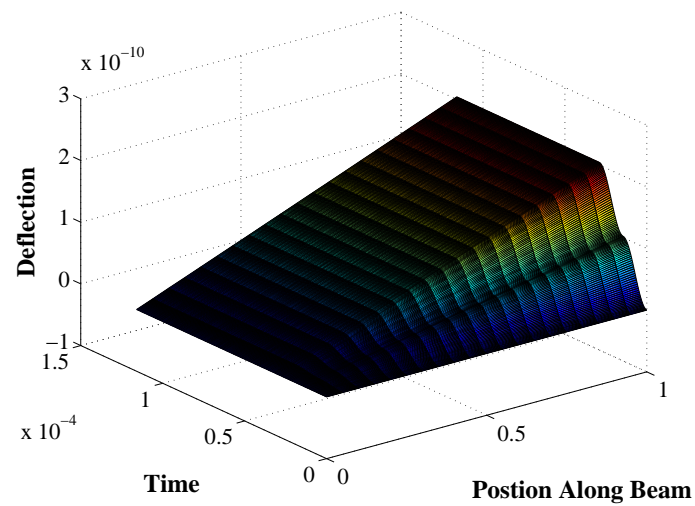
Figure A.48: Zero Vibration Derivative Acceleration Response of Longitudinal Beam with Attached Mass.
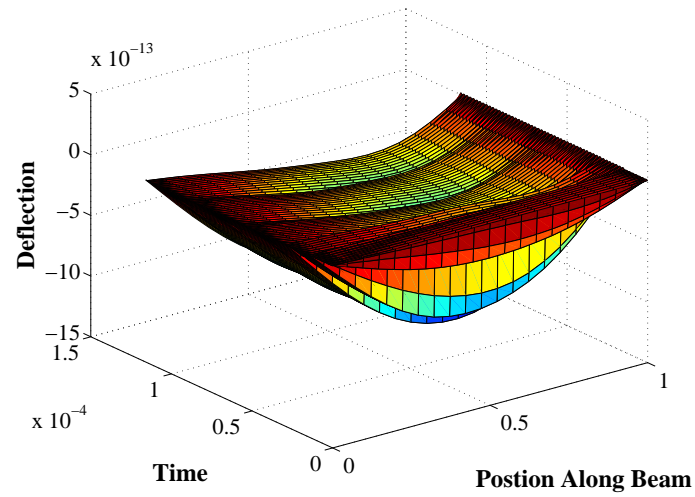
Figure A.49: Modes 2 through 5 ZVD Acceleration Response of Longitudinal Beam with Attached Mass.
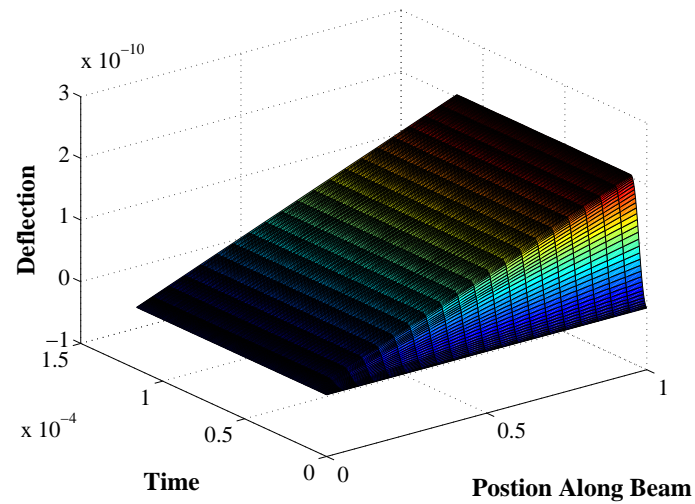
Figure A.50: UMZV Acceleration Response of Longitudinal Beam with Attached Mass.
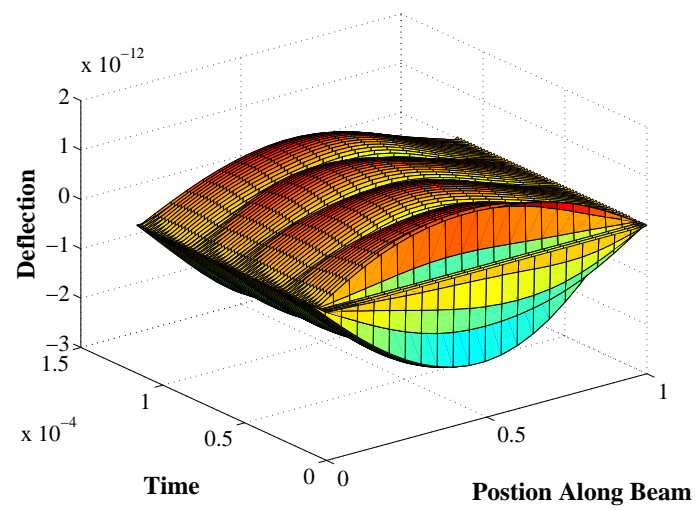
Figure A.51: Modes 2 through 5 UMZV Acceleration Response of Longitudinal Beam with Attached Mass

APPENDIX B

BEAM DESIGN

B.1 Longitudinal Beam Frequency Relationships
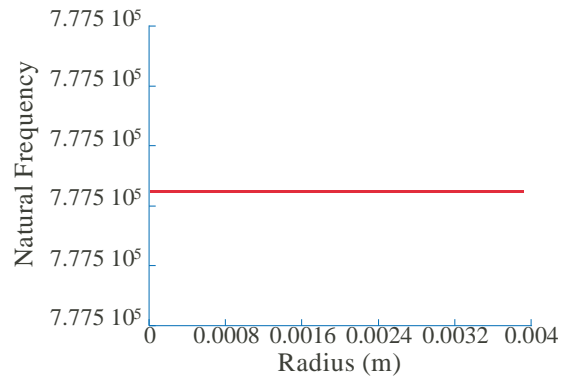
Figure B.1: Longitudinal Beam: Frequency Variation with Diameter.
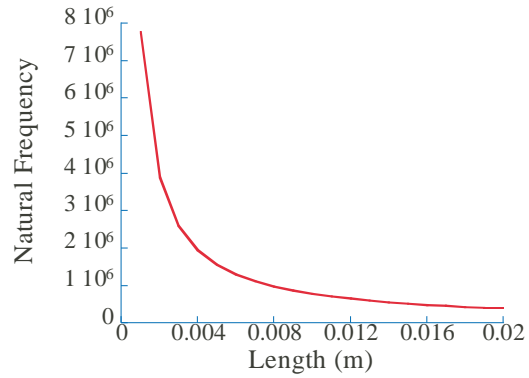
Figure B.2: Longitudinal Beam: Frequency Variation with Length.
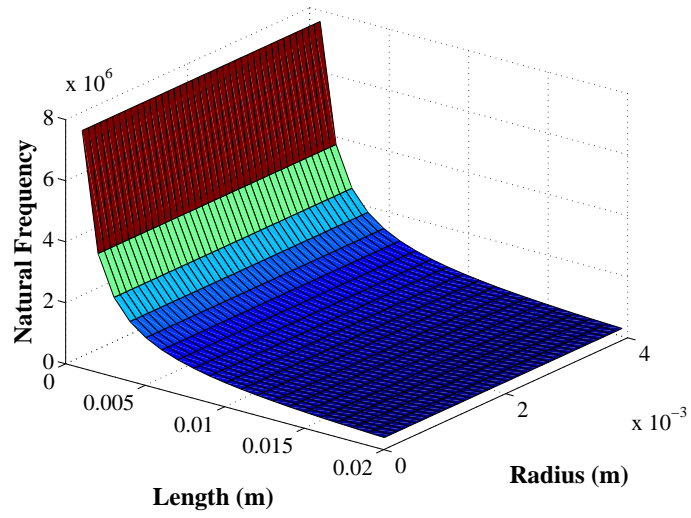
Figure B.3: Longitudinal Beam: Frequency Variation with Length and Diameter.
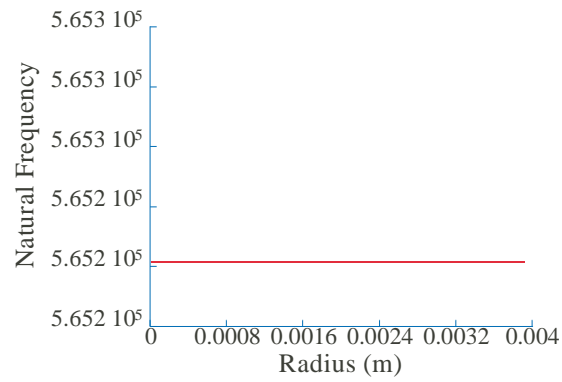
Figure B.4: Longitudinal Beam with Mass: Frequency Variation with Diameter.
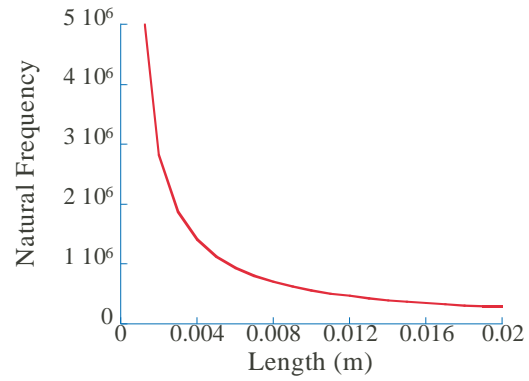
Figure B.5: Longitudinal Beam with Mass: Frequency Variation with Length.
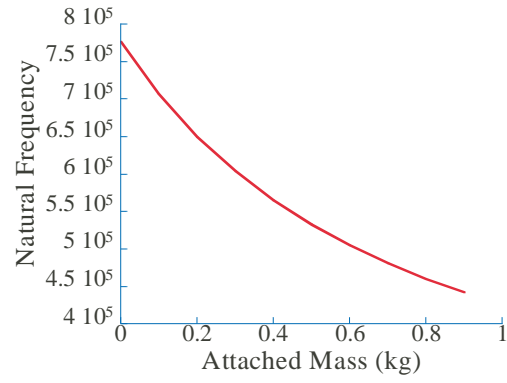
Figure B.6: Longitudinal Beam with Mass: Frequency Variation with Mass.
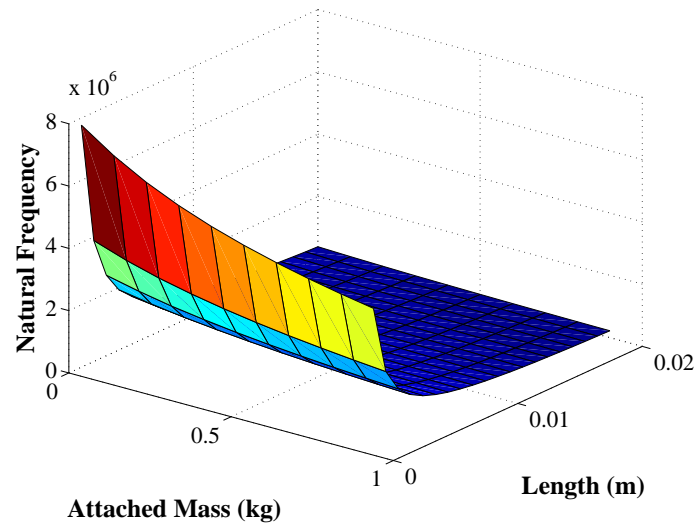
Figure B.7: Longitudinal Beam with Mass: Frequency Variation with Length and Mass.
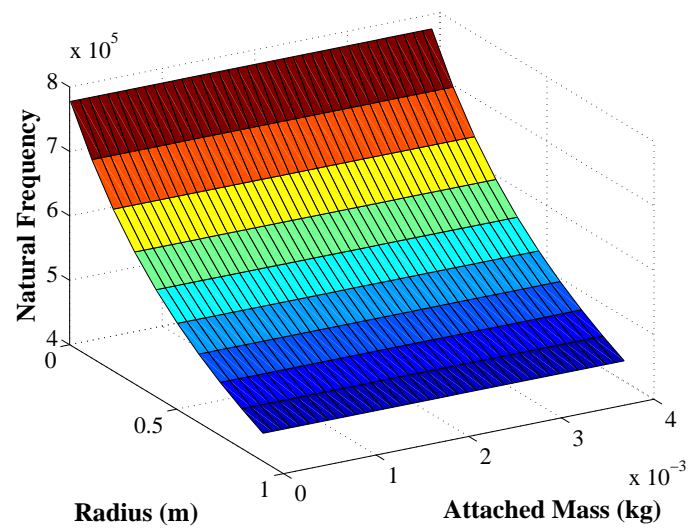
Figure B.8: Longitudinal Beam with Mass: Frequency Variation with Diameter and Mass.

REFERENCES

[1] ABE, M. and IGUSA, T., "Semi-active dynamic vibration absorbers for controlling transient response," *Journal of Sound and Vibration*, vol. 198, no. 5, pp. 547–569, 1996.

[2] ABRARIA, F., ELBESTAWI, M. A., and SPENCEA, A. D., "On the dynamics of ball end milling: modeling of cutting forces and stability analysis," *International Journal of Machine Tool Manufacture*, vol. 38, no. 3, pp. 215–237, 1998.

[3] ADHIKARI, S. and WOODHOOUSE, J., "Identification of damping: Part 1, viscous damping," *Journal of Sound and Vibration*, vol. 243, no. 1, pp. 43–61, 2001.

[4] ADHIKARI, S. and WOODHOOUSE, J., "Identification of damping: Part 2, non-viscous damping," *Journal of Sound and Vibration*, vol. 243, no. 1, pp. 63–68, 2001.

[5] AGRAWAL, A. K. and HE, W., "Control of seismically excited cable-stayed bridge using a resetting semi-active stiffness damper," in *American Control Conference*, (Arlington, VA), pp. 1103–1108, 2001.

[6] AGRAWAL, S. K. and POTA, H. R., "A flatness based approach to residual motion suppression of highrise elevators," in *American Control Conference*, (Philadelphia, PA), 1998.

[7] ALLI, H. and SINGH, T., "On the feedback control of the wave equation," *Journal of Sound and Vibration*, vol. 234, no. 4, pp. 625–640, 2000.

[8] ALTINAS, Y., *Manufacturing Automation: Metal Cutting Mechanics, Machine Tool Vibrations, and CNC Design.* New York: Cambridge University Press, 2000.

[9] ANDERSON, J., SEMERCIGIL, S. E., and TURAN, O. F., "A standing-wave-type sloshing absorber to control transient oscillations," *Journal of Sound and Vibration*, vol. 232, no. 5, pp. 839–856, 2000.

[10] ANDRESEN, U. and SINGHOSE, W., "A simple cam design procedure for automatic screw machines with flexible dynamics," in *Japan-USA Symp. on Flexible Automation*, (Hiroshima, Japan), 2002.

[11] ARMSTRONG-HELOUVRY, B., DUPONT, P., and CANUDAS DE WIT, C., "A survey of models, analysis tools and compensation methods for control of machines with friction," *Automatica*, vol. 30, no. 7, pp. 1083–1138, 1994.

[12] ASAMI, T., WAKASONO, T., KAMEOKA, K., HASEGAWA, M., and SEKIGUCHI, H., "Optimum design of dynamic absorbers for a system subjected to random excitation," *JSME International Journal*, vol. 34, no. 2, pp. 218–226, 1991.

[13] BALACHANDRAN, B., LI, Y.-Y., and FANG, C.-C., "A mechanical filter concept for control of non-linear crane-load oscillations," *Journal of Sound and Vibration*, vol. 228, no. 3, pp. 651–682, 1999.

[14] BALANDIN, D. V., BOLOTNIK, N. N., and PILKEY, W. D., *Optimal Protection From Impact, Shock, and Vibration.* Amsterdam: Gordon and Breach, 2001.

[15] BALANDIN, D., "Optimal vibration isolation of multi-mass elastic structure," in *American Controls Conference*, (San Diego California), 1999.

[16] BAO, W. Y. and TANSEL, I. N., "Modeling micro-end-milling operations. part i: analytical cutting force model," *International Journal of Machine Tools and Manufacture*, vol. 40, no. 15, pp. 2155–2173, 2000.

[17] BAO, W. Y. and TANSEL, I. N., "Modeling micro-end-milling operations. part iii: influence of tool wear," *International Journal of Machine Tools and Manufacture*, vol. 40, pp. 2193–2211, 2000.

[18] BAO, W. and TANSEL, I., "Modeling micro-end-milling operations. part ii:tool run-out," *International Journal of Machine Tools and Manufacture*, vol. 40, pp. 2175–2192, 2000.

[19] BARTEL, D. L. and KRAUTER, A. I., "Time domain optimization of a vibration absorber," *Transactions of the ASME, Journal of Engineering for Industry*, vol. 93, no. 3, pp. 799–804, 1971.

[20] BAUMGART, M. and PAO, L. Y., "Cooperative multi-input shaping for arbitrary inputs," in *American Control Conference*, (Arlington, VA), 2001.

[21] BAUMGART, M. and PAO, L. Y., "Discrete time-optimal command shapers and controls for multi-input multi-output systems," in *American Control Conference*, vol. 3, (Anchorage, AK), 2002.

[22] BELDIMAN, O. V., WANG, H. O., and BUSHNELL, L. G., "Trajectory generation of high-rise/high-speed elevators," in *American Control Conference*, (Philadelphia, PA), 1998.

[23] BELVIN, W. K. and PARK, K. C., "Structural tailoring and feedback control synthesis: An interdisciplinary approach," *Journal of Guidance, Control, Dynamics*, vol. 13, no. 3, pp. 424–429, 1990.

[24] BHAT, B. R. and WAGNER, H., "Natural frequencies of a uniform cantilever with a tip mass slender in the axial direction," *Journal of Sound and Vibration*, vol. 45, no. 2, pp. 304–307, 1976.

[25] BHAT, S. P. and MIU, D. K., "Point-to-point positioning of flexible structures using a time domain lqr smoothness constraint," *J. of Dynamic Sys., Meas., and Control*, vol. 114, pp. 416–421, 1992.

[26] BHAT, S. P., TANAKA, M., and MIU, D. K., "Experiments on point-to-point position control of a flexible beam using laplace transform technique-part 1: Open-loop," *Journal of Dynamic Systems, Measurement, and Control*, vol. 113, pp. 432–437, 1991.

[27] BHAT, S. P. and MIU, D. K., "Precise point-to-point positioning control of flexible structures," *J. of Dynamic Sys., Meas., and Control*, vol. 112, no. 4, pp. 667–674, 1990.

[28] BIANCHI, G., PAOLUCCI, F., VAN DEN BRAEMBUSSCHE, P., and VAN BRUSSEL, H., "Towards virtual engineering in machine tool design," *Annals of the CIRP*, vol. 45, no. 1, pp. 381–384, 1996.

[29] BIEDIGER, E. A. O., *Vibration Reduction Using Command Generation in Formation Flying Satellites.* Phd., Georgia Institute of Technology, 2005.

[30] BLACKWOOD, G. H. and VON FLOTOW, A. H., "Active control for vibration isolation despite resonant structural dynamics: A trade study of sensors, actuators and configurations," in *Recent Advances in Active Control of Sound and Vibration*, Blacksburg VA: Virginia Polytechnic Insitute, 1993.

[31] BOE, F. and HANNAFORD, B., "On-line improvement of speed and tracking performance on repetetive paths," *IEEE Transactions on Control Systems Technology*, vol. 6, no. 3, pp. 350–358, 1998.

[32] BOHEZ, E. L. J., "Five-axis milling machine tool kinematic chain design and analysis," *International Journal of Machine Tools and Manufacture*, vol. 42, pp. 505–520, 2002.

[33] BOOK, W. J., "Controlled motion in an elastic world," *Journal of Dynamic Systems, Measurement, and Control*, vol. 115, p. 252261, 1993.

[34] BRACKETT, L. C., DENOYER, K., JACOBS, J., and DAVIS, T., "Miniature vibration isolation system (mvis)," in *IEEE Aerospace Conference*, vol. 4, pp. 335–344, 2000.

[35] BROGAN, J., FORTGANG, J., and SINGHOSE, W., "Experimental verification of vibration absorbers combined with input shaping for oscillatory systems," in *American Controls Conference*, (Denver, CO), 2003.

[36] CARR, J. W. and FEGER, C., "Ultraprecision machining of polymers," *Precision Engineering*, vol. 15, no. 4, pp. 221–237, 1993.

[37] CARRILLO, F., HADDOUCHE, K., and ROTELLA, F., "Hybrid real time adaptive pid control system for turning," in *IEEE International Conference on Control Applications*, (Dearborn, MI), 1996.

[38] CASELLA, F., LOCATELLI, A., and SCHIAVONI, N., "Modeling and control for vibration suppresion in large flexible structure with jet thrusters and piezoactuators," *IEEE Transactions on Control Systems Technology*, vol. 10, no. 4, pp. 589–599, 2002.

[39] CHANG, S. B., WU, S. H., and HU, Y. C., "Submicrometer overshoot control of rapid and precise positioning," *Precision Engineering*, vol. 20, pp. 161–170, 1997.

[40] CHAO, C.-P. and SHAW, S. W., "The effects of imperfections on the performance of the subharmonic vibration absorber system," *Journal of Sound and Vibration*, vol. 215, no. 5, pp. 1065–1099, 1998.

[41] CHAO, C.-P. and SHAW, S. W., "The dynamics respose of multiple pairs of subharmonic torsional vibration absorbers," *Journal of Sound and Vibration*, vol. 231, no. 2, pp. 411–431, 2000.

[42] CHAO, C.-P., SHAW, S., and LEE, C.-T., "Stability of the unison response for a rotating system with multiple tautochronic pendulum vibration absorbers," *Journal of Applied Mechanics*, vol. 64, no. March, pp. 149–156, 1997.

[43] CHEN, T.-Y., WEI, W.-J., and TSAI, J.-C., "Optimum design of headstocks of precision lathes," *International Journal of Machine Tools and Manufacture*, vol. 39, pp. 1961–1977, 1999.

[44] CHEN, Y.-Y., HUANG, P.-Y., and YEN, J.-Y., "Frequency-domain algorithms for servo systems with friction," *IEEE Transactions on Control Systems Technology*, vol. 10, no. 5, pp. 654–665, 2002.

[45] CHEN, Z., VICKERS, G. W., and DONG, Z., "A new principle of cnc tool path planning for three-axis sculptured part machining -a steepest-ascending tool path," *Journal of Manufacturing Science and Engineering*, vol. 126, pp. 515–523, 2004.

[46] CHEUNG, C. and LEE, W. B., "A multi-spectrum analysis of surface roughness formation in ultra-precision machining," *Precision Engineering*, vol. 24, pp. 77–87, 2000.

[47] CHEW, M.; CHUANG, C., "Minimizing residual vibration in high-speed cam-follower systems over a range of speeds," *Transactions of ASME*, vol. 117, no. March, pp. 166–172, 1995.

[48] CHOI, I.-H. and KIM, J.-D., "Development of monitoring system on the diamond tool wear," *International Journal of Machine Tools and Manufacture*, vol. 39, pp. 505–515, 1999.

[49] CREDE, C. E., *Vibration and Shock Isolation*. New York: John Wiley and Sons, 1951.

[50] CREDE, C. E., *Shock and Vibration Concepts in Engineering Design*. Englewood Cliffs, NJ: Prentice-Hall, 1965.

[51] CUBALCHINI, R., "Technology and design needs for precision pointing systems," in *IEEE Conference on Descision and Control*, (New Orleans, LA), pp. 162–767, 1995.

[52] CUSIMANO, G., "A procedure for a suitable selection of laws of motion and electric drive systems under inertia loads.," *Mechanism and Machine Theory*, vol. 38, pp. 519–533, 2003.

[53] CUVALCI, O., "The effect of detuning parameters on the absorption region for a coupled system: a numerical and experimental study," *Journal of Sound and Vibration*, vol. 229, no. 4, pp. 837–857, 2000.

[54] DEQUIDT, A., CASTELAIN, J.-M., and VALDES, E., "Mechanical pre-design of high performance motion servomechanism," *Mechanism and Machine Theory*, vol. 35, pp. 1047–1063, 2000.

[55] DEWEY, J. S., LEANG, K., and DEVASIA, S., "Experimeintal and theoretical results in output-trajectory redesign for flexible structures," *Journal of Dynamic Systems, Measurement, and Control*, vol. 120, pp. 456–461, 1998.

[56] DICKENS, J. D., "Dynamic model of vibration isolator under static load," *Journal of Sound and Vibration*, vol. 236, no. 2, pp. 323–337, 2000.

[57] DICKENS, J. D. and NORWOOD, C. J., "Universal method to measure dynamic performance of vibration isolators under static load," *Journal of Sound and Vibration*, vol. 244, no. 4, pp. 685–696, 2001.

[58] DOHDA, K., NI, J., and ROOIJ, N. D., "Micro/meso-scale manufacturing," *Journal of Manufacturing Science and Engineering*, vol. 126, p. 641, 2004.

[59] DOW, T., MILLER, E., and GARRARD, K., "Tool force and deflection compensation for small milling tools," *Precision Engineering*, vol. 28, pp. 31–45, 2004.

[60] DRAPEAU, V. and WANG, D., "Verification of a closed-loop shaped-input controller for a five-bar-linkage manipulator," in *IEEE Int. Conf. on Robotics and Automation*, vol. 3, (Atlanta, GA), pp. 216–221, IEEE, 1993.

[61] DRESNER, T. L. and BARKAN, P., "New methods for the dynamic analysis of flexible single-input and multi-input cam-follower systems," *Transactions of the ASME*, vol. 117, no. March, pp. 150–155, 1995.

[62] EASTEP, F., KHOT, N. S., and GRANDHI, R., "Improving the active vibrational control of large space structures through structural modifications," *Acta Astronautica*, vol. 15, no. 6/7, pp. 383–389, 1987.

[63] EDHI, E. and HOSHI, T., "Stability of high frequency machining vibration by extened chatter model," *Precision Engineering*, vol. 26, pp. 204–213, 2002.

[64] EHMANN, K. F., DEVOR, R. E., and KAPOOR, S. G., "Micro/meso-scale mechanical manufacturing -opportunities and challenges-," in *SME/ASME International Conferencer on Materials and Processing*, vol. 1, (Honolulu, HI), pp. 6–13, 2002.

[65] ELOUNDOU, R. and SINGHOSE, W., "Interpretation of smooth reference commands as input-shaped function," in *American Controls Conference*, (Anchorage, AK), 2002.

[66] ELOUNDOU, R. and SINGHOSE, W., "Justification for using step-function reference commands: Comparison to s-curves," in *2nd IFAC on Mechatronic Systems*, (Berkeley, CA), 2002.

[67] ELWANY, M. H. S. and BARR, A. D. S., "Optimal design of beams under flexural vibration," *Journal of Sound and Vibration*, vol. 88, no. 2, pp. 175–195, 1983.

[68] EMA, S. and MARUI, E., "Suppression of chatter vibration in drilling," *Journal of Manufacturing Science and Engineering*, vol. 120, pp. 200–202, 1998.

[69] EMA, S. and MARUI, E., "Suppression of chatter vibration of boring tools using impact dampers," *International Journal of Machine Tools and Manufacture*, vol. 40, pp. 1141–1156, 2000.

[70] ERKORKMAZ, K. and ALTINTAS, Y., "High speed cnc system design. part i: Jerk limited trajectory generation and quintic spline interpolation," *International Journal of Machine Tools and Manufacture*, vol. 41, pp. 1323–1345, 2001.

[71] ERKORKMAZ, K. and ALTINTAS, Y., "High speed cnc system design. part ii: Modeling and indentification of feed drives," *International Journal of Machine Tools and Manufacture*, vol. 41, pp. 1487–1509, 2001.

[72] ESKICIOGLU, H., AKKOK, M., and YILDIZ, O. H., "Computer aided selection of machine tool spindle and bearing arrangements," *PD Vol. 64-8.1, Engineering Systems Design and Analysis, ASME*, vol. 8, no. Part A, pp. 181–187, 1994.

[73] FARDANESH, B. and RASTEGAR, J., "A new model-based tracking controller for robot manipulators using trajectory pattern inverse dynamics," *IEEE Trans. on Robotics and Automation*, vol. 8, no. 2, pp. 279–285, 1992.

[74] FEDDEMA, J. T., "Digital filter control of remotely operated flexible robotic structures," in *American Control Conf.*, vol. 3, (San Francisco, CA), pp. 2710–2715, ACC, 1993.

[75] FEINERMAN, A. D., LAJOS, R. E., WHITE, V., and DENTON, D. D., "X-ray lathe: An x-ray lithographic exposure tool for nonplanar objects," *Journal of Microelectromechanical Systems*, vol. 5, no. 4, pp. 250–255, 1996.

[76] FENG, H.-Y. and MENQ, C.-H., "A flexible ball-end milling system model for cutting force and machining error prediction," *Journal of Manufacturing Science and Engineering*, vol. 118, pp. 461–469, 1996.

[77] FERRETTI, G., MAGNANI, G., and RIO, A. Z., "Impact modeling and control for industrial manipulators," *IEEE Control Systems Magazine*, vol. 18, no. 4, pp. 65–71, 1998.

[78] FILIPOVIC, D. and OLGAC, N., "Torsional delayed resonator with velocity feedback," *IEEE/ASME Transactions on Mechatronics*, vol. 3, no. 1, pp. 67–72, 1998.

[79] FORTGANG, J., MARQUEZ, J., and SINGHOSE, W., "Application of command shaping on micro-mills," in *2004 Japan-USA Flexible Symposium on Automation*, (Denver, CO), 2004.

[80] FORTGANG, J. and SINGHOSE, W., "Input shaping for continuum beams under longitudinal vibration," in *IEEE/ASME International Conference on Advanced Intelligent Mechatronics*, (Monterey, California), 2005.

[81] FORTGANG, J., SINGHOSE, W., MARQUEZ, J., and PEREZ, H., "Command shaping for micro-mills and cnc controllers," in *American Controls Conference*, (Portland, Oregon), 2005.

[82] FORTGANG, J., "Concurrent design of input shaping and vibration absorbers," tech. rep., Georgia Institute of Technology, 2002.

[83] FORTGANG, J., PATRANGENARU, V., and SINGHOSE, W., "Scheduling of input shaping and transient vibration absorbers for high-rise elevators," in *16th IFAC World Congress*, (Prague, Czech Republic), 2005.

[84] FORTGANG, J. and SINGHOSE, W., "The combined use of input shaping and nonlinear vibration absorbers," in *5th IFAC Symposium on Nonlinear Control*, (Saint-Petersburg, Russia), 2001.

[85] FORTGANG, J. and SINGHOSE, W., "Design of vibration absorbers for step motions and step disturbances," in *ASME 2001 DETC*, (Pittsburg, Pennsylvania), 2001.

[86] FORTGANG, J. and SINGHOSE, W., "Concurrent design of input shaping and vibration absorbers," in *American Control Conference*, (Anchorage, Alaska), 2002.

[87] FORTGANG, J. and SINGHOSE, W., "Concurrent design of vibration absorbers and input shaping," *Accepted to the Journal of Dynamic Systems, Measurement, and Control*, 2004.

[88] FORTGANG, J. and SINGHOSE, W., "Improving trajectory following by controlling internal deflections through input shaping," in *MOVIC 2004 (Motion and Vibration Control)*, (St. Louis), 2004.

[89] FORTGANG, J. and SINGHOSE, W., "Design of vibration absorbers for step motions and step disturbances," *Journal of Mechanical Design*, vol. 127, no. 1, pp. 160–163, 2005.

[90] FRAHAM, H., "Device for damping vibration in bodies," April 18, 1911 1911.

[91] FRAKES, D., GROSSER, K., FORTGANG, J., and SINGHOSE, W., "Simulating motion of an operator-controlled gantry crane in a cluttered work environment," in *2000 International Mechanical Congress and Exposition*, (Orlando, FL), 2000.

[92] FRANKLIN, G. F., POWELL, J. D., and EMAMI-NAEINI, A., *Feedback control of Dynamic Systems*. New York: Addison-Wesley Publishing Group, 3rd ed., 1995.

[93] FRANSE, J., ROBLEE, J. W., and MODEMANN, K., "Dynamic characteristics of the lawrence livermore national laboratory precision engineering research lathe," *Precision Engineering*, vol. 13, no. 3, pp. 196–202, 1991.

[94] FRIEDRICH, C. R., COANE, P., GOETTERT, J., and GOPINATHIN, N., "Direct fabrication of deep x-ray lithography masks by micromechanical milling," *Precision Engineering*, vol. 22, pp. 164–173, 1998.

[95] FRIEDRICH, C. R. and VASILE, M. J., "Development of the micromilling process for high-aspect-ratio microstructures," *Journal of Microelectromechanical Systems*, vol. 5, no. 1, pp. 33–38, 1996.

[96] FUH, K.-H. and HWANG, R.-M., "A predicted milling force model for high-speed end milling operations," *International Journal of Machine Tool Manufacture*, vol. 37, no. 7, pp. 969–979, 1997.

[97] FUTAMI, S., FURUTANI, A., and YOSHIDA, S., "Nanometer positioning and its microdynamics," *Nanotechnology*, vol. 1, pp. 31–37, 1990.

[98] GARDONIO, P. and ELLIOTT, S. J., "Passive and active isolation of structural vibration transmission between two plates connected by a set of mounts.," *Journal of Sound and Vibration*, vol. 273, no. 3, pp. 483–511, 2000.

[99] GEORGE, L., FORTGANG, J., and BOOK, W. J., "Practical implementation of a dead zone inverse on a hydraulic wrist," in *ASME Mechanical Engineering Conference*, (New Orleans, LA), 2002.

[100] GOEL, R. P., "Transverse vibrations of tapered beams," *Journal of Sound and Vibration*, vol. 47, no. 1, pp. 1–7, 1976.

[101] GONG, Y. and EHMANN, K. F., "Mechanistic model for dynamic forces in micro-drilling," in *ASME International Mechanical Engineering Congress and Exposition*, (New York, NY), 2001.

[102] GONSALVES, D., NEILSON, R., and BARR, A., "The dynamics of a non-linear vibration absorber," *Procedings of the Institution of Mechanical Engineers. Journal of Mechanical Engineering Science*, vol. 207, no. C6, pp. 363–374, 1993.

[103] GROSSER, K., FORTGANG, J., and SINGHOSE, W., "Limiting high mode vibration and rise time in flexible telerobotic arms," in *Conf. on Systems, Cybernetics, and Informatics*, (Orlando, FL), 2000.

[104] GROSSER, K. and SINGHOSE, W., "Command generation for flexible telerobtic arms," in *International Symposium on Motion and Vibration Control in Mechatronics*, (Tokyo, Japan), pp. 51–56, 1999.

[105] GU, U. C. and CHENG, C. C., "Vibration analysis of a high-speed spindle under the action of a moving mass," *Journal of Sound and Vibration*, vol. 278, pp. 1131–1146, 2004.

[106] GURGOZE, M., "Proportionally damped systems subjected to damping modifications by several viscous dampers," *Journal of Sound and Vibration*, vol. 255, no. 2, pp. 407–412, 2002.

[107] HABER, R. and ALIQUE, J., "Nonlinear internal model control using neural networks: an application for machining processes," *Neural Computing and Applications*, vol. 13, no. 1, pp. 47–55, 2004.

[108] HAENER, J., "Formulas for the frequencies including higher frequencies of uniform cantilever and free-free beams with additional masses at the ends," *Journal of Applied Mechanics*, vol. September, 1958, p. 412, 1958.

[109] HAHN, R., "Design of lanchester damper for elimination of metal-cutting chatter," *Transactions of the ASME*, vol. 73, pp. 331–335, 1951.

[110] HALE, A. L., LISOWSKI, R. J., and DAHL, W. E., "Optimal simultaneous structual control design of maneuvering flexible spacecraft," *Journal of Guidance, Control, Dynamics*, vol. 8, no. 1, pp. 86–93, 1985.

[111] HARTOG, J. P. D., *Mechanical Vibrations*. New York: Dover Publications, Inc., 1985.

[112] HASKEW, T. A. and SCHINSTOCK, D. E., "Optimal design of electromechanical actuators for active loads," *IEEE/ASME Transactions on Mechatronics*, vol. 3, no. 2, pp. 129–137, 1998.

[113] HITCHCOCK, P., GLANVILLE, M., KWOK, K., WATKINS, R., and SAMALI, B., "Damping properties and wind-induced response of a steel frame tower fitted with liquid column vibration absorbers," *Journal of Wind Engineering and Industrial Aerodynamics*, vol. 83, pp. 183–196, 1999.

[114] HONDA, H., OHKAWA, F., HAGIHARA, J., and OGURO, R., "A positioning control for serial twin linear sliders with linear motor drives," in *Japan-USA Symposium on Flexible Automation*, (Denver, CO), 2004.

[115] HONG, J.-P., HA, K.-H., and LEE, J., "Stator pole and yoke design for vibration reduction of switched reluctance motor," *IEEE Transactions on Magnetics*, vol. 38, no. 2, pp. 929–932, 2002.

[116] HOSEK, M., OLGAC, N., and ELMALI, H., "Torsional vibration control of mdof systems using the centrifugal delayed resonator," in *IEEE Int. Conf. on Control Applications*, (Hartford, CT), 1997.

[117] HOUSNER, G. W. and KEIGHTLEY, W. O., "Vibrations of linearly tapered cantilever beams," *Journal of the Engineering Mechanics Division*, vol. April, 1962, 1962.

[118] HSUEH, W.-J., "Analysis of vibration isolation systems using a graph model," *Journal of Sound and Vibration*, vol. 216, no. 3, pp. 399–412, 1998.

[119] HSUEH, W.-J., "Vibration transmillibility of a unidirectional multi-degree-of-freedom system with multiple dynamic absorbers," *Journal of Sound and Vibration*, vol. 229, no. 4, pp. 793–805, 2000.

[120] HUEY, J. and SINGHOSE, W., "The application of input shaping to wire-driven mechanisms," in *6th International Conference on Motion and Vibration Control*, (Saitama, Japan), 2002.

[121] HUEY, J. and SINGHOSE, W., "Effect of vertical acceleration on the frequency of a pendulum: Inpact on input shaping," in *IEEE Conference on Control Applications*, (Istanbul, Turkey), 2003.

[122] HUNT, J. B., *Dynamic Vibration Absorbers*. London: Mech. Eng. Publications LTD, 1979.

[123] HYDE, J. M. and SEERING, W. P., "Using input command pre-shaping to suppress multiple mode vibration," in *IEEE Int. Conf. on Robotics and Automation*, vol. 3, (Sacramento, CA), pp. 2604–2609, IEEE, 1991.

[124] IKAWA, N., DONALDSON, R., KOMANDURI, R., KONIG, W., AACHEN, T., MCKEOWN, P., MORIWAKI, T., and STOWERS, I., "Ultraprecision metal cutting - the past, the present and the future," *Annals of the CIRP*, vol. 40, no. 2, pp. 587–594, 1991.

[125] IKENAGA, S., LEWIS, F. L., DAVIS, L., CAMPOS, J., EVANS, M., and SCULLY, S., "Active suspension control using a novel strut and active filtered feedback: Design and implementation," in *1999 IEEE International Conference on Control Applications*, (Kohala Coast, HI), pp. 1502–1508, 1999.

[126] IKUA, B. W., TANAKA, H., OBATA, F., and SAKAMOTO, S., "Prediction of cutting forces and maching error in ball end milling of curved surfaces -i theoretical analysis," *Precision Engineering*, vol. 25, pp. 266–273, 2001.

[127] IMAMURA, F. and KAUFMAN, H., "Time optimal contour tracking for machine tool controllers," *IEEE Control System*, pp. 11–17, 1991.

[128] INMAN, D. J., *Engineering Vibrations*. Upper Saddle River, New Jersey: Prentice Hall, 2 ed., 2001.

[129] ISHKAWA, Y. and KITAHARA, T., "Present and future of micromechatronics," in *International Symposium on Micromechatronics and Human Science*, 1997.

[130] ISMAIL, F. and BASTAMI, A., "Improving stability of slender end mills againts chatter," *Journal of Engineering for Industry*, vol. 108, pp. 264–268, 1986.

[131] JANGID, R., "Optimum damping in a non-linear base isolation system," *Journal of Sound and Vibration*, vol. 189, no. 4, pp. 477–487, 1996.

[132] JOHNSON, C. D., "Design of passive damping systems," *Journal of Mechanical Design*, vol. 117, pp. 171–176, 1995.

[133] JONES, S. and ULSOY, A., "An approach to control input shaping with application to coordinate measuring machines," *J. of Dynamics, Measurement and Control*, vol. 121, no. June, pp. 242–247, 1999.

[134] KANE, T. R., RYAN, R. R., and BANERJEE, A. K., "Dynamics of a cantilever beam attached to a moving base," *Journal of Guidance, Control, Dynamics*, vol. 10, no. 2, pp. 139–151, 1987.

[135] KARNOPP, D., "Active and semi-active vibration isolation," *Journal of Mechanical Design*, vol. 117, pp. 177–185, 1995.

[136] KARNOVSKY, I. A. and LEBED, O. I., *Formulas for structural dynamics : tables, graphs and solutions*. London: McGraw-Hill, 2000.

[137] KAWAI, T., SAWADA, K., and TAKEUCHI, Y., "Ultra-precision micro structuring by means of mechanical machining," in *International Conference on MEMS*, pp. 22 –25, 2001.

[138] KENISON, M. and SINGHOSE, W., "Concurrent design of input shaping and feedback control for insensitivity to parameter variations," in *6th International Workshop on Advanced Motion Control*, (Nagoya, Japan), 2000.

[139] KENISON, M. and SINGHOSE, W., "Concurrent design of input shaping and proportional plus derivative feedback control," *ASME J. of Dynamic Systems, Measurement, and Control*, vol. 124, no. 3, pp. 398–405, 2002.

[140] KHOT, N. S., "Structural/control optimization to improve the dynamic response of space structures," *Computational Mechanics*, vol. 3, pp. 179–186, 1988.

[141] KHOT, N. S. and ABHYANKAR, N. S., "Integrated optimum structural and control design," in *Structural optimization : status and promise* (KAMAT, M. P., ed.), vol. 150, pp. 743–767, Washington, DC: American Institute of Aeronautics and Astronautics, 1993.

[142] KHOT, N. S., VENKAYYA, V., and EASTEP, F., "Optimal structral modifications to enhance the active vibration control of flexible structures," *AIAA Journal*, vol. 24, no. 8, pp. 1368–1373, 1986.

[143] KIM, C.-J., J, R. M., and NI, J., "A static model of chip formation in microscale milling," *Journal of Manufacturing Science and Engineering*, vol. 126, pp. 710–718, 2004.

[144] KIM, J.-D. and KIM, D.-S., "Development of a combined-type tool dynamoter witha piezo-film accelerometer for an ultra-precision lathe," *Journal of Materials Processing Technology*, vol. 71, pp. 360–366, 1997.

[145] KIM, J.-D. and KIM, D.-S., "Waviness compensation of precision machining by peizo-electric micro cutting device," *International Journal of Machine Tools and Manufacture*, vol. 38, pp. 1305–1322, 1998.

[146] KIM, K. and HA, J., "Suppression of machine tool chatter using a viscoelastic dynamic damper," *Journal of Engineering for Industry*, vol. 109, pp. 58–65, 1987.

[147] KIMURA, J., HARADA, S., and SAEKI, M., "Proposal of a parallel supporting damper with tendon and robust control system design," in *International Conference on Control Applications*, (Kohala Coast, HA), pp. 1412–1417, 1999.

[148] KORENEV, B. G. and REZNIKOV, L. M., *Dynamic Vibration Absorbers:Theory and Technical Applications*. New York: John Wiley and Sons, 1993.

[149] KOZAK, K., EBERT-UPHOFF, I., and SINGHOSE, W., "Analysis of varying natural frequencies and damping ratios of a sample parallel manipulator throughout its workspace using linearized equations of motion," in *ASME Design Engineering Technical Conferences*, (Pittsburgh, PA), 2001.

[150] KOZAK, K., HUEY, J., and SINGHOSE, W., "Performance measures for input shaping," in *IEEE Conf. on Control Applications*, (Istanbul, Turkey), 2003.

[151] KULIK, V. and PEDCHENKO, A., "Simplified design calculation schemes for machine tool mechanisms," *Soviet Engineering Research*, vol. 9, no. 5, pp. 81–86, 1989.

[152] LAUDERBAUGH SANDERS, L. K., "Process dynamics models for the control of end milling," in *American Control Conference*, (Chicago IL), pp. 2563–2567, 2000.

[153] LAURA, P. A. A., POMBO, J. L., and SUSEMIHL, E. A., "A note of the vibration of a clamped-free beam with a mass at the end," *Journal of Sound and Vibration*, vol. 37, no. 2, pp. 161–168, 1974.

[154] LAWRENCE, J. and SINGHOSE, W., "Decreasing effects of coulomb friction in precision positioning using input shaping: Experimental verifications," in *Japan-USA Symp. on Flexible Automation*, (Hiroshima, Japan), 2002.

[155] LEE, H. S. and TOMIZUKA, M., "Robust motion controller design for high-accuracy positioning systems," *IEEE Transactions on Industrial Electronics*, vol. 43, no. 1, pp. 48–55, 1996.

[156] LEE, W. B., "Prediction of microcutting force variation in ultra-precision machining," *Precision Engineering*, vol. 12, no. 1, pp. 25–28, 1990.

[157] LEE, W. Y., KIM, K. W., and SIN, H. C., "Design and analysis of a milling cutter with improved dynamic characteristics," *International Journal of Machine Tools and Manufacture*, vol. 42, pp. 961–967, 2002.

[158] LEE, W., CHEUNG, C., CHIU, W., and LEUNG, T., "An investigation of residual form error compensation in ultra-precision machining of aspheric surfaces," *Journal of Materials Processing Technology*, vol. 99, pp. 129–134, 2000.

[159] LI, C. F., JOHNSON, D. B., and KOVACEVIC, R., "Modeling of waterjet guided laser grooving of silicon," *International Journal of Machine Tools and Manufacture*, vol. 43, pp. 925–936, 2003.

[160] LI, C. J. and LI, S., "To improve workpiece roundness in precision diamond turning by in situ measurement and repetitive control," *Mechatronics*, vol. 6, no. 5, pp. 523–535, 1996.

[161] LI, J., NIEMANN, D., and WANG, H. O., "Robust tracking for high-rise/high-speed elevators," in *American Control Conference*, (Philadelphia, PA), 1998.

[162] LI, P., DAI, S., CHAI, S., and LI, Y., "High damping al-fe-mo-si/zn-al composites produced by rapidly solidified powdered metallurgy process," *Scripta Materialia*, vol. 42, pp. 955–960, 2000.

[163] LI, Q., TSO, S., GUO, L., and ZHANG, W., "Improving motion tracking of servomotor-driven closed-loop mechanisms using mass-redistribution," *Mechanism and Machine Theory*, vol. 35, pp. 1033–1045, 2000.

[164] LI, Q., ZHANG, W., and CHEN, L., "Design for control- a concurrent engineering approach for mechatronic systems design," *IEEE/ASME Transactions on Mechatronics*, vol. 6, no. 2, pp. 161–169, 2001.

[165] LI, S., LIU, R., and ZHANG, A., "Study on an end milling generation surface model and simulations taking into account of main axle's tolerance," *Journal of Materials Processing Technology*, vol. 129, pp. 86–90, 2002.

[166] LI, Y. Y., "Analytical study of a system with a mechanical filter," *Journal of Sound and Vibration*, vol. 274, no. 4, pp. 633–653, 2001.

[167] LIANG, Y., MORONUKI, N., and FURUKAWA, Y., "Calculations of the effect of material anisotropy on microcutting processes," *Precision Engineering*, vol. 16, no. 2, pp. 132–138, 1994.

[168] LIAO, Y. J. G. and HU, S. J., "Flexible multibody dynamics based fixture-workpiece analysis model for fixturing stability," *International Journal of Machine Tools and Manufacture*, vol. 40, pp. 343–362, 2000.

[169] LILIEN, J.-L. and VINOGRADOV, A. A., "Full-scale tests of torsional damper and detuner (tdd) antigalloping device," *IEEE Transactions on Power Delivery*, vol. 17, no. 2, pp. 638–643, 2002.

[170] LIM, E. M. and MENQ, C.-H., "Integrated planning for precision machining of complex surfaces. part 1: Cutting-path and feedrate optimization," *International Journal of Machine Tool Manufacture*, vol. 37, no. 1, pp. 61–75, 1997.

[171] LIM, K. B. and JUNKINS, J. L., "Robustness optimization of structural and controller parameters," *Journal of Guidance, Control, Dynamics*, vol. 12, no. 1, pp. 89–96, 1989.

[172] Liu, X., DeVor, R., Kapoor, S. G., and Ehmann, K. F., "The mechanics of machining at the microscale: Assessment of the current state of the science," *Journal of Manufacturing Science and Engineering*, vol. 126, pp. 666–678, 2004.

[173] Longoria, R. and Narayanan, V., "Modeling and design of an inertial vibration reflector," *Journal of Mechanical Design*, vol. 119, no. March, pp. 20–27, 1997.

[174] Lucca, D., Seo, Y., and Rhorer, R., "Aspects of surface generation in orthogonal ultraprecision machining," *Annals of the CIRP*, vol. 43, no. 1, pp. 43–46, 1994.

[175] Lust, R. V. and Schmit, L., "Control-augmented structural synthesis," *AIAA Journal*, vol. 26, no. 1, pp. 86–95, 1988.

[176] Magee, D. P. and Book, W. J., "Filtering micro-manipulator wrist commands to prevent flexible base motion," in *American Control Conf.*, (Seattle, WA), 1995.

[177] Magee, D. P. and Book, W. J., "Optimal filtering to minimize the elastic behavior in serial link manipulators," in *American Control Conference*, (Philadelphia, PA), 1998.

[178] Magee, D. P., Cannon, D. W., and Book, W. J., "Combined command shaping and inertial damping for flexure control," in *American Control Conference*, (Albuquerque, NM), 1997.

[179] Manning, R. and Schmit, L., "Control augmented structural synthesis with transient response constraints," *AIAA Journal*, vol. 28, no. 5, pp. 883–891, 1990.

[180] Marinescu, I. D., Ispas, C., and Boboc, D., *Handbook of Machine Tool Analysis*. New York: Marcel Dekker, Inc., 2002.

[181] Marquez, J., Fortgang, J., Singhose, W., and Perez, H., "Optimizacion del proceso de microfresado mediante el empleo de tecnicas de reduccion activa de vibraciones," in *XVI National Conference of Mechanical Engineering (Spain)*, (Leon, Spain), pp. 2709–2714, 2004.

[182] Marui, E., Ema, S., Hashimoto, M., and Wakasawa, Y., "Plate insertion as a means to improve the damping capacity of a cutting tool system," *International Journal of Machine Tools and Manufacture*, vol. 38, pp. 1209–1220, 1998.

[183] Masuzawa, T. and Tonshoff, H., "Three-dimensional micromachining by machine tools," *Annals of the CIRP*, vol. 46, no. 2, pp. 621–658, 1997.

[184] Matsumura, T., Hanawa, T., Ninomiya, Y., and Shirakashi, T., "Machining system for micro fabrication on glass," in *Japan-USA Symposium on Flexible Automation*, (Denver, CO), 2004.

[185] McInroy, J. E., "Modeling and design of flexure jointed stewart platforms for control purposes," *IEEE/ASME Transactions on Mechatronics*, vol. 7, no. 1, pp. 95–99, 2002.

[186] Meckl, P. H., Arestides, P. B., and Woods, M. C., "Optimized s-curve motion profiles for minimum residual vibration," in *American Controls Conference*, (Philadelphia, PA), 1998.

[187] MEKID, S., "High precision linear slide. part i: design and construction," *International Journal of Machine Tools and Manufacture*, vol. 40, pp. 1039–1050, 2000.

[188] MENON, K. and KRISHNAMURTHY, K., "Control of low velocity friction and gear backlash in a machine tool feed drive," *Mechatronics*, vol. 9, pp. 33–52, 1999.

[189] MIRZAEI, S., SAGHAIANNEJAD, S., TAHANI, V., and MOALLEM, M., "Electromagnetic shock absorber," in *Electric Machines and Drives Conference*, pp. 760 –764, 2001.

[190] MISHIMA, N., "Concept proposal of a modular micro machine tool and its design evaluation," in *Japan-USA Symposium on Flexible Automation*, (Denver, CO), 2004.

[191] NAKAMURA, Y., CHUNG, W., and SORDALEN, O. J., "Design and control of the nonholonomic manipulator," *IEEE Transactions on Robotics and Automation*, vol. 17, no. 1, pp. 48–59, 2001.

[192] NASHIF, A. D., JONES, D. I. G., and HENDERSON, J. P., *Vibration Damping*. New York: John Wiley and Sons, 1985.

[193] NATSIAVAS, S., "Steady state oscillations and stability of non-linear dynamic vibration absorbers," *Journal of Sound and Vibration*, vol. 156, no. 2, pp. 227–245, 1992.

[194] NIGAM, N. and NARAYANAN, S., *Applications of Random Vibrations*. New York: Springer-Verlag and Narosa Publishing House, 1994.

[195] NISHIMURA, H. and KOJIMA, A., "Robust vibration isolation control for a multi-degree-of-freedom structure," in *IEEE International Conference on Control Applications*, (Trieste Italy), 1998.

[196] NISHIMURA, H. and KOJIMA, A., "Seismic isolation control for a buildinglike structure," *IEEE Control System*, vol. December, pp. 38–44, 1999.

[197] NIU, W. and TOMIZUKA, M., "A new approach of coordinated motion control subjected to actuator constraints," *ASME J. of Dynamic Systems, Measurement, and Control*, vol. 123, no. 3, 2001.

[198] OGATA, K., *System Dynamics*. Englewood Cliffs, NJ: Prentice Hall, Inc, 2nd ed., 1992.

[199] OGURA, I. and OKAZAKI, Y., "Profile generation for brittle materials by using ultra-precision lathe with on-machine measurement system," in *American Society for Precision Engineering Annual Meeting*, (Crystal City, Virginia), 2001.

[200] OKAZAKI, Y., "A micro-positioning tool post using a piezoelectric actuator for diamond turning machines," *Precision Engineering*, vol. 12, no. 3, pp. 151–516, 1990.

[201] OKAZAKI, Y., "Fast tool servo system and its application ot three dimensional fine surface figures," in *American Society for Precision Engineering*, 1998.

[202] OKAZAKI, Y., "Raster-scan machining for rapid generation of three-dimensional fine surface figures," in *Japan-USA Flexible Automation Conference*, (Ann Arbor, Michigan), 2000.

[203] OKAZAKI, Y., "Desk-top ultra high-speed milling machine," in *3rd International Workshop on Microfactories*, (Minneapolis, MN), pp. 41–44, 2002.

[204] OKAZAKI, Y., MORI, T., and NORITA, N., "Desk-top nc milling machine with 200 krpm spindle," in *ASPE 2001 Annual Meeting*, (Crystal City, VA), pp. 192–195, 2001.

[205] ONISZCZUK, Z., "Damped vibration analysis of two-degree-of-freedom discrete system," *Journal of Sound and Vibration*, vol. 257, no. 2, pp. 391–403, 2002.

[206] ONODA, J. and HAFTKA, R. T., "An approach to structural/control simultaneous optimization for large flexible spacecraft," *AIAA Journal*, vol. 25, no. 8, pp. 1133–1138, 1987.

[207] OUEINI, SHAFIC S.; CHIN, C.-M. N. A. H., "Dynamics of a cubic nonlinear vibration absorber," *Nonlinear Dynamics*, vol. 20, pp. 283–295, 1999.

[208] OZISIK, H. and KELTIE, R., "Implementation of an open-loop control technique for high-speed micropositioning in a single-point diamond turning process," *Precision Engineering*, vol. 13, no. 2, pp. 83–94, 1991.

[209] PAHL, G. and BEITZ, W., *Engineering design*. New York: Design Council, 1984.

[210] PAN, G., XU, H., KWAN, C. M., LIANG, C., HAYNES, L., and GENG, Z., "Modeling and intelligent chatter control strategies for a lathe machine," in *IEEE International Conference on Control Applications*, (Dearborn, MI), 1996.

[211] PAO, L. Y., "Multi-input shaping design for vibration reduction," *Automatica*, vol. 35, no. 1, pp. 81–89, 1999.

[212] PARK, J.-H. and ASADA, H., "Concurrent design optimization of mechanical structure and control for high speed robots," *Journal of Dynamic Systems, Measurement, and Control*, vol. 116, pp. 344–354, 1994.

[213] PARK, U. H., LEE, J. W., LIM, B. D., and SUNG, Y. G., "Design and sensitivity analysis of an input shaping filter in the z-plane," *J. of Sound and Vibration*, vol. 243, pp. 157–171, 2001.

[214] PARKER, R. G., "A physical explanation for the effectiveness of planet phasing to suppress planetary gear vibration," *Journal of Sound and Vibration*, vol. 236, no. 4, pp. 561–573, 2000.

[215] PEI, Z. and FERREIRA, P., "An experimental investigation of rotary ultrasonic face milling," *International Journal of Machine Tools and Manufacture*, vol. 39, pp. 1327–1344, 1999.

[216] PEI, Z., KHANNA, N., and FERREIRA, P., "Rotary ultrasonic machining of structural ceramics - a review," *Ceramic Engineering and Science Proceedings*, vol. 16, no. 1, pp. 259–278, 1995.

[217] PENNESTRI, E., "An application of chebyshev's min-max criterion to the optimal design of a damped dynamic vibration absorber," *Journal of Sound and Vibration*, vol. 217, no. 4, pp. 757–765, 1998.

[218] PICARD, Y., ADAMS, D., VASILE, M., and RITCHEY, M., "Focused ion beam-shaped microtools for ulta-precision machining of cylindrical components," *Precision Engineering*, vol. 27, pp. 56–69, 2003.

[219] POIGNET, P., GAUTIER, M., KHALIL, W., and PHAM, M. T., "Modeling, simulation and control of high speed machine tools using robotics formalism," *Mechatronics*, vol. 12, pp. 461–487, 2002.

[220] RANDALL, S. E., "Optimum vibration absorbers for linear damped systems," *Journal of Mechanical Design*, vol. 103, no. October, pp. 908–913, 1981.

[221] RAO, S., "Combined structural and control optimization of flexible strucures," *Engineering Optimization*, vol. 13, pp. 1–16, 1988.

[222] RAO, S., PAN, T. S., and VENKAYYA, V., "Robustness improvement of actively controlled structures through structural modifications," *AIAA Journal*, vol. 28, no. 2, pp. 353–361, 1990.

[223] RASTEGAR, J., KHORRAMI, F., and RETCHKIMAN, Z., "Inversion of nonlinear systems via the trajectory patten method," in *Decision and Control*, (Lake Buena Vista, FL), 1994.

[224] RASTEGAR, J. S., LIU, L., and YIN, D., "Task-specific optimal simultaneos kinematic, dynamic, and control design of high-performance robotic systems," *IEEE/ASME Transactions on Mechatronics*, vol. 4, no. 4, pp. 387–395, 1999.

[225] RAYLEIGH, J. W., *The Theory of Sound*, vol. 1. New York: Dover Publications, second ed., 1945.

[226] REDDY, V. R. and SHARAN, A. M., "The finite element modelled design of lathe spindles: The static and dynamic analyses," *Journal of Vibration, Acoustics, Stress, and Reliability in Design*, vol. 109, pp. 407–415, 1987.

[227] REYER, J. A. and PAPLAMBROS, P. Y., "Combined optimal design and control with application to an electric dc motor," *Journal of Mechanical Design*, vol. 124, pp. 183–191, 2002.

[228] RIVIN, E. I., "Vibration isolation of precision equipment," *Precision Engineering*, vol. 17, pp. 41–56, 1995.

[229] RIVIN, E. I., *Stiffness and Damping in Mechanical Design.* New York: Marcel Dekker, Inc., 1999.

[230] RIVIN, E. I. and KANG, H., "Enhancement of dynamic stability of cantilever tooling structures," *International Journal of Machine Tool Manufacture*, vol. 32, no. 4, pp. 539–561, 1992.

[231] RO, P. I. and HUBBEL, P. I., "Nonlinear micro-dynamic behavior of a ball-screw driven precision slide system," *Precision Engineering*, vol. 14, no. 4, pp. 229–236, 1992.

[232] ROBERTS, R., "Control of high-rise/high-speed elevators," in *American Control Conference*, (Philadelphia, PA), 1998.

[233] SADEGHIPOUR, K., "Dynamic modelling and modal flexibility sharing of vibrating machine tool system," in *Manufacturing International*, (Atlanta), 1990.

[234] SADEGHIPOUR, K. and COWLEY, A., "Receptance sensitivity and the effect of concentrated mass inserts on the modal balance of spindle-bearing systems," *International Journal of Machine Tool Design and Research*, vol. 26, no. 4, pp. 415–429, 1986.

[235] SASTRY, S., KAPOOR, S. G., and DEVOR, R. E., "Compensation of progressive radial run-out in face-milling by spindle speed variation," *International Journal of Machine Tools and Manufacture*, vol. 40, pp. 1121–1139, 2000.

[236] SAWADA, K., ODAKA, S., KAWAI, T., HIRAI, T., TAKEUCHI, Y., and SATA, T., "Manufacture of diffraction grating on tiny parts by means of ultraprecision milling," *Microsystem Technologies*, vol. 5, pp. 157–160, 1999.

[237] SAWADA, K., KAWAI, T., SATA, T., and TAKEUCHI, Y., "Development of ultraprecision micro grooving (manufacture of v-shaped groove)," *JSME International Journal Series C.*, vol. 43, no. 1, pp. 170–176, 2000.

[238] SCHALLER, T., BOHN, L., MAYER, J., and SCHUBERT, K., "Microstructure grooves with a width of less than 50 micrometers cut with ground hard metal micro end mills," *Precision Engineering*, vol. 23, pp. 229–235, 1999.

[239] SCHMITENDORF, W. E., "Designing tuned mass dampers ia static output feedback: a numerical approach," *Earthquake Engineering and Structural Dynamics*, vol. 29, pp. 127–137, 2000.

[240] SCHOUTEN, C., ROSIELLE, P., and SCHELLEKENS, P., "Design of a kinematic coupling for precision applications," *Precision Engineering*, vol. 20, pp. 46–52, 1997.

[241] SETH, N., RATTAN, K., and BRANDSTETTER, R., "Vibration control of a coordinate measuring machine," in *IEEE Conf. on Control Apps.*, (Dayton, OH), pp. 368–73, 1993.

[242] SHAW, J., SHAW, S. W., and HADDOW, A. G., "On the response of the non-linear vibration absorber," *International Journal of Non-Linear Mechanics*, vol. 24, no. 4, pp. 281–293, 1989.

[243] SHEKAR, N. C., HATWAL, H., and MALLIK, A. K., "Performance of non-linear isolators and absorbers to shock excitations," *Journal of Sound and Vibration*, vol. 227, no. 2, pp. 293–307, 1999.

[244] SHIN, Y. and WANG, K., "Design of an optimal damper to minimize the vibration of machine tool structures subject to random excitation," *Engineering with Computers*, vol. 7, no. 4, pp. 199–208, 1991.

[245] SIMONS, D. and ISIK, C., "Optimal trigonometric robot joint trajectories," *Robotica*, vol. 9, pp. 379–386, 1991.

[246] SINGER, N. C., *Residual vibration reduction in computer controlled machines.* Phd., M. I. T., 1988.

[247] SINGER, N., SINGHOSE, W., and KRIIKKU, E., "An input shaping controller enabling cranes to move without sway," in *ANS 7th Topical Meeting on Robotics and Remote Systems*, (Augusta, GA), 1997.

[248] SINGER, N. C. and SEERING, W. P., "Preshaping command inputs to reduce system vibration," *J. of Dynamic Sys., Measurement, and Control*, vol. 112, no. March, pp. 76–82, 1990.

[249] SINGH, G. and BEOHAR, S., "Synthesis of profile actuated lathe tool slide mechanism using information theory," *Journal of the Franklin Institute*, vol. 334B, no. 3, pp. 377–388, 1997.

[250] SINGH, T. and ALLI, H., "Exact time-optimal control of the wave equation," *Journal of Guidance, Control, Dynamics*, vol. 19, no. 1, pp. 130–134, 1996.

[251] SINGH, T. and HEPPLER, G. R., "Shaped inputs for a multimode system," in *Proceedings of the IEEE International Conference on Robotics and Automation*, vol. 3, (Atlanta, GA), pp. 484–489, IEEE, 1993.

[252] SINGH, T. and SINGHOSE, W., "Tutorial on input shaping/time delay control of maneuvering flexible structures," in *American Control Conference*, (Anchorage, AK), 2002.

[253] SINGHOSE, W. and CHUANG, T., "Reducing deviations from trajectory components with input shaping," in *American Control Conference*, vol. 1, (Seattle, WA), pp. 929–33, 1995.

[254] SINGHOSE, W., SEERING, W., and SINGER, N., "Residual vibration reduction using vector diagrams to generate shaped inputs," *J. of Mechanical Design*, vol. 116, no. June, pp. 654–659, 1994.

[255] SINGHOSE, W. and SINGER, N., "Effects of input shaping on two-dimensional trajectory following," *IEEE Trans. on Robotics and Automation*, vol. 12, no. 6, pp. 881–887, 1996.

[256] SINGHOSE, W., SINGER, N., and SEERING, W., "Improving repeatability of coordinate measuring machines with shaped command signals," *Precision Engineering*, vol. 18, no. April, pp. 138–146, 1996.

[257] SINGHOSE, W., SINGER, N., and SEERING, W., "Time-optimal negative input shapers," *J. of Dynamic Systems, Measurement, and Control*, vol. 119, no. June, pp. 198–205, 1997.

[258] SINGHOSE, W. E., *Command Generation for Flexible Systems*. Ph.d., PhD. Thesis, Massachusetts Institute of Technology, 1997.

[259] SINGHOSE, W. E., CRAIN, E. A., and SEERING, W. P., "Convolved and simultaneous two-mode input shapers," *Control Theory and Applications*, no. Nov., pp. 515–520, 1997.

[260] SINGHOSE, W. E., PAO, L. Y., and SEERING, W. P., "Slewing multi-mode flexible spacecraft using zero derivative robustness constraints," *J. Guidance, Control, and Dynamics*, vol. 20, no. 1, pp. 204–206, 1997.

[261] SINGHOSE, W. E., PORTER, L. J., and SEERING, W. P., "Input shaped control of a planar gantry crane with hoisting," in *American Control Conf.*, (Albuquerque, NM), 1997.

[262] SINGHOSE, W. E., SEERING, W. P., and SINGER, N. C., "Shaping inputs to reduce vibration: A vector diagram approach," in *IEEE Int. Conf. on Robotics and Automation*, vol. 2, (Cincinnati, OH), pp. 922–927, IEEE, 1990.

[263] SINGHOSE, W. E., SEERING, W. P., and SINGER, N. C., "Input shaping for vibration reduction with specified insensitivity to modeling errors," in *Japan-USA Sym. on Flexible Automation*, (Boston, MA), 1996.

[264] SINGHOSE, W. E., SINGER, N. C., DEREZINSKI, S. J., RAPPOLE, B. W., and KENNETH, P., "Method and apparatus for minimizing unwanted dynamics in a physical system," June 10, 1997 1997.

[265] SLOCUM, A. H., "Design of three-groove kinematic couplings," *Precision Engineering*, vol. 14, pp. 67–73, 1992.

[266] SLOCUM, A. H., *Precision Machine Design*. Englewood Cliffs, NJ: Prentice-Hall, Inc., 1992.

[267] SLOCUM, A. H., MARSH, E. R., and SMITH, D. H., "A new damper design for machine tool structures: the replicated internal viscous damper," *Precision Engineering*, vol. 16, no. 3, pp. 174–183, 1994.

[268] SMITH, A. and TLUSTY, J., "An overview of modeling and simulation of the milling process," *Journal of Engineering for Industry*, vol. 113, pp. 169–175, 1991.

[269] SMITH, M. H., ANNASWAMY, A. M., and SLOCUM, A. H., "Adaptive control strategies for a precision machine tool axis," *Precision Engineering*, vol. 17, pp. 192–206, 1995.

[270] SMITH, O. J. M., "Posicast control of damped oscillatory systems," *Proceedings of the IRE*, vol. 45, no. September, pp. 1249–1255, 1957.

[271] SNOWDON, J. C., *Vibration and Shock in Damped Mechanical Systems*. New York: John Wiley and Sons, Inc., 1968.

[272] SNOWDON, J. C., "Vibration isolation: Use and characterization," *Journal of the Acoustical Society of America*, vol. 66, no. 5, pp. 124–1274, 1979.

[273] SOONS, J. A., THEUWS, F. C., and SCHELLEKENS, P. H., "Modeling the errors of multi-axis machines: a general methodology," *Precision Engineering*, vol. 14, no. 1, pp. 5–19, 1992.

[274] SPANOS, J., RAHMNA, Z., and BLACKWOOD, G., "A soft 6-axis active vibration isolator," in *American Control Conference*, (Seattle, Washington), pp. 412–416, 1995.

[275] SUBRAHMANIAN, R. and EHMANN, K. F., "Development of a meso-scale machine tool (mmt) for micro-machining," in *Japan-USA Symposium on Flexible Automation*, vol. 1, (Hiroshima, Japan), pp. 163–169, 2002.

[276] SUN, J., JOLLY, M., and NORRIS, M. A., "Passive, adaptive, and active tuned vibration absorbers- a survey," *Journal of Vibration and Acoustics*, vol. 117, pp. 234–242, 1995.

[277] SUTHERLAND, J. and DEVOR, R., "An improved method for cutting force and surface error prediction in flexible end milling systems," *Journal of Engineering for Industry*, vol. 108, pp. 269–279, 1986.

[278] TAKENAKA, Y., KOBORI, T., ISHII, K., YAMADA, T., ARITA, T., TANIDA, K., KOIKE, Y., MUTAGUCHI, M., MURATA, T., and MARUOKA, M., "Development and application of v-shaped hybrid mass damper for high-rise buildings," in *MOVIC*, (Yokohama, Japan), 1994.

[279] TAKEUCHI, Y., SAWADA, K., and SATA, T., "Ultraprecision 3d micromachining of glass," *Annals of the CIRP*, vol. 45, no. 1, pp. 401–404, 1996.

[280] TAKEUCHI, Y., KATO, K., KAWAKITA, S., SAWADA, K., and SATA, T., "Generation of sculptured surfaces by means of an ultraprecision milling machine," *Annals of the CIRP*, vol. 41, no. 1, pp. 611–614, 1993.

[281] TAKEUCHI, Y., SAWADA, K., and SATA, T., "Computer aided ultra-precision micromachining of metallic materials," in *IEEE International Conference on Robotics and Automation*, pp. 67 –72, 1995.

[282] TANIDA, K., KOIKE, Y., MUTAGUCHI, M., MURATA, T., and IMAZEKI, M., "Development of v-shaped hybrid mass damper and application of high-rise building," *IHI Engineering Review*, vol. 29, no. 2, pp. 72–78, 1996.

[283] TAYLOR, J. B. and TU, J. F., "Precision x-y microstage with maneuverable kinematic coupling mechanism," *Precision Engineering*, vol. 18, pp. 85–94, 1996.

[284] TAYLOR, S., KHOO, B. T., and WALTON, D., "Microcomputer optimization of machine tool spindle stiffness," *International Journal of Machine Tool Manufacture*, vol. 30, no. 1, pp. 151–159, 1990.

[285] THOMAS, R., FORTGANG, J., and SINGHOSE, W., "Optimization of lightly damped pick-and-place processes using optimal dynamic-vibration-absorbers," in *MOVIC 2002*, (Saitama Japan), 2002.

[286] THOMSEN, J. J., "Vibration suppression by using self-arranging mass: Effects of adding restoring force," *Journal of Sound and Vibration*, vol. 197, no. 4, pp. 403–425, 1996.

[287] TLUSTY, J. and MACNEIL, P., "Dynamics of cutting forces in end milling," *Annals of the CIRP*, vol. 24, no. 1, pp. 21–25, 1975.

[288] TOBIAS, S. A., *Machine-Tool Vibrations*. New York: John Wiley and Sons, 1965.

[289] TOMIZUKA, M., "Zero phase error tracking algorithm for digital control," *Journal of Dynamic Systems, Measurement, and Control*, vol. 109, pp. 65–68, 1987.

[290] TONGUE, B. H., *Principles of Vibration*. New York: Oxford University Press, 1996.

[291] TOUNSI, A., BAILEY, T., and ELBESTAWI, M. A., "Indentification of acceleration deceleration profiles of feed drive systems in cnc machines," *International Journal of Machine Tools and Manufacture*, vol. 43, pp. 441–451, 2003.

[292] TOUTANT, R., BALAKRISHNAN, S., ONYSHKO, S., and POPPLEWELL, N., "Feedrate compensation for constant cutting force turning," *IEEE Control System*, vol. December, pp. 44–47, 1993.

[293] TSAI, Y.-C. and HSIEH, J.-M., "A study of a design and nc manufacturing model of ball-end cutters," *Journal of Materials Processing Technology*, vol. 117, pp. 183–192, 2001.

[294] TU, Q. and RASTEGAR, J., "The effects of manipulator type on the vibrational excitation during motion," *Mechanism and Machine Theory*, vol. 32, no. 2, pp. 221–234, 1997.

[295] TUNG, E., TOMIZUKA, M., and URUSHISAKI, Y., "High-speed end milling using a feedforward control architecture," *Journal of Manufacturing Science and Engineering*, vol. 118, pp. 178–187, 1996.

[296] TUTTLE, T. D. and SEERING, W. P., "A zero-placement technique for designing shaped inputs to suppress mulitple-mode vibration," in *American Controls Conference*, (Baltimore, MD), 1994.

[297] TZES, A. and YURKOVICH, S., "An adaptive input shaping control scheme for vibration suppression in slewing flexible structures," *IEEE Transactions on Control Systems Technology*, vol. 1, no. June, pp. 114–121, 1993.

[298] TZOU, H. S., "Design of a piezoelectric exciter/actuator for micro-displacement control: theory and experiment," *Precision Engineering*, vol. 13, no. 2, pp. 104–110, 1991.

[299] VAN BRUSSEL, H., "Mechatronics-a powerful concurrent engineering framework," *IEEE/ASME Transactions on Mechatronics*, vol. 1, no. 2, pp. 127–136, 1996.

[300] VAN BRUSSEL, H., SAS, P., NEMETH, I., DE FONSECA, P., and VAN DE BRAEMBUSSCHE, P., "Towards a mechatronic compiler," *IEEE/ASME Transactions on Mechatronics*, vol. 6, no. 1, pp. 90–105, 2001.

[301] VARANASI, K. K. and NAYSEH, S. A., "The dynamics of lead-screw drives: Low-order modeling and experiments," *Journal of Dynamic Systems, Measurement, and Control*, vol. 126, pp. 388–396, 2004.

[302] VASILE, M., FRIEDRICH, C. R., KIKKERI, B., and McELHANNON, R., "Micrometer-scale machining: tool fabrication and initial results," *Precision Engineering*, vol. 19, pp. 180–186, 1996.

[303] VENKATESH, S. R. and CHO, Y. M., "Identification and control of high-rise elevators," in *American Control Conference*, (Philadelphia, PA), 1998.

[304] VOGLER, M. P., DEVOR, R. E., and KAPOOR, S. G., "On the modeling and analysis of machining performance in micro-endmilling, part 1: Surface generation," *Journal of Manufacturing Science and Engineering*, vol. 126, pp. 685–694, 2004.

[305] VOGLER, M. P., KAPOOR, S. G., and DeVOR, R. E., "On the modeling and analysis of machining performance in micro-endmilling, part 2: Cutting force prediction," *Journal of Manufacturing Science and Engineering*, vol. 126, pp. 695–705, 2004.

[306] VOGLER, M. P., LIU, X., KAPOOR, S. G., and DeVOR, R. E., "Development of meso-scale machine tool (mmt) systems," *Transactions of NAMRI/SME*, vol. 30, pp. 653–66, 2002.

[307] WAKASAWA, Y., HASHIMOTO, M., and MARUI, E., "Damping capacity improvement of machine structures by close packing with balls," *International Journal of Machine Tools and Manufacture*, vol. 42, pp. 467–472, 2002.

[308] WALSH, P. L. and LAMANCUSA, J. S., "A variable stiffness vibration absorber for minimization of transient vibrations," *Journal of Sound and Vibration*, vol. 158, no. 2, pp. 195–211, 1992.

[309] WANG, A., FUNG, R., and HUANG, S., "Dynamic analyis of a tall building with a tuned-mass-damper device subjected to earthquake excitations," *Journal of Sound and Vibration*, vol. 244, no. 1, pp. 123–136, 2001.

[310] WANG, J. J., LIANG, S., and BOOK, W. J., "Convolution analysis of milling force pulsation," *Journal of Engineering for Industry*, vol. 116, pp. 17–25, 1994.

[311] WANG, M. and FEI, R., "Chatter suppression based on nonlinear vibration characteristic of electrorheological fluids," *International Journal of Machine Tools and Manufacture*, vol. 39, pp. 1925–1934, 1999.

[312] WARBURTON, G. B.; AYORINDE, E., "Optimum absorber parameters for simple systems," *Earthquake Engineering And Structural Dynamics*, vol. 8, pp. 197–217, 1980.

[313] WEAVER, W. J., TIMOSHENKO, S. P., and YOUNG, D. H., *Vibration Problems in Engineering*. New York: John Wiley and Sons, fifth ed., 1990.

[314] WEI, C. and LIN, J. F., "Kinematic analysis of the ball screw mechanism considering variable contact anfles and elastic deformation," *Journal of Mechanical Design*, vol. 125, pp. 717–733, 2003.

[315] WELBOURN, D. B. and SMITH, J. D., *Machine-tool dynamics: An introduction*. London: Cambridge University Press, 1970.

[316] WU, B.-C., YOUNG, G.-S., and HUANG, T.-Y., "Application of a two-level optimization process to conceptual structual design of a machine tool," *International Journal of Machine Tools and Manufacture*, vol. 40, pp. 783–794, 2000.

[317] XU, A.-P., QU, Y. X., ZHANG, D.-W., and HUANG, T., "Simulation and experimental investigation of the end milling process considering cutter flexibility," *International Journal of Machine Tools and Manufacture*, vol. 43, pp. 283–292, 2003.

[318] XUE, S. D., KO, J. M. ., and XU, Y. L., "Optimum parameters of a tuned liquid column damper for suppressing pitching vibration of an undamped structure," *Journal of Sound and Vibration*, vol. 235, no. 4, pp. 639–653, 2000.

[319] Ya, W., Shiqiu, K., Shuzi, Y., Qilin, Z., Shanxiang, X., and Yaozu, W., "An experimental study of cutting noise dynamics," in *ASME Design Technical Conferences*, (Miami, FL), 1991.

[320] Yang, L.-F., Chew, M.-S., and Juang, J.-N., "Concurrent mechanism and control design for slewing of flexible space structures," *Journal of Mechanical Design*, vol. 116, no. September, pp. 944–951, 1994.

[321] Yeh, J. and Liou, F., "Contact condition modelling for machining fixture setup processes," *International Journal of Machine Tools and Manufacture*, vol. 39, pp. 787–903, 1999.

[322] Yen, H.-Y. and Shen, M.-H. H., "Passive vibration suppression of beams and blades using magnetomechanical coating," *Journal of Sound and Vibration*, vol. 245, no. 4, pp. 701–714, 2001.

[323] Yoshimura, M., "Evaluation of forced and self-excited vibrations at the design stage of machine-tool structures," *Journal of Mechanisms, Transmissions, and Automation in Design*, vol. 108, no. 3, pp. 323–329, 1986.

[324] Youcef-Toumi, K., "Modeling, design, and contol intergration: A necessary step in mechatronics," *IEEE/ASME Transactions on Mechatronics*, vol. 1, no. 1, pp. 29–38, 1996.

[325] Yu, J.-H., Postrkhin, E., Ma, K. B., Wei-KanChu, and Wilson, T., "Vibration isolation for space structures using hts-magnet interaction," *IEEE Transactions on Applied Superconductivity*, vol. 9, no. 2, pp. 908–910, 1999.

[326] Yun, W.-S., Ko, J. H., Lee, H. U., Cho, D.-W., and Ehmann, K. F., "Development of a virtual machining system, part 3: Cutting process simulation in transient cuts," *International Journal of Machine Tools and Manufacture*, vol. 42, pp. 1617–1626, 2002.

[327] Zhang, G. P., Huang, Y. M., Shi, W. H., and Fu, W. P., "Predicting dynamic behaviors of a whole machine tool structure based on computer-aided engineering," *International Journal of Machine Tools and Manufacture*, vol. 43, pp. 699–706, 2003.

[328] Zhang, W. J., Li, Q., and Guo, L. S., "Integrated design of mechanical structure and control algorithm for a programmable four-bar linkage," *IEEE/ASME Transactions on Mechatronics*, vol. 4, no. 4, pp. 354–362, 1999.

[329] Zhu, W.-H., Jun, M. B., and Altinas, Y., "A fast tool servo design for precision turning of shafts on conventional cnc lathes," *International Journal of Machine Tools and Manufacture*, vol. 41, pp. 953–965, 2001.